Università degli Studi di Palermo

AREA QUALITÀ, PROGRAMMAZIONE E SUPPORTO STRATEGICO
SETTORE STRATEGIA PER LA RICERCA
U. O. DOTTORATI

Dottorato di Ricerca in "Scienze della Terra e del Mare"
Dipartimento di Scienze della Terra e del Mare (DiSTeM)
GEO/08 Geochimica e Vulcanologia

CHEMICAL AND ISOTOPIC CHARACTERISATION OF THE ATMOSPHERIC DEPOSITION IN VOLCANIC, URBAN, INDUSTRIAL, AND RURAL ENVIRONMENTS IN SICILY, ITALY

IL DOTTORE
DOTT. FILIPPO BRUGNONE

IL COORDINATORE
PROF. ALESSANDRO AIUPPA

IL TUTOR
PROF. FRANCESCO PARELLO

CO TUTORS
PROF. SERGIO CALABRESE

DOTT. WALTER D'ALESSANDRO

CICLO XXXVI
ANNO CONSEGUIMENTO TITOLO 2024

Università degli Studi di Palermo

AREA QUALITÀ, PROGRAMMAZIONE E SUPPORTO STRATEGICO
SETTORE STRATEGIA PER LA RICERCA
U. O. DOTTORATI

Dottorato di Ricerca in "Scienze della Terra e del Mare"
Dipartimento di Scienze della Terra e del Mare (DiSTeM)
GEO/08 Geochimica e Vulcanologia

CHEMICAL AND ISOTOPIC CHARACTERISATION OF THE ATMOSPHERIC DEPOSITION IN VOLCANIC, URBAN, INDUSTRIAL, AND RURAL ENVIRONMENTS IN SICILY, ITALY

IL DOTTORE
DOTT. FILIPPO BRUGNONE

IL COORDINATORE
PROF. ALESSANDRO AIUPPA

IL TUTOR
PROF. FRANCESCO PARELLO

CO TUTORS
PROF. SERGIO CALABRESE

DOTT. WALTER D'ALESSANDRO

CICLO XXXVI
ANNO CONSEGUIMENTO TITOLO 2024

Università degli Studi di Palermo

AREA QUALITÀ, PROGRAMMAZIONE E SUPPORTO STRATEGICO
SETTORE STRATEGIA PER LA RICERCA
U. O. DOTTORATI

Dottorato di Ricerca in "Scienze della Terra e del Mare"
Dipartimento di Scienze della Terra e del Mare (DiSTeM)
GEO/08 Geochimica e Vulcanologia

CHEMICAL AND ISOTOPIC CHARACTERISATION OF THE ATMOSPHERIC DEPOSITION IN VOLCANIC, URBAN, INDUSTRIAL, AND RURAL ENVIRONMENTS IN SICILY, ITALY

IL DOTTORE
DOTT. FILIPPO BRUGNONE

IL COORDINATORE
PROF. ALESSANDRO AIUPPA

IL TUTOR
PROF. FRANCESCO PARELLO

CO TUTORS
PROF. SERGIO CALABRESE

DOTT. WALTER D'ALESSANDRO

CICLO XXXVI
ANNO CONSEGUIMENTO TITOLO 2024

A Noemi

Table of content

Abstract

The chemical composition of atmospheric deposition is influenced by several factors, including the chemical composition of gases and particulate matter from natural and anthropogenic sources, chemical and physical reactions during pollutant transport, and removal processes. This study aimed at investigating the atmospheric deposition by analysing rainwater pH and the concentration of major (F^-, Cl^-, HCO_3^-, NO_3^-, SO_4^{2-}, Na^+, K^+, NH_4^+, Ca^{2+}, and Mg^{2+}), trace (Li, B, Al, Si, Ti, V, Cr, Mn, Fe, Co, Ni, Cu, Zn, As, Se, Br, Rb, Sr, Mo, Cd, Sn, Sb, Cs, Ba, Tl, Pb, U), ultra-trace elements (Sc, Ge, Te, Y, Nb, Zr, Hf, Th, La, Ce, Pr, Nd, Sm, Eu, Gd, Tb, Dy, Ho, Er, Tm, Yb, Lu), and of the isotopic composition of B ($\delta^{11}B/^{10}B$) and Sr ($^{87}Sr/^{86}Sr$). A network of fifteen bulk collectors was used to collect 301 monthly atmospheric deposition samples for almost two years from four different contexts: urban, industrial, rural, and volcanic. Different techniques, including titration, ionic chromatography, inductively coupled plasma-optical emission and mass spectrometry, and multi-collector mass spectrometry, were employed to analyse these samples.

The results showed that the natural acidity of rainwater in the Etna area was derived from the dissolution of volcanic acid gases, while in urban and industrial areas, the acidity was increased by the dissolution of anthropogenic SOx and NOx and generally neutralised by Ca^{2+} and Mg^{2+} of crustal origin. Principal Component Analysis and Positive Matrix Factorisation were used to process the major ion concentrations, revealing that natural sources were responsible for the emissions of Na^+, Cl^-, and partly Mg^{2+} (dissolution of sea-salt aerosols), Ca^{2+}, HCO_3^- and, to some extent, Mg^{2+} and K^+ (dissolution of crustal materials), and of F^-, and partly Cl^-, and SO_4^{2-} (volcanic emissions). Conversely, K^+ (biomass burning), NH_4^+ (agricultural activities), NO_3^- and SO_4^{2-} (domestic heating, vehicular traffic, industrial emissions) were derived, mainly, from anthropogenic sources. Deposition rates of major ions were also calculated, with the highest values observed at coastal sites for Na^+ and Cl^-, and close to Mt. Etna for F^- and SO_4^{2-}.

In terms of trace elements, volcanic activity significantly contributed to the enrichment of rainwater in many trace elements, especially during the paroxysms that occurred between 2021 and 2022, resulting in intense volcanic ash deposition. The industrial area of Milazzo had the highest deposition fluxes of Br and B (marine source), as well as Ni, Mo, and Cr (industrial emissions). The urban area of Palermo had the highest flux of Sb, resulting from vehicle brake wear and tear. Comparing our data to those obtained for some trace elements in European rainwater showed that lower concentrations of Pb, Fe, and Al were found for rainwater in Sicily than in Europe, not considering the rainwater samples from Etna in which strong Fe and Al enrichments were measured. On the contrary, significant enrichments were observed for Zn, V, Cu, Ni, Cr, and As due to local inputs from urban and industrial emissions.

The concentration of trace elements in rainwater obtained from filtered (0.45 μm) aliquots only allows quantification of the contribution of the most soluble atmospheric particulate fraction. To have a complete picture of atmospheric deposition, it is necessary to measure the less soluble atmospheric particulate fraction in rainwater. This can be done by measuring the concentration of trace elements in two additional matrices: (i) solution obtained by the acidic mineralisation of the insoluble fraction deposited on the filters, and (ii) solution obtained by the dissolution of the material adhering to the surface of the bulk collector at the end of each sampling period. The insoluble fraction constituted for many elements the main contribution to the bulk atmospheric deposition, reaching up to 96.3%, 95.5%, and 86.8% for Ti, Fe, and Al, respectively. The relative contributions of the recovery solution reached values up to 9.37% for Pb. The samples obtained during dry and rainy periods revealed significant differences.

Technology-Critical Elements (TCEs) include ultra-trace elements, Sc, Zr, Nb, Ge, Y, Te, Hf, and Th, and the lanthanoids, La, Ce, Pr, Nd, Sm, Eu, Gd, Tb, Dy, Ho, Er, Tm, Yb, and Lu. Rainwater in urban areas had the highest concentrations of Sc, Zr, Nb, and Hf, while that of the Etna area had the highest concentrations of Ge, Y, and Te. Concentrations of Th were similar between the different

contexts. Rainwater from Etna had the highest concentrations of all lanthanoids, indicating that volcanic sources and leaching of volcanic ash enriched rainwater in these usually very low-concentration elements.

Boron and strontium isotopic compositions in rainwater samples were different in the Mt. Etna area compared to other study areas. Two sources of atmospheric emissions of B and Sr were identified. The marine source was predominant in urban and industrial areas close to the coastline, while the volcanic isotopic signature was prevalent at all sites on Mt. Etna and detectable up to 35 km from the summit craters.

Acknowledgements

I wish to express my deepest grateful to Prof. Francesco Parello, Prof. Sergio Calabrese, and Dott. Walter D'Alessandro for having supported and guided me during the PhD journey. Thanks to all the knowledge I have received from them, I had the opportunity to gain many new experiences, which made me grow both personally and professionally.

I want to extend special thanks to Prof. Filippo Saiano and Dott.ssa Maddalena Pennisi for welcoming me to their laboratories and making me feel at home from the first moment. A warm thank also goes to Dott. Matteo Salvadori for having supported and endured me during the laboratory activities carried out together.

Many thanks go to Dott. Lorenzo Brusca, Dott. Marcello Liotta, Dott. Sergio Bellomo and Dott. Vincenzo Prano who supported me during my crazy experiments and always kindly answered all my questions.

Many thanks also to Dott.ssa Anna Maria Abita and the staff of ARPA Sicilia for the availability and support offered during the sampling campaigns.

I would like to express my gratitude also to the coordinator of the PhD course, Prof. Alessandro Aiuppa, and to the administrative staff of the Dipartimento di Scienze della Terra e del Mare and of the Istituto Nazionale di Geofisica e Vulcanologia of Palermo for their support in handling the paperwork and duties of doctoral students.

My acknowledgements are also extended to Prof. Orlando Vaselli and Prof. Andri Stefánsson for having had the patience to revise this (excessively) long manuscript.

Great thanks go to all my dear officemates and friends both from the University of Palermo and the University of Florence, who made my PhD journey lighter by sharing, sometimes unknowingly, all my ups and downs. Special thanks go to Lorenza Li Vigni, a valuable assistant in the lab whenever I needed help. Thanks also extended to Salvatore, Brigida, Joaquin, Patrick, Antonio, Jacopo, Stefania, Rebecca, Francesco, and Simone.

Loving thanks go to my mother, my brother, and Noemi's family, for their unconditional love and support. I leave last, but not least, my most affectionate thanks to Noemi, to whom this work is dedicated, without which I would not have been able to recover in difficult times.

1. Introduction

1.1 Atmospheric deposition: definitions

Atmospheric deposition is one of the main ways through which a wide variety of chemicals, such as sea spray, geogenic dust, anthropogenic particulate matter, polycyclic aromatic hydrocarbons, volcanic ash, etc., reach terrestrial and aquatic ecosystems. Nowadays, this research subject is receiving more and more attention from the scientific community.

Atmospheric deposition occurs through two main mechanisms: (i) dry deposition and (ii) wet deposition (*Dollard et al., 1983*; *Seinfeld & Pandis, 1998*). Together these two forms of deposition constitute the bulk deposition. Dry deposition is the flux of gases and particles falling from the atmosphere in the absence of precipitation and occurs with several mechanisms like turbulent diffusion, sedimentation, Brownian diffusion, interception, inertial forces, electrical migration, thermophoresis, and diffusionphoresis (*Amodio et al., 2014*). Wet deposition is the flux from the atmosphere through water (rain, snow, hail, fog), being the most effective mechanism for removing particles and soluble gaseous pollutants from the atmosphere through scavenging mechanisms (*Mishra et al., 2012*; *Wang et al., 2019*). There are two main scavenging mechanisms involved (*Gong et al., 2011*; *Kajino & Aikawa, 2015*): one is called *rainout*, the in-cloud scavenging process which mainly absorbs or dissolves gases and fine particles within cloud droplets, and the second one, called *washout*, the below-cloud scavenging, which is an efficient process to remove coarse particles. The scavenging process in-cloud removes more than 70% of aerosol particles by number and more than 99% by mass (*Amodio et al., 2014*), and it is related to the activation of cloud condensation nuclei, aerosol particles, with diameters between 0.01 and a few hundreds of μm, which mostly consist of $(NH_4)_2SO_4$ and NH_4NO_3. Since water droplets form by homogeneous nucleation only in air supersaturated by 300-400%, the cloud condensation nuclei play a fundamental role in allowing the condensation of the droplets at supersaturation conditions usually lower than 1% (i.e., heterogeneous nucleation) (*Houze, 1993*; *Liotta et al., 2017*). Conversely, the washout process

occurs during the fall of raindrops from the base of the clouds to the ground. When the droplets become big enough, ~ 1 mm, they can fall as raindrops. Weak precipitation having less than 0.1 mm h^{-1} intensity can remove 50-80% of the below-cloud aerosol, in both number and mass, within four hours (*Andronache, 2004*; *Zhang et al., 2004*; *Amodio et al., 2014*).

The contribution of each form (wet and dry) of atmospheric deposition to the bulk deposition is strongly depending on the characteristics of the area and, especially, on its meteorological conditions (*Sickles et al., 2003*; *Tang et al., 2005*; *Arsene et al., 2007*). In rainy areas, the contribution of dry deposition is almost negligible compared to the contribution of wet deposition (*Loye-Pilot & Martin, 1996*); on the contrary, in arid or semi-arid areas, where processes such as erosion and geogenic dust transport are very pronounced, dry deposition prevails over wet deposition strongly contributing to the chemical composition of total deposition. The wet deposition also shows a seasonal variability, representing the main contribution of bulk deposition during the rainy season (usually from September to March for the southern Mediterranean area), while it contributes little to the chemical composition of bulk deposition during the drier season (in the southern Mediterranean area from April to August) (*Avila & Alarcón, 1999*; *Pulido-Villena et al., 2006*).

1.2 Chemical composition of atmospheric deposition

The composition of atmospheric deposition depends on the chemistry of gases and the mineralogy of particulate matter emitted by the different sources, on the source amplitude, on the chemical and physical reactions that occur during local and regional scale pollutant transport, and on removal processes (*Galy-Lacaux et al., 2009*; *D'Alessandro et al., 2013*). Atmospheric aerosol particles including sea salts, crustal dust (usually, the prominent aerosols in the atmosphere - *Schlesinger, 1997*; *Amodio et al., 2014*), volcanic emissions, wildfires, biogenic material, and anthropogenic pollutants, are the main sources of chemical elements to the atmosphere.

Different sources, both natural and anthropogenic, can emit gaseous and particulate matter with very similar chemical compositions, both in terms of major and trace constituents. One of the aims of environmental studies of the atmosphere, sometimes not easy to achieve, is to discriminate, through specific chemical or isotopic tracers, the main sources of the chemical elements present in atmospheric deposition.

The main dissolved inorganic chemical components of rainwater derive primarily from particles in the air (Na^+, K^+, Ca^{2+}, Mg^{2+}, and Cl^-), and atmospheric gases (SO_4^{2-}, NH_4^+, NO_3^-). Sodium (Na^+), chloride (Cl^-), magnesium (Mg^{2+}), and sea salt sulfate (ss-SO_4^{2-}), are enriched in sea salt (*Keene et al., 1986*; *Moreda-Piñeiro et al., 2017*; *Ye et al., 2018*), and represent the main part of the total ions content of rainwater in coastal areas (*Arimoto et al., 1987*; *Berner & Berner, 1987*; *Halstead et al., 2000*). The ionic ratios of these ions in rainfall in coastal areas are similar to those in seawater. An enrichment of Cl^- may be attributed to its anthropogenic sources such as incineration operations (*Wang et al., 2008*), but also to volcanic emissions (*Calabrese et al., 2011*). Calcium (Ca^{2+}), magnesium (Mg^{2+}), and to some extent, potassium (K^+) and sodium (Na^+) are typical crustal species (*Berner & Berner, 1996*; *Amodio et al., 2014*), and especially non-sea-salt calcium (nss-Ca^{2+}) is one of the main contributors to the neutralisation of rainwater acidity (*Brugnone et al., 2023a*). On the contrary, non-sea-salt sulfate SO_4^{2-} (nss-SO_4^{2-}) and nitrate (NO_3^-), usually considered the main ones responsible for the acidification processes, are markers of anthropogenic pollution. These ion species come from anthropogenic sources such as energy production plants, urban transport, and agriculture activities, but also from biological emissions (*Berner & Berner, 1996*; *Zufall & Davidson, 1998*). The deposition of ammonium (NH_4^+) mainly originated through ammonia volatilisation from N-fertilisation in agricultural fields and animal farming (*Amodio et al., 2014*; *Huang et al., 2017*). Ammonium is another chemical species that can contribute to the neutralisation of rainwater acidity, but it can, on the contrary, also cause acidification of rainwater if oxidised to form nitric acid (HNO_3) (*Wu et al., 2012*). The abundance of potassium (K^+) in the atmospheric

deposition could be attributed especially to biomass burning, the use of fertilisers, and other agricultural activities (*Berner & Berner, 1996*; *Chandra Mouli et al., 2005*; *Viana et al., 2008*). Biomass burning is also responsible for the emissions of NO_3^-, NH_4^+, SO_4^{2-}, Ca^{2+}, Na^+, and Mg^{2+}. Gaseous and particulate fluoride (F^-) are derived from anthropogenic emissions, such as coal burning, ceramic, brick, and cement factories, but also from natural sources like volcanoes (*Bellomo et al., 2007*; *Brugnone et al., 2020*; *Brugnone et al., 2023a*), and seawater spray (*Ge et al., 2016*).

The study of the chemical composition of atmospheric deposition not only concerns major ions but also minor and trace elements. Concentrations of trace elements in atmospheric deposition have been widely investigated, mainly for elements or metalloids that represent a risk to human health and ecosystems due to their toxicity, such as mercury (Hg), lead (Pb), cadmium (Cd), chromium (Cr), copper (Cu), among others (*Pearson et al., 2019*; *Cao et al., 2020*). Due to industrialisation and urban growth, the abundance of these potentially toxic elements has increased in recent decades (*Nicholson et al., 2003*). Some elements, such as Cu and Zn, are essential nutrients but they can cause harmful effects depending on their concentration levels (*Amodio et al., 2014*). For example, cadmium is considered very toxic because of its high solubility and is classified as potentially carcinogenic (*Fraga, 2005*; *Ye et al., 2018*). It is also ecologically hazardous because of its easy uptake by plants, its tendency to accumulate in crops, and its persistent nature once it is in the environment (*Ye et al., 2018*). Lead is the most widespread toxic metal on Earth due to anthropogenic activities (*Ye et al., 2018*), and it is also recognised by the World Health Organization as one of the most dangerous chemical elements for human health (*Silbergeld et al., 2000*; *Fewtrell et al., 2003*). Copper, chromium, cadmium, lead, and zinc are trace elements of mainly anthropogenic origin, and they are emitted into the atmosphere from various industrial processes, motor vehicle traffic, and agricultural activities (*Duan & Tan, 2013*; *Shao et al., 2013*). Indeed, copper, chromium, and lead are derived from diesel exhaust from vehicles and lubricant oil combustion (*Pulles et al., 2012*; *Adamiec et al., 2016*). Chromium can also be a waste product of

coal combustion and is also used in the textile industry (*Ye et al., 2018*). Lead is also widely used in the ceramics industry (*Tan et al., 2014*). Cadmium comes mainly from vehicular emissions and partly from industrial emissions (*Hu & Cheng, 2013*). Aucélio et al., 2007, and Hjortenkrans et al., 2007, verified that cadmium comes from lubricating oil and tyre wear from vehicles. Finally, zinc is widely used in agriculture, in the form of zinc salt (e.g., $ZnSO_4$) and/or ZnO aqueous solutions (*Ye et al., 2018*).

The current Italian legislation on environmental protection (*Decreto Legislativo 13/08/2010, n.155*), implemented by European legislation (*2008/50/CE*), provides for the monitoring of atmospheric deposition of only a few trace metals (As, Cd, Hg, Ni, Pb). Considering the development in recent years of new technological and energy-related applications (e.g., solar panels, high-efficiency batteries, electronic equipment, catalytic converters) and the consequent exponential increase in the use and demand of a specific group of less-studied trace elements, the current legislation is affected by significant gaps. The massive requirements of these trace elements led to their extensive extraction from the lithosphere and resulted in the worldwide dispersion and remobilisation of these elements within the atmosphere and the biosphere. Indeed, recent studies draw attention to a group of trace elements known as Technology-Critical Elements (TCEs), including tellurium (Te), germanium (Ge), gallium (Ga), indium (In), niobium (Nb), tantalum (Ta), the platinum group elements (PGEs: Pt, Pd, Rh, Os, Ir, Ru), and the rare earth elements (YREEs: La, Ce, Pr, Nd, Sm, Eu, Gd, Tb, Dy, Y, Ho, Er, Tm, Yb, Lu) (*Cobelo-García et al., 2015*). A Technology-Critical Element (TCE) is a chemical element that is critical to modern and emerging technologies, resulting in a striking increase in its usage (*U.S. Department of Energy. Critical Materials Strategy. Washington, D.C.*). The lanthanoids in rainwater originate from a variety of natural and anthropogenic processes. Accurately determining the concentrations of these elements in rainwater has become of increasing interest because they provide important information about the geochemical cycling of metals, anthropogenic inputs, and atmospheric pollution (*Arslan et al.,*

2018). It has recently been recognised that lanthanoids in atmospheric particles and rainwater have a significant impact on the geochemical cycle of the same elements in the hydrosphere (*Zhu et al., 2016*). These elements are present in rainwater with very low average concentrations of less than a microgram per litre.

An important question concerns which form (soluble or insoluble) major and trace elements are found in atmospheric deposition. The different elements in the atmospheric deposition have different degrees of solubility, which vary as the physic-chemical characteristics, such as acidity, of the rainwater. Therefore, bulk atmospheric deposition is composed of both soluble and insoluble fractions. Most of the studies found in the literature were focused on the soluble fraction of the atmospheric trace element deposition (*Azimi et al., 2003*; *Avila & Rodrigo, 2004*; *Hou et al., 2005*; *Sakata et al., 2006*; *Moaref et al., 2014*), but some researchers have paid more attention to the insoluble fraction (*Guerzoni et al., 1999*; Báez et al., 2007; *Fernández-Olmo et al., 2014, 2015; Ye et al., 2018*; *Brugnone et al., 2023b*). Lead, aluminium, iron, and silicon, for example, exist mainly in poorly soluble forms (*Guerzoni et al., 1999*; *Ye et al., 2018*), while trace elements such as zinc, cadmium, and chromium are very soluble and this reason represents a high risk for human health and, in general, for many environmental matrices. Cadmium and lead have low solubility at high mass particle concentrations (*Guerzoni et al., 1999*). In dry atmospheric deposition, the contribution of the soluble fraction is usually less than that of the insoluble fraction for all trace elements (*Ye et al., 2018*). Evaluation of the trace element soluble and particulate fractions is essential since the soluble and particulate forms have different fates in the environment, especially concerning bioavailability (*Theodosi et al., 2010*). A European norm (*EN 15841:2009*) defines the methodology to be followed for the determination of the concentration of certain heavy metals (As, Cd, Pb, and Ni) in both the soluble and insoluble fractions.

1.3 Chemical – physical parameters of rainwater

The pH is an important parameter controlling the chemical composition of a solution. The natural acidity of rainwater may be controlled by the dissolution of acidic gases, or by basic species able to buffer the acidity, such as carbonate particulates. The stability ranges of the aqueous species of trace elements are strongly influenced by the acidic conditions of the solution, and the degree of mobility of the elements in the environment depends on their amplitude. The slight acidity of natural rainwater in the background atmosphere is at first approximation controlled by the dissociation of dissolved atmospheric carbon dioxide ($CO_{2(g)}$). Assuming an equilibrium at 25 °C between pure water and atmospheric CO_2, with a partial pressure of $10^{-4.0}$ atm (~ 400 ppm CO_2), the equilibrium pH of the solution will be ~ 5.60 (USGS PHREEQC Version 3 calculation). Many authors evidenced widespread acid-rain neutralisation by atmospheric carbonate dust over the entire Mediterranean basin induced by the frequent arrival of Saharan dust (*Al-Momani et al., 1995*; *Guerzoni et al., 1999*; *Galy-Lacaux et al., 2009*; *Laouali et al., 2012*) and widespread outcrops of limestone formations (*D'Alessandro et al., 2013*; *Al-Momani et al., 2008*). Natural rain with a pH greater than 5.60 is generally the result of the dissolution of $CaCO_3$:

$$CaCO_3(s) + H^+(sol) \rightarrow Ca^{2+}(sol) + HCO_3^-(sol) \quad (1)$$

Neutralisation of natural acidity in rainwater may also occur by reaction with ammonia gas (NH_3), deriving from the decomposition of urea in soil and agricultural environments (*Charlson & Rodhe, 1982*; *Stumm & Morgan, 1996*).

Water droplets (10 - 50 μm in diameter) condense on aerosol particles and can absorb naturally occurring gases such as CO_2, NO_X, SO_2, HCl and organic acids, responsible for the pH decreasing, up to pH values of no less than ~ 4.5, and/or NH_3 that neutralises mineral acids and buffers the solution phase. Values of pH < 4.5 can indicate the local influence of anthropogenic or volcanic sources. Sulfate of non-marine origin (non-sea-salt sulfate, nss-SO_4^{2-}), and nitrate are principally derived from the conversion of anthropogenic gaseous precursors (e.g., SO_2 and NOx,

Seinfeld & Pandis, 1998). SO_2 and nss-SO_4^{2-} are emitted by coal-fired power stations, ore smelting, and petrochemical plants. Gaseous NOx is mainly emitted as NO from natural (biogenic emissions and biomass burning during wildfires), and anthropogenic sources (household combustion, fossil fuel combustion in urban transport) (*Conradie et al., 2016*). Usually, sulfur and nitrogen components are considered the main responsible for the acidification of rainwater (*Seinfeld & Pandis, 1998*; *Huang et al., 2008*). One of the main effects of volcanic emissions on rainwater chemistry is the drastic increase of its acidity, as a direct consequence of the interaction with plume-derived strongly acidic gases, mainly SO_2, HCl, HF, and HBr. The result is the formation of sulfuric, hydrochloric, hydrofluoric, and hydrobromic acids in the atmosphere (*Calabrese et al., 2011*).

1.4 Boron and strontium isotopes

Boron is a trace element in the atmosphere and is mainly found in the form of gaseous constituents such as boric acid (90 - 95%) or particulate boron (5 - 10%) (*Fogg & Duce, 1985*). Boron concentrations in the atmosphere are generally very low, between 0.1 μg L^{-1} and a few hundred μg L^{-1}. Boron has two stable isotopes, ^{11}B and ^{10}B, and the atomic weight resulting from the weighted mean of the two isotopes is 10,811 u. The global B cycle is primarily driven by a large flux, i.e., 1.44 Tg a^{-1} through the atmosphere derived from sea salt aerosols. Other significant sources of atmospheric B include emissions during the combustion of biomass (0.26 - 0.43 Tg a^{-1}), and coal, which adds 0.20 Tg a^{-1} as an anthropogenic contribution. A global B flux of 0.022 Tg a^{-1} can be attributed to the volcanic source (*Fogg & Duce, 1985*). There are few works found in the literature in which B isotopes have been investigated in rainwater samples (*Spivack, 1986*; *Xiao et al., 1992*; *Eisenhut & Heumann, 1997*; *Barth, 1998*; *Miyata et al., 2000*; *Demuth & Heumann, 1999*; *Chetelat et al., 2005*; *Rose-Koga et al., 2006*; *Millot et al., 2010*; *Zhao & Liu, 2010*).

Strontium is also a trace element in the atmosphere and the concentrations generally range from 1 μg L^{-1} to over 1000 μg L^{-1} in rainwaters. It has four natural isotopes, three stable (^{84}Sr, ^{86}Sr,

^{88}Sr) and one radiogenic (^{87}Sr). Radiogenic strontium isotope ratios ($^{87}Sr/^{86}Sr$) are a particularly useful tracer of atmospheric aerosols as the globally homogenous $^{87}Sr/^{86}Sr$ composition of seawater (0.70917; *Hodell et al., 1990*) enables the contribution of sea-salt to be readily distinguished from terrestrial and anthropogenic components that have more variable $^{87}Sr/^{86}Sr$ ratios (e.g., *Négrel & Roy, 1998*; *Derry & Chadwick, 2007*; *Négrel et al., 2007*). Only a few researchers have worked on the determination of the isotopic composition of strontium in rainwater (*Herut et al., 1993*; *Négrel & Roy, 1998*; *Han & Liu, 2006*; *Négrel et al., 2007*; *Xu et al., 2009*; *Xu & Han, 2009*; *Han et al., 2010, 2012*; *Xu et al., 2012*; *Pearce et al., 2015*).

1.5 Role of atmospheric deposition studies for environmental research

The atmospheric deposition is a source of nutrients, (e.g., nitrogen, sulfur, carbon, and base metals - *Duce et al., 2009*), but it can also contribute to a variety of environmental issues including acid rain, aquatic eutrophication, disturbances of biogeochemical cycles, global climate change (*Wang et al., 2019*), as well as damages to buildings and architectural heritage (*Montana et al., 2012*; *Conradie et al., 2016; Comite et al., 2020*). The experimental results demonstrated that atmospheric deposition is also a relevant source of chemical elements in the soil (*Grey et al., 2003*; *Nicholson et al., 2003*; *Gandois et al., 2010*; *Shen et al., 2016*). Pollution phenomena in many environmental compartments and the human health impact on the exposed population may be linked to atmospheric deposition (*Amodio et al., 2014*). Long-term variations in the chemical characteristics of atmospheric deposition provide important tools to define the temporal evolution of atmospheric pollution and can be used as an indicator to discriminate natural processes from anthropogenic influences (*Tang et al., 2005*). The knowledge of the chemical composition of atmospheric deposition plays an important role because, being the initial solvent in water-rock interaction processes, rainwaters can also be considered the "titrant" in hydrogeochemical processes (*Edmunds, 2010*). Environmental studies of the chemical composition of the atmosphere, in areas characterised by the presence of active

volcanoes, cannot be separated from the characterisation of volcanic emissions. Volcanic emissions are an important source of gases and particles in the atmosphere, contributing significantly to the natural geochemical cycles of all elements (*Cadle, 1980*; *Nriagu, 1989*; *Hinkley et al., 1999*; *Oppenheimer, 2003*). Many studies have been carried out on the main volcanic emitters of the world, to estimate and characterise their emissions (*Cadle et al., 1973*; *Buat-Menard & Arnold, 1978*; *Chuan et al., 1986; Crowe et al., 1987*; *Pennisi et al., 1988*; *Kyle et al., 1990*; *Symonds et al., 1992*; *Andres et al., 1993*; *Toutain et al., 1995*; *Rubin, 1997*; *Galindo et al., 1998*; *Gauthier & Le Cloarec, 1998*; *Cheynet et al., 2000*; *Allard et al., 2000*; *Aiuppa et al., 2003, 2004*; *Bagnato et al., 2007*; *Calabrese et al., 2011*; *Tassi et al., 2013*; *Tamburello et al., 2014*; *D'Aleo et al., 2016*; *Liotta et al., 2017, 2021*; *Inguaggiato et al., 2023*; *Xochilt et al., 2023*; *Federico et al., 2023*). By contrast, the atmospheric deposition of major ions and trace elements around active volcanoes is poorly constrained. Although active volcanoes are widely distributed in the world and their emissions play a key role in the global geochemical cycles of many elements, only Hawaiian, Japanese, Italian and a few Central American volcanoes have been studied from the point of view of major species atmospheric deposition. In the last thirty years, the study of major and trace elements in atmospheric deposition has progressed enormously, thanks to the development of new sampling methodologies and analytical techniques with high-performance instruments (*Capasso et al., 1993*; *Rowe et al., 1995*; *Scholl et al., 1995*; *Cimino et al., 1998*; *Aiuppa et al., 2001*; *Delmelle et al., 2001*; *Hayashi & Okazaki, 2002*; *Bellomo et al., 2003*; *Aiuppa et al., 2003, 2006*; *Edmonds et al., 2003*; *Okuda et al., 2005*; *Liotta et al., 2006, 2017*; *Moune et al., 2006*; *Sakata et al., 2008*; *Madonia & Liotta, 2010*; C*alabrese et al., 2011*; *Mather et al., 2012*; *Cangemi et al., 2017*).

1.6 Main aims and structure of the thesis

A lot of research on the chemical characterisation of atmospheric deposition, both in terms of major and trace elements, has been carried out in the last thirty years. From the literature, it is

possible to derive the concentrations and the deposition fluxes of many ionic species and metals in various contexts, urban, industrial, rural, remote, and volcanic. Nevertheless, from a literature review, an unclear distinction between the soluble and insoluble fractions of atmospheric deposition, also in the reference norms, was recognised. More, only a few works have investigated both fractions in depth. To fill this gap, the first part of this work focuses on the characterisation of the chemical composition of the bulk atmospheric deposition in four different environments, volcanic, urban, industrial, and rural, characterised by very different sources of gaseous species and atmospheric particulate matter. The location of the study areas within the Mediterranean Basin placed them under the influence of not only local-scale sources, but also regional-scale sources such as the marine source, the geogenic source related to Saharan dust, and the anthropogenic source related to European-scale emissions. Major ion concentrations and deposition fluxes were investigated in the soluble fraction of the bulk atmospheric deposition, while trace elements were analysed both in the soluble and insoluble fractions. The main aims of the first part of this work were to identify the chemical signatures and the relative contributions of each source in the different environments, and investigate, both qualitatively and quantitatively, the distribution of trace elements between the soluble and insoluble fractions of bulk atmospheric deposition. Due to the intense paroxysmal activity at Mt. Etna between 2021 and 2022, the study of the impact of volcanic activity on the chemical composition of both fractions, soluble and insoluble, of atmospheric deposition was added.

Few works in the literature focus on the determination of the concentration of ultra-trace elements and lanthanoids in rainwater (*Asaf et al., 2005*; *Iwashita et al., 2011*; *Zhu et al., 2016*; *Garcia et al., 2022*) and, to the best of my knowledge, the concentrations of TCEs in this matrix have never been determined. The second part of this thesis illustrates the concentrations of TCEs in bulk atmospheric deposition samples collected in the different environments mentioned above.

Apart from the water itself, the isotopic signatures of many other elements dissolved in rainwater can provide important information about sources of gaseous and particulate emissions,

transport pathways, and deposition processes. The last part of this thesis focuses on the isotopic signature of boron and strontium to recognise the main sources from which these and related elements originate.

The scientific evidence provided by this PhD research expands our current knowledge of the chemical and isotopic compositions of the bulk atmospheric deposition in the Mediterranean Basin. Thanks to the detailed description of the characteristics of the different sources present in the study areas, the chemical characterisation of the soluble and insoluble fraction of atmospheric deposition, the determination of the concentrations of TCEs in rainwater, and B and Sr isotopic analyses, this work might offer a useful tool for future investigations on atmospheric deposition.

1.7 References

Adamiec, E., Jarosz-Krzemińska, E., Wieszała, R. (2016). Trace elements from non-exhaust vehicle emissions in urban and motorway road dusts. Environ. Monit. Assess., 188, 369. https://doi.org/10.1007/S10661-016-5377-1.

Aiuppa, A., Bonfanti, P., Brusca, L., D'Alessandro, W., Federico, C., Parello, F. (2001). Evaluation of the environmental impact of volcanic emissions from the chemistry of rainwater: Mount Etna area (Sicily). Appl. Geochem., 16, 7–8, pp. 985-1000. https://doi.org/10.1016/S0883-2927(00)00075-5.

Aiuppa, A., Dongarrà, G., Federico, C., Pecoraino, G., Valenza, M. (2003). Degassing of trace volatile metals during the 2001 eruption of Etna. In: Robock, A., Oppenheimer, C. (Eds.), Volcanism and the Earth's Atmosphere. Geophysical Monograph, 139. https://doi.org/10.1029/139GM03.

Aiuppa, A., Bellomo, S., D'Alessandro, W., Federico, C., Ferm, M., Valenza, M. (2004). Volcanic plume monitoring at Mount Etna by diffusive (passive) sampling. J. Geophys. Res., 109. https://doi.org/10.1029/2003JD004481.

Aiuppa, A., Bellomo, S., Brusca, L., D'Alessandro, W., Paola, R., Longo, M. (2006). Major-ion bulk deposition around an active volcano (Mt. Etna, Italy). B. Volcanol., 68, pp. 255-265. https://doi.org/10.1007/s00445-005-0005-x.

Allard, P., Aiuppa, A., Loyer, H., Carrot, F., Gaudry, A., Pinte, G., Michel, A., Dongarrà, G. (2000). Acid gas and metal emission rates during long-lived basalt degassing at Stromboli volcano. Geophys. Res. Lett., 27, pp. 1207–1210. https://doi.org/10.1029/1999GL008413.

Al-Momani, I. F.; Ataman, O. Y.; Anwari, A. M.; Tuncel, S.; Köse, C.; Tuncel, G. (1995). Chemical composition of precipitation near an industrial area at Izmir, Turkey. Atmos. Environ., 29, pp. 1131–1143. https://doi.org/10.1016/1352-2310(95)00027-V.

Al-Momani, I. F.; Momani, K. A.; Jaradat, Q. M.; Massadeh, A. M.; Yousef, Y. A.; Alomary, A. A. (2008). Atmospheric deposition of major and trace elements in Amman, Jordan. Environ. Monit. Assess., 136, pp. 209–218. https://doi.org/10.1007/s10661-007-9676-4.

Amodio, M., Catino, S., Dambruoso, P. R., De Gennaro, G., Di Gilio, A., Giungato, P., Laiola, E., Marzocca, A., Mazzone, A., Sardaro, A., Tutino, M. (2014). Atmospheric deposition: Sampling procedures, analytical methods, and main recent findings from the scientific literature. In Advances in Meteorology. https://doi.org/10.1155/2014/161730.

Andres, R. J., Kyle, P. R., Chuan, R. L. (1993). Sulphur dioxide, particle and elemental emissions from Mount Etna, Italy during July 1987. Geol. Rundsch., 82, pp. 687–695. https://doi.org/10.1007/BF00191496.

Andronache, C. (2004). Estimates of sulfate aerosol wet scavenging coefficient for locations in the Eastern United States. Atmos. Environ., 38(6). https://doi.org/10.1016/j.atmosenv.2003.10.035.

Arimoto, R., Duce, R. A., Ray, B. J., Hewitt, A. D., Williams, J. (1987). Trace elements in the atmosphere of American Samoa: Concentrations and deposition to the tropical South Pacific. J. Geophys. Res., 92(D7), 8465. https://doi.org/10.1029/JD092iD07p08465.

Arsene, C., Olariu, R. I., Mihalopoulos, N. (2007). Chemical composition of rainwater in northeastern Romania, Iasi region (2003-2006). Atmos. Environ., 41(40), pp. 9452–9467. https://doi.org/10.1016/j.atmosenv.2007.08.046.

Arslan, Z., Oymak T., White J. (2018). Triethylamine-assisted $Mg(OH)_2$ coprecipitation/preconcentration for determination of trace metals and rare earth elements in seawater by inductively coupled plasma mass spectrometry (ICP-MS). Anal. Chim. Acta., 1008, pp. 18-28. https://doi.org/10.1016/j.aca.2018.01.017.

Asaf, L., Nativ, R., Hassan, M., Shain, D., Geyer, S., Ziv, B. (2005). Influence of small- and large-scale variables on the chemical and isotopic compositions of urban rainwater, as illustrated by a case study in Ashdod, Israel. J. Geophys. Res., 110(11). https://doi.org/10.1029/2004JD005414.

Aucélio, R. Q., de Souza, R. M., de Campos, R. C., Miekeley, N.; da Silveira, C. L. P. (2007). The determination of trace elements in lubricating oils by atomic spectrometry. Spectrochim. Acta Part B At. Spectrosc., 62, 952–961. https://doi.org/10.1016/J.SAB.2007.05.003.

Avila, A. & Alarcón, M. (1999). Relationship between precipitation chemistry and meteorological situations at a rural site in NE Spain. Atmos. Environ., 33(11), 1663–1677. https://doi.org/10.1016/S1352-2310(98)00341-0.

Avila, A. & Rodrigo, A. (2004). Trace metal fluxes in bulk deposition, throughfall and stemflow at two evergreen oak stands in NE Spain subject to different exposure to the industrial environment. Atmos. Environ., 38, 171–180. https://doi.org/10.1016/J.ATMOSENV.2003.09.067.

Azimi, S., Ludwig, A., Thévenot, D. R., Colin, J. L. (2003). Trace metal determination in total atmospheric deposition in rural and urban areas. Sci. Total Environ., 308, 247–256. https://doi.org/10.1016/S0048-9697(02)00678-2.

Báez, A., Belmont, R., García, R., Padilla, H., Torres, M. C. (2007). Chemical composition of rainwater collected at a southwest site of Mexico City, Mexico. Atmos. Res., 86, 61–75. https://doi.org/10.1016/J.ATMOSRES.2007.03.005.

Bagnato, E., Aiuppa, A., Parello, F., Calabrese, S., D'Alessandro, W., Mather, T. A., McGonigle, J. S., Pyle, D. M., Wangberg, I. (2007). Degassing of gaseous (elemental and reactive) and particulate mercury from Mount Etna volcano (Southern Italy). Atmos. Environ., 41, 35, pp. 7377-7388. https://doi.org/10.1016/j.atmosenv.2007.05.060.

Barth, S. (1998). $^{11}B/^{10}B$ variations of dissolved boron in a freshwater–seawater mixing plume (Elbe Estuary, North Sea). Mar. Chem., 62, 1-2, pp. 1–14. https://doi.org/10.1016/S0304-4203(98)00023-1.

Bellomo, S., D'Alessandro, W., Longo, M. (2003). Volcanogenic fluorine in rainwater around active degassing volcanoes: Mt. Etna and Stromboli Island, Italy. Sci. Total Environ., 301, 1-3, pp. 175-185. https://doi.org/10.1016/S0048-9697(02)00284-X.

Bellomo, S., Aiuppa, A., D'Alessandro, W., Parello, F. (2007). Environmental impact of magmatic fluorine emission in the Mt. Etna area. J. Volcanol. Geotherm. Res., 165(1-2), pp. 87-101. https://doi.org/10.1016/j.jvolgeores.2007.04.013.

Berner, E. K. & Berner, R. A. (1987). Global Water Cycle: Chemical composition and Environment. Prentice-Hall, Inc., Englewood Cliffs, New Jersey. p. 397.

Berner, E. K. & Berner, R. A. (1996). Global Environment: Water, Air, and Geochemical Cycles: Upper Saddle River, NJ, Prentice Hall.

Brugnone, F., D'Alessandro, W., Calabrese, S., Li Vigni, L., Bellomo, S., Brusca, L., Prano, V., Saiano, F., Parello, F. (2020). A Christmas gift: Signature of the 24th December 2018 eruption of Mt. Etna on the chemical composition of bulk deposition in eastern Sicily. Italian Journal of Geosciences, 139, pp. 341-358. https://doi.org/10.3301/IJG.2020.08.

Brugnone, F., D'Alessandro, W., Parello, F., Liotta, M., Bellomo, S., Prano, V., Li Vigni, L., Sprovieri, M., Calabrese, S. (2023a). Atmospheric Deposition around the Industrial Areas of Milazzo and Priolo Gargallo (Sicily–Italy)-Part A: Major Ions. Int. J. Environ. Res. Public Health, 20(5), 3898. https://doi.org/10.3390/ijerph20053898.

Brugnone, F., D'Alessandro, W., Parello, F., Brusca, L., Saiano, F., Li Vigni, L., Sprovieri, M., Calabrese, S. (2023b). Atmospheric Deposition around the Industrial Areas of Milazzo and Priolo Gargallo (Sicily–Italy)—Part B: Trace Elements. Atmosphere, 14, 737. https://doi.org/10.3390/atmos14040737.

Buat-Ménard, P. & Arnold, M. (1978). The heavy metal chemistry of atmospheric particulate matter emitted by Mount Etna volcano. Geophys. Res. Lett., 5–4, pp. 245–248. https://doi.org/10.1029/GL005i004p00245.

Cadle, R. D., Wartburg, A. F., Pollok, W. H., Gandrud, B. W., Shedlovky, J. P. (1973). Trace constituents emitted to the atmosphere by Hawaiian volcanoes. Chemosphere. 6, pp. 231-234. https://doi.org/10.1016/0045-6535(73)90046-5.

Cadle, R. D. (1980). A comparison of volcanic with other fluxes at atmospheric trace gas constituents. Rev. Geophys. Space Phys., 18, pp. 746-752. https://doi.org/10.1029/RG018i004p00746.

Calabrese, S., Aiuppa, A., Allard, P., Bagnato, E., Bellomo, S., Brusca, L., Parello, F. (2011). Atmospheric sources and sinks of volcanogenic elements in a basaltic volcano (Etna, Italy). Geochim. Cosmochim. Acta, 75(23), pp. 7401–7425. https://doi.org/10.1016/j.gca.2011.09.040.

Cao, X., Tan, C., Wu, L., Luo, Y., He, Q., Liang, Y., Peng, B., Christie, P. (2020). Atmospheric deposition of cadmium in an urbanized region and the effect of simulated wet precipitation on the uptake performance of rice. Sci. Total Environ., 700, 134513. https://doi.org/10.1016/J.SCITOTENV.2019.134513.

Cangemi, M., Madonia, P., Favara, R. (2017). Chemical characterisation of rainwater at Stromboli Island (Italy): The effect of post-depositional processes. J. Volcanol. Geoth. Res., 335, pp. 82-91. https://doi.org/10.1016/j.jvolgeores.2017.01.023.

Capasso, G., Dongarrà, G., Favara, R., Francoforte, S., Hauser, S. (1993). Composition of bulk precipitation on island of Vulcano (Aeolian I. Italy). Naturalistica sicil., S. IV, XVII (1-2), pp. 33-43.

Chandra Mouli, P., Venkata Mohan, S., & Reddy, S. J. (2005). Rainwater chemistry at a regional representative urban site: Influence of terrestrial sources on ionic composition. Atmos. Environ., 39(6). https://doi.org/10.1016/j.atmosenv.2004.10.036.

Charlson, R. J. & Rodhe, H. (1982). Factors controlling the acidity of natural rainwater. Nature, 295, pp. 683–685. https://doi.org/10.1038/295683a0.

Cheynet, B., Dall'Aglio, M., Garavelli, A., Grasso, M. F., Vurro, F. (2000). Trace elements from fumaroles at Vulcano Island (Italy): rates of transport and a thermochemical model. J. Volcanol. Geotherm. Res., 95, pp. 273–283. https://doi.org/10.1016/S0377-0273(99)00122-5.

Chetelat, B., Gaillardeta, J., Freydierb, T. R., Négrel, P. (2005). Boron isotopes in precipitation: Experimental constraints and field evidence from French Guiana. Earth Planet Sc. Lett., 235, pp. 16-30. https://doi.org/10.1016/j.epsl.2005.02.014.

Chuan, R. L., Palais, J. M., Rose, W. I. (1986). Fluxes, sizes, morphology and compositions of particles in the Mt. Erebus Volcanic Plume, December 1983. J. Atmos. Chem., 4, pp. 467-477. https://doi.org/10.1007/BF00053846.

Cimino, G. & Toscano, G. (1998). Dissolution of trace metals from lava ash: influence on the composition of rainwater in the Mount Etna volcanic area. Environ. Pollut., 99, 3, pp. 389-393. https://doi.org/10.1016/S0269-7491(98)00004-9.

Cobelo-García, A., Filella, M., Croot, P., Frazzoli, C., Du Laing, G., Ospina-Alvarez, N., Rauch, S., Salaun, P., Schafer, J., Zimmermann, S. (2015). COST action TD1407: network on technology-critical elements (NOTICE)-from environmental processes to human health threats. Environ. Sci. Pollut. Res., 22(19), pp. 15188–15194. https://doi.org/10.1007/s11356-015-5221-0.

Comite, V., Ricca, M., Ruffolo, S. A., Graziano, S. F., Rovella, N., Rispoli, C., Gallo, C., Randazzo, L., Barca, D., Cappelletti, P., La Russa, M. F. (2020). Multidisciplinary Approach for Evaluating the Geochemical Degradation of Building Stone Related to Pollution Sources in the Historical Center of Naples (Italy). Appl. Sci., 10(12), 4241. https://doi.org/10.3390/app10124241.

Conradie, E. H., Van Zyl, P. G., Pienaar, J. J., Beukes, J. P., Galy-Lacaux, C., Venter, A. D., Mkhatshwa, G. V. (2016). The chemical composition and fluxes of atmospheric wet deposition at four sites in South Africa. Atmos. Environ., 146, pp. 113–131. https://doi.org/10.1016/j.atmosenv.2016.07.033.

Crowe, B. M., Finnegan, D. L., Zoller, W. H., Boyton, W. V. (1987). Trace element geochemistry of volcanic gases and particles from 1983-1984 eruptive episodes of Kilauea volcano. J. Geophys. Res., 92, pp. 13708-13714. https://doi.org/10.1029/JB092iB13p13708.

D'Aleo, R., Bitetto, M., Delle Donne, D., Tamburello, G., Battaglia, A., Coltelli, M., Patanè, D., Prestifilippo, M., Sciotto, M., Aiuppa, A. (2016). Spatially resolved SO_2 flux emissions from Mt Etna. Geophys. Res. Lett., 43, pp. 7511–7519. https://doi.org/10.1002/2016GL069938.

D'Alessandro, W., Katsanou, K., Lambrakis, N., Bellomo, S., Brusca, L., Liotta, M. (2013). Chemical and isotopic characterisation of bulk deposition in the Louros basin (Epirus, Greece). Atmos. Res., 132–133, pp. 399–410. https://doi.org/10.1016/j.atmosres.2013.07.007.

Decreto Legislativo 13/08/2010, n.155 "Attuazione Della Direttiva 2008/50/CE Relativa Alla Qualità Dell'aria Ambiente e per Un'aria più Pulita in Europa (10G0177) (GU Serie Generale n.216 del 15/09/2010—Suppl. Ordinario n.217. Available online: https://www.gazzettaufficiale.it/eli/id/2010/09/15/010G0177/sg (accessed on 10 January 2023).

Delmelle, P., Stix, J., Bourque, C. P.-A., Baxter, P. J., Garcia-Alvarea, J., Barqueror, J. (2001). Dry deposition and heavy acid loading in the vicinity of Masaya Volcano, a major sulfur and chlorine source in Nicaragua. Envir. Sci. Tech., 35 (7), pp. 1289 – 1293. https://doi.org/10.1021/es000153m.

Demuth, N., Heumann, K. G. (1999). Determination of trace amounts of boron in rainwater by ICP-IDMS and NTI-IDMS and the dependence on meteorological and anthropogenic influences. J. Anal. At. Spectrom., 14, pp. 1449–1453. https://doi.org/10.1039/A901515I.

Derry, L. A. & Chadwick, O. A. (2007). Contributions from Earth's atmosphere to soil. Elements, 3(5), pp. 333–338. https://doi.org/10.2113/gselements.3.5.333.

Dollard, G. J., Unsworth, M. H., & Harve, M. J. (1983). Pollutant transfer in upland regions by occult precipitation. Nature, 302(5905), pp. 241-243. https://doi.org/10.1038/302241a0.

Duan, J. & Tan, J. (2013). Atmospheric trace elements and Arsenic in China: Situation, sources, and control policies. Atmos. Environ., 74, 93–101. https://doi.org/10.1016/J.ATMOSENV.2013.03.031.

Duce, R. A., Galloway, J. N., Liss, P. S. (2009). The impacts of atmospheric deposition to the ocean on marine ecosystems and climate. World Meteorological Organization (WMO) Bulletin, 58(1), 61.

Edmonds, M., Oppenheimer, C., Pyle, D., Richard, H. (2003). Rainwater and ash leachate analysis as proxies for plume chemistry at Soufriere Hills Volcano, Montserrat. Geological Society Special Publication, 213, pp. 203-218. https://doi.org/10.1144/GSL.SP.2003.213.01.12.

Edmunds, W. M. (2010). Conceptual models for recharge sequences in arid and semi-arid regions using isotopic and geochemical methods. In: Weather, H.S., Mathias, S.A., Li, X. (Eds.), Groundwater Modelling in Arid and Semi-arid Areas. Cambridge University Press, Cambridge, pp. 21–37.

Eisenhut, S. & Heumann, K. G. (1997). Identification of ground water contaminations by landfills using precise boron isotope ratio measurements with negative thermal ionization mass spectrometry. Freseneius J. Anal. Chem., 359, pp. 375–377. https://doi.org/10.1007/s002160050590.

EN 15841:2009. Ambient air quality - Standard method for determination of arsenic, cadmium, lead and nickel in atmospheric deposition.

Federico, C., Inguaggiato, S., Liotta, M., Rizzo, A. L., Vita, F. (2023). Decadal monitoring of the hydrothermal system of Stromboli volcano, Italy. Geochemistry, Geophysics, Geosystems, 24, e2023GC010931. https://doi.org/10.1029/2023GC010931.

Fernández-Olmo, I., Puente, M., Montecalvo, L., Irabien, A. (2014). Source contribution to the bulk atmospheric deposition of minor and trace elements in a Northern Spanish coastal urban area. Atmos. Res., 145–146, pp. 80–91. https://doi.org/10.1016/J.ATMOSRES.2014.04.002.

Fernández-Olmo, I., Puente, M., Irabien, A. (2015). A comparative study between the fluxes of trace elements in bulk atmospheric deposition at industrial, urban, traffic, and rural sites. Environ. Sci. Pollut. Res., 22, pp. 13427–13441. https://doi.org/10.1007/s11356-015-4562-z.

Fewtrell, L., Kaufman, R., Prüss-Üstün, A. (2003). Lead: Assessing the Environmental Burden of Diseases at National and Local Levels; WHO: Geneva, Switzerland.

Fogg, T. R. & Duce, R. A. (1985). Boron in troposphere: distribution and fluxes. J. Geophys. Res. Atmos., 90(D2), pp. 3781-3796. https://doi.org/10.1029/JD090iD02p03781.

Fraga, C. G. (2005). Relevance, essentiality, and toxicity of trace elements in human health. Mol. Asp. Med., 26, 235–244. https://doi.org/10.1016/j.mam.2005.07.013.

Galindo, I., Ivlev, L. S., González, A., Ayala, R. (1998). Airborne measurements of particle and gas emissions from the December 1994–January 1995 eruption of Popocatépetl volcano (Mexico). J. Volcanol. Geoth. Res., 83, 3-4, pp. 197-217. https://doi.org/10.1016/S0377-0273(98)00033-X.

Galy-Lacaux, C., Laouali, D., Descroix, L., Gobron, N., Liousse, C. (2009). Long-term precipitation chemistry and wet deposition in a remote dry savanna site in Africa (Niger). Atmos. Chem. Phys., 9(5), pp. 1579–1595. https://doi.org/10.5194/acp-9-1579-2009.

Gandois, L., Nicolas, M., VanderHeijden, G., Probst, A. (2010). The importance of biomass net uptake for a trace metal budget in a forest stand in north-eastern France. Sci. Total Environ., 408(23), pp. 5870–5877. https://doi.org/10.1016/J.SCITOTENV.2010.07.061.

Garcia, M. G., Lecomte, K. L., Depetris, P. J. (2022). Natural and anthropogenic sources of solutes in the wet precipitation of a densely populated city of Southern South America. Chemosphere, 287(3). https://doi.org/10.1016/j.chemosphere.2021.132307.

Gauthier, P.-J. & Le Cloarec, M.-F. (1998). Variability of alkali and heavy metal fluxes released by Mt. Etna volcano, Sicily, between 1991 and 1995. J. Volcanol. Geoth. Res., 81, pp. 311–326. https://doi.org/10.1016/S0377-0273(98)00002-X.

Ge, B., Wang, Z., Gbaguidi, A. E., Zhang, Q. (2016). Source Identification of Acid Rain Arising over Northeast China: Observed Evidence and Model Simulation. Aerosol Air Qual. Res., 16(6), 1366–1377. https://doi.org/10.4209/AAQR.2015.05.0294.

Gong, W., Stroud, C., Zhang, L. (2011). Cloud processing of gases and aerosols in air quality modelling. Atmosphere, 2(4). https://doi.org/10.3390/atmos2040567.

Gray, C. W., McLaren, R. G., Roberts, A. H. C. (2003). Atmospheric accessions of trace elements to some New Zealand pastoral soils. Sci. Total Environ., 305(1–3), pp. 105–115. https://doi.org/10.1016/S0048-9697(02)00404-7.

Guerzoni, S., Molinaroli, E., Rossini, P., Rampazzo, G., Quarantotto, G., De Falco, G., Cristini, S. (1999). Role of desert aerosol in metal fluxes in the Mediterranean area. Chemosphere, 39, pp. 229–246. https://doi.org/10.1016/S0045-6535(99)00105-8.

Halstead, M. J. R., Cunninghame, R. G., Hunter, K. A. (2000). Wet deposition of trace metals to a remote site in Fiordland, New Zealand. Atmos. Environ., 34(4). https://doi.org/10.1016/S1352-2310(99)00185-5.

Hayashi, K. & Okazaki, M. (2002). Effect of volcanic fumes from Mt. Oyama, Miyakejima Island, on atmospheric deposition, soil solution, and soil properties in Kumagaya, central Japan. Soil Sci Plant Nutr., 48, pp. 401-411. https://doi.org/10.1080/00380768.2002.10409218.

Han, G., Liu, C-Q. (2006). Strontium isotope and major ion chemistry of the rainwaters from Guiyang, Guizhou Province, China. Sci. Total. Environ., 364, pp. 165-174. https://doi.org/10.1016/j.scitotenv.2005.06.025.

Han, G., Tang, Y., Wu, Q., Tan, Q. (2010). Chemical and strontium isotope characterization of rainwater in karst virgin forest, Southwest China. Atmos. Environ., 44, pp. 174-181. https://doi.org/10.1016/j.atmosenv.2009.10.019.

Han, G., Wu, Q., Tang, Y. (2012). Acid rain and alkalization in southwestern China: chemical and strontium isotope evidence in rainwater from Guiyang. J. Atmos. Chem., 68, pp. 139-155. https://doi.org/10.1007/s10874-012-9213-x.

Herut, B., Starinsky, A., Katz, A. (1993). Strontium in rainwater from Israel: Sources, isotopes and chemistry. Earth Planet. Sc. Lett., 120(1,2), pp. 77-84.

Hinkley, T. K., Lamothe, P. J., Wilson, S. A., Finnegan, D. L., Gerlach, T. M. (1999). Metal emissions from Kilauea, and a suggested revision of the estimated worldwide metal output by quiescent degassing of volcanoes. Earth Planet. Sci. Lett., 170, pp. 315–325. https://doi.org/10.1016/S0012-821X(99)00103-X.

Hjortenkrans, D. S. T., Bergbäck, B. G., Häggerud, A. V. (2007). Metal emissions from brake linings and tires: Case studies of Stockholm, Sweden 1995/1998 and 2005. Environ. Sci. Technol., 41, 5224–5230. https://doi.org/10.1021/ES070198O.

Hodell, D. A., Mead, G. A., Mueller, P. A. (1990). Variation in the strontium isotopic composition of seawater (8 Ma to present): implications for chemical weathering rates and dissolved fluxes to the oceans. Chem. Geol., 80, pp. 291–307.

Hou, H., Takamatsu, T., Koshikawa, M. K., Hosomi, M. (2005). Trace elements in bulk precipitation and throughfall in a suburban area of Japan. Atmos. Environ., 39, 3583–3595. https://doi.org/10.1016/J.ATMOSENV.2005.02.035.

Houze, R. A., Jr. (1993). Cloud Dynamics. Academic Press, San Diego, 573 pp.

Hu, Y., Cheng, H. (2013). Application of stochastic models in identification and apportionment of trace element pollution sources in the surface soils of a large-scale region. Environ. Sci. Technol., 47, 3752–3760. https://doi.org/10.1021/ES304310K.

Huang, Y. L., Wang, Y. L., Zhang, L. P. (2008). Long-term trend of the chemical composition of wet atmospheric precipitation during 1986-2006 at Shenzhen City, China. Atmos. Environ., 42, 16, pp. 3740-3750. https://doi.org/10.1016/j.atmosenv.2007.12.063.

Huang, J., Duan, Y-H., Xu, M-G., Zhai, L-M., Zhang, X-B., Wang, B-R., Zhang, Y-Z., Gao, S-D., & Sun, N. (2017). Nitrogen mobility, ammonia volatilization, and estimated leaching loss from long-term manure incorporation in red soil. Journal of Integrative Agriculture, 16(9), 2082–2092. https://doi.org/10.1016/S2095-3119(16)61498-3.

Inguaggiato, S., Liotta, M., Rouwet, D., Tassi, F., Vita, F., Schiavo, B., Ono, S., Keller, N. S. (2023). Sulfur origin and flux variations in fumarolic fluids of Vulcano Island, Italy. Front. Earth Sci., 11. https://doi.org/10.3389/feart.2023.1197796.

Iwashita, M., Saito, A., Arai, M., Furusho, Y., Shimamura, T. (2011). Determination of Rare Earth Elements in Rainwater Collected in Suburban Tokyo. Geochem. J., 45(187), https://doi.org/10.2343/geochemj.1.0121.

Kajino, M. & Aikawa, M. (2015). A model validation study of the washout/rainout contribution of sulfate and nitrate in wet deposition compared with precipitation chemical composition data in Japan. Atmos. Environ., 117, 124–134. https://doi.org/10.1016/j.atmosenv.2015.06.042.

Keene, W. C., Pszenny, A. A. P., Galloway, J. N., Hawley, M. E. (1986). Sea-salt corrections and interpretation of constituent ratios in marine precipitation. J. Geophys. Res. Atmos., 91(D6), 6647–6658. https://doi.org/10.1029/JD091ID06P06647.

Kyle, P. R., Meeker, K., Finnegan, D. (1990), Emission rates of sulfur dioxide, trace gases and metals from Mount Erebus, Antarctica. Geophys. Res. Lett., 17, pp. 2125-2128. https://doi.org/10.1029/GL017i012p02125.

Laouali, D.; Galy-Lacaux, C.; Diop, B.; Delon, C.; Orange, D.; Lacaux, J. P.; Akpo, A.; Lavenu, F.; Gardrat, E.; Castera, P. (2012). Long-term monitoring of the chemical composition of precipitation and wet deposition fluxes over three Sahelian savannas. Atmos. Environ. 50, pp. 314–327. https://doi.org/10.1016/j.atmosenv.2011.12.004.

Liotta, M., Brusca, L. Grassa, F., Inguaggiato, S., Longo, M., Madonia, P. (2006). Geochemistry of rainfall at Stromboli volcano (Aeolian Islands): Isotopic composition and plume-rain interaction. Geochem. Geophys. Geosyst., 7, Q07006, https://doi.org/10.1029/2006GC001288.

Liotta, M., Shamavu, P., Scaglione, S., D'Alessandro, W., Bobrowski, N., Bruno Giuffrida, G., Tedesco, D., Calabrese, S. (2017). Mobility of plume-derived volcanogenic elements in meteoric water at Nyiragongo volcano (Congo) inferred from the chemical composition of single rainfall events. Geochim. Cosmochim. Acta, 217, pp. 254–272. https://doi.org/10.1016/j.gca.2017.08.001.

Liotta, M., Cruz, M. M., Ferrufino, A., Rüdiger, J., Gutmann, A., Rojas Cerda, K. V., Bobrowski, N., Maarten de Moor, J. (2021). Magmatic signature in acid rain at Masaya volcano, Nicaragua:

Inferences on element volatility during lava lake degassing. Chemical Geology, 585, 120562. https://doi.org/10.1016/j.chemgeo.2021.120562.

Loye-Pilot M. D. & Martin J. M. (1996). The Impact of Desert Dust Across the Mediterranean. Edited by S. Guerzoni and S. Chester, Kluwer Academic Publishers, Dordrecht, The Netherlands.

Madonia, P. & Liotta, M. (2010). Chemical composition of precipitation at Mt. Vesuvius and Vulcano Island, Italy: Volcanological and environmental implications. Environ. Earth Sci., 61(1), pp 159-171. https://doi.org/10.1007/s12665-009-0333-9.

Mather, T. A., Witt, M. L. I., Pyle, D. M., Quayle, B. M., Aiuppa, A., Bagnato, E., Martin, R. S., Sims, K. W. W., Edmonds, M., Sutton, A. J., Ilyinskaya, E. (2012). Halogens and trace metal emissions from the ongoing 2008 summit eruption of Kīlauea volcano, Hawai`i. Geochim. Cosmochim. Ac., 83, pp. 292-323. https://doi.org/10.1016/j.gca.2011.11.029.

Millot, R., Petelet-Giraud, E., Guerrot, C., Négrel, P. (2010). Multi-isotopic composition (^{7}Li– δ^{11}B– δD– δ^{18}O) of rainwaters in France: Origin and spatio-temporal characterization. Appl. Geochem., 25, pp. 1510-1524. https://doi.org/10.1016/j.apgeochem.2010.08.002.

Mishra, A., Singh, A. K., Singh, K. A., Pandey, P., Yadav, S., Khan, A. H., Barman, S. C. (2012). Urban Air Pollution and their Effects on RainWater Characteristics in Lucknow City, India. Journal of Environmental Research and Development, 6, 4.

Miyata, Y., Tokieda, T., Amakawa, H., Uematsu, M., Nozaki, Y. (2000). Boron isotope variations in the atmosphere. Tellus, 52B, pp. 1057-1065. https://doi.org/10.3402/tellusb.v52i4.17083.

Moaref, S., Sekhavatjou, M. S., Alhashemi, A. H. (2014). Determination of trace elements concentration in wet and dry atmospheric deposition and surface soil in the largest industrial city, southwest of Iran. Int. J. Environ. Res., 8, 335–346. https://doi.org/10.22059/ijer.2014.724.

Montana, G., Randazzo, L., Mazzoleni, P. (2012). Natural and anthropogenic sources of total suspended particulate and their contribution to the formation of black crusts on building stone materials of Catania (Sicily). Environ. Earth Sci., 67(4), pp. 1097-1110. https://doi.org/10.1007/s12665-012-1554-x.

Moreda-Piñeiro, J., Alonso-Rodríguez, E., Turnes-Carou, I., Moscoso-Pérez, C., Blanco-Heras, G., Tellado, L. G., López-Mahía, P., Muniategui-Lorenzo, S., Prada-Rodríguez, D. (2017). Inorganic ions and trace metals bulk deposition at an Atlantic Coastal European region. Journal of Atmospheric Chemistry, 74(1). https://doi.org/10.1007/s10874-016-9338-4.

Moune, S., Gauthier, P.-J., Gislason, S., Sigmarsson, O. (2006). Trace element degassing and enrichment in the eruptive plume of the 2000 eruption of Hekla volcano, Iceland. Geochim. Cosmochim. Ac., 70, pp. 461-479. https://doi.org/10.1016/j.gca.2005.09.011.

Négrel, P. & Roy, S. (1998). Chemistry of rainwater in the Massif Central (France): a strontium isotope and major element study. Appl. Geochem., 13(8), pp. 941-952. https://doi.org/10.1016/S0883-2927(98)00029-8.

Négrel, P., Guerrot, C., Millot, R. (2007). Chemical and strontium isotope characterization of rainwater in France: influence of sources and hydrogeochemical implications. Isot. Environ. Health S., 43(3), pp. 179-196. https://doi.org/10.1080/10256010701550773.

Nicholson, F. A., Smith, S. R., Alloway, B. J., Carlton-Smith, C., & Chambers, B. J. (2003). An inventory of trace elements inputs to agricultural soils in England and Wales. Sci. Total Environ., 311(1–3), pp. 205–219. https://doi.org/10.1016/S0048-9697(03)00139-6.

Nriagu J. O. (1989). A global assessment of natural sources of atmospheric trace metals. Nature, 338, pp. 47–49. https://doi.org/10.1038/338047a0.

Okuda, T., Iwase, T., Ueda, H., Suda, Y., Tanaka, S., Dokiya, Y., Fushimi, K., Hosoe, M. (2005). The impact of volcanic gases from Miyake Island on the chemical constituents in precipitation in the Tokyo metropolitan area. Sci Total Environ., 341(1-3), pp. 185-97. https://doi.org/10.1016/j.scitotenv.2004.09.036.

Oppenheimer, C. (2003). Volcanic degassing. In: Rudnick, R.L. (Ed.), The Crust, Holland, H.D., Turekian, K.K. Treatise on Geochemistry, vol. 3. Elsevier-Pergamon, Oxford, pp. 123– 166. https://doi.org/10.1016/B0-08-043751-6/03020-6.

Pearce, C. R., Parkinson, I. J., Gaillardet, J., Chetelat, B., Burton, K. W. (2015). Characterising the stable ($\delta^{88}/^{86}Sr$) and radiogenic ($^{87}Sr/^{86}Sr$) isotopic composition of strontium in rainwater. Chem. Geol., 409, pp. 54-60. http://dx.doi.org/10.1016/j.chemgeo.2015.05.010.

Pearson, C., Howard, D., Moore, C., Obrist, D. (2019). Mercury and trace metal wet deposition across five stations in Alaska: Controlling factors, spatial patterns, and source regions. Atmos. Chem. Phys., 19, 6913–6929. https://doi.org/10.5194/acp-19-6913-2019.

Pennisi, M., Le Cloarec, M. F., Lambert, G., Le Roulley, J. C. (1988). Fractionation of metals in volcanic emissions. Earth Planet. Sci. Lett., 88, pp. 284–288. https://doi.org/10.1016/0012-821X(88)90085-4.

Pulido-Villena, E., Reche, I., Morales-Baquero, R. (2006). Significance of atmospheric inputs of calcium over the southwestern Mediterranean region: High Mountain lakes as tools for detection. Glob. Biogeochem. Cycles, 20(2). https://doi.org/10.1029/2005GB002662.

Pulles, T., Denier van der Gon, H., Appelman, W., Verheul, M. (2012). Emission factors for trace elements from diesel and petrol used in European vehicles. Atmos. Environ., 61, 641–651. https://doi.org/10.1016/J.ATMOSENV.2012.07.022.

Rose-Koga, E. F., Sheppard, S. M. F., Chaussidon, M., Carignan, J. (2006). Boron isotopic composition of atmospheric precipitations and liquid–vapour fractionations. Geochim. Cosmochim. Ac., 70, 7, pp. 1603-1615. https://doi.org/10.1016/j.gca.2006.01.003.

Rowe, G. L., Brantley, S. L. Fernandez, J. F., Borgia, A. (1995). The chemical and hydrologic structure of Poa´s Volcano, Costa Rica. J. Volcanol. Geoth. Res., 64, 3–4, pp. 233-267. https://doi.org/10.1016/0377-0273(94)00079-V.

Rubin, K. (1997). Degassing of metals and metalloids from erupting seamount and mid-ocean ridge volcanoes: Observations and predictions. Geochim. Cosmochim. Acta, 61, pp. 3525-3542. https://doi.org/10.1016/S0016-7037(97)00179-8.

Sakata, M., Marumoto, K., Narukawa, M., Asakura, K. (2006). Regional variations in wet and dry deposition fluxes of trace elements in Japan. Atmos. Environ., 40, 521–531. https://doi.org/10.1016/J.ATMOSENV.2005.09.066.

Sakata, M., Tani, Y., Takagi, T. (2008). Wet and dry deposition fluxes of trace elements in Tokyo Bay. Atmos. Environ., 42, 23, pp. 5913-5922. https://doi.org/10.1016/j.atmosenv.2008.03.027.

Schlesinger, W. H. (1997). Biogeochemistry: An Analysis of Global Change. Academic Press, New York, NY, USA.

Scholl, M. A. & Ingebritsen, S. E. (1995). Total and non-sea salt sulfate and chloride measured in bulk precipitation samples from the Kilauea Volcano area, Hawaii. Water-Resources Investigations Report 95-4001. https://doi.org/10.3133/wri954001.

Seinfeld, J. H. & Pandis, S. N. (1998). Atmospheric Chemical Composition and Physics from air pollution to climate change. New York. John Wiley and Sons, Incorporated.

Shao, X., Cheng, H., Li, Q., Lin, C. (2013). Anthropogenic atmospheric emissions of cadmium in China. Atmos. Environ., 79, 155–160. https://doi.org/10.1016/J.ATMOSENV.2013.05.055.

Shen, F., Li, Y., Zhang, M., Awasthi, M. K., Ali, A., Li, R., Wang, Q., Zhang, Z. (2016). Atmospheric Deposition-Carried Zn and Cd from a Zinc Smelter and Their Effects on Soil Microflora as Revealed by 16S rDNA. Sci. Rep., 6(1), pp. 1–13. https://doi.org/10.1038/srep39148.

Sickles, J. E. & Grimm, J. W. (2003). Wet deposition from clouds and precipitation in three high-elevation regions of the Eastern United States. Atmos. Environ., 37, pp. 277-288. https://doi.org/10.1016/S1352-2310(02)00823-3.

Silbergeld, E. K., Waalkes, M., Rice, J. M. (2000). Lead as a carcinogen: Experimental evidence and mechanisms of action. American. J. Ind. Med., 38, 316–323.

Spivack, A. J. (1986). Boron isotope geochemistry. PhD Thesis. MIT-WHOI Joint Program in Oceanography, Cambridge, Massachusetts, USA. http://hdl.handle.net/1721.1/15187.

Symonds, R. B., Reed, M. H., Rose, W. I. (1992). Origin, speciation, and fluxes of trace element gases at Augustine volcano, Alaska: Insights into magma degassing and fumarolic processes. Geochim. Cosmochim. Acta, 56, pp. 633-657. https://doi.org/10.1016/0016-7037(92)90087-Y.

Stumm, W. & Morgan, J. J. (1996). Aquatic chemistry: chemical equilibria and rates in natural waters. Wiley Interscience.

Tamburello, G., Hansteen, T. H., Bredemeyer, S., Aiuppa, A., Tassi, F. (2014). Gas emissions from five volcanoes in northern Chile and implications for the volatiles budget of the Central Volcanic Zone. Geophys. Res. Lett., 41. https://doi.org/10.1002/2014GL060653.

Tan, J. H., Duan, J. C., Ma, Y. L., Yang, F. M., Cheng, Y., He, K. B., Yu, Y. C., Wang, J. W. (2014). Source of atmospheric trace elements in winter in Foshan, China. Sci. Total Environ., 493, 262–270. https://doi.org/10.1016/J.SCITOTENV.2014.05.147.

Tang, A., Zhuang, G., Wang, Y., Yuan, H., Sun, Y. (2005). The chemistry of precipitation and its relation to aerosol in Beijing. Atmos. Environ., 39(19), pp. 3397–3406. https://doi.org/10.1016/j.atmosenv.2005.02.001.

Tassi, F., Capecchiacci, F., Cabassi, J., Calabrese, S., Vaselli, O., Rouwet, D., Pecoraino, G., Chiodini, G. (2012). Geogenic and atmospheric sources for volatile organic compounds in fumarolic emissions from Mt. Etna and Vulcano Island (Sicily, Italy). J. Geophys. Res., 117., P20. https://doi.org/10.1029/2012JD017642.

Theodosi, C., Markaki, Z., Tselepides, A., Mihalopoulos, N. (2010). The significance of atmospheric inputs of soluble and particulate major and trace elements to the eastern Mediterranean seawater. Mar. Chem., 120, 154–163. https://doi.org/10.1016/J.MARCHEM.2010.02.003.

Toutain, J. P., Quisefit, J.P., Briole, P., Aloupogiannis, P., Blanc, P., Robaye, G. (1995). Mineralogy and chemistry of solid aerosols emitted from Mount Etna. Geochem. J., 29, pp. 163-173. https://doi.org/10.2343/geochemj.29.163.

Viana, M., López, J. M., Querol, X., Alastuey, A., García-Gacio, D., Blanco-Heras, G., López-Mahía, P., Piñeiro-Iglesias, M., Sanz, M. J., Sanz, F., Chi, X., Maenhaut, W. (2008). Tracers and impact of open burning of rice straw residues on PM in Eastern Spain. Atmos. Environ., 42(8). https://doi.org/10.1016/j.atmosenv.2007.11.012.

Wang, Y., Wai, K. M., Gao, J., Liu, X., Wang, T., Wang, W. (2008). The impacts of anthropogenic emissions on the precipitation chemistry at an elevated site in North-eastern China. Atmos. Environ., 42(13), 2959–2970. https://doi.org/10.1016/J.ATMOSENV.2007.12.051.

Wang, L., Shen, Z., Lu, D., Zhang, Q., Zhang, T., Lei, Y., Xu, H. (2019). Water-soluble components in rainwater over Xi'an in northwest China: Source apportionment and pollution controls effectiveness evaluation. Atmos. Poll. Res., 10(2). https://doi.org/10.1016/j.apr.2018.08.011.

Wu, Q., Han, G., Tao, F., Tang, Y. (2012). Chemical composition of rainwater in a karstic agricultural

area, Southwest China: The impact of urbanization. Atmos. Res., 111, pp. 71–78. https://doi.org/10.1016/j.atmosres.2012.03.002.

Xiao, Y., Sun, D., Wang, Y., Qi, H., Jin, L. (1992). Boron isotopic compositions of brine, sediments, and source water in Da Qaidam Lake, Qinghai, China. Geochim. Cosmochim. Ac., 56, 4, pp. 1561-1568. https://doi.org/10.1016/0016-7037(92)90225-8.

Xochilt, G., Bobrowski, N., Rüdiger, J., Liotta, M., Geil, B., Hoffmann, T., Gutiérrez, E., Dinger, F., Montalvo, F., Villalobos, M., Escobar, D. (2023). Geochemical characterization of volcanic gas emissions at Santa Ana and San Miguel volcanoes, El Salvador, using remote-sensing and in situ measurements. Front. Earth Sci., 11. https://doi.org/10.3389/feart.2023.1049670.

Xu, Z. & Han, G. (2009). Chemical and strontium isotope characterization of rainwater in Beijing, China. Atmos. Res., 43, pp. 1954-1961. https://doi.org/10.1016/j.atmosenv.2009.01.010.

Xu, Z., Li, Y., Tang, Y., Han, G. (2009). Chemical and strontium isotope characterization of rainwater at an urban site in Loess Plateau, Northwest China. Atmos. Res., 94, pp. 481-490. https://doi.org/10.1016/j.atmosres.2009.07.005.

Xu, Z., Tang, Y., Ji, J. (2012). Chemical and strontium isotope characterization of rainwater in Beijing during the 2008 Olympic year. Atmos. Res., 107, pp. 115-125. https://doi.org/10.1016/j.atmosres.2012.01.002.

Ye, L., Huang, M., Zhong, B., Wang, X., Tu, Q., Sun, H., Wang, C., Wu, L., Chang, M. (2018). Wet and dry deposition fluxes of trace elements in Pearl River Delta Region (China): Characteristics, ecological risk assessment, and source apportionment. Journal of Environmental Sciences (China), 70. https://doi.org/10.1016/j.jes.2017.11.019.

Zhao, Z-Q., Liu, C-Q. (2010). Anthropogenic inputs of boron into urban atmosphere: Evidence from boron isotopes of precipitations in Guiyang City, China. Atmos. Environ., 44, pp. 4165-4171. https://doi.org/10.1016/j.atmosenv.2010.07.035.

Zhang, L., Michelangeli, D. V., Taylor, P. A. (2004). Numerical studies of aerosol scavenging by low-level, warm stratiform clouds and precipitation. Atmos. Environ., 38(28). https://doi.org/10.1016/j.atmosenv.2004.05.042.

Zhu, Z., Liu, C-Q., Wang, Z-L., Liu, X., Li, J. (2016). Rare earth elements concentrations and speciation in rainwater from Guiyang, an acid rain impacted zone of Southwest China. Chem. Geol., 442, pp. 23-34. https://doi.org/10.1016/j.chemgeo.2016.08.038.

Zufall, M. J. & Davidson, C. I. (1998). Dry deposition of particles. In: Atmospheric Particles. R. M. Harrison and R. van Grieken, Eds., IUPAC Series on Analytical and Physical Chemistry of Environmental Systems 5, pp. 425–473, John Wiley & Sons, Chichester, UK.

2. Study areas

2.1 General overview

To provide an exhaustive overview of the characteristics, properties, and behaviour of major ions, minor and trace elements, and boron and strontium isotopes, in Mediterranean atmospheric deposition, sampling campaigns were carried out in four different environments study areas properly selected to include different geological settings and different natural and anthropogenic sources of gases and particulate matter into the atmosphere.

Selected sites, all located in Sicily (Italy), and reported in Figure 1, were, as follows: (i) a volcanic area, i.e., Mt. Etna, located on the east coast; (ii) two urban areas, Palermo and Catania, located in the northwest and the east coast, respectively; (iii) two industrial districts, Milazzo and Priolo Gargallo, respectively located in the northeast and the southeast coast; (iv) a rural area, Mt. Soro, located in the Nebrodi Regional Natural Park.

In the current chapter, geological and anthropogenic backgrounds for each study area are reported. Being very important for the identification of sources of gases and particulate matter, a brief climatic description of the study areas is also given in this chapter.

Figure 1 - Distribution of the monitoring areas.

2.2 Mt. Etna

Mt. Etna is in eastern Sicily (Italy). Its elevation (> 3300 m) and areal extent (~ 1250 km^2) make it the biggest active European volcano (*Branca et al., 2004*). It is also one of the most active volcanoes in the world (*Cappello et al., 2013*). Because of its persistent state of activity during historical times, it is intensely monitored by numerous national and international institutes of research, i.e., the Istituto Nazionale di Geofisica e Vulcanologia-Osservatorio Etneo (INGV-OE), via the collection of geochemical, volcanological, geophysical, and remote sensing data, together with a regular sampling of volcanic solid products (ash, lapilli, etc), of all eruptive events (*Bonaccorso et al., 2004*; *Calabrese et al., 2011; Aiuppa et al., 2019; Corsaro & Miraglia, 2022*).

Figure 2 - Mt. Etna bulk collector's network. (a) Zafferana Etnea; (b) Citelli; (c) Mt. Intraleo; (d) Cratere 2001. Photos are by Sergio Calabrese, Filippo Brugnone and Walter D'Alessandro.

Etna is a large 0.57 Ma old stratovolcano built upon tensional faults cutting a ~ 20 km thick continental crust (*Chester et al., 1985*), and formed after the break-up of the African plate margin during its collision with the European continental block since the Upper Miocene (*Barberi et al.*,

1974). Etna's recent volcanic activity consists of persistent passive degassing at the summit craters, and from the upper flanks as diffuse soil emanations (*Allard et al., 1991*; *Allard 1997*), occasionally interrupted by lava emissions associated with paroxysmal eruptions, including strong strombolian and violent lava-fountaining events (*Bonaccorso et al., 2004; Branca & Del Carlo, 2004*; *Ferlito et al., 2014*; *Aiuppa et al., 2019; Corsaro & Miraglia, 2022*). These emissions result from degassing of alkali basalt-hawaiite magma which rises from a shallow mantle diapir (*D'Alessandro et al., 1997*; *Hirn et al., 1997*). Mt. Etna is known as one of the largest global contributors of magmatic gases such as CO_2, SO_2, and halogens (HF, HCl, HBr) (*Allard et al., 1991*; *Allard, 1997*; *Bruno et al., 1996*; *Caltabiano et al., 2004*; *Aiuppa et al., 2005*). The SO_2 flux from Mt. Etna's plume has been routinely measured by remote sensing techniques since 1987 (*Caltabiano et al., 2004*). SO_2 flux ranges between 600 to 25000 t day^{-1}; fluxes greater than 10000 t day^{-1} were mostly measured during eruptive events (*Caltabiano et al., 2004*). Detailed research on Mt. Etna demonstrated that volatile heavy metals, such as Bi, Cu, Cd, Sn, Zn, Tl, and Te are also strongly enriched in their gaseous emissions (*Gauthier & Le Cloarec, 1998*). The monitoring sites of Mt. Etna are shown in Figures 2a, b, c, and d.

2.2.1 Etna's paroxysmal activity 2021-2022

The summit area of Mt. Etna comprises four active vents: Voragine (VOR), Bocca Nuova (BN), North-East Crater (NEC), and South-East Crater (SEC). Among these, SEC represents the youngest, but also the most active crater (*Andronico & Corsaro, 2011*; *Di Renzo et al., 2019*; *Corsaro & Miraglia, 2022*). SEC has often produced cyclical or episodic eruptive activity (*Parfitt & Wilson, 1994*; *Spina et al., 2019*), characterised by a series of paroxysmal lava fountaining events with very short repose times (*Andronico & Corsaro 2011; Spina et al., 2019; Corsaro & Miraglia 2022*). This is exemplified by 23 lava fountain episodes in 1998 (*Neri et al., 2011*), the 64 paroxysms in 2000 (*Andronico & Corsaro, 2011*; *Calabrese et al., 2011*), and the 44 fountaining events between

January 2011 and December 2013 (*Calvari et al., 2018*; *Calvari et al., 2021*; *Bonaccorso et al., 2021*). During the long-standing effusive phase that occurred on the upper SE flank of Mt. Etna from 2004 to 2008, a lateral eruptive event occurred at SEC from 14 to 24 July 2006, where new active vents produced strombolian activity and lava effusion.

A new cyclical eruptive phase started at the SEC on 13 December 2020, producing over 60 paroxysms up to 21 February 2022 (*Andronico et al., 2021*; *Bonaccorso et al., 2021*; *Marchese et al., 2021*; *Calvari & Nunnari, 2022*; *Musu et al., 2023*). The activity went through a relatively intense sequence from 16 February to 01 April 2021, with a paroxysm occurring every 1.85 days (± 0.67 days) until 19 March and longer repose times for the last two events (23-24 March and 31 March – 01 April). for a total of 17 paroxysmal events (*De Gori et al., 2021*; *Marchese et al., 2021*; *Calvari & Nunnari, 2022*; *Corsaro & Miraglia, 2022*). Each paroxysmal event followed the typical pattern observed at the SEC in recent decades (*Alparone et al., 2003*; *Andronico & Corsaro 2011*; *Calvari et al., 2011, 2021*; *Calvari & Nunnari, 2022*; *Corsaro & Miraglia, 2022*), with an intensification of strombolian activity which culminated in the fountaining event (*Calvari & Nunnari, 2022*; *Corsaro & Miraglia, 2022*). During the fountaining activity, a sustained eruption column was generated, which could extend to several kilometres in height (*Andronico et al., 2021; Calvari et al., 2021; Calvari & Nunnari, 2022*), and with a duration from ~ 50 minutes to a maximum of ~ 13 hours, with a median duration of ~ 2.7 hours (*Calvari & Nunnari, 2022*). Figure 3 shows the pyroclastic column and the ash fallout associated with the paroxysm of 04 March 2021.

Figure 3 – The pyroclastic column and the ash fallout associated with the paroxysm of 04 March 2021. Photo taken from the village of Cesarò (Mt. Nebrodi). Photo is by Filippo Brugnone.

2.3 Palermo and Catania urban areas

Palermo is a city of 630.167 inhabitants (*ISTAT* – 01 January 2023), located on the northwest coast of Sicily. The metropolitan area of Palermo is surrounded by mountains, which result from the piling up of deep-water and carbonate platform tectonic units (Imerese and Panormide - *Catalano et al., 2013*). The Sicilian orogen links the Southern Apennine and the Calabrian Arc to the Tellian and Atlas systems of North Africa. The Sicilian Fold and Thrust Belt is a segment of the Apennine-Tyrrhenian System, which refers both to the post-collisional convergence between Africa and a complex European crust (*Bonardi et al., 2003*) and to the coeval roll-back of the subduction hinge of the Adriatic Ionian-African lithosphere (*Doglioni et al., 1999*; *Catalano et al., 2013*).

Catania is a city of 298.762 inhabitants (*ISTAT* - 01 January 2023), located on the east coast of Sicily, ~ 27 kilometres southeast of Mt. Etna. The Catania plain, located between Mt. Etna and the Hyblean Foreland, lies within the Plio-Quaternary foredeep (*Lentini, 1982*; *Lentini et al., 1994*) that

originated from the collapse of the northern margin of the Hyblean Plateau due to extensional faulting (*Grasso, 1993*). The geological and geophysical data suggest that this collapse occurred after the Late Pliocene (*Torelli et al., 1998*) as a result of the progressive migration of the Maghrebian thrust wedge (the "Gela Nappe" front) toward the foreland (*Butler et al., 1992*). Data from hydrocarbon exploration drilling revealed the presence of ~ 600 m of Plio-Pleistocene sediments (*Yellin-Dror et al., 1997*). The most recent unit of this succession, on which the clastic deposits of the plain lie, is represented by Pleistocene marine marly clays, which also constitute a part of the sedimentary basement of Etna.

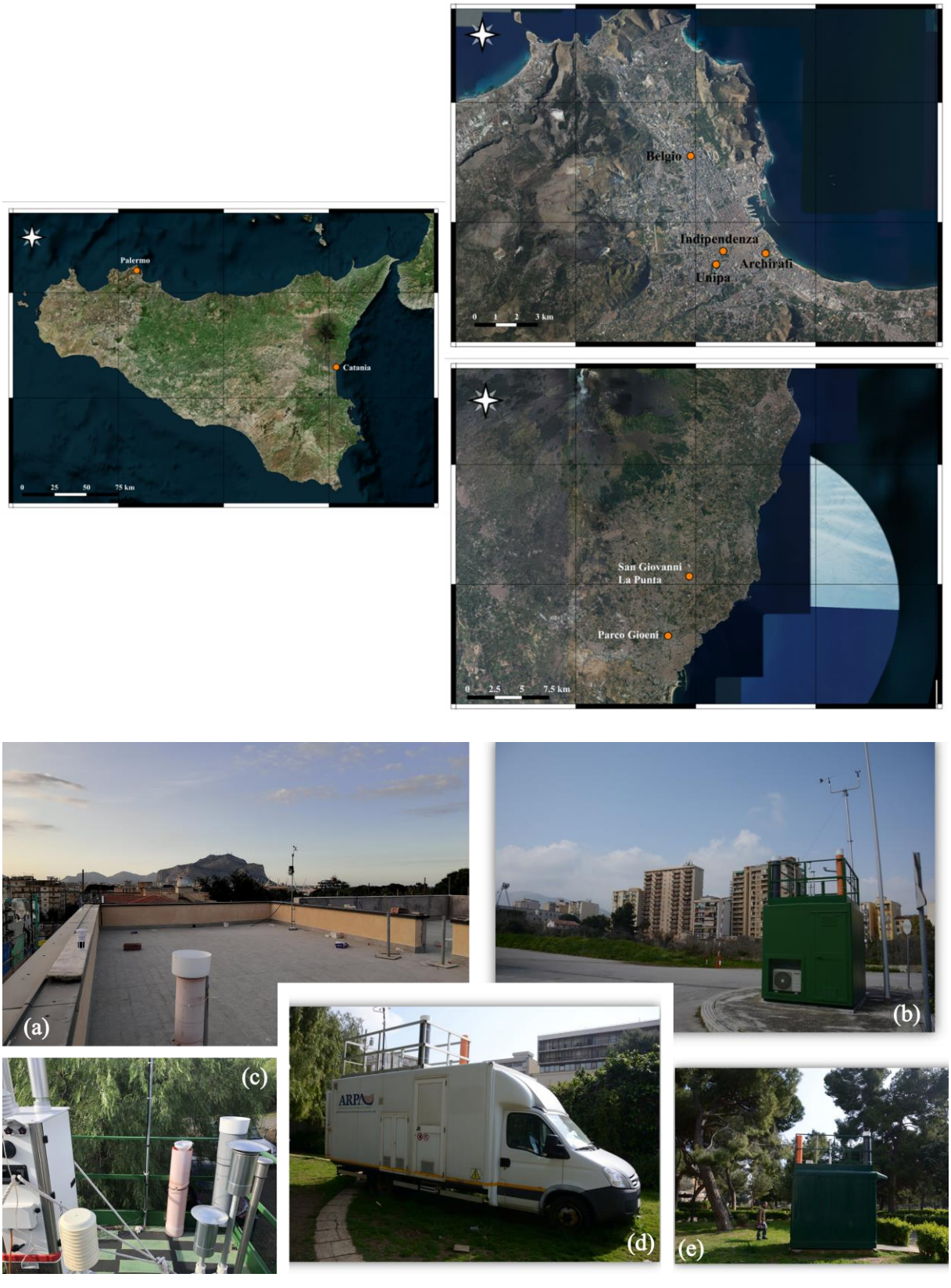

Figure 4 - Palermo (top right) and Catania (bottom right) bulk collector networks. (a) Archirafi; (b) Unipa; (c) Catania; (d) Belgio; (e) Indipendenza. Photos are by Sergio Calabrese and Filippo Brugnone.

Both study areas have a high population density and are among the most important cultural and commercial centres in Sicily. The main sources of gas and atmospheric particulate emissions are vehicle traffic, domestic heating, and ships, such as cruise ships, that crowd the ports of both cities throughout the year, but especially in summer. The monitoring sites of the two urban areas are shown in Figures 4a, b, c, d, e, and f.

2.4 Milazzo and Priolo Gargallo industrial areas

The city of Milazzo, located on the northern coast of Sicily, has 30043 inhabitants (*ISTAT* - 01 January 2023). Industrial development abruptly increased during the 1950s and 1960s, with a steel factory, energy production plants, and the largest single oil refinery in Europe, which produces low-sulfur diesel and unleaded gasoline (*Duplay et al., 2008*; *Bevilacqua & Braglia, 2014*), and which are still in operation. The industrial area covers a surface of ~ 5.5 km^2. Epidemiological information reported an increasing number of cancers and lung infections in this region (*Fano et al., 2019*), as well as an excess of diseases in the urinary system (*Zona et al., 2016*).

The urban and industrial area of Priolo Gargallo is located on the south-eastern coast of Sicily, covers a surface of 55 km^2, and comprises the municipalities of Priolo Gargallo (11,249 inhabitants), Augusta (34,658 inhabitants), Melilli (13,171 inhabitants), Siracusa (116,244 inhabitants), Floridia (21,182 inhabitants), and Solarino (7,513 inhabitants). All population data are from ISTAT, 01 January 2023. The industrial district of Priolo Gargallo includes a huge petrochemical district (the widest in Europe, ~ 27 km^2) that extends from the north of Siracusa to Augusta, where the main industrial activities include oil refineries, processing of oil-related products, and energy production. Until 1986, an asbestos treatment/processing plant of the Italian company Eternit operated in the area.

Figure 5 - Milazzo (top right) and Priolo Gargallo (bottom right) bulk collector networks. (a) Contrada Gabbia – Milazzo; (b) Priolo Gargallo; (c) Augusta; (d) Siracusa. Photos are by Sergio Calabrese.

The heavy industrialisation and dense urbanisation, coupled with a low water turnover, especially in Augusta Bay, have promoted a very high state of degradation. The urban and industrial areas of Milazzo and Priolo Gargallo were classified by the Italian Ministry of the Environment as areas at high risk of environmental crisis. These sites were defined as highly contaminated areas where industrial pollution may cause an important impact in terms of human health and ecological risk, as well as a detrimental impact on cultural and environmental heritage (*ISPRA, 2002*). The monitoring sites of the two urban areas are shown in Figure 5a, b, c, and d.

2.5 Mt. Soro (Nebrodi) background area

The Mt. Soro sampling site is in northeastern Sicily, within the Nebrodi Regional Natural Park, which covers an area of ~ 500 km^2. The Nebrodi Regional Natural Park includes a section of the Mountain chain that runs in an east-west direction along the northern coast of Sicily and that was formed by the overlap of different trust belts during the Alpine orogenesis (*Lentini & Carbone, 2014*). Morphologically, due to the dominance in this part of the chain of various flysch successions with prevailing clayey lithology, the Mountain slopes are not very steep. Notwithstanding, the area comprises the second-highest massif along the chain (Mt. Soro, 1847 m a.s.l.). Geologically the area belongs to the different sedimentary units almost exclusively represented by their Tertiary Flysch covers (*Lentini & Carbone, 2014*) and is comprised of other two main geological units: the Calabride units to the north-west mainly composed of metamorphic lithologies and the Mt. Etna volcanic district to the south-west.

This monitoring site (Fig. 6), being located within a natural park, is relatively far from urban settlements, the nearest being San Teodoro (1220 inhabitants), 8.5 km southeast. It is also 16.8 km from the Tyrrhenian Sea and approximately 35 km from the summit craters of Mt. Etna. The altitude above sea level is 1552 m.

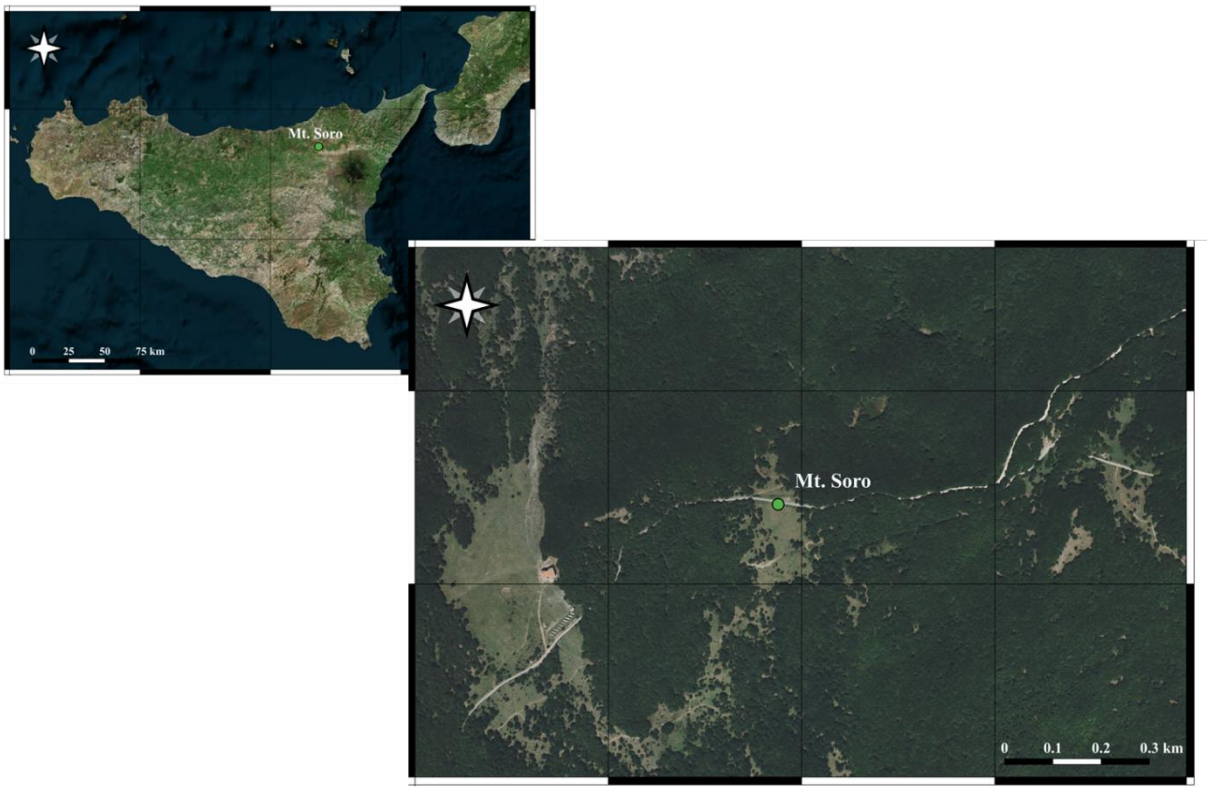

Figure 6 - Mt. Soro sampling site. Photo is by Filippo Brugnone

2.6 Climate Setting

Sicily is in a central position in the Mediterranean basin, which is characterised by the homonymous climate. During the summer season, the southern Mediterranean area is characterised by the presence of subtropical high-pressure cells, which ensure stable weather conditions, dominated by the breeze, which blows from the sea to the coast during the day, and from the inland to the sea during the night. During winter the protagonists of the weather are the cyclonic storms coming from the Atlantic Ocean (*Bolle, 2003*), the prevailing wind direction is from the north and the west, and the mean wind speed is higher than in summer.

The Mediterranean Sea is an important source of energy and moisture due to evaporation, which is highest during winter as a consequence of the interaction between the sea and the cold and dry air masses coming from the north. Energy and moisture released by the sea represent important elements for cyclogenesis, which, due to climate change, increased its intensity in the last years (*Mariotti et al., 2002*; *Lionello et al., 2006*; *Gaertner et al., 2007*).

In Palermo, Catania, Milazzo, and Priolo Gargallo the highest temperatures are measured during the summer months, from June to August, with values sometimes exceeding 40 °C during intense heat waves of sub-tropical origin. The lowest temperatures are measured during the winter, from December to February, with values that frequently fall even below 10 °C at all the sampling sites. Precipitations are concentrated during autumn and spring, often associated with intense but short-lived thunderstorms, while during the winter and especially during the summer there is less rainfall. Thirty-year (1970-2000) rainfall average amounts are 610 mm, 447 mm, 907 mm, and 526 mm for Palermo, Catania, Milazzo, and Priolo Gargallo areas, respectively.

Mt. Etna and Mt. Soro areas display peculiar climatic conditions with respect to the Mediterranean climate of the surrounding areas, due to their altitude and geographical position. In these two areas, temperatures do not only vary between seasons but also as the altitude and the

exposure of the slopes change. During the winter, at all monitoring sites of these two areas, temperatures frequently drop below 0 °C and precipitation occurs in the form of snow or hail.

Precipitations too are strongly influenced by elevation and exposure of the flanks to the dominant winds. For Mt. Etna, the most important wet air masses come from the eastern sector (Ionian Sea), so most of the rainfall is concentrated on the eastern flank of the volcano, as the volcano itself induces condensation. The heaviest rainfall is measured on the East flank, between 600 and 700 m of elevation, with a median value (1970-2000) of up to 1300 mm (Zafferana Etnea). For Mt. Soro the wet air masses come from the north coast (Terranean Sea), so most of the rainfall is concentrated on the northern slopes. Rainfall amounts reach values of ~ 1200 mm. Precipitations are concentrated during autumn and winter in both areas, while they are scarce during summer and only occur in the form of diurnal heat storms.

Using wind data at the isobaric altitude of 850 hPa (approx. 1450 m a.s.l.), taken from the database of the European Centre for Medium-Range Weather Forecasts (ECMWF), an average wind direction of 266° was calculated for the period 01 March 2021 - 31 March 2023, with an average wind speed of 7.2 m s^{-1}. These values were calculated for a point on the vertical of the city of Palermo.

2.7 References

Aiuppa, A., Federico, C., Franco, A., Giudice, G., Guerrieri, S., Inguaggiato, S., Liuzzo, M., McGonigle, A.J.S., Valenza, M. (2005). Emission of bromine and iodine from Mt. Etna volcano. Geochem. Geosyst., 6, Q08008. https://doi.org/10.1029/2005GC000965.

Aiuppa, A., Fischer, T.P., Plank, T., Bani, P. CO_2 flux emissions from the Earth's most actively degassing volcanoes, 2005–2015. (2019). Sci. Rep., 9, 5442. https://doi.org/10.1038/s41598-019-41901-y.

Allard, P., Carbonelle, J., Dajlevic, D., Le Bronec, J., Morel, P., Robe, M.C., Maurenas, J.M., Faivre-Pierret, R., Martin, R., Sabroux, D., Zettwoog, P. (1991). Eruptive and diffuse emissions of CO_2 from Mt. Etna. Nature, 351, pp. 387-391. https://doi.org/10.1038/351387a0.

Allard, P. (1997). Endogenous magma degassing and storage at Mt. Etna. Geophys. Res. Lett., 24(17), pp. 2219-2222. https://doi.org/10.1029/97GL02101.

Alparone, S., Andronico, D., Lodato, L., Sgroi, T. (2003). Relationship between tremor and volcanic activity during the Southeast Crater eruption on Mt. Etna in early 2000. J. Geophys. Res. Solid Earth 108(B3). https://doi.org/10.1029/2002JB001866.

Andronico, D. & Corsaro, R. A. (2011). Lava fountains during the episodic eruption of South–East Crater (Mt. Etna), 2000: insights into magma-gas dynamics within the shallow volcano plumbing system. Bull. Volcanol., 73, pp. 1165–1178. https://doi.org/10.1007/s00445-011-0467-y.

Barberi, F., Civetta, L., Gasparini, P., Innocenti, F., Scandone, R., Villari L. (1974). Evolution of a section of the Africa-Europe plate boundary: Paleomagnetic and volcanological evidence from Sicily. Earth Planet. Sci. Lett., 22(2), pp. 123-132. https://doi.org/10.1016/0012-821X(74)90072-7.

Bevilacqua, M. & Braglia, M. (2014). Environmental efficiency analysis for ENI oil refineries. J. Clean. Prod., 10, pp. 85–92. https://doi.org/10.1016/S0959-6526(01)00022-1.

Bolle, H. J. (2003). Climate, Climate Variability, and Impacts in the Mediterranean Area: An Overview. In Mediterranean Climate. Regional Climate Studies. Springer, Berlin, Heidelberg. https://doi.org/10.1007/978-3-642-55657-9_2.

Bonaccorso, A., Calvari, S., Coltelli, M., Del Negro, C., and Falsaperla, S. (Eds): (2004) Mt. Etna: Volcano Laboratory. Am. Geophys. Union Geophys. Monog., Ser., 143.

Bonaccorso, A., Carleo, L., Currenti, G., Sicali, A. (2021). Magma migration at shallower levels and lava fountains sequence as revealed by borehole dilatometers on Etna volcano. Front. Earth Sci., 800. https://doi.org/10.3389/feart.2021.740505.

Bonardi, G., De Capoa, P., Staso, A. Di, Estévez, A., Martín-Martín, M., Martín-Rojas, I., Tent-Manclús, J. E. (2003). Oligocene-to-early miocene depositional and structural evolution of the Calabria-Peloritani Arc southern terrane (Italy) and geodynamic correlations with the Spain betics and Morocco Rif. Geodin. Acta, 16(2–6), pp. 149–169. https://doi.org/10.1016/j.geoact.2003.06.001.

Branca, S. & Del Carlo, P. (2004). Eruptions of Mt Etna during the past 3.200 years: a revised compilation integrating the Historical and stratigraphic records. In: Mt. Etna: Volcano Laboratory. Am. Geophys. Union Geophys. Monog, pp 1–27. https://doi.org/10.1029/143GM02.

Branca, S., Coltelli, M., Groppelli, G. (2004). Geological evolution of Etna volcano. Washington DC Am. Geophys. Union Geophys. Monog. Ser., 143, pp. 49–63. https://doi.org/10.1029/143GM04.

Bruno, N., Caltabiano, T., Grasso, F., Porto, M., Romano, R. (1996). Degassing of SO_2 and CO_2 at Mt. Etna volcano during the 1991-1993 eruption: correlations and considerations. Acta Vulcanol., 4, pp. 143-147. https://doi.org/10.1016/S0377-0273(01)00201-3.

Butler, R. W. H., Grasso, M., La Manna F. (1992). Origin and deformation of the Neogene–Recent Maghrebian foredeep at the Gela Nappe, SE Sicily. Journal of the Geological Society,149 (4), pp. 547–556. https://doi.org/10.1144/gsjgs.149.4.0547.

Calabrese, S., Aiuppa, A., Allard, P., Bagnato, E., Bellomo, S., Brusca, L., Parello, F. (2011). Atmospheric sources and sinks of volcanogenic elements in a basaltic volcano (Etna, Italy). Geochim. Cosmochim. Acta, 75(23), pp. 7401–7425. https://doi.org/10.1016/j.gca.2011.09.040.

Calvari, S., Salerno, G. G., Spampinato, L., Gouhier, M., La Spina, A., Pecora, E., Harris, A. J. L., Labazuy, P., Biale, E., Boschi E. (2011). An unloading foam model to constrain Etna's 11-13 January 2011 lava fountaining episode. J. Geophys. Res. Solid Earth, 116. https://doi.org/10.1029/2011JB008407.

Calvari, S., Cannavò, F., Bonaccorso, A., Spampinato L., Pellegrino A., G. (2018). Paroxysmal explosions, lava fountains and ash plumes at Etna Volcano: eruptive processes and hazard implications. Front. Earth Sci., 6(107). https://doi.org/10.3389/feart.2018.00107.

Calvari, S., Bonaccorso, A., Ganci, G. (2021). Anatomy of a paroxysmal lava fountain at Etna volcano: the case of the 12 March 2021. Remote Sens., 13(15), 3052. https://doi.org/10.3390/rs13153052.

Calvari, S. & Nunnari, G. (2022). Comparison between automated and manual detection of lava fountains from fixed monitoring thermal cameras at Etna volcano. Remote Sens., 14(10), 2392. https://doi.org/10.3390/rs14102392.

Cappello, A., Bilotta, G., Neri, M., Negro, C. D. (2013). Probabilistic modelling of future volcanic eruptions at Mt. Etna. J. Geophys. Res. Solid. Earth, 118, pp. 1925–1935. https://doi.org/10.1002/jgrb.50190.

Catalano, R., Agate, M., Albanese, C., Avellone, G. Basilone, L., Gasparo Morticelli, M., Gugliotta, C., Sulli, A. Valenti, V., Gibilaro, C., Pierini, S. (2013). Walking along a crustal profile across the Sicily Fold and Thrust Belt. AAPG International Conference & Exhibition, 23-26 October 2011, Milan, Italy, Post-Conference Field Trip 4/27-29 October 2011. Geol. F. Trips 5, no. 2.3, pp. 61-78. http://dx.doi.org/10.3301/GFT.2013.05.

Caltabiano, T., Burton, M., Giammanco, S., Allard, P., Bruno, N., Mure, F., Romano, R. (2004). Volcanic gas emissions from the summit craters and flanks of Mt. Etna, 1987–2000. In: Bonaccorso A, Calvari S, Coltelli M, Del Negro C, Falsaperla S (eds). Mt. Etna: Volcano Laboratory. Union Geophys. Monog. Ser., 143. https://doi.org/10.1029/143GM08.

Chester, D. K., Duncan, A. M., Guest, J. E., Kilbum, C. R. J. (1985). Mt. Etna: The Anatomy of a Volcano. Chapman & Hall, London.

Corsaro, R. A. & Miraglia, L. (2022). Near real-time petrologic monitoring on volcanic glass to infer magmatic processes during the February–April 2021 Paroxysms of the South-East Crater, Etna. Front. Earth Sci. 10:828026. https://doi.org/10.3389/feart.2022.828026.

D'Alessandro, W., Giammanco, S., Parello, F., Valenza, M., (1997). CO_2 output and $\delta^{13}C$ (CO_2) from Mt. Etna as indicators of degassing of shallow asthenosphere. Bull. Volcanol., 58, pp. 455-458. https://doi.org/10.1007/s004450050154.

De Gori, P., Giampiccolo, E., Cocina, O., Branca S., Doglioni C., Chiarabba C. (2021). Re-pressurized magma at Mt. Etna, Italy, may feed eruptions for years. Communications Earth & Environment, 2, pp. 1–9. https://doi.org/10.1038/s43247-021-00282-9.

Di Renzo, V., Corsaro, R. A., Miraglia, L., Pompilio, M., Civetta, L. (2019). Long and short-term magma differentiation at Mt Etna as revealed by Sr-Nd isotopes and geochemical data. Earth-Sci. Rev., 190, pp. 112–130. https://doi.org/10.1016/j.earscirev.2018.12.008.

Doglioni, C., Merlini, S., & Cantarella, G. (1999). Foredeep geometries at the front of the Apennines in the Ionian Sea (central Mediterranean). Earth Planet. Sci. Lett., 168, pp. 243-254.

Duplay, J., Semhi, K., Mey, M., Messina, A., Quaranta, G., Huber, F., Aubert, A. (2008). Geogenic versus anthropogenic geochemical influence on trace elements contents in soils from the Milazzo Peninsula. Geochemistry, 74, pp. 691–704. https://doi.org/10.1016/j.chemer.2014.04.006.

Fano, V., Cernigliaro, A., Scondotto, S., Pollina Addario, S., Caruso, S., Mira, A., Forastiere, F., Perucci, C.A. (2019). Stato di Salute Della Popolazione Residente Nelle Aree ad Elevato Rischio Ambientale e nei siti di Interesse Nazionale Della Sicilia: Analisi Della Mortalità (aa 1995–2000) e dei Ricoveri Ospedalieri (aa 2001–2003); Report: Epidemiologia Sviluppo Ambientale 2019; Assessorato Sanità Dipartimento Osservatorio Epidemiologico (Regione Siciliana); Dipartimento di Epidemiologia ASL RME. Available online: https://www.epicentro.iss.it/ambiente/sicilia_sintesi (accessed on 1 November 2022).

Ferlito, C., Coltorti, M., Lanzafame, G., Giacomoni, P. P. (2014). The volatile flushing triggers eruptions at open conduit volcanoes: evidence from Mt. Etna volcano (Italy). Lithos., 184, pp. 447–455. https://doi.org/10.1016/j.lithos.2013.10.030.

Gaertner, M. A., Jacob, D., Gil, V., Domínguez, M., Padorno, E., Sánchez, E., Castro, M. (2007). Tropical cyclones over the Mediterranean Sea in climate change simulations. Geophys. Res. Lett., 34(14). https://doi.org/10.1029/2007GL029977.

Gauthier Pierre, J. & Le Cloarec M. F. (1998). Variability of alkali and heavy metal fluxes released by Mt. Etna volcano, Sicily, between 1991 and 1995. J. Volcanol. Geotherm. Res., 81, pp. 311–326. https://doi.org/10.1016/S0377-0273(98)00002-X.

Grasso, M. (1993). Pleistocene structures along the Ionian side of the Hyblean Plateau (SE Sicily): Implications for the tectonic evolution of the Malta Escarpment. Geological development of the Sicilian-Tunisia Platform. pp. 49-54.

Hirn, A., Nicolich, R., Galart, J., Laigle, M., Cernobori, L., ETNASEIS Scientific Group. (1997). Roots of Etna volcano in faults of great earthquakes. Earth Planet. Sci. Lett., 148, pp. 171-191. https://doi.org/10.1016/S0012-821X(97)00023-X.

ISPRA 2002. Available online: https://www.isprambiente.gov.it/it/attivita/suolo-e-territorio/siti-contaminati/siti-di-interessenazionale-sin (accessed on 12 December 2022).

Lentini, F. (1982). The geology of Mt. Etna basement. Mem. Soc. Geol. It. 23. pp. 7-25.

Lentini, F., Carbone, S., Catalano, S. (1994). Main structural domains of the Central Mediterranean Region and their Neogene tectonic evolution. Bollettino di Geofisica Teorica ed Applicata. 36, pp. 103-125.

Lentini, F. & Carbone, S. (2014). Geology of Sicily. Italian Geological Survey – ISPRA, Mem. Descr. Carta Geol. d'It. XCV, pp. 7-414.

Lionello, P., J. Bhend, J., Buzzi, A., Della-Marta, P.M., Krichak, S.O., Jansa`, A., Maheras, P., Sanna, A., Trigo, I.F., Trigo R. (2006). Cyclones in the Mediterranean region: Climatology and effects on the environment. Developments in Earth and Environmental Sciences, Elsevier, (4), pp. 325-372. https://doi.org/10.1016/S1571-9197(06)80009-1.

Marchese, F., Filizzola, C., Lacava, T., Falconeri, A., Faruolo, M., Genzano, N., Mazzeo, G., Pietrapertosa, C., Pergola, N., Tramutoli, V., Neri, M. (2021). Mt. Etna paroxysms of February–April 2021 monitored and quantified through a multiplatform satellite observing system. Remote Sens., 13. https://doi.org/10.3390/rs13163074.

Mariotti, A., Struglia, M. V., Zeng, N., & Lau, K. M. (2002). The hydrological cycle in the Mediterranean region and implications for the water budget of the Mediterranean Sea. J. Clim., 15(13), pp. 1674–1690. https://doi.org/10.1175/15200442(2002)015<1674:THCITM>2.0.CO;2.

Musu, A., Corsaro, R. A., Higgins, O., Jorgenson, C., Petrelli, M., Caricchi, L. (2023). The magmatic evolution of South-East Crater (Mt. Etna) during the February–April 2021 sequence of lava fountains from a mineral chemistry perspective. Bull. Volcanol., 85(33). https://doi.org/10.1007/s00445-023-01643-2.

Neri, M., Acocella, V., Behncke, B. Giammanco, S., Mazzarini, F., Rust, D. (2011). Structural analysis of the eruptive fissures at Mt. Etna (Italy). Ann. Geophys., 54, pp. 464–479. https://doi.org/10.4401/ag-5332.

Parfitt, E. A. & Wilson, L. (1994). The 1983–86 Pu'u 'O'o eruption of Kilauea Volcano, Hawaii: a study of dike geometry and eruption mechanisms for a long-lived eruption. J. Volcanol. Geotherm. Res., 59, pp. 179–205. https://doi.org/10.1016/0377-0273(94)90090-6.

Spina, L., Cannata, A., Morgavi, D., Perugini, D. (2019). Degassing behaviour at basaltic volcanoes: new insights from experimental investigations of different conduit geometry and magma viscosity. Earth Sci. Rev., 192, pp. 317–336. https://doi.org/10.1016/j.earscirev.2019.03.010.

Torelli, L., Grasso, M., Mazzoldi, G., Peis, D. (1998). Plio-Quaternary tectonic evolution and structure of the Catania foredeep, the northern Hyblean Plateau, and the Ionian shelf (SE Sicily). Tectonophysics, 298, pp. 209-221. https://doi.org/10.1016/S0040-1951(98)00185-1.

Yellin-Dror, A., Grasso, M., Ben-Avraham, Z., Tibor, G. (1997). The subsidence history of the northern Hyblean plateau margin, southeastern Sicily. Tectonophysics, 282, pp. 277-289. https://doi.org/10.1016/S0040-1951(97)00228-X.

Zona, A., Iavarone, I., Buzzoni, C., Conti, S., Santoro, M., Fazzo, L., Pasetto, R., Pirastu, R., Bruno, C., Ancona, C., et al. (2016). SENTIERI Epidemiological Study of Residents in National Priority Contaminated Sites. Fifth Report. Epidemiol. & Prev., 43 (Suppl. S1), pp. 1–208. https://doi.org/10.19191/EP19.2-3.S1.032.

3. Materials and Methods: sampling, sample processing, analysis, statistical elaborations

3.1 General overview

This chapter is devoted to the description of all the methodologies employed for (i) the sampling of atmospheric deposition samples, (ii) the laboratory pre-treatment of the rainwater samples, (iii) the laboratory procedure for mineralisation of the insoluble fraction, (iv) the chemical and the isotopic analysis of the different sub-samples.

Several sampling procedures and analytical methods for monitoring major ions and minor and trace elements in atmospheric deposition have been developed in the last decades. The type of collector to be used varies depending on whether you want to acquire only dry deposition, only wet deposition, or both (bulk deposition). All collectors shall have a cylindrical vertical section of sufficient height to avoid sampling losses resulting from splashing and the diameter for the opening area and the volume of the collector need to be selected to collect all the precipitation for the required sampling duration (*Amodio et al., 2014*). The laboratory analytical procedures, the number, and type of aliquots produced from each sample collected, and the number and type of instrumental analyses to be performed depending on the type of atmospheric deposition sampled, the type and number of elements whose concentrations are to be determined and, therefore, on the purpose of the research.

In this PhD research project, the rainwater samples were collected through the implementation of a sampling network of bulk collectors, similar to those used for previous research (*Aiuppa et al., 2001*; *Aiuppa et al., 2006*; *Muezzinoglu & Cizmecioglu, 2006; Liotta et al., 2006*, *2017*; *Soriano et al., 2012*; *Calabrese et al., 2011*; *D'Alessandro et al., 2013*; *Brugnone et al., 2020*; *Brugnone et al., 2023a*, *2023b*). The sampling and analytical methods used are summarised below.

3.2 Atmospheric deposition sampling and laboratory methods

Rainwater samples were collected in four different contexts, from March 2021 to April 2023, by using a network of fifteen bulk collectors (Tab. 1). The collecting systems used for the present research were “bulk collectors”, which remained open during the whole sampling period, thus receiving both wet and dry deposition. A total of 301 samples were collected with sampling procedures following published protocols for atmospheric composition monitoring (*Harmens et al., 2004; EN 15841:2009; EMEP/CCC, 2009; WMO, 2018*). The device was based on the standard EN 15841:2009 (standard method for determination of arsenic, cadmium, lead, and nickel in atmospheric deposition). Although some errors in assessing atmospheric deposition with the surrogate approach could result from poor sampling properties and defective sampling strategies (*Dammgen et al., 2005*), the European Committee for Standardization (CEN) recommends bulk (bottle/funnel) samplers to collect and assess the atmospheric deposition of metals. Aas et al. (2009) evaluated sampler uncertainties of different collectors (wet only, bulk, Bergerhoff, and bulk bottle/funnel); the authors showed that the lowest uncertainty was found for the bulk bottle/funnel sampler. This sampler is recommended to measure total atmospheric deposition at industrial and urban sites, mainly when total deposition is not only due to precipitation events (*Aas et al., 2009*).

Therefore, each bulk collector consisted of a 10 L bottle (made of High-Density Polyethylene, HDPE) and a Büchner type funnel (Ø 240 mm, made of polypropylene, PP - Kartell™ Polypropylene Buchner Funnels). The design and installation of the bulk collectors conformed to EMEP/CCC (European Monitoring and Evaluation Programme/Chemical Coordinating Center) site requirements for precipitation gauges (*EMEP/CCC-Report, 2009*): at least 10 metres away from vertical obstacles, such as buildings or trees, which would prevent the accumulation of rain or snow, especially in the case of cross rainfall. To minimise the contamination by soil dust of local origin, and to protect the collected rain from direct sunlight, the collecting system was positioned at least 1.5 m above the ground level into a matt PVC tube. All funnels had a cylindrical vertical section of

sufficient height to avoid sampling losses resulting from splashing and the diameter for the opening area and the volume of the collector have been selected to collect all the precipitation for the required sampling duration (*Amodio et al., 2014*). Only in a few cases (20), due to unexpected strong rainfall or unwanted extension of the sampling period, the sampled water was greater than the volume of the collector.

All the equipment of the bulk collectors (funnels and bottles) was cleaned before the field exposure, with a 2% w/v HNO_3 (Merck Suprapur) solution, and then rinsed several times with deionised water (18.2 MΩ cm resistance, Milli-Q water-purification system, Millipore), and dried under a hood for 24 h. Afterwards, the bulk collectors were assembled and stored in clean plastic bags until their exposure in the field. In all monitoring campaigns, bottles and funnels were removed and replaced by clean ones at the end of the sampling period. All the operations described above were performed wearing powder-free latex gloves.

3.1.1 Atmospheric deposition sampling network

Based on previous work (*Aiuppa et al., 2001*, *2006*; *Bellomo et al., 2007*; *Martin et al., 2009*; *Calabrese et al., 2011*), three bulk collectors were installed on the down-wind (south-eastern, eastern, and north-eastern) flanks, at different distances from summit craters. The first one was installed at the beginning of April 2021, near "Cratere 2001", a few hundred meters upstream of the "Rifugio Sapienza", at an altitude of 2581 m above sea level. This was the closest sampling point to the summit craters (3.0 km). Eighteen samples were sampled until April 2023. Sampling was carried out monthly, except for the periods December 2021 - February 2022 and November 2022 - April 2023, during which it was not possible to reach the monitoring site due to the high thickness of the snow on the ground. The second and the third ones were installed at Zafferana Etnea (altitude of 850 m a.s.l. and 10.0 km from the summit craters), and Citelli (1688 m a.s.l. and 5.4 km from the summit craters). Both were installed at the beginning of March 2021. In the former, twenty-three samples

were sampled until mid-February 2023, with an average sampling interval of thirty-one days; in the latter, twenty-three samples were sampled until the end of March 2023, with an average sampling interval of thirty-three days. To define the local atmospheric background, the fourth bulk collector was installed in a site up-wind, in a rural area poorly affected by volcanic emissions (*Bellomo et al., 2007*; *Calabrese et al., 2011*), near Mt. Intraleo. Twenty-one samples were sampled at this site from late April 2021 to mid-February 2023, with an average sampling interval of thirty-one days. All these collectors were at least 9 km from the nearest urban settlement except that of Zafferana Etnea which was less than 2 km from the outskirts of the homonymous town.

Four bulk collectors were installed, at the beginning of March 2021, in the City of Palermo. One was installed on the roof of the "Emilio Segré" building in "Via Archirafi no. 36" (Dipartimento di Scienze della Terra e del Mare, Università degli Studi di Palermo), and three on the roof of as many air quality monitoring stations of the Agenzia Regionale per la Protezione Ambientale (ARPA Sicilia), two of which are located at major road junctions ("Via Belgio" and "Piazza Indipendenza"), and the third in an urban area with little vehicular traffic ("Viale delle Scienze"). At the "Via Archirafi", "Piazza Indipendenza", and "Viale delle Scienze" sites, the bulk collectors worked until mid-February 2023, sampling twenty-three samples at each site, with an average of one sample every thirty days. At the "Via Belgio" site, the bulk collectors worked until the end of February 2022, sampling twelve samples, with an average of one sample every thirty days. These sampling sites were selected to monitor the urban anthropogenic impact (i.e., vehicular traffic, ship transport, domestic heating), and the influence of the marine source on the chemical composition of atmospheric deposition in the city of Palermo.

Two bulk collectors were installed from the end of April 2021 until mid-February 2023, in the area of Catania, one in "Parco Gioeni", an urban park located in the northern part of the city, and one at San Giovanni la Punta (23,454 inhabitants), a town ~ 6 km north of Catania. Twenty-one and twenty samples, at a frequency of one sample every thirty-one and thirty-three days, were sampled at

these two sites, respectively. These were two monitoring sites in urbanised areas with moderate vehicular traffic. These sampling sites were chosen to characterise anthropogenic, marine, and volcanic contributions to the chemical composition of atmospheric deposition, given their distance from the coastline (2.5 km and 5.0 km, respectively) and Mt. Etna's summit craters (26.0 km and 21.5 km, respectively). These collectors were placed also on the roof of air quality monitoring stations of ARPA Sicilia.

One bulk collector was installed, between the beginning of March 2021 and the end of April 2022, in “Contrada Gabbia”, “Giammoro - Milazzo”, a small settlement surrounded by the industrial area of Milazzo (ME). Fifteen samples were sampled at a frequency of twenty-eight days. This monitoring site was chosen to characterise the anthropogenic industrial contribution to atmospheric deposition in this area.

Three bulk collectors were installed on the roof of air quality monitoring stations of ARPA Sicilia in the Siracusa area for monitoring the industrial impact on the atmosphere of one of the largest refineries in Europe. At the “Siracusa” and the “Priolo Gargallo” monitoring sites a total of forty-six rainwater samples were collected between the beginning of March 2021 and the middle of February 2023, while at “Augusta” site twelve samples were collected in one year, between March 2021 and the end of February 2022. At all the sites, the sampling frequency was thirty days. A total of twenty-two samples, with a frequency of thirty-one days, were collected at the Mt. Soro background area between March 2021 and February 2023.

Table 1 summarises the geographical information of all the sampling sites.

Table 1 - The collectors' network and information of monitoring sites.

ID	Site	Type of Site	Position UTM WGS84	Altitude (m a.s.l.)	Elevation from the ground (m)	Distance from the sea (km)	Distance from Etna's summit craters (km)
CIT	Citelli	Volcanic	33S 504769 4180074	1688	1.5	13.3	5.4
ZAF	Zafferana Etnea	Volcanic	33S 508202 4173454	850	1.5	9.9	10.0
CRT	Cratere 2001	Volcanic	33S 500537 4174966	2581	1.5	17.6	3.6
INT	Mt. Intraleo	Volcanic	33S 492899 4175099	1514	1.5	25.4	7.5
ARC	Palermo - Archirafi	Urban	33S 357403 4219295	33	22	0.5	147.9
UNI	Palermo - Unipa	Urban	33S 355032 4218766	42	3.5	2.7	150.1
IND	Palermo - Indipendenza	Urban	33S 355392 4219342	38	3.5	1.7	149.9
BEL	Palermo - Belgio	Urban	33S 353812 4223960	41	3.5	3.4	152.7
CAT	Catania	Urban	33S 507169 4153592	138	3.5	2.6	26.0
GLP	S. Giovanni La Punta	Urban	33S 508926 4159074	345	3.5	5.3	21.5
GAB	Milazzo	Industrial/Urban	33S 527148 4228670	9	3.5	0.4	57.3
SIR	Siracusa Belvedere	Industrial/Urban	33S 518528 4105315	150	3.5	3.5	75.5
AUG	Augusta	Industrial/Urban	33S 519569 4119118	5	3.5	0.1	62.6
PRI	Priolo Gargallo	Industrial/Urban	33S 516974 4112227	19	3.5	1.1	68.4
CES	Mt. Soro	Rural	33S 470287 4197501	1524	3.5	16.8	35.0

3.1.2 Laboratory pre-treatment of rainwater samples (soluble fraction)

At the end of the sampling period, the collection bottles were capped and carried to the laboratory. The quantity of water was measured gravimetrically to calculate the amount of rainwater. The collected water samples were split into sub-samples. One untreated aliquot (100 mL) was immediately used for the determination of pH and electric conductivity (EC) (*UNI EN ISO 10523:2009; EN 7888:1985*). Another untreated aliquot (100 mL) was taken for total alkalinity determination (expressed as mg(HCO_3^-) L^{-1}). Subsequently, the remaining rainwater sample was filtered using a 0.45 µm pore size, 47 mm diameter, cellulose nitrate membrane, to remove any solid material and to stabilise the solution for the subsequent analysis. From the filtered aliquot, two sub-samples were obtained: (i) 50 mL for major anions (NO_3^-, SO_4^{2-}, Cl^-, and F^-) determinations; 50 mL acidified sample, with 100 µL of Ultrapure HNO_3, for major cations (Na^+, K^+, NH_4^+, Ca^{2+}, Mg^{2+}), and a large suite of minor and trace elements (Li, Be, B, Al, Si, Ti, V, Cr, Mn, Fe, Co, Ni, Cu, Zn, As, Se, Br, Rb, Sr, Mo, Cd, Sn, Sb, Cs, Ba, Tl, Pb, Bi, U). For selected samples, those in which a

sufficient volume of water was present, the filtered water not used for the preparation of the above aliquots, was split into other two sub-samples: (i) determination of the Technology-Critical Elements – TCEs (Sc, Ge, Te, Y, Nb, Zr, Hf, Th, La, Ce, Pr, Nd, Sm, Eu, Gd, Tb, Dy, Ho, Er, Tm, Yb, Lu) concentrations; (ii) determination of the isotopic composition of B and Sr. All samples were stored dark and refrigerated (4 °C) until analysis.

During the dry period (no rain in the collectors), dry deposition was recovered following the method described by Menichini et al. (2006): 300 mL of ultrapure water was used to slowly wash both the funnel and the sampling bottle, and the obtained solution/suspension of the dry deposition was treated as described above.

Furthermore, for each site and each sampling period, the bulk collector systems were first rinsed with 150 mL of 2% w/v HNO_3 (Merck Suprapur) solution and then with 150 mL of deionised water (Milli-Q). 50 ml of the resulting washing solutions were recovered in 50 ml centrifuge tubes and refrigerated at 4 ºC before being analysed for the concentration determination of minor and trace elements (Li, B, Al, Ti, V, Cr, Mn, Fe, Co, Ni, Cu, Zn, As, Se, Br, Rb, Sr, Mo, Cd, Sn, Sb, Cs, Ba, Tl, Pb, and U). As this procedure has never been tried before, only a few (25) of the prepared samples were analysed and the results will be presented in this thesis. The remaining samples will be analysed, if possible, after the end of the PhD project.

Sample manipulations were carried out in clean rooms and all plastic wares were washed with deionised water (Milli-Q). Pre-treatment of the rainwater samples was performed in the laboratories of the “Dipartimento di Scienze della Terra e del Mare - DiSTeM” of the University of Palermo.

3.1.3 Laboratory procedure for mineralisation of the insoluble fraction

Cellulose nitrate membranes, with 0.45 μm pore size and 47 mm diameter, were used for the filtration of the rainwater samples. All solid material with a diameter larger than that of the pores was

retained by the membranes. The filter residue membrane was processed based on the *UNI EN 14902:2005* normative and the US Environmental Protection Agency (EPA) Method 3051 (*US EPA, 2007*). The microwave-assisted method with nitric acid HNO_3 (Merck Suprapur) was applied. The samples were treated at the laboratory of the "Dipartimento di Scienze Agrarie, Alimentari e Forestali – SAAF" of Palermo, according to the procedure described below. The total weight of the retained material was calculated by subtracting the original weight of the membrane before filtration from the weight of the membrane after filtration. For each rainwater sample, more than one membrane could have been used for the filtration. All membranes used for a water sample were considered one sample if the total weight (membrane + solid material) was ≤ 0.5 g, otherwise the same membranes were divided into two or more sub-samples with a maximum weight of 0.5 g. Mineralisation was performed by a Microwave Digestion System CEM Mars 5 with temperature control. Twenty-four Polytetrafluoroethylene vessels were used, after being thoroughly cleaned with 2% w/v HNO_3 (Merck Suprapur) solution and then rinsed with deionised water (MilliQ). Each sample was placed inside a vessel, with 4 mL of Ultrapure 67% w/v HNO_3 and 3 mL of 32% w/v Ultrapure H_2O_2. The vessels were placed in the microwave digestion system, configured with a program that included a twenty-minute heating ramp up to a temperature of 200 °C and a pressure of 800 psi, forty minutes of holding these conditions, and, finally, a cooling period of twenty minutes. The mineralised samples were recovered in a 50 mL centrifuge tube; the vessels were washed with 10 mL of deionised water (MilliQ) water and these solutions were added to the sample. The samples were brought to a final volume of 20 mL using deionised water (MilliQ). The presence of a solid residue, almost certainly of silicate composition, was observed in many samples. To remove this, which could be a problem during instrumental analysis, all samples were centrifuged for 3 minutes at 5000 rpm using an ALC 4222 MK II centrifuge. The supernatant was recovered in 15 mL vessel tubes and subsequently analysed for the determination of minor and trace element concentrations (Li, B, Al, Ti, V, Cr, Mn, Fe, Co, Ni, Cu, Zn, As, Sr, Mo, Ba, and Pb).

3.1.4 Laboratory Procedure for Technology-Critical Elements (TCEs)

Despite instrumental advancements, accurate determination of Technology-Critical Elements (including lanthanoids) in rainwater samples remains a challenge. This is mostly because of very low elemental concentrations ranging from nanograms per litre to low micrograms per litre. Among various instrumental approaches, inductively coupled plasma mass spectrometry (ICP-MS) is a powerful technique offering excellent sensitivity and multielement detection capability. Nevertheless, direct determinations from rainwater by ICP-MS are often hampered by spectral and non-spectral interferences. Coprecipitation methods have been attractive means for eliminating the salt matrix and preconcentrating the trace elements in rainwater. Coprecipitation as metal hydroxides has also an added advantage for ICP-MS since acid dissolution yields metal ions in a slightly acid solution. $Mg(OH)_2$ coprecipitation has been popular for TCEs and lanthanoids as it uses Mg^{2+} available in seawater (*Arslan et al., 2018*). In this paragraph, an $Mg(OH)_2$ coprecipitation method using Triethylamine (TEA), an aprotic base, for scavenging the trace elements, the TCEs, and the lanthanoid from the rainwater will be presented. The coprecipitation with TEA afforded quantitative scavenging of a large suite of elements, including those that form ammonia complexes, i.e., Cd, Cu, Co, Ni, and Zn.

The methodology comprises a series of steps that are summarised below. 50 mL of filtered sample was first spiked with 500 μL of $MgCl_2$ x $6H_2O$ (final concentration in the sample 344 μg L^{-1}), being the starting solution insufficiently rich in magnesium, and with 200 μL of pure (~ 99%) TEA, to cause the coprecipitation of $Mg(OH)_2$, on whose surface the elements of interest will be adsorbed. After sitting for fifteen minutes, the colloidal solution was centrifuged at 4800 rpm on an ALC 4218-D centrifuge for 30 minutes. The supernatant solution was poured off and the precipitate was dissolved first in 1.5 mL of 7% HNO_3. The solution was recovered in a clean 10 mL centrifuge tube. 1.5 mL of 1% HNO_3 was poured into the original tube to remove any residue, and the solution was

recovered in the 10 mL tube. The last step was repeated a second time. 4.0 mL of deionised water (Milli-Q) was poured into the original tube and the solution was added to the sample. The sample was brought up to a volume of 10 mL with deionised water (Milli-Q) and refrigerated at 4 ºC before the chemical analysis.

3.3 Chemical analyses

The analytical methods used are summarised in Table 2. Chemical analyses were performed in the laboratories of the "Dipartimento di Scienze della Terra e del Mare - DiSTeM" of the University of Palermo, and in the laboratories of the "Istituto Nazionale di Geofisica e Vulcanologia, section of Palermo.

Table 2 - Methods and instruments for chemical analysis of atmospheric precipitation.

Constituent and parameter	Method	Instrument	Laboratory
Conductivity	Conductimetry at 25 °C	VWR Symphony model 11388-372	Water Geochemistry – University of Palermo
Hydrogen ion (H^+)	Potentiometry (glass electrode)	VWR Symphony model 662-1807	Water Geochemistry – University of Palermo
Total Alkalinity mg(HCO_3^-)	Titration (0.1N) HCl	Titrando 888 Metrohm	Water Geochemistry – University of Palermo
Cations (Na^+, K^+, Mg^{2+}, Ca^{2+}, NH_4^+)	Ion Chromatography (IC) & Inductively coupled optical emission Spectrometry (IPS-OES)	Thermo Scientific Dionex ICS-5000+ Agilent Technologies 5900	Istituto Nazionale di Geofisica e Vulcanologia – Section of Palermo
Anions (F^-, SO_4^{2-}, Cl^-, NO_3^-)	Ion Chromatography (IC)	Thermo Scientific Dionex ICS-5000+	Istituto Nazionale di Geofisica e Vulcanologia – Section of Palermo
Minor and Trace elements (Li, Be, B, Al, Ti, V, Cr, Mn, Fe, Co, Ni, Cu, Zn, As, Se, Br, Rb, Sr, Mo, Cd, Sn, Sb, Cs, Ba, Tl, Pb, Bi, U)	Inductively coupled plasma-mass spectrometry (ICP-MS) & Inductively coupled optical emission Spectrometry (IPS-OES)	Agilent Technologies 7800 Agilent Technologies 5900	Istituto Nazionale di Geofisica e Vulcanologia – Section of Palermo
Technology Critical Elements - TCEs (Sc, Ge, Te, Y, Nb, Zr, Hf, Th, La, Ce, Pr, Nd, Sm, Eu, Gd, Tb, Dy, Ho, Er, Tm, Yb, Lu)	Inductively coupled plasma-mass spectrometry (ICP-MS)	Agilent Technologies 7800	Istituto Nazionale di Geofisica e Vulcanologia – Section of Palermo
B & Sr isotopes	High Resolution Multi-collector Inductively coupled plasma-mass spectrometry (HR-MC-ICP-MS)	Thermo Scientific Neptune Plus™	Istituto di Geoscienze e Georisorse (IGG) - Consiglio Nazionale delle Ricerche (CNR)

The pH values were determined by a pH meter with a glass electrode (VWR Symphony

model 662-1807), previously calibrated with buffer solutions (pH 4, 7, and 10). The conductivity of the samples was measured by a portable Conductimeter with automatic correction of the temperature (VWR Symphony model 11388-372), previously calibrated with a solution of 84 μS cm^{-1} @20 °C, similar to the average conductivity expected for the sampled rainwaters.

Total alkalinity, expressed as mg(HCO_3^-) L^{-1}, was determined through an automatic titrator (Titrando 888 Metrohm), using 0.1 N HCl. To determine the concentration of HCO_3^- in very dilute solutions, such as rainwater, without having to change the concentration of the titrating acid, an analytical method was developed in which the HCl was added very slowly to the solution (maximum of 5 mL $min.^{-1}$). The detection limit was 8.0 μeq L^{-1}.

Ion chromatography technique was used for the determination of major anions (NO_3^-, SO_4^{2-}, Cl^-, and F^-), and major cations (Ca^{2+}, K^+, Mg^{2+}, Na^+, NH_4^+) concentrations, with an ion chromatograph Thermo Scientific Dionex ICS-5000+. The anion chromatograph, equipped with an anion column (Dionex IonPac AS19-4μm), a pre-column (Dionex IonPac AG19-4μm), and a suppressor (ASRS-500 4 mm), worked under a continuous flow of carbonate-bicarbonate eluent (Na_2CO_3/$NaHCO_3$), for major anions determination (*UNI EN ISO 10304-1:2009*). The cation chromatograph, equipped with a cationic column (Dionex IonPac CS16-5μm), a pre-column (Dionex IonPac CG16-5μm), and a suppressor (CSRS-500 4 mm), worked under a continuous flow of Methanesulphonic acid (MSA) for ammonium determination (*UNI EN ISO 14911-1:2001*). The detection limits (LOD) (μeq L^{-1}) were 1 for NO_3^- and SO_4^{2-}, 0.3 for Cl^-, F^- and NH_4^+, 0.1 for Ca^{2+}, Mg^{2+}, K^+, and Na^+. Calibration solutions for all the investigated ions were prepared by diluting stock standard solutions (Merck). Calibration curves were made with 7 calibration levels and precision was always < 2% for cations, and < 3% for anions, except for fluoride (~ 9%). The accuracy of the method was checked by analysing certified reference materials of natural waters (Environment Canada Ontario 99 and NWLON-7) at regular intervals. For further details, the reader is invited to see Table 3.

Due to a technical problem with the ion chromatograph used for cation analysis, samples from the period June 2022 - April 2023, i.e., from series no. 17 to series no. 23, were analysed for major cations (Na^+, K^+, Mg^{2+}, and Ca^{2+}) at the Istituto Nazionale di Geofisica e Vulcanologia by inductively coupled optical emission spectrometry (IPS-OES) using an ICP-OES Agilent 5900. The detection limits (LOD) (μeq L^{-1}) were 0.1 for Ca^{2+} and Mg^{2+}, and 0.005 for K^+ and Na^+. Each analytical session involves a calibration routine for all the elements to be quantified, through the analysis of working standards at increasing concentrations, which can vary in number from a minimum of 6 to a maximum of 12 to cover 3 to 6 orders of magnitude of concentrations, i.e., from a few tens of ng L^{-1} up to mg L^{-1}. The calibration curves were evaluated according to various parameters such as the linear regression (R), the value of the calculated concentration versus the chemical concentration of each standard, the precision of the value (R. S. D.) and the signal stability of the internal standard. Different internal standards (Y, Rh, In, Re) were used during the analytical runs to control the matrix effect and were introduced directly online into the introduction system via a T-connector that ensures a constant and continuous introduction. For a correct evaluation of the data, precision and accuracy were always considered. The concentrations of ammonium for these samples were not determined. For further details, the reader is invited to see Table 3.

Minor and trace elements (Li, Be, B, Al, Ti, V, Cr, Mn, Fe, Co, Ni, Cu, Zn, As, Se, Br, Rb, Sr, Mo, Cd, Sn, Sb, Cs, Ba, Tl, Pb, Bi, U), Technology-Critical Elements - TCEs (Te, Sc, Ge, Y, Nb, Zr, Hf, Th) and lanthanoids (La, Ce, Pr, Nd, Sm, Eu, Gd, Tb, Dy, Ho, Er, Tm, Yb, Lu) were analysed by inductively coupled plasma-mass spectrometry with an ICP-MS instrument (Agilent Technologies 7800) (*UNI EN 16171:2016*). The detection limits (LOD) were calculated using the method of blank variability for each investigated element. The detection limits (μg L^{-1}) were: 0.20 for Fe, 0.10 for Li, B, Al, Zn, and Br, 0.05 for Be, Ti, V, Cr, Mn, Ba, and Pb, 0.03 for Ni and Cu, 0.02 for Co, As, Se, Rb, Sr, and Mo, 0.01 for Cd, Sn, and Sb, 0.005 for Zr, 0.003 for Tl and Bi, 0.001 for Y, Te, Cs, and U, 0.0005 for La, Ce, Pr, Nd, Sm, Eu, Gd, Tb, Dy, Ho, Er, Tm, Yb, and Lu, 0.0003 for Ge, 0.0002 for

Sc, and, finally, 0.0001 for Nb, Hf, and Th.

External multi-element calibrations were performed with standard solutions obtained by mixing and diluting multi and single-element work solutions (100 mg L^{-1}, and 1000 mg L^{-1}, CertiPUR ICP Standards Merck). The calibration routine was done on selected isotopes for each element with 11 calibration points prepared daily in 10 mL polyethene tubes by dilution with 2% w/v HNO_3 solution, treated as a blank solution. Element contents in the analysed samples were calculated using the spectrometer software (ICP Mass Hunter, version B.01.01). The sensitivity variations were monitored by ^{103}Rh, ^{115}In, and ^{185}Re with 10 μg L^{-1} concentration as an internal standard added directly online. The reproducibility of the chemical analysis was verified by 5 replications for each sample and standard and the R. S. D. were always < 20% for trace elements, and < 30% for ultra-trace elements. QA/QC for the investigated elements was evaluated by the analysis of four Certified Reference Materials (SpectraPure SPSSW1 and SPSSW2, Environment Canada TM 27.3, TM 61.2, TM35), specific to the analysis of trace elements in fresh and rainwater and accuracies between ±10 to ±20% for B, Cr, Fe, Ni, Zn, As, Se, Te, and Bi, and below than ±10% for the other elements, were calculated. For further details, the reader is invited to see Table 3. Argon gas of high purity grade (99.99%) was used as the gas carrier.

The concentration of minor and trace elements in the insoluble fraction solutions (Li, B, Al, Ti, V, Cr, Mn, Fe, Co, Ni, Cu, Zn, As, Sr, Mo, Ba, Pb) was determined by an inductively coupled optical emission spectrometry (IPS-OES) using an ICP-OES Agilent 5900. The quality control procedures were analogous to those described for the ICP-MS. For the detection limits, the accuracy and the R. S. D. for each element, the reader is invited to see Table 3.

3.4 Laboratory procedure for B and Sr isotopes

Determining the isotopic composition of B and Sr requires precise sample pre-treatment procedures, especially when working with matrices where these elements are present in low

concentrations, as in the case of rainwaters. For B, it is crucial to separate it from the matrix to inhibit the "mass bias" during mass spectrometer analysis (*Guerrot et al., 2011*). Whereas, for Sr, it is essential to separate it from rubidium (Rb), which has a naturally weakly radioactive isotope (^{87}Rb) with the same atomic weight as the isotope ^{87}Sr. All laboratory procedures were performed at the "Istituto di Geoscienze e Georisorse" of the Italian National Research Council (IGG-CNR) in Pisa (Italy). The preparation of the samples was performed in two cleanrooms, one ISO 6 and the other ISO 5 (*UNI EN ISO 14644-1*), using B-free and Sr-free ultrapure reagents. Ultrapure water was obtained starting from Milli-Q water (resistivity of 18.2 MΩ cm^{-1}), and subsequent sub-boiled distillation using Savillex DST-1000; ultrapure HNO_3 (2N) solution was obtained starting from Suprapur HNO_3 and two subsequent steps of sub-boiled distillation using Savillex DST-1000; ultrapure B-free NH_4OH (2N) was obtained with the sub-boiled distillation of Ultrapure NH_4OH, adding mannitol to the starting solution to prevent B volatilisation.

The methodology used for the separation of B from the matrix provided a series of steps that are summarised below. The first step was to take enough previously filtered rainwater (see paragraph 3.1.2 "Laboratory pre-treatment of rainwater samples"). For a successful isotopic analysis, it is necessary to introduce in column a quantity of B equal to 800 - 1000 ng. Therefore, it was essential to know the concentration of B in the samples. The concentration of B was determined by analysis of the filtered and acidified samples, prepared according to the procedure described in paragraph 3.1.2 "Laboratory pre-treatment of rainwater samples", and analysed according to the methodology presented in section 3.2 "Chemical analysis". Speciation of B in aqueous fluids is highly dependent on pH conditions, and B in solution is found as a borate ion only at pH > 8 (*Tonarini et al., 1997*). For the methodology used was necessary to have B in this ionic form, therefore the samples were conditioned with 1 mL of NH_4OH (2N) for 100 mL of sample to raise the pH of the solution to a value ≥ 10. Six columns in Polytetrafluoroethylene (PTFE), with a volume of 2 mL, were prepared for the separation of B by anionic exchange. The columns were first washed with a 2% w/v HNO_3

(Merck Suprapur) solution, then rinsed with enough sub-boiled water, and left to dry under a laminar flow hood. Once dry the columns were placed on a clean Polymethylmethacrylate (PMMA) rack. The lower portion of each column was then filled with enough amount of an anionic resin "Amberlite® IRA743 free base". For this step, a pipette and SB water, previously spiked with NH_4OH (2N) to bring its pH to a value ≥ 8, were used. The columns and the resin have been washed with 3 mL of HCl (2N); this wash makes the environment inside the columns slightly acidic. To raise the pH, 2 mL of pH ≥ 8 SB water were then introduced. The resin was then conditioned with 1 mL of NH_4OH (2N) and then with 2 mL of pH ≥ 8 SB water. Then the samples were loaded into the columns. The sample passed through the anionic resin, which trapped the B in solution as a borate ion, thus separating it from the matrix. To ensure complete absorption of the borate ion by the resin, the samples released from the columns in the first step were recovered and loaded back into the columns. To ensure the removal of all other anions from the resin, the same was then washed again with 2 mL of pH ≥ 8 SB water, 1 mL of NH_4OH (2N), and finally 3 mL of pH ≥ 8 SB water. 15 mL centrifuge tubes, before being cleaned with HNO_3 (2N) and rinsed with plenty of SB water, were put under the columns. The elution of the borate ion was performed by washing each column with 5 mL of HNO_3 (2N). In this last step, it was essential not to miss even a drop of sample; the first drop released from the resin contained almost all the B. The resin first releases the isotope ^{11}B, then the isotope ^{10}B, therefore it was still necessary to recover all 5 mL of the solution.

The first steps of the methodology used for analysing the isotopic composition of Sr were the same as those illustrated for B. Once the necessary amount of filtered samples had been taken, they were evaporated. Polytetrafluoroethylene beakers were used to evaporate the samples, and they were washed according to the procedure illustrated below. After an initial rinse with SB water, successively 3 mL of HCl (6.60N), 3 mL of HNO_3 (2N), and 3 mL of SB water were placed inside each baker. Between each solution, the bakers were placed on a hot plate under a laminar hood for approximately 6 hours. After adequate drying on the hot plate, the bakers were ready to be used.

Evaporation of the samples was carried out on a hot plate, under a laminar hood, at a temperature between 60 °C and 95 °C. The precipitate from the evaporation was recovered with 2 mL of HNO_3 (2N), and this solution was centrifuged for 12 minutes. At this point, ten columns, before being cleaned with the same procedure used for the columns for B, were prepared for ion exchange chromatography. An "Eichhorn Strontium Resin" was placed inside each column, and they were conditioned with 1 mL of HNO_3 (2M). The samples were loaded into the columns. Sr was retained by the resin and the columns were cleaned with the following acid sequence: 1 mL of HNO_3 (2M), 3 mL of HNO_3 (7M), and 0.5 mL of HNO_3 (2M). 15 mL centrifuge tubes, previously cleaned with HNO_3 (2N) and rinsed with plenty of SB water, were put under the columns. The elution of the strontium ion was performed by washing each column with 3 mL of HNO_3 (0.05M).

3.5 Isotopic analysis

Isotopic analyses were performed in the laboratories of the "Istituto di Geoscienze e Georisorse" of the Italian National Research Council (IGG-CNR) in Pisa (Italy). A multi-collector mass spectrometer (Thermo Scientific Neptune Plus™ HR-MC-ICP-MS) was used for B and Sr isotopic ratios determination. An Argon flow rate of 100 μL $minute^{-1}$ was set for both element analyses. The appropriate detectors were positioned such that just the elemental ion of interest can enter the detector whereas the interfering ions were stopped on one side of the detector slit. To check that the signal peaks were "flat-top type", a "mass scan" and a "peak scan" were performed. The peaks were centred ("peak centre") and the mass corresponding to the centre of the peak was used for positioning the collectors. The appropriate positioning of collectors was performed by using four high-precision "stepper motors".

For B isotopic ratios analysis, Faraday cups H3-L3 were selected and coupled to an Amplifier 10^{13} Ω, to reach the maximum $\delta^{11}B/^{10}B$ stability. After B concentration measurements, all the samples were diluted to a B concentration of ≈ 25 μg L^{-1} and bracketed with 25 μg L^{-1} solution of

NIST NBS 951 boric acid standard, similar to the B concentration expected in the rainwater samples. NIST NBS 951 was made from an original lot of pure H_3BO_3 of more than 200 kg in 22 containers, which was free from impurities and largely homogeneous throughout the lot (except for one container) (*Coplen et al., 2002*) and has been chosen as the reference to which the B isotopic ratios should be reported ($\delta^{11}B_{nbs951}$ = 0‰). Therefore, the given delta notation ($\delta^{11}B$) represents the deviation (‰) from the NIST NBS 951 standard, with a certified $\delta^{11}B/^{10}B$ ratio of 4.0436255 ± 0.013 (2Ω).

The analytical procedure for B isotope analysis consisted of sample-reference bracketing, using NIST NBS 951, and an on-peak zero blank correction (*Guerrot et al., 2011*). A triplicate of analysis was done for each sample during the same analytical session. The result is given as an average delta value without further normalisation. Because of the large mass fractionation during MC-ICP-MS analyses of boron, the instrument was tuned before each analytical session for maximum stability rather than maximum intensity adjusting the sample gas flow following the procedure suggested by Foster (2008). A wash time of 250 s after each sample and reference analysis to overcome the well-known wash-out problem of boron (*Al-Ammar et al., 2000*). Boron isotopic ratio analyses were performed in three different rounds. In the first and third rounds H skimmer cones were used, and a low resolution was set. In the second round Jet sample cones were used, and a medium resolution was set. The Jet sample cones arrangement significantly enhanced the B signal sensitivities, compared to the standard cone arrangement (H skimmer cone + standard sample cone). With the H skimmer cones a signal of 65 mV was measured for the NIST NBS 951 Standard, while with the Jet sample cones, a signal of 210 mV was achieved. However, the use of Jet sample cones, and the consequent use of medium resolution, led to a lower stability of the sample gas flow rate. At non-optimum sample gas flow rates, the B isotopic ratios deviated from the reference value. Another problem that was considered when setting up the instrument was the “memory effect”. The “memory effect” is due to the tendency of boron to volatilise in the form of boric acid, which coats the walls of

the “spray chamber”, thus contaminating the next sample analysed. To reduce this effect an appropriate washing time before the introduction of each new sample was set. To estimate the error due to the “memory effect”, a blank solution was analysed. Very low signals were measured for the blank solution, 1.1 mV and 4.0 mV with the H skimmer cones and the Jet sample cones configurations, respectively. Several samples of another Standard solution were analysed, IAEA-B-1, which is a seawater sample from the Ligurian Sea, north of the island of Elba (Italy). It has a B concentration of 5 mg L^{-1} and an isotopic $\delta^{11}B$ ratio of +38.6‰ ± 1.66‰ (2Ω) (*Gonfantini et al., 2003*).

For Sr isotopic ratios analysis Faraday cups H3-L3 were selected and coupled to an Amplifier 10^{12} Ω for Sr mass and 10^{13} Ω for Kr and Rb masses. Strontium isotopic ratio analyses were performed in two different rounds. In the first, H skimmer cones were used, and a low resolution was set. In the second round Jet sample cones were used, and a medium resolution was set. As observed for B isotopic analysis, also for Sr the Jet sample cones arrangement significantly enhanced the Sr signal sensitivities, compared to the standard cone arrangement (H skimmer cone + standard sample cone). With the H skimmer cones a signal of 2.1 V was measured for the NIST NBS 987 Standard solution (100 μg L^{-1} of Sr), while with the Jet sample cones, a signal of 2.8 V was achieved. For Sr isotopic analysis a blank solution was analysed, measuring signals from less than 1.0 mV to 4.5 mV, equal to 0.048 μg L^{-1} – 0.216 μg L^{-1} of Sr, which were negligible concentrations for the analysed samples.

3.6 Quality control assurance

The detection limits, the analytical methods used, the accuracy and the precision values (R. S. D.) for each investigated element are shown in Table XX. The R. S. D. values are the averages of the calculated values, for each element, in each analysed sample. Accuracy is not indicated (n.d.) where it could not be calculated, as the element is absent in the Certified Reference Material (CRM) used.

Table 3 - Methods, Limit of Detection (LOD), Accuracy, and Relative Standard Deviation (R. S. D.) for each investigated element. For B and Sr isotopes, accuracy and precision are reported as absolute values.

Elements	Unit	Methods	LOD	Accuracy	R. S. D.
F^-	µeq L^{-1}	IC	0.30	± 0.5%	< 10%
Cl^-	µeq L^{-1}	IC	0.30	± 3.8%	< 3%
NO_3^-	µeq L^{-1}	IC	1.00	n.d.	< 3%
SO_4^{2-}	µeq L^{-1}	IC	1.00	± 2.3%	< 3%
HCO_3^-	µeq L^{-1}	Titration	8.00	n.d.	< 10%
Na^+	µeq L^{-1}	IC & ICP-OES	0.10 - 0.005	± 1.2%	< 2%
K^+	µeq L^{-1}	IC & ICP-OES	0.10 - 0.005	± 1.3%	< 2%
NH_4^+	µeq L^{-1}	IC	0.30	n.d.	< 2%
Mg^{2+}	µeq L^{-1}	IC & ICP-OES	0.10 - 0.10	± 3.3%	< 2%
Ca^{2+}	µeq L^{-1}	IC & ICP-OES	0.10 - 0.10	± 1.7%	< 2%
Li	µg L^{-1}	ICP-MS & ICP-OES	0.10 - 2.00	± 5.2%	4.1%
Be	µg L^{-1}	ICP-MS	0.05	< 10%	~ 5%
B	µg L^{-1}	ICP-MS & ICP-OES	0.10 - 0.50	± 12%	6.0%
Al	µg L^{-1}	ICP-MS & ICP-OES	0.10 - 10.0	± 5.6%	4.5%
Sc	ng L^{-1}	ICP-MS	0.20	± 1.8%	27%
Ti	µg L^{-1}	ICP-MS & ICP-OES	0.05 - 1.00	± 6.5%	4.1%
V	µg L^{-1}	ICP-MS & ICP-OES	0.05 - 0.90	± 0.5%	5.2%
Cr	µg L^{-1}	ICP-MS & ICP-OES	0.05 - 0.50	± 11%	4.4%
Mn	µg L^{-1}	ICP-MS & ICP-OES	0.05 - 0.10	± 4.4%	3.8%
Fe	µg L^{-1}	ICP-MS & ICP-OES	0.20 - 1.00	± 13%	3.4%
Co	µg L^{-1}	ICP-MS & ICP-OES	0.02 - 0.60	± 5.6%	10%
Ni	µg L^{-1}	ICP-MS & ICP-OES	0.03 - 0.60	± 14%	5.1%
Cu	µg L^{-1}	ICP-MS & ICP-OES	0.03 - 1.00	± 8.2%	3.7%
Zn	µg L^{-1}	ICP-MS & ICP-OES	0.10 - 1.00	± 15%	3.3%
Ge	ng L^{-1}	ICP-MS	0.30	n.d.	29%
As	µg L^{-1}	ICP-MS & ICP-OES	0.02 - 3.00	± 19%	23%
Se	µg L^{-1}	ICP-MS	0.02	10 - 15%	12%
Br	µg L^{-1}	ICP-MS	0.10	< 10%	14%
Rb	µg L^{-1}	ICP-MS	0.02	< 10%	15%
Sr	µg L^{-1}	ICP-MS & ICP-OES	0.02 - 0.02	± 10%	5.4%
Y	ng L^{-1}	ICP-MS	1.00	± 4.9%	6.6%
Zr	ng L^{-1}	ICP-MS	5.00	n.d.	5.1%
Nb	ng L^{-1}	ICP-MS	0.10	n.d.	15%
Mo	µg L^{-1}	ICP-MS & ICP-OES	0.02 - 0.70	± 6.2%	19%
Cd	µg L^{-1}	ICP-MS	0.01	< 10%	4.6%
Sn	µg L^{-1}	ICP-MS	0.01	< 10%	5.0%
Sb	µg L^{-1}	ICP-MS	0.01	< 10%	8.1%
Te	ng L^{-1}	ICP-MS	1.00	± 14%	21%
Cs	µg L^{-1}	ICP-MS	0.001	< 10%	2.8%
Ba	µg L^{-1}	ICP-MS & ICP-OES	0.05 - 0.05	± 1.4%	3.5%
La	ng L^{-1}	ICP-MS	0.50	± 0.8%	5.2%
Ce	ng L^{-1}	ICP-MS	0.50	± 3.4%	7.2%
Pr	ng L^{-1}	ICP-MS	0.50	± 6.5%	12%
Nd	ng L^{-1}	ICP-MS	0.50	± 2.9%	13%
Sm	ng L^{-1}	ICP-MS	0.50	± 1.5%	17%
Eu	ng L^{-1}	ICP-MS	0.50	± 8.1%	21%
Gd	ng L^{-1}	ICP-MS	0.50	± 0.2%	14%
Tb	ng L^{-1}	ICP-MS	0.50	± 5.4%	20%
Dy	ng L^{-1}	ICP-MS	0.50	± 0.7%	11%
Ho	ng L^{-1}	ICP-MS	0.50	± 3.6%	24%
Er	ng L^{-1}	ICP-MS	0.50	± 2.0%	13%
Tm	ng L^{-1}	ICP-MS	0.50	± 0.1%	14%
Yb	ng L^{-1}	ICP-MS	0.50	± 5.3%	11%
Lu	ng L^{-1}	ICP-MS	0.50	± 40%	18%
Hf	ng L^{-1}	ICP-MS	0.10	n.d.	20%
Tl	µg L^{-1}	ICP-MS	0.003	< 10%	3.6%
Pb	µg L^{-1}	ICP-MS & ICP-OES	0.05 - 4.00	± 8.3%	6.8%
Bi	µg L^{-1}	ICP-MS	0.003	10 - 15%	1.2%
Th	ng L^{-1}	ICP-MS	0.10	± 0.7%	21%
U	µg L^{-1}	ICP-MS	0.001	< 10%	7.8%
$\delta^{11}B$	‰	HR-MC-ICP-MS	/	0.11‰	± 0.14‰
$^{87}Sr/^{86}Sr$	/	HR-MC-ICP-MS	/	0.000043	± 0.000008

Different blank solutions were prepared and analysed to control the quality of sampling and analytical procedures. Every chemical reagent used and every sampling and laboratory material that comes into contact with the sample can modify the concentration of the elements in the sample.

Regarding the concentration of minor and trace elements in rainwater, three different blank solutions were prepared:

- Rain method-blank I (R I), an aliquot of 50 mL of filtered (0.45 μm) deionised water (MilliQ), stored in a previously cleaned 50 mL centrifuge tube and then acidified with 200 μL of 65% w/v HNO_3 (Merck Suprapur).
- Rain method-blank II (R II), 300 mL of deionised water was poured onto the previously cleaned bulk collector and 50 mL of this solution, previously filtered (0.45 μm) was stored in a previously cleaned 50 mL centrifuge tube and then acidified with 200 μL of 65% w/v HNO_3 (Merck Suprapur).
- Rain method-blank III (R III), 150 mL of deionised water and 150 mL of 2% w/v HNO_3 (Merck Suprapur) solution were poured into the filtration system with a previously installed 0.45 μm membrane filter, and 50 mL of this solution was stored into a previously cleaned 50 mL centrifuge tube.

Regarding the concentration of minor and trace elements in the insoluble fraction, four different blank solutions were prepared:

- Membrane method-blank I (MI), 7 mL solution of deionised water (MilliQ), placed into a previously cleaned vessel, mineralised as a sample, and finally increased to a volume of 20 mL using sufficient MilliQ.
- Membrane method-blank II (M II), 4 mL of ultrapure 67% w/v HNO_3 (4 mL), plus 3 mL of ultrapure H_2O_2 (3 mL), mineralised as a sample, and finally increased to a volume of 20 mL using sufficient MilliQ.
- Membrane method-blank III (M III), mineralisation of blank membrane filters from

different manufacturers.

- Membrane method-blank IV (M IV), mineralisation of the membrane filters used for the preparation of the blank solutions R III.

Concerning the concentration of the Technology-Critical Elements, a blank solution was prepared by performing the entire procedure, using a deionised water solution (MilliQ), as a rainwater sample. The blank solution was analysed only for some of the TCEs (Y, La, Ce, Pr, Nd, Sm, Eu, Gd, Tb, Dy, Ho, Er, Tm, Yb, and Lu).

As regards the isotopic composition of Sr and B in the rainwater samples, using international standard solutions of known concentration and isotopic composition (NIST NBS 951 and IAEA B1 for B, and NIST SRM 987 for Sr), different standard solutions were prepared by performing the entire procedures described for the rainwater samples.

For the NIST NBS 951 and the IAEA B1, standard solutions with a boron concentration of 25 μg L^{-1} were prepared. The accuracy of the measurement was monitored by twenty-seven replicate analyses of shelf NIST NBS 951 gave an average $\delta^{11}B$ of − 0.04‰ ± 0.12‰ (2σ), fifty-six replicate analyses of NIST NBS 951, after full chemistry, gave an average $\delta^{11}B$ of + 0.64‰, and fifteen replicate analyses of the IAEA standard B1 (seawater), which gave an average $\delta^{11}B$ of + 39.76‰ ± 0.13‰ (2σ). Within run errors on individual runs (n = 3) were in the order of 0.1 ± 0.2‰ (2σ). For the NIST NBS 987 Standard, solutions diluted to Sr concentrations of 65 μg L^{-1} and 100 μg L^{-1}, similar to the Sr concentration expected in the rainwater samples, were prepared and analysed. NIST SRM 987 is recommended for radiogenic and stable strontium-isotope studies as the zero-delta reference (*Moore et al., 1982*; *Walder & Freedman, 1992*). NIST NBS 987 Standard solution was analysed eleven times. An average value of $^{87}Sr/^{86}Sr$ = 0.710291 ± 0.000008 (2σ; n = 11) was measured. Measured values were adjusted at 0.710248, which is the $^{87}Sr/^{86}Sr$ isotopic ratio of the NIST SRM 987 (*McArthur et al., 2000*).

3.6.1 Blank solutions

The main descriptive statistical parameters (minimum, median, maximum, and standard deviation) for each blank solution, prepared as described before, are shown in the following tables (Tab. 4, 5, and 6) and figures (Fig. 7, 8, and 9). For each blank solution, the number of samples analysed is reported, as well as the number of samples in which the element concentration was below the quantification limit (< LOQ). The results for each sample analysed can be found in Supplementary materials (Tab. S.8).

As regards the rainwater blank solutions, great variability was observed for all the analysed elements, both considering the same type of blank solution and between different solutions. In all the analysed solutions, the concentrations for Ni, Se, Mo, Cd, Sb, Cs, and Tl were usually below the limit of quantification (Tab. 4). In the blank solution R I the highest median concentrations for Mo and Sb were measured, while for V, Cr, Mn, Ni, Br, Rb, and Sr the highest median concentrations were measured in the R II blank solution. Equal median concentrations of Co were measured in the blank solutions R I and R II. For the other elements, i.e., Li, B, Al, Ti, Fe, Cu, Zn, As, Se, Cd, Ba, Pb, and U the highest median concentrations were measured in the R III blank solution. For Cs and Tl equal median values were measured in R I and R III blank solutions. Finally, the concentrations of Sn were determined only in the R III solution (Fig. 7).

Table 4 - Main statistical parameters for minor and trace element concentrations in the blank solutions R I, R II, and R III. All values are expressed as µg L^{-1}.

	R I (n = 9)				R II (n = 4)				R III (n = 10)			
	Min.	Median	Max.	Dev. Std.	Min.	Median	Max.	Dev. Std.	Min.	Median	Max.	Dev. Std.
Li	<LOQ (7)	0.005	0.0500	0.0169	0.0130	0.0220	0.0440	0.0147	<LOQ (4)	0.00800	0.0340	0.0100
B	<LOQ (6)	0.0500	1.40	0.442	0.396	1.03	2.19	0.883	<LOQ (5)	0.106	35.0	12.9
Al	<LOQ (1)	0.986	3.19	1.09	1.31	8.89	10.5	4.29	0.4010	13.1	43.9	18.4
Ti	<LOQ (6)	0.00500	0.228	0.0733	0.0580	0.163	0.249	0.0823	0.0310	0.103	0.810	0.273
V	<LOQ (1)	0.0110	0.0970	0.0327	<LOQ (1)	0.0205	0.100	0.0442	<LOQ (4)	0.00900	0.0330	0.0100
Cr	<LOQ (1)	0.0400	1.49	0.625	0.055	0.0990	0.170	0.0577	0.0100	0.0455	0.289	0.100
Mn	0.0146	0.222	0.698	0.224	0.148	0.259	0.855	0.333	0.0240	0.0710	0.267	0.085
Fe	0.05	0.293	3.50	1.47	2.96	5.00	10.0	3.22	0.0100	2.63	22.0	7.13
Co	0.00200	0.0150	0.0260	0.00659	<LOQ (1)	0.0150	0.0420	0.0181	<LOQ (6)	0.00500	0.0260	0.00705
Ni	<LOQ (2)	0.0495	3.79	1.55	<LOQ (1)	0.155	0.365	0.146	<LOQ (4)	0.0355	0.495	0.148
Cu	<LOQ (2)	0.175	0.663	0.211	<LOQ (2)	0.905	8.44	4.00	<LOQ (2)	1.80	14.7	5.10
Zn	<LOQ (1)	2.36	17.8	5.63	0.849	4.39	17.6	7.60	<LOQ (1)	4.88	10.7	3.78
As	0.00400	0.00796	0.0241	0.00742	0.005	0.00700	0.00700	0.00100	<LOQ (5)	0.00650	0.0310	0.00831
Se	<LOQ (2)	0.0694	0.217	0.0819	<LOQ (4)	n.d.	n.d.	n.d.	<LOQ (4)	0.0780	0.201	0.0670
Br	<LOQ (2)	0.160	1.28	0.525	8.68	14.6	27.7	8.37	<LOQ (10)	n.d.	n.d.	n.d.
Rb	<LOQ (4)	0.00700	0.0259	0.00757	0.0230	0.0390	0.0640	0.0214	<LOQ (6)	0.00500	0.0300	0.00781
Sr	<LOQ (1)	0.0973	2.71	1.05	0.0840	0.726	1.40	0.622	<LOQ (1)	0.424	0.962	0.285
Mo	<LOQ (3)	0.0931	0.353	0.140	<LOQ (3)	0.00500	0.0150	0.00500	<LOQ (9)	0.00500	0.00500	n.d.
Cd	<LOQ (5)	0.00100	0.0118	0.00445	<LOQ (3)	0.00100	0.0170	0.00800	<LOQ (4)	0.00400	0.0210	0.00686
Sn	n.d.	n.d.	n.d.	n.d.	n.d.	n.d.	n.d.	n.d.	<LOQ (9)	0.00500	0.0160	0.00348
Sb	<LOQ (1)	0.00964	0.0217	0.00641	<LOQ (2)	0.00550	0.00900	0.00189	<LOQ (8)	0.00500	0.00900	0.00149
Cs	<LOQ (3)	0.00100	0.00319	0.00102	<LOQ (4)	n.d.	n.d.	n.d.	<LOQ (8)	0.000500	0.00200	0.000632
Ba	0.06	0.452	3.47	1.36	0.177	0.620	0.900	0.365	0.0480	0.454	3.09	0.896
Tl	<LOQ (5)	0.00150	0.0160	0.00510	<LOQ (4)	n.d.	n.d.	n.d.	<LOQ (10)	n.d.	n.d.	n.d.
Pb	0.005	0.0110	0.0554	0.0152	0.0120	0.0665	0.296	0.127	0.0110	0.247	0.854	0.295
U	<LOQ (5)	0.000500	0.00596	0.00181	0.00100	0.00150	0.00200	0.000577	<LOQ (4)	0.00200	0.00800	0.00272

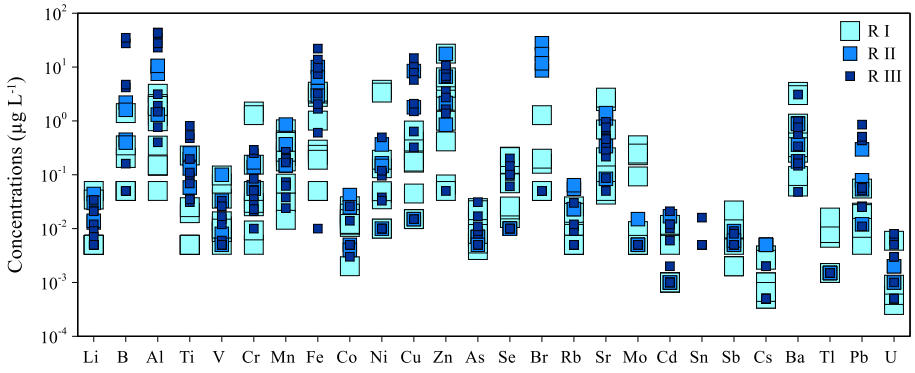

Figure 7 - Minor and trace element concentrations (µg L^{-1}) in the blank solutions R I, R II, and R III.

As regards the membrane filter blank solutions, great variability was observed for all the analysed elements, both considering the same type of blank solution and between different solutions. In all the analysed solutions, the concentrations for Li, B, and Tl were usually below the limit of quantification. Thallium and boron equal median concentrations were measured in M I and M IV

solutions, while they were not determined in M II and M III solutions. In the blank solution M II were measured the highest median concentrations for Li and As. The highest median concentration for Mo was measured in the blank solution M III. The highest median concentrations for the other analysed elements were measured in the M IV blank solution (Tab. 5 and Fig. 8).

Table 5 - Main statistical parameters for minor and trace element concentrations in the blank solutions M I, M II, M III, and M IV. All values are expressed as µg L^{-1}.

	M I (n = 3)				M II (n = 4)				M III (n = 7)				M IV (n = 24)			
	Min.	Median	Max.	Dev. Std.	Min.	Median	Max.	Dev. Std.	Min.	Median	Max.	Dev. Std.	Min.	Median	Max.	Dev. Std.
Li	<LOQ (2)	0.00500	0.398	0.227	<LOQ (2)	0.114	0.340	0.167	<LOQ (4)	0.00500	0.701	0.00500	<LOQ (15)	0.00500	1.15	0.336
B	<LOQ (2)	0.0500	1.87	1.05	<LOQ (4)	n.d.	n.d.	n.d.	<LOQ (7)	n.d.	n.d.	n.d.	<LOQ (18	0.0500	163	35.5
Al	4.91	32.0	87.0	41.8	11.9	46.9	178	75.8	30.6	62.8	131	30.6	35.3	224	1697	411
Ti	0.258	1.87	2.40	1.12	0.631	12.2	74.7	33.7	0.544	2.82	7.72	0.544	1.14	30.5	231	57.6
V	0.0640	0.335	0.361	0.164	0.140	0.430	0.936	0.335	0.232	0.247	0.491	0.232	0.199	0.659	3.60	0.852
Cr	0.206	0.213	0.260	0.0295	0.150	0.818	2.23	0.877	1.44	2.76	22.3	1.44	2.28	4.22	27.9	7.79
Mn	0.0730	0.176	2.30	1.26	0.173	0.670	2.87	1.26	0.144	0.669	3.25	0.144	0.443	2.98	17.5	3.78
Fe	1.98	5.30	355	203	25.9	90.2	179	71.3	24.2	33.8	75.2	24.2	32.3	218	1140	300
Co	<LOQ (1)	0.0170	0.791	0.450	<LOQ (3)	0.00500	0.0448	0.0199	0.0363	0.0645	0.503	0.0363	<LOQ (8)	0.0897	0.988	0.238
Ni	0.343	0.622	1.54	0.627	<LOQ (1)	0.555	3.92	1.84	0.956	1.58	2.63	0.956	<LOQ (2)	3.10	7.33	1.88
Cu	<LOQ (1)	0.338	0.686	0.336	0.0490	1.13	2.98	1.22	<LOQ (2)	0.478	2.48	0.0150	0.511	2.90	18.2	3.59
Zn	5.20	8.92	10.9	2.89	1.90	5.27	8.30	2.62	19.5	26.9	138	19.5	6.90	69.3	196	50.7
As	0.00500	0.0670	0.941	0.524	<LOQ (1)	0.102	1.51	0.724	0.0182	0.0677	0.136	0.0182	<LOQ (8)	0.0186	0.465	0.147
Sr	0.179	2.53	3.50	1.71	0.416	1.45	4.55	1.92	1.23	2.44	13.6	1.23	0.964	4.67	12.7	3.06
Mo	<LOQ (1)	0.213	1.50	0.808	<LOQ (2)	0.148	0.295	0.166	0.301	0.634	1.35	0.301	<LOQ (2)	0.285	1.71	0.402
Ba	<LOQ (2)	0.000500	0.00100	0.000289	<LOQ (3)	0.00050	0.00100	0.000250	0.00100	0.00100	0.00700	0.00100	<LOQ (8)	0.00450	0.111	0.0249
Pb	<LOQ (2)	0.00150	0.0100	0.00491	<LOQ (4)	n.d.	n.d.	n.d.	<LOQ (7)	n.d.	n.d.	n.d.	<LOQ (18)	0.00150	0.0130	0.00335

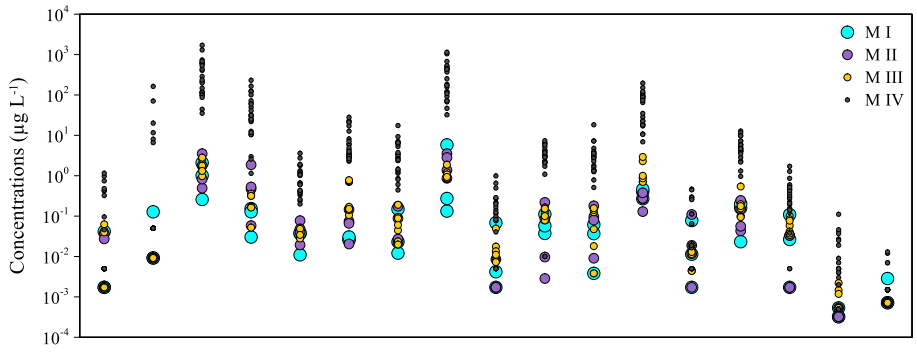

Figure 8 - Minor and trace element concentrations (µg L^{-1}) in the blank solutions M I, M II, M III, and M IV.

As regards the Technology-Critical Elements, it was possible to quantify the concentrations only for Y and the lanthanoids. The highest median concentrations were measured for La, Ce, Y, Nd, and Sm, up to one order of magnitude higher than the median concentrations measured for the other elements (Tab. 6 and Fig. 9).

Table 6 - Main statistical parameters for some TCE concentrations in the blank solutions. All values are expressed as ng L^{-1}.

	TCEs Blank (n = 3)			
	Min.	Median	Max.	Dev. Std.
Sc	n.d.	n.d.	n.d.	n.d.
Ge	n.d.	n.d.	n.d.	n.d.
Y	0.246	0.347	0.419	0.0869
Zr	n.d.	n.d.	n.d.	n.d.
Te	n.d.	n.d.	n.d.	n.d.
Hf	n.d.	n.d.	n.d.	n.d.
Th	n.d.	n.d.	n.d.	n.d.
La	0.349	0.551	0.561	0.120
Ce	0.183	0.495	0.795	0.306
Pr	0.0430	0.0470	0.108	0.0364
Nd	0.106	0.296	0.368	0.135
Sm	0.131	0.236	0.288	0.0800
Eu	0.00300	0.00707	0.0160	0.00665
Gd	0.0230	0.0320	0.0340	0.00586
Tb	0.0150	0.0260	0.0290	0.00737
Dy	0.0707	0.0707	0.0707	0.0000
Ho	0.00800	0.0180	0.0230	0.00764
Er	0.0530	0.0860	0.123	0.0350
Tm	0.0200	0.0210	0.0220	0.00100
Yb	0.0970	0.0990	0.181	0.0479
Lu	0.0220	0.0280	0.0290	0.00379

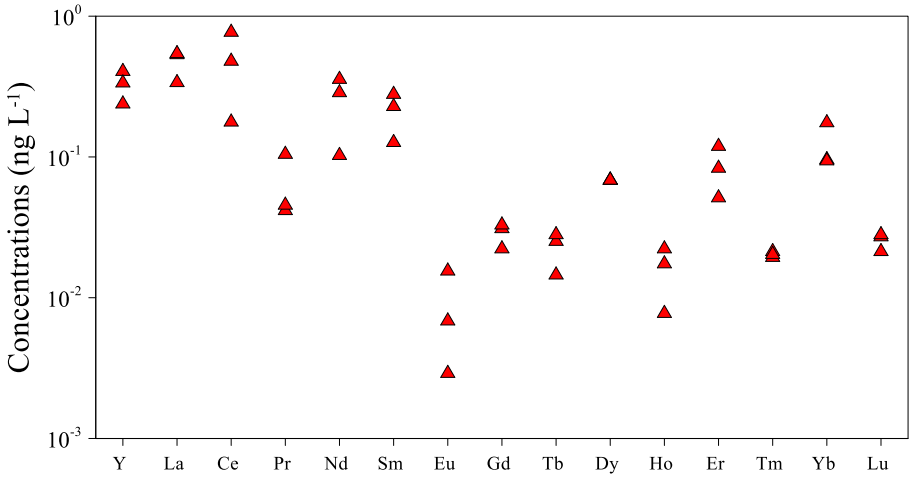

Figure 9 - Technology-Critical Elements concentrations (ng L^{-1}) in the blank solutions.

3.7 Statistical elaborations of the results

The annual volume-weighted mean (VWM) concentration values for major ions, minor and trace elements, and Technology-Critical Elements, were calculated by using the following equation:

$$\text{VWM}=\frac{\sum_{i=1}^{n} CiPi}{\sum_{i=1}^{n} Pi} \quad (2),$$

where C*i* represents the concentration of the specific component in the ^{i}th sample, P*i* is the rainfall depth (L m^{-2}) during the *i*th sampling period and *n* is the total number of rainfall events (*Keresztesi et al., 2020*). This parameter was used to reduce the potential effect of different precipitation amounts on each ion and each element concentration.

For the comparison with the rainwater samples, the concentrations of minor and trace elements measured in the insoluble fraction solutions were normalised with respect to the volume of filtered rain.

According to the electroneutrality principle, the sum of positive and negative charges within the water sample should be zero. The acceptable range of ion difference in rainwater samples is 10% or ± 200 µeq L^{-1} (*Alastuey et al., 1999; Chandra et al., 2005; Laouali et al., 2012*). The charge balance error of each sample was calculated according to the equation:

$$\text{B. C. (\%)} = \{((\frac{\sum anions}{\sum cations}) - 1) \times 100\} \quad (3).$$

To estimate the contribution of the marine source and anthropogenic sources toward the different major ionic species, the non-sea-salt fractions ((X)nss) were calculated by the following equation:

$$(\text{X})\text{nss} = (\text{X})\text{rain} - ((\text{Na}^{+})\text{rain} \times \left[\frac{X}{Na^{+}}\right] SW \quad (4),$$

where (X)rain is the concentration of species X in rainwater, and (X)nss is the non-sea salt contribution of species X in meq L^{-1} (*Loye-Pilot & Martin, 1996*). The use of the previous equation assumes that all the sodium in rainwater comes from the sea and that no chemical fractionation

occurs between chloride and the other ions after sea salt injection into the atmosphere (*D'Alessandro et al., 2013*).

The neutralisation factors (NFx) of the different chemical components of interest were estimated using the equation suggested by Possanzini et al. 1988:

$$NFx = \frac{[X]}{[nss{-}SO_4^{2-} + NO_3^-]} \quad (5),$$

where [X] denotes the chemical component of interest, i.e., nss-Ca^{2+}, nss-Mg^{2+}, NH_4^+, etc.

The equilibrium between acidity and alkalinity was evaluated using NP/AP, calculated as:

$$\frac{NP}{AP} = \frac{nss{-}Ca^{2+} + NH_4^+}{nss{-}SO_4^{2+} + NO_3^-} \quad (6).$$

Through the measured concentrations of each element, it is possible to calculate the deposition rates by using the following relation:

$$\Phi x = \frac{C_x \, x \, P}{T} \quad (7),$$

where Cx is the concentration of each element "x" in rain, expressed as μeq L^{-1} for major ions, μg L^{-1} for minor and trace elements, ng L^{-1} for the Technology-Critical Elements; P is the amount of precipitation (L m^{-2}), and T is the exposition time of the collectors (d).

Relationships between each major ion, minor and trace elements, and each Technology-Critical Element were investigated using Pearson's correlation coefficients and Principal Component Analysis (PCA). For each constituent, when the concentrations were below the detection limit, values equal to the detection limits divided by a factor 2 were considered. A Varimax rotation to a set of orthogonal axes was selected. Varimax rotation was applied because orthogonal rotation minimizes the number of variables with high loading on each component and facilitates the interpretation of results. The purpose of the analysis is to obtain a small number of factors which account for most of the variability in the variables set. The KMO (Kaiser-Meyer-Olkin) test was used to test the applicability of Principal Component Analysis to the dataset of this research.

To investigate the sources of major ions and trace elements in the bulk atmospheric deposition, a Positive Matrix Factorisation (PFM) model was applied. The PMF model is a mathematical factor-based receptor model that interprets source types with a robust uncertainty estimate. PMF can be solved with the Multilinear Engine (ME-2) developed by Paatero (1999) and implemented in version 5 of US EPA PMF (*Khan et al., 2016*; *Ye et al., 2018; Amato et al., 2024*). In this study, the US EPA PMF v5 was applied to determine the source apportionment of dry and wet deposition of major ions. This statistical methodology must be used with caution because the selection of tracers for each source is crucial for the final source apportionment outputs, not only in terms of number of sources identified but also, consequently, in the source contributions estimates (*Amato et al., 2024*). The input data included concentrations of chemical species and equation-based uncertainties. The equation-based uncertainty includes detection limits and error fractions (10%). If the concentration was less than or equal to the detection limit (LOD) provided, the uncertainty (Unc) was calculated using a fixed fraction of the LOD (8):

$$\text{Unc} = \frac{5}{6} X\ LOD \quad (8).$$

If the concentration was greater than the LOD provided, the uncertainty was calculated using Equation (9):

$$\text{Unc} = \sqrt{(Error\ Fraction\ x\ concentration)^2 + (0.5\ X\ LOD)^2} \quad (9).$$

3.7.1 Charge balance

The concentration of the total cation was slightly higher than that of the total anion for all the investigated areas (Fig. 10). The charge balances, calculated with equation (3), showed that 41% of the analysed rainwater samples fall within the acceptable range (± 200 μeq L^{-1}) for dilute waters. The anionic species, such as CH_3COO^-, $HCOO^-$, $C_2O_4^{2-}$, and PO_4^{3-}, contributed by the organic components (e.g., plant and soil released oxalate) was a possible explanation for the relatively lower total anion concentration (*Chandra et al., 2005*).

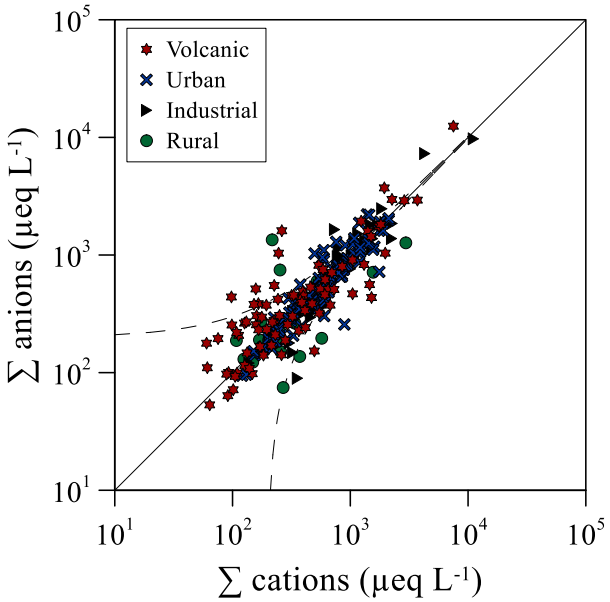

Figura 10 - Charge balance of anions and cations (µeq L^{-1}). The continuous line is the ratio 1:1 between anions and cations. The two dotted curves delimited the area with a difference between ∑ cations and ∑ anions of 200 µeq L^{-1}.

3.8 References

Aas, W., Alleman, L. Y., Bieber, E., Gladtke, D., Houdret, J. L., Karlsson, V., Monies, C. (2009). Comparison of methods for measuring atmospheric deposition of arsenic, cadmium, nickel and lead. J. Environ. Monitor., 11, pp. 1276–1283. https://doi.org/10.1039/B822330K.

Aiuppa, A., Bonfanti, P., Brusca, L., D'Alessandro, W., Federico, C., Parello, F. (2001). Evaluation of the environmental impact of volcanic emissions from the chemistry of rainwater: Mt. Etna area (Sicily). Appl. Geochem., 16(7-8), pp. 985-1000. https://doi.org/10.1016/S0883-2927(00)00075-5.

Aiuppa A., Bellomo S., Brusca L., D'Alessandro W. Di Paola R., Longo M., (2006). Major-ion bulk deposition around an active volcano (Mt. Etna, Italy). Bull. Volcanol., 68, pp. 255-265. https://doi.org/10.1007/s00445-005-0005-x.

Al-Ammar, A., Reitznerová, E., Barnes, R. M. (2000). Improving boron isotope ratio measurement precision with quadrupole inductively coupled plasma-mass spectrometry. Spectrochim. Acta Part B: At. Spectros. 55, 1861–1867. https://doi.org/10.1016/S0584-8547(00)00282-2.

Alastuey, A., Querol, X., Chaves, A., Ruiz, C. R., Carratala, A., Lopez-Soler, A. (1999). Bulk deposition in a rural area located around a large coal-fired power station, northeast Spain. Environ. Pollut., 106(3), pp. 359-367. https://doi.org/10.1016/S0269-7491(99)00103-7.

Amato, F., van Drooge, B. L., Jaffrezo, J. L., Favez, O., Colombi, C., Cuccia, E., Reche, C., Ippolito, F., Ridolfo, S., Lara, R., Uzu, G., Ngoc, T. V. D., Dominutti, P., Darfeuil, S., Albinet, A., Srivastava, D., Karanasiou, A., Lanzani, G., Alastuey, A., Querol, X. (2024) Aerosol source apportionment uncertainty linked to the choice of input chemical components. Environ Int., 12, 184, 108441. https://doi: 10.1016/j.envint.2024.108441.

Amodio, M., Catino, S., Dambruoso, P. R., De Gennaro, G., Di Gilio, A., Giungato, P., Laiola, E., Marzocca, A., Mazzone, A., Sardaro, A., Tutino, M. (2014). Atmospheric deposition:

Sampling procedures, analytical methods, and main recent findings from the scientific literature. In Advances in Meteorology. https://doi.org/10.1155/2014/161730.

Arslan, Z., Oymak T., White J. (2018). Triethylamine-assisted $Mg(OH)_2$ coprecipitation/preconcentration for determination of trace metals and rare earth elements in seawater by inductively coupled plasma mass spectrometry (ICP-MS). Anal. Chim. Acta., 1008, pp. 18-28. https://doi.org/10.1016/j.aca.2018.01.017.

Bellomo, S., Aiuppa, A., D'Alessandro, W., Parello, F. (2007). Environmental impact of magmatic fluorine emission in the Mt. Etna area. J. Volcanol. Geotherm. Res., 165(1-2), pp. 87-101. https://doi.org/10.1016/j.jvolgeores.2007.04.013.

Brugnone, F., D'Alessandro, W., Calabrese, S., Li Vigni, L., Bellomo, S., Brusca, L., Prano, V., Saiano, F., Parello, F. (2020). A Christmas gift: Signature of the 24th December 2018 eruption of Mt. Etna on the chemical composition of bulk deposition in eastern Sicily. Italian Journal of Geosciences, 139, pp. 341-358. https://doi.org/10.3301/IJG.2020.08.

Brugnone, F., D'Alessandro, W., Parello, F., Liotta, M., Bellomo, S., Prano, V., Li Vigni, L., Sprovieri, M., Calabrese, S. (2023a). Atmospheric Deposition around the Industrial Areas of Milazzo and Priolo Gargallo (Sicily–Italy)-Part A: Major Ions. Int. J. Environ. Res. Public Health, 20(5), 3898. https://doi.org/10.3390/ijerph20053898.

Brugnone, F., D'Alessandro, W., Parello, F., Brusca, L., Saiano, F., Li Vigni, L., Sprovieri, M., Calabrese, S. (2023b). Atmospheric Deposition around the Industrial Areas of Milazzo and Priolo Gargallo (Sicily–Italy)—Part B: Trace Elements. Atmosphere, 14, 737. https://doi.org/10.3390/atmos14040737.

Calabrese, S., Aiuppa, A., Allard, P., Bagnato, E., Bellomo, S., Brusca, L., Parello, F. (2011). Atmospheric sources and sinks of volcanogenic elements in a basaltic volcano (Etna, Italy). Geochim. Cosmochim. Acta, 75(23), pp. 7401–7425. https://doi.org/10.1016/j.gca.2011.09.040.

Chandra Mouli, P., Venkata Mohan, S., & Reddy, S. J. (2005). Rainwater chemistry at a regional representative urban site: Influence of terrestrial sources on ionic composition. Atmos. Environ., 39(6). https://doi.org/10.1016/j.atmosenv.2004.10.036.

Coplen, T. B., Böhlke, J. K., De Bièvre, P., Ding, T., Holden, N. E., Hopple, J. A., Krouse, H. R., Lamberty, A., Peiser, H. S., Révész, K., Rieder, S. E., Rosman, K. J. R., Roth, E., Taylor, P. D. P., Vocke, R. D. JR., Xiao J. K. (2002). Isotope-Abundance variations of selected elements (IUPAC Technical Report). Pure Appl. Chem., 74(10), pp. 1987–2017.

D'Alessandro, W., Katsanou, K., Lambrakis, N., Bellomo, S., Brusca, L., Liotta, M. (2013). Chemical and isotopic characterisation of bulk deposition in the Louros basin (Epirus, Greece). Atmos. Res., 132–133, pp. 399–410. https://doi.org/10.1016/j.atmosres.2013.07.007.

Dammgen, U., Erisman, J. W., Cape, J. N., Grunhage, L., Fowler, D. (2005). Practical considerations for addressing uncertainties in monitoring bulk deposition. Environ. Pollut., 134(3), pp. 535–548. https://doi.org/10.1016/j.envpol.2004.08.013.

EMEP/CCC. Manual for Sampling and Chemical Analysis. EMEP Cooperative Program for Monitoring and Heavy Metals and POP Measurements 2009; EMEP/CCC: 2009; NILU: Oslo, Norway, 2009.

EN 7888:1985. Water quality – Determination of electrical conductivity.

EN 15841:2009. Ambient air quality - Standard method for determination of arsenic, cadmium, lead and nickel in atmospheric deposition.

Gonfiantini, R., Tonarini, S., Gröning, M., Adorni-Braccesi, A., Al-Ammar, A.S., Astner, M., Bächler, S., Barnes, R.M., Bassett, R.L., Cocherie, A., Deyhle, A., Dini, A., Ferrara, G., Gaillardet, J., Grimm, J., Guerrot, C., Krähenbühl, U., Layne, G., Lemarchand, D., Meixner, A., Northington, D.J., Pennisi, M., Reitznerová, E., Rodushkin, I., Sugiura, N., Surberg, R.,

Tonn, S., Wiedenbeck, M., Wunderli, S., Xiao, Y. and Zack, T. (2003). Intercomparison of Boron Isotope and Concentration Measurements. Part II: Evaluation of Results. Geostandards Newsletter, 27: 41-57. https://doi.org/10.1111/j.1751-908X.2003.tb00711.x.

Guerrot, C., Millot, R., Robert, M., Négrel, P. (2011). Accurate and high-precision determination of boron isotopic ratios at low concentrations by MC-ICP-MS (Neptune). Geostandards and Geoanalytical Research, 35(2), pp. 275-284. https://doi.org/10.1111/j.1751-908X.2010.00073.x.

Harmens, H., Mills, G., Hayes, F., Williams, P. ICP Vegetation Annual Report–2003/2004. ICP Vegetation 2004. Available online: https://icpvegetation.ceh.ac.uk/icp-vegetation-annual-report-20032004 (accessed on 13 December 2022).

Keeler, G. J., Landis, M. S., Norris, G. A., Christianson, E. M., Dvonch, J. T. (2006). Sources of mercury wet deposition in eastern Ohio, USA. Environ. Sci. Technol., 40, pp. 5874-5881. https://doi.org/10.1021/es060377q.

Keresztesi, Á., Nita, I. A., Réka, K., Birsan, M. V., Bodor, Z. Robert, S. (2020). Spatial and long-term analysis of rainwater chemistry over the conterminous United States. Environ. Res., 188, 109872. https://doi.org/10.1016/j.envres.2020.109872.

Khan, M. F., Latif, M. T., Saw, W. H., Amil, N., Nadzir, M. S. M., Sahani, M., Tahir, N. M., and Chung, J. X. (2016). Fine particulate matter in the tropical environment: monsoonal effects, source apportionment, and health risk assessment, Atmos. Chem. Phys., 16, pp. 597–617. https://doi.org/10.5194/acp-16-597-2016, 2016.

Laouali, D., Galy-Lacaux, C., Diop, B., Delon, C., Orange, D., Lacaux, J. P., Akpo, A., Lavenu, F., Gardrat, E., Castera, P. (2012). Long term monitoring of the chemical composition of precipitation and wet deposition fluxes over three Sahelian savannas. Atmos. Environ., 50, pp. 314–327. https://doi.org/10.1016/j.atmosenv.2011.12.004.

Liotta, M., Brusca, L. Grassa, F., Inguaggiato, S., Longo, M., Madonia, P. (2006). Geochemistry of rainfall at Stromboli volcano (Aeolian Islands): Isotopic composition and plume-rain interaction. Geochem. Geophys. Geosyst., 7, Q07006, https://doi.org/10.1029/2006GC001288.

Liotta, M., Shamavu, P., Scaglione, S., D'Alessandro, W., Bobrowski, N., Bruno Giuffrida, G., Tedesco, D., Calabrese, S. (2017). Mobility of plume-derived volcanogenic elements in meteoric water at Nyiragongo volcano (Congo) inferred from the chemical composition of single rainfall events. Geochim. Cosmochim. Acta, 217, pp. 254–272. https://doi.org/10.1016/j.gca.2017.08.001.

Loÿe-Pilot, M. D., Martin, J. M., Morelli, J. (1986). Influence of Saharan dust on the rain acidity and atmospheric input to the Mediterranean. Nature, 321, pp. 427–428. https://doi.org/10.1038/321427a0.

Martin, R. S., Mather, T. A., Pyle, D. M., Watt, S. F. L., Day, J., Collins, S. J, Wright, T. E, Aiuppa, A., Calabrese, S. (2009). Sweet chestnut (Castanea sativa) leaves as a bio-indicator of volcanic gas, aerosol, and ash deposition onto the flanks of Mt Etna in 2005-2007. J. Volcanol. Geotherm. Res., 179, pp. 107–119. https://doi.org/10.1016/j.jvolgeores.2008.10.012.

McArthur, J. M., Donovan, D. T., Thirlwall, M. F., Fouke, B. W., Mattey, D. (2000). Strontium isotope profile of the early Toarcian (Jurassic) oceanic anoxic event, the duration of ammonite biozones, and belemnite palaeotemperatures. Earth Planet. Sci. Lett., 179(2), pp. 269-285, https://doi.org/10.1016/S0012-821X(00)00111-4.

Menichini, E., Settimo, G., Viviano, G. (2006). Methods for the determination of arsenic, cadmium, nickel, and polycyclic aromatic hydrocarbons in atmospheric depositions. Istituto Superiore di Sanità. "Metodiche per il rilevamento delle emissioni in atmosfera da impianti industriali"

2006, v, 23 p. Rapporti ISTISAN 06/38 (in Italian). Accessed online in https://www.iss.it/ on 17/05/2023).

Moore, L. J., Murphy, T. J., Barnes, I. L., Paulsen, P. J. (1977). Absolute Isotopic Abundance Ratios and Atomic Weight of a Reference Sample of Strontium. J Res Natl Bur Stand., 1982, (1):1-8. https://doi.org/10.6028/jres.087.001.

Muezzinoglu, A. & Cukurluoglu, S. (2006). Deposition of heavy metals in a Mediterranean climate area. Atmos. Res., 81,1-16. https://doi.org/10.1016/j.atmosres.2005.10.004.

Possanzini, M., Buttini, P., Di Paolo, V. (1988). Characterization of a rural area in terms of dry and wet deposition. Science of Total Environ., 74, pp. 111-120. https://doi.org/10.1016/0048-9697(88)90132-5.

Soriano, A., Pallarés, S., Pardo, F., Vicente, A. B., Sanfeliu, T., Bech, J. (2012). Deposition of heavy metals from particulate settleable matter in soils of an industrialised area. J. Geochem. Explor., 113, pp. 36-44. https://doi.org/10.1016/j.gexplo.2011.03.006.

Tonarini, S., Pennisi, M., Adorni-Braccesi, A., Dini, A., Ferrara, G., Gonfantini, R, Wiedenbeck, M, Gröning, M. (2003). Intercomparison of Boron Isotope and Concentration Measurements. Part I: Selection, Preparation, and Homogeneity Tests of the Intercomparison Materials. Geostandards Newsletter, 27(1), pp. 21-39. https://doi.org/10.1111/j.1751-908X.2003.tb00710.x

UNI EN 16171:2016. Sludge, treated biowaste, and soil - Determination of elements using inductively coupled plasma mass spectrometry (ICP-MS).

UNI EN ISO 14911:2001. Water quality - Determination of dissolved Li^+, Na^+, NH_4^+, K^+, Mn^{2+}, Ca^{2+}, Mg^{2+}, Sr^{2+}, and Ba^{2+} using ion chromatography – method for water and wastewater.

UNI EN ISO 14902:2005. Ambient air quality - Standard method for the measurement of Pb, Cd, As and Ni in the PM10 fraction of suspended particulate matter.

UNI EN ISO 10523:2009. Water quality – Determination of pH.

UNI EN ISO 10304-1:2009. Water quality - Determination of dissolved anions by liquid chromatography of ions - Part 1: Determination of bromide, chloride, fluoride, nitrate, nitrite, phosphate, and sulfate.

UNI EN ISO 14644-1:2016. Cleanrooms and associated controlled environments Classification of air cleanliness by particle concentration.

US EPA, 2007. Method 3051 Microwave Assistant Acid Digestion of Sediments, Sludges, Soils and Oils. U.S. Environmental Protection Agency, Washington, DC.

Walder, A. J. & Freedman, P. A. (1992). Communication. Isotopic ratio measurement using a double-focusing magnetic sector mass analyser with an inductively coupled plasma as an ion source. J. Anal. At. Spectrom., 7, pp. 571-575. https://doi.org/10.1039/JA9920700571.

Wang, Q., Liu, M., Li, Y., Liu, Y., Li, S., Ge, R. (2016). Dry and wet deposition of polycyclic aromatic hydrocarbons and comparison with typical media in urban system of Shanghai, China. Atmos. Environ., 144, pp. 175-181. https://doi.org/10.1016/j.atmosenv.2016.08.079.

WMO. Guide to Meteorological Instrument and Observing Practice; WMO No. 8 2018; WMO: Geneva, Switzerland, 2018.

Ye, L., Huang, M., Zhong, B., Wang, X., Tu, Q., Sun, H., Wang, C., Wu, L., Chang, M. (2018). Wet and dry deposition fluxes of heavy metals in Pearl River Delta Region (China): Characteristics, ecological risk assessment, and source apportionment. J. Environ. Sci., 70, pp. 106-123. https://doi.org/10.1016/j.jes.2017.11.019.

4. Results

4.1General overview

This chapter sets out the results from the laboratory analyses of the chemical and isotopic composition of the atmospheric deposition samples collected in the investigated areas. This chapter is subdivided into sections, corresponding to the four investigated contexts. In these four sections, the results of chemical-physical parameters (pH and Electric Conductivity), major ions, minor and trace elements, among them Technology-Critical Elements (TCEs), and B and Sr isotopic ratios are reported. The concentrations of beryllium and bismuth, analysed in the soluble fraction of atmospheric deposition, were not included in the results and commented on in the discussion as they were almost always below the limit of quantification (< LOQ for 88.7% and 98.7%, respectively).

As described in chapter 3, "Materials and Methods: Sampling, Preparation, and Analysis", the minor and trace elements concentrations were measured in three different types of samples: rainwater; solutions obtained by the mineralisation of membrane filters after filtering and blocking the insoluble fraction (henceforth, "insoluble fraction"); solution obtained by the recovery of the soluble fraction of the dry deposition and the materials on the surfaces of the collectors (henceforth, "recovery"). Therefore, a further subdivision is performed in the minor and trace elements subsections, which describe the results from (i) the concentrations in the soluble fraction (rainwater); (ii) the concentrations in the insoluble fraction solutions; (iii) the concentrations in the rinse solutions.

All the results obtained, and discussed below, can be found in the Supplementary materials:

(i) typology of samples and the number of samples analysed for each typology (Tab. S.1);

(ii) pH, Electric Conductivity, and major ions in rainwater samples (Tab. S.2);

(iii) minor and trace elements in rainwater samples (Tab. S.3);

(iv) minor and trace elements in rinse solutions (Tab. S.4);

(v) minor and trace elements in the insoluble fraction solutions (Tab. S.5);

(vi) TCEs (Tab. S.6);

(vii) boron and strontium isotopes (Tab. S.7).

4.2 Mt. Etna

The sequential number of samples and their sampling periods, for each monitoring site in the Etna area, are shown in Table 7.

Table 7 - Sequential number of samples and sampling periods for Citelli, Zafferana Etnea, Cratere 2001 and Intraleo sampling sites.

Site	No. Sample	Installed	Sampled	Time Exp. (day)
Citelli	1	02/03/2021	30/03/2021	28
	2	30/03/2021	27/04/2021	28
	3	27/04/2021	26/05/2021	29
	4	26/05/2021	29/06/2021	34
	5	29/06/2021	02/08/2021	34
	6	02/08/2021	01/09/2021	30
	7	01/09/2021	13/10/2021	42
	8	13/10/2021	01/11/2021	19
	9	01/11/2021	24/11/2021	23
	10	24/11/2021	21/12/2021	27
	11	21/12/2021	19/01/2022	29
	12	19/01/2022	22/02/2022	34
	13	22/02/2022	28/03/2022	34
	14	28/03/2022	27/04/2022	30
	15	27/04/2022	24/05/2022	27
	16	24/05/2022	14/07/2022	51
	17	14/07/2022	23/08/2022	40
	18	23/08/2022	27/09/2022	35
	19	27/09/2022	25/10/2022	28
	20	25/10/2022	21/11/2022	27
	21	21/11/2022	19/12/2022	28
	22	19/12/2022	24/01/2023	36
	23	24/01/2023	28/03/2023	63

Site	No. Sample	Installed	Sampled	Time Exp. (day)
Zafferana Etnea	1	02/03/2021	30/03/2021	28
	2	30/03/2021	27/04/2021	28
	3	27/04/2021	27/05/2021	30
	4	27/05/2021	29/06/2021	33
	5	29/06/2021	03/08/2021	35
	6	03/08/2021	01/09/2021	29
	7	01/09/2021	12/10/2021	41
	8	12/10/2021	01/11/2021	20
	9	01/11/2021	24/11/2021	23
	10	24/11/2021	21/12/2021	27
	11	21/12/2021	19/01/2022	29
	12	19/01/2022	23/02/2022	35
	13	23/02/2022	28/03/2022	33
	14	28/03/2022	27/04/2022	30
	15	27/04/2022	24/05/2022	27
	16	24/05/2022	14/07/2022	51
	17	14/07/2022	24/08/2022	41
	18	24/08/2022	27/09/2022	34
	19	27/09/2022	26/10/2022	29
	20	26/10/2022	21/11/2022	26
	21	21/11/2022	19/12/2022	28
	22	19/12/2022	25/01/2023	37
	23	25/01/2023	13/02/2023	19

Site	No. Sample	Installed	Sampled	Time Exp. (day)
Cratere 2001	2	01/04/2021	28/04/2021	27
	3	28/04/2021	27/05/2021	29
	4	27/05/2021	30/06/2021	34
	5	30/06/2021	03/08/2021	34
	6	03/08/2021	01/09/2021	29
	7	01/09/2021	13/10/2021	42
	8	13/10/2021	01/11/2021	19
	9	01/11/2021	23/11/2021	22
	12	23/11/2021	23/02/2022	92
	13	23/02/2022	28/03/2022	33
	14	28/03/2022	27/04/2022	30
	15	27/04/2022	24/05/2022	27
	16	24/05/2022	15/07/2022	52
	17	15/07/2022	24/08/2022	40
	18	24/08/2022	27/09/2022	34
	19	27/09/2022	25/10/2022	28
	21	25/10/2022	19/12/2022	55
	23	19/12/2022	20/04/2023	122

Site	No. Sample	Installed	Sampled	Time Exp. (day)
Mt. Intraleo	3	27/04/2021	26/05/2021	29
	4	26/05/2021	29/06/2021	34
	5	29/06/2021	03/08/2021	35
	6	03/08/2021	01/09/2021	29
	7	01/09/2021	13/10/2021	42
	8	13/10/2021	01/11/2021	19
	9	01/11/2021	22/11/2021	21
	10	22/11/2021	21/12/2021	29
	11	21/12/2021	19/01/2022	29
	12	19/01/2022	22/02/2022	34
	13	22/02/2022	28/03/2022	34
	14	28/03/2022	26/04/2022	29
	15	26/04/2022	24/05/2022	28
	16	24/05/2022	14/07/2022	51
	17	14/07/2022	23/08/2022	40
	18	23/08/2022	27/09/2022	35
	19	27/09/2022	25/10/2022	28
	20	25/10/2022	21/11/2022	27
	21	21/11/2022	19/12/2022	28
	22	19/12/2022	24/01/2023	36
	23	24/01/2023	13/02/2023	20

4.2.1 Chemical-physical parameters (pH, EC)

4.2.1.1 The acidity of rainwater

The pH values of the rainwater samples collected at four sites at Mt. Etna showed great variability during the two years of monitoring, ranging from 3.1 to 7.7, with a median value of 5.6. The frequency distribution of pH in rainwater samples in this study area was bimodal and showed two different groups: acidic and neutral-alkaline precipitation samples (Fig. 11).

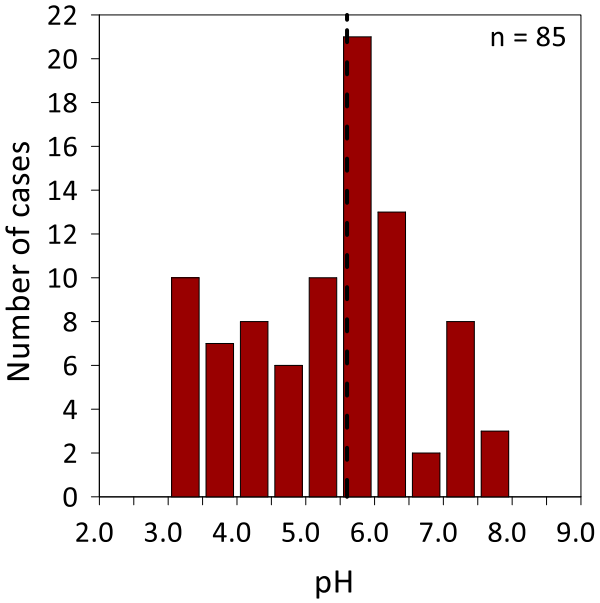

Figure 11 - Frequency distribution of pH in Etna's rainwater samples (85 cases). The black dashed line is the median.

The class with the highest frequency lies in the pH range of 5.5 – 6.0, with a frequency value of ~ 25%. The pH values for each monitoring site in the Mt. Etna area are reported in Table 8 and shown in Figure 12.

Table 8 - Statistical parameters for rainwater's pH at Mt. Etna

Study area	Site	Min	Max	Median	Q1	Q3
Mt. Etna	CIT	3.1	7.3	4.4	3.7	7.3
	ZAF	3.4	7.6	5.7	4.9	6.0
	CRT	3.1	7.2	5.5	4.2	6.2
	INT	4.0	7.7	5.6	5.1	5.8

The lowest median pH value was measured at the Citelli site (4.4), while the highest median pH value was measured at Mt. Intraleo (5.6). Quartiles showed that the rainwater at Citelli had a strong acid composition, indeed 25% of the samples had a pH value below 3.7, and ~ 64% of the cases had a pH value below the natural pH of rainwater (5.6). A balance between the number of samples with a pH below and above 5.6 (~ 48% and 50%, respectively) can be observed in Zafferana and Cratere 2001. At Mt. Intraleo, on the other hand, the pH was below 5.6 in the ~ 43% of the samples. Except for Citelli, at all monitoring sites in this area, the highest pH value was measured during the third sampling period, between 27 April and 26 May 2021. At Citelli, the highest pH value was measured during the fifth sampling period, between 29 June and 2 August 2021. At Citelli, Zafferana Etnea, Cratere 2001, and Mt. Intraleo, the lowest pH values were measured during the following periods: 24 November - 24 December 2021, 14 July - 24 August 2022, 19 December 2022 - 20 April 2023, 21 November - 19 December 2022. Please refer to Table 7 for the correspondence between the sampling period and the sequential sample number.

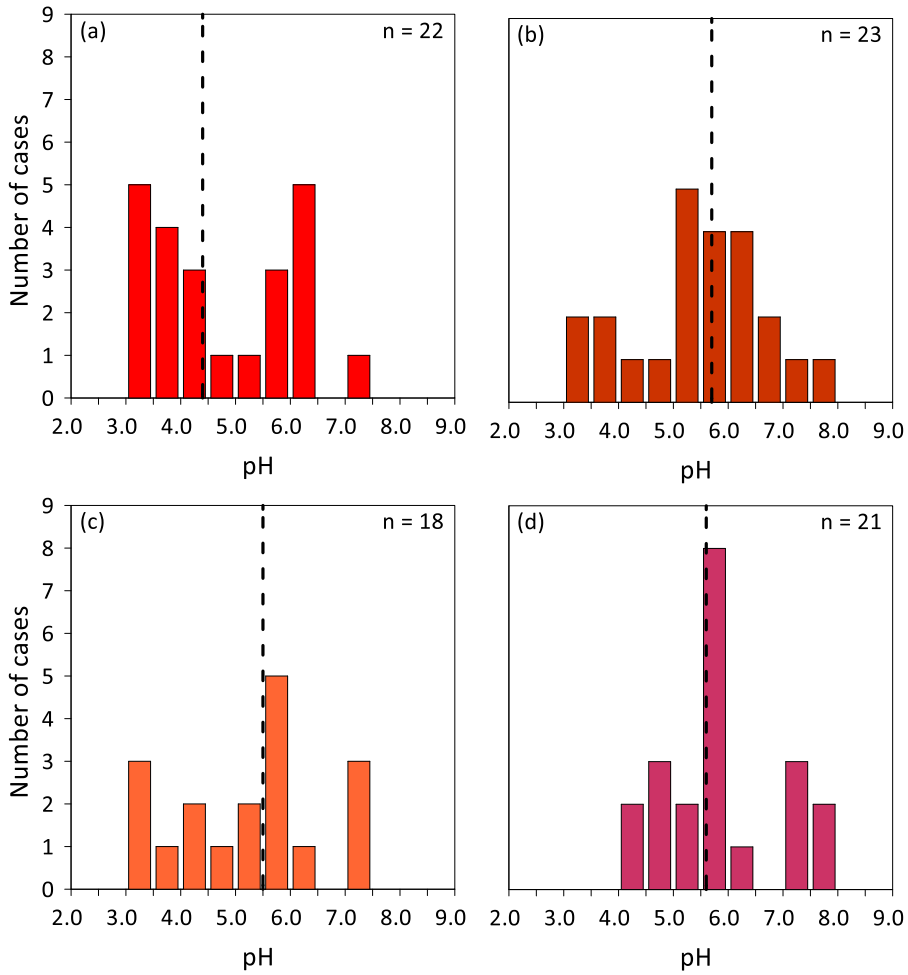

Figure 12 - Frequency distribution of pH in (a) Citelli, (b) Zafferana Etnea, (c) Cratere 2001, and (d) Mt. Intraleo rainwater samples. The black dashed lines are the median values.

4.2.1.2 The Electric Conductivity (EC) of rainwater

The EC values of the rainwater samples collected at Mt. Etna (four sites), showed great variability during the two years of monitoring, ranging from 4.5 to 457 µS cm^{-1}, with a median of 47.9 µS cm^{-1}. For a better graphical representation, the Log_{10} of the electric conductivity values were calculated. The probability distribution was unimodal, and the class with the highest frequency (~ 38%) lies in the EC range of 1.4-1.8. Electric conductivity values were generally low in all the sampling sites, with values below 2 (on a Log_{10} basis) for ~ 76% of the entire population (Fig. 13). These EC values are typical of rain with a relatively low amount of dissolved ions.

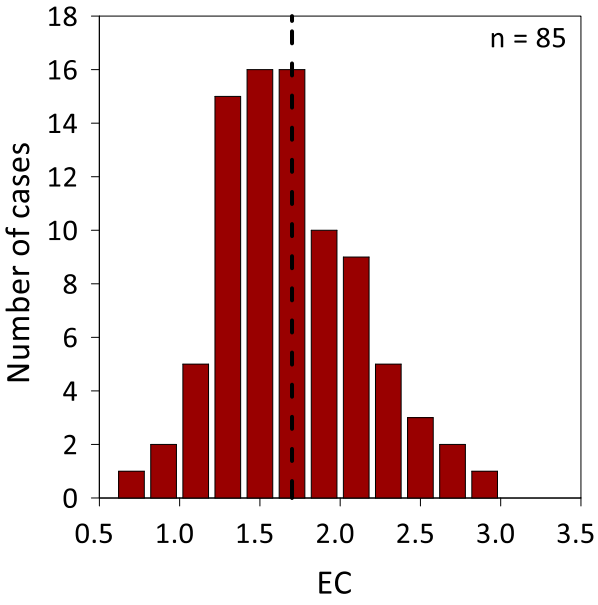

Figure 13 - Frequency distribution of EC (Log_{10}) in Etna's rainwater samples (85 cases). The black dashed line is the geometric mean.

The EC values for each monitoring site in the Mt. Etna area are reported in Table 9 and shown in Figure 14.

Table 9 - Statistical parameters for rainwater's EC (Log_{10}) and at Mt. Etna.

Study area	Site	Min	Max	Median	Q1	Q3
Mt. Etna	CIT	1.36	2.45	1.81	1.56	1.94
	ZAF	0.653	2.20	1.53	1.40	2.09
	CRT	1.23	2.66	1.78	1.53	1.74
	INT	0.851	2.27	1.43	1.20	2.26

The lowest median EC value was measured in the Mt. Intraleo sampling site (1.43), while the highest median EC value was measured at Citelli (1.81), one of the sampling sites most exposed to the fallout of volcanic ash. The lowest value was measured in Zafferana (0.699) during the sampling period of 3 August - 1 September 2021, while the highest value (2.66) was measured in the Cratere 2001 rainwater sample for the period 15 July - 24 August 2022. Very similar values, considering all the descriptive statistical parameters reported in Table 5, were measured at the Zafferana Etnea and

the Mt. Intraleo sites. For Citelli and Zafferana Etna, the highest frequencies were measured in the EC interval 1.4 – 1.6 (~ 27% and ~ 26%, respectively), while at Cratere 2001 in the interval 1.6 – 1.8 (~ 22%), and at Mt. Intraleo in two different intervals, between 1.2 and 1.4 and from 1.6 to 1.8 (~ 24%).

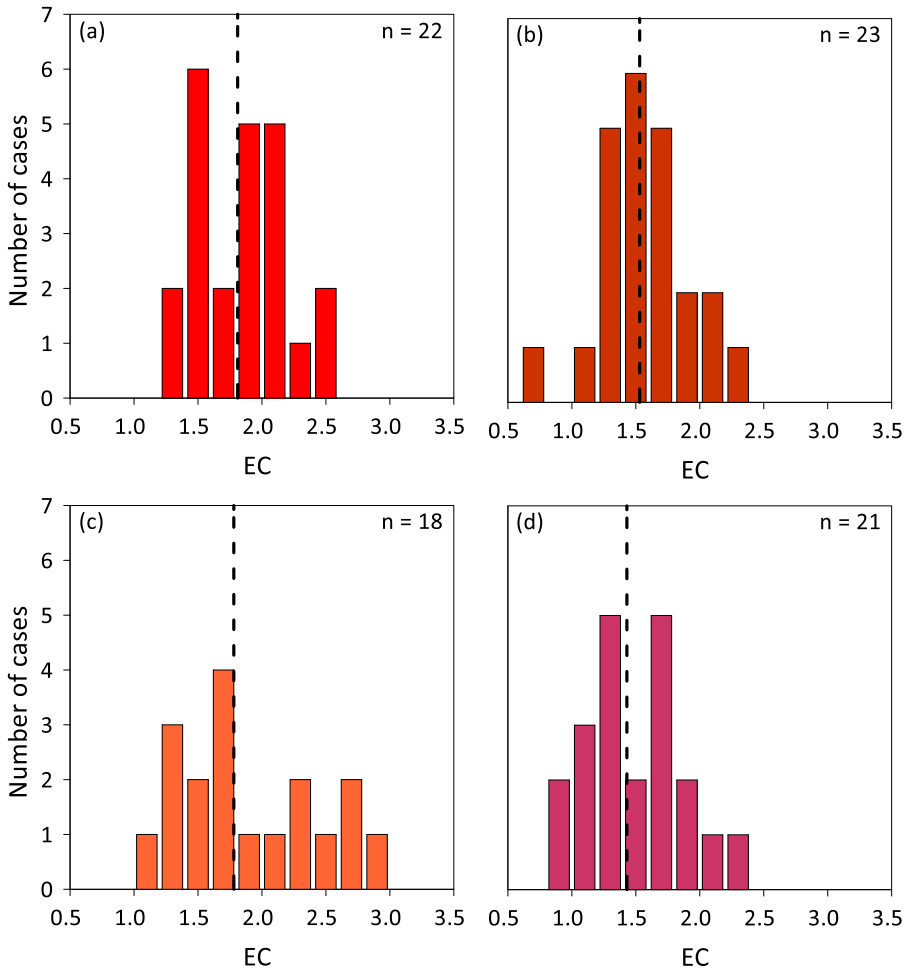

Figure 14 - Frequency distribution of EC in (a) Citelli, (b) Zafferana Etnea, (c) Cratere 2001, and (d) Mt. Intraleo rainwater samples. The black dashed lines are the geometric mean values.

4.2.2 Major inorganic ions

A total of 85 rainwater samples were analysed for major ions. A statistical summary of the major ions in rainwater samples from Mt. Etna is provided in Table 10. Volume-weighted mean and non-sea-salt concentrations were calculated using equations (2) and (4) reported in section 3.7.

Twenty-three rainwater samples from Mt. Etna had a pH value below 4.3 and in them, the HCO_3- concentration was zero. In the remaining samples, the HCO_3^- concentration was determined in ~ 58% of the cases. For NH_4^+ in ~ 11% of the analysed samples, the concentration was below the limit of quantification, while for NO_3^-, K^+, F^-, Cl^-, and SO_4^{2-} it was 8.2%, 3.5%, 3.5%, 2.4%, and 1.2%, respectively. In all the analysed samples was possible to quantify the concentrations of Na^+, Mg^{2+}, and Ca^{2+}.

Table 10 - Statistical parameters for major ions ($\mu eq\ L^{-1}$) in Mt. Etna rainwater samples.

Site		F^-	Cl^-	NO_3^-	SO_4^{2-}	HCO_3^-	Na^+	K^+	NH_4^+	Mg^{2+}	Ca^{2+}
Citelli	Min	0.780	< LOQ	< LOQ	30.3	0.00	9.78	3.30	< LOQ	15.5	32.4
	Max	242	1295	78.3	513	500	684	230	303	347	729
	VWM	67.8	286	11.8	93.8	23.9	70.9	16.7	54.8	43.9	127
	ss (%)	0	28.8	0	9.2	1.4	100	9.3	0	36.2	2.5
	nss (%)	100	71.2	100	90.8	98.6	0	90.7	100	63.8	97.5
Zafferana Etnea	Min	0.38	30.7	< LOQ	21.7	0.00	28.3	1.40	< LOQ	9.80	9.61
	Max	1270	1452	126	267	226	618	341	743	557	1455
	VWM	25.3	123	16.6	65.4	49.9	84.3	11.6	34.6	35.3	89.5
	ss (%)	0	79.7	0	15.6	0.807	100	15.8	0	53.4	4.13
	nss (%)	100	20.3	100	84.4	99.2	0	84.2	100	46.6	95.9
Cratere 2001	Min	< LOQ	< LOQ	< LOQ	< LOQ	0.00	23.2	< LOQ	< LOQ	15.2	50.4
	Max	2607	6360	73.0	11507	274	3912	780	735	1540	7370
	VWM	289	618	17.2	922	40.0	268	57.4	52.1	107	398
	ss (%)	0	50.5	0	3.5	3.2	100	10.2	0	56.0	3.0
	nss (%)	100	49.5	100	96.5	96.8	0	89.8	100	44.0	97.0
Mt. Intraleo	Min	< LOQ	15.3	< LOQ	12.0	0.00	8.52	< LOQ	< LOQ	9.40	14.7
	Max	129	456	168	489	533	396	364	566	312	934
	VWM	5.82	84.2	20.0	54.0	38.3	53.5	15.4	30.7	32.8	115
	ss (%)	0.1	73.9	0.00	12.0	0.7	100	7.6	0.00	36.4	2.0
	nss (%)	99.9	26.1	100	88.0	99.3	0.00	92.4	100	63.6	98.0

Chemical abundances are represented by Tukey box plots, for each monitored site (Fig. 15). The whiskers are drawn from the ends of the box, each extending 1.5 times the width of the box towards the maximum and minimum values; the values outside of these whiskers are defined as outliers (*Reimann et al., 1997*).

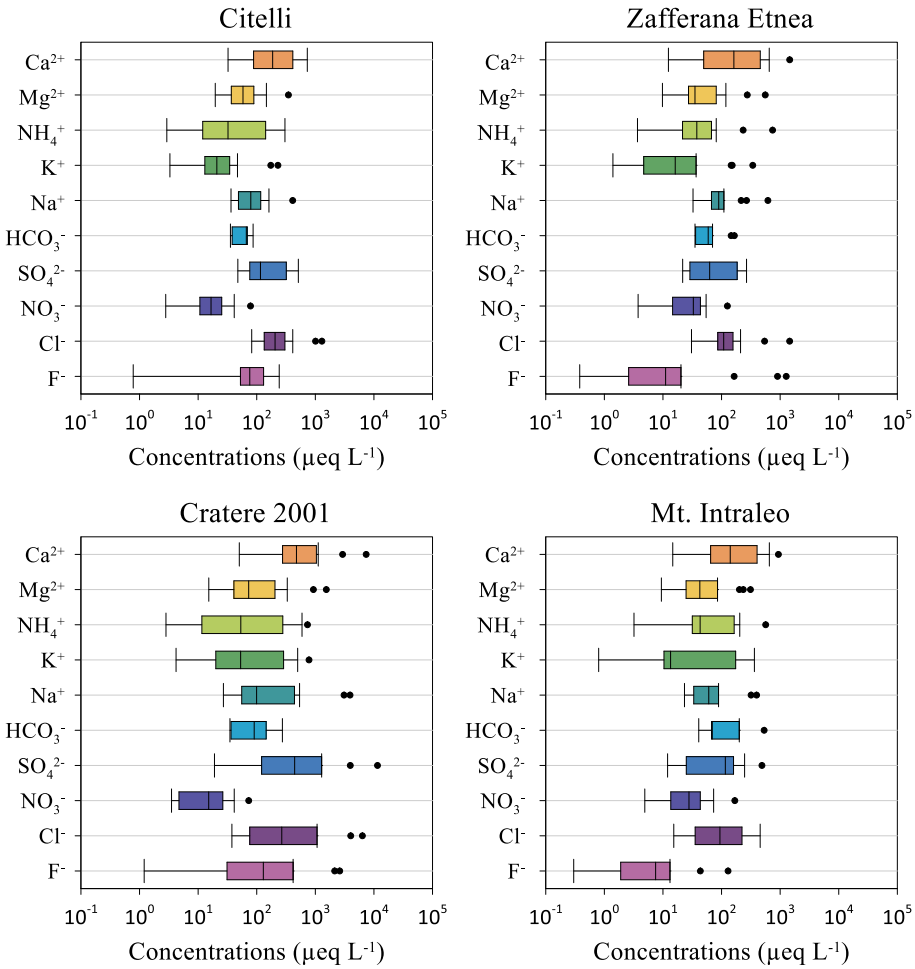

Figure 15 - Major ion concentrations (µeq L^{-1}) in Mt. Etna's rainwater samples.

The most concentrated sample, in terms of total dissolved solids (TDS), was collected at the Cratere 2001, with a value of 19959 µeq L^{-1} (618 mg L^{-1}), in the sampling period 23 November 2021– 23 February 2022. The less concentrated rainwater sample was collected at Mt. Intraleo, with a value of 117 µeq L^{-1} (3.48 mg L^{-1}), in the sampling period of 22 November – 21 December 2021.

At Citelli, the relative VWM concentrations of the major anions follow the sequence Cl^- > SO_4^{2-} > F^- > HCO_3^- > NO_3^-. Similar sequences were observed in the Zafferana Etnea and Mt. Intraleo sites. In the former the sequence was Cl^- > SO_4^{2-} > HCO_3^- > F^- > NO_3^-, while in the latter it was Cl^- > SO_4^{2-} > HCO_3^- > NO_3^- > F^-. A different sequence was observed for Cratere 2001: SO_4^{2-} > Cl^- > F^- > HCO_3^- > NO_3^-. Therefore, chloride was the main anion, with relative abundances of 59.2%, 43.9%, and 41.6% at Citelli, Zafferana Etnea, and Mt. Intraleo, respectively (Fig 16).

Nevertheless, the highest chloride VWM concentration was measured at Cratere 2001, with a value of 618 μeq L^{-1}. In the Cratere 2001 site, the most abundant anion was sulfate (SO_4^{2-}), with a median VMW concentration of 922 μeq L^{-1} and a relative contribution of 49.4%. Relevant relative contributions, between 19.4% and 26.7%, were calculated for SO_4^{2-} in the other Mt. Etna sampling sites (Fig. 16). Fluoride was relatively abundant in Cratere 2001 and Citelli sampling sites, with VWM concentrations of 67.8 μeq L^{-1} and 289 μeq L^{-1}, respectively. Lower VMW concentrations, 25.3 μeq L^{-1} and 5.82 μeq L^{-1} were calculated for Zafferana Etnea and Mt. Intraleo, respectively (Fig. 16). Although fluoride concentrations were lowest in the Mt. Intraleo samples, their relative contribution to the anion summation is not negligible (2.9%). A significant relative contribution of HCO_3^- was observed for the Zafferana Etnea and Mt. Intraleo sites, amounting to 17.8% and 18.9%, respectively. Lower contributions were observed at Citelli (4.9%) and Cratere 2001 (2.1%), (Fig. 16). The highest HCO_3^- VWM concentration was calculated for the samples collected at Mt. Intraleo in the period 28 March – 26 April 2022, equal to 18.9 μeq L^{-1}. Nitrate (NO_3^-) showed low relative contributions, ranging between 0.9% (Cratere 2001) and 9.9% (Mt. Intraleo), with a VMW concentration of 20.0 μeq L^{-1} in the latter (Fig. 16). Please refer to Table 7 for the correspondence between the sampling period and the sequential sample number.

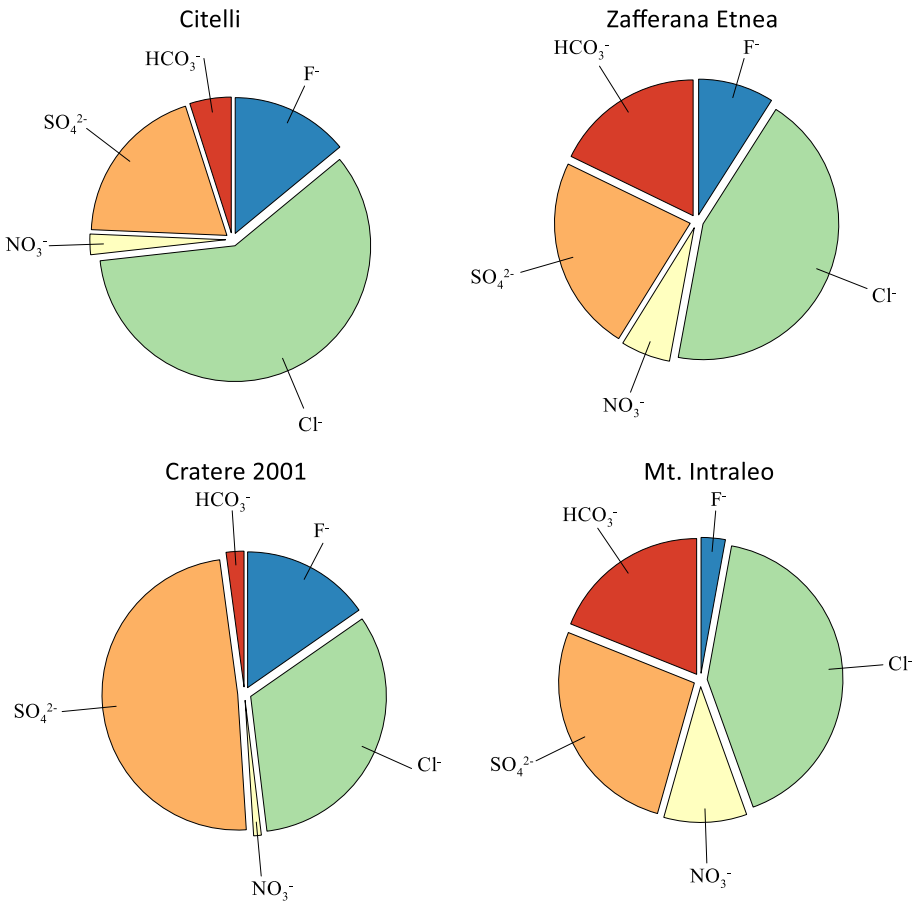

Figure 16 - Relative abundances (Eq%) of any major anions in Mt. Etna sampling sites.

As regards major cations, the sequence of relative abundances was Ca^{2+} > Na^{+} > Mg^{2+} > NH_4^{+} > K^{+}, for all the Mt. Etna sampling sites, except for Citelli, where the relative contribution of NH_4^{+} (17.5%) was higher than that of Mg^{2+} (14.0%), and for Cratere 2001, where the relative contribution of K^{+} (6.5%) was slightly higher than that of NH_4^{+} (5.9%). Therefore, calcium was the main cation, with relative abundances of 40.4%, 35.1%, 45.1%, and 46.5% in Citelli, Zafferana Etnea, Cratere 2001, and Mt. Intraleo sampling sites, respectively (Fig 17). The highest calcium VWM concentration was measured at Cratere 2001, with a value of 398 μeq L^{-1}. For the same site, the highest VMW concentrations for all the major cations were calculated, equal to 268, 107, and 57.4 μeq L^{-1}, for Na^{+}, Mg^{2+}, and K^{+} respectively. The only exception was the ammonium ion, for which the highest VWM concentration was calculated for the Citelli site, equal to 54.8 μeq L^{-1}.

Relevant relative contributions, between 12.2% and 14.0%, were calculated for Mg^{2+}, and between 5.9% and 17.5% for NH_4^+. Usually, the less abundant major cation was K^+, with a relative contribution of up to 6.5% (Fig. 17).

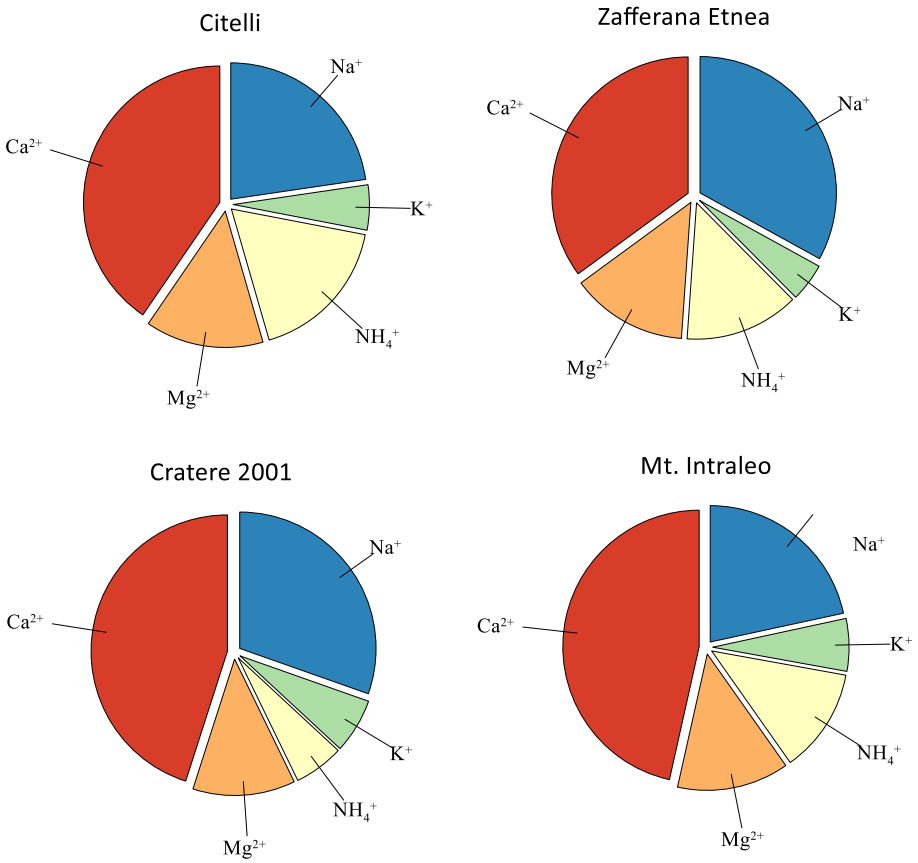

Figure 17 - Relative abundances (Eq%) of any major cations in Mt. Etna sampling sites.

4.2.3 Minor and trace elements concentrations

4.2.3.1 Rainwater samples

A summary of statistical parameters of the analysed minor and trace elements in the rainwater samples from Mt. Etna sampling sites is provided in Table 11, and Figure 18. A total of 85 rainwater samples were analysed for minor and trace elements; it was not possible to determine the concentration of Sn and Cs in 80% and in ~ 16% of the cases. For Al, V, Fe, Zn, As, Rb, Sr, Sb, and

Ba, it was always possible to determine the concentration, while for the other elements, it was not possible to do so in between approximately 1% and 10% of the samples.

Table 11 - Statistical parameters for minor and trace element concentrations (µg L^{-1}) in Citelli, Zafferana Etnea, Cratere 2001, and Mt. Intraleo sampling sites. Sample n. is the number of samples in which the maximum concentration was measured for each element.

	Element	Li	B	Al	Ti	V	Cr	Mn	Fe	Co	Ni	Cu	Zn	As
Citelli	Min	< LOQ	< LOQ	29.2	0.0810	0.253	0.0310	0.523	2.47	0.0330	0.118	0.307	0.256	0.0720
	Max	2.36	8.37	2742	166	7.49	0.741	146	2043	1.69	1.61	47.9	120	1.79
	Sample n.	16	05	10	10	10	14	16	10	16	16	16	16	17
	VWM	0.334	2.85	497	17.9	1.64	0.0991	20.2	240	0.281	0.373	9.83	14.0	0.404
	Element	Se	Br	Rb	Sr	Mo	Cd	Sn	Sb	Cs	Ba	Tl	Pb	U
	Min	0.142	< LOQ	0.295	4.66	< LOQ	0.0350	< LOQ	0.0150	< LOQ	0.862	0.0210	< LOQ	0.00300
	Max	4.89	146	32.0	102	0.778	1.85	0.0270	1.93	0.148	89.4	2.71	1.99	0.0810
	Sample n.	16	16	16	16	05	16	07	18	16	04	16	07	10
	VWM	0.680	18.3	2.09	18.6	0.105	0.246	0.00703	0.164	0.0214	10.7	0.272	0.605	0.0184

	Element	Li	B	Al	Ti	V	Cr	Mn	Fe	Co	Ni	Cu	Zn	As
Zafferana Etnea	Min	< LOQ	1.09	2.41	< LOQ	0.0790	< LOQ	0.356	0.284	< LOQ	< LOQ	< LOQ	1.20	0.0300
	Max	9.49	21.9	2402	47.3	11.3	0.302	304	325	1.77	1.03	47.4	50.9	1.11
	Sample n.	04	05	19	04	04	16	02	04	06	04	04	04	04
	VWM	0.188	3.43	75.3	0.605	0.645	0.0524	9.29	15.5	0.0885	0.166	3.63	6.93	0.171
	Element	Se	Br	Rb	Sr	Mo	Cd	Sn	Sb	Cs	Ba	Tl	Pb	U
	Min	0.101	< LOQ	0.0420	2.54	< LOQ	< LOQ	< LOQ	0.0170	< LOQ	0.412	0.0140	< LOQ	< LOQ
	Max	13.6	40.5	14.6	251	3.36	0.527	0.0440	0.936	0.309	33.9	1.35	1.28	0.0350
	Sample n.	05	05	04	04	17	04	17	17	04	04	04	05	05
	VWM	0.465	12.1	0.725	12.3	0.0902	0.0755	0.00669	0.120	0.0115	4.87	0.113	0.238	0.00434

	Element	Li	B	Al	Ti	V	Cr	Mn	Fe	Co	Ni	Cu	Zn	As
Cratere 2001	Min	0.0490	1.09	5.33	< LOQ	0.260	0.0220	1.73	2.41	0.0140	0.0840	0.518	0.162	0.0730
	Max	17.4	61.0	57291	25.6	97.2	1.08	1095	3633	10.6	6.80	980	227	11.3
	Sample n.	16	23	16	16	16	17	16	16	17	16	12	16	16
	VWM	1.10	5.53	3007	2.50	3.09	0.185	69.6	317	0.904	0.768	51.4	20.6	0.934
	Element	Se	Br	Rb	Sr	Mo	Cd	Sn	Sb	Cs	Ba	Tl	Pb	U
	Min	0.114	1.52	0.177	3.21	0.0210	< LOQ	< LOQ	0.0190	< LOQ	1.51	0.0190	< LOQ	0.00200
	Max	17.7	549	84.3	1111	19.6	6.98	0.0790	0.565	0.807	110	9.78	2.43	0.979
	Sample n.	17	12	16	16	23	16	16	17	16	16	16	12	12
	VWM	2.14	38.0	7.45	61.3	0.504	0.670	0.00936	0.0707	0.0661	14.9	0.682	0.373	0.0802

	Element	Li	B	Al	Ti	V	Cr	Mn	Fe	Co	Ni	Cu	Zn	As
Mt. Intraleo	Min	< LOQ	< LOQ	1.81	0.0140	0.0510	0.0220	< LOQ	1.39	< LOQ	< LOQ	0.475	1.89	0.0200
	Max	0.562	36.4	217	1.08	2.33	5.55	74.1	80.3	0.595	3.43	27.5	102	0.980
	Sample n.	16	13	16	16	16	16	03	16	16	16	16	16	16
	VWM	0.0869	3.07	24.9	0.154	0.351	0.185	5.00	6.10	0.0556	0.367	2.88	7.81	0.178
	Element	Se	Br	Rb	Sr	Mo	Cd	Sn	Sb	Cs	Ba	Tl	Pb	U
	Min	< LOQ	2.83	0.0270	1.57	< LOQ	< LOQ	< LOQ	0.0180	< LOQ	0.477	< LOQ	< LOQ	< LOQ
	Max	0.958	71.4	10.7	78.5	0.815	0.295	0.0500	1.64	0.0420	48.6	0.500	0.764	0.0370
	Sample n.	16	13	16	16	13	16	13	16	16	16	15	16	05
	VWM	0.240	8.98	0.847	10.7	0.0554	0.0673	0.00630	0.192	0.00461	3.75	0.0734	0.111	0.00371

In the Citelli sampling site, the VWM concentrations for minor and trace elements ranged from 0.007 µg L^{-1} (Sn) to 497 µg L^{-1} (Al), at Zafferana Etnea from 0.004 µg L^{-1} (U) to 75.3 µg L^{-1} (Al), at Cratere 2001 from 0.009 µg L^{-1} (Sn) to 3007 µg L^{-1} (Al), and at Mt. Intraleo from 0.004 µg L^{-1} (U) to 24.9 µg L^{-1} (Al). Therefore, the lowest VWM concentrations were calculated for Sn and U, while the highest VWM concentrations were calculated for Al. For all the analysed elements, the highest VWM concentrations were calculated for the Cratere 2001 sampling site, except Ti, Sb, and

Pb, for which the highest values, equal to 17.9 µg L^{-1}, 0.16 µg L^{-1}, and 0.60 µg L^{-1} were calculated for Citelli. At the Zafferana Etnea and Mt. Intraleo sites, VWM concentrations were lower than at the other two sites in the Etna area, in some cases even by two orders of magnitude. The concentrations of the elements analysed did not only show great differences between the different sites. A relevant intra-site variability, up to three orders of magnitude, was observed for different periods of sampling (Fig. 18).

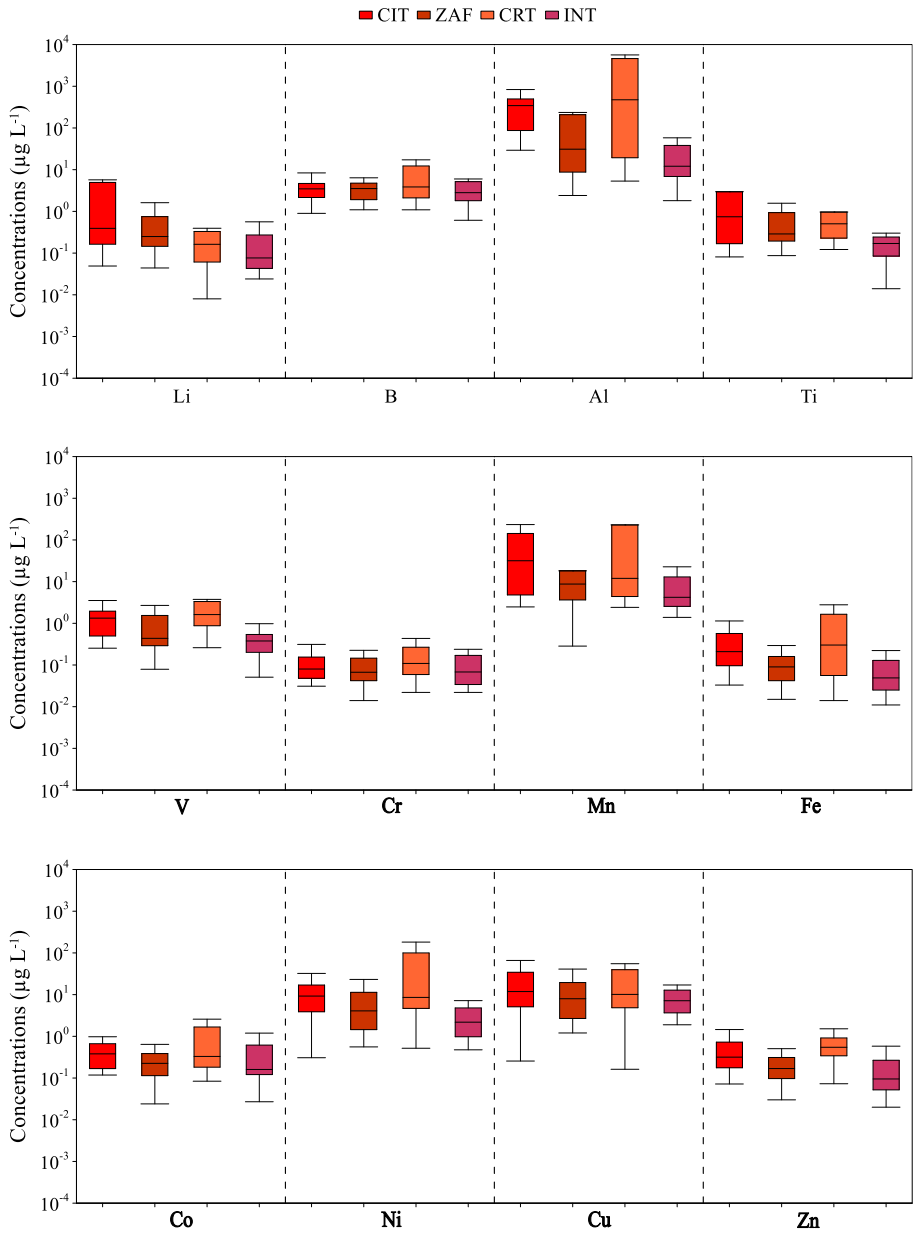

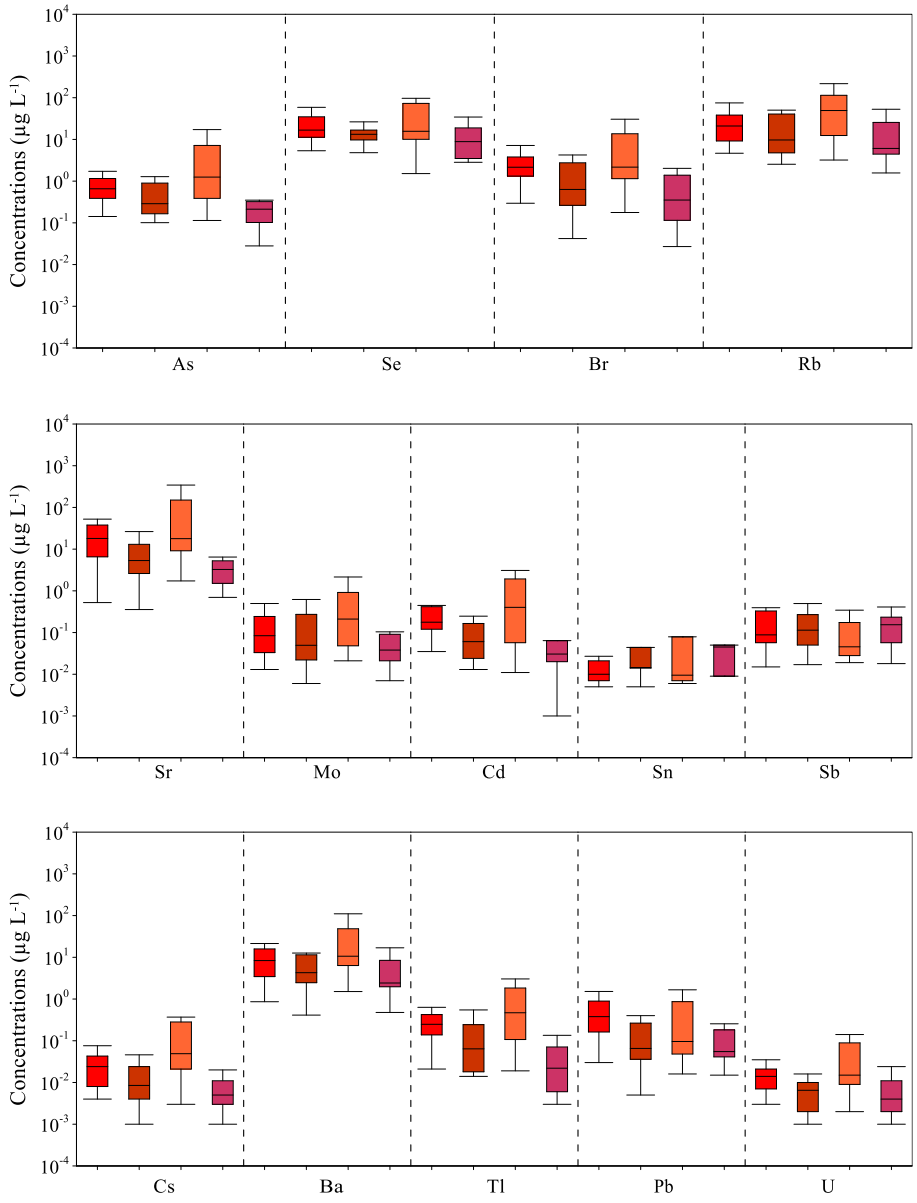

Figure 18 - Minor and trace element concentrations (µg L^{-1}) in rainwater samples from the Mt. Etna area. The elements are ordered from highest to lowest atomic weight.

4.2.3.2 Insoluble fraction

To characterise the chemical composition of the insoluble fraction of the atmospheric deposition, the material retained by the membrane filters (> 0.45 µm) was mineralised according to the procedure described in paragraph 3.1.3. A summary of statistical parameters of the analysed minor and trace elements in the solutions derived from the mineralisation of the insoluble fraction is provided in Table 12 and Figure 19. A total of 85 insoluble fraction solutions were analysed for

minor and trace element concentrations. It was not possible to determine the concentration of As in the 3.5% of the samples, of Mo in the 2.3% of the cases, and of B and Co in the 1.2% of the samples. For the remaining elements, the concentrations were quantified in all the samples.

Table 12 - Statistical parameters for minor and trace element concentrations in the insoluble fraction solutions of Citelli, Zafferana Etnea, Cratere 2001, and Mt. Intraleo. The concentrations are in µg L^{-1}, except for Al, Ti, Fe, and Zn (mg L^{-1}).

	Element	Li	B	Al	Ti	V	Cr	Mn	Fe	Co	Ni	Cu	Zn	As
Citelli	Min	1.10	9.13	0.814	0.0432	19.6	10.9	16.9	0.790	1.77	8.10	26.3	0.0528	1.97
	Max	728	985	1442	106	2725	993	15772	991	302	381	6824	3.57	152
	Median	45.9	109	114	9.21	337	70.4	1310	98.8	41.2	41.9	292	0.369	16.0
	Element	Se	Br	Rb	Sr	Mo	Cd	Sn	Sb	Cs	Ba	Tl	Pb	U
	Min	n.d.	n.d.	n.d.	10.1	1.28	n.d.	n.d.	n.d.	n.d.	16.6	n.d.	6.56	n.d.
	Max	n.d.	n.d.	n.d.	11771	27.1	n.d.	n.d.	n.d.	n.d.	5594	n.d.	425	n.d.
	Median	n.d.	n.d.	n.d.	1200	6.13	n.d.	n.d.	n.d.	n.d.	691	n.d.	56.6	n.d.

	Element	Li	B	Al	Ti	V	Cr	Mn	Fe	Co	Ni	Cu	Zn	As
Zafferana Etnea	Min	2.37	4.36	2.53	0.0842	15.3	6.21	43.0	2.81	1.00	6.35	23.0	0.104	0.964
	Max	331	418	565	37.1	1361	492	8881	474	197	242	3549	3.12	60.9
	Median	24.9	40.8	35.4	2.52	96.2	44.9	434	35.1	12.9	29.7	196	0.330	6.67
	Element	Se	Br	Rb	Sr	Mo	Cd	Sn	Sb	Cs	Ba	Tl	Pb	U
	Min	n.d.	n.d.	n.d.	14.1	0.163	n.d.	n.d.	n.d.	n.d.	31.1	n.d.	5.55	n.d.
	Max	n.d.	n.d.	n.d.	6821	37.2	n.d.	n.d.	n.d.	n.d.	3625	n.d.	291	n.d.
	Median	n.d.	n.d.	n.d.	287	4.14	n.d.	n.d.	n.d.	n.d.	180	n.d.	43.6	n.d.

	Element	Li	B	Al	Ti	V	Cr	Mn	Fe	Co	Ni	Cu	Zn	As
Cratere 2001	Min	35.6	106	84.6	3.89	211	33.7	1012	84.5	27.6	32.7	338	0.278	13.1
	Max	897	1550	2167	104	5352	1130	31342	1878	595	476	10672	5.80	379
	Median	188	332	390	25.8	1054	204	5222	363	125	115	1243	0.898	78.9
	Element	Se	Br	Rb	Sr	Mo	Cd	Sn	Sb	Cs	Ba	Tl	Pb	U
	Min	n.d.	n.d.	n.d.	569	3.61	n.d.	n.d.	n.d.	n.d.	478	n.d.	35.0	n.d.
	Max	n.d.	n.d.	n.d.	16741	59.0	n.d.	n.d.	n.d.	n.d.	9303	n.d.	662	n.d.
	Median	n.d.	n.d.	n.d.	3580	13.3	n.d.	n.d.	n.d.	n.d.	2300	n.d.	180	n.d.

	Element	Li	B	Al	Ti	V	Cr	Mn	Fe	Co	Ni	Cu	Zn	As
Mt. Intraleo	Min	1.28	2.17	2.86	0.161	6.82	6.73	25.9	3.14	0.574	3.70	12.6	0.0729	0.661
	Max	376	539	574	25.2	1223	581	5677	515	174	237	1216	1.92	69.9
	Median	17.9	34.1	23.8	0.936	50.7	43.2	281	21.8	7.66	23.4	136	0.311	5.28
	Element	Se	Br	Rb	Sr	Mo	Cd	Sn	Sb	Cs	Ba	Tl	Pb	U
	Min	n.d.	n.d.	n.d.	16.4	0.302	n.d.	n.d.	n.d.	n.d.	14.9	n.d.	3.42	n.d.
	Max	n.d.	n.d.	n.d.	1968	9.61	n.d.	n.d.	n.d.	n.d.	1660	n.d.	256	n.d.
	Median	n.d.	n.d.	n.d.	114	1.60	n.d.	n.d.	n.d.	n.d.	128	n.d.	29.3	n.d.

In Citelli site, the median concentrations ranged from 6.13 µg L^{-1} for Mo to 114 mg L^{-1} for Al, at Zafferana Etnea from 4.14 µg L^{-1} (Mo) to 35.4 mg L^{-1} (Al), at Cratere 2001 from 13.3 µg L^{-1} (Mo) to 390 mg L^{-1} (Al), and at Mt. Intraleo from 1.60 µg L^{-1} (Mo) to 23.8 mg L^{-1} (Al). Therefore, the lowest median concentrations were calculated for Mo, while the highest median concentrations were calculated for Al. For all the analysed elements, the highest median concentrations were calculated for the Cratere 2001 sampling site. At the Zafferana Etnea and Mt. Intraleo sites, median

concentrations were lower than at the other two sites in the Etna area, in some cases even by two orders of magnitude.

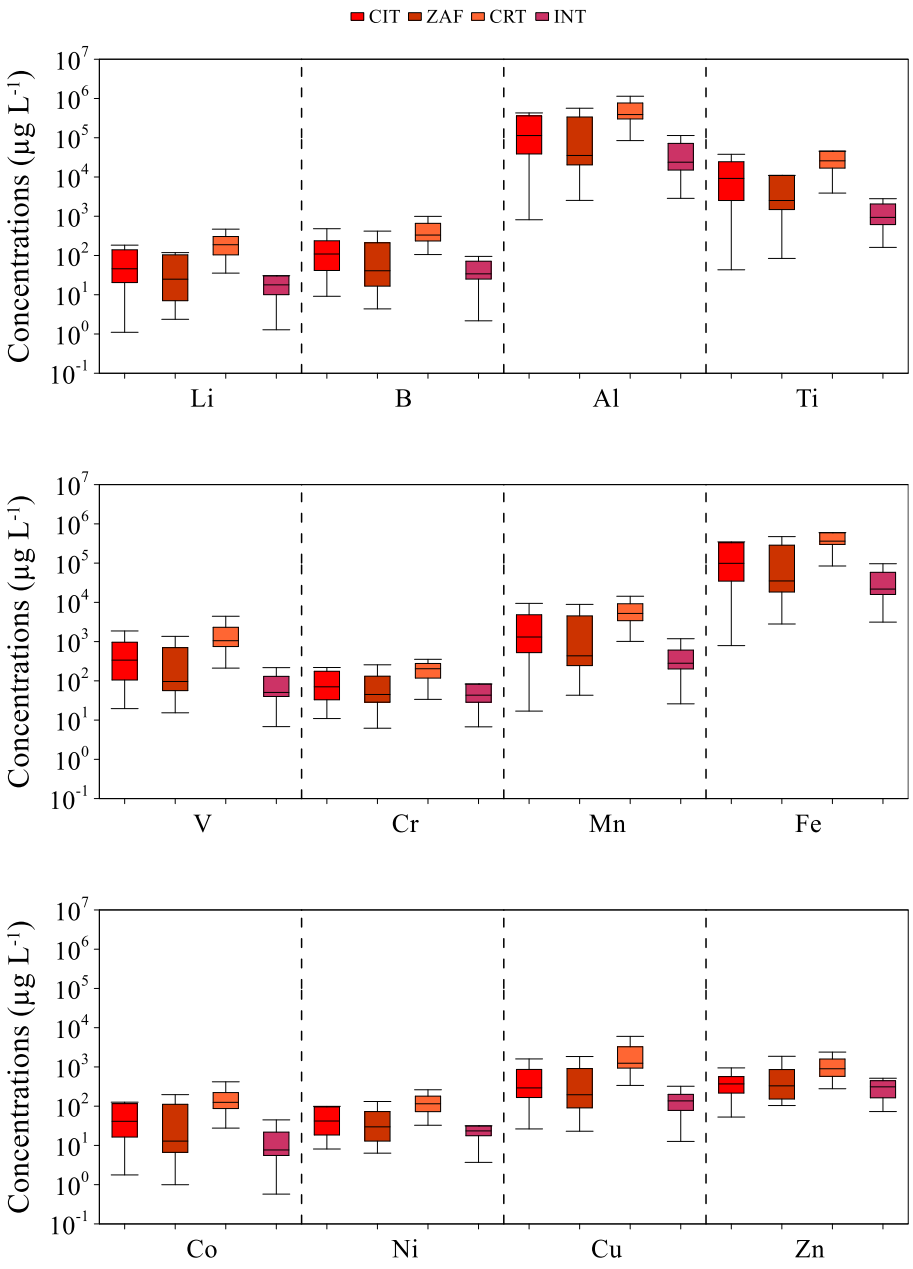

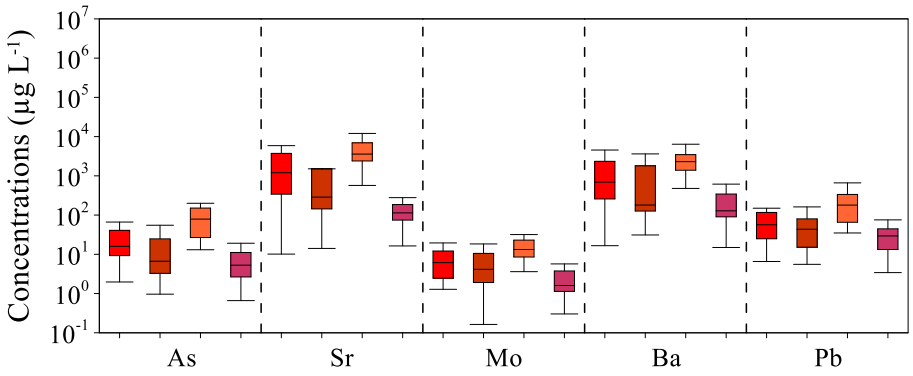

Figure 19 - Minor and trace element concentrations (µg L^{-1}) in the Mt. Etna insoluble fraction solutions. The elements are ordered from highest to lowest atomic weight.

4.2.3.3 Rinse solutions

To determine the concentration of minor and trace elements in the material remaining adhered to the surfaces of the bulk collector, a rinse aliquot was prepared according to the procedure described in paragraph 3.1.2. The concentration of the analysed minor and trace elements in the rinse solutions from Mt. Etna sampling sites, excluding the Cratere 2001 site, is provided in Table 13. A total of six rinse solutions, two for each site, were analysed for minor and trace element concentrations. The concentration of Sn was always below the limit of quantification, while it was not possible to determine the concentration of Br, Li, and Cd in 50%, ~ 32%, and ~ 18% of the samples, respectively. For the other elements, the concentrations were always quantified.

Table 13 - Minor and trace element concentrations (µg L^{-1}) in Citelli, Zafferana Etnea, and Mt. Intraleo rinse solutions.

Citelli	Li	B	Al	Ti	V	Cr	Mn	Fe	Co	Ni	Cu	Zn	As
	0.180	6.15	507	11.1	1.93	0.0520	10.8	127	0.114	0.0820	28.3	10.1	0.150
	0.189	35.8	452	3.88	2.48	0.384	16.1	141	0.116	0.303	23.5	14.1	0.332
	Se	Br	Rb	Sr	Mo	Cd	Sn	Sb	Cs	Ba	Tl	Pb	U
	0.741	32.9	1.20	10.3	0.0850	0.0570	<LOQ	0.0270	0.0280	11.8	0.203	0.717	0.0470
	0.878	<LOQ	6.56	12.1	0.110	0.179	<LOQ	0.263	0.0350	9.56	0.263	3.50	0.0590

Zafferana Etnea	Li	B	Al	Ti	V	Cr	Mn	Fe	Co	Ni	Cu	Zn	As
	<LOQ	6.50	67.0	2.19	0.0620	0.150	1.54	19.4	0.0320	0.228	0.692	12.3	0.0430
	0.174	39.1	691	5.77	2.51	0.274	20.9	133	0.242	0.720	26.5	39.9	0.284
	Se	Br	Rb	Sr	Mo	Cd	Sn	Sb	Cs	Ba	Tl	Pb	U
	0.133	27.6	0.134	0.499	0.0190	0.0230	<LOQ	0.443	0.00300	0.896	0.0340	0.838	0.00300
	2.10	<LOQ	2.30	18.7	0.0990	0.320	<LOQ	0.208	0.0270	24.5	0.0840	6.49	0.120

Mt. Intraleo	Li	B	Al	Ti	V	Cr	Mn	Fe	Co	Ni	Cu	Zn	As
	<LOQ	5.73	28.7	0.737	0.0830	0.0590	0.692	12.9	0.0120	0.193	2.31	1.17	0.0310
	0.289	41.7	613	5.94	2.77	0.499	17.8	174	0.186	0.446	28.4	23.0	0.559
	Se	Br	Rb	Sr	Mo	Cd	Sn	Sb	Cs	Ba	Tl	Pb	U
	0.142	33.2	0.0940	0.292	0.0230	<LOQ	<LOQ	0.0110	0.0170	0.265	0.0240	0.347	0.00300
	2.10	<LOQ	3.85	17.6	0.143	0.659	<LOQ	0.242	0.0510	14.9	0.768	6.06	0.0900

Minor and trace element concentrations in the rinse solutions ranged from 0.003 µg L^{-1} for uranium and caesium to 691 µg L^{-1} for aluminium. Relevant differences were observed between the sampling sites and the samples analysed, up to one order of magnitude. For Li, B, Cr, As, Se, Br, Cd, Cs, and Tl the highest mean concentrations were measured at Mt. Intraleo. For Al, Ti, V, Mn, Fe, Cu, Rb, Sr, and Mo the highest mean concentrations were measured at Citelli, while at Zafferana Etnea were measured the highest mean concentrations for Co, Ni, Zn, Sb, Ba, Pb, and U.

4.2.4 Technology-Critical Elements (TCEs)

From the Mt. Etna study area, 29 preconcentrated rainwater samples, prepared according to the procedure illustrated in paragraph 3.1.4, were analysed for the concentrations of the TCEs, including the lanthanoids. It was not possible to determine the concentration of Nb in 31% of the sample, of Sc and Lu in the 10% of the cases, of Th and Er in the 6.9% of the samples and for Ge, Te, Hf, Tb, Dy, Ho, Tm, and Yb in the 3.4% of the samples. For the remaining elements, the concentrations were quantified in all the samples. A summary of the statistical parameters of the analysed TCEs is provided in Table 14 and Figure 20.

Table 14 - Statistical parameters for TCE concentrations (ng L^{-1}) in Citelli, Zafferana Etnea, Cratere 2001, and Mt. Intraleo preconcentrated rainwater samples.

Citelli	Element	Sc	Ge	Y	Zr	Nb	Te	Hf	Th	La	Ce	Pr
	Min	3.48	3.62	17.9	52.1	0.273	5.24	0.654	0.366	18.2	12.4	3.28
	Max	35.3	50.2	757	293	2.63	75.7	4.95	14.6	1276	2208	245
	Median	5.63	9.19	34.2	125	1.22	20.4	2.52	1.40	56.5	56.7	7.42
	Element	Nd	Sm	Eu	Gd	Tb	Dy	Ho	Er	Tm	Yb	Lu
	Min	18.4	2.83	1.21	3.33	0.474	2.01	0.412	1.53	0.0710	0.895	0.182
	Max	929	124	45.7	154	17.5	117	16.6	45.5	5.56	32.7	4.62
	Median	30.3	5.72	1.46	5.29	0.674	3.64	0.766	2.49	0.303	2.07	0.391

Zafferana Etnea	Element	Sc	Ge	Y	Zr	Nb	Te	Hf	Th	La	Ce	Pr
	Min	0.842	1.05	5.13	5.05	0.0260	2.89	0.0520	0.497	3.77	8.31	1.15
	Max	5.25	7.57	47.0	241	1.68	31.8	3.58	2.21	95.5	104	15.4
	Median	2.78	2.99	8.37	50.5	0.642	4.63	0.757	1.00	18.0	15.6	1.71
	Element	Nd	Sm	Eu	Gd	Tb	Dy	Ho	Er	Tm	Yb	Lu
	Min	4.22	0.767	0.288	0.684	0.0950	0.737	0.127	0.359	0.0620	0.488	0.0400
	Max	66.0	10.3	2.84	8.77	0.988	5.31	1.17	3.34	0.442	2.55	0.415
	Median	11.0	1.74	0.557	1.74	0.277	1.69	0.205	0.889	0.142	0.751	0.123

Cratere 2001	Element	Sc	Ge	Y	Zr	Nb	Te	Hf	Th	La	Ce	Pr
	Min	1.92	2.75	2.91	10.2	0.160	1.71	0.216	0.224	3.21	5.10	0.576
	Max	12.7	33.4	178	280	4.19	117	5.29	3.02	197	326	38.4
	Median	4.36	5.44	19.5	100	0.926	6.80	0.863	1.43	25.4	22.5	3.81
	Element	Nd	Sm	Eu	Gd	Tb	Dy	Ho	Er	Tm	Yb	Lu
	Min	2.68	0.591	0.143	0.648	0.0150	0.341	0.0800	0.222	0.0320	0.220	0.155
	Max	150	31.8	7.85	27.0	3.95	21.2	3.85	10.2	1.28	7.74	1.34
	Median	17.7	3.53	0.974	3.44	0.449	2.60	0.601	1.59	0.229	1.54	0.388

Mt. Intraleo	Element	Sc	Ge	Y	Zr	Nb	Te	Hf	Th	La	Ce	Pr
	Min	0.987	0.933	6.86	25.4	0.766	1.55	0.341	1.09	8.32	8.92	1.35
	Max	4.14	6.18	11.6	181	1.26	30.6	2.64	3.85	21.0	30.1	2.84
	Median	2.30	3.25	10.1	98.1	0.847	3.40	1.52	1.56	18.0	16.9	2.24
	Element	Nd	Sm	Eu	Gd	Tb	Dy	Ho	Er	Tm	Yb	Lu
	Min	6.02	1.42	0.274	1.42	0.188	1.16	0.215	0.629	0.0880	0.627	0.115
	Max	11.3	2.48	0.602	2.30	0.315	1.76	0.349	0.967	0.184	0.812	0.246
	Median	9.57	2.20	0.534	1.89	0.284	1.40	0.263	0.784	0.111	0.729	0.124

Among the TCEs, the highest concentration was measured for Ce, up to values of 2208 ng L^{-1} at the Citelli sampling site, and a median concentration of 27.9 ng L^{-1} by considering all the sampling sites. The highest median concentration, instead, was measured for Zr, equal to 93.5 ng L^{-1}. The lowest median concentration was measured for Tm (0.111 ng L^{-1}) at the Mt. Intraleo sampling site. For Sc (5.63 ng L^{-1}), Ge (9.19 ng L^{-1}), Y (34.2 ng L^{-1}), Zr (125 ng L^{-1}), Nb (1.22 ng L^{-1}), Te (20.4 ng L^{-1}), and Hf (2.52 ng L^{-1}) the highest median concentrations were measured at the Citelli sampling site. For Th, similar median concentrations were calculated for Citelli (1.40 ng L^{-1}) and Cratere 2001 (1.43 ng L^{-1}) rainwater samples. The median concentrations of lanthanoid follow this order: La > Ce > Nd > Pr ≈ Sm > Gd > Dy > Yb ≈ Er > Eu > Ho > Tb > Lu ≈ Tm. For all lanthanoids, the highest concentrations were measured in rainwater samples at the Citelli monitoring site. The sampling site with the lowest lanthanoid median concentrations was Mt. Intraleo.

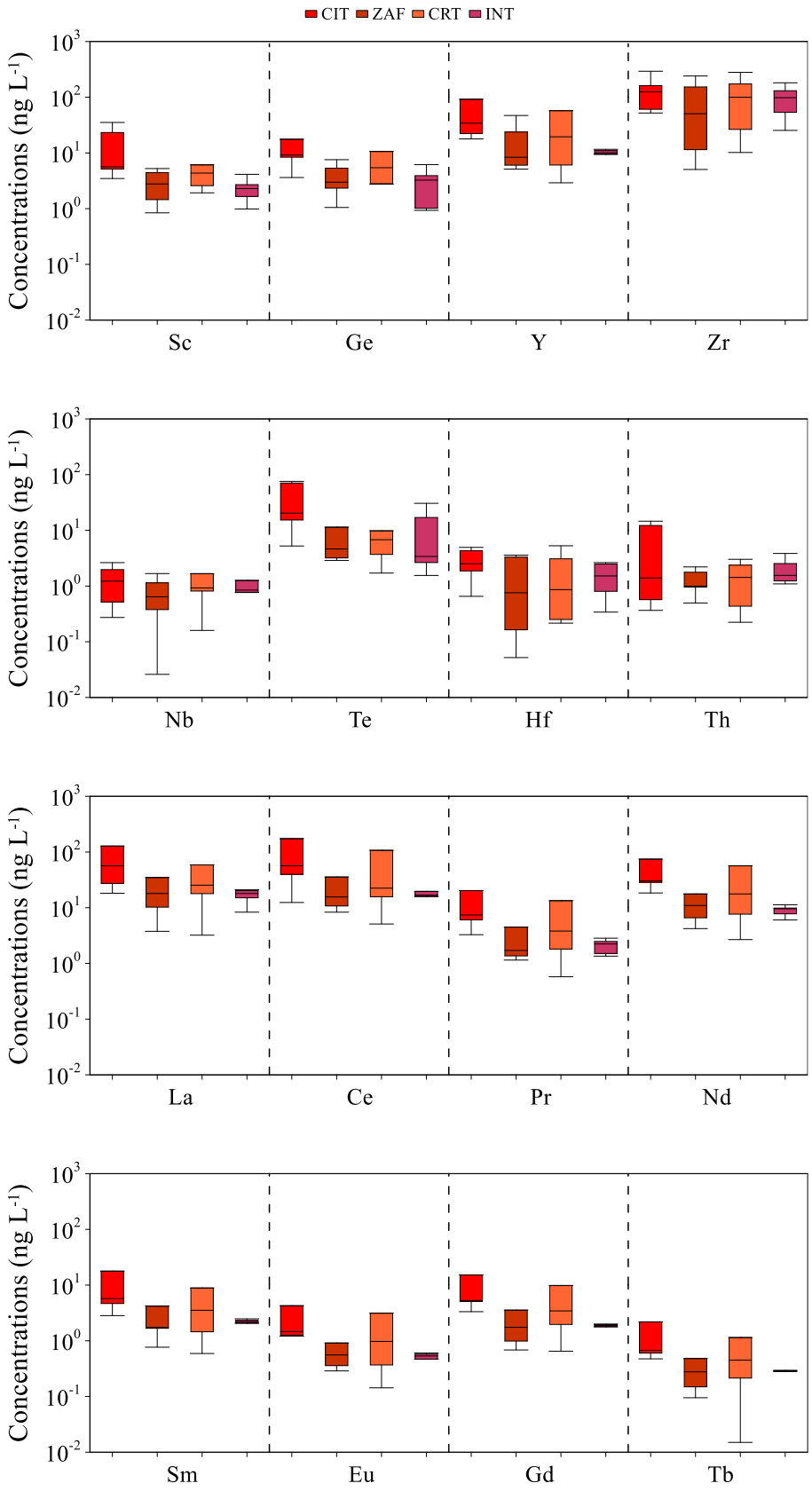
CIT ZAF CRT INT
Concentrations (ng L-1)
Sc
Ge
Y
Zr
Nb
Te
Hf
Th
La
Ce
Pr
Nd
Sm
Eu
Gd
Tb

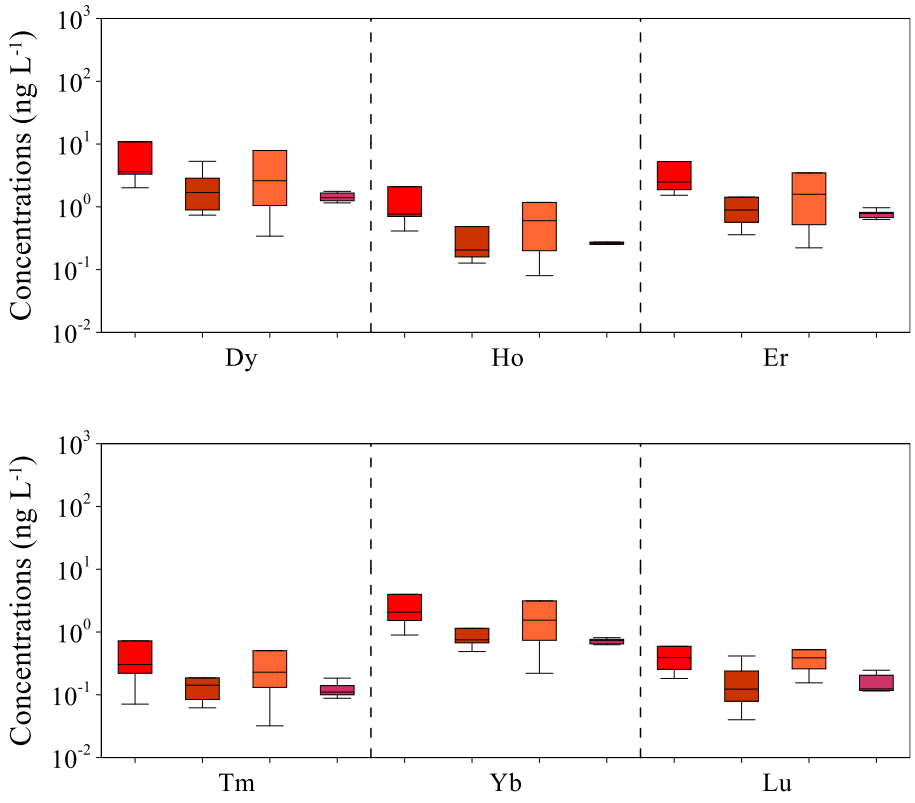

Figure 20 - TCE concentrations (ng L^{-1}) in Mt. Etna rainwater samples. The elements are ordered from highest to lowest atomic weight.

4.2.5 Boron and strontium isotopic composition

Boron ($\delta^{11}B/^{10}B$) and Strontium ($^{87}Sr/^{86}Sr$) isotopic composition were measured in 10 selected rainwater samples. The main statistical parameters (minimum, median, maximum) are given in Table 15.

Table 15 - Main statistical parameters for boron ($\delta^{11}B$‰) and strontium ($^{87}Sr/^{86}Sr$) in Etna's rainwater samples. Dev. Std. is the Standard Deviation for boron isotopic composition, while Std. Err. is the Standard Error for strontium ratio measurements.

Site	$^{87}Sr/^{86}Sr$			
	Min	Median	Max	Std. Err.
Zafferana Etnea	0.703865	0.708064	0.708144	0.000007
Cratere 2001	0.703728	0.704334	0.708083	0.000007
Intraleo	0.708803	0.709583	0.710363	0.000007
Site	$\delta^{11}B$ (‰)			
	Min	Median	Max	Dev. Std.
Zafferana Etnea	22.88	38.05	42.90	0.21
Cratere 2001	1.29	16.96	31.51	0.21
Intraleo	30.07	32.05	34.04	0.09

Very low $\delta^{11}B$ values were measured in some samples from Cratere 2001 (+1.29‰ ± 0.21‰) and Zafferana Etnea (+22.9‰ ± 0.21‰) sampling sites. The lowest $\delta^{11}B$ median value (+16.96‰ ± 0.21‰) was measured in Cratere 2001. The highest absolute $\delta^{11}B$ value was measured in a rainwater sample from Zafferana Etnea (+42.90‰ ± 0.21‰). Two replicates for sample no. 4 of Cratere 2001 were analysed for boron isotopic composition, to verify the stability in the measurement of a repeated sample; $\delta^{11}B$ values of +10.64‰ ± 0.42‰ and +11.45‰ ± 0.07‰ were measured. For the rainwater sample no. 13 of the same survey site, two different aliquots were analysed, obtained from two separate chemical procedures; $\delta^{11}B$ values of +16.96‰ ± 0.11‰ and +16.86‰ ± 0.15‰ were measured.

Strontium isotopic composition ranged from 0.70373 ± 0.00001 (Cratere 2001) to 0.71036 ± 0.00001 (Mt. Intraleo). The lowest and the highest median $^{87}Sr/^{86}Sr$ ratio were measured for Cratere 2001 (0.70433 ± 0.00001) and Mt. Intraleo (0.70958 ± 0.00001) sampling sites, respectively. To verify the stability in the measurement of a repeated sample, two replicates of the rainwater sample no. 13 of Cratere 2001 were analysed, obtained from two separate chemical procedures; $^{87}Sr/^{86}Sr$ ratios of 0.704334 ± 0.000009 and 0.704343 ± 0.000007 were measured.

4.3 Palermo and Catania urban areas

The sequential number of samples and their sampling periods, for each monitoring site in the Etna area, are shown in Table 16.

Table 16 - Sequential number of samples and sampling periods for Archirafi, Unipa, Indipendenza, and Belgio sampling sites.

Site	No. Sample	Installed	Sampled	Time Exp. (day)
Palermo - Archirafi	1	01/03/2021	30/03/2021	29
	2	30/03/2021	26/04/2021	27
	3	26/04/2021	27/05/2021	31
	4	27/05/2021	28/06/2021	32
	5	28/06/2021	02/08/2021	35
	6	02/08/2021	03/09/2021	32
	7	03/09/2021	11/10/2021	38
	8	11/10/2021	25/10/2021	14
	8bis	25/10/2021	03/11/2021	9
	9	03/11/2021	22/11/2021	19
	10	22/11/2021	13/12/2021	21
	11	13/12/2021	18/01/2022	36
	12	18/01/2022	22/02/2022	35
	13	22/02/2022	30/03/2022	36
	14	06/04/2022	26/04/2022	20
	15	26/04/2022	23/05/2022	27
	16	23/05/2022	20/07/2022	58
	17	20/07/2022	23/08/2022	34
	18	23/08/2022	28/09/2022	36
	19	28/09/2022	25/10/2022	27
	20	25/10/2022	23/11/2022	29
	21	23/11/2022	20/12/2022	27
	22	20/12/2022	01/02/2023	43
	23	01/02/2023	16/02/2023	15

Site	No. Sample	Installed	Sampled	Time Exp. (day)
Palermo - Indipendenza	1	01/03/2021	30/03/2021	29
	2	30/03/2021	26/04/2021	27
	3	26/04/2021	27/05/2021	31
	4	27/05/2021	28/06/2021	32
	5	28/06/2021	02/08/2021	35
	6	02/08/2021	03/09/2021	32
	7	03/09/2021	11/10/2021	38
	8	11/10/2021	03/11/2021	23
	9	03/11/2021	22/11/2021	19
	10	22/11/2021	17/12/2021	25
	11	17/12/2021	18/01/2022	32
	12	18/01/2022	25/02/2022	38
	13	25/02/2022	30/03/2022	33
	14	30/03/2022	26/04/2022	27
	15	26/04/2022	23/05/2022	27
	16	23/05/2022	20/07/2022	58
	17	20/07/2022	23/08/2022	34
	18	23/08/2022	28/09/2022	36
	19	28/09/2022	27/10/2022	29
	20	27/10/2022	23/11/2022	27
	21	23/11/2022	20/12/2022	27
	22	20/12/2022	26/01/2023	37
	23	26/01/2023	16/02/2023	21

Site	No. Sample	Installed	Sampled	Time Exp. (day)
Palermo - Unipa	1	01/03/2021	30/03/2021	29
	2	30/03/2021	26/04/2021	27
	3	26/04/2021	27/05/2021	31
	4	27/05/2021	28/06/2021	32
	5	28/06/2021	02/08/2021	35
	6	02/08/2021	03/09/2021	32
	7	03/09/2021	11/10/2021	38
	8	11/10/2021	03/11/2021	23
	9	03/11/2021	22/11/2021	19
	10	22/11/2021	17/12/2021	25
	11	17/12/2021	18/01/2022	32
	12	18/01/2022	25/02/2022	38
	13	25/02/2022	30/03/2022	33
	14	30/03/2022	26/04/2022	27
	15	26/04/2022	23/05/2022	27
	16	23/05/2022	20/07/2022	58
	17	20/07/2022	23/08/2022	34
	18	23/08/2022	28/09/2022	36
	19	28/09/2022	27/10/2022	29
	20	27/10/2022	23/11/2022	27
	21	23/11/2022	20/12/2022	27
	22	20/12/2022	26/01/2023	37
	23	26/01/2023	16/02/2023	21

Site	No. Sample	Installed	Sampled	Time Exp. (day)
Palermo - Belgio	1	01/03/2021	30/03/2021	29
	2	30/03/2021	26/04/2021	27
	3	26/04/2021	27/05/2021	31
	4	27/05/2021	28/06/2021	32
	5	28/06/2021	02/08/2021	35
	6	02/08/2021	03/09/2021	32
	7	03/09/2021	11/10/2021	38
	8	11/10/2021	03/11/2021	23
	9	03/11/2021	22/11/2021	19
	10	22/11/2021	17/12/2021	25
	11	17/12/2021	18/01/2022	32
	12	18/01/2022	25/02/2022	38

4.3.1 Chemical-physical parameters (pH, EC)

4.3.1.1 The acidity of rainwater

The pH values of the rainwater samples collected in Palermo (four sites), and Catania (two sites) showed great variability during the two years of monitoring, respectively ranging from 4.2 to

7.9, with a median value of 6.6, and between 5.0 to 7.8, with a median of 6.2. The frequency distributions of pH in rainwater samples were unimodal in Palermo, with the highest frequency (~ 38%) in the pH range 6.5 – 7.0 (Fig. 21a), and bimodal in Catania, with the highest frequencies in the pH range 5.5 – 6.0 (~ 32%) and between 7.0 and 7.5 (~ 20%) (Fig. 21b).

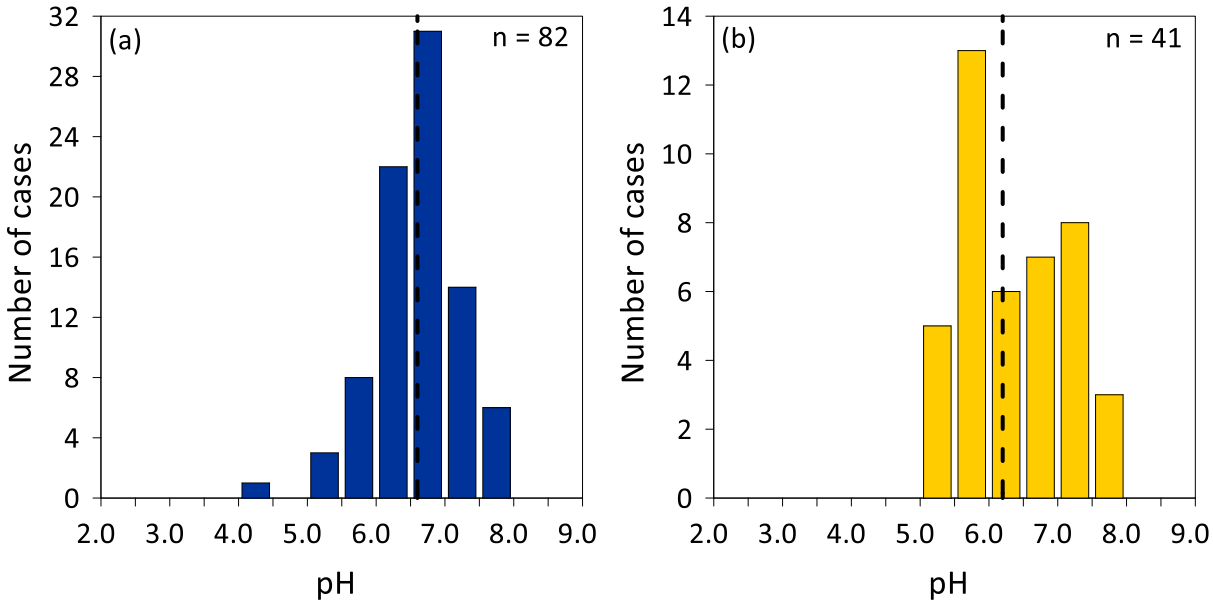

Figure 21 - Frequency distribution of pH in Palermo (a - 82 cases) and Catania (b - 41 cases) rainwater samples. The black dashed lines are the medians.

In both the Palermo and Catania areas, only a few rainwater samples had pH values below 5.6, ~ 5% in the former and ~ 22% in the latter study area. The pH values for each monitoring site in the Palermo and Catania areas are reported in Table 17 and shown in Figure 22 and Figure 23.

Table 17 - Statistical parameters for rainwater's pH in the Palermo and Catania urban areas.

Study area	Site	Min	Max	Median	Q1	Q3
Palermo	ARC	5.2	7.9	6.6	6.0	6.9
	UNI	5.1	7.5	6.6	6.1	7.1
	IND	5.4	7.8	6.7	6.2	7.0
	BEL	4.2	7.7	6.5	6.0	6.9
Catania	GLP	5.0	7.8	6.2	5.6	6.1
	CAT	5.3	7.5	6.2	5.8	6.9

In Palermo and Catania, no major differences were observed in the pH values measured at the different monitoring sites. The lowest median value was calculated for Catania and San Giovanni La Punta (6.2), while median values between 6.5 and 6.7 were calculated for the Palermo sites. At the Archirafi, Unipa and Indipendenza sites, the lowest pH values were 5.2, 5.1 and 5.4 respectively, all measured in the rainwater sample from the last sampling period, 26 January - 16 February 2023. The highest pH values of 7.9 (Archirafi), 7.5 (Unipa), 7.8 (Indipendenza), and 7.7 (Belgio), were measured in the rainwater of the fourth sampling period (27 May - 28 June 2021) for Archirafi and Indipendenza, and the fifth sampling period (28 June - 02 August 2021) for the other two sites. The median pH value calculated for Belgio, which is lower than those of the other sites in the Palermo area, is caused by a very low pH value of 4.2 measured in the rainwater sample from 03/11/2021 – 22/11/2021. Except for the Archirafi site, where the highest frequency falls between pH values of 6.0 and 6.5 (25%) (Fig. 22a), for the other sites in the Palermo area, the highest frequency falls between pH values of 6.5 and 7.0 (~ 43% for Unipa and Indipendenza, and ~ 33% for Belgio) (Fig. 22b, c, d). Except for these differences, homogeneity in the pH values measured at the various monitoring sites in the Palermo area can also be found in the values calculated for the first and third quartiles. In both the sampling sites from the Catania areas, the lowest pH values were measured in the last period, from 26 January to 14 February 2023. The highest pH value (7.8) in the Catania sampling site was measured in the period 25 May – 14 July 2022, while the highest pH value (7.5) in the San Giovanni La Punta sampling site was measured in the period 26 May – 30 June 2021. The highest frequency falls between pH values of 5.5 and 6.0 for both sampling sites (~ 33% and 30% for Catania and San Giovanni La Punta, respectively). A higher third quartile value (6.9) was calculated for the pH value of rainwater from the Catania site, compared to the value calculated for the San Giovanni La Punta site (6.1). Please refer to Table 16 for the correspondence between the sampling period and the sequential sample number.

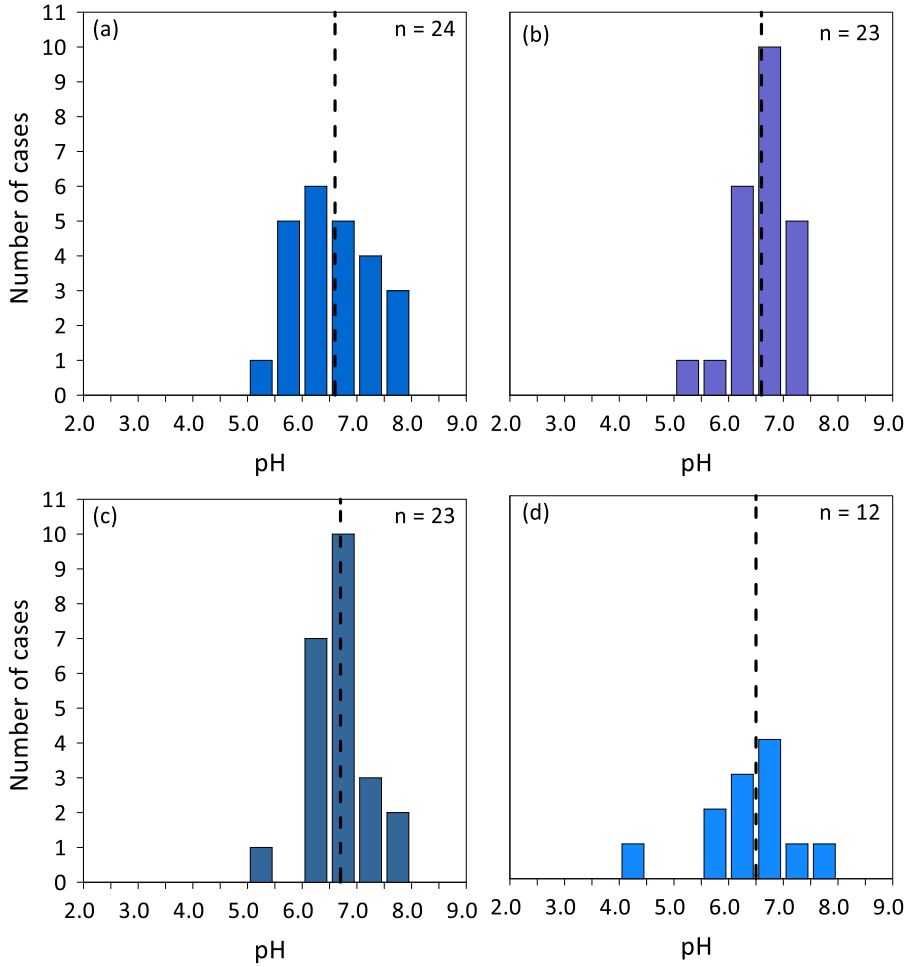

Figure 22 - Frequency distribution of pH in (a) Archirafi, (b) Unipa, (c) Indipendenza, and (d) Belgio rainwater samples. The black dashed lines are the median values.

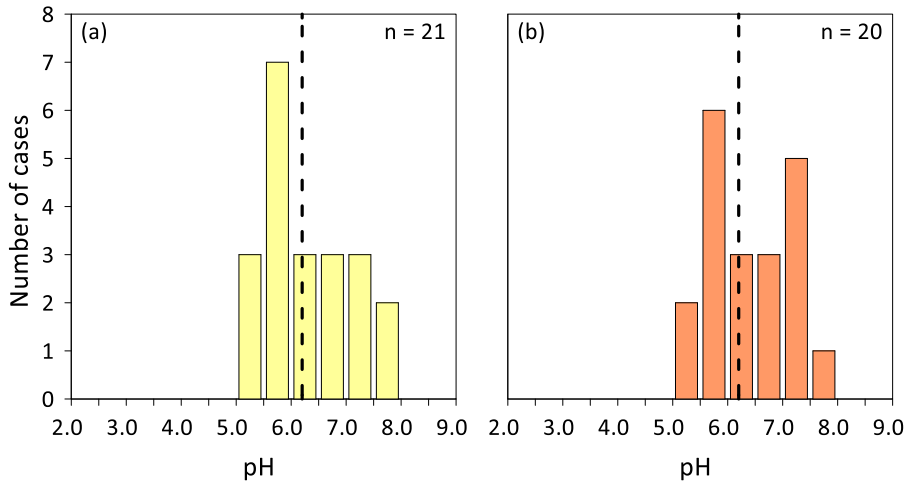

Figure 23 - Frequency distribution of pH in (a) Catania and (b) San Giovanni La Punta rainwater samples. The black dashed lines are the median values.

4.3.1.2 The Electric Conductivity (EC) of rainwater

The EC values of the rainwater samples collected in the two urban areas (six sites), showed great variability during the two years of monitoring, ranging from 10.7 to 305 µS cm^{-1}, with a median of 54.8 µS cm^{-1}. For a better graphical representation, the Log_{10} of the electric conductivity values were calculated. The probability distribution was unimodal for the Palermo area, and bimodal for the Catania area. In the former, the class with the highest frequency (~ 44%) lies in the EC range of 1.4 – 1.8, and in the latter lies in the range of 1.2 – 1.4, with a frequency of ~ 22%. The Electric Conductivity values were generally low in all the sampling sites, with values below 2 (on a Log_{10} basis) for almost 80% of the entire population (Fig. 24a, b). These EC values are typical of rain with a relatively low amount of dissolved ions.

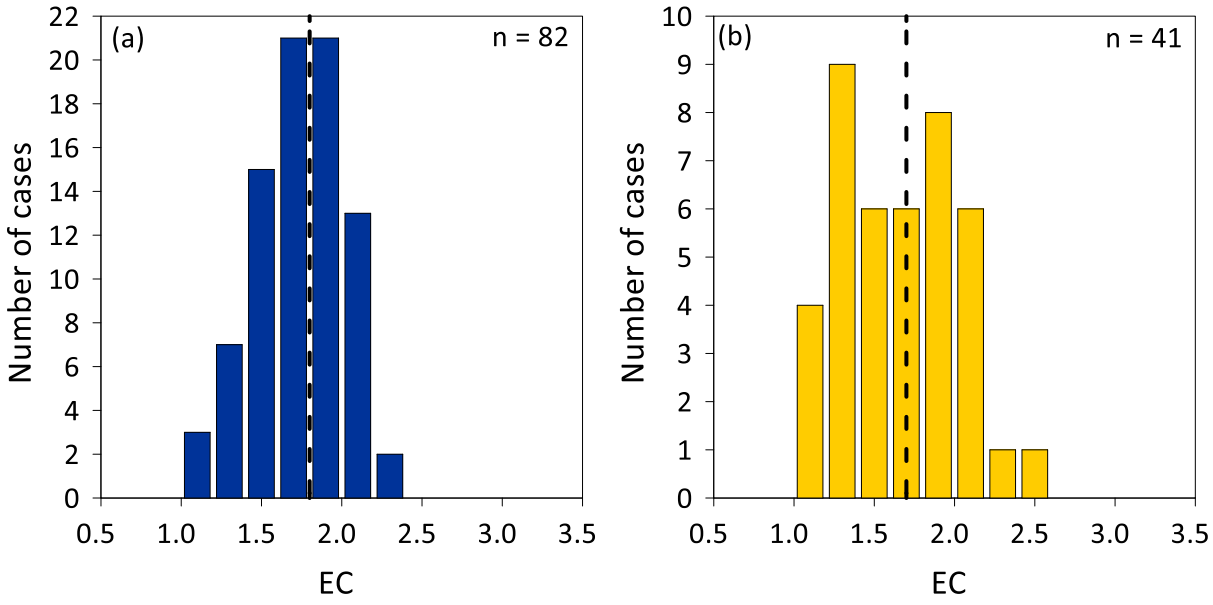

Figure 24 - Frequency distribution of EC (Log_{10}) in Palermo (a) and Catania (b) rainwater samples. The black dashed lines are the geometric means.

The EC values for each monitoring site in the Palermo and Catania urban areas are reported in Table 18 and shown in Figure 25 and Figure 26.

Table 18 - Statistical parameters for rainwater's EC (Log_{10}) at Palermo and Catania urban areas.

Study area	Site	Min	Max	Median	Q1	Q3
Palermo	ARC	1.08	2.33	1.79	1.59	1.73
	UNI	1.23	2.26	1.75	1.64	1.96
	IND	1.38	2.15	1.79	1.53	1.93
	BEL	1.04	1.96	1.75	1.41	1.92
Catania	CAT	1.04	2.16	1.63	1.36	1.86
	GLP	1.04	2.20	1.77	1.30	1.77

The lowest median EC value was measured in the Catania sampling site (1.63), while the highest median EC values were measured at the Archirafi and Indipendenza sites (1.79). The lowest (1.04) values were measured in the Belgio, Catania, and San Giovanni La Punta sampling sites, and the highest (2.33) at the Archirafi sampling site. Very similar values, considering all the descriptive statistical parameters reported in Table 18, were measured in the two sampling sites of the Catania urban area. For the Archirafi sampling sites, the highest frequencies were measured in the EC intervals 1.6 – 1.8 and 1.8 – 2.0 (25%), at Unipa in the interval 1.6 – 1.8 (~ 35%), at Indipendenza in the interval 1.4 – 1.6 (~ 30%), and at Belgio in the interval 1.8 – 2.0 (~ 33%). For the Catania sampling site, the highest frequency was measured in the EC intervals 1.2 – 1.4 and 1.8 – 2.0 (~ 19%), while in the San Giovanni sampling site, it lies in the EC interval 1.2 – 1.4, with a frequency of 25%.

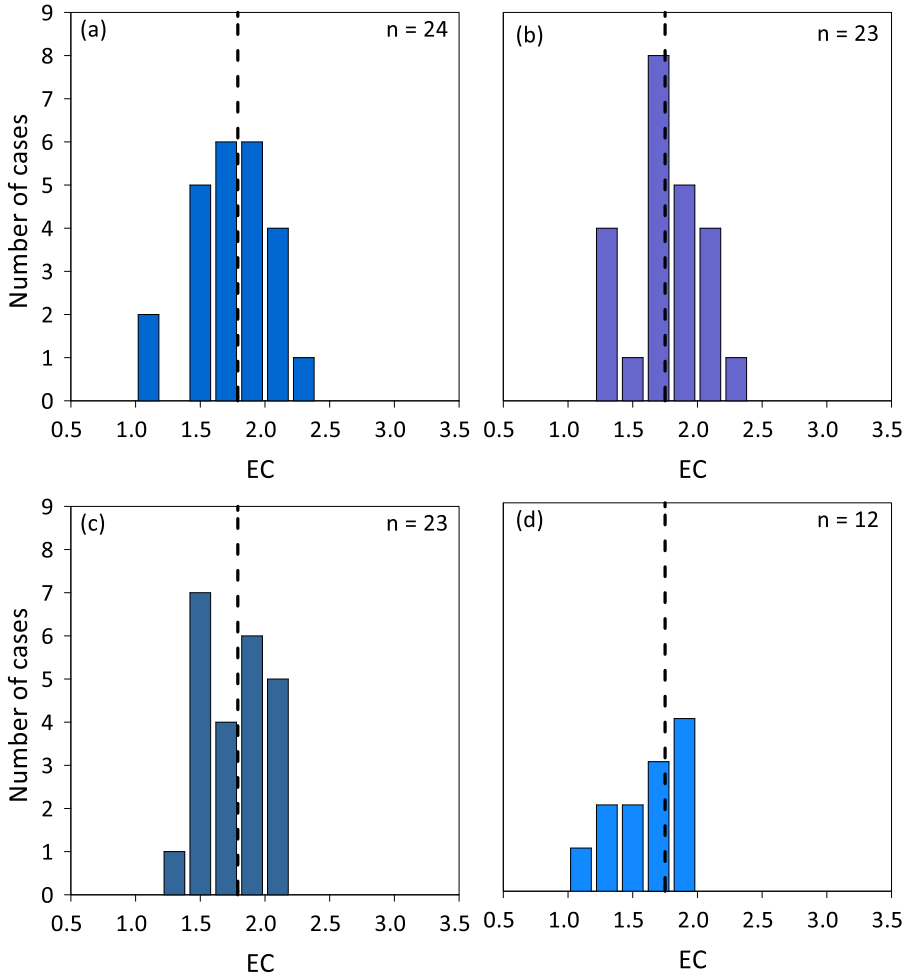

Figure 25 - Frequency distribution of EC in (a) Archirafi, (b) Unipa, (c) Indipendenza, and (d) Belgio rainwater samples. The black dashed lines are the geometric mean values.

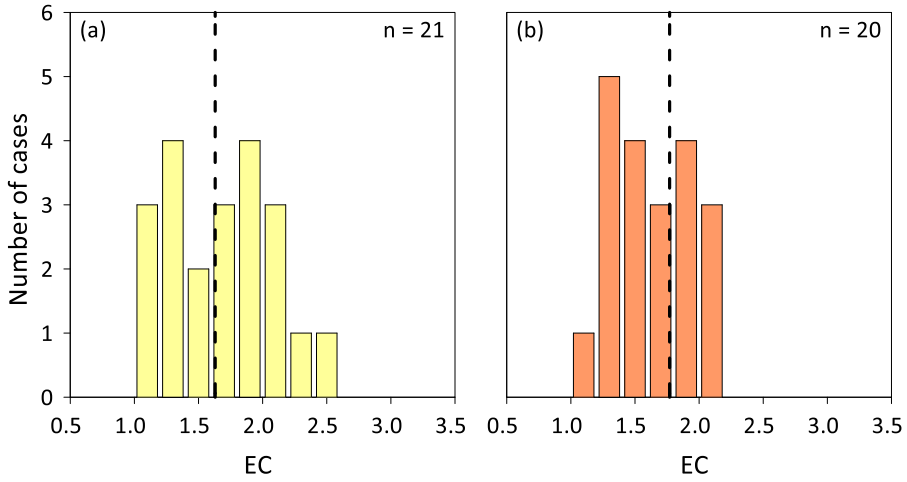

Figure 26 - Frequency distribution of EC in (a) Catania, and (b) San Giovanni La Punta rainwater samples. The black dashed lines are the geometric mean values.

4.3.2 Major inorganic ions

A summary of statistical parameters of the analysed major ions in rainwater samples from Palermo and Catania sampling sites is provided in Table 19. Volume-weighted mean and non-sea-salt concentrations were calculated using equation (2) and (4), respectively. A total of 82 (Palermo urban area) and 41 (Catania urban area) rainwater samples were analysed for major ions. For the F^- the concentration could not be determined in ~ 39% of the samples from the study area of Palermo, while the percentage was 22% for the study area of Catania. Only one rainwater sample collected at the Belgio site had a pH value close to 4.3; in this sample, the HCO_3^- concentration was determined. The HCO_3^- concentration was not determined in ~ 5% and ~ 24% of the samples from the study area of Palermo and Catania, respectively. For NH_4^+ the percentages of < LOQ were ~ 27% and ~ 15% for the two urban areas. For SO_4^{2-} and NO_3^-, only in the Palermo study area, it was not possible to determine the concentrations in ~ 5% and ~ 1% of the cases, respectively. In the Catania study area, it was not possible to quantify the K^+ concentration in ~ 5% of the samples. Finally, in all the analysed samples was possible to quantify the concentrations of Cl^-, Na^+, Mg^{2+}, and Ca^{2+}.

Table 19 - Statistical parameters for major ions (μeq L^{-1}) in Palermo and Catania rainwater samples.

Site		F^-	Cl^-	NO_3^-	SO_4^{2-}	HCO_3^-	Na^+	K^+	NH_4^+	Mg^{2+}	Ca^{2+}
Archirafi	Min	<LOQ	13.4	<LOQ	<LOQ	<LOQ	25.9	2.30	<LOQ	31.8	51.5
	Max	6.00	587	270	328	1059	508	92.9	129	221	1314
	VWM	0.579	240	23.7	48.7	181	224	9.68	13.2	80.2	218
	ss (%)	5.6	100	0	55.9	0.6	100	50.6	0	62.5	4.5
	nss (%)	94.4	0	100	44.1	99.4	0	49.4	100	37.5	95.5
Unipa	Min	<LOQ	13.3	<LOQ	<LOQ	<LOQ	29.5	2.56	<LOQ	31.7	39.4
	Max	8.00	885	185	332	724	786	150	155	214	949
	VWM	0.937	241	31.8	49.9	154	224	8.27	12.7	83.1	169
	ss (%)	3.5	100	0	54.6	0.7	100	59.2	0	60.3	5.8
	nss (%)	96.5	0	100	45.4	99.3	0	40.8	100	39.7	94.2
Indipendenza	Min	<LOQ	13.3	4.55	<LOQ	<LOQ	26.3	3.40	<LOQ	34.0	41.5
	Max	7.10	678	293	320	1411	594	244	171	206	1000
	VWM	1.13	226	32.1	46.4	192	206	14.1	28.3	82.7	228
	ss (%)	2.7	100	0	54.1	0.5	100	31.9	0	55.8	4.0
	nss (%)	97.3	0	100	45.9	99.5	0	68.1	100	44.2	96.0
Belgio	Min	< LOQ	39.0	2.78	< LOQ	40.7	48.0	2.56	< LOQ	32.1	44.5
	Max	15.3	493	231	362	1403	446	139	34.2	197	1428
	VWM	0.451	199	24.5	44.9	172	178	8.11	8.89	76.0	181
	ss (%)	5.8	99.8	0	48.2	0.5	100	48.0	0	52.5	4.3
	nss (%)	94.2	0.2	100	51.8	99.5	0	52.0	100	47.5	95.7

Site		F^-	Cl^-	NO_3^-	SO_4^{2-}	HCO_3^-	Na^+	K^+	NH_4^+	Mg^{2+}	Ca^{2+}
Catania	Min	< LOQ	10.9	5.50	20.2	< LOQ	27.1	< LOQ	< LOQ	18.3	25.3
	Max	321	644	553	733	951	553	145	122	321	1494
	VWM	3.84	169	37.9	67.7	59.2	159	9.49	15.1	53.3	137
	ss (%)	0.6	100	0.00	28.5	1.3	100	36.6	0.00	66.9	5.1
	nss (%)	99.4	0.00	100	71.5	98.7	0.00	63.4	100	33.1	94.9
San Giovanni La Punta	Min	< LOQ	62.0	7.30	22.1	< LOQ	57.0	< LOQ	< LOQ	18.2	33.7
	Max	316	360	272	526	674	338	139	186	203	1199
	VWM	2.63	151	23.7	51.4	69.9	140	7.32	27.7	44.6	126
	ss (%)	0.8	100	0.00	33.0	1.0	100	41.6	0.00	70.1	4.9
	nss (%)	99.2	0.00	100	67.0	99.0	0.00	58.4	100	29.9	95.1

Chemical abundances, expressed as μeq L^{-1}, are represented by Tukey box plots, one set for each monitored site (Fig. 27).

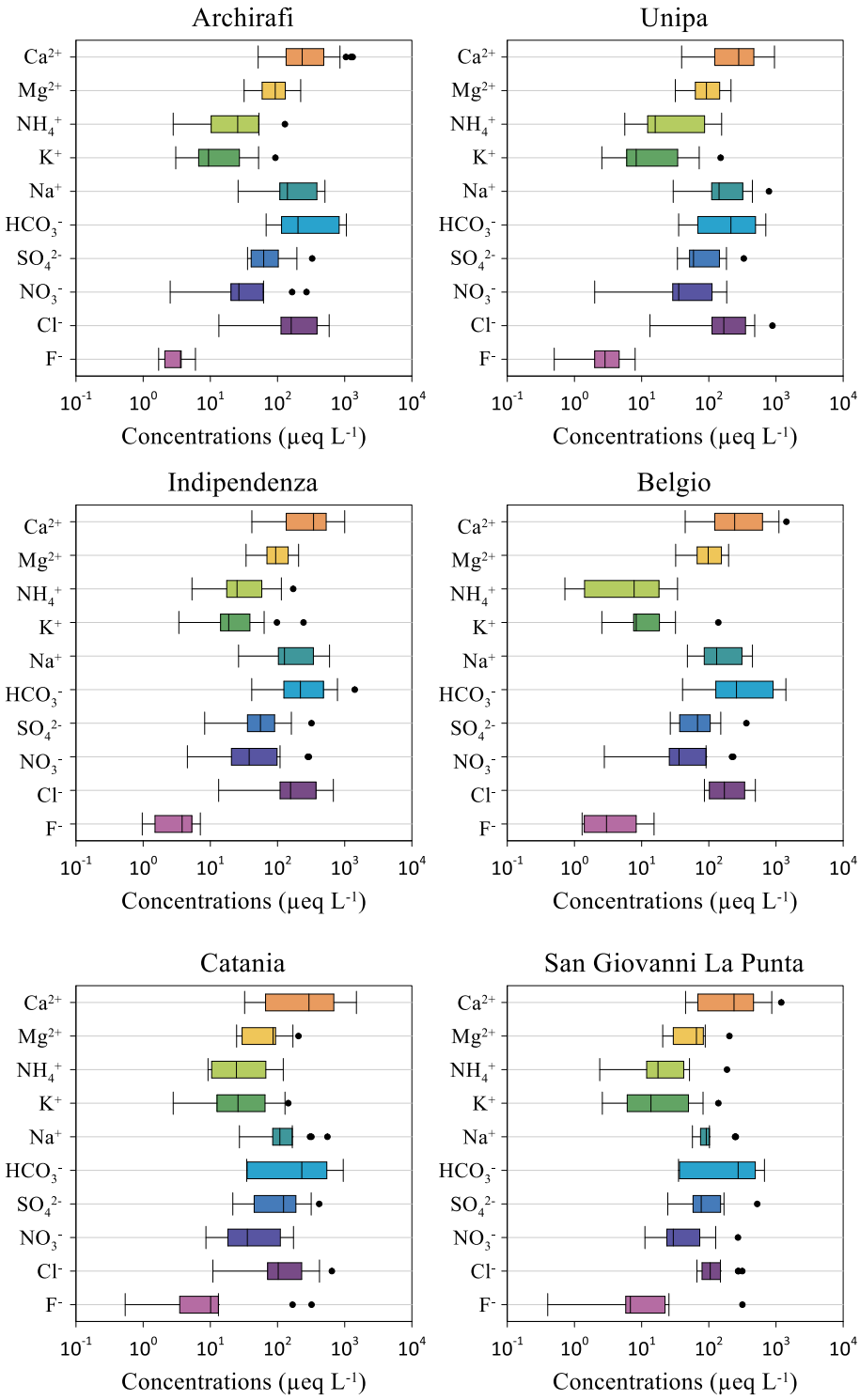

Figure 27 - Major ion concentrations (µeq L^{-1}) in Palermo (four sites) and Catania (two sites) rainwater samples.

The most saline rainwater sample, in terms of Total Dissolved Solids (TDS), was collected at the Catania sampling site, with a value of 4165 µeq L^{-1} (143 mg L^{-1}), in the sampling period 14 July

– 25 August 2022. The less saline rainwater sample was collected in the same site, with a value of 215 μeq L^{-1} (6.39 mg L^{-1}), in the sampling period of 22 November – 20 December 2022. Please refer to Table 16 for the correspondence between the sampling period and the sequential sample number.

In all the sampling sites, the relative VWM concentrations of the major anions follow the sequence $Cl^- > HCO_3^- > SO_4^{2-} > NO_3^- > F^-$, except for the Catania sampling site, where the relative contribution of sulfate (20.0%) was higher than that of bicarbonate (17.5%). Therefore, chloride was the main anion, with relative abundances of 48.6%, 50.6%, 45.5%, 46.2%, 50.1%, and 50.6% in Archirafi, Unipa, Indipendenza, Belgio, Catania, and San Giovanni La Punta, respectively (Fig. 28). The highest bicarbonate VWM concentration was measured at Indipendenza, with a value of 192 μeq L^{-1}, and the lowest at Catania (59.2 μeq L^{-1}). The highest chloride VWM concentration was measured at the Archirafi and the Unipa sampling site, with a value of ~ 241 μeq L^{-1}, the lowest at San Giovanni La Punta (151 μeq L^{-1}). Similar relative contributions were observed for sulfate in the Palermo urban area, up to 10.4% for the Unipa sampling site. Higher relative contributions were observed for the same ion in the Catania urban area (20.0%, and 17.2% at the Catania and San Giovanni La Punta sampling sites, respectively). Consequently, the highest VWM concentration was measured at the Catania sampling site (67.7 μeq L^{-1}), and the lowest at Belgio (44.9 μeq L^{-1}). Relative contributions between 4.79% (Archirafi), and 11.2% (Catania) were observed for nitrate, with the highest VMW concentration measured in the Catania sampling site (37.9 μeq L^{-1}), and the lowest (23.7 μeq L^{-1}) at Unipa and San Giovanni La Punta sampling sites. Fluoride was the less abundant ion in all the sampling sites. Very low relative contributions, up to 0.226% (Indipendenza) were observed for the Palermo urban area, with the highest VMW concentration measured at Indipendenza (1.13 μeq L^{-1}). Higher relative contributions were observed in the urban area of Catania, both at the Catania site (1.14%) and the San Giovanni La Punta (0.879%), and VWM concentrations up to 3.84 μeq L^{-1} in the former.

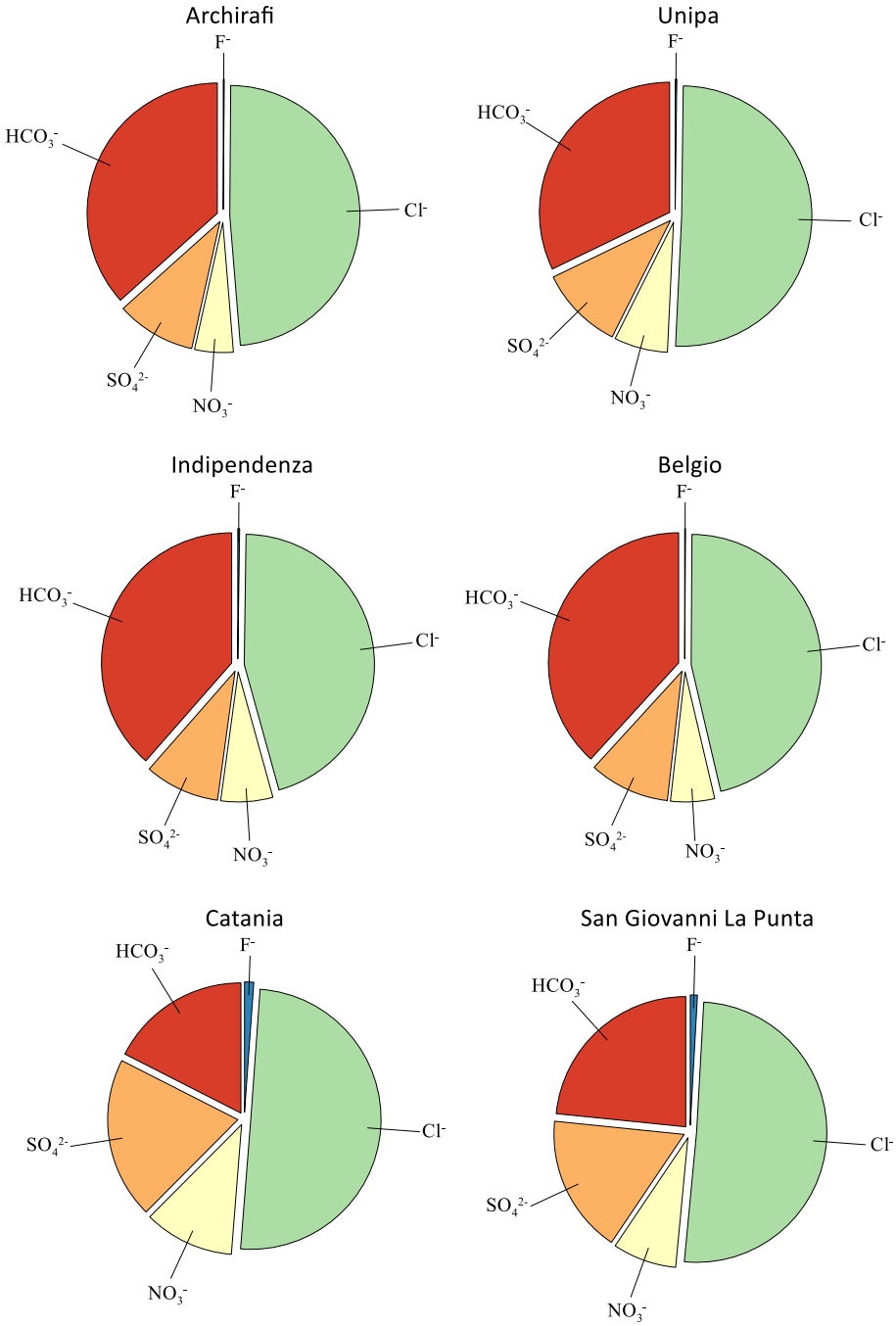

Figure 28 - Relative abundances (Eq%) of any major anions in rainwater samples from Palermo and Catania urban areas.

As regards major cations, the sequence of relative abundances was $Na^+ > Ca^{2+} > Mg^{2+} > NH_4^+ > K^+$ for the Archirafi, Unipa, Catania, and San Giovanni La Punta sampling sites. A similar sequence was observed for the Indipendenza and Belgio sampling sites, where the relative abundances of Ca^{2+} (40.7% and 40.0%) were slightly higher than that of Na^+ (36.9% and 39.4%).

Therefore, sodium and calcium were the main cations, with relative abundances of 41.1%, 45.0%, 36.9%, 39.4%, 42.6%, and 40.5% for the former, and 40.0%, 34.0%, 40.7%, 40.0%, 36.7%, and 36.5% for the latter, in Archirafi, Unipa, Indipendenza, Belgio, Catania, and San Giovanni La Punta sampling sites, respectively (Fig. 29).

The highest calcium VWM concentration was measured at Indipendenza, with a value of 233 μeq L^{-1}, and the lowest was measured at San Giovanni La Punta (126 μeq L^{-1}). For sodium, the highest VWM concentrations were calculated for Archirafi and Unipa sampling sites (224 μeq L^{-1}), while the lowest was at San Giovanni La Punta (140 μeq L^{-1}). Very similar relative contributions were observed for magnesium, between 12.9% (San Giovanni La Punta), and 16.8% (Belgio), with the lowest VWM concentration (44.6 μeq L^{-1}) measured in the former. The highest VWM concentration for Mg^{2+} was calculated for the Indipendenza site (84.5 μeq L^{-1}). Low relative contributions were calculated for NH_4^+, up to 8.03% at San Giovanni La Punta. Nevertheless, the highest VWM concentration of this cation was calculated at the Indipendenza sampling site, equal to 28.3 μeq L^{-1}. Potassium relative contributions were very low, up to 2.53% at the Indipendenza and Catania sampling sites. The highest VMW concentration for K^+ (14.1 μeq L^{-1}) was calculated for the Indipendenza site. The lowest K^+ VMW concentration was calculated for San Giovanni La Punta, equal to 7.32 μeq L^{-1}.

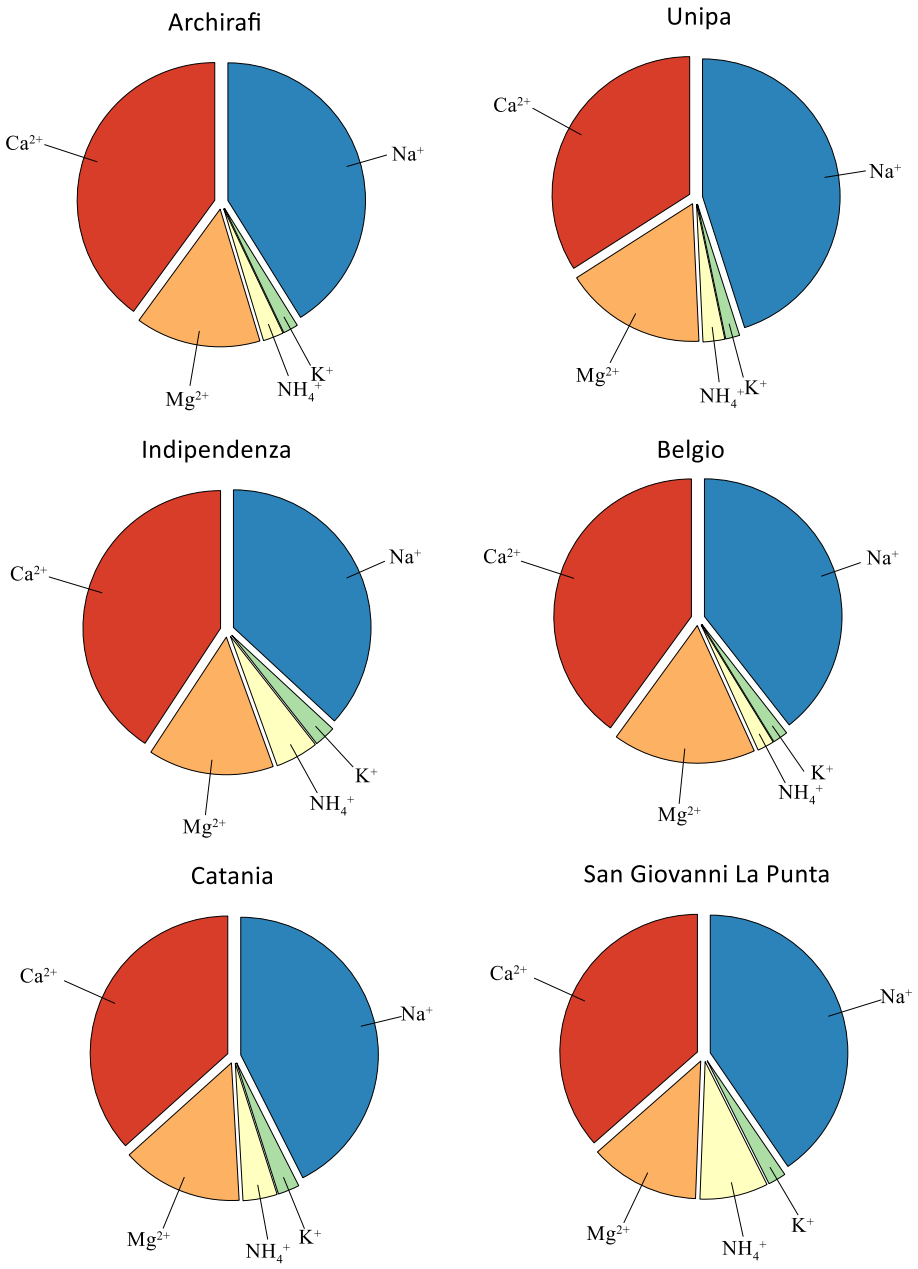

Figure 29 - Relative abundances (Eq%) of any major cations in rainwater samples from Palermo and Catania urban areas.

4.3.3 Minor and trace elements concentrations

4.3.3.1 Rainwater samples

A summary of statistical parameters of the analysed minor and trace elements in the rainwater samples from Palermo and Catania urban areas is provided in Table 20 and Figure 30. A total of 82 (Palermo urban area) and 41 (Catania urban area) rainwater samples were analysed for minor and

trace elements. In the Palermo rainwater samples, it was not possible to determine the concentration of Sn and Cs in ~ 66% and in ~ 48% of the cases. For B, Al, V, Cr, Cu, Zn, As, Rb, Sr, Mo, and Sb it was always possible to determine the concentrations, while for the other elements, it was not possible to do so in between approximately 1% and 25% of the cases. For the rainwater samples of the Catania urban area, it was not possible to determine the concentration of Sn and Cs in ~ 56% and ~ 37% of the cases, respectively. For B, Al, V, Cr, Fe, Ni, Cu, Zn, As, Rb, Sr, Mo, Sb, Ba, and Tl it was always possible to determine the concentrations, while for the other elements, it was not possible to do so in between approximately 1% and 10% of the cases.

Table 20 - Statistical parameters for minor and trace element concentrations (µg L^{-1}) in the sampling sites of the Palermo and Catania urban areas. Sample n. is the number of samples in which the maximum concentration was measured for each element.

Archirafi	Element	Li	B	Al	Ti	V	Cr	Mn	Fe	Co	Ni	Cu	Zn	As
	Min	< LOQ	3.11	0.680	< LOQ	0.0840	0.0180	< LOQ	0.619	< LOQ	0.0310	0.349	0.380	0.0290
	Max	1.64	23.5	135	1.62	2.54	0.473	24.6	18.1	0.308	1.34	12.4	33.5	0.511
	Sample n.	17	03	16	06	16	06	06	04	06	04	17	06	16
	VWM	0.181	6.18	20.5	0.189	0.371	0.100	1.20	3.51	0.0175	0.244	1.95	6.87	0.0963
	Element	Se	Br	Rb	Sr	Mo	Cd	Sn	Sb	Cs	Ba	Tl	Pb	U
	Min	< LOQ	< LOQ	0.154	5.76	0.0150	0.00700	< LOQ	0.0750	< LOQ	1.52	< LOQ	< LOQ	< LOQ
	Max	0.421	56.2	10.2	79.4	0.468	0.0630	0.0440	1.28	0.0370	80.9	0.0310	1.71	0.0650
	Sample n.	16	22	17	03	06	07	06	16	17	02	03	06	16
	VWM	0.143	25.5	0.525	13.9	0.126	0.0198	0.00629	0.202	0.00317	8.59	0.00611	0.0458	0.00411

Unipa	Element	Li	B	Al	Ti	V	Cr	Mn	Fe	Co	Ni	Cu	Zn	As
	Min	< LOQ	2.28	1.22	< LOQ	0.0720	0.0220	< LOQ	0.373	< LOQ	< LOQ	0.319	1.89	0.00900
	Max	0.401	16.5	36.3	1.02	1.63	2.14	44.6	19.7	0.510	2.20	23.2	29.2	0.231
	Sample n.	13	13	15	04	04	20	04	04	04	20	04	17	04
	VWM	0.126	6.47	7.10	0.133	0.323	0.241	1.08	2.45	0.0142	0.297	1.75	5.64	0.0783
	Element	Se	Br	Rb	Sr	Mo	Cd	Sn	Sb	Cs	Ba	Tl	Pb	U
	Min	0.0320	< LOQ	0.0840	4.63	0.0110	< LOQ	< LOQ	0.0500	< LOQ	1.88	< LOQ	< LOQ	< LOQ
	Max	0.485	82.3	1.51	68.9	0.269	0.0710	0.0290	1.83	0.00900	114	0.0190	0.292	0.0210
	Sample n.	13	13	04	04	04	18	04	18	13	02	23	04	04
	VWM	0.137	26.6	0.260	12.2	0.0434	0.0159	0.00535	0.322	0.00213	8.41	0.00607	0.0321	0.00250

Indipendenza	Element	Li	B	Al	Ti	V	Cr	Mn	Fe	Co	Ni	Cu	Zn	As
	Min	< LOQ	2.78	0.942	< LOQ	0.0900	0.0190	< LOQ	0.976	< LOQ	0.0380	0.870	2.46	0.0160
	Max	0.661	20.8	105	2.19	1.73	1.07	36.2	70.8	0.429	1.91	19.1	18.9	0.472
	Sample n.	03	16	07	03	04	16	04	07	03	16	16	06	17
	VWM	0.160	6.89	16.1	0.276	0.351	0.121	1.46	8.14	0.0258	0.178	2.61	5.65	0.101
	Element	Se	Br	Rb	Sr	Mo	Cd	Sn	Sb	Cs	Ba	Tl	Pb	U
	Min	< LOQ	< LOQ	0.125	4.90	0.0170	< LOQ	< LOQ	0.0810	< LOQ	1.18	< LOQ	< LOQ	< LOQ
	Max	0.326	69.6	3.64	77.0	0.679	0.0490	0.0830	0.798	0.0100	27.3	0.0320	0.800	0.0300
	Sample n.	11	13	03	04	03	14	03	22	13	03	18	07	03
	VWM	0.130	25.5	0.395	13.3	0.0799	0.0147	0.00751	0.224	0.00234	6.05	0.00773	0.0949	0.00315

Belgio	Element	Li	B	Al	Ti	V	Cr	Mn	Fe	Co	Ni	Cu	Zn	As
	Min	0.0300	4.21	1.21	< LOQ	0.0850	0.0330	0.310	1.03	< LOQ	0.0780	0.753	1.31	0.0260
	Max	0.654	27.5	50.4	1.59	1.92	29.0	35.5	548	0.328	2.24	17.4	22.4	0.349
	Sample n.	04	04	09	04	04	02	04	02	04	06	04	06	04
	VWM	0.114	6.39	9.03	0.0670	0.320	1.65	2.11	33.2	0.0370	0.288	2.67	7.34	0.0703
	Element	Se	Br	Rb	Sr	Mo	Cd	Sn	Sb	Cs	Ba	Tl	Pb	U
	Min	< LOQ	5.56	0.125	5.19	0.0260	< LOQ	< LOQ	0.0660	< LOQ	1.37	< LOQ	< LOQ	< LOQ
	Max	0.612	46.7	1.67	88.0	2.97	0.263	0.0560	1.58	0.00300	42.9	0.0190	0.427	0.0360
	Sample n.	04	11	03	04	02	06	06	04	09	02	04	09	05
	VWM	0.127	21.7	0.235	11.0	0.220	0.0163	0.00684	0.246	0.000937	7.62	0.00396	0.0737	0.00285

Catania	Element	Li	B	Al	Ti	V	Cr	Mn	Fe	Co	Ni	Cu	Zn	As
	Min	< LOQ	2.22	3.40	0.0690	0.0720	0.0300	0.0490	1.67	< LOQ	0.0570	0.187	0.939	0.0280
	Max	1.11	34.7	183	4.77	5.04	3.22	98.3	78.8	0.777	3.26	82.9	140	1.44
	Sample n.	17	17	05	04	17	14	17	14	17	17	17	17	17
	VWM	0.111	6.09	13.2	0.259	0.459	0.185	5.46	6.96	0.0572	0.293	3.79	11.4	0.122
	Element	Se	Br	Rb	Sr	Mo	Cd	Sn	Sb	Cs	Ba	Tl	Pb	U
	Min	0.0330	< LOQ	0.114	3.61	0.00900	< LOQ	< LOQ	0.0370	< LOQ	1.04	0.00300	0.0150	< LOQ
	Max	3.66	54.1	10.4	161	1.08	0.416	0.0600	4.28	0.0460	29.8	0.525	0.214	0.0560
	Sample n.	04	12	17	15	17	17	17	17	17	17	17	03	15
	VWM	0.275	20.9	0.616	15.2	0.0722	0.0327	0.00817	0.307	0.00442	4.40	0.0285	0.0573	0.00424

San Giovanni La Punta	Element	Li	B	Al	Ti	V	Cr	Mn	Fe	Co	Ni	Cu	Zn	As
	Min	< LOQ	1.84	1.61	< LOQ	0.101	0.0280	< LOQ	1.48	< LOQ	0.0500	0.180	1.45	0.0410
	Max	0.634	16.5	99.8	2.11	4.63	0.621	38.2	30.0	0.357	0.768	21.3	29.8	0.839
	Sample n.	04	04	05	03	12	12	05	03	03	03	04	11	04
	VWM	0.0847	4.84	13.1	0.171	0.446	0.0765	2.67	3.94	0.0288	0.182	2.22	8.94	0.107
	Element	Se	Br	Rb	Sr	Mo	Cd	Sn	Sb	Cs	Ba	Tl	Pb	U
	Min	< LOQ	2.40	0.108	4.01	0.0130	0.00500	< LOQ	0.0450	< LOQ	1.50	0.000160	< LOQ	< LOQ
	Max	6.84	48.5	5.72	120	1.75	0.115	0.159	1.49	0.0150	21.7	0.200	0.128	0.0790
	Sample n.	04	23	17	04	04	11	06	20	17	04	04	03	04
	VWM	0.185	18.5	0.430	11.7	0.0813	0.0246	0.00713	0.203	0.00256	4.02	0.0190	0.0464	0.00476

In all Palermo's sampling sites, the lowest VWM concentrations were calculated for caesium, between 0.0009 µg L^{-1} (Belgio) and 0.003 µg L^{-1} (Archirafi), the highest for bromide, with values from 21.7 µg L^{-1} (Belgio) and 26.6 µg L^{-1} (Unipa). In the Catania sampling site, the lowest VWM concentration was calculated for uranium and caesium (0.004 µg L^{-1}), the highest for bromide (20.9 µg L^{-1}), while in the San Giovanni La Punta sampling site, the lowest VWM concentration was calculated for caesium (0.002 µg L^{-1}), and the highest for bromide (18.6 µg L^{-1}).

For V, Mn, Co, Cu, Zn, As, Se, Rb, Sr, Cd, Cs, and Tl the highest VWM concentrations were calculated for the Catania sampling site. For Li, Al, and Ba the highest VWM concentrations were calculated for the Archirafi sampling site, while for Ni, Br, and Sb in the Unipa sampling site, and Cr, Fe, and Mo in the Belgio sampling site. Finally, the highest VWM concentrations of B, Ti, and Pb were calculated for the Indipendenza site. The VMW concentrations of Sn were similar in the Indipendenza and Catania sampling sites. Uranium concentrations were similar in all the sampling sites. The concentrations of the elements analysed did not only show great differences between the different sites. A relevant intra-site variability, up to three orders of magnitude, was observed for different periods of sampling (Fig. 30).

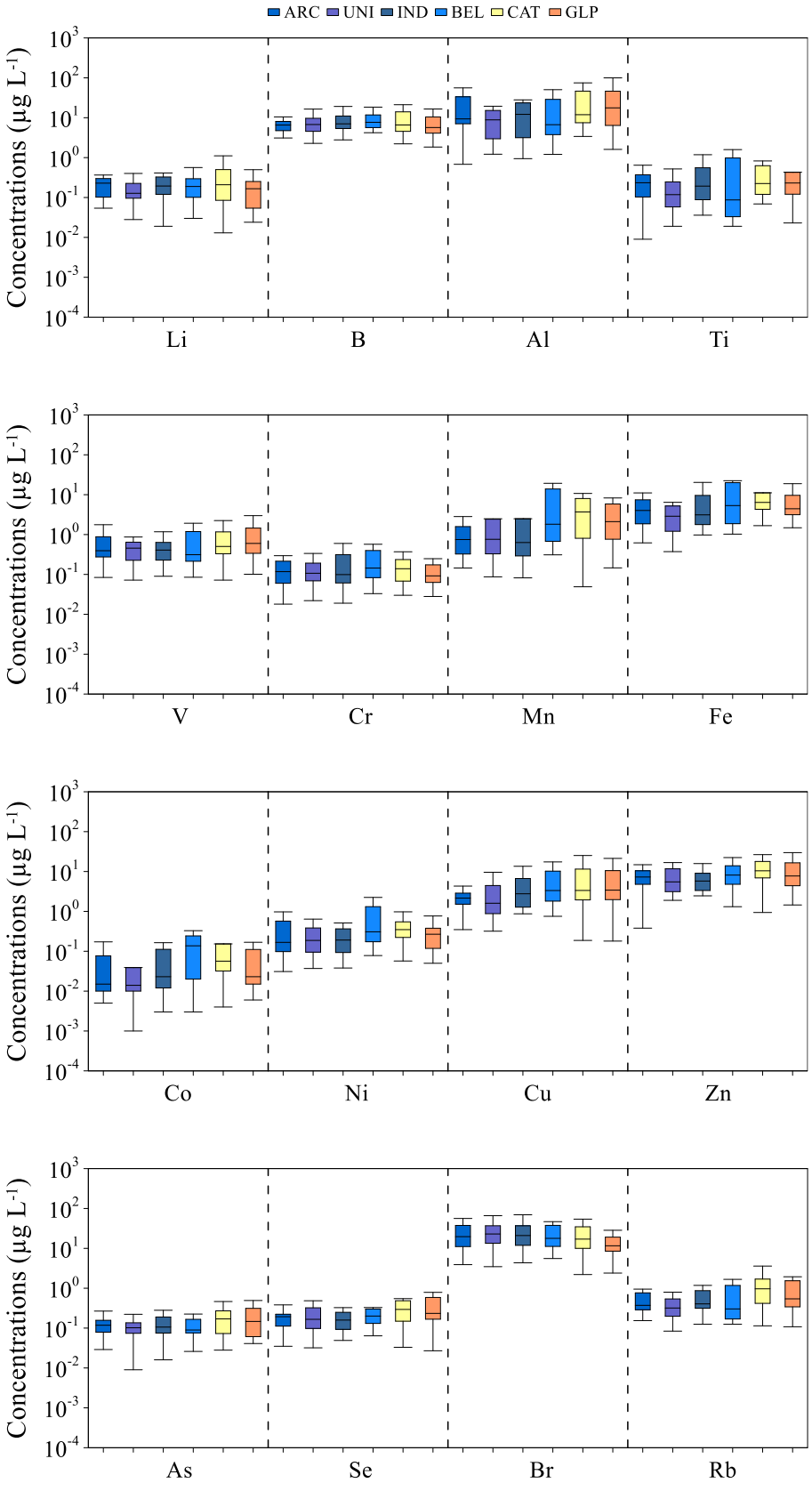
ARC UNI IND BEL CAT GLP
Concentrations (µg L-1)
Li
B
Al
Ti
V
Cr
Mn
Fe
Co
Ni
Cu
Zn
As
Se
Br
Rb

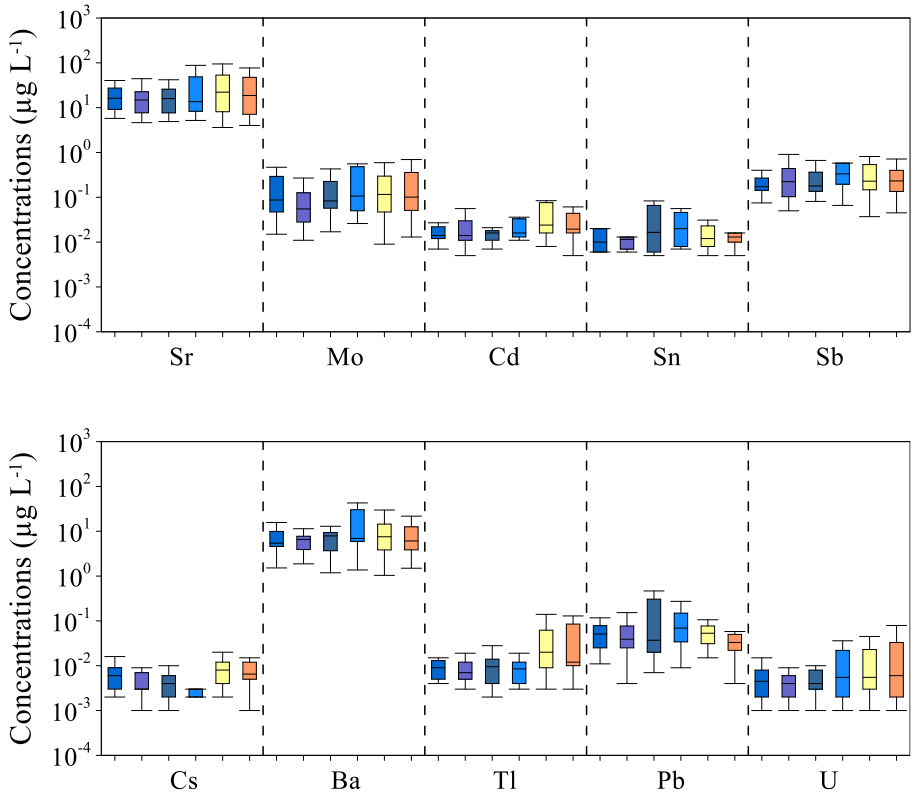

Figure 30 - Minor and trace element concentrations (µg L^{-1}) in the rainwater samples from the Palermo and Catania urban areas. The elements are ordered from highest to lowest atomic weight.

4.3.3.2 Insoluble fraction

As discussed in paragraph 3.1.3, to evaluate the contribution of the insoluble fraction of the atmospheric deposition, water samples were filtered to separate the insoluble particles (> 0.45 µm). A statistical summary of the analysed minor and trace elements in the insoluble fraction solutions is provided in Table 21, and Figure 31. A total of 81 and 41 insoluble fraction solutions were analysed for minor and trace element concentrations from the Palermo and the Catania urban areas, respectively. For As, Mo, and Co it was not possible to determine the concentration in the ~ 12%, ~ 2%, and ~ 1% of the samples. For the remaining elements, the concentrations were quantified in all the samples. For the Catania urban area, it was always possible to quantify the concentrations of all the minor and trace elements, except for As (~ 5%).

Table 21 - Statistical parameters for minor and trace element concentrations in Archirafi, Unipa, Indipendenza, Belgio, Catania, and San Giovanni La Punta insoluble fraction solutions. The concentrations are in µg L^{-1}, except for Al, Ti, Fe, and Zn (mg L^{-1}).

	Element	Li	B	Al	Ti	V	Cr	Mn	Fe	Co	Ni	Cu	Zn	As
Archirafi	Min	1.23	6.63	1.01	0.0410	2.37	6.85	38.6	1.74	0.696	6.33	23.6	0.111	0.396
	Max	56.3	87.9	53.0	2.25	100	125	897	53.7	22.8	64.7	505	1.30	11.4
	Median	10.5	27.2	13.7	0.445	28.9	52.2	251	14.8	5.94	21.9	106	0.509	3.62
	Element	Se	Br	Rb	Sr	Mo	Cd	Sn	Sb	Cs	Ba	Tl	Pb	U
	Min	n.d.	n.d.	n.d.	13.8	0.347	n.d.	n.d.	n.d.	n.d.	16.1	n.d.	11.0	n.d.
	Max	n.d.	n.d.	n.d.	323	7.12	n.d.	n.d.	n.d.	n.d.	520	n.d.	134	n.d.
	Median	n.d.	n.d.	n.d.	54.8	1.45	n.d.	n.d.	n.d.	n.d.	125	n.d.	36.9	n.d.

	Element	Li	B	Al	Ti	V	Cr	Mn	Fe	Co	Ni	Cu	Zn	As
Unipa	Min	1.60	1.61	1.69	0.0579	3.36	7.35	35.0	1.85	0.395	6.53	30.0	0.125	0.145
	Max	172	255	285	19.0	751	313	3870	264	100	162	1691	2.14	37.0
	Median	19.6	30.3	17.9	0.402	38.9	50.0	269	17.2	7.70	23.7	105	0.392	4.91
	Element	Se	Br	Rb	Sr	Mo	Cd	Sn	Sb	Cs	Ba	Tl	Pb	U
	Min	n.d.	n.d.	n.d.	11.4	0.478	n.d.	n.d.	n.d.	n.d.	22.7	n.d.	6.99	n.d.
	Max	n.d.	n.d.	n.d.	2645	10.7	n.d.	n.d.	n.d.	n.d.	1657	n.d.	213	n.d.
	Median	n.d.	n.d.	n.d.	50.5	1.76	n.d.	n.d.	n.d.	n.d.	156	n.d.	38.2	n.d.

	Element	Li	B	Al	Ti	V	Cr	Mn	Fe	Co	Ni	Cu	Zn	As
Indipendenza	Min	1.76	5.82	2.34	0.0700	4.82	12.1	33.0	2.52	0.730	6.59	53.7	0.188	0.136
	Max	174	387	188	3.42	316	440	2677	174	58.3	223	1166	2.65	39.0
	Median	24.4	57.7	27.8	0.652	56.0	105	425	27.7	10.6	37.9	251	0.603	8.05
	Element	Se	Br	Rb	Sr	Mo	Cd	Sn	Sb	Cs	Ba	Tl	Pb	U
	Min	n.d.	n.d.	n.d.	15.7	0.426	n.d.	n.d.	n.d.	n.d.	25.2	n.d.	10.5	n.d.
	Max	n.d.	n.d.	n.d.	429	15.3	n.d.	n.d.	n.d.	n.d.	1112	n.d.	399	n.d.
	Median	n.d.	n.d.	n.d.	109	4.37	n.d.	n.d.	n.d.	n.d.	247	n.d.	86.8	n.d.

	Element	Li	B	Al	Ti	V	Cr	Mn	Fe	Co	Ni	Cu	Zn	As
Belgio	Min	3.11	4.88	4.23	0.113	10.0	32.7	54.7	5.11	1.15	11.7	86.5	0.144	1.42
	Max	101	169	104	3.56	240	289	1501	109	42.5	107	1311	1.67	23.4
	Median	13.7	37.1	15.8	0.429	34.4	96.9	229	16.7	5.37	23.7	196	0.522	3.59
	Element	Se	Br	Rb	Sr	Mo	Cd	Sn	Sb	Cs	Ba	Tl	Pb	U
	Min	n.d.	n.d.	n.d.	29.5	1.33	n.d.	n.d.	n.d.	n.d.	33.6	n.d.	13.1	n.d.
	Max	n.d.	n.d.	n.d.	423	19.8	n.d.	n.d.	n.d.	n.d.	763	n.d.	220	n.d.
	Median	n.d.	n.d.	n.d.	57.8	3.74	n.d.	n.d.	n.d.	n.d.	156	n.d.	40.9	n.d.

	Element	Li	B	Al	Ti	V	Cr	Mn	Fe	Co	Ni	Cu	Zn	As
Catania	Min	1.17	7.85	3.34	0.268	9.46	7.58	43.9	3.23	0.553	4.15	32.1	0.0770	0.0349
	Max	388	676	1222	92.1	3344	509	19097	1179	437	259	2999	2.08	63.7
	Median	25.8	60.8	39.5	2.27	91.2	67.6	589	36.0	14.2	36.9	196	0.479	6.79
	Element	Se	Br	Rb	Sr	Mo	Cd	Sn	Sb	Cs	Ba	Tl	Pb	U
	Min	n.d.	n.d.	n.d.	2.33	0.382	n.d.	n.d.	n.d.	n.d.	32.3	n.d.	4.22	n.d.
	Max	n.d.	n.d.	n.d.	12760	12.7	n.d.	n.d.	n.d.	n.d.	3461	n.d.	196	n.d.
	Median	n.d.	n.d.	n.d.	325	3.46	n.d.	n.d.	n.d.	n.d.	277	n.d.	43.7	n.d.

	Element	Li	B	Al	Ti	V	Cr	Mn	Fe	Co	Ni	Cu	Zn	As
San Giovanni La Punta	Min	9.82	19.8	17.0	1.00	38.8	27.9	26.6	16.6	6.07	15.8	89.9	0.226	2.31
	Max	437	680	1091	77.4	2339	523	18238	898	301	288	3335	9.05	105
	Median	104	178	198	12.1	474	132	2831	176	70.3	82.2	644	1.28	20.6
	Element	Se	Br	Rb	Sr	Mo	Cd	Sn	Sb	Cs	Ba	Tl	Pb	U
	Min	n.d.	n.d.	n.d.	106	1.16	n.d.	n.d.	n.d.	n.d.	125	n.d.	18.8	n.d.
	Max	n.d.	n.d.	n.d.	8550	51.4	n.d.	n.d.	n.d.	n.d.	5549	n.d.	458	n.d.
	Median	n.d.	n.d.	n.d.	1474	9.89	n.d.	n.d.	n.d.	n.d.	1346	n.d.	91.5	n.d.

In the Archirafi sampling site the median concentrations ranged from 1.45 µg L^{-1} for Mo to 14.8 mg L^{-1} for Fe, at Unipa from 1.76 µg L^{-1} for Mo to 17.9 mg L^{-1} for Al, from 4.37 µg L^{-1} (Mo) to 27.8 mg L^{-1} (Al) at Indipendenza, and from 3.59 µg L^{-1} (As) to 16.7 mg L^{-1} (Fe) at the Belgio sampling site. At the Catania sampling site, the median concentrations ranged from 3.46 µg L^{-1} (Mo) to 39.5 mg L^{-1} (Al) and at San Giovanni La Punta they ranged from 9.89 µg L^{-1} (Mo) to 198 mg L^{-1}

(Al). Therefore, the lowest median concentrations were calculated for Mo and As, while the highest median concentrations were calculated for Al and Fe. For all the analysed elements, the highest median concentrations were calculated for the San Giovanni La Punta sampling site, up to one order of magnitude higher than the other urban sampling sites. At Archirafi the median concentrations were generally lower than at the other urban sites.

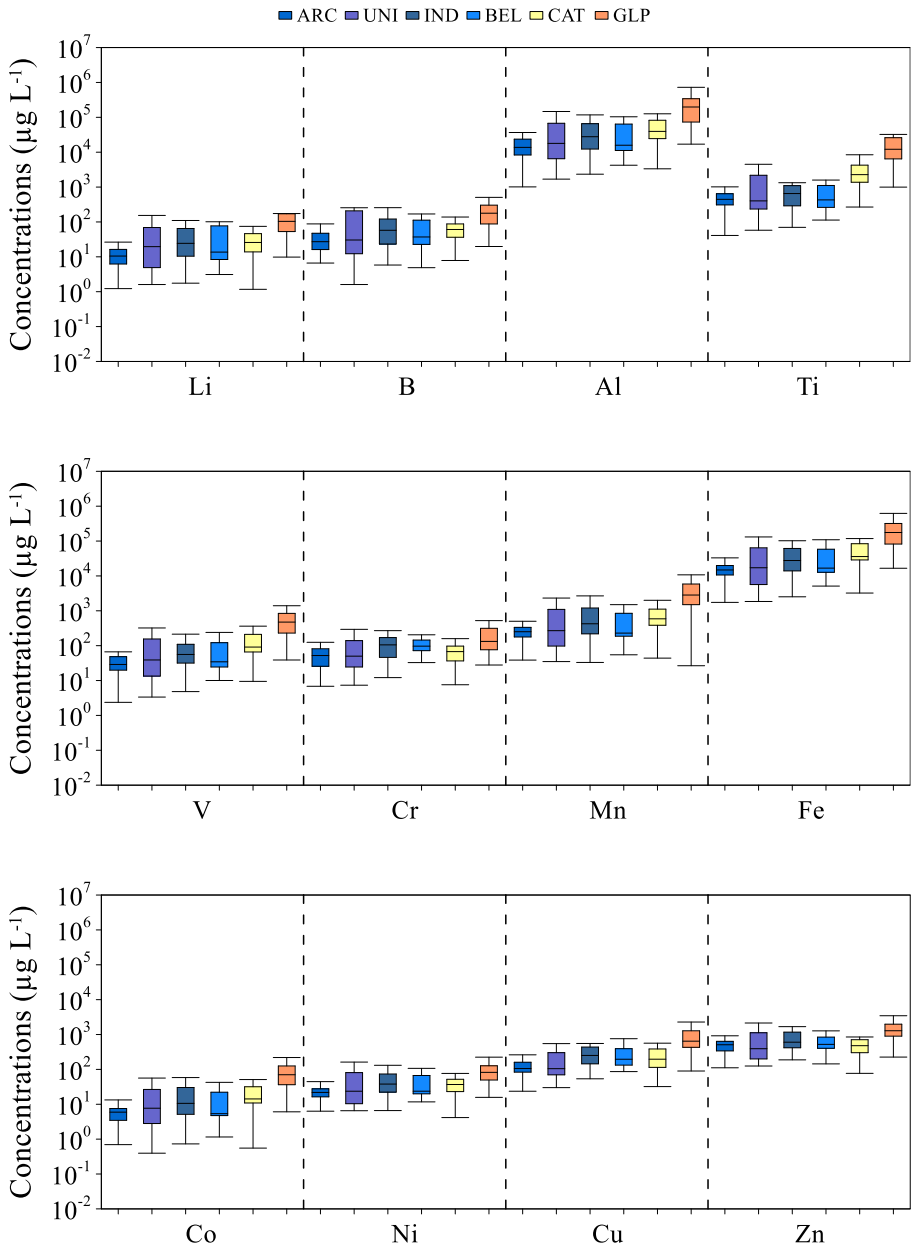

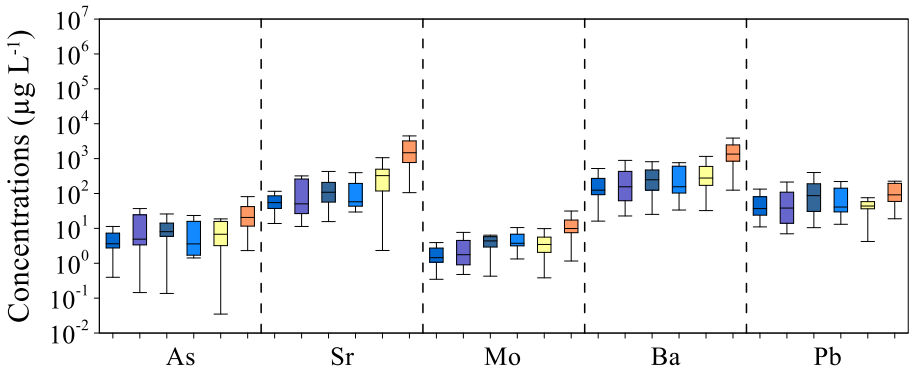

Figure 31 - Minor and trace element concentrations (µg L^{-1}) in the insoluble fraction solutions at the Palermo and Catania urban areas. The elements are ordered from highest to lowest atomic weight.

4.3.3.3 Rinse solutions

The concentration of minor and trace elements in the material remaining adhered to the surfaces of the bulk collector was quantified by analysing a rinse aliquot prepared according to the procedure described in paragraph 3.1.2. The concentrations of the analysed minor and trace elements in the rinse solutions from the Palermo and Catania urban areas are provided in Table 22. A total of seven (Palermo urban area) and four (Catania urban area) rinse solutions, two for each site, except for Belgio, were analysed for minor and trace element concentrations. The concentration of Sn was always below the limit of quantification. It was not possible to determine the concentration of Br and Li in ~ 71% and ~ 57% of the samples and Cs and Ti in ~ 43% of the cases. For the other elements, the concentrations were always quantified.

Table 22 - Minor and trace element concentrations (µg L^{-1}) in Archirafi, Unipa, Indipendenza, Belgio, Catania, and San Giovanni La Punta rinse solutions.

Archirafi	Li	B	Al	Ti	V	Cr	Mn	Fe	Co	Ni	Cu	Zn	As
	<LOQ	7.89	72.4	1.64	0.143	0.110	6.57	21.6	0.0650	0.212	4.38	13.0	0.0280
	0.757	36.7	421	4.75	1.14	0.570	30.4	172	0.366	0.959	31.7	86.5	0.238
	Se	Br	Rb	Sr	Mo	Cd	Sn	Sb	Cs	Ba	Tl	Pb	U
	0.219	<LOQ	0.158	6.07	0.0230	0.0310	<LOQ	0.0820	0.00800	9.63	0.0160	2.38	0.0190
	0.657	<LOQ	1.07	17.4	0.0860	0.0970	<LOQ	0.441	0.0210	30.1	0.0230	13.1	0.114

Unipa	Li	B	Al	Ti	V	Cr	Mn	Fe	Co	Ni	Cu	Zn	As
	<LOQ	7.76	75.2	0.879	0.130	0.143	4.77	35.2	0.0480	0.159	2.43	8.78	0.0390
	0.118	39.4	239	2.57	0.501	0.374	16.1	112	0.175	0.639	11.9	31.5	0.125
	Se	Br	Rb	Sr	Mo	Cd	Sn	Sb	Cs	Ba	Tl	Pb	U
	0.111	1.39	0.0850	3.99	0.0270	0.0190	<LOQ	0.141	0.00500	4.91	<LOQ	2.80	0.0130
	0.537	<LOQ	0.654	11.5	0.0560	0.106	<LOQ	0.377	0.0130	17.9	0.0140	5.12	0.0540

Indipendenza	Li	B	Al	Ti	V	Cr	Mn	Fe	Co	Ni	Cu	Zn	As
	<LOQ	5.93	84.5	1.58	0.138	0.189	4.61	27.9	0.128	0.178	3.31	48.7	0.0320
	0.195	42.2	477	3.91	1.24	0.725	52.3	223	0.556	1.28	35.1	91.8	0.260
	Se	Br	Rb	Sr	Mo	Cd	Sn	Sb	Cs	Ba	Tl	Pb	U
	0.222	<LOQ	0.124	4.07	0.132	0.0170	<LOQ	0.100	0.00500	5.32	0.00500	2.12	0.0110
	0.938	1.14	1.45	27.1	0.175	0.211	<LOQ	0.416	0.0140	40.8	0.0150	17.1	0.113

Belgio	Li	B	Al	Ti	V	Cr	Mn	Fe	Co	Ni	Cu	Zn	As
	<LOQ	5.81	86.5	0.821	0.131	0.231	5.23	30.7	0.0520	0.276	5.80	16.1	0.0330
	Se	Br	Rb	Sr	Mo	Cd	Sn	Sb	Cs	Ba	Tl	Pb	U
	0.114	<LOQ	0.0790	4.00	0.0400	0.0250	<LOQ	0.157	0.00500	5.06	0.00500	2.33	0.0120

Catania	Li	B	Al	Ti	V	Cr	Mn	Fe	Co	Ni	Cu	Zn	As
	<LOQ	7.42	64.5	0.654	0.0400	0.106	0.864	19.3	0.0120	0.121	1.00	6.20	0.0240
	0.342	46.6	940	5.94	4.32	0.590	74.7	247	0.795	1.01	29.8	85.7	0.393
	Se	Br	Rb	Sr	Mo	Cd	Sn	Sb	Cs	Ba	Tl	Pb	U
	0.133	20.5	<LOQ	0.527	0.00900	<LOQ	<LOQ	0.0620	0.00200	1.03	0.00300	1.21	<LOQ
	1.42	1.90	3.90	51.6	0.170	0.235	<LOQ	0.326	0.0270	46.3	0.0850	5.51	0.112

San Giovanni La Punta	Li	B	Al	Ti	V	Cr	Mn	Fe	Co	Ni	Cu	Zn	As
	<LOQ	6.54	58.2	0.889	0.0330	0.109	1.27	200	0.0210	2.47	19.0	3.05	0.162
	0.272	43.6	1037	10.2	4.10	0.435	40.1	227	0.478	0.933	30.6	86.3	0.372
	Se	Br	Rb	Sr	Mo	Cd	Sn	Sb	Cs	Ba	Tl	Pb	U
	0.134	14.3	<LOQ	0.358	0.0150	0.00800	<LOQ	0.119	0.00200	0.762	0.00300	0.772	0.00300
	1.39	2.56	2.99	36.1	0.256	0.217	<LOQ	0.219	0.0280	47.5	0.0810	5.11	0.221

Minor and trace element concentrations in the rinse solutions ranged from 0.00200 µg L^{-1} for caesium to 1037 µg L^{-1} for aluminium. Relevant differences were observed between the sampling sites and the samples analysed, up to two orders of magnitude. For a lot of elements, i.e., B, Al, Ti, V, Mn, Fe, Co, As, Se, Br, Rb, Sr, Cd, Ba, Tl, and U the highest mean concentrations were measured for the rinse solutions from San Giovanni La Punta. For Cr, Ni, Cu, Zn, Mo, and Pb the highest mean concentrations were measured at Indipendenza, while at the Archirafi sampling site were measured the highest mean concentrations for Li and Sb. For Cs equal mean concentrations were measured at Archirafi and San Giovanni La Punta sampling sites.

4.3.4 Technology-Critical Elements (TCEs)

Twenty-two (Palermo) and 13 (Catania) preconcentrated rainwater samples were prepared, according to the procedure illustrated in paragraph 3.1.4, for the determination of the concentrations of the Technology-Critical Elements, including the lanthanoids. For the Palermo study area, it was not possible to determine the concentration of Nb in ~ 32% of the sample, of Ge, Hf, Pr, Sm, Gd, Tb, Dy, Ho, Er, Tm, and Lu, in ~ 18% of the cases, of Sc, Te, and Eu in ~ 14% of the samples, and Zr, Th, and Yb in ~ 9%, ~ 5%, and ~ 5% of the cases, respectively. For the remaining elements, the concentrations were quantified in all the samples. For the Catania urban area, it was not possible to determine the concentration of Nb in ~ 31% of the sample, of Tm in 23% of the cases, of Te in ~ 15 % of the samples, and of Sc, Ge, Hf, Dy, Ho, Er, and Lu in ~ 8% of the cases. For the remaining elements, the concentrations were quantified in all the samples. A summary of statistical parameters of the analysed TCEs is provided in Table 23, and Figure 32.

Table 23 - Statistical parameters for TCE concentrations (ng L^{-1}) in Archirafi, Unipa, Indipendenza, Belgio, Catania, and San Giovanni La Punta preconcentrated rainwater samples.

Archirafi	Element	Sc	Ge	Y	Zr	Nb	Te	Hf	Th	La	Ce	Pr
	Min	0.419	0.617	2.51	283	1.24	1.43	4.62	0.160	3.73	2.68	1.48
	Max	24.7	16.2	29.1	1620	3.60	3.96	29.3	5.39	52.3	31.7	4.35
	Median	15.9	4.29	8.93	479	1.60	2.49	7.04	1.02	19.9	12.0	2.89
	Element	Nd	Sm	Eu	Gd	Tb	Dy	Ho	Er	Tm	Yb	Lu
	Min	4.07	0.943	0.311	1.28	0.136	1.23	0.276	0.654	0.0800	0.236	0.120
	Max	19.7	4.30	1.06	3.55	0.556	3.87	0.739	2.11	0.302	2.10	0.427
	Median	7.22	2.76	0.544	2.30	0.292	1.86	0.427	1.07	0.163	0.542	0.133

Unipa	Element	Sc	Ge	Y	Zr	Nb	Te	Hf	Th	La	Ce	Pr
	Min	0.496	1.67	2.54	10.7	0.658	1.06	0.316	0.518	4.87	7.79	1.00
	Max	13.1	4.84	23.8	285	1.51	6.61	4.91	3.55	37.3	19.2	3.08
	Median	7.73	2.33	7.75	120	1.43	1.58	3.09	1.26	16.9	13.8	1.66
	Element	Nd	Sm	Eu	Gd	Tb	Dy	Ho	Er	Tm	Yb	Lu
	Min	4.17	0.826	0.176	0.582	0.134	1.03	0.181	0.581	0.0870	0.254	0.0770
	Max	12.7	2.96	0.771	2.48	0.313	2.13	0.459	1.08	0.170	0.971	0.213
	Median	5.59	1.97	0.351	1.69	0.225	1.41	0.236	0.856	0.118	0.736	0.136

Indipendenza	Element	Sc	Ge	Y	Zr	Nb	Te	Hf	Th	La	Ce	Pr
	Min	2.11	1.40	2.06	7.39	0.146	1.60	0.136	0.647	2.45	1.54	0.857
	Max	7.81	5.76	18.6	324	1.62	2.96	5.89	1.97	22.3	24.3	3.63
	Median	4.47	1.98	7.34	42.2	0.750	2.57	1.53	1.22	13.9	8.26	1.55
	Element	Nd	Sm	Eu	Gd	Tb	Dy	Ho	Er	Tm	Yb	Lu
	Min	3.56	0.244	0.161	0.686	0.0620	0.600	0.109	0.344	0.0550	0.338	0.0300
	Max	14.4	3.57	0.755	3.02	0.425	2.70	0.446	1.53	0.226	1.08	0.211
	Median	4.52	1.44	0.416	1.41	0.229	1.30	0.272	0.845	0.109	0.471	0.114

	Element	Sc	Ge	Y	Zr	Nb	Te	Hf	Th	La	Ce	Pr
Belgio	Min	0.216	1.04	4.51	2.48	0.606	1.54	0.0190	0.358	3.86	7.22	0.911
	Max	5.60	7.69	48.4	264	0.959	2.54	4.20	0.851	52.9	60.6	7.99
	Median	2.98	1.75	10.5	176	0.640	2.08	2.69	0.516	23.3	11.8	1.75
	Element	Nd	Sm	Eu	Gd	Tb	Dy	Ho	Er	Tm	Yb	Lu
	Min	3.81	0.930	0.120	0.865	0.107	0.450	0.142	0.278	0.0610	0.501	0.0450
	Max	35.1	7.27	1.67	7.58	0.952	5.53	1.09	3.18	0.390	2.68	0.417
	Median	7.50	1.89	0.395	1.48	0.197	1.36	0.258	0.642	0.111	0.773	0.0920

	Element	Sc	Ge	Y	Zr	Nb	Te	Hf	Th	La	Ce	Pr
Catania	Min	0.148	0.525	3.24	14.1	0.509	1.06	0.193	0.357	3.78	4.92	0.787
	Max	9.58	11.1	15.1	234	5.15	13.5	4.72	3.98	32.3	33.0	3.26
	Median	4.27	3.45	10.6	133	1.08	3.62	2.25	1.45	22.7	15.4	2.58
	Element	Nd	Sm	Eu	Gd	Tb	Dy	Ho	Er	Tm	Yb	Lu
	Min	3.41	0.919	0.220	0.557	0.110	0.478	0.111	0.425	0.115	0.291	0.0550
	Max	19.0	3.24	0.715	2.87	0.381	2.25	0.427	1.45	0.185	1.28	0.208
	Median	11.8	2.18	0.557	2.22	0.308	1.79	0.313	0.874	0.137	0.655	0.149

	Element	Sc	Ge	Y	Zr	Nb	Te	Hf	Th	La	Ce	Pr
San Giovanni La Punta	Min	1.27	1.06	5.47	21.8	0.697	1.11	0.188	0.450	6.44	7.63	1.24
	Max	7.98	5.62	20.5	250	5.40	18.8	4.33	2.84	39.2	30.7	5.48
	Median	2.37	3.71	9.63	139	3.10	3.09	2.35	2.04	22.2	11.6	2.36
	Element	Nd	Sm	Eu	Gd	Tb	Dy	Ho	Er	Tm	Yb	Lu
	Min	4.84	1.23	0.317	1.01	0.164	0.854	0.125	0.514	0.0760	0.336	0.0590
	Max	22.6	4.32	1.00100	3.61	0.549	2.96	0.576	1.75	0.278	1.82	0.370
	Median	10.2	2.14	0.594	2.33	0.286	1.34	0.335	0.735	0.133	0.842	0.138

Among the TCEs, the highest concentration was measured for Zr, up to values of 1620 ng L^{-1} at the Archirafi sampling site, and a median concentration of 182 ng L^{-1} by considering all the sampling sites. The lowest median concentration was measured for Lu (0.0920 ng L^{-1}) at the Belgio sampling site. For Sc (15.9 ng L^{-1}), Ge (4.29 ng L^{-1}), Zr (479 ng L^{-1}), and Hf (7.04 ng L^{-1}) the highest median concentrations were measured at the Archirafi sampling site. For Y (10.6 ng L^{-1}) and Te (3.62 ng L^{-1}), the highest median concentrations were measured at the Catania sampling site. Finally, for Nb (3.10 ng L^{-1}) and Th (2.04 ng L^{-1}), the highest median concentrations were measured at the San Giovanni La Punta sampling site. The median concentrations of lanthanoid follow this order: La > Ce > Nd > Pr ≈ Sm > Gd > Dy > Er ≈ Yb > Eu > Ho ≈ Tb > Tm ≈ Lu. For all lanthanoids, very similar median concentrations were measured in rainwater samples from the Palermo and Catania urban areas.

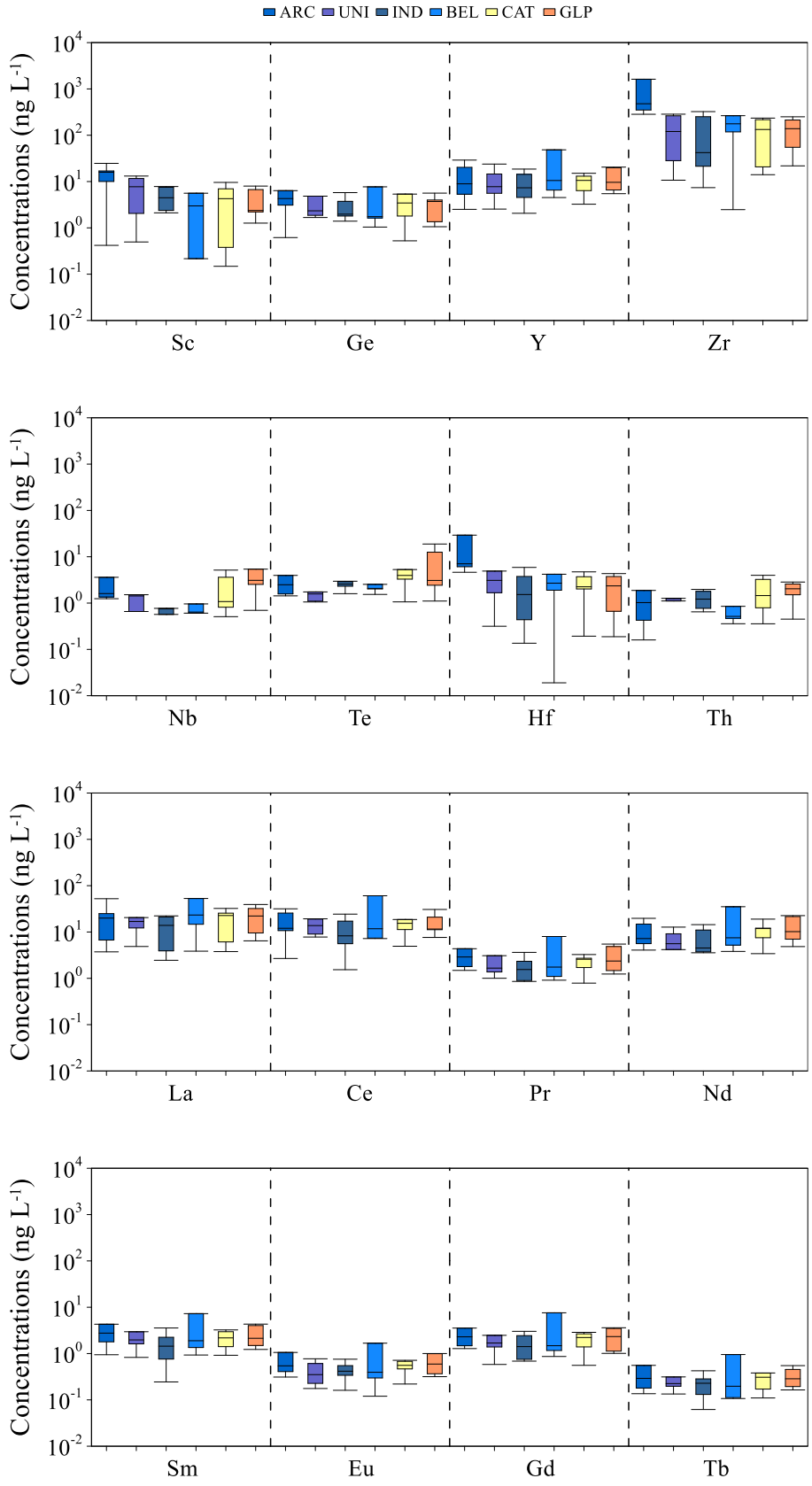
ARC
UNI
IND
BEL
CAT
GLP
Concentrations (ng L-1)
Sc
Ge
Y
Zr
Nb
Te
Hf
Th
La
Ce
Pr
Nd
Sm
Eu
Gd
Tb

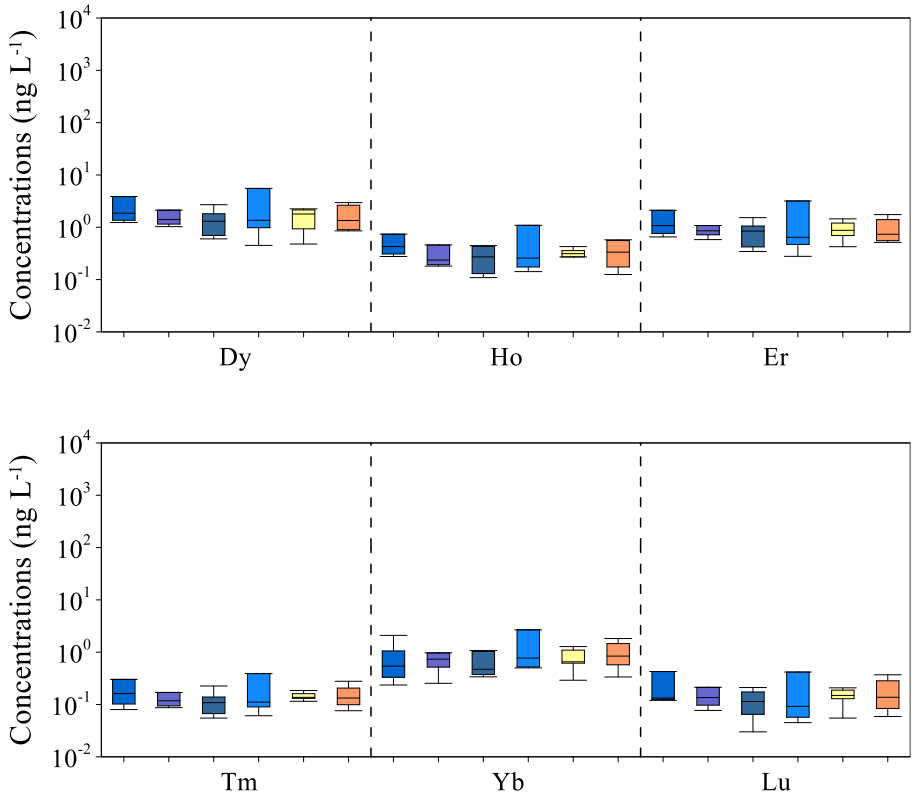

Figure 32 - TCE concentrations (ng L^{-1}) in the rainwater samples from the Palermo and Catania urban areas. The elements are ordered from highest to lowest atomic weight.

4.3.5 Boron and strontium isotopic composition

Boron ($\delta^{11}B/^{10}B$) and Strontium ($^{87}Sr/^{86}Sr$) isotopic composition were measured in 6 and 4 rainwater samples, for the Palermo and the Catania urban areas, respectively. The main statistical parameters (minimum, median, maximum) are given in Table 24.

Table 24 - Main statistical parameters for boron ($\delta^{11}B$‰) and strontium ($^{87}Sr/^{86}Sr$) in the Palermo and the Catania urban areas rainwater samples. Dev. Std. is the Standard Deviation for boron isotopic composition, while Std. Err. is the Standard Error for strontium ratio measurements.

Site	$^{87}Sr/^{86}Sr$			
	Min	Median	Max	Std. Err.
Archirafi	0.708882	0.709002	0.709122	0.000009
Unipa	0.709608	0.709608	0.709608	0.000008
Indipendenza	0.708874	0.708895	0.708916	0.000008
Belgio	0.708858	0.708858	0.708858	0.000008
Catania	0.708495	0.709208	0.709921	0.000007
San Giovanni La Punta	0.706475	0.706938	0.707401	0.000010
Site	$\delta^{11}B$ (‰)			
	Min	Median	Max	Dev. Std.
Archirafi	38.32	38.70	39.07	0.21
Unipa	37.93	37.93	37.93	0.09
Indipendenza	25.58	29.88	34.19	0.21
Belgio	28.78	28.78	28.78	0.05
Catania	31.60	35.97	40.33	0.17
San Giovanni La Punta	22.00	25.59	29.17	0.27

Very low $\delta^{11}B$ values were measured in some samples from San Giovanni La Punta, up to +22.00‰ ± 0.27‰. The lowest $\delta^{11}B$ median value (+25.59‰ ± 0.27‰) was measured in the same sampling site. The highest absolute $\delta^{11}B$ value was measured in a rainwater sample from Catania (+40.33‰ ± 0.17‰). The highest median $\delta^{11}B$ value was measured in the rainwater sampled from Archirafi (+38.70‰ ± 0.21‰). Two replicates for sample no.12 of the Archirafi site were analysed for boron isotopic composition, to verify the stability in the measurement of a repeated sample; $\delta^{11}B$ values of +38.32‰ ± 0.26‰ and +38.15‰ ± 0.13‰ were measured.

Strontium isotopic composition ranged from 0.706475 ± 0.000010 (San Giovanni La Punta) to 0.709921 ± 0.000007 (Catania). The lowest and the highest median $^{87}Sr/^{86}Sr$ ratios were measured for San Giovanni La Punta (0.706938 ± 0.000010) and Unipa (0.709608 ± 0.000008) sampling sites, respectively.

4.4 Milazzo and Priolo Gargallo industrial areas

The sequential number of samples and their sampling periods, for each monitoring site in the Etna area, are shown in Table 25.

Table 25 - Sequential number of samples and sampling periods for Milazzo, Siracusa, Augusta, and Priolo Gargallo sampling sites.

Site	No. Sample	Installed	Sampled	Time Exp. (day)
Palermo - Archirafi	1	01/03/2021	30/03/2021	29
	2	30/03/2021	26/04/2021	27
	3	26/04/2021	27/05/2021	31
	4	27/05/2021	28/06/2021	32
	5	28/06/2021	02/08/2021	35
	6	02/08/2021	03/09/2021	32
	7	03/09/2021	11/10/2021	38
	8	11/10/2021	25/10/2021	14
	8bis	25/10/2021	03/11/2021	9
	9	03/11/2021	22/11/2021	19
	10	22/11/2021	13/12/2021	21
	11	13/12/2021	18/01/2022	36
	12	18/01/2022	22/02/2022	35
	13	22/02/2022	30/03/2022	36
	14	06/04/2022	26/04/2022	20
	15	26/04/2022	23/05/2022	27
	16	23/05/2022	20/07/2022	58
	17	20/07/2022	23/08/2022	34
	18	23/08/2022	28/09/2022	36
	19	28/09/2022	25/10/2022	27
	20	25/10/2022	23/11/2022	29
	21	23/11/2022	20/12/2022	27
	22	20/12/2022	01/02/2023	43
	23	01/02/2023	16/02/2023	15

Site	No. Sample	Installed	Sampled	Time Exp. (day)
Palermo - Indipendenza	1	01/03/2021	30/03/2021	29
	2	30/03/2021	26/04/2021	27
	3	26/04/2021	27/05/2021	31
	4	27/05/2021	28/06/2021	32
	5	28/06/2021	02/08/2021	35
	6	02/08/2021	03/09/2021	32
	7	03/09/2021	11/10/2021	38
	8	11/10/2021	03/11/2021	23
	9	03/11/2021	22/11/2021	19
	10	22/11/2021	17/12/2021	25
	11	17/12/2021	18/01/2022	32
	12	18/01/2022	25/02/2022	38
	13	25/02/2022	30/03/2022	33
	14	30/03/2022	26/04/2022	27
	15	26/04/2022	23/05/2022	27
	16	23/05/2022	20/07/2022	58
	17	20/07/2022	23/08/2022	34
	18	23/08/2022	28/09/2022	36
	19	28/09/2022	27/10/2022	29
	20	27/10/2022	23/11/2022	27
	21	23/11/2022	20/12/2022	27
	22	20/12/2022	26/01/2023	37
	23	26/01/2023	16/02/2023	21

Site	No. Sample	Installed	Sampled	Time Exp. (day)
Palermo - Unipa	1	01/03/2021	30/03/2021	29
	2	30/03/2021	26/04/2021	27
	3	26/04/2021	27/05/2021	31
	4	27/05/2021	28/06/2021	32
	5	28/06/2021	02/08/2021	35
	6	02/08/2021	03/09/2021	32
	7	03/09/2021	11/10/2021	38
	8	11/10/2021	03/11/2021	23
	9	03/11/2021	22/11/2021	19
	10	22/11/2021	17/12/2021	25
	11	17/12/2021	18/01/2022	32
	12	18/01/2022	25/02/2022	38
	13	25/02/2022	30/03/2022	33
	14	30/03/2022	26/04/2022	27
	15	26/04/2022	23/05/2022	27
	16	23/05/2022	20/07/2022	58
	17	20/07/2022	23/08/2022	34
	18	23/08/2022	28/09/2022	36
	19	28/09/2022	27/10/2022	29
	20	27/10/2022	23/11/2022	27
	21	23/11/2022	20/12/2022	27
	22	20/12/2022	26/01/2023	37
	23	26/01/2023	16/02/2023	21

Site	No. Sample	Installed	Sampled	Time Exp. (day)
Palermo - Belgio	1	01/03/2021	30/03/2021	29
	2	30/03/2021	26/04/2021	27
	3	26/04/2021	27/05/2021	31
	4	27/05/2021	28/06/2021	32
	5	28/06/2021	02/08/2021	35
	6	02/08/2021	03/09/2021	32
	7	03/09/2021	11/10/2021	38
	8	11/10/2021	03/11/2021	23
	9	03/11/2021	22/11/2021	19
	10	22/11/2021	17/12/2021	25
	11	17/12/2021	18/01/2022	32
	12	18/01/2022	25/02/2022	38

4.4.1 Chemical-physical parameters (pH, EC)

4.4.1.1 The acidity of rainwater

The pH values of the rainwater samples collected in Milazzo (one site), and Priolo Gargallo (three sites) showed great variability during the two years of monitoring, respectively ranging from

5.0 to 7.8, with a median value of 6.5, and between 5.2 to 7.6, with a median of 6.5. The frequency distributions of pH in rainwater samples were bimodal in Milazzo, with the highest frequencies in the pH range 5.0 – 5.5 (20%) and between 7.0 and 7.5 (20%) (Fig. 33a), and unimodal in Priolo Gargallo study area, with the highest frequency in the pH range 6.5 – 7.5 (~ 52%) (Fig. 33b).

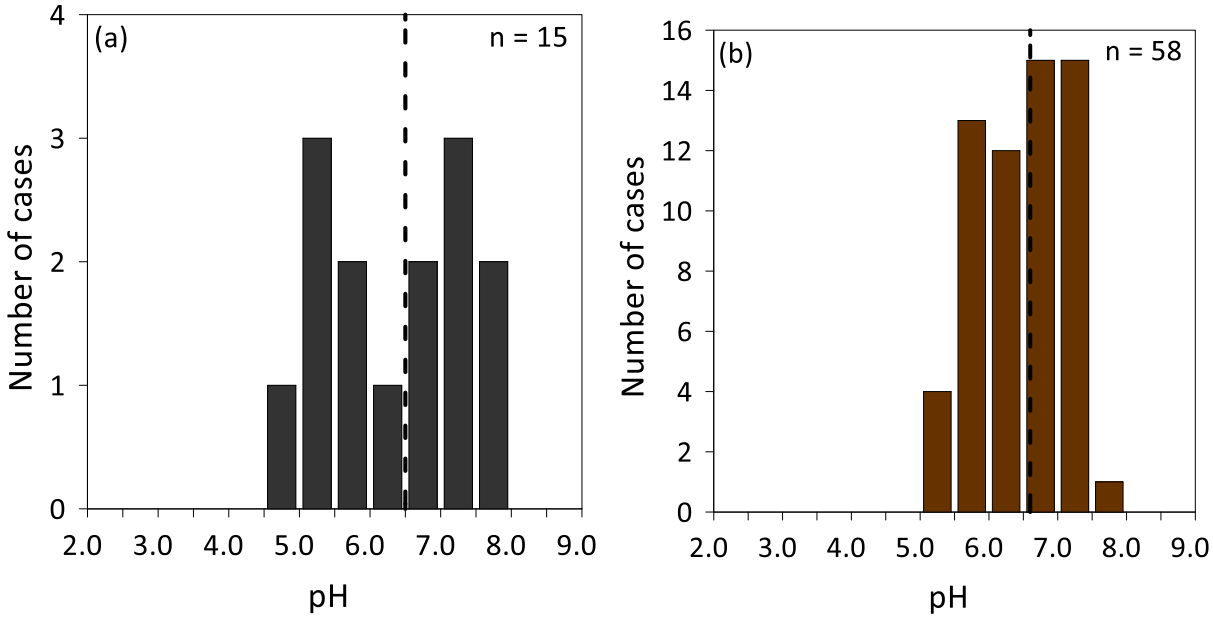

Figure 33 - Frequency distribution of pH in Milazzo (a - 15 cases) and Priolo Gargallo (b - 58 cases) rainwater samples. The black dashed lines are the medians.

In both the Milazzo and Priolo Gargallo study areas, only a few rainwater samples had pH values below 5.6, ~ 33% in the former and ~ 14% in the latter study area, respectively. The pH values for each monitoring site in the Priolo Gargallo industrial area are reported in Table 26 and shown in Figure 34.

Table 26 - Statistical parameters for rainwater's pH in the Milazzo and Priolo Gargallo industrial areas.

Study area	Site	Min	Max	Median	Q1	Q3
Milazzo	GAB	5.0	7.8	6.5	5.5	7.0
Priolo Gargallo	SIR	5.2	7.6	6.7	6.1	6.8
	AUG	5.3	7.2	6.3	5.7	7.0
	PRI	5.5	7.5	6.6	5.8	6.8

No major differences were observed in the pH values measured at the different monitoring sites. The lowest median value was calculated for Augusta (6.3), while the highest at Siracusa (6.7). The lowest pH value at Milazzo was measured in the rainwater sample from the period 02/11/2021 – 23/11/2021, and the highest in the sample from the period 28/04/2021 – 27/05/2021. At the Siracusa, Augusta, and Priolo Gargallo sampling sites, the lowest pH values were 5.2, 5.3 and 5.5 respectively, measured in the rainwater samples from the period 22/12/2021 – 20/01/2022 at Siracusa, and from the period 07/09/2021 – 12/10/2021 at Augusta and Priolo Gargallo. At the same sampling sites, the highest pH values of 7.6, 7.2, and 7.5, were measured in the rainwater samples from the periods 26/05/2021 – 29/06/2021, 31/03/2021 – 27/04/2021, and 29/03/2022 – 28/04/2022, respectively. Please refer to Table 25 for the correspondence between the sampling period and the sequential sample number. At Siracusa the highest frequency falls in the pH ranges 6.0 – 6.5 (~ 26%) and 7.0 – 7.5 (~ 26%), at Augusta in the pH range 5.5 – 6.0 (~ 33%), and at Priolo Gargallo in the pH range 5.5 – 6.0 (~ 30%) (Fig. 32a, b, c). A lower first quartile pH value (5.7) was calculated for the rainwaters from the Augusta site, compared to the values calculated for Siracusa (6.1) and Priolo Gargallo (5.8) sampling sites, but higher than those calculated for Milazzo (5.5).

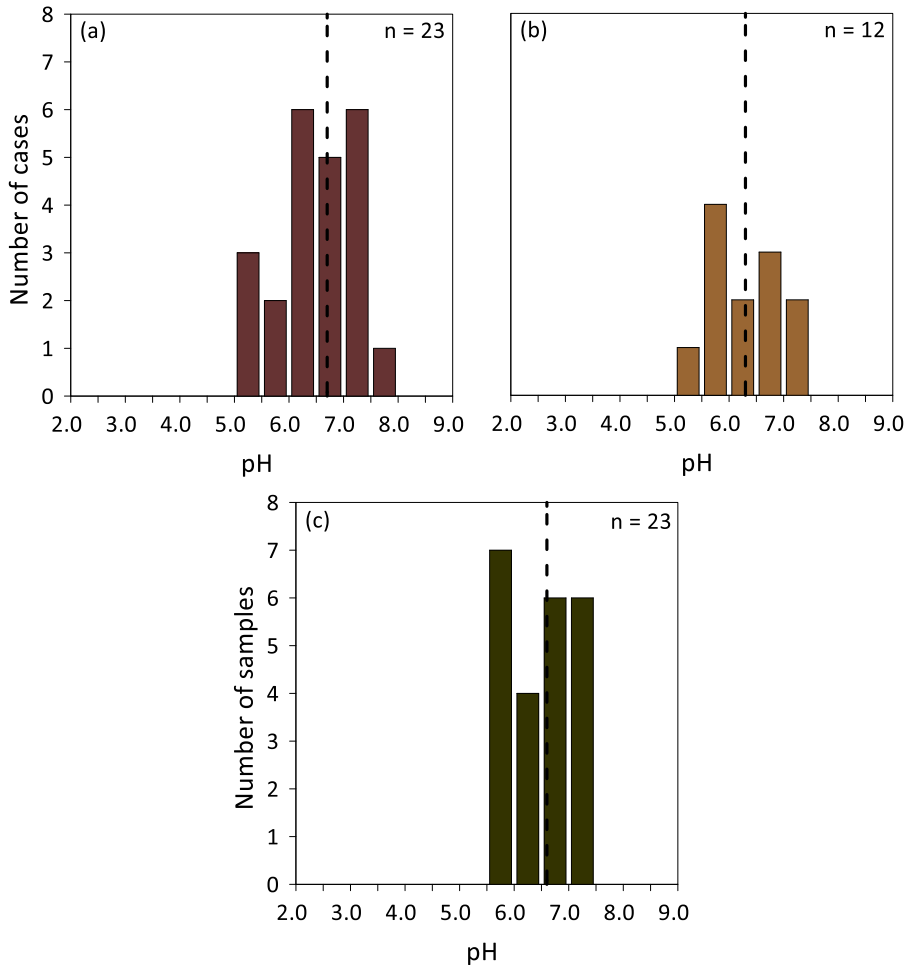

Figure 34 - Frequency distribution of pH in (a) Siracusa, (b) Augusta, and (c) Priolo Gargallo rainwater samples. The black dashed lines are the median values.

4.4.1.2 The Electric Conductivity (EC) of rainwater

The EC values of the rainwater samples collected in the two industrial areas, showed great variability during the two years of monitoring, ranging from 5.8 to 1032 µS cm^{-1}, with a median of 64.4 µS cm^{-1}. For a better graphical representation, the Log_{10} of the electric conductivity values were calculated. The probability distribution was unimodal for the Priolo Gargallo industrial area, and the class with the highest frequency (~ 45%) lies in the EC range of 1.8 – 2.2. The Electric Conductivity values were generally low in all the sampling sites, with values below 2 (on a Log_{10} basis) for almost 66% of the entire population (Fig. 35a, b). These EC values are typical of rain with a relatively low amount of dissolved ions.

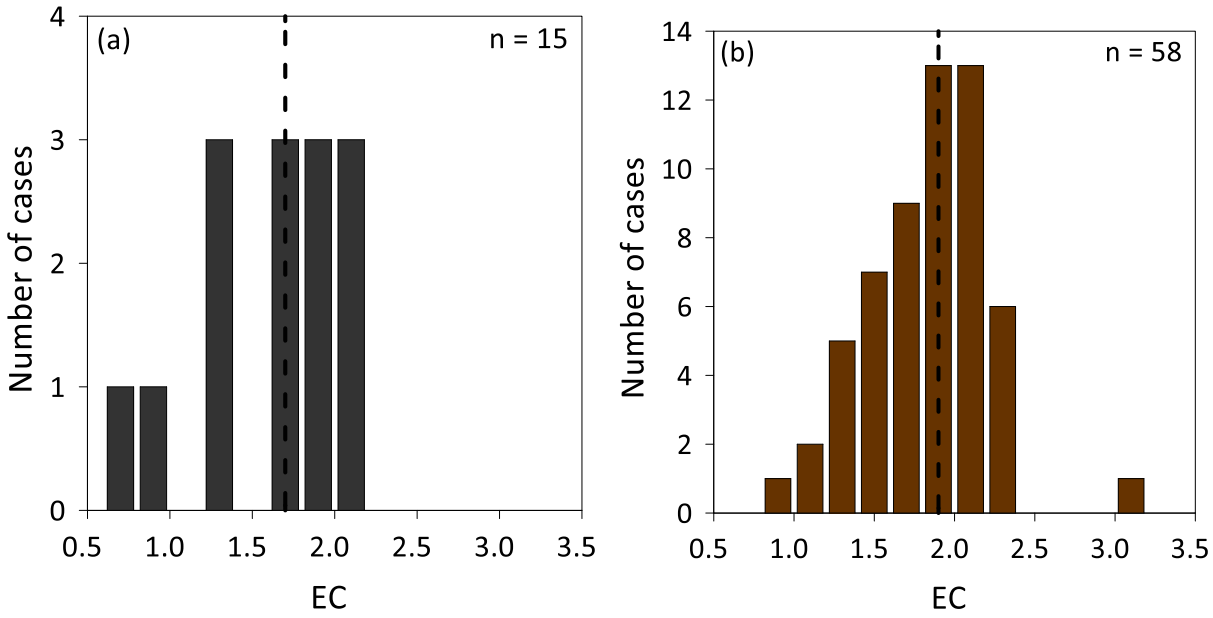

Figure 35 - Frequency distribution of EC (Log_{10}) in Milazzo (a) and Priolo Gargallo (b) rainwater samples. The black dashed lines are the geometric means.

The EC values for each monitoring site in the Priolo Gargallo industrial area are reported in Table 27 and shown in Figure 36.

Table 27 - Statistical parameters for rainwater's EC (Log_{10}) at Milazzo and Priolo Gargallo industrial areas.

Study area	Site	Min	Max	Median	Q1	Q3
Milazzo	GAB	0.763	2.18	1.70	1.34	2.09
Priolo Gargallo	SIR	1.04	2.27	1.88	1.51	1.91
	AUG	1.20	2.39	1.89	1.73	2.04
	PRI	0.959	2.30	1.88	1.52	2.03

The lowest value was measured at Milazzo and the highest at Augusta. The lowest median EC value was measured in the Milazzo sampling site (1.70), while the highest median EC value was measured at the Augusta sites (1.89). Very similar values, considering all the descriptive statistical parameters reported in Table 23, were calculated for all the sampling sites of the Priolo Gargallo

industrial area. Lower values were measured and calculated for the Milazzo site. For the Siracusa sampling sites, the highest frequencies were measured in the EC intervals 1.8 – 2.0 and 2.0 – 2.2 (~ 22%), at Augusta in the interval 2.0 – 2.2 (~ 33%), and at Priolo Gargallo in the interval 1.8 – 2.0 (~ 22%).

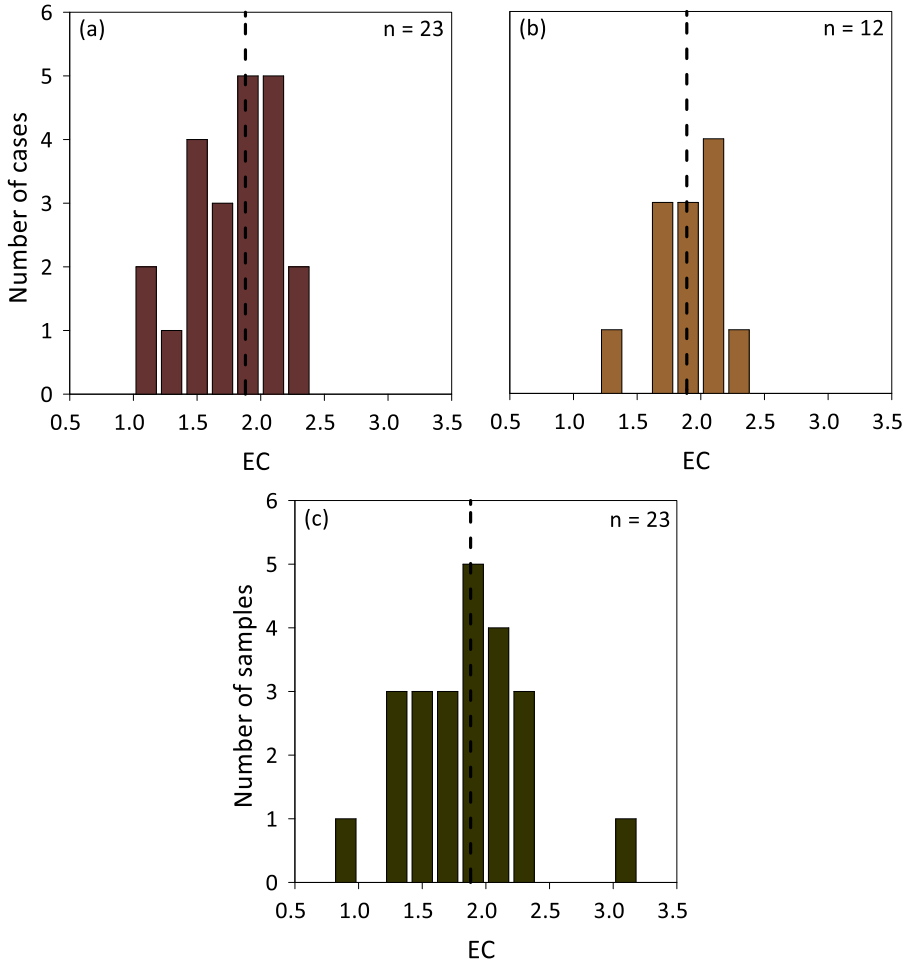

Figure 36 - Frequency distribution of EC in (a) Siracusa, (b) Augusta, and (c) Priolo Gargallo rainwater samples. The black dashed lines are the geometric mean values.

4.4.2 Major inorganic ions

A summary of statistical parameters of the analysed major ions in rainwater samples from Milazzo and Priolo Gargallo industrial areas is provided in Table 28. Volume-weighted mean and non-sea-salt concentrations were calculated using equation (2) and (4), respectively. A total of 14

(Milazzo) and 58 (Priolo Gargallo industrial area) rainwater samples were analysed for major ions. For the NH_4^+ the concentration could not be determined in ~ 29% of the samples from Milazzo, while the percentage was ~ 14% for the study area of Priolo Gargallo. Although no rainwater sample had a pH below 4.3, the concentration of HCO_3^- was < LOQ in ~ 23% and ~ 20% of the samples from Milazzo and Priolo Gargallo, respectively. The determination of the bicarbonate ion concentration was not performed in 1 sample collected in the Milazzo area and 3 samples (sampling period no. 12) from the Priolo Gargallo industrial area. For F^- the percentages of < LOQ were ~ 29% and ~ 22% for the two industrial areas, while for K^+ they were ~ 14% and ~ 3.5%. Only for the study area of Milazzo, it was not possible to quantify the concentration of SO_4^{2-} and Cl^- in ~ 7% of the rainwater samples. Finally, in all the analysed samples was possible to quantify the concentrations of Na^+, Mg^{2+}, and Ca^{2+}.

Table 28 - Statistical parameters for major ions ($\mu eq\ L^{-1}$) in Milazzo and Priolo Gargallo rainwater samples.

Site		F^-	Cl^-	NO_3^-	SO_4^{2-}	HCO_3^-	Na^+	K^+	NH_4^+	Mg^{2+}	Ca^{2+}
Milazzo	Min	< LOQ	< LOQ	8.50	< LOQ	< LOQ	75.2	< LOQ	< LOQ	27.8	48.3
	Max	12.9	776	229	508	500	684	77.5	63.5	233	1638
	VWM	1.99	312	28.5	77.9	63.1	294	11.0	15.5	85.7	165
	ss (%)	2.2	100	0	45.9	2.2	100	58.2	0	76.8	7.8
	nss (%)	97.8	0	100	54.1	97.8	0	41.8	100	23.2	92.2

Site		F^-	Cl^-	NO_3^-	SO_4^{2-}	HCO_3^-	Na^+	K^+	NH_4^+	Mg^{2+}	Ca^{2+}
Siracusa	Min	< LOQ	30.5	1.26	33.2	< LOQ	43.0	< LOQ	< LOQ	26.4	45.8
	Max	61.0	4650	682	1890	1344	2140	85.8	378	547	1520
	VWM	1.96	349	32.3	93.0	136	303	10.2	33.9	82.1	218
	ss (%)	2.2	100	0	39.6	1.1	100	65.1	0	82.5	6.1
	nss (%)	97.8	0	100	60.4	98.9	0	34.9	100	17.5	93.9
Augusta	Min	< LOQ	116	8.80	46.3	< LOQ	116	< LOQ	< LOQ	42.7	57.8
	Max	138	1668	100	373	1673	1479	580	275	335	607
	VWM	0.608	380	26.2	82.8	62.5	331	27.1	34.6	94.0	139
	ss (%)	7.9	100	0	48.6	2.5	100	26.7	0	78.8	10.4
	nss (%)	92.1	0	100	51.4	97.5	0	73.3	100	21.2	89.6
Priolo Gargallo	Min	< LOQ	29.7	4.70	24.5	< LOQ	38.1	2.80	< LOQ	24.3	26.6
	Max	36.9	6890	871	1920	1087	6050	246	75.8	1470	3316
	VWM	2.20	445	36.8	101	84.0	386	14.6	14.7	104	187
	ss (%)	2.6	100	0	46.4	2.2	100	57.6	0	83.2	9.0
	nss (%)	97.4	0	100	53.6	97.8	0	42.4	100	16.8	91.0

Chemical abundances, expressed as μeq L^{-1}, are represented by Tukey box plots, one set for each monitored site (Fig. 37).

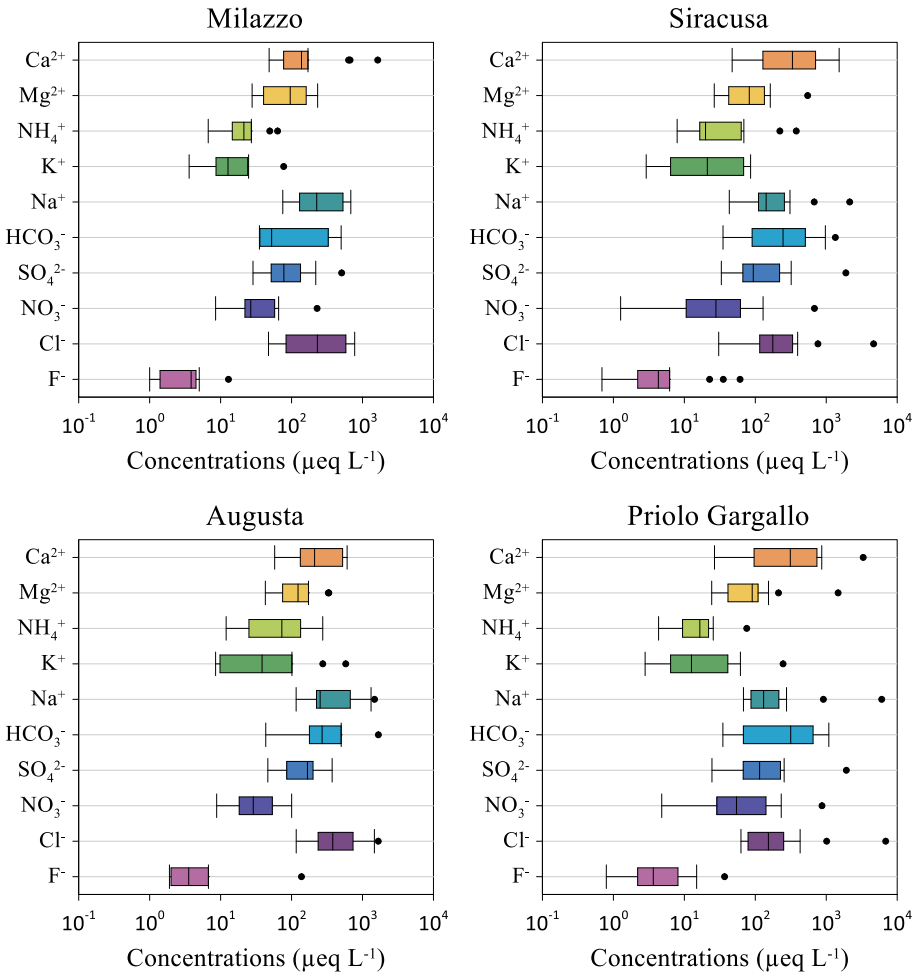

Figure 37 - Major ion concentrations (μeq L^{-1}) in Milazzo (one site) and Priolo Gargallo (three sites) rainwater samples.

The most saline rainwater sample, in terms of Total Dissolved Solids (TDS), was collected at the Priolo Gargallo sampling site, with a value of 20800 μeq L^{-1} (625 mg L^{-1}), in the sampling period 20/01/2022 – 24/02/2022. The less saline rainwater sample was collected in the same site, with a value of 258 μeq L^{-1} (7.79 mg L^{-1}), in the sampling period of 02/11/2021 – 23/11/2021. Please refer to Table 25 for the correspondence between the sampling period and the sequential sample number.

In all the sampling sites, the relative VWM concentrations of the major anions follow the sequence $Cl^- > SO_4^{2-} > HCO_3^- > NO_3^- > F^-$, except for Siracusa, where the relative contribution of HCO_3^- (22.2%) was higher than that of SO_4^{2-} (15.2%). Therefore, chloride was the main anion in all the sampling sites, with relative abundances of 64.5%, 57.0%, 68.8%, and 66.5%, in Milazzo, Siracusa, Augusta, and Priolo Gargallo sampling sites, respectively (Fig. 38). The highest chloride VWM concentration was measured at the Priolo Gargallo sampling site, with a value of 445 μeq L^{-1}, the lowest at Milazzo (312 μeq L^{-1}). Bicarbonate relative abundances were 13.1%, 22.2%, 11.3%, and 12.5%, in Milazzo, Siracusa, Augusta, and Priolo Gargallo sampling sites, respectively (Fig. 37). The highest bicarbonate VWM concentration was measured at Siracusa, with a value of 136 μeq L^{-1}, and the lowest at the Augusta and Milazzo sampling sites (~ 63 μeq L^{-1}). Similar relative contributions were observed for sulfate in both industrial areas, up to 16.1% for the Milazzo sampling site. The highest sulfate VWM concentration was measured at the Priolo Gargallo sampling site (101 μeq L^{-1}), and the lowest was at Milazzo (77.9 μeq L^{-1}). Relative contributions between 4.75% (Augusta), and 5.90% (Milazzo) were observed for nitrate. Nevertheless, the highest nitrate VMW concentration was measured at Priolo Gargallo (36.8 μeq L^{-1}), and the lowest (26.2 μeq $L^{-}1$) at Augusta. Fluoride was the less abundant ion in all the sampling sites. Very low relative contributions, up to 0.431% (Siracusa) were observed, with the highest VMW concentration measured at Priolo Gargallo (2.20 μeq L^{-1}), and the lowest at Augusta (0.608 μeq L^{-1}).

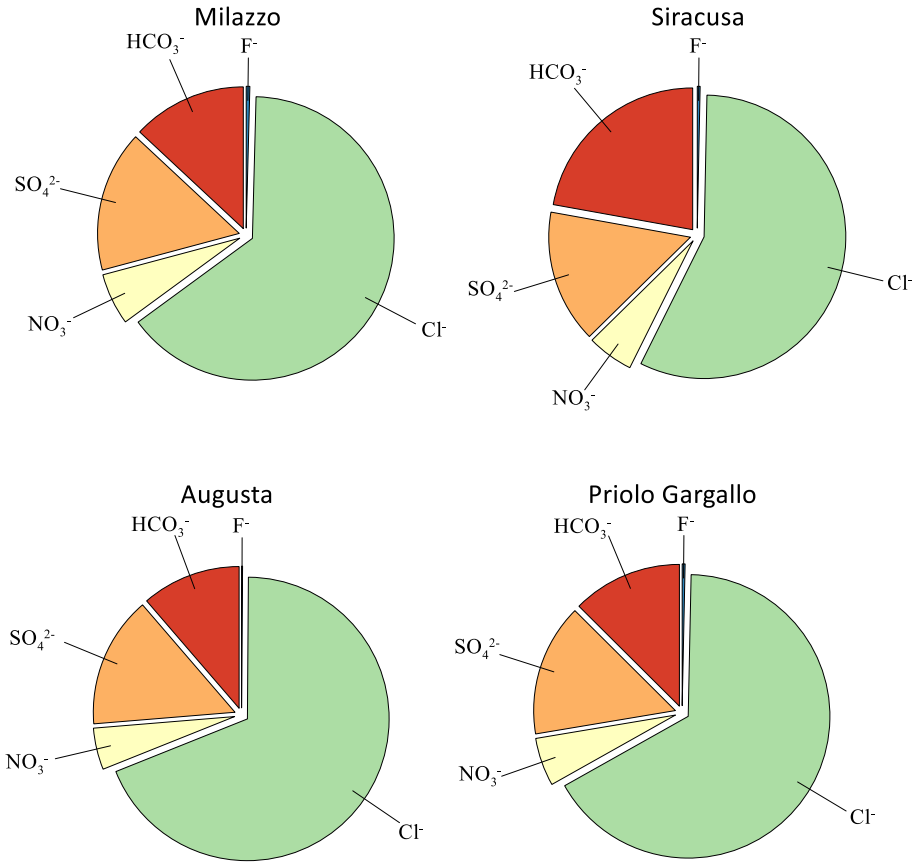

Figure 38 - Relative abundances (Eq%) of any major anions in the rainwater samples from Milazzo and Priolo Gargallo industrial areas.

As regards major cations, the sequence of relative abundances was $Na^+ > Ca^{2+} > Mg^{2+} > NH_4^+ > K^+$, for all the sampling sites, except Priolo Gargallo where the relative contribution of K^+ (2.07%) was equal to that of NH_4^+. Therefore, sodium was the main cation, with relative abundances of 51.5%, 46.8%, 52.9%, and 54.7%, in Milazzo, Siracusa, Augusta, and Priolo Gargallo sampling sites, respectively (Fig. 39). The highest sodium VWM concentration was measured at Priolo Gargallo, with a value of 386 μeq L^{-1}, and the lowest was measured at Milazzo (294 μeq L^{-1}). For calcium, the highest VWM concentration was measured at Siracusa (218 μeq L^{-1}), and the lowest at Augusta (139 μeq L^{-1}). Very similar relative contributions were observed for magnesium, between 12.7% (Siracusa), and 15.0% (Milazzo and Augusta), with the lowest VWM concentration (82.1 μeq L^{-1}) calculated for the former, while the highest (104 μeq L^{-1}), was calculated for the Priolo Gargallo sampling site. The highest relative contribution for ammonium was calculated at Augusta (5.52%),

with a VWM concentration of 34.6 μeq L^{-1}. The lowest VWM concentration was calculated for Priolo Gargallo (14.7 μeq L^{-1}). Potassium relative contributions were very low, up to 4.33% at Augusta, where the highest VMW concentration was calculated (27.1 μeq L^{-1}). The lowest potassium VMW concentration was calculated for Siracusa, equal to 10.2 μeq L^{-1}.

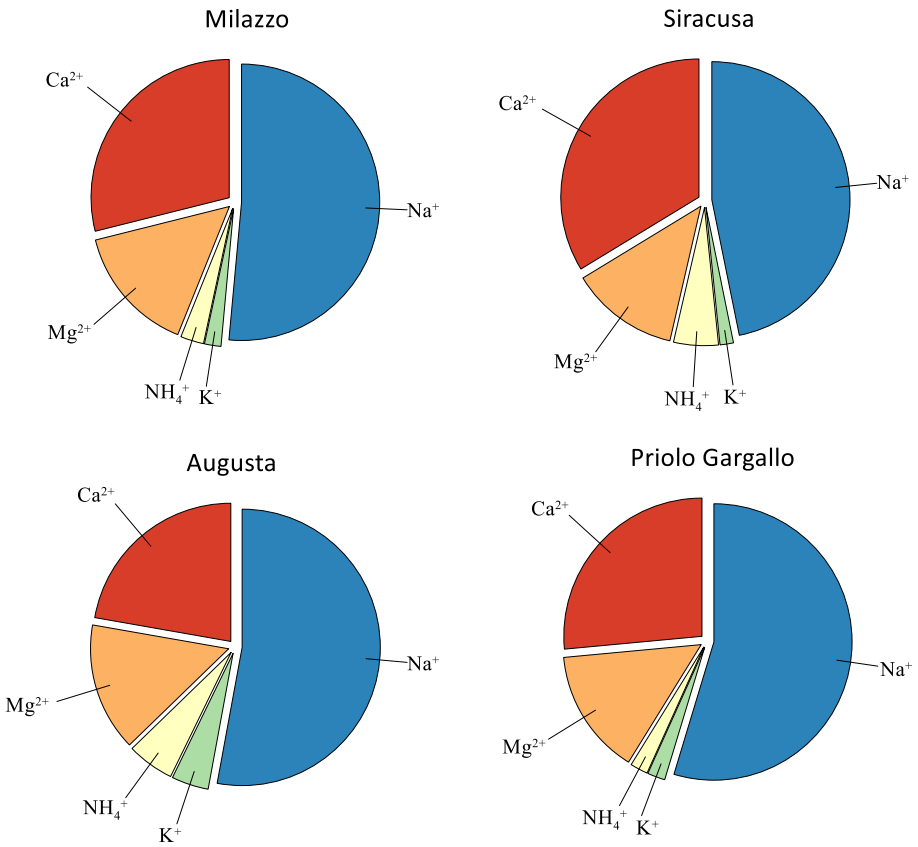

Figure 39 - Relative abundances (Eq%) of any major cations in the rainwater samples from Milazzo and Priolo Gargallo industrial areas.

4.4.3 Minor and trace elements concentrations

4.4.3.1 Rainwater samples

A summary of statistical parameters of the analysed minor and trace elements in the rainwater samples from the Milazzo and Priolo Gargallo industrial areas is provided in Table 29, and Figure 40. A total of 14 (Milazzo) and 57 (Catania urban area) rainwater samples were analysed for minor and trace elements. In the Milazzo rainwater samples, it was not possible to determine the

concentration of Sn, Cs, and Pb in ~ 93%, ~ 64%, and ~ 43% of the cases. For Li, B, Al, V, Cr, Ni, Cu, Zn, As, Br, Rb, Sr, Mo, Cd, Sb, Ba, and Tl it was always possible to determine the concentrations, while for the other elements, it was not possible to do so in between approximately 7% and 29% of the cases. For the rainwater samples of the Priolo Gargallo industrial area, it was not possible to determine the concentration of Sn and Cs in ~ 67% and ~ 46% of the cases, respectively. For B, Al, V, Cr, Fe, Ni, Cu, Zn, As, Rb, Sr, Sb, and Ba it was always possible to determine the concentrations, while for the other elements, it was not possible to do so in between approximately 2% and 17% of the cases.

Table 29 - Statistical parameters for minor and trace element concentrations (µg L^{-1}) in the sampling sites of the Milazzo and Priolo Gargallo industrial areas. Sample n. is the number of samples in which the maximum concentration was measured for each element.

Siracusa	Element	Li	B	Al	Ti	V	Cr	Mn	Fe	Co	Ni	Cu	Zn	As
	Min	< LOQ	1.04	1.81	< LOQ	0.159	0.0380	< LOQ	1.13	0.00400	0.105	0.251	3.70	0.0240
	Max	2.60	64.9	69.5	5.23	9.36	2.32	55.2	53.6	0.895	13.1	32.8	189	1.03
	Sample n.	12	12	12	05	12	13	04	13	13	12	12	12	12
	VWM	0.167	7.25	12.9	0.183	0.820	0.220	1.71	4.18	0.0563	0.738	1.93	39.1	0.158
	Element	Se	Br	Rb	Sr	Mo	Cd	Sn	Sb	Cs	Ba	Tl	Pb	U
	Min	< LOQ	< LOQ	0.0820	4.43	< LOQ	< LOQ	< LOQ	0.0770	< LOQ	2.47	< LOQ	< LOQ	< LOQ
	Max	3.23	233	4.05	181	2.88	0.160	0.0350	9.08	0.0180	135	0.154	0.272	0.132
	Sample n.	12	12	12	12	12	12	12	12	20	15	12	03	12
	VWM	0.187	39.9	0.374	17.7	0.0902	0.0168	0.00878	0.568	0.00246	13.1	0.0106	0.0630	0.00654

Augusta	Element	Li	B	Al	Ti	V	Cr	Mn	Fe	Co	Ni	Cu	Zn	As
	Min	0.0680	5.37	0.259	0.0100	0.202	0.0250	0.769	0.163	0.00800	0.0260	0.555	7.21	0.0360
	Max	0.966	18.9	96.9	3.02	1.56	0.396	38.0	53.3	0.749	1.36	30.0	1185	0.367
	Sample n.	12	04	05	05	05	05	04	02	04	04	12	12	04
	VWM	0.151	7.19	7.23	0.131	0.410	0.0516	3.62	4.15	0.0569	0.290	2.91	159	0.0832
	Element	Se	Br	Rb	Sr	Mo	Cd	Sn	Sb	Cs	Ba	Tl	Pb	U
	Min	0.0470	4.23	0.107	7.51	0.0140	0.0110	< LOQ	0.0670	< LOQ	2.97	< LOQ	< LOQ	< LOQ
	Max	1.43	150	3.99	56.4	0.567	0.164	0.0430	0.358	0.0140	15.5	0.137	0.692	0.0350
	Sample n.	05	10	04	04	04	12	02	02	12	04	05	2	02
	VWM	0.170	37.9	0.326	19.8	0.0478	0.0245	0.00688	0.148	0.00277	5.57	0.00980	0.153	0.00362

Priolo Gargallo	Element	Li	B	Al	Ti	V	Cr	Mn	Fe	Co	Ni	Cu	Zn	As
	Min	< LOQ	1.44	1.50	< LOQ	0.0950	0.0190	< LOQ	0.982	< LOQ	0.0310	0.146	1.33	0.0250
	Max	0.664	28.3	200	29.9	5.14	0.654	38.1	205	0.351	1.92	32.2	58.4	0.410
	Sample n.	20	20	05	05	20	03	04	05	03	20	20	20	20
	VWM	0.159	6.98	8.45	0.142	0.514	0.0748	1.92	3.28	0.0332	0.254	2.21	6.38	0.0827
	Element	Se	Br	Rb	Sr	Mo	Cd	Sn	Sb	Cs	Ba	Tl	Pb	U
	Min	< LOQ	< LOQ	0.0670	3.88	0.0140	< LOQ	< LOQ	0.0240	< LOQ	1.12	< LOQ	< LOQ	< LOQ
	Max	1.36	128	3.05	138	0.388	0.0590	0.0430	32.7	0.0270	202	0.0460	0.264	0.0320
	Sample n.	05	21	20	07	20	10	20	07	20	07	05	14	20
	VWM	0.205	44.2	0.333	26.1	0.0551	0.0167	0.00640	2.87	0.00205	19.9	0.00849	0.0615	0.00334

Milazzo	Element	Li	B	Al	Ti	V	Cr	Mn	Fe	Co	Ni	Cu	Zn	As
	Min	0.0310	2.91	0.112	< LOQ	0.288	0.0490	0.225	< LOQ	< LOQ	0.0850	0.491	1.10	0.0580
	Max	0.482	17.8	37.6	0.214	2.61	2.54	7.67	22.3	0.110	2.82	6.64	26.6	0.437
	Sample n.	03	03	09	07	04	03	12	13	13	03	07	13	03
	VWM	0.151	6.61	9.83	0.0892	0.824	0.155	3.88	5.37	0.0510	0.709	2.24	10.5	0.156
	Element	Se	Br	Rb	Sr	Mo	Cd	Sn	Sb	Cs	Ba	Tl	Pb	U
	Min	< LOQ	6.15	0.0940	5.05	0.0350	0.00700	< LOQ	0.0350	< LOQ	2.00	0.00500	< LOQ	< LOQ
	Max	0.506	67.2	1.52	111	1.24	0.0650	0.0120	0.511	0.0120	32.4	0.0460	1.18	0.0240
	Sample n.	03	13	03	03	03	13	07	13	07	03	01	13	03
	VWM	0.155	29.7	0.257	17.0	0.153	0.0259	0.00572	0.139	0.00179	8.19	0.0159	0.122	0.00179

In Milazzo, the lowest VWM concentration was calculated for Cs and U (0.00179 µg L^{-1}), and the highest for bromide (29.7 µg L^{-1}). In all the sampling sites from the Priolo Gargallo industrial area, the lowest VWM concentrations were calculated for Cs (between 0.00205 and 0.00277 µg L^{-1}), while the highest for bromide (between 37.9 to 44.2 µg L^{-1}). For V, Mn, Fe, Mo, Cd, and Tl the highest VWM concentrations were calculated for Milazzo. For Li, B, Al, Ti, Cr, Ni, As, Rb, Sn, and U were calculated for Siracusa, for Co, Cu, Zn, Cs, and Pb in the Augusta sampling sites and, finally, for Se, Br, Sr, Sb, and Ba for the Priolo Gargallo sampling site. The concentrations of the elements analysed did not only show great differences between the different sites. A relevant intra-site variability, up to three orders of magnitude, was observed for different periods of sampling (Fig. 40).

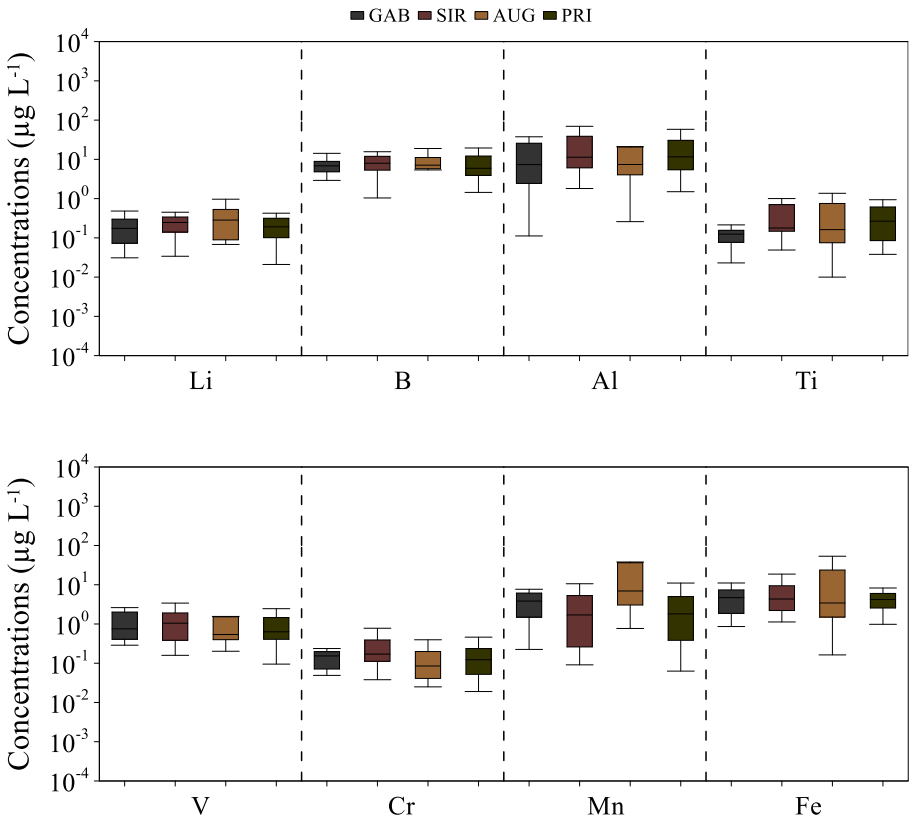

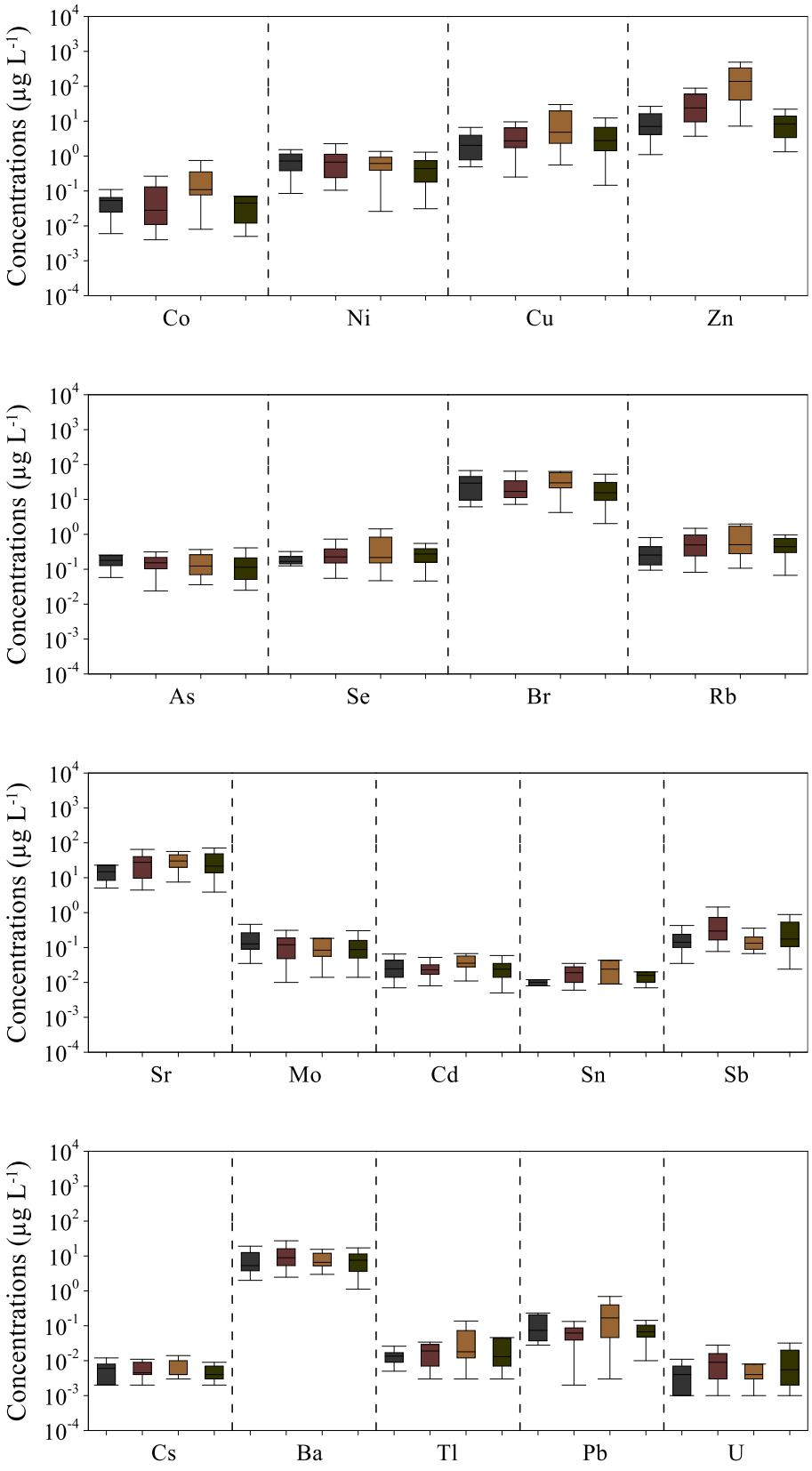

Figure 40 - Minor and trace element concentrations (µg L^{-1}) in the rainwater samples from the Milazzo and Priolo Gargallo industrial areas. The elements are ordered from highest to lowest atomic weight.

4.4.3.2 Insoluble fraction

To characterise the chemical composition of the insoluble fraction of the atmospheric deposition, the material retained by the membrane filters (> 0.45 µm) was mineralised according to the procedure described in paragraph 3.1.3. A summary of statistical parameters of the analysed minor and trace elements in the insoluble fraction solutions is provided in Table 30, and Figure 41. A total of 14 and 58 insoluble fraction solutions were analysed for minor and trace element concentrations from the Milazzo and the Priolo Gargallo industrial areas, respectively. It was not possible to determine the concentration in the ~ 14%, and ~ 7% of the samples. For the remaining elements, the concentrations were quantified in all the samples.

Table 30 - Statistical parameters for minor and trace element concentrations in the insoluble fraction solutions at Milazzo, Siracusa, Augusta, and Priolo Gargallo. The concentrations are in µg L^{-1}, except for Al, Ti, Fe, and Zn (mg L^{-1}).

	Element	Li	B	Al	Ti	V	Cr	Mn	Fe	Co	Ni	Cu	Zn	As
Milazzo	Min	2.77	6.40	3.29	0.131	8.11	12.5	68.8	3.07	0.946	11.2	21.9	0.0502	1.62
	Max	166	298	345	25.4	924	347	5077	308	115	180	1522	1.75	39.9
	Median	24.6	75.0	28.3	1.00	107	147	434	35.6	12.4	60.4	185	0.429	15.1
	Element	Se	Br	Rb	Sr	Mo	Cd	Sn	Sb	Cs	Ba	Tl	Pb	U
	Min	n.d.	n.d.	n.d.	2.55	0.789	n.d.	n.d.	n.d.	n.d.	29.5	n.d.	3.56	n.d.
	Max	n.d.	n.d.	n.d.	3703	15.0	n.d.	n.d.	n.d.	n.d.	2658	n.d.	177	n.d.
	Median	n.d.	n.d.	n.d.	66.7	9.03	n.d.	n.d.	n.d.	n.d.	251	n.d.	76.4	n.d.

	Element	Li	B	Al	Ti	V	Cr	Mn	Fe	Co	Ni	Cu	Zn	As
Siracusa	Min	2.15	4.12	3.49	0.146	8.32	8.33	40.1	3.11	1.15	7.92	36.4	0.139	2.92
	Max	265	407	620	48.9	1715	413	8553	529	219	311	1445	7.72	84.1
	Median	35.5	71.4	45.5	1.89	128	95.8	999	47.6	21.6	62.5	216	0.890	21.7
	Element	Se	Br	Rb	Sr	Mo	Cd	Sn	Sb	Cs	Ba	Tl	Pb	U
	Min	n.d.	n.d.	n.d.	21.6	0.421	n.d.	n.d.	n.d.	n.d.	31.5	n.d.	7.55	n.d.
	Max	n.d.	n.d.	n.d.	6138	17.7	n.d.	n.d.	n.d.	n.d.	4304	n.d.	575	n.d.
	Median	n.d.	n.d.	n.d.	267	3.57	n.d.	n.d.	n.d.	n.d.	458	n.d.	66.9	n.d.

	Element	Li	B	Al	Ti	V	Cr	Mn	Fe	Co	Ni	Cu	Zn	As
Augusta	Min	0.966	5.52	1.61	0.138	5.19	24.0	22.8	1.53	0.770	3.42	18.3	0.0890	3.24
	Max	142	188	155	12.7	422	345	2208	145	58.7	118	464	8.37	58.8
	Median	52.1	112	76.7	2.73	182	110	898	69.7	26.2	61.4	279	1.38	17.0
	Element	Se	Br	Rb	Sr	Mo	Cd	Sn	Sb	Cs	Ba	Tl	Pb	U
	Min	n.d.	n.d.	n.d.	35.8	0.405	n.d.	n.d.	n.d.	n.d.	22.8	n.d.	4.23	n.d.
	Max	n.d.	n.d.	n.d.	1879	11.3	n.d.	n.d.	n.d.	n.d.	1171	n.d.	279	n.d.
	Median	n.d.	n.d.	n.d.	364	5.30	n.d.	n.d.	n.d.	n.d.	499	n.d.	71.5	n.d.

	Element	Li	B	Al	Ti	V	Cr	Mn	Fe	Co	Ni	Cu	Zn	As
Priolo Gargallo	Min	1.73	4.90	3.79	0.0788	6.48	7.34	22.7	2.01	0.857	5.92	17.8	0.101	0.402
	Max	358	811	1045	97.5	3088	502	16351	993	386	276	2751	2.25	65.9
	Median	24.1	49.3	33.6	1.28	79.1	63.5	550	31.9	14.1	50.8	158	0.601	16.1
	Element	Se	Br	Rb	Sr	Mo	Cd	Sn	Sb	Cs	Ba	Tl	Pb	U
	Min	n.d.	n.d.	n.d.	28.7	0.118	n.d.	n.d.	n.d.	n.d.	33.4	n.d.	3.28	n.d.
	Max	n.d.	n.d.	n.d.	11256	32.0	n.d.	n.d.	n.d.	n.d.	3123	n.d.	186	n.d.
	Median	n.d.	n.d.	n.d.	134	2.62	n.d.	n.d.	n.d.	n.d.	217	n.d.	42.0	n.d.

In the Milazzo sampling site the median concentrations ranged from 9.03 µg L^{-1} for Mo to 35.6 mg L^{-1} for Fe, at Siracusa from 3.57 µg L^{-1} for Mo to 47.6 mg L^{-1} for Fe, from 5.30 µg L^{-1} (Mo) to 77.6 mg L^{-1} (Al) at Augusta, and from 2.62 µg L^{-1} (Mo) to 33.6 mg L^{-1} (Al) at the Priolo Gargallo sampling site. Therefore, the lowest median concentrations were calculated for Mo, while the highest median concentrations were calculated for Al and Fe. For many of the analysed elements, the highest median concentrations were calculated for the Augusta sampling site. Exceptions were Cr, Mo, and Pb, for which the highest median values were calculated at Milazzo, and Mn, Ni, and As, for which the highest median values were calculated for the Siracusa sampling site. At Priolo Gargallo the median concentrations were generally lower than at the other industrial sites.

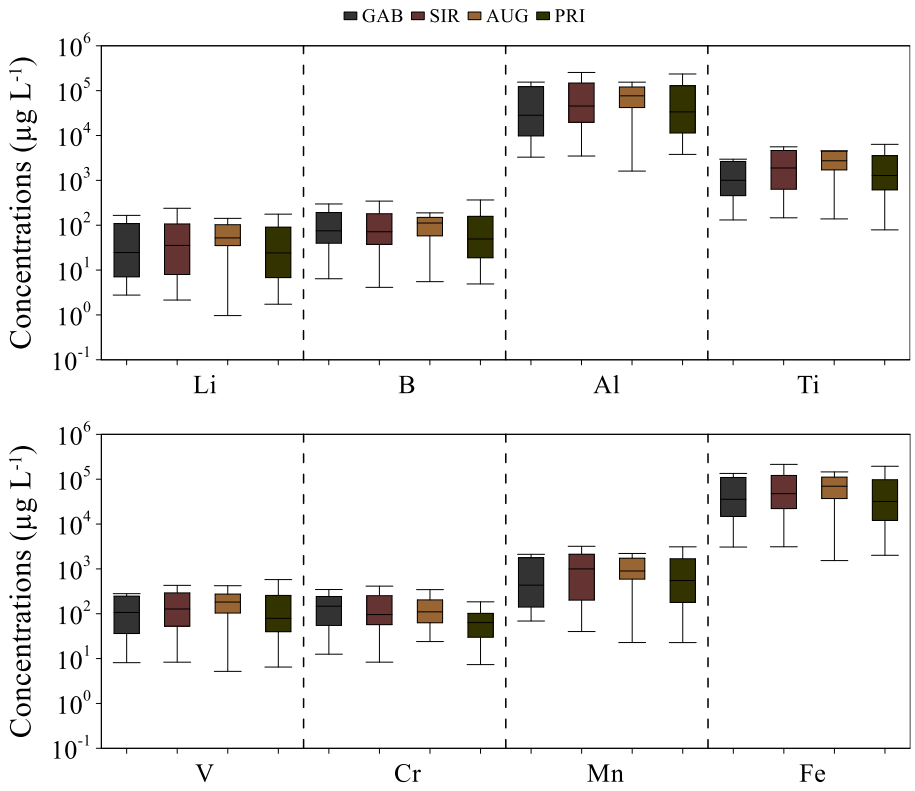

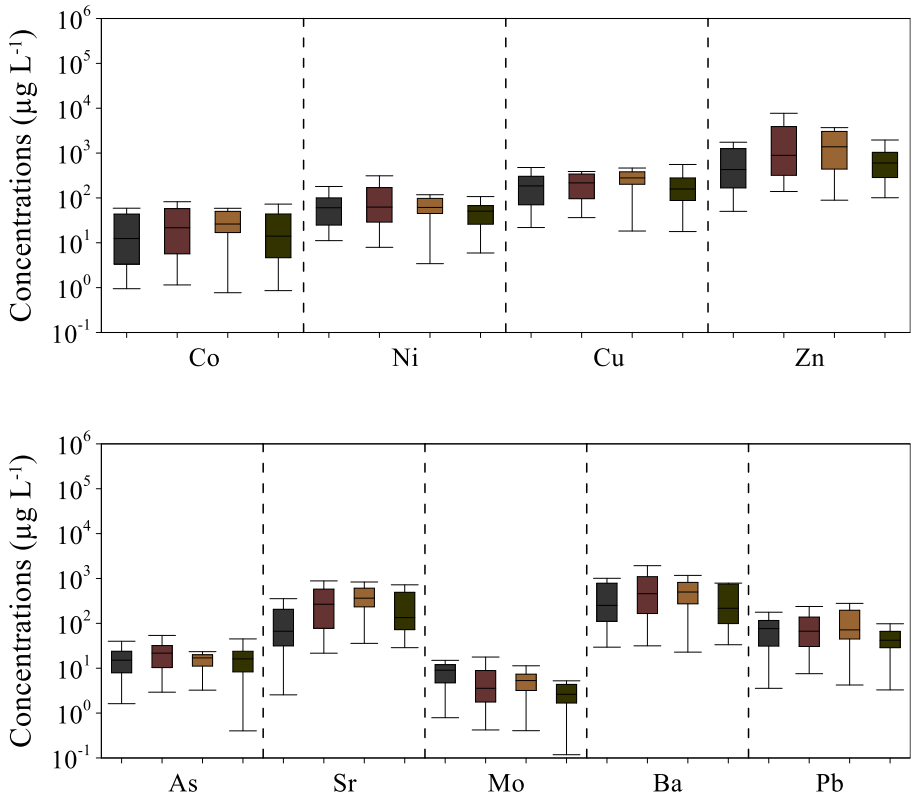

Figure 41 - Minor and trace element concentrations (µg L^{-1}) in the Milazzo and Priolo Gargallo insoluble fraction solutions. The elements are ordered from highest to lowest atomic weight.

4.4.3.3 Rinse solutions

To determine the concentration of minor and trace elements in the material remaining adhered to the surfaces of the bulk collector, a rinse aliquot was prepared according to the procedure described in paragraph 3.1.2. The concentrations of the analysed minor and trace elements in the rinse solutions from the Milazzo and Priolo Gargallo industrial areas are provided in Table 31. Only one and five rinse solutions from Milazzo and Priolo Gargallo industrial areas were analysed for minor and trace element concentrations. The concentration of Sn was always below the limit of quantification. For the sample from Milazzo, it was not possible to quantify the concentration also for Li, Co, Cd, Tl, and U. For the samples from the Priolo Gargallo study area, it was not possible to determine the concentration of Li, Br and Tl in 60% of the cases, of Cs in 40% of the samples, and of Rb and U in 20% of the samples. For the other elements, the concentrations were always quantified.

Table 31 - Minor and trace element concentrations (µg L^{-1}) in Milazzo, Siracusa, Augusta, and Priolo Gargallo rinse solutions.

Milazzo	Li	B	Al	Ti	V	Cr	Mn	Fe	Co	Ni	Cu	Zn	As
	<LOQ	5.03	17.6	0.381	0.0940	0.0800	0.570	9.78	<LOQ	0.0730	0.599	6.17	0.0270
	Se	Br	Rb	Sr	Mo	Cd	Sn	Sb	Cs	Ba	Tl	Pb	U
	0.132	23.3	0.0130	2.43	0.0250	<LOQ	<LOQ	0.0570	0.00200	0.643	<LOQ	0.895	<LOQ
Siracusa	Li	B	Al	Ti	V	Cr	Mn	Fe	Co	Ni	Cu	Zn	As
	<LOQ	8.13	95.6	1.86	0.112	0.210	1.73	26.3	0.0220	0.188	1.20	12.9	0.0260
	0.090	33.1	360	2.90	2.25	0.376	26.8	97.0	0.274	1.64	11.9	141	0.249
	Se	Br	Rb	Sr	Mo	Cd	Sn	Sb	Cs	Ba	Tl	Pb	U
	0.336	<LOQ	0.0560	1.53	0.0260	0.0290	<LOQ	0.110	0.00500	2.05	0.00500	3.35	0.0130
	0.852	1.08	0.936	19.1	0.0870	0.125	<LOQ	0.190	0.0100	114	0.0200	3.84	0.0820
Augusta	Li	B	Al	Ti	V	Cr	Mn	Fe	Co	Ni	Cu	Zn	As
	<LOQ	4.32	40.6	0.520	0.0590	0.0690	0.936	10.6	0.0170	0.139	0.935	14.5	0.00600
	Se	Br	Rb	Sr	Mo	Cd	Sn	Sb	Cs	Ba	Tl	Pb	U
	0.130	<LOQ	0.0200	1.80	0.0100	0.0100	<LOQ	0.0660	0.00100	0.880	<LOQ	2.21	0.00400
Priolo Gargallo	Li	B	Al	Ti	V	Cr	Mn	Fe	Co	Ni	Cu	Zn	As
	<LOQ	5.48	24.1	0.341	0.0490	0.136	0.807	13.4	0.00900	0.133	0.887	4.23	0.0180
	0.204	43.1	511	3.97	1.79	0.406	33.7	139	0.405	1.07	18.0	68.9	0.236
	Se	Br	Rb	Sr	Mo	Cd	Sn	Sb	Cs	Ba	Tl	Pb	U
	0.141	4.55	<LOQ	0.616	0.0150	0.0110	<LOQ	0.0440	<LOQ	0.615	<LOQ	0.703	<LOQ
	1.19	<LOQ	1.41	21.9	0.0970	0.122	<LOQ	0.219	0.0150	28.1	0.0280	3.92	0.100

Minor and trace element concentrations in the rinse solutions ranged from 0.00100 µg L^{-1} for caesium to 511 µg L^{-1} for aluminium. Relevant differences were observed between the sampling sites and the samples analysed, up to two orders of magnitude. The highest mean concentrations for each minor and trace element were measured at Siracusa or Priolo Gargallo sampling sites. Lower concentrations were measured for the rinse solutions from Milazzo and Augusta. Specifically, for Li, B, Al, Mn, Fe, Co, Cu, Se, Rb, Sr, Cs, Tl, and U the highest mean concentration were measured at Priolo Gargallo, while for the other elements at Siracusa. The only exception was Br for which the highest concentration was measured at the Milazzo sampling site.

4.4.4 Technology-Critical Elements concentrations

Seven (Milazzo) and 19 (Priolo Gargallo) preconcentrated rainwater samples, prepared according to the procedure illustrated in paragraph 3.1.4, were analysed for the determination of the concentrations of the Technology-Critical Elements, including the lanthanoids. For the Milazzo sampling site, it was not possible to determine the concentration of Th in only one sample (14.3%), For the remaining elements, the concentrations were quantified in all the samples. For the Priolo Gargallo industrial area, it was not possible to determine the concentration of Nb in 20% of the sample, of Te and Lu in 15% of the cases, of Hf, Dy, Ho, Er, and Tm in 10 % of the samples, and of Sc, Ge, Y, Zr, Th, Pr, Sm, Eu, Gd, and Tb in 5% of the cases. For La, Ce, Nd, and Yb, the concentrations were quantified in all the samples.

A summary of the statistical parameters of the analysed TCEs is provided in Table 32, and Figure 42.

Table 32 - Statistical parameters for TCE concentrations (ng L^{-1}) in Milazzo, Siracusa, Augusta, and Priolo Gargallo preconcentrated rainwater samples.

Milazzo	Element	Sc	Ge	Y	Zr	Nb	Te	Hf	Th	La	Ce	Pr
	Min	1.11	1.24	3.38	11.8	0.0430	1.56	0.124	0.0930	3.16	4.62	0.574
	Max	6.40	7.24	19.7	392	2.16	6.91	6.43	2.79	25.9	22.8	3.54
	Median	2.65	2.86	6.40	98.7	0.535	1.91	1.96	0.276	13.8	8.07	1.24
	Element	Nd	Sm	Eu	Gd	Tb	Dy	Ho	Er	Tm	Yb	Lu
	Min	2.58	0.685	0.168	0.590	0.0310	0.465	0.115	0.320	0.0360	0.365	0.00500
	Max	15.1	3.13	0.781	3.52	0.477	2.45	0.552	1.39	0.241	1.54	0.260
	Median	5.09	1.35	0.317	1.32	0.159	0.900	0.172	0.518	0.0890	0.695	0.0960

Siracusa	Element	Sc	Ge	Y	Zr	Nb	Te	Hf	Th	La	Ce	Pr
	Min	1.62	1.42	2.11	51.3	0.511	1.58	1.26	0.0500	9.68	7.85	0.738
	Max	12.8	5.47	12.8	290	1.10	7.67	4.37	2.36	69.7	16.3	2.50
	Median	5.10	2.83	10.6	160	0.895	3.26	2.50	1.18	26.6	11.7	1.67
	Element	Nd	Sm	Eu	Gd	Tb	Dy	Ho	Er	Tm	Yb	Lu
	Min	2.30	0.611	0.244	0.527	0.00200	0.330	0.0660	0.220	0.0320	0.272	0.0990
	Max	11.3	3.52	0.583	2.20	0.322	2.02	0.421	1.28	0.182	0.933	0.302
	Median	8.72	1.63	0.426	1.59	0.207	1.30	0.295	0.775	0.0985	0.748	0.158

Augusta	Element	Sc	Ge	Y	Zr	Nb	Te	Hf	Th	La	Ce	Pr
	Min	2.34	1.66	8.44	14.4	0.0820	1.52	0.157	0.616	17.0	11.5	1.70
	Max	5.98	4.16	17.9	217	1.79	4.28	4.48	3.79	51.9	24.7	3.27
	Median	3.97	2.84	13.8	155	0.820	2.50	2.62	2.26	31.3	19.7	2.57
	Element	Nd	Sm	Eu	Gd	Tb	Dy	Ho	Er	Tm	Yb	Lu
	Min	7.30	1.71	0.415	1.57	0.206	1.20	0.254	0.666	0.0740	0.525	0.0640
	Max	14.8	3.82	0.697	3.11	0.400	2.59	0.455	1.34	0.206	1.27	0.282
	Median	10.6	2.20	0.533	2.28	0.307	1.93	0.396	0.945	0.170	0.744	0.115

Priolo Gargallo	Element	Sc	Ge	Y	Zr	Nb	Te	Hf	Th	La	Ce	Pr
	Min	1.32	0.862	4.17	25.9	0.396	1.08	0.239	0.0740	15.4	11.2	0.750
	Max	9.88	3.09	16.1	247	1.30	5.17	4.08	5.17	376	198	2.77
	Median	5.06	1.88	8.78	118	0.763	1.92	2.11	0.727	44.0	18.0	1.71
	Element	Nd	Sm	Eu	Gd	Tb	Dy	Ho	Er	Tm	Yb	Lu
	Min	4.31	0.806	0.351	0.880	0.0650	0.619	0.144	0.276	0.0600	0.372	0.0330
	Max	11.9	3.27	0.705	2.42	0.384	2.07	0.409	1.07	0.138	0.847	0.215
	Median	7.98	1.45	0.457	1.65	0.222	1.28	0.231	0.845	0.0980	0.601	0.146

Among the TCEs, the highest concentration was measured for Zr, up to values of 392 ng L^{-1} at the Milazzo sampling site, and a median concentration of 133 ng L^{-1} by considering all the sampling sites. Nevertheless, the higher median concentration (160 ng L^{-1}) was calculated for the Siracusa sampling site The lowest median concentration was measured for Tm (0.0890 ng L^{-1}) at the Milazzo sampling site. For Sc (5.10 ng L^{-1}), Nb (0.895 ng L^{-1}), and Te (3.26 ng L^{-1}) the highest median concentrations were measured at the Siracusa sampling site. For Y (13.8 ng L^{-1}), Hf (2.62 ng L^{-1}), and Th (2.26 ng L^{-1}), the highest median concentrations were measured at the Augusta sampling site. Finally, for Ge (2.86 ng L^{-1}), the highest median concentration was measured at the Milazzo sampling site. The median concentrations of lanthanoid follow this order: La > Ce > Nd > Pr ≈ Sm > Gd > Dy > Er ≈ Yb > Eu > Ho ≈ Tb > Tm ≈ Lu. For all lanthanoids, similar median concentrations were measured in rainwater samples from the two industrial areas.

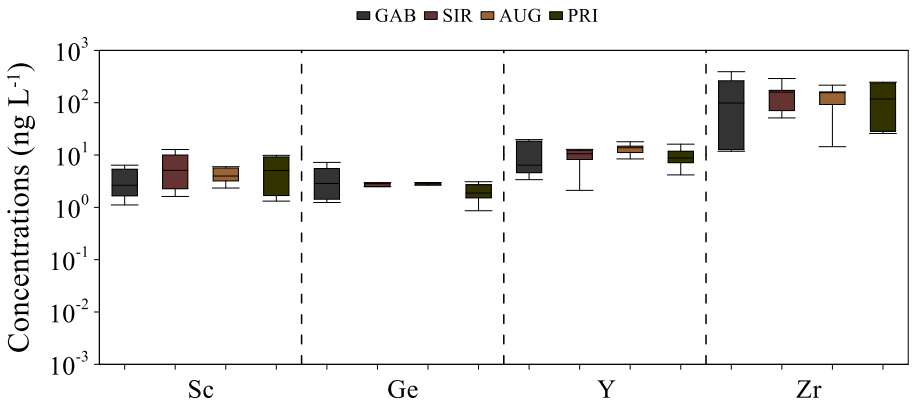

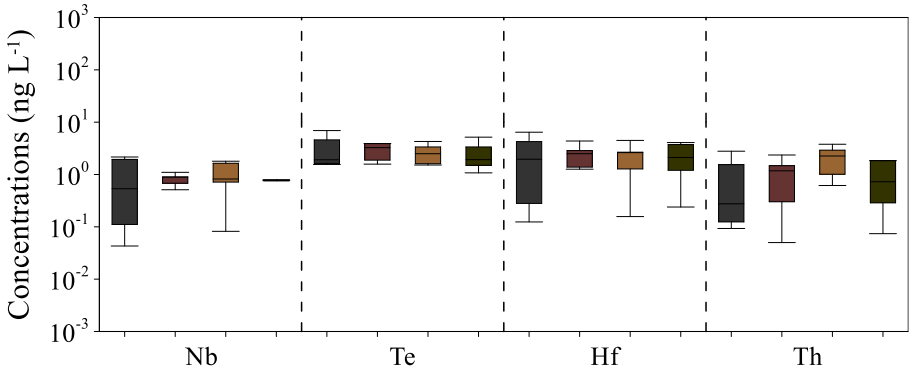
Concentrations (ng L-1)
10^3
10^2
10^1
10^0
10^-1
10^-2
10^-3
Nb
Te
Hf
Th

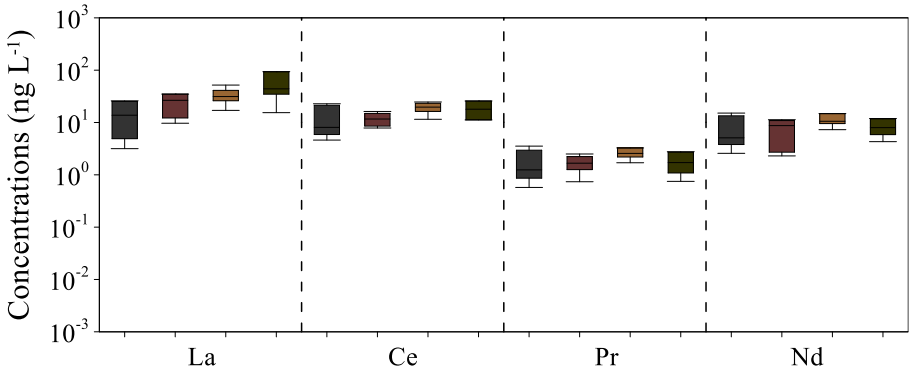
Concentrations (ng L-1)
10^3
10^2
10^1
10^0
10^-1
10^-2
10^-3
La
Ce
Pr
Nd

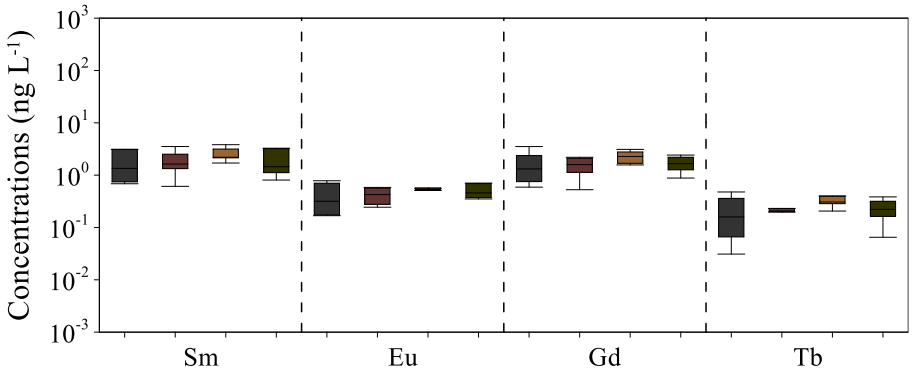
Concentrations (ng L-1)
10^3
10^2
10^1
10^0
10^-1
10^-2
10^-3
Sm
Eu
Gd
Tb

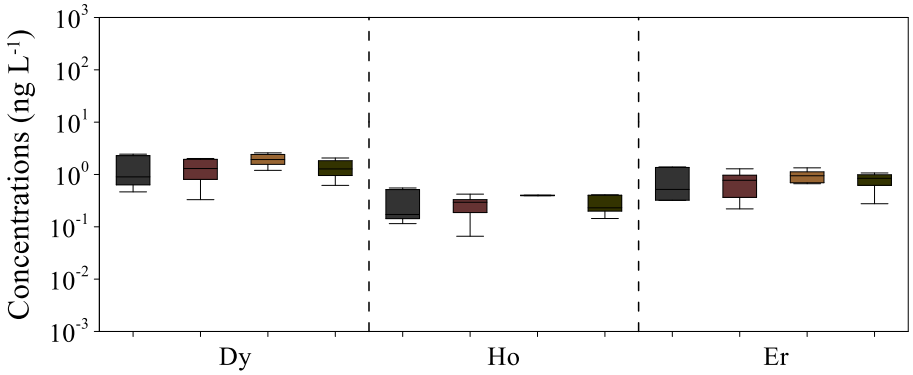
Concentrations (ng L-1)
10^3
10^2
10^1
10^0
10^-1
10^-2
10^-3
Dy
Ho
Er

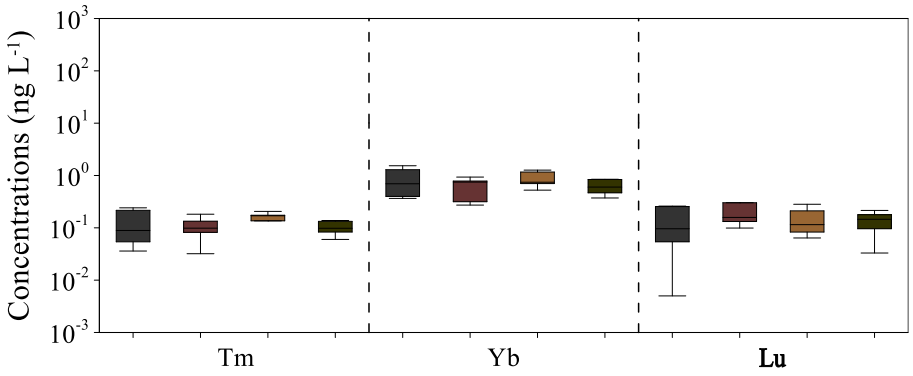

Figure 42 - TCE concentrations (ng L^{-1}) in the rainwater samples from the Milazzo and Priolo Gargallo industrial areas. The elements are ordered from highest to lowest atomic weight.

4.4.5 Boron and strontium isotopic composition

Boron ($\delta^{11}B/^{10}B$) and Strontium ($^{87}Sr/^{86}Sr$) isotopic composition were measured in 2 and 3 rainwater samples, respectively for the Milazzo and the Priolo Gargallo industrial areas. The main statistical parameters (minimum, median, maximum) are given in Table 33.

Table 33 - Main statistical parameters for boron ($\delta^{11}B$‰) and strontium ($^{87}Sr/^{86}Sr$) in the Milazzo and the Priolo Gargallo industrial areas rainwater samples. Dev. Std. is the Standard Deviation for boron isotopic composition, while Std. Err. is the Standard Error for strontium ratio measurements.

Site	$^{87}Sr/^{86}Sr$			
	Min	Median	Max	Std. Err.
Milazzo	0.708768	0.708946	0.709125	0.000009
Siracusa	0.708572	0.708631	0.708690	0.000011
Priolo Gargallo	0.709919	0.709919	0.709919	0.000007
Site	$\delta^{11}B$ (‰)			
	Min	Median	Max	Dev. Std.
Milazzo	30.91	32.30	33.68	0.08
Siracusa	27.41	31.86	36.32	0.19
Priolo Gargallo	37.82	37.82	37.82	0.23

The lowest $\delta^{11}B$ values were measured in the samples from Siracusa, up to +27.41‰ ± 0.19‰. The lowest $\delta^{11}B$ median value (+31.86‰ ± 0.19‰) was measured in the same sampling site. The highest absolute $\delta^{11}B$ value was measured in the rainwater sample from Priolo Gargallo

(+37.82‰ ± 0.23‰).

Strontium isotopic composition ranged from 0.708557 ± 0.000011 (Siracusa) to 0.709919 ± 0.000007 (Priolo Gargallo). The lowest and the highest median $^{87}Sr/^{86}Sr$ ratios were measured for Siracusa (0.708572 ± 0.000011) and Priolo Gargallo (0.709923 ± 0.000007) sampling sites, respectively. To verify the stability in the measurement of a repeated sample, two replicates of the rainwater sample no. 4 of the Siracusa site were analysed; $^{87}Sr/^{86}Sr$ ratios of 0.708572 ± 0.000011 and 0.708557 ± 0.000015 were measured. Two replicates of the rainwater sample no. 13 of the Priolo Gargallo site were prepared with two different chemical procedures and were analysed for the strontium isotopic composition. $^{87}Sr/^{86}Sr$ ratios of 0.709919 ± 0.000005 and 0.709926 ± 0.000008 were measured.

4.5 Mt. Soro (Nebrodi) background area

The sequential number of samples and their sampling periods, for each monitoring site in the Etna area, are shown in Table 34.

Table 34 - Sequential number of samples and sampling periods for the Mt. Soro sampling site.

Site	No. Sample	Installed	Sampled	Time Exp. (day)
Mt. Soro	1	04/03/2021	30/03/2021	26
	2	30/03/2021	28/04/2021	29
	3	28/04/2021	27/05/2021	29
	4	27/05/2021	30/06/2021	34
	5	30/06/2021	01/08/2021	32
	6	01/08/2021	/	/
	7	21/09/2021	13/10/2021	22
	8	13/10/2021	01/11/2021	19
	9	01/11/2021	22/11/2021	21
	10	22/11/2021	21/12/2021	29
	11	21/12/2021	18/01/2022	28
	12	18/01/2022	24/02/2022	37
	13	24/02/2022	29/03/2022	33
	14	29/03/2022	26/04/2022	28
	15	26/04/2022	25/05/2022	29
	16	25/05/2022	23/08/2022	90
	17	23/08/2022	27/09/2022	35
	18	27/09/2022	27/10/2022	30
	19	27/10/2022	21/11/2022	25
	20	21/11/2022	20/12/2022	29
	21	20/12/2022	24/01/2023	35
	22	24/01/2023	13/02/2023	20

4.5.1 Chemical-physical parameters (pH, EC)

4.5.1.1 The acidity of rainwater

The pH values of the rainwater samples collected in the Mt. Soro sampling site showed great variability during the two years of monitoring, ranging from 4.5 to 7.6, with a median value of 6.2. The pH values are reported in Table 35 and shown in Figure 43. The frequency distribution of pH was unimodal, with the highest frequency in the pH range 6.0 – 6.5 (~ 32%) (Fig. 43). In the Mt. Soro background study area, only a few rainwater samples had pH values below 5.6 (~ 10%).

Table 35 - Statistical parameters for rainwater's pH in the Mt. Soro background area.

Study area	Site	Min	Max	Median	Q1	Q3
Mt. Soro	CES	4.5	7.6	6.2	5.9	7.2

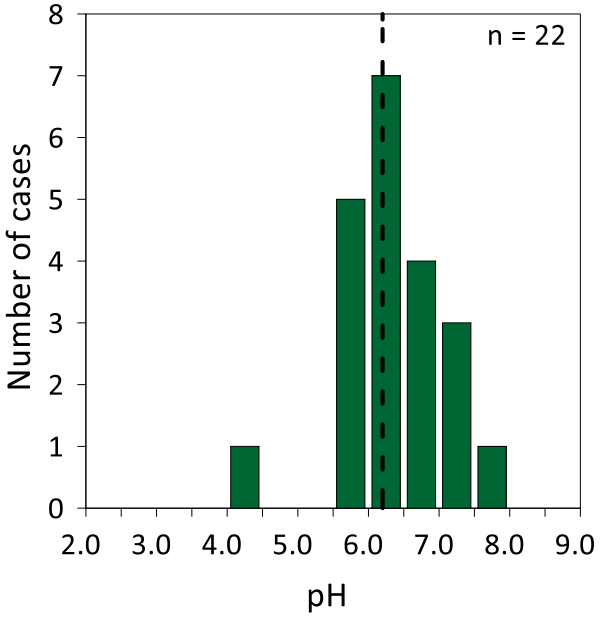

Figure 43 - Frequency distribution of pH in Mt. Soro (22 samples) rainwater samples. The black dashed line is the median.

The lowest pH value at the Mt. Soro sampling site was measured in the rainwater sample from the last sampling period (24/01/2023 – 13/02/2023), the highest in sample no. 03 (period 28/04/2021 – 27/05/2021).

4.5.1.2 The Electric Conductivity (EC) of rainwater

The EC values of the rainwater samples collected in the Mt. Soro background area, showed great variability during the two years of monitoring, ranging from 8.4 to 121 µS cm^{-1}, with a median of 27.2 µS cm^{-1}. For a better graphical representation, the Log_{10} of the electric conductivity values were calculated. The statistical parameters for the EC are reported in Table 36 and the measured values are shown in Figure 44.

Table 36 - Statistical parameters for rainwater's EC (Log_{10}) at Mt. Soro background area.

Study area	Site	Min	Max	Median	Q1	Q3
Mt. Soro	CES	0.924	2.08	1.43	1.18	1.83

The probability distribution was unimodal and the class with the highest frequency (~ 23%) lies in the EC range of 1.4 – 1.6. The Electric Conductivity values were generally low, with values below 2 (on a Log_{10} basis) for almost 95% of the entire population (Fig. 44). These EC values are typical of rain with a relatively low amount of dissolved ions.

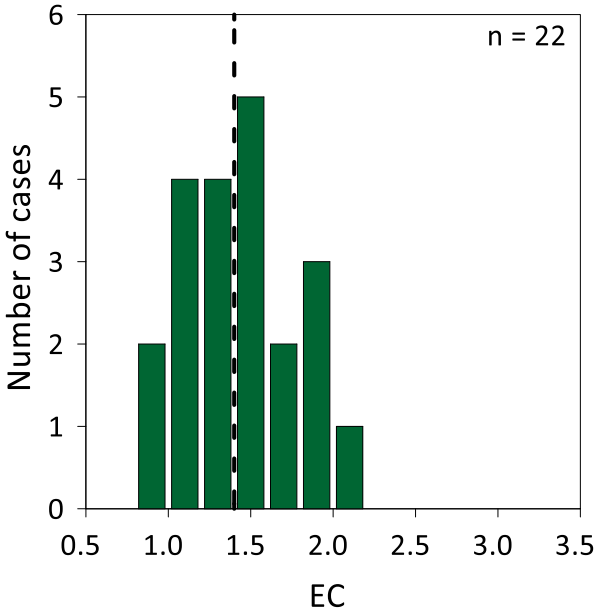

Figure 44 - Frequency distribution of EC (Log_{10}) in Mt. Soro rainwater samples (22 cases). The black dashed line is the geometric mean.

4.5.2 Major inorganic ions

A summary of statistical parameters of the analysed major ions in rainwater samples from the Mt. Soro background area is provided in Table 37. Volume-weighted mean and non-sea-salt concentrations were calculated using equation (2) and (4), respectively. A total of 21 rainwater samples were analysed for major ions. For F^- the concentration could not be determined in ~ 38% of the samples. No rain sample had a pH below 4.3, nevertheless for HCO_3^- the percentage of < LOQ was ~ 19%. For NH_4^+ and SO_4^{2-} the < LOQ was ~ 10%. For NO_3^- and Cl^- it was not possible to quantify the concentrations in ~ 5% of the rainwater samples. Finally, in all the analysed samples was possible to quantify the concentrations of K^+, Na^+, Mg^{2+}, and Ca^{2+}.

Table 37 - Statistical parameters for major ions ($\mu eq\ L^{-1}$) in Mt. Soro rainwater samples.

Site		F^-	Cl^-	NO_3^-	SO_4^{2-}	HCO_3^-	Na^+	K^+	NH_4^+	Mg^{2+}	Ca^{2+}
	Min	<LOQ	<LOQ	<LOQ	<LOQ	<LOQ	34.0	3.07	<LOQ	15.1	17.7
	Max	32.8	383	285	158	1166	363	139	141	304	2068
Mt. Soro	VWM	2.06	101	25.6	37.6	162	114	8.42	29.8	38.8	121
	ss (%)	0.8	100	0	36.9	0.3	100	29.6	0	65.9	4.1
	nss (%)	99.2	0	100	63.1	99.7	0	70.4	100	34.1	95.9

Chemical abundances, expressed as μeq L^{-1}, are represented by a Tukey box plot (Fig. 45).

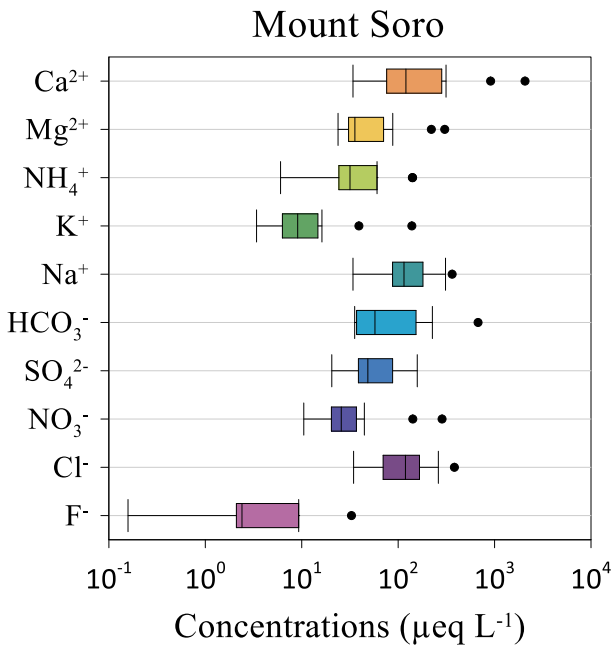

Figure 45 - Major ion concentrations (μeq L^{-1}) in Mt. Soro rainwater samples.

The most saline rainwater sample, in terms of Total Dissolved Solids (TDS), with a value of 4230 μeq L^{-1} (130 mg L^{-1}), was collected in the sampling period no. 04 (27/05/2021 – 30/06/2021) The less saline rainwater sample, with a value of 255 μeq L^{-1} (8.12 mg L^{-1}), was collected in the sampling period no. 23 (24/01/2023 – 13/12/2023).

The relative VWM concentrations of the major anions follow the sequence HCO_3^- > Cl^- > SO_4^{2-} > NO_3^- > F^-. Therefore, bicarbonate was the main anion, with a relative abundance of 49.3% (Fig. 46), and a VWM concentration of 162 μeq L^{-1}. The relative contributions were 30.7%, 14.5%, 7.82%, and 0.629%, while the VWM concentrations were 101 μeq L^{-1}, 37.6 μeq L^{-1}, 25.6 μeq L^{-1}, and 2.06 μeq L^{-1}, for Cl^-, SO_4^{2-}, NO_3^-, and F^-, respectively.

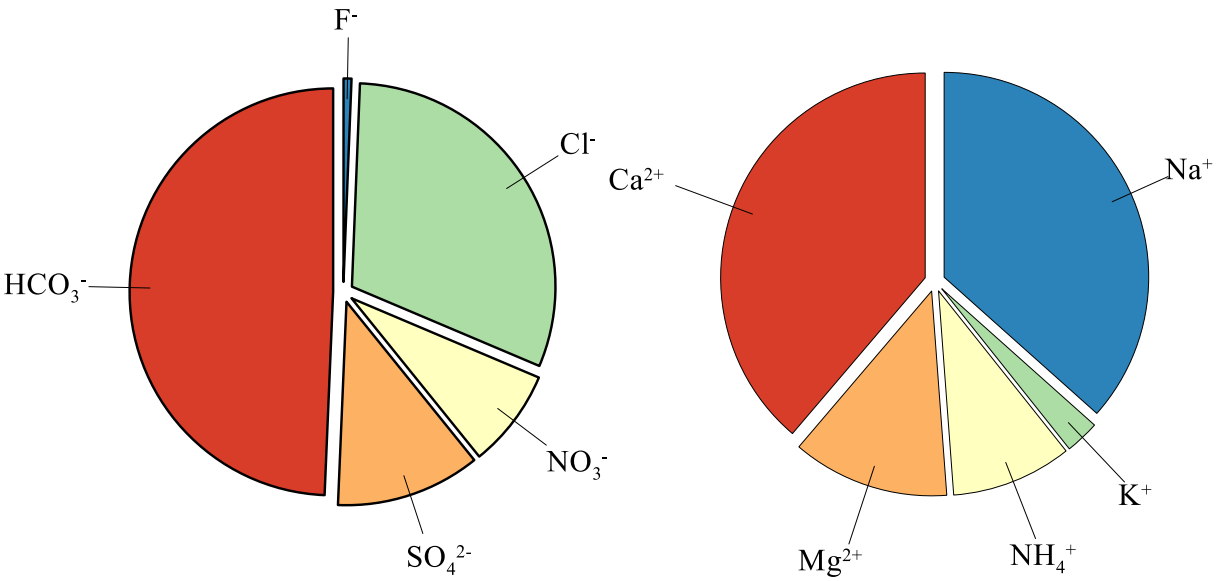

Figure 46 - Relative abundances (Eq%) of major anions and cations in the rainwater samples from the Mt. Soro background area.

As regards major cations, the sequence of relative abundances was Ca^{2+} > Na^{+} > Mg^{2+} > NH_4^{+} > K^{+}. Therefore, calcium was the main cation, with relative abundances of 38.8% (Fig. 46), and a VWM concentration of 121 μeq L^{-1}. The relative contributions were 36.6%, 12.4%, 9.53%, and 2.70%, while the VWM concentrations were 114 μeq L^{-1}, 38.8 μeq L^{-1}, 29.8 μeq L^{-1}, and 8.42 μeq L^{-1}, for Na^{+}, Mg^{2+}, NH_4^{+}, and K^{+}, respectively.

4.5.3 Minor and trace elements concentrations

4.5.3.1 Rainwater samples

A summary of statistical parameters of the analysed minor and trace elements in the rainwater samples from the Mt. Soro background area is provided in Table 38, and Figure 47. A total of 21 rainwater samples were analysed for minor and trace elements. It was not possible to determine the concentration of Sn and Cs in ~ 76% and in ~ 29% of the cases. For B, Al, V, Cr, Ni, Cu, Zn, As, Rb, Se, Sb, and Ba it was always possible to determine the concentrations, while for the other elements, it was not possible to do so in between approximately 5% and 19% of the cases.

Table 38 - Statistical parameters for minor and trace element concentrations (µg L^{-1}) in the sampling site of Mt. Soro. Sample n. is the number of samples in which the maximum concentration was measured for each element.

Mt. Soro	Element	Li	B	Al	Ti	V	Cr	Mn	Fe	Co	Ni	Cu	Zn	As
	Min	< LOQ	0.578	0.556	< LOQ	0.108	0.0170	< LOQ	< LOQ	< LOQ	0.0280	0.0360	1.99	0.0230
	Max	1.11	30.2	123	0.618	2.31	0.369	11.4	16.5	0.176	1.26	6.68	25.7	0.464
	Sample n.	03	04	12	09	04	14	13	17	14	04	04	07	04
	VWM	0.0692	3.69	11.3	0.190	0.293	0.0647	2.86	5.22	0.0323	0.328	1.77	7.49	0.0790
	Element	Se	Br	Rb	Sr	Mo	Cd	Sn	Sb	Cs	Ba	Tl	Pb	U
	Min	< LOQ	< LOQ	0.0770	2.67	< LOQ	< LOQ	< LOQ	0.0270	< LOQ	1.02	< LOQ	< LOQ	< LOQ
	Max	0.824	37.9	1.69	94.2	0.311	0.0720	0.0600	0.913	0.0130	24.7	0.124	0.970	0.0220
	Sample n.	12	04	04	04	04	12	09	04	04	04	12	09	04
	VWM	0.155	12.3	0.232	9.84	0.0347	0.0217	0.00925	0.103	0.00252	3.62	0.0137	0.0878	0.00234

The lowest VWM concentration was calculated for U (0.00234 µg L^{-1}), and the highest for bromide (12.3 µg L^{-1}). A relevant intra-site variability, up to two orders of magnitude, was observed for different periods of sampling (Fig. 47).

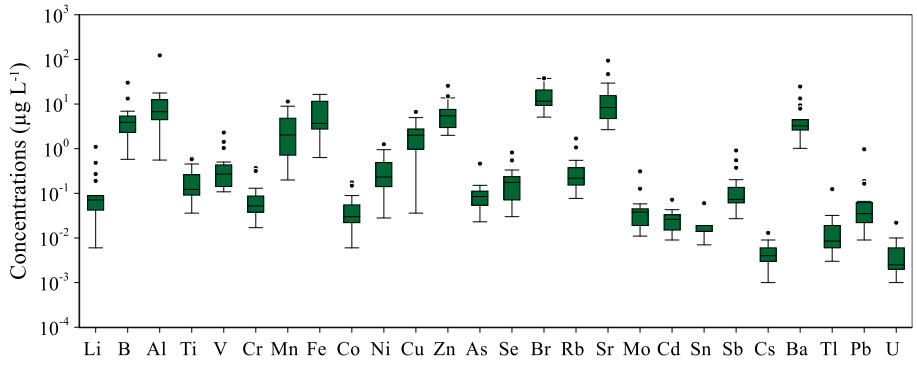

Figure 47 - Minor and trace element concentrations (µg L^{-1}) in Mt. Soro rainwater samples.

4.5.3.2 Insoluble fraction

To characterise the chemical composition of the insoluble fraction of the atmospheric deposition, the material retained by the membrane filters (> 0.45 µm) was mineralised according to the procedure described in paragraph 3.1.3. A summary of statistical parameters of the analysed minor and trace elements in the insoluble fraction solutions is provided in Table 39, and Figure 48. A total of 21 insoluble fraction solutions were analysed for minor and trace element concentrations. Only for Mo (~ 14%), and As (~ 10%) it was not possible to determine the concentration in some

samples. For the remaining elements, the concentrations were quantified in all the samples. The median concentrations ranged from 2.47 µg L^{-1} for Mo to 30.7 mg L^{-1} for Al.

Table 39 - Statistical parameters for minor and trace element concentrations in the insoluble fraction solutions of Mt. Soro. The concentrations are in µg L^{-1}, except for Al, Ti, Fe, and Zn (mg L^{-1}).

	Element	Li	B	Al	Ti	V	Cr	Mn	Fe	Co	Ni	Cu	Zn	As
Mt. Soro	Min	2.55	2.10	3.74	0.120	8.08	10.8	29.8	3.39	0.605	5.92	17.1	0.0749	0.221
	Max	360	567	1161	78.9	2852	514	15360	889	317	253	2976	3.94	62.2
	Median	18.0	41.0	30.7	0.653	49.6	79.3	357	24.6	7.19	24.3	121	0.420	7.59
	Element	Se	Br	Rb	Sr	Mo	Cd	Sn	Sb	Cs	Ba	Tl	Pb	U
	Min	13.9	0.327	n.d.	n.d.	n.d.	n.d.	22.1	n.d.	5.08	n.d.	n.d.	n.d.	n.d.
	Max	13081	24.8	n.d.	n.d.	n.d.	n.d.	6774	n.d.	188	n.d.	n.d.	n.d.	n.d.
	Median	n.d.	n.d.	n.d.	64.3	2.47	n.d.	n.d.	n.d.	n.d.	140	n.d.	26.2	n.d.

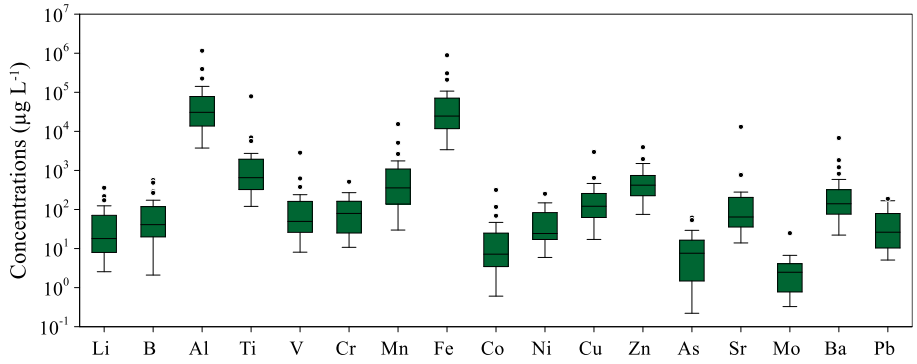

Figure 48 - Minor and trace element concentrations (µg L^{-1}) in the insoluble fraction solutions of Mt. Soro.

4.5.3.3 Rinse solutions

The concentration of minor and trace elements in the material remaining adhered to the surfaces of the bulk collector was quantified by analysing a rinse aliquot prepared according to the procedure described in paragraph 3.1.2. The concentrations of the analysed minor and trace elements in the rinse solutions from the Mt. Soro background area are provided in Table 40. Two rinse solutions were analysed for minor and trace element concentrations. It was not possible to quantify the concentration of Li and Sn, and of Co, Tl, and U it was possible to do that only for one sample. For the other elements, it was always possible to determine the concentrations.

Table 40 - Statistical parameters for minor and trace element concentrations (µg L^{-1}) in Mt. Soro rinse solutions.

Mt. Soro	Li	B	Al	Ti	V	Cr	Mn	Fe	Co	Ni	Cu	Zn	As
	<LOQ	8.31	23.8	0.367	0.0170	0.152	1.10	12.9	0.00500	0.189	1.05	17.6	0.0150
	<LOQ	41.0	198	1.12	0.290	0.164	21.3	46.5	0.145	0.575	9.79	44.0	0.105
	Se	Br	Rb	Sr	Mo	Cd	Sn	Sb	Cs	Ba	Tl	Pb	U
	0.0800	2.76	0.0220	0.903	0.0250	0.0240	<LOQ	0.132	0.00100	1.462	<LOQ	0.362	<LOQ
	0.469	2.24	1.13	11.7	0.0240	0.158	<LOQ	0.176	0.0100	17.5	0.0160	2.73	0.0420

At the Mt. Soro site, the concentrations for minor and trace elements in the rinse solutions were between 0.0100 µg L^{-1} for Cs to 198 µg L^{-1} for Al. High concentrations were also measured for B, Fe, Mn, and Zn.

4.5.4 Technology-Critical Elements concentrations

Eight preconcentrated rainwater samples were prepared, according to the procedure illustrated in paragraph 3.1.4, for the determination of the concentrations of the Technology-Critical Elements, including the lanthanoids. It was not possible to determine the concentration of Nb, Ge, and Tm in ~ 38%, 25%, and 25% of the samples, respectively. For Y, Te, Hf, Ce, Pr, Sm, Eu, Gd, Tb, Dy, Ho, Er, Yb, and Lu, it was not possible to quantify the concentrations in only one sample (12.5%). For the remaining elements, the concentrations were quantified in all the samples. A summary of the statistical parameters of the analysed TCEs is provided in Table 41, and Figure 49.

Table 41 - Statistical parameters for TCE concentrations (ng L^{-1}) in the Mt. Soro preconcentrated rainwater samples.

Mt. Soro	Element	Sc	Ge	Y	Zr	Nb	Te	Hf	Th	La	Ce	Pr
	Min	0.482	0.834	5.58	2.02	0.250	0.815	0.109	0.153	1.46	6.93	0.802
	Max	4.99	5.18	22.9	202	2.18	4.24	3.73	7.89	35.7	42.9	4.59
	Median	1.75	1.08	9.85	22.1	0.315	1.85	0.299	1.41	9.89	17.3	2.14
	Element	Nd	Sm	Eu	Gd	Tb	Dy	Ho	Er	Tm	Yb	Lu
	Min	2.40	0.722	0.259	0.911	0.141	0.613	0.123	0.451	0.0570	0.344	0.0380
	Max	21.9	5.50	1.39	5.57	0.681	3.39	0.701	1.47	0.249	1.65	0.282
	Median	7.10	1.83	0.478	1.63	0.213	1.50	0.258	0.732	0.0945	0.606	0.113

Among the TCEs, the highest concentration was measured for Zr, up to values of 202 ng L^{-1} and a median concentration of 22.1 ng L^{-1}. The lowest median concentration was measured for Tm (0.0945 ng L^{-1}). The median concentrations of lanthanoid follow this order: La > Ce > Nd > Pr ≈ Sm > Gd > Dy > Er ≈ Yb > Eu > Ho ≈ Tb > Tm ≈ Lu. A great variability, up to two orders of magnitude for Zr, was observed during the two years of monitoring.

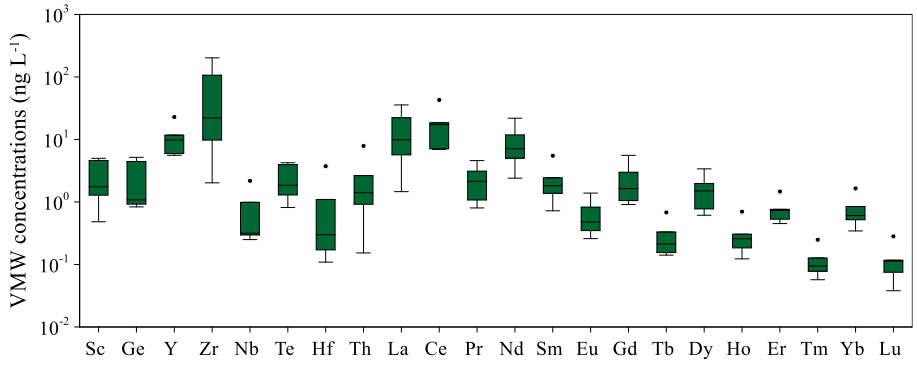

Figure 49 - TCE concentrations (ng L^{-1}) in the Mt. Soro sampling site.

4.5.5 Boron and strontium isotopic composition

Boron ($\delta^{11}B/^{10}B$) and Strontium ($^{87}Sr/^{86}Sr$) isotopic composition were measured in 4 rainwater samples. The main statistical parameters (minimum, median, maximum) are given in Table 42.

Table 42 - Main statistical parameters for boron ($\delta^{11}B$‰) and strontium ($^{87}Sr/^{86}Sr$) in the Mt. Soro rainwater samples. Dev. Std. is the Standard Deviation for boron isotopic composition, while Std. Err. is the Standard Error for strontium ratio measurements.

Site	$^{87}Sr/^{86}Sr$			
	Min	Median	Max	Std. Err.
Mount Soro	0.707193	0.709031	0.709283	0.000010
Site	$\delta^{11}B$ (‰)			
	Min	Median	Max	Dev. Std.
Mount Soro	22.61	39.37	40.33	0.17

The $\delta^{11}B$ values were between +22.61 and +40.33 ± 0.17‰, with a median value of +39.40 ± 0.17‰. To verify the stability in the measurement of a repeated sample, two replicates of the rainwater sample no.12 were analysed; $\delta^{11}B$ values of +38.30‰ ± 0.14‰ and +38.85‰ ± 0.23‰ were measured.

Strontium isotopic composition ranged from 0.707193 to 0.709283 ± 0.000010, with a median of 0.709031 ± 0.000010.

5. Discussion

5.1 Buffering of the natural acidity of rainwater

The acidity of natural pristine rainwater in the background atmosphere is mainly controlled by the dissociation of dissolved atmospheric CO_2. Assuming an equilibrium at 25 °C between pure water and atmospheric CO_2, with a partial pressure of $10^{-4.0}$ atm, the equilibrium pH of the solution will be ~ 5.60. Anthropogenic emissions are considered the main acidifying agent of rainwater (*Seinfeld & Pandis, 1998*) although some natural processes may also contribute (e.g., acid gases of volcanic emissions - *Calabrese et al., 2011*). Organic acid produced by biomass burning may also contribute to the lowering of the pH of rainwater (*Berner & Berner, 1987; Brugnone et al., 2020*). High acidities in precipitation could enhance the mobility of trace metals, by increasing the stability of their aqueous species. On the contrary, in the Mediterranean area, as well as in other areas with an extensive presence of geogenic dust, mainly deriving from limestone formations (*Al-Momani et al., 2008; D'Alessandro et al., 2013*), rainwater is prevailingly alkaline due to the titration of the acidity by the carbonate particles (*Al-Momani et al., 2008*; *D'Alessandro et al., 2013*; *Brugnone et al., 2020; 2023a*). The wash-out of below-cloud alkaline aerosols neutralises natural rainwater acidity (*D'Alessandro et al., 2013; Amodio et al., 2014; Brugnone et al., 2023a*). Previous authors evidenced widespread acid-rain neutralisation by atmospheric carbonate dust over the entire Mediterranean basin, induced by the frequent arrival of Saharan dust (*Al-Momani et al., 1995*; *Guerzoni et al., 1999*; *Galy-Lacaux et al., 2009*; *Laouali et al., 2012*). Therefore, the chemical composition of water droplets reflects the direction taken by the acid-base titration.

The rainwater samples were divided into two groups: alkaline and acidic. In the Mt. Etna study area, the acidic group accounted approximately for 51% of the entire population, and this was probably the result of the interaction with volcanic-derived CO_2, SO_2, and especially with halogen gases (HCl, HF, HBr). The consequence was the formation of sulfuric, hydrochloric, and

hydrofluoric acids. Conversely, the alkaline group accounted approximately for 49% of the entire population. In the Palermo urban area, only 4.9% of the population belonged to the acidic group, while in the Catania urban area, the percentage of samples belonging to this group was 29%. These results highlight a strong neutralisation of the natural acidity of rainwater during the wash-out of below-cloud alkaline aerosols. The differences observed between the Palermo area and the Catania area may be explained by a greater contribution of gaseous species able to produce a decrease in the pH of rainwater, both attributable to anthropogenic sources and, in some periods, also to the volcanic source (Mt. Etna), in the latter more than in the former. Another explanation can be sought in the different geological contexts in which the two study areas fall. As illustrated in section 2.3 "Palermo and Catania urban areas", indeed, in the Palermo area there are extensive carbonate and limestone outcrops, while in the Catania area, the prevalent lithology (excluding volcanic rocks) is that of marly clays. In the Milazzo and Priolo Gargallo industrial areas, only 18% of the rainwater samples belonged to the acidic group. The observed acidity of these samples was due to the influence of anthropogenic (urban and/or industrial) NO_X and SO_X gaseous pollutants, deriving from a combination of local and regional sources (*Xing et al., 2017*; *Brugnone et al., 2023a*). The results observed for these two industrial areas agree with those observed by Brugnone et al. (2023a) in the same areas (20%). Finally, in the Mt. Soro background area, only one of the twenty-two rainwater samples collected (~ 5%) had a pH value below 5.6. This study area is mainly characterised by flysch successions with prevailing clayey lithology and the absence of acidifying sources.

By using equation (5) in section 3.6, the neutralisation factors of the acidity of rainwater were calculated for each study area and different cations (K^+, NH_4^+, Mg^{2+}, and Ca^{2+}). As regards the Mt. Etna study area, values obtained from the VWM concentrations ranged from 0.06 to 0.21 for K^+, from 0.06 to 0.52 for NH_4^+, from 0.11 to 0.44 for Mg^{2+}, and from 0.42 to 1.56 for Ca^{2+} (Fig. 50a). For each major cation, the lowest neutralisation factor was calculated for the Cratere 2001 site and the highest for the Mt. Intraleo sampling site. The results suggest that Ca^{2+} was the major

neutralising agent in the area. Furthermore, the neutralisation of the acidity of the rainwater samples from the Cratere 2001 sampling site was only partial due to the very high concentration of nss-sulfate, which showed a VWM concentration of 889 μeq L^{-1}. In the Palermo urban area, the neutralisation factors were between 0.10 and 0.18 for K^+, 0.13 and 0.36 for NH_4^+, 1.02 and 1.11 for Mg^{2+}, and between 2.07 and 3.01 for Ca^{2+} (Fig 50b). In the Catania urban area, the neutralisation factors were between 0.09 and 0.10 for K^+, between 0.14 and 0.37 for NH_4^+, 0.50 and 0.59 for Mg^{2+}, and between 1.30 and 1.68 for Ca^{2+} (Fig. 50b). Higher neutralisation ratios were calculated for the study area of Palermo, than for the Mt. Etna and the Catania areas, especially for Mg^{2+} and Ca^{2+}. The main contribution of Mg^{2+} and Ca^{2+} to the rainwater of the Palermo urban area originated from the erosion of the extensive outcrops of carbonate rocks and soils. As regards the Milazzo and the Priolo Gargallo industrial areas, the neutralisation factors ranged from 0.08 to 0.25 for K^+, from 0.11 to 0.32 for NH_4^+, from 0.66 to 0.86 for Mg^{2+}, and from 1.28 to 1.74 for Ca^{2+} (Fig. 50c). Brugnone et al. (2023a) observed similar ratios in the same industrial areas, in a different period of study. Finally, for the Mt. Soro background area, neutralisation factors of 0.13, 0.47, 0.61, and 1.92 were calculated for K^+, NH_4^+, Mg^{2+}, and Ca^{2+}, respectively (Fig 50d).

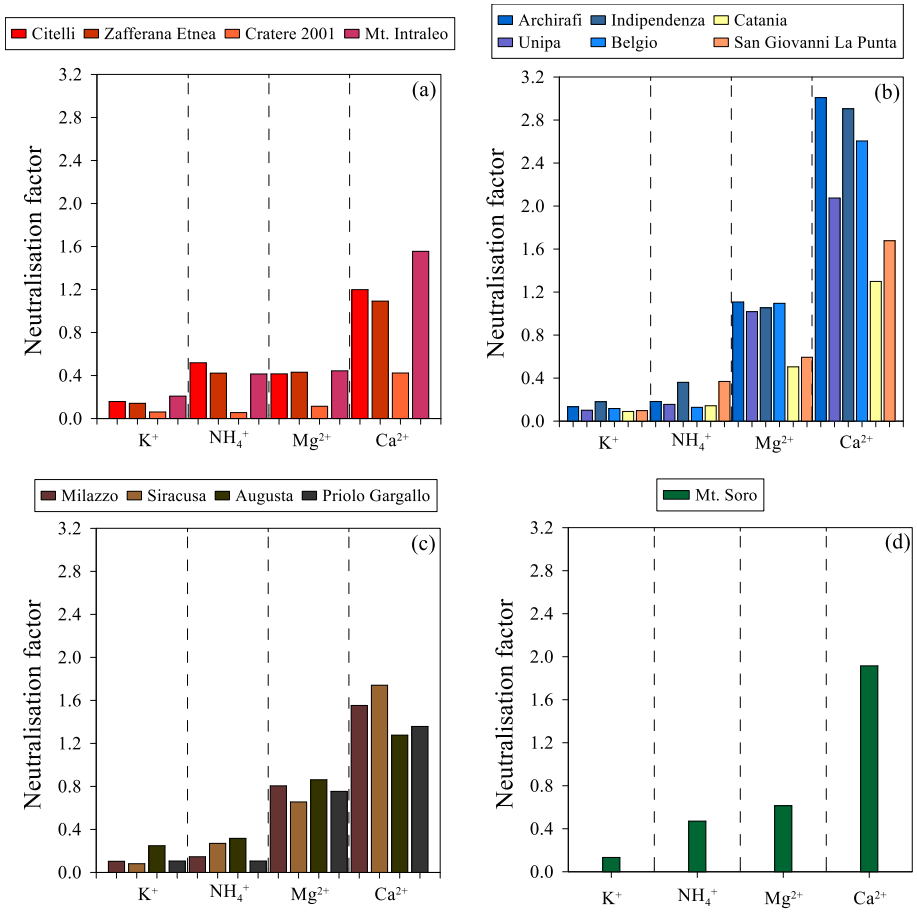

Figure 50 - Neutralisation factors for K^+, NH_4^+, Mg^{2+}, and Ca^{2+} in Mt. Etna (a), Palermo and Catania (b), Milazzo and Priolo Gargallo (c), and Mt. Soro (d) study areas.

Considering the results from all study areas, it can be observed that Ca^{2+} and Mg^{2+} were the two species that contributed the most to the neutralisation of rainwater acidity. For Ca^{2+}, seasonal variability in the magnitude of the neutralisation factors was observed, with the maximum effect observed during periods with frequent high-intensity winds from southern directions and a reduced number of precipitation events. During periods characterised by low rainfall, soils with reduced moisture levels are affected by strong erosive processes, particularly if high-intensity winds occur during dry periods.

Therefore, in this research, Ca^{2+} and Mg^{2+} were considered the primary neutralising components of rainwater (NP), while $nssSO_4^{2-}$ and NO_3^- acted as the primary acidifying components of rain (AP) (*Huang et al., 2008*). The equilibrium between acidity and alkalinity (NP/AP) was

evaluated using equation (6) in section 3.6. The results are shown in Figure 51. In the Mt. Etna study area, the ratio NP/AP varied from 0.54 (Cratere 2001) to 2.00 (Mt. Intraleo). For the Palermo urban area from 3.09 (Unipa) to 4.12 (Archirafi), while for the Catania urban area from 1.80 (Catania) to 2.27 (San Giovanni La Punta). For Milazzo and Priolo Gargallo industrial areas, the NP/AP ratios were between 2.11 (Priolo Gargallo) and 2.40 (Siracusa). Finally, in the Mt. Soro background area, the NP/AP ratio was 2.53.

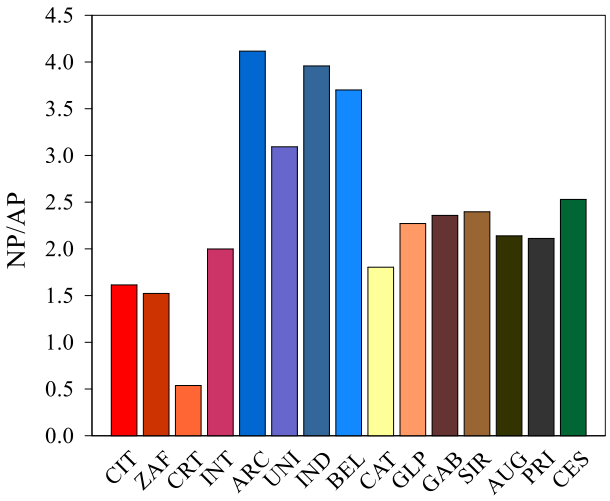

Figure 51 - Neutralising/acidifying component ratios in all the sampling sites.

As observed for the neutralisation factors, the neutralisation of the acidity of the rainwater samples from the Cratere 2001 sampling site was only partial. Nevertheless, the lowest median pH value was recorded at the Citelli site (4.4) and not at the Cratere 2001 site (5.5), highlighting a greater influence by volcanic acidic species such as HCl, HF, and HBr on the rainwater chemistry of the former rather than the latter study site. The stronger neutralisation of Mt. Etna's rainwater acidity was observed for the Mt. Intraleo site. The site of Citelli was on the downwind sector, the Mt. Intraleo site on the up-wind flank and can be considered as representative of the local background. The measured pH values confirm earlier findings (*Aiuppa et al., 2006*; *Calabrese et al., 2011*), that the prevailing wind direction plays a key role in the chemical composition of rainwater. In other

words, pH measurement provides clues on the degree of interaction, evidencing that volcanic emissions of Mt. Etna have a strong influence on the acidity of rainwater. Overall, the most intense neutralisation of rainwater acidity was observed for the urban area of Palermo, the study area most influenced by the outcrop of rocks and soils with a carbonate composition. The results confirm the buffering role of the natural acidity of rainwater by the atmospheric geogenic particulate matter (with a high content of Ca^{2+} and Mg^{2+}), which represents a significant source of CCNs of raindrops. Also, NH_4^+ can act as a neutralisation factor, and it was derived mainly from anthropogenic sources, such as agricultural practices. It would be important to distinguish whether ammonia dissolves in rainwater as a gas or as solid particles of $(NH_4)_2SO_4$ or NH_4Cl since the effects are opposite in the two cases (*Dongarrà & Francofonte, 1995*).

A weak positive Pearson correlation (R = 0.291, p-value < 0.0001) was observed between Ca^{2+} and SO_4^{2-} (Fig. 52a) and between pH and Ca^{2+} (R = 0.243, p-value < 0.0001), (Fig. 52b). No correlation was found between pH and SO_4^{2-} (R = 0.037, p-value = 0.5324), (Fig. 52c).

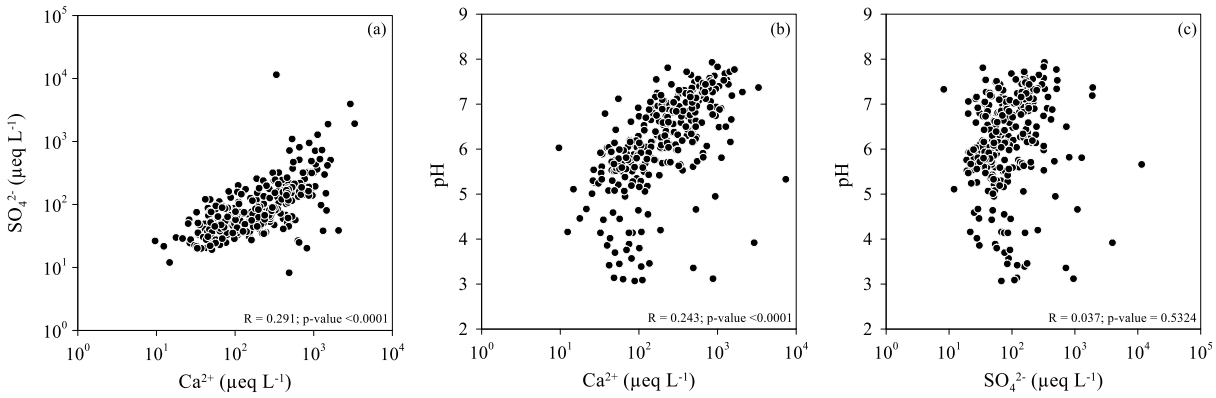

Figure 52 - Pearson correlations between (a) Ca^{2+} and SO_4^{2-} ($\mu eq\ L^{-1}$) and between pH and (b) Ca^{2+} ($\mu eq\ L^{-1}$), and (c) SO_4^{2-} ($\mu eq\ L^{-1}$).

Rainwater samples characterised by a high load of SO_4^{2-}, for which we could expect relatively low pH values, usually also show a high load of Ca^{2+}, thus suggesting that the residual

acidity from SO_2-derived SO_4^{2-} was neutralised by the high load of Ca^{2+}; contrarily, low concentrations of Ca^{2+} correspond to low pH values because of limited buffering effects.

5.2 Major constituents in rainwater

5.2.1 Sources apportionment

All the rainwater samples were characterised by variable amounts of dissolved ions. Great variability was observed between different monitoring sites, and intra-site variability during the study period. The scatter plots in Figure 53a show the total dissolved solids, expressed as μeq L^{-1}, for each sample, related to the amount of rainfall (L m^{-2}) in each sampling period. A weak inverse correlation between the two parameters was observed ($R = 0.272$; p-value < 0.001). Instead, a stronger correlation between the TDS (μeq L^{-1}) and the EC (μS cm^{-1}) was found ($R = 0.571$; p-value < 0.001) (Fig. 53b). Therefore, an increase in the amount of substances in solution was reflected in an increase in the electrical conductivity value. This makes it possible to have, employing a simple measurement carried out directly in the field, an initial idea of the total concentration of dissolved elements in solution.

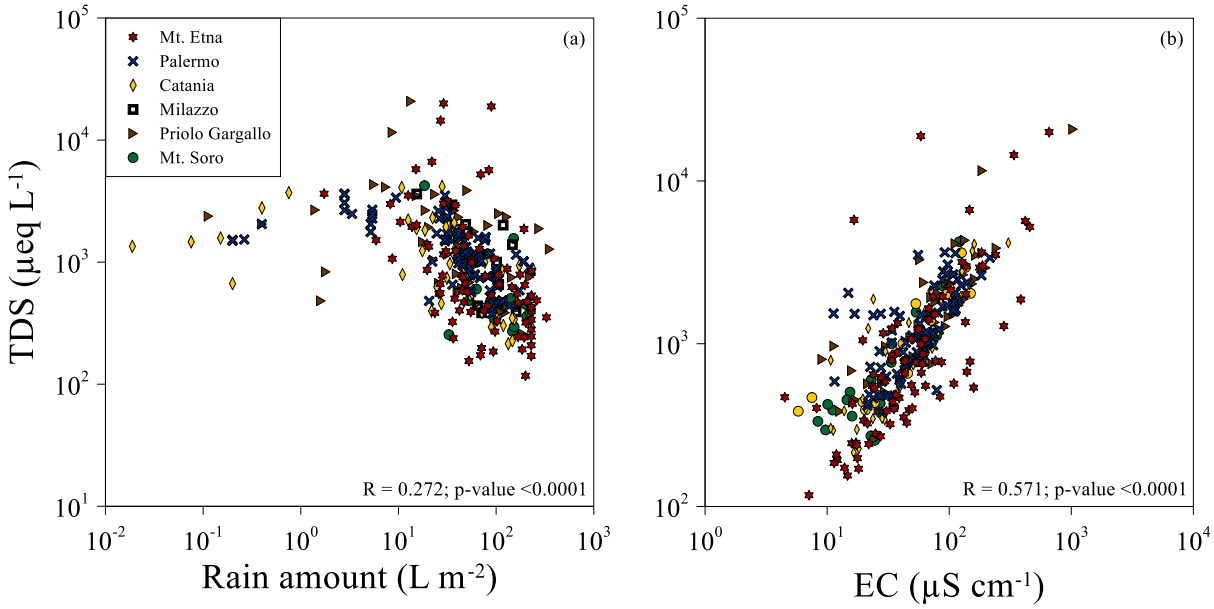

Figure 53 – (a) Total Dissolved Solids (TDS - µeq L^{-1}) versus rain amount (L m^{-2}) and (b) versus EC (µS cm^{-1}) for the Mt. Etna, Palermo, Catania, Milazzo, Priolo Gargallo, and Mt. Soro study areas.

The bar plots in Figure 54 show the volume-weighted mean concentrations (µeq L^{-1}) of major anions (a) and cations (b) in the rainwater samples of each study area. Fluoride concentrations in the study areas of Palermo, Catania, Milazzo, Priolo Gargallo, and Mt. Soro have been multiplied by a factor of 10 for better graphical display.

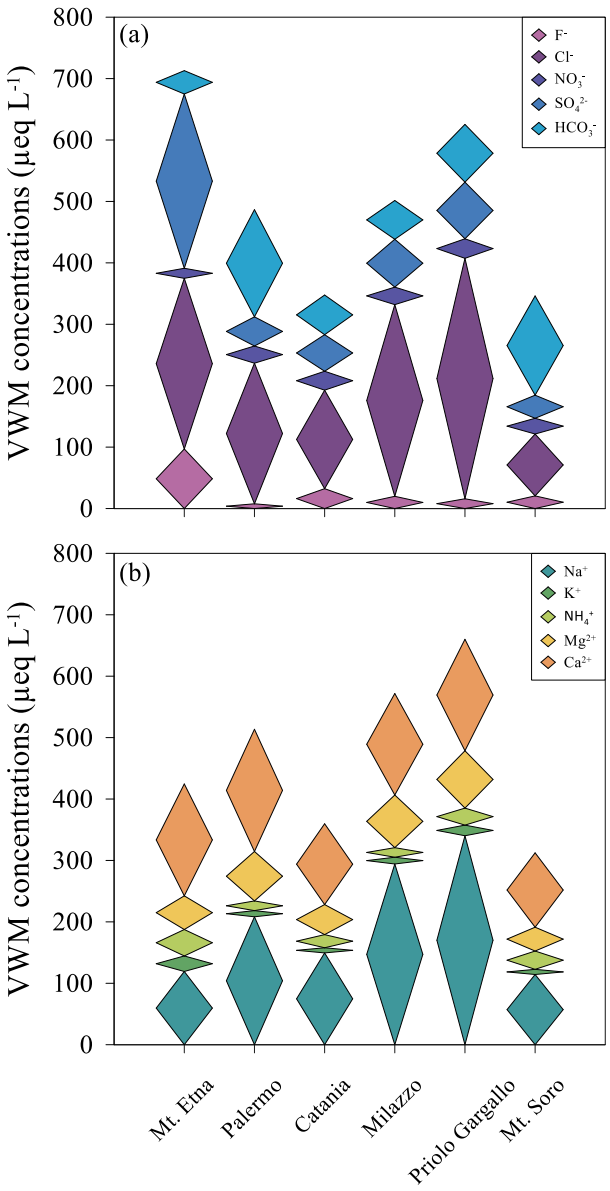

Figure 54 - Sum of the volume-weighted mean (VWM) concentrations (μeq L^{-1}) for (a) major anions and (b) major cations in all the study areas. Fluoride concentrations in the study areas of Palermo, Catania, Milazzo, Priolo Gargallo, and Mt. Soro have been multiplied by a factor of 10.

The highest average VWM concentrations of fluoride (97.0 μeq L^{-1}) and sulfate (284 μeq L^{-1}) were calculated for the Mt. Etna area, one order of magnitude higher than the other study areas. This can be explained considering that Mt. Etna is a fluoride source orders of magnitude greater than any other natural or anthropogenic source in the Sicilian Island (*Bellomo et al., 2003, 2007*; *Calabrese et al., 2011*; *Brugnone et al., 2020*), and its concentration in rainwater decreases rapidly moving away from the volcanic source. For chloride, the highest VWM concentration (403 μeq L^{-1}) was calculated

for the Cratere 2001 sampling site. High VWM concentrations of chloride were calculated also for the coastal sites of the Palermo urban area, and Milazzo and Priolo Gargallo industrial areas. For chloride, different sources can be considered, such as marine, volcanic, and anthropogenic inputs. For bicarbonate, the highest value was calculated for the Palermo study area (192 μeq L^{-1}) further underscoring the geogenic carbonate source of the area. Similar VWM concentrations were calculated for nitrate in the Milazzo sampling site (28.5 μeq L^{-1}) and Priolo Gargallo industrial area (31.8 μeq L^{-1}), followed by the Palermo urban area, with an average value of 28.0 μeq L^{-1}. This reflects a clear anthropogenic derivation for nitrate (from NOx emissions).

Sodium was the main cation in the rainwater samples of the two industrial areas, Milazzo and Priolo Gargallo, with VWM concentrations of 294 μeq L^{-1} and 340 μeq L^{-1}, respectively. Its origin can be ascribed, mainly, to the sea salt contribution. For the Palermo urban area, the main cations were sodium (209 μeq L^{-1}) and calcium (200 μeq L^{-1}). Calcium origin can be ascribed to several sources, the main one being geogenic (re-suspended dust from carbonate rocks). The remaining cations showed low VWM concentrations, up to 107 μeq L^{-1} (Cratere 2001), 54.8 μeq L^{-1} (Citelli), and 57.4 μeq L^{-1} (Cratere 2001) for magnesium, ammonium, and potassium, respectively.

Known sources of Na^+ and Cl^- in the atmosphere are sea salt (*Thurston & Spengler, 1985*), and crustal aerosols (*Calabrese et al., 2011*; *Brugnone et al., 2023a*). Typically, sodium is used as a reference to determine the sea-salt component in aerosol particles since the water-soluble Na^+ is assumed to originate solely from seawater (*Chesselet et al., 1972*). Seawater influence is highlighted in Figure 55, where nearly all rainwater samples show Na^+/Cl^- ratios similar to that of seawater, with a high linear positive correlation ($R = 0.879$; p-value < 0.0001).

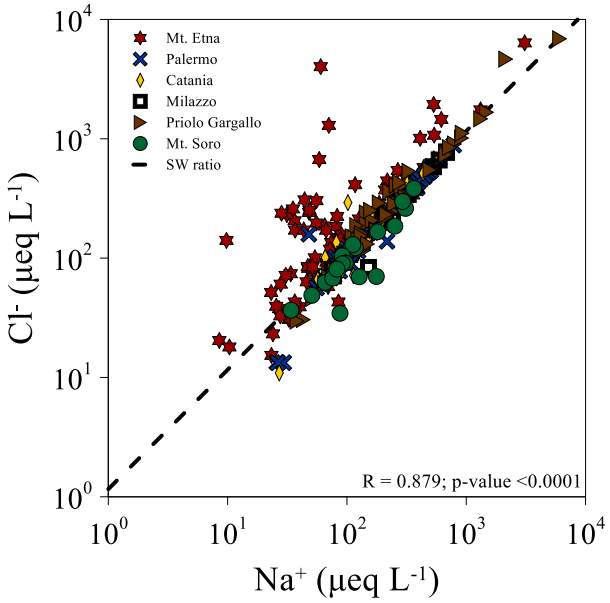

Figure 55 - Correlation between Na^+ and Cl^- ($\mu eq\ L^{-1}$) in the rainwater samples.

Therefore, the high load of Na^+ and Cl^- in all the study areas was due, mainly, to their closeness to the coast. Indeed, the highest VWM concentrations for both sodium and chloride were calculated for the Milazzo and Priolo Gargallo industrial areas, located at an average distance from the coast of 0.4 and 1.5 km, respectively. Conversely, the lowest VWM concentrations for these two species were calculated for the Catania urban area (average distance from the coast of 4.0 km) and the Mt. Soro sampling site (17 km away from the coast). This evidence indicates that sea-derived CCN strongly contributed to the chemical composition of the rainwater. Some samples of the Palermo urban area showed a general tendency towards a Na^+ excess with respect to the seawater ratio. The sodium excess can be attributed to a geogenic contribution or human activities, such as emissions from cement or detergent factories. On the contrary, other samples, mainly for the Mt. Etna study area, showed an excess in chloride, which likely suggests an important volcanic contribution in the form of gaseous HCl emissions.

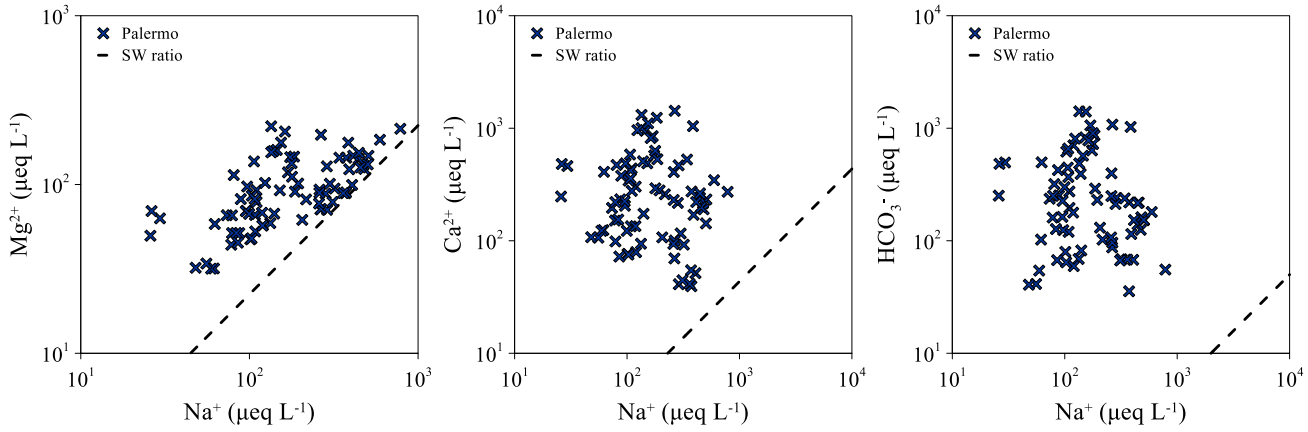

Figure 56 - Correlation between Na^+ and Mg^{2+}. Ca^{2+}, and HCO_3^- ($\mu eq\ L^{-1}$) in the Palermo rainwater samples.

In the Na^+ vs. Mg^{2+}, Ca^{2+}, and HCO_3^- diagrams (Fig. 56), samples from the Palermo urban area showed that these major ions were enriched relative to the marine contribution calculated from the Na^+/ion ratios, highlighting the great contribution of the geogenic source to the chemical composition of the rainwater. Indeed, these three species (Mg^{2+}, Ca^{2+}, and HCO_3^-) derived mainly from the weathering of the carbonate rocks which crop out extensively in the study area. The terrigenous contribution to the chemical composition of rainwater was linked also to Saharan dust species, e.g., calcite, dolomite, gypsum, illite, smectite, and palygorskite (*Alaimo & Ferla, 1979; Badalamenti et al., 1984*). Seasonally, several tons of dust particles are carried by southerly winds from the Sahara Desert reaching the entire Mediterranean basin and sometimes much of the European continent. Only for Mg the marine source becomes prevailing in some of the collected samples which show a Na^+/Mg^{2+} ratio close to that of seawater.

In the Cl^- vs. SO_4^{2-} diagram, Mt. Etna rainwater samples plot in an intermediate position between the Cl/S ratios typical of Mt. Etna's plume, suggesting the involvement of the volcanic source (Fig. 57). Chloride/sulfur ratios in the Etna's plume are from Aiuppa et al. (2004).

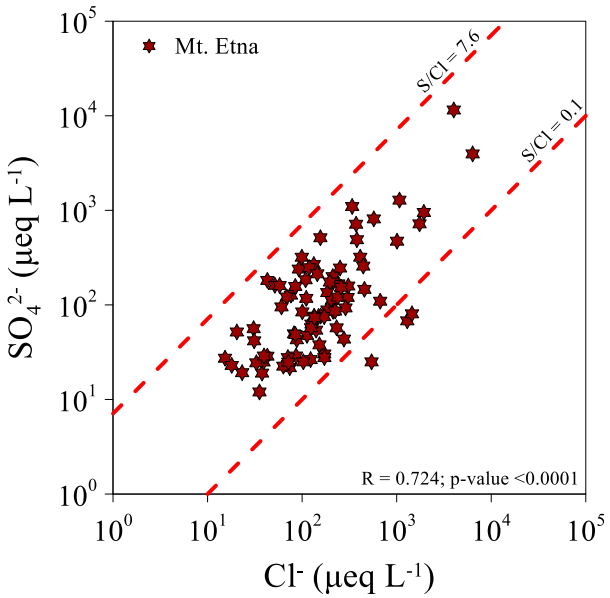

Figure 57 - Correlation between Cl^- and SO_4^{2-} (µeq L^{-1}) in the Mt. Etna rainwater samples. The two red dotted lines are representative of the ratios between the two species in Etna's plume during quiet periods (ratio 0.1) and eruptive periods (ratio 7.6).

In addition to the marine and volcanic sources, sulfate may derive from different anthropogenic sources. Non-sea-salt and non-volcanic sulfate, and nitrate, can be attributed mainly to local fossil fuel combustion sources (*Mphepya et al., 2004*; *Tan et al., 2014*; *Ye et al., 2018*), but also the long-range transport from most heavily industrialised parts of Europe. They result from emissions of gaseous sulfur dioxide (SO_2) and gaseous NOx during the combustion of fossil fuels (oil, coal, and diesel) and sulphide ore smelting. Gaseous NOx is emitted also as nitrogen oxide (NO) from natural (such as biomass burning), as well as other anthropogenic sources (vehicular traffic and household combustion). In the atmosphere, gaseous SO_2 is oxidised to sulfate, while NOx can be oxidised to nitrate (NO_3^-). As observed by Brugnone et al. (2023a), both the Milazzo and Priolo Gargallo industrial areas have important sources of anthropogenic sulfur species (SOx) and nitrogen species (NOx), which could explain the higher sulfate and nitrate concentrations in these two study areas compared to the others. The positive linear correlation between nitrate and sulfate (R = 0.650; p-value < 0.0001), shown in Figure 58, corroborates the hypothesis that these species can be partially attributed to the same fossil fuel combustion sources. The linear positive correlation between the two

species was higher for the Milazzo and the Priolo Gargallo industrial areas, with a correlation coefficient R = 0.939 (p-value < 0.001).

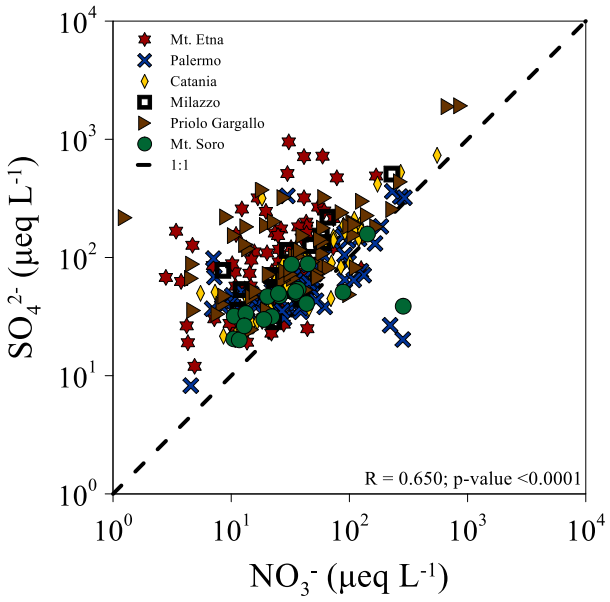

Figure 58 - Correlation between NO_3^- and SO_4^{2-} (µeq L^{-1}) in rainwater samples. The dotted line is the ratio 1:1 between the two species.

The sulfate enrichments were related to contributions from non-anthropogenic sources. The high sulfate concentrations in the Etna area are not matched by high nitrate concentrations, the sources being quite distinct: predominantly volcanic and partly marine for the former, anthropogenic for the latter. Nitrate enrichments observed for some samples from the urban area of Palermo were related to the emission of nitrogen species by vehicular traffic and domestic heating.

Fluoride concentrations were generally low in all the monitoring sites, except for the Mt. Etna study area. Gaseous fluoride compounds may derive from anthropogenic sources, but volcanic emissions from Mt. Etna represent an important natural source of this ion, emitted in a very soluble form (mainly HF), allowing a rapid removal from the atmosphere close to the emission points by rainwater (*Pennisi et al., 1998*). Bellomo et al. (2007) reported that of the ~ 200 Mg of fluoride (as HFg) emitted daily by Mt. Etna, 1.6 ± 2.7 Mg are deposited by wet and dry deposition. Longer dry

spells may favour its travel to sampling sites further away from Mt. Etna. Additionally, condensation and reaction of HF on the surface of ash particles is a very effective scavenging mechanism (*Oskarsson, 1980; Witham et al., 2005; Bellomo et al., 2007*). The good positive correlation between fluoride and sulfate for the Mt. Etna rainwater (R = 0.838; p-value < 0.0001) strengthens the hypothesis of a common volcanic origin (Fig. 59).

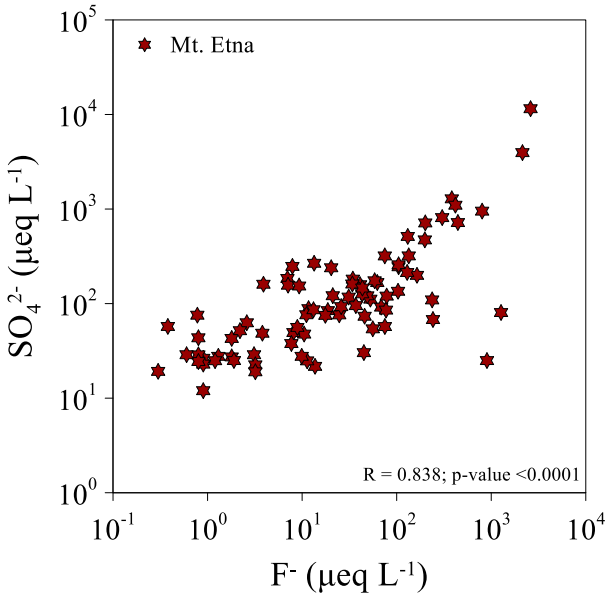

Figure 59 - Correlation between F^- and SO_4^{2-} (µeq L^{-1}) in Mt. Etna rainwater samples.

Considering all study areas, seawater can be considered a minor source of fluoride due to the very low correlation with Na^+ (R = 0.242; p-value = 0.0001) (Tab. 43). Additionally, the Na/F ratio, on an equivalent basis, was equal to 100, very different from that for seawater (8720). Coal burning, ceramic industries, and cement production are the main human activities that emit fluoride into the atmosphere in urban and industrial areas (*Niren et al., 2001*).

The highest VWM concentration of K^+ was calculated for the Cratere 2001 sampling site (57.4 µeq L^{-1}), while the lowest was calculated for the San Giovanni La Punta site (7.32 µeq L^{-1}). Multiple sources may be considered for potassium in rainwater: volcanic, terrigenous, marine, and anthropogenic (agricultural activities).

Ammonium resulted from anthropogenic emissions of gaseous ammonia (NH_3) and particulates containing NH_4^+, principally related to agricultural activities. Quite similar VWM concentrations of NH_4^+ were calculated for all the study areas, with the highest value at the Citelli site (54.8 μeq L^{-1}), and the lowest at the Belgio sampling site (8.9 μeq L^{-1}). The good positive correlation between K^+ and NH_4^+ ($R = 0.744$; p-value < 0.0001) (Tab. 43), could testify to a common source, at least to some extent.

5.2.2 Sea salt and non-sea salt fractions

To discriminate the contribution of the marine source from other sources, the non-sea-salt fractions ((X)nss) were calculated using equation (4) in section 3.6. The use of the previous equation assumes that all the sodium in rainwater comes from the sea and that no chemical fractionation occurs between chloride and the other ions after sea salt injection into the atmosphere (*D'Alessandro et al., 2013*). This assumption was not always true, especially for the Mt. Etna sampling sites, where a volcanic contribution for sodium was observed. For this reason, in some cases, the sea salt contribution for some elements (e.g., chloride) was greater than 100%; in these cases, a value of 100% was imposed.

For Na^+ (100%), Cl^- (88.8%), and Mg^{2+} (62.5%) the predominant source was marine, for NH_4^+ (100%), NO_3^- (100%), HCO_3^- (98.7%), F^- (97.7%), Ca^{2+} (94.8%), SO_4^{2-} (64.5%), and K^+ (63.5%) the prevalent source was non-marine (Fig. 60).

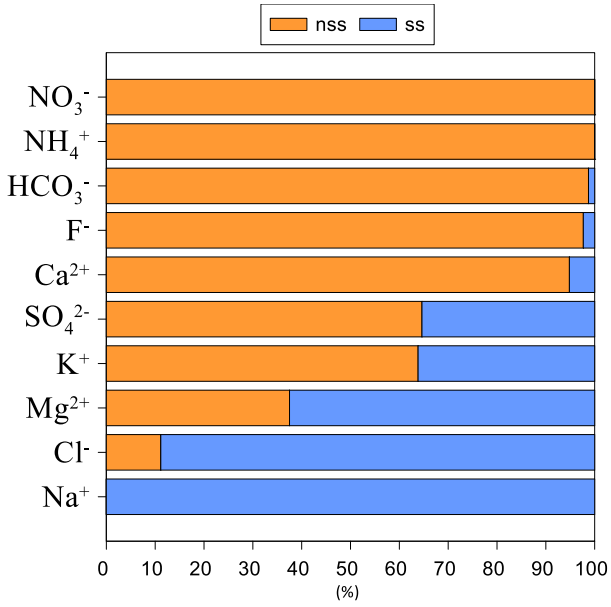

Figure 60 - Non-sea-salt (orange) and sea-salt (blue) fractions (%) for each major ion.

Among the sampling sites, a large difference in the marine and non-marine fractions of individual ionic species, and a clear correlation between distance from the coast and the altitude can be observed. For all the monitoring sites, chloride was derived exclusively from sea salt contribution. Exceptions were the Mt. Etna sampling sites, for which the marine contribution varied from 28.8% at Citelli to 79.7% at Zafferana Etnea. The former was the site most exposed to the volcanic source, due to both its short distance from Etna's summit craters (5.4 km) and the direction of dispersion of volcanic products; the latter was the site located closest to the sea (9.9 km), and the greatest distance from Etna's summit craters (10.0 km). The nss-chloride in the Etna area had a clear volcanic origin. Similar considerations can be made for magnesium and sulfate. For the Etna sites, an average relative contribution from the marine source of 45.5% and 10.1% were calculated for Mg^{2+} and SO_4^{2-}, respectively, in contrast to the other monitoring sites, where average ss-Mg^{2+} and ss-SO_4^{2-} fractions of 68.7% and 44.7% were calculated. Especially for sulfate, the predominant source at the Etna sites was once again represented by volcanic emissions. Rainwater from the Etna area showed the lowest ss-fraction content for all the major ions. In contrast, the sites of Milazzo and Augusta showed the greatest contribution from the marine source.

5.2.3 Statistical analysis of major ions

5.2.3.1 Pearson correlation coefficients

The Pearson's correlation coefficients for each major ion, for each rainwater sample (n = 301), were calculated, and reported in Table 43.

Table 43 - Pearson's correlation coefficients for major ions in rainwater. Bold values have p-value ≤ 0.0001.

	F^-	Cl^-	NO_3^-	SO_4^{2-}	HCO_3^-	Na^+	K^+	NH_4^+	Mg^{2+}	Ca^{2+}
F^-		**0.603**	0.024	**0.815**	-0.046	**0.242**	**0.417**	0.200	**0.370**	**0.339**
Cl^-	**0.603**		**0.628**	**0.620**	-0.003	**0.879**	**0.431**	0.145	**0.831**	**0.559**
NO_3^-	0.024	**0.628**		**0.650**	**0.482**	**0.621**	**0.303**	0.149	**0.712**	**0.739**
SO_4^{2-}	**0.815**	**0.620**	**0.650**		0.047	**0.273**	**0.234**	0.046	**0.298**	**0.291**
HCO_3^-	-0.046	-0.003	**0.482**	0.047		-0.036	**0.277**	**0.243**	0.164	**0.348**
Na^+	**0.242**	**0.879**	**0.621**	**0.273**	-0.036		**0.521**	**0.407**	**0.910**	**0.668**
K^+	**0.417**	**0.431**	**0.303**	**0.234**	**0.277**	**0.521**		**0.744**	**0.727**	**0.705**
NH_4^+	0.200	0.145	0.149	0.046	**0.243**	**0.407**	**0.744**		**0.628**	**0.558**
Mg^{2+}	**0.370**	**0.831**	**0.712**	**0.298**	0.164	**0.910**	**0.727**	**0.628**		**0.863**
Ca^{2+}	**0.339**	**0.559**	**0.739**	**0.291**	**0.348**	**0.668**	**0.705**	**0.558**	**0.863**	

Fluoride was correlated with sulfate (0.815), and partially with chloride (0.603). Chloride was correlated especially with sodium (0.879) and magnesium (0.831). Nitrate was correlated with calcium (0.739), magnesium (0.712), and partially with sulfate (0.650). No strong correlation was found for bicarbonate. The stronger correlations for potassium were with ammonium (0.744), magnesium (0.727) and calcium (0.705).

5.2.3.2 Principal Component Analysis (PCA)

Relationships between major ions may be also estimated through the Principal Component Analysis (PCA). For each ion, when the concentrations were below the detection limit, values equal

to the detection limits (LOD) divided by a factor 2 were considered. It was decided to make the statistical analysis for each study context, separately. The results followed by Varimax rotation to a set of orthogonal axes for a total of 301 rainwater samples are presented in Tables 44a, b, c, and d.

Table 44 - The results from Principal Component Analysis (PCA) for Mt. Etna (a), Palermo and Catania (b), Milazzo and Priolo Gargallo (c), and Mt. Soro (d) rainwater samples. Factors loadings greater than 0.700 are in bold.

(a) Variable	PC1	PC2	PC3	(b) Variable	PC1	PC2	PC3
F^-	0.207	**0.952**	-0.006	F^-	0.514	0.025	-0.112
Cl^-	0.273	**0.891**	-0.053	Cl^-	0.044	**0.987**	0.068
NO_3^-	0.113	0.066	**0.905**	NO_3^-	**0.826**	0.135	-0.084
SO_4^{2-}	0.000	**0.914**	-0.173	SO_4^{2-}	**0.832**	0.262	0.038
HCO_3^-	0.023	0.228	-0.422	HCO_3^-	**0.772**	-0.145	0.006
Na^+	**0.910**	0.219	-0.149	Na^+	-0.002	**0.990**	0.032
K^+	**0.925**	0.191	0.194	K^+	**0.714**	0.018	0.376
NH_4^+	**0.739**	-0.001	0.348	NH_4^+	-0.012	0.101	**0.969**
Mg^{2+}	**0.969**	0.189	0.033	Mg^{2+}	**0.703**	0.611	0.150
Ca^{2+}	**0.960**	0.077	-0.117	Ca^{2+}	**0.901**	0.011	0.104
Variance (%)	47.9	22.7	11.0	Variance (%)	43.9	21.9	10.6

(c) Variable	PC1	PC2	PC3	(d) Variable	PC1	PC2	PC3
F^-	0.226	0.114	**0.873**	F^-	0.010	**0.888**	0.001
Cl^-	**0.974**	-0.036	0.038	Cl^-	0.275	**0.919**	-0.049
NO_3^-	**0.899**	-0.028	0.269	NO_3^-	**0.928**	0.259	0.181
SO_4^{2-}	**0.917**	0.096	0.284	SO_4^{2-}	0.406	0.414	-0.563
HCO_3^-	-0.107	**0.793**	0.329	HCO_3^-	0.346	0.062	**0.714**
Na^+	**0.966**	-0.021	-0.051	Na^+	0.429	**0.846**	-0.039
K^+	0.364	**0.813**	0.003	K^+	**0.898**	0.223	0.269
NH_4^+	-0.058	**0.830**	-0.041	NH_4^+	**0.901**	0.110	-0.295
Mg^{2+}	**0.974**	0.094	0.038	Mg^{2+}	**0.928**	0.350	0.000
Ca^{2+}	**0.787**	0.228	0.361	Ca^{2+}	**0.957**	0.158	0.176
Variance (%)	56.0	20.7	8.53	Variance (%)	58.9	18.3	9.36

The KMO (Kaiser-Meyer-Olkin) test returned values of 0.687, 0.619, 0.748, and 0.648 for Mt. Etna, Palermo and Catania, Milazzo and Priolo Gargallo, and Mt. Soro study areas, respectively.

Bartlett's sphericity test had a significance value of < 0.001, confirming the applicability of PCA, for each dataset analysed. For each context, three principal components (PC) were extracted, explaining 81.6%, 76.4%, 85.2%, and 86.6% of the total variances.

For the Mt. Etna volcanic area, the PC1 accounts for 47.9% of the total variance and has high loadings for Mg^{2+}, Ca^{2+}, Na^{+}, K^{+}, and NH_4^{+}. For the first four cations, a main geogenic origin may be assumed, linked to the deposition or resuspension of ash and other volcanic products and their dissolution in rainwater. For sodium, especially in the Zafferana Etnea sampling site, due to its minor distance from the coastline, a marine contribution cannot be excluded. For NH_4^{+}, and partially also for K^{+}, an anthropogenic source, i.e., agricultural practices, may be assumed. Sulfate, chloride, and fluoride had higher loadings in the principal component 2. This component accounts for 22.7% of the total variance. Volcanic emissions of SO_2, HCl, and HF were the main sources for these ionic species in the rainwater of the Etna area. Nitrate was loaded only in PC3 (11.0% of the total variance); an anthropogenic origin may be assumed for this anion.

For the Palermo and Catania urban areas, the PC1 accounts for 43.9% of the total variance and has high loadings for Ca^{2+}, HCO_3^{-}, SO_4^{2-}, NO_3^{-}, Mg^{2+} and K^{+}. For the first two species, a prevalent geogenic origin may be assumed, although a small part of the calcium may also be derived from the marine source. Sulfate and nitrate had an anthropogenic origin, deriving from urban vehicular and household emissions of gaseous SOx and NOx. Sulfate may be derived also from the marine source, especially for the Palermo urban area, while a small contribution from the volcanic source may be hypothesized for the Catania urban area. Finally, for Mg^{2+} and K^{+} marine and geogenic sources were mainly responsible for their emission into the atmosphere. The PC2 accounts for 21.9% of the total variance and has high loadings for chloride and sodium, clearly of marine origin. Nitrate was loaded only in PC3 (10.6% of the total variance). For the two urban areas, the nitrate has an almost exclusively anthropogenic origin, deriving directly from agricultural activities or the secondary transformation of gaseous NOx.

For the Milazzo and the Priolo Gargallo industrial areas, the PC1 accounts for 56.0% of the total variance and has high loadings for Cl^-, Mg^{2+}, Na^+, SO_4^{2-}, NO_3^-, and Ca^{2+}. A main marine origin can be assumed for the first three species, as confirmed by the Na^+/Cl^- (0.884) and the Na^+/Mg^{2+} (3.12) ratios, close to those of seawater. Sulfate and nitrate had an anthropogenic origin, related to the emissions of NOx and SOx arising from the industrial activities in the two study areas (Brugnone et al., 2023b). For Ca^{2+} a prevalent geogenic, and partially marine contribution, may be called upon. Bicarbonate, ammonium, and potassium had the higher loadings in the PC2, which accounts for 20.7% of the total variance. A common anthropogenic source, i.e., agricultural practices, may be assumed for NH_4^+ and K^+. Potassium could also be partly of geogenic origin, and this would explain the bicarbonate loading in this component. Fluoride was loaded only in PC3 (8.53% of the total variance). Gaseous and particulate fluoride may be derived from anthropogenic emissions, such as ceramic and brick factories for the Milazzo area, and cement factories for the Priolo Gargallo area (*Brugnone et al., 2023a*). Fluoride concentrations in the two study areas were usually very low and often below the instrumental quantification limit. However, peaks of concentrations (up to 138 μeq L^{-1}) were measured in the Priolo Gargallo area during the paroxysmal events that characterised Etna's volcanic activity between 2021 and 2022. Several times, Etna's plume and volcanic ash were dispersed southwards by winds at high altitudes, contributing to the chemical composition of rainwater even at great distances from emission centres. The high correlation coefficient between fluoride and nss-sulfate (volcanic and/or anthropogenic) reinforces the previous hypothesis. Similar scientific evidence, for these two areas, has been identified by Brugnone et al. (2020, 2023a).

Finally, for the Mt. Soro background area, the PC1 accounts for 58.9% of the total variance and had high loadings for Ca^{2+}, Mg^{2+}, NO_3^-, NH_4^+, and K^+. Geogenic source for the first two cations, and anthropogenic source (i.e., agricultural practices) for the remaining ions, may be assumed. The PC2 accounts for 18.3% of the total variance and had a high load of Na^+, Cl^-, and F^-. Sodium and chloride had a common marine source, as verified by the high correlation coefficient (R = 0.936; p-

value < 0.0001). In addition, chloride may have, at least partly, a volcanic origin. Fluoride, which was loaded into this component and showed a high correlation coefficient with chloride (R = 0.747; p-value = 0.002) could had the same origin. Two times, during the monitoring period, the plume and volcanic products of Etna were dispersed north/west, reaching the area of Mt. Soro. In particular, during Etna's paroxysmal eruption of 10 February 2022, fine ash fell into the bulk collector installed on this site. In the rainwater sample no. 12, covering the period 18 January - 24 February 2022, the highest concentrations of chloride (383 μeq L^{-1}) and fluoride (32.8 μeq L^{-1}) were measured, for the latter an order of magnitude greater than the concentrations measured in the other samples. Bicarbonate was loaded in PC3 (9.36% of the total variance) and had a geogenic origin.

5.2.3.3 Positive Matrix Factorization (PMF) analysis

Major ions were added to improve the model calculation in the EPA PMF analysis. Initially, PMF factors were resolved using the numbers from 100 runs. The number of factors was changed to optimise the goodness-of-fit parameter Q over the theoretical Q (Qrobust/Qexpected < 2), and the strong and weak variables were determined with the signal-to-noise (S/N) ratio (*Khan et al., 2016*; *Ye et al., 2018; Amato et al., 2024*). The PMF analysis was conducted separately for each sampling site. The results are reported in Table 45. Ammonium was determined in 219 of the 301 rainwater samples collected during this research. For samples in which the ammonium concentration was not measured, a value equal to the median of the values measured at each sampling site was used. For the Citelli sampling site, bicarbonate was not considered because the S/N ratio was very low, equal to 0.30. For the Zafferana Etnea, Mt. Intraleo, and Cratere 2001 sampling sites, bicarbonate was set to a weak category, due to S/N ratios equal to 0.6, 0.7, and 0.9, respectively.

Table 45 - The results from Positive Matrix Factorization (PMF) analysis for each sampling site. The values are in %. BB and biomass burn = Biomass burning; Sec = Secondary formation; Cer/Cem = Ceramic and/or cement industries. Bold values are the maximum for each ion in each sampling site.

Site	Factor	Source	F^-	Cl^-	NO_3^-	SO_4^{2-}	HCO_3^-	Na^+	K^+	NH_4^+	Mg^{2+}	Ca^{2+}
Citelli	1	Volcanic	**54.5**	**68.3**	/	6.10	/	13.4	8.70	0.80	16.3	/
	2	Marine	/	24.6	9.20	16.1	/	**60.3**	/	13.8	19.2	6.80
	3	Geogenic	43.9	/	/	28.2	/	21.5	34.2	/	**43.5**	**61.8**
	4	Anthropogenic	/	/	**62.1**	2.30	/	/	7.20	0.10	1.80	/
	5	Agricultural	1.60	/	10.3	2.70	/	/	5.50	**76.5**	6.00	7.30
	6	BB/Sec	/	7.10	18.4	**44.5**	/	4.90	**44.4**	8.90	13.3	24.1

Site	Factor	Source	F^-	Cl^-	NO_3^-	SO_4^{2-}	HCO_3^-	Na^+	K^+	NH_4^+	Mg^{2+}	Ca^{2+}
Zafferana Etnea	1	Volcanic	**90.7**	32.1	12.5	/	/	23.3	**41.8**	/	**32.4**	23.7
	2	BB/Sec	/	/	4.60	32.9	/	8.60	33.7	3.40	12.1	12.2
	3	Geogenic	1.70	6.20	/	15.9	**100**	11.4	/	/	17.8	**35.0**
	4	Agricultural	7.60	15.5	20.7	/	/	5.20	20.9	**75.1**	20.0	27.3
	5	Anthropogenic	/	10.5	**62.1**	**34.3**	/	5.60	2.80	6.10	/	1.80
	6	Marine	/	**35.7**	0.10	16.9	/	**46.0**	0.80	15.3	17.7	/

Site	Factor	Source	F^-	Cl^-	NO_3^-	SO_4^{2-}	HCO_3^-	Na^+	K^+	NH_4^+	Mg^{2+}	Ca^{2+}
Cratere 2001	1	Volcanic	**56.5**	29.1	/	**67.9**	**50.2**	/	2.00	0.50	0.60	2.60
	2	Agricultural	0.20	0.10	1.30	0.10	32.3	5.30	12.8	**77.7**	6.10	2.70
	3	Marine	26.4	**45.7**	/	29.0	/	38.6	37.6	2.50	34.0	28.3
	4	BB/Others	16.8	24.3	2.30	2.30	/	17.3	/	5.90	3.50	/
	5	Anthropogenic	/	0.40	**95.4**	0.40	17.5	0.10	5.20	1.80	1.30	3.70
	6	Geogenic	0.20	0.40	1.00	0.3	/	**38.7**	**42.4**	11.7	**54.5**	**62.7**

Site	Factor	Source	F^-	Cl^-	NO_3^-	SO_4^{2-}	HCO_3^-	Na^+	K^+	NH_4^+	Mg^{2+}	Ca^{2+}
Mt. Intraleo	1	Agricultural	/	1.00	/	7.70	/	/	**61.9**	**56.6**	16.5	/
	2	Anthropogenic	4.00	/	**72.9**	23.1	3.60	21.2	/	32.4	18.4	18.2
	3	Geogenic	/	7.30	11.8	**47.5**	13.9	/	24.1	/	**33.9**	**70.2**
	4	Others	21.5	34.0	1.40	14.4	**82.6**	/	/	11.4	2.50	11.6
	5	Volcanic	**74.4**	0.50	13.2	1.10	/	/	14.0	/	7.70	/
	6	Marine	/	**57.2**	0.70	6.10	/	**78.8**	/	/	21.0	/

Site	Factor	Source	F^-	Cl^-	NO_3^-	SO_4^{2-}	HCO_3^-	Na^+	K^+	NH_4^+	Mg^{2+}	Ca^{2+}
Archirafi	1	Anthropogenic	/	3.70	**59.1**	**52.8**	28.0	5.00	/	/	/	15.7
	2	Biomass burn	1.60	/	18.1	0.40	/	0.10	**54.8**	/	9.80	/
	3	Agricultural	/	4.60	0.40	17.5	/	4.60	/	**88.9**	5.40	2.20
	4	Others	**84.8**	11.3	22.4	/	6.60	9.70	/	3.10	9.40	5.60
	5	Marine	10.4	**80.4**	/	10.4	/	**77.3**	19.0	8.00	**45.9**	7.90
	6	Geogenic	3.20	/	/	18.9	**65.4**	3.30	26.2	/	29.5	**68.5**

Site	Factor	Source	F^-	Cl^-	NO_3^-	SO_4^{2-}	HCO_3^-	Na^+	K^+	NH_4^+	Mg^{2+}	Ca^{2+}
Unipa	1	Geogenic	1.20	7.50	3.90	/	**77.9**	12.2	5.30	5.10	**45.5**	**60.6**
	2	Agricultural	18.4	/	/	18.7	/	0.90	/	**90.1**	11.1	15.0
	3	Others	**76.0**	8.10	15.1	/	6.10	9.00	21.3	4.90	1.40	/
	4	Biomass burn	3.20	3.40	/	21.6	6.40	0.50	**73.4**	/	/	11.9
	5	Anthropogenic	1.10	5.90	**71.1**	**42.3**	9.60	4.00	/	/	/	11.0
	6	Marine	0.10	**75.1**	9.80	17.4	/	**73.3**	/	/	42.0	1.40

Site	Factor	Source	F^-	Cl^-	NO_3^-	SO_4^{2-}	HCO_3^-	Na^+	K^+	NH_4^+	Mg^{2+}	Ca^{2+}
Indipendenza	1	Agricultural	0.30	9.10	2.10	/	/	8.30	19.8	**74.7**	13.2	14.3
	2	Biomass burn	20.2	4.60	32.0	/	3.10	4.30	**49.2**	0.20	8.50	/
	3	Others	**67.0**	1.20	5.40	14.70	18.1	3.40	/	6.60	9.40	14.9
	4	Marine	/	**71.8**	7.20	23.9	1.70	**70.6**	8.90	18.0	**37.0**	/
	5	Anthropogenic	12.5	6.60	**52.2**	**61.3**	18.3	5.50	/	/	7.90	21.9
	6	Geogenic	/	6.70	1.10	/	**58.8**	7.90	22.1	0.50	24.0	**48.9**

Site	Factor	Source	F^-	Cl^-	NO_3^-	SO_4^{2-}	HCO_3^-	Na^+	K^+	NH_4^+	Mg^{2+}	Ca^{2+}
Belgio	1	Geogenic	23.1	1.10	15.5	5.50	**56.5**	/	0.60	/	**36.9**	**47.1**
	2	Marine	/	**58.1**	1.80	10.7	8.20	**67.7**	13.7	1.60	35.1	6.50
	3	Agricultural	1.10	12.6	1.30	3.80	4.90	7.40	5.70	**92.0**	7.00	/
	4	Anthropogenic	8.60	8.30	32.7	**50.4**	/	1.60	3.80	5.10	7.70	31.1
	5	Biomass burn	9.00	12.6	**35.2**	0.20	21.1	12.2	**76.1**	1.30	13.4	14.1
	6	Others	**58.2**	7.30	13.5	29.5	9.20	11.1	/	/	/	1.20

Site	Factor	Source	F^-	Cl^-	NO_3^-	SO_4^{2-}	HCO_3^-	Na^+	K^+	NH_4^+	Mg^{2+}	Ca^{2+}
Catania	1	Volcanic	**77.6**	/	/	10.3	16.7	6.50	11.4	2.00	11.0	17.6
	2	Biomass burn	/	26.1	8.30	16.5	7.20	5.30	**57.9**	/	5.40	/
	3	Geogenic	0.10	1.70	28.5	19.7	**70.0**	2.80	/	/	18.5	**45.9**
	4	Marine	/	**64.4**	/	11.9	3.30	**65.7**	/	21.6	**26.7**	2.10
	5	Anthropogenic	22.3	7.90	**58.9**	**38.6**	2.30	16.1	0.40	4.20	25.8	25.7
	6	Agricultural	/	/	4.30	3.00	0.50	3.60	30.3	**72.1**	12.6	8.80

Site	Factor	Source	F^-	Cl^-	NO_3^-	SO_4^{2-}	HCO_3^-	Na^+	K^+	NH_4^+	Mg^{2+}	Ca^{2+}
San Giovanni La Punta	1	Anthropogenic	7.10	35.4	**60.6**	**36.8**	7.80	24.9	0.10	/	**36.0**	26.8
	2	Volcanic	**86.9**	5.60	19.9	28.9	15.0	4.40	34.2	1.00	13.5	20.1
	3	Biomass burn	0.20	/	2.20	5.40	1.70	2.10	**48.6**	3.00	5.80	0.30
	4	Agricultural	2.40	8.60	7.80	8.10	8.30	8.00	/	**92.8**	10.0	9.20
	5	Marine	3.30	**50.2**	4.60	11.5	0.30	**55.9**	5.90	/	24.7	3.20
	6	Geogenic	0.10	0.10	4.90	9.30	**66.8**	4.80	11.1	3.10	10.1	**40.5**

Site	Factor	Source	F^-	Cl^-	NO_3^-	SO_4^{2-}	HCO_3^-	Na^+	K^+	NH_4^+	Mg^{2+}	Ca^{2+}
Milazzo	1	Agricultural	/	9.50	14.0	**28.0**	1.00	/	7.20	**77.4**	5.90	/
	2	Cer/Cem	**56.0**	0.70	6.90	/	3.10	/	0.10	/	1.30	4.60
	3	Marine	18.9	**80.1**	/	26.2	1.80	**77.5**	/	12.6	**47.5**	2.30
	4	Biomass burn	/	0.20	27.1	/	4.60	17.9	**60.4**	8.70	16.3	18.4
	5	Geogenic	15.1	9.50	13.4	18.1	**82.5**	/	32.3	/	18.5	**47.0**
	6	Anthropogenic	10.0	/	**38.5**	27.7	7.00	4.70	/	1.30	10.6	27.7

Site	Factor	Source	F^-	Cl^-	NO_3^-	SO_4^{2-}	HCO_3^-	Na^+	K^+	NH_4^+	Mg^{2+}	Ca^{2+}
Siracusa	1	Agricultural	6.50	1.40	0.30	1.74	4.50	2.10	/	**88.6**	4.70	/
	2	Marine	0.40	**79.7**	10.6	25.9	/	**75.9**	24.1	/	**50.9**	7.60
	3	Anthropogenic	/	/	**77.0**	**32.7**	/	3.10	6.20	2.10	14.9	30.2
	4	Biomass burn	6.20	7.80	0.10	21.3	34.3	3.70	**58.6**	0.90	16.8	20.3
	5	Geogenic	/	10.6	0.90	7.70	**59.2**	12.3	4.60	8.50	9.10	**40.5**
	6	Volcanic	**86.9**	0.40	11.1	10.7	2.10	3.00	6.50	/	3.70	1.50

Site	Factor	Source	F^-	Cl^-	NO_3^-	SO_4^{2-}	HCO_3^-	Na^+	K^+	NH_4^+	Mg^{2+}	Ca^{2+}
Augusta	1	Volcanic	**87.3**	/	/	3.90	3.40	1.90	/	12.6	2.70	9.60
	2	Geogenic	10.6	6.10	/	36.5	**93.4**	0.60	42.9	2.00	17.4	**37.4**
	3	Anthropogenic	/	0.10	**68.1**	13.2	/	1.70	/	/	4.80	30.8
	4	Marine	/	**83.1**	19.1	**38.4**	3.10	**78.5**	/	/	**67.6**	13.9
	5	Agricultural	1.30	/	/	7.90	/	14.9	/	**76.9**	0.20	4.50
	6	Biomass burn	0.80	10.7	12.8	/	0.10	2.40	**57.1**	8.50	7.40	3.80

Site	Factor	Source	F^-	Cl^-	NO_3^-	SO_4^{2-}	HCO_3^-	Na^+	K^+	NH_4^+	Mg^{2+}	Ca^{2+}
Priolo Gargallo	1	Marine	14.7	**84.9**	0.70	**26.7**	/	**83.2**	14.1	/	**60.1**	12.3
	2	Anthropogenic	/	1.30	**48.5**	18.1	4.80	3.90	/	1.80	13.3	38.9
	3	Volcanic	**73.3**	7.80	7.40	5.10	/	8.70	0.80	/	6.50	5.00
	4	Agricultural	/	/	/	10.3	/	1.00	16.3	**91.6**	2.10	/
	5	Biomass burn	0.10	5.50	43.3	23.9	2.10	3.20	**62.1**	0.40	8.80	3.00
	6	Geogenic	11.9	0.50	/	16.0	**93.1**	/	6.70	6.20	9.20	**40.8**

Site	Factor	Source	F^-	Cl^-	NO_3^-	SO_4^{2-}	HCO_3^-	Na^+	K^+	NH_4^+	Mg^{2+}	Ca^{2+}
Mt. Soro	1	Marine	/	**36.4**	/	8.10	2.00	**35.8**	16.7	2.80	21.2	8.30
	2	Geogenic	14.2	5.30	29.4	/	/	20.1	**61.4**	13.6	44.5	**69.5**
	3	Others	3.50	1.10	/	/	**79.1**	/	3.60	5.00	1.00	1.80
	4	Volcanic	**77.3**	22.7	/	7.00	/	11.0	6.60	2.70	6.10	/
	5	Agricultural/Sec	/	7.20	18.1	37.8	/	/	11.7	**76.0**	5.80	/
	6	Anthropogenic	4.90	27.4	**52.5**	**47.0**	18.9	33.0	/	/	**21.4**	20.4

The main sources identified by the model PMF are marine, geogenic, volcanic, agricultural, anthropogenic, and biomass combustion. In some cases (Citelli and Mt. Soro), and for some ions (sulfate and ammonium), secondary chemical reactions may have contributed, at least in part, to the concentration of the same ions in the atmosphere. For the Milazzo site, moreover, a well-defined industrial contribution has been isolated, connected to the production activities of ceramics and cement, insistent in the study area. The contribution of other sources, such as long-range transport and secondary chemical transformation, cannot be excluded for almost all monitoring sites. The following factor profiles, one for the regional background area of Mt. Soro (Fig. 61), one for the local background site of Mt. Intraleo (Fig. 62), one for the urban context (Indipendenza – Fig. 63), one for the industrial area of Priolo Gargallo (Fig. 64), one for the industrial area of Milazzo (Fig. 65) and, finally, one for the volcanic area (Cratere 2001 – Fig. 66), show that: (i) sodium and chloride were the distinctive ionic species of the marine source; (ii) crustal/geogenic source was identified by high load of calcium and usually also bicarbonate and magnesium; (iii) fluoride and sometimes chloride and sulfate were the distinctive ions of the volcanic source; (iv) ammonium was the marker of emissions related to agricultural activities; (v) potassium was the marker of the biomass burning; (vi) anthropogenic emissions were characterised by high load of nitrate and sulfate; (vii) in the Milazzo industrial area, the higher than background concentrations of fluoride have been

attributed to emissions from the ceramic and cement production industries, thus being able to discriminate this specific source on a local scale.

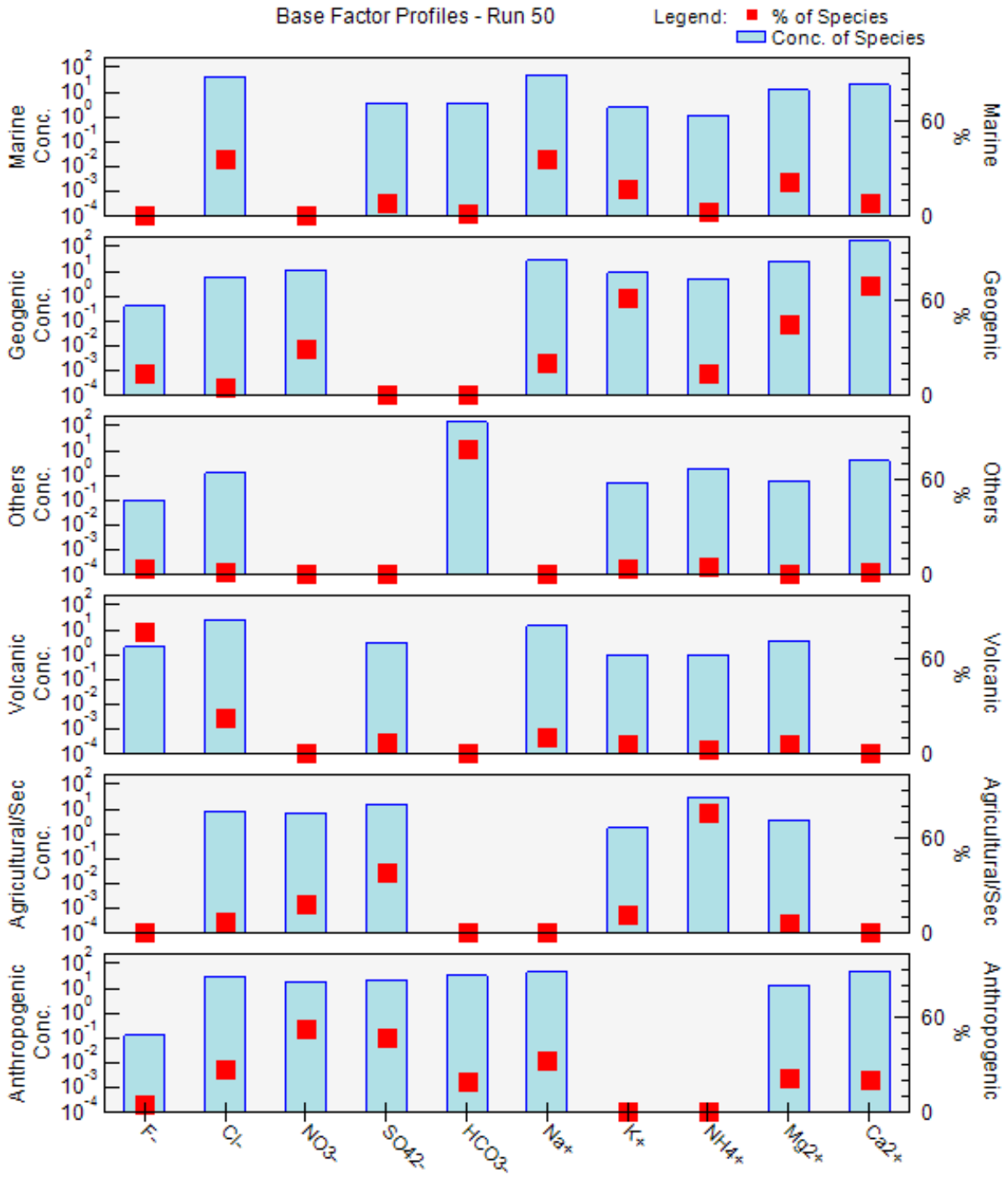

Figure 61 - Factor profiles (% of species and concentrations) obtained from the US Environmental Protection Agency (EPA) PMF model in the Mt. Soro sampling site.

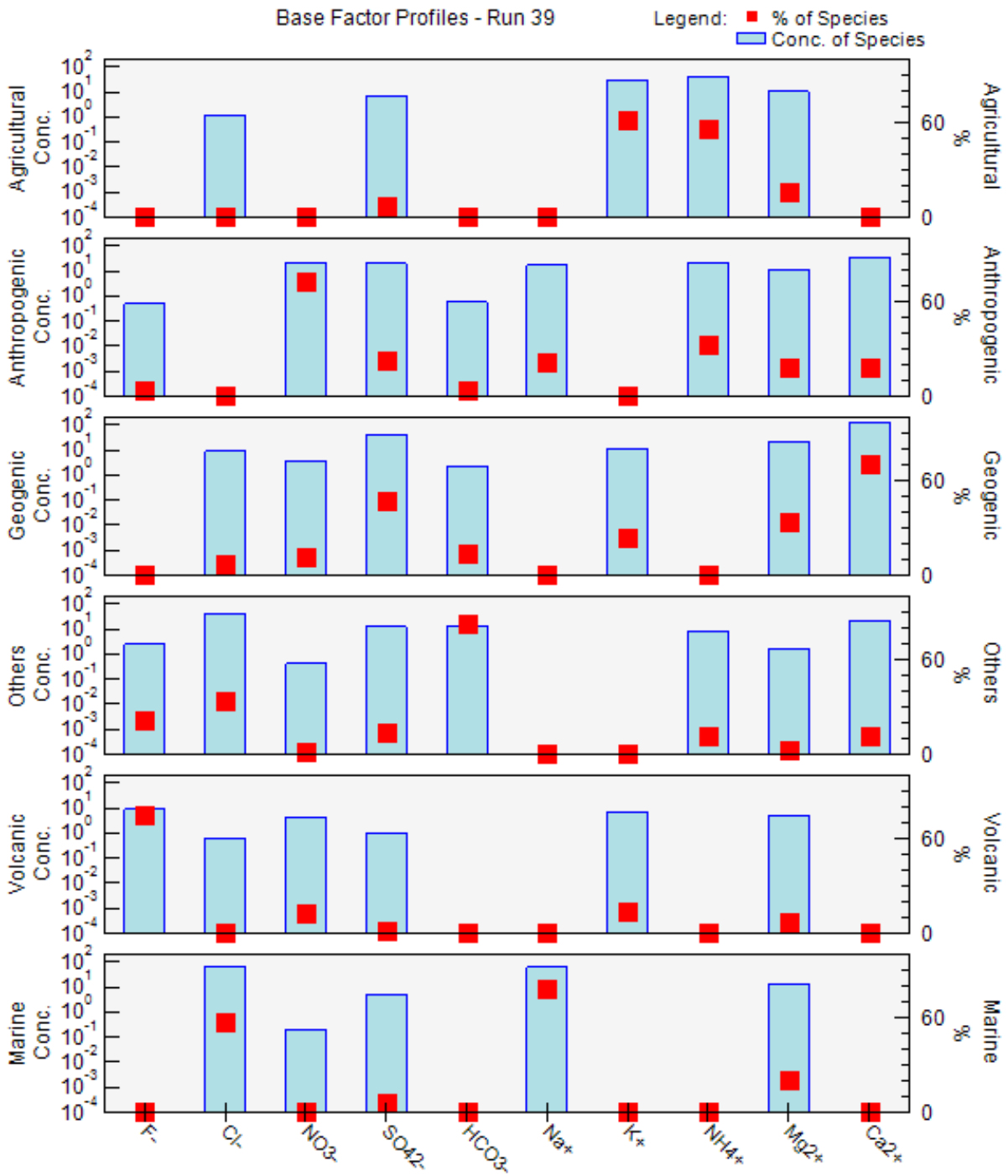

Figure 62 - Factor profiles (% of species and concentrations) obtained from the US Environmental Protection Agency (EPA) PMF model in the Mt. Intraleo sampling site.

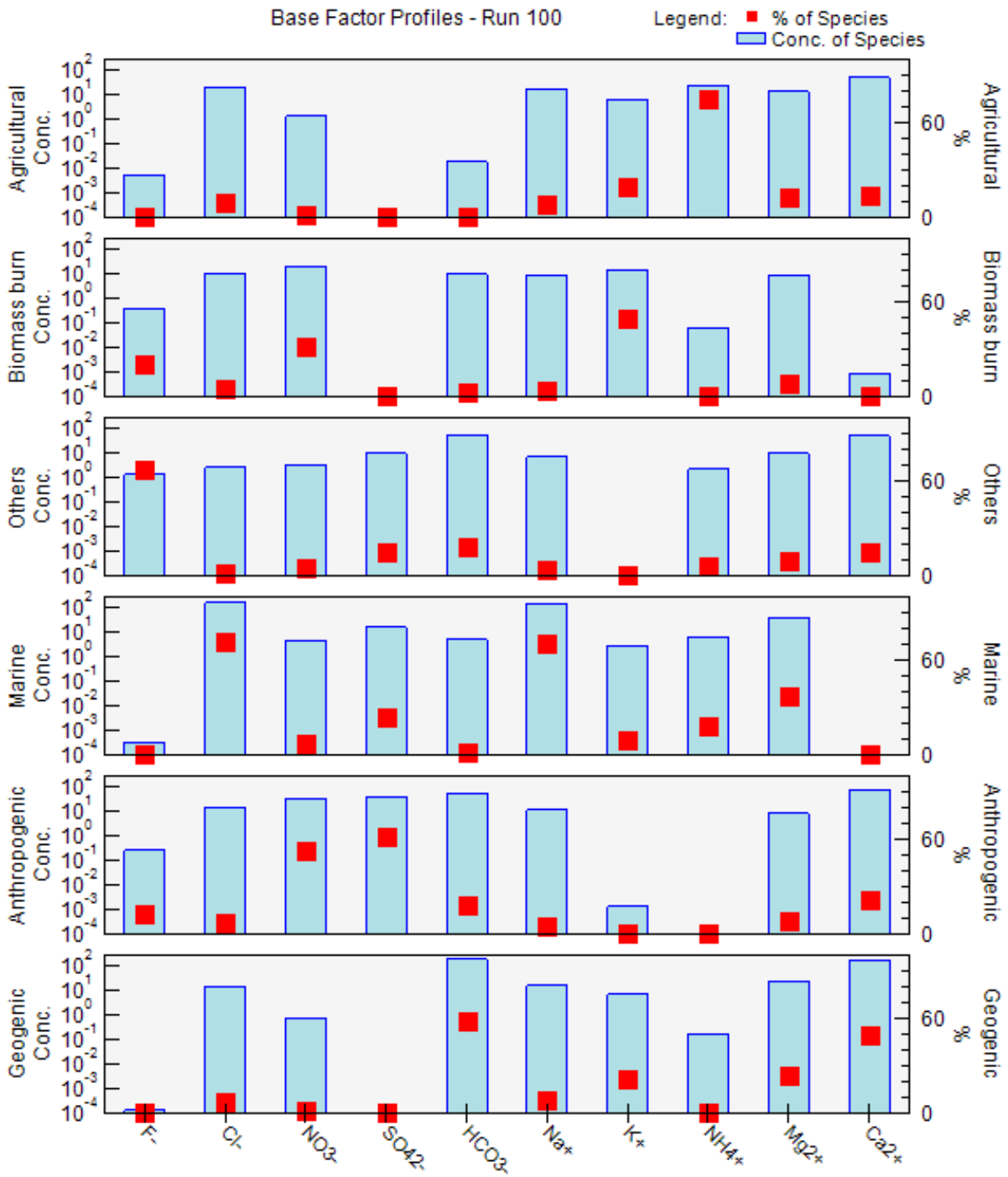

Figure 63 - Factor profiles (% of species and concentrations) obtained from the US Environmental Protection Agency (EPA) PMF model in the Indipendenza sampling site.

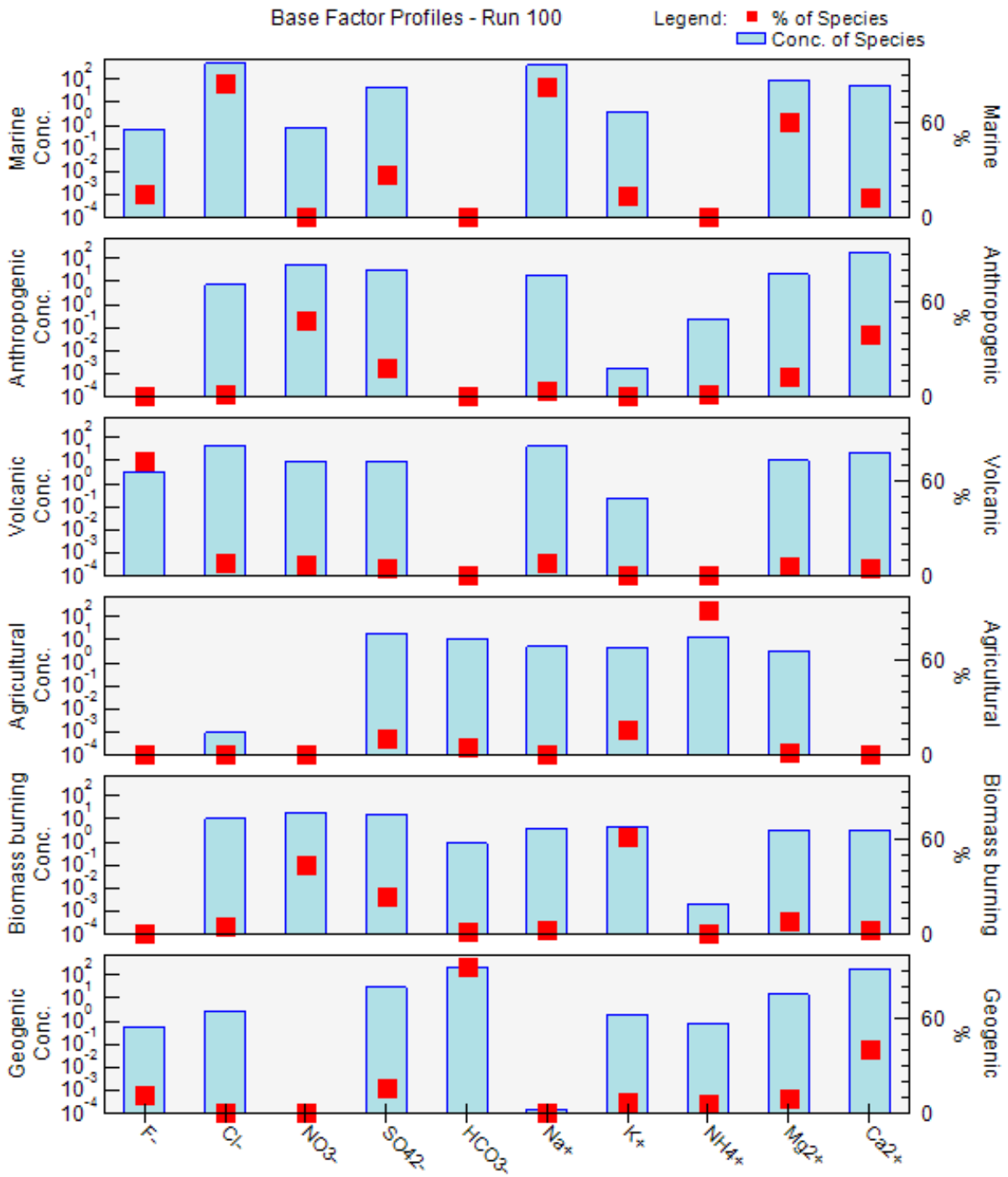

Figure 64 - Factor profiles (% of species and concentrations) obtained from the US Environmental Protection Agency (EPA) PMF model in the Priolo Gargallo sampling site.

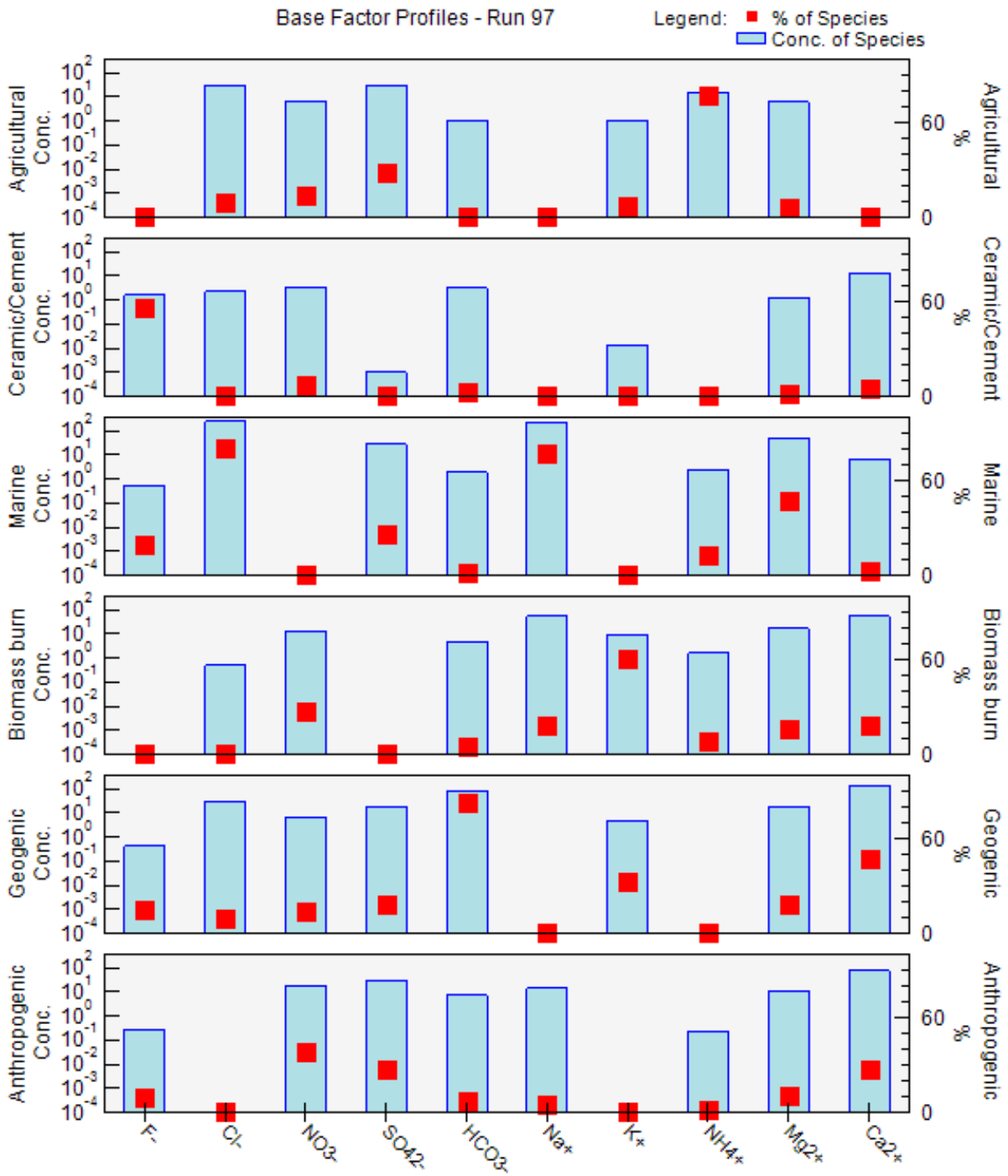

Figure 65 - Factor profiles (% of species and concentrations) obtained from the US Environmental Protection Agency (EPA) PMF model in the Milazzo sampling site.

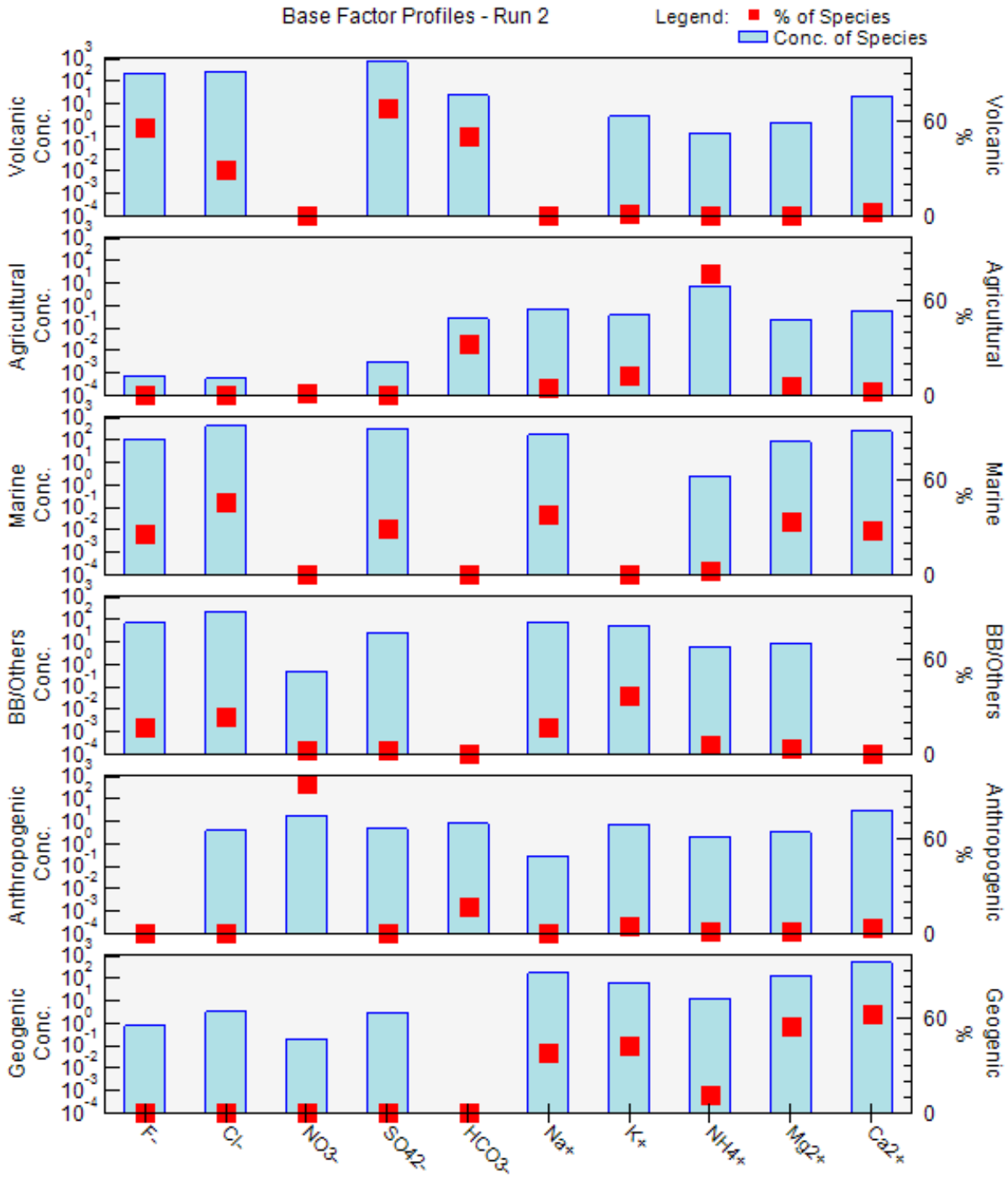

Figure 66 - Factor profiles (% of species and concentrations) obtained from the US Environmental Protection Agency (EPA) PMF model in Cratere 2001 sampling site.

For sodium and chloride, the main source was sea-salt aerosols in all the coastal sites, i.e., Palermo and Catania urban areas and Milazzo and Priolo Gargallo industrial areas. The highest marine contribution for sodium was estimated for the Priolo Gargallo sampling site (83.2%), while the lowest was for the Mt. Soro sampling site (35.8%), (Fig. 67). Other sources for sodium were

agricultural practices, up to 14.9% at Augusta, anthropogenic activities, up to 33.0% at Mt. Soro, biomass burning, up to 17.9% at Milazzo, geogenic materials, up to 38.7% at Cratere 2001, and volcanic emissions, up to 23.3% at Zafferana Etnea. The highest marine contribution for chloride was estimated for the Priolo Gargallo sampling site (84.9%), while the lowest was for the Citelli sampling site (24.6%), (Fig. 68). Other sources for chloride were agricultural practices, up to 15.5% at Zafferana Etnea, anthropogenic activities, up to 35.4% at San Giovanni La Punta, biomass burning, up to 26.1% at Catania, geogenic materials, up to 10.6% at Siracusa, and volcanic emissions, up to 68.3% at Citelli.

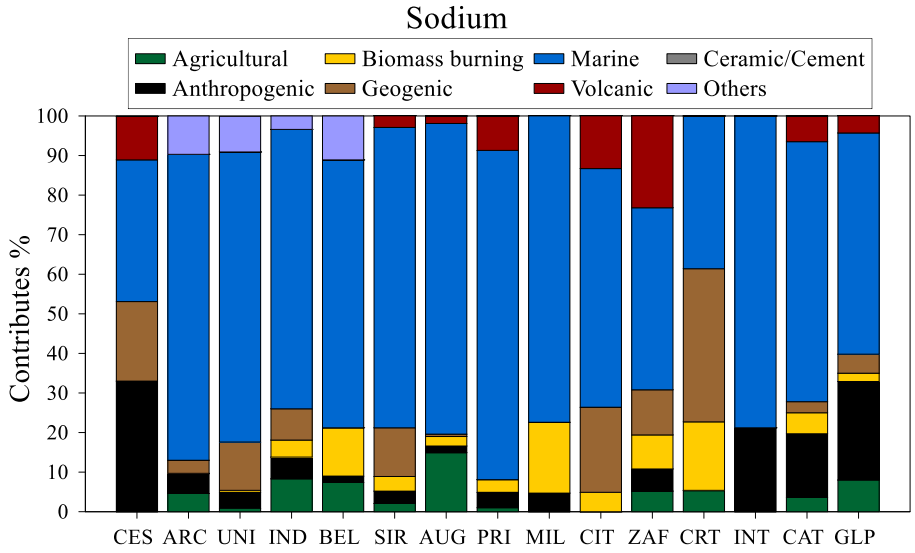

Figure 67 - Sodium contributes (%) for each main source and each sampling site calculated from the US Environmental Protection Agency (EPA) PMF model.

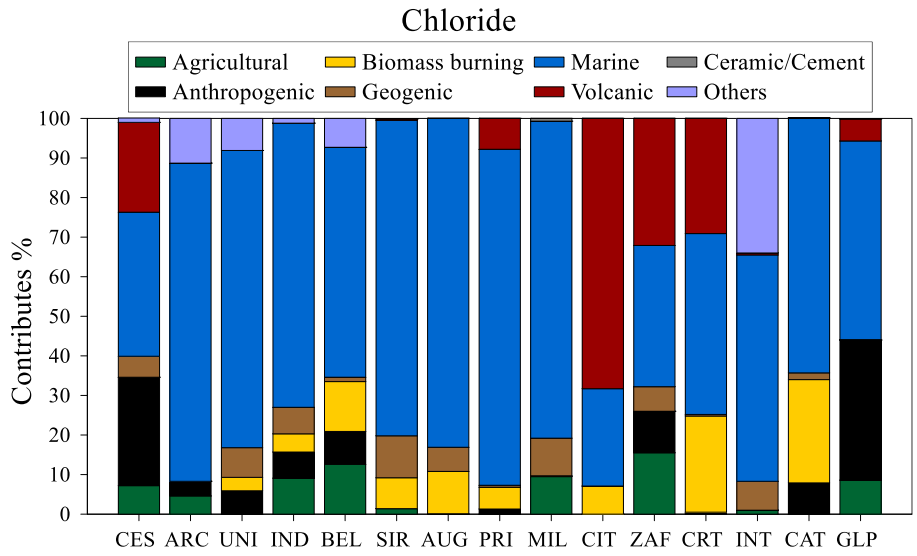

Figure 68 - Chloride contributes (%) for each main source and each sampling site calculated from the US Environmental Protection Agency (EPA) PMF model.

For magnesium, the main source was sea-salt aerosols in many of the sampling sites, ranging from 17.7% (Zafferana Etnea) to 67.6% (Augusta). Other sources of magnesium were agricultural practices, up to 20.0% at Zafferana Etnea, anthropogenic activities, up to 36.0% at San Giovanni La Punta, biomass burning, up to 16.8% at Siracusa, geogenic materials, up to 54.5% at Cratere 2001, and volcanic emissions, up to 32.4% at Zafferana Etnea. At the Milazzo sampling site, 1.3% of magnesium emissions could come from industrial activities related to the production of ceramics and cement (Fig. 69).

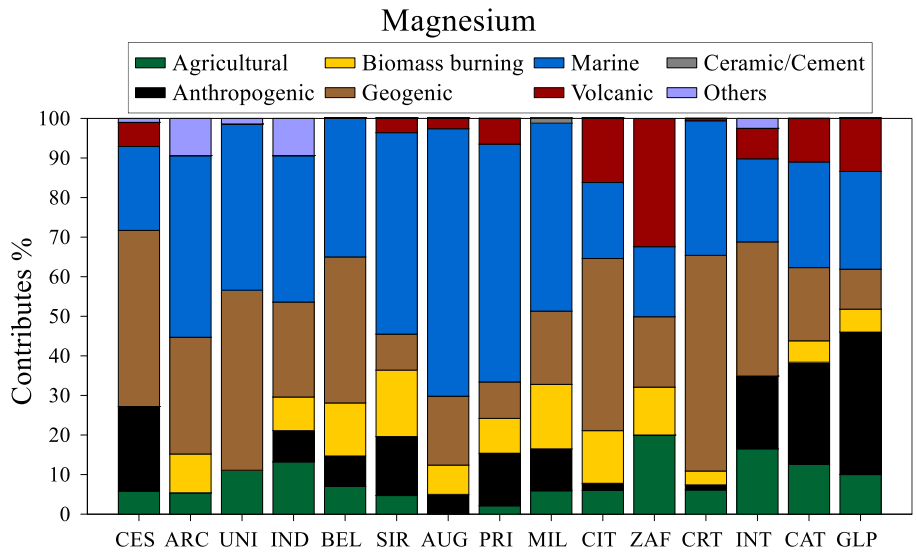

Figure 69 - Magnesium contributes (%) for each main source and each sampling site calculated from the US Environmental Protection Agency (EPA) PMF model.

For potassium, the main source was biomass burning at many of the sampling sites, with relative contributions up to 73.4% for the Unipa sampling site. No contributions attributable to this source were estimated for the Mt. Soro, Cratere 2001, and Mt. Intraleo sampling sites. In the first two sites, the main source of potassium was the geogenic materials (61.4% and 42.4%, respectively). At the Mt. Intraleo sampling site, the main source was agricultural practices (61.9%). Other sources for potassium were anthropogenic activities, up to 7.2% at Citelli, sea salt aerosols, with contributions up to 37.6% at Cratere 2001, and volcanic emissions, up to 41.8% at Zafferana Etnea (Fig. 70).

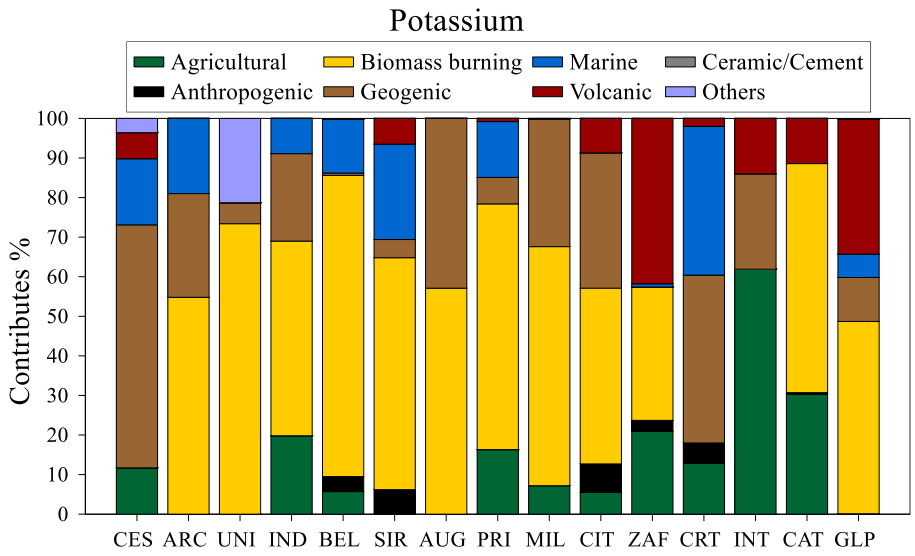

Figure 70 - Potassium contributes (%) for each main source and each sampling site calculated from the US Environmental Protection Agency (EPA) PMF model.

For ammonium, the main source was related to agricultural practices, for which contributions between 56.6% (Mt. Intraleo) to 92.0% (Belgio) were estimated (Fig. 71). A relevant anthropogenic contribution was estimated for the Mt. Intraleo sampling site (32.4%), while geogenic contributions reached values up to 11.7% and 13.6% at Cratere 2001 and Mt. Soro sampling sites, respectively. Marine contributions were very low, up to 21.6% at the Catania sampling site, while volcanic relative contribution was important in the sampling site of Augusta (12.6%).

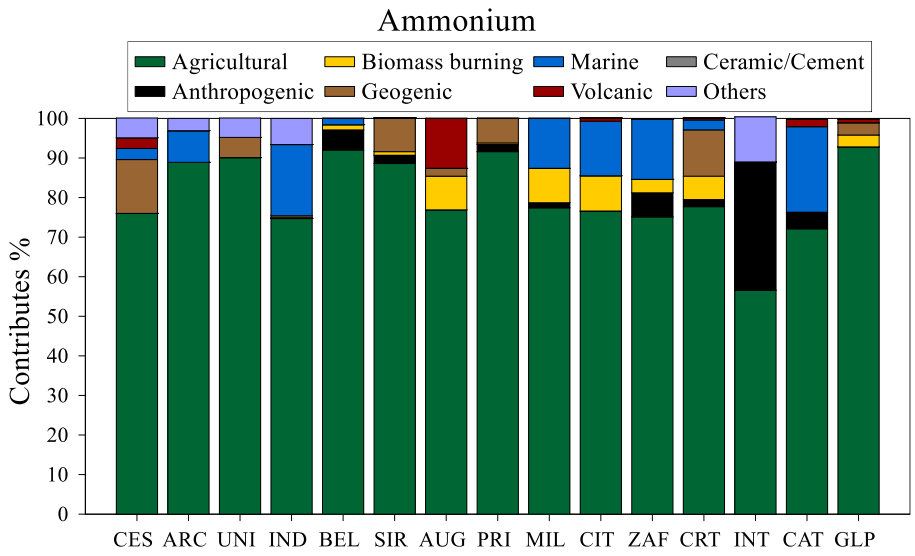

Figure 71 - Ammonium contributes (%) for each main source and each sampling site calculated from the US Environmental Protection Agency (EPA) PMF model.

For calcium and bicarbonate, the main source was related to the uplift and dispersion of geogenic materials, with relative contributions between 35.0% (Zafferana Etnea) and 69.5% (Mt. Soro) for the former and up to 100% (Zafferana Etnea) for the latter. Other sources for calcium were anthropogenic activities, up to 38.9% at Priolo Gargallo, biomass burning, up to 24.1% at Citelli, sea salt aerosols, with relative contributions up to 28.3% at Cratere 2001, and volcanic emissions, up to 23.7% at Zafferana Etnea. At the Milazzo sampling site, 4.6% of calcium concentration could come from industrial activities related to the production of ceramics and cement (Fig. 72). Other sources for bicarbonate were anthropogenic activities, up to 28.0% at the Archirafi sampling site, volcanic emissions, up to 50.2% at Cratere 2001, biomass burning, up to 34.3% at Siracusa, and agricultural activities, with relative contributions up to 32.3% at Cratere 2001. For the Mt. Intraleo sampling site, other sources, not well recognised, were responsible for 82.6% of the total contribution of bicarbonate. At the Milazzo sampling site, 3.1% of the bicarbonate concentration could come from industrial activities related to the production of ceramics and cement (Fig. 73).

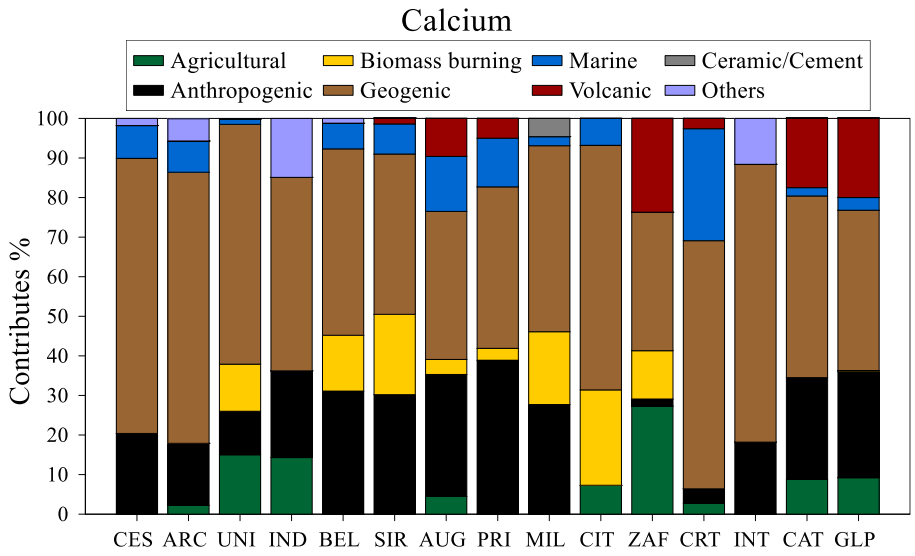

Figure 72 - Calcium contributes (%) for each main source and each sampling site calculated from the US Environmental Protection Agency (EPA) PMF model.

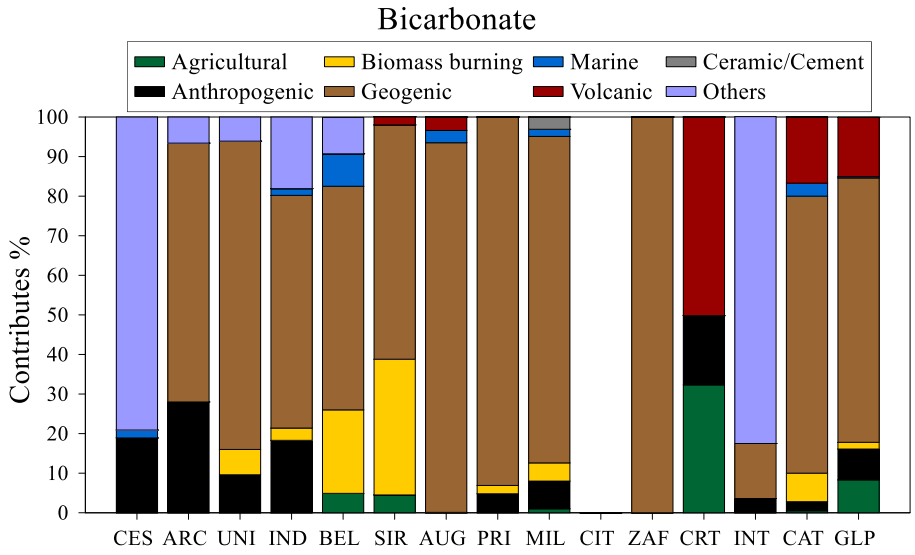

Figure 73 - Bicarbonate contributes (%) for each main source and each sampling site calculated from the US Environmental Protection Agency (EPA) PMF model.

For fluoride, the main source was the volcanic emissions in many of the sampling sites, with relative contributions up to 90.7% for the Zafferana Etnea sampling site (Fig. 74). No volcanic contributions were estimated for the Palermo urban area and the Milazzo sampling site, for which the main sources of fluoride were the industrial activities related to the production of ceramics and cement. Agricultural activities contributed to 18.4% of the fluoride concentration in the Unipa

sampling site. Anthropogenic contributions were relevant for the Indipendenza (12.5%) and the Catania (22.3%) sampling sites. Biomass burning was an important source of fluoride in the Indipendenza (20.2%) and the Cratere 2001 (16.8%) sampling sites. Other sources for fluoride were geogenic materials, up to 43.9% at Citelli, and sea salt contributions, up to 26.4% at Cratere 2001. Other sources, not well recognised, were responsible for the emissions of fluoride in the urban area of Palermo, with a mean relative contribution of 71.5%.

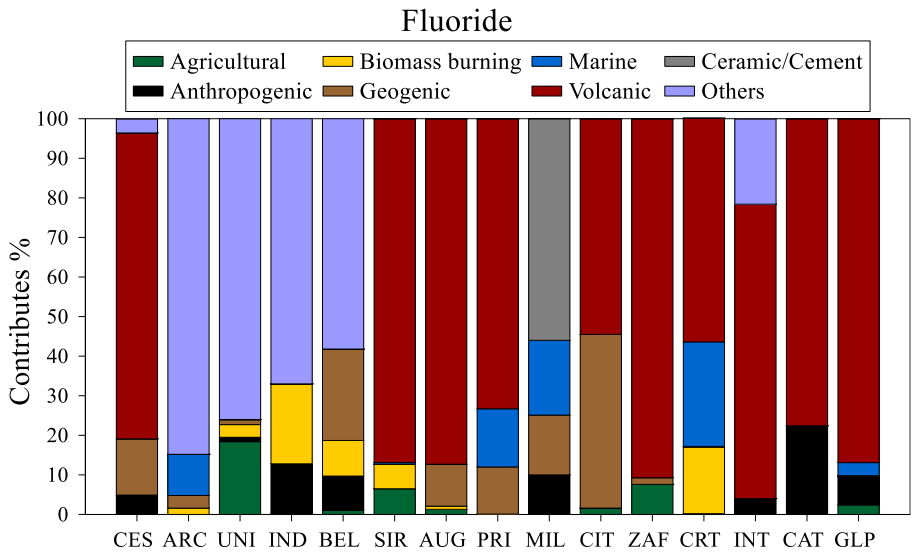

Figure 74 - Fluoride contributes (%) for each main source and each sampling site calculated from the US Environmental Protection Agency (EPA) PMF model.

For sulfate and nitrate, the main source was related to the anthropogenic activities, with relative contributions between 0.4% (Cratere 2001) and 61.3% (Indipendenza) for the former and between 32.7% (Belgio) and 95.4% (Cratere 2001) for the latter. Other sources for sulfate were sea salt aerosols, up to 38.4% at Augusta, geogenic materials, up to 47.5% at Mt. Intraleo sampling site, biomass burning, with relative contributions of up to 44.5% at Citelli, agricultural activities, up to 37.8% at Mt. Soro, and volcanic emissions, with relative contributions up to 67.9% at the Cratere 2001 sampling site (Fig. 75). Other sources for nitrate were biomass burning, up to 35.2% at Belgio, sea salt aerosols, geogenic materials, with relative contributions up to 29.4% at Mt. Soro, agricultural

activities, up to 20.7% at Zafferana Etnea, volcanic emissions, up to 19.9% at San Giovanni La Punta, and sea salt aerosols, with relative contributions up to 19.1% at Augusta. At the Milazzo sampling site, 6.9% of nitrate concentration could come from industrial activities related to the production of ceramics and cement. Long-range transport and secondary chemical transformations could explain the contribution of up to 22.4% of the total nitrate in the Palermo urban area (Fig. 76).

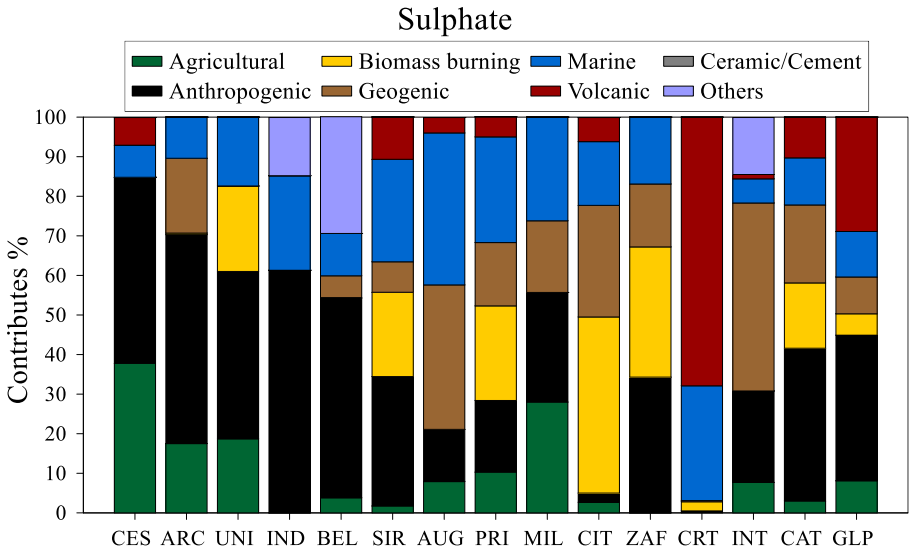

Figure 75 - Sulfate contributes (%) for each main source and each sampling site calculated from the US Environmental Protection Agency (EPA) PMF model.

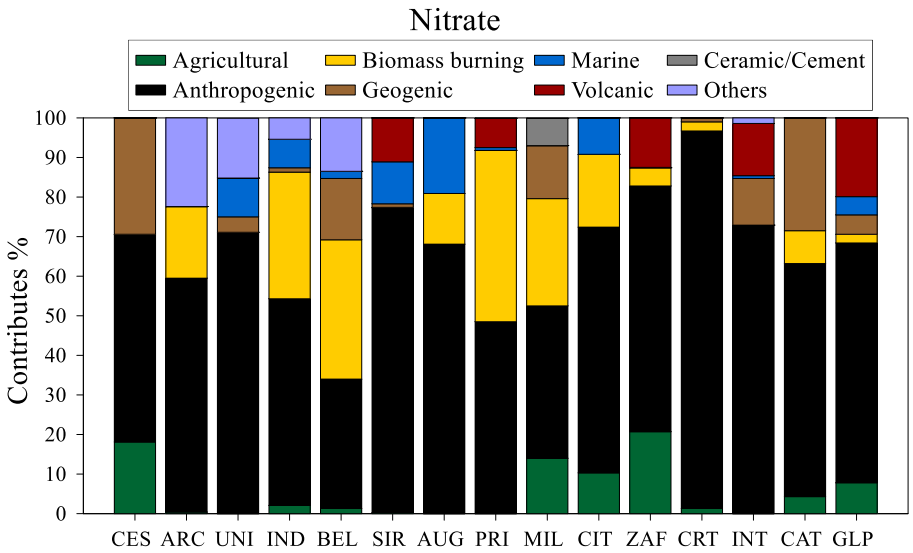

Figure 76 - Nitrate contributes (%) for each main source and each sampling site calculated from the US Environmental Protection Agency (EPA) PMF model.

In conclusion, the large quantities of Na^+, Cl^- and partly Mg^{2+} found in the coastal sites of both urban and industrial areas can be attributed to the marine source. The imprint of this source was also present, albeit attenuated, in the Etna and background sites. Another very influential and spatially widespread natural source was the geogenic one, to which the concentrations of Ca^{2+}, HCO_3^- and, to some extent, Mg^{2+} and K^+ can be attributed. The last natural source, able to condition the chemical composition of atmospheric deposition in the Etna sites, in those of the urban area of Catania, in those of the industrial area of Priolo Gargallo and, occasionally, also in the Mt. Soro background site, was the volcanic source. Its contribution was observed for all the ionic species analysed, especially for F^-, Cl^-, and SO_4^{2-}. Remarkable was the contribution of anthropogenic sources, such as biomass combustion, from which derived part of the quantities of K^+ found in rainwater, agricultural activities, responsible for the emission of nitrogen species found in rainwater as NH_4^+, urban emissions (domestic heating, vehicular traffic) and industrial emissions of NOx and SOx, from which derived part of the NO_3^- and SO_4^{2-} concentrations found in rainwater. At a very specific industrial activity, the production of ceramics and cement can be attributed the F^- found in the rainwater in the Milazzo area. It was not possible to discriminate the contribution of other natural and anthropogenic sources, for which the term "others" was chosen, such as the transport of dust of Saharan origin and the long-range transport of particulate matter.

5.2.4 Atmospheric deposition fluxes for major ions

Rainwater is an effective means of transport of elements to the earth's surface. The chemical flux of major ions (μeq m^2 d^{-1}) can be determined by knowing the concentrations (μeq L^{-1}), the exposure time (d) of the collector, and the amount of precipitation (L m^{-2}). The average deposition rates of the major ions during the study period were computed for each site using equation (7) in section 3.6, and the results are shown in Figure 77. Atmospheric deposition values followed the concentrations of each ion but also depended on the precipitation amounts.

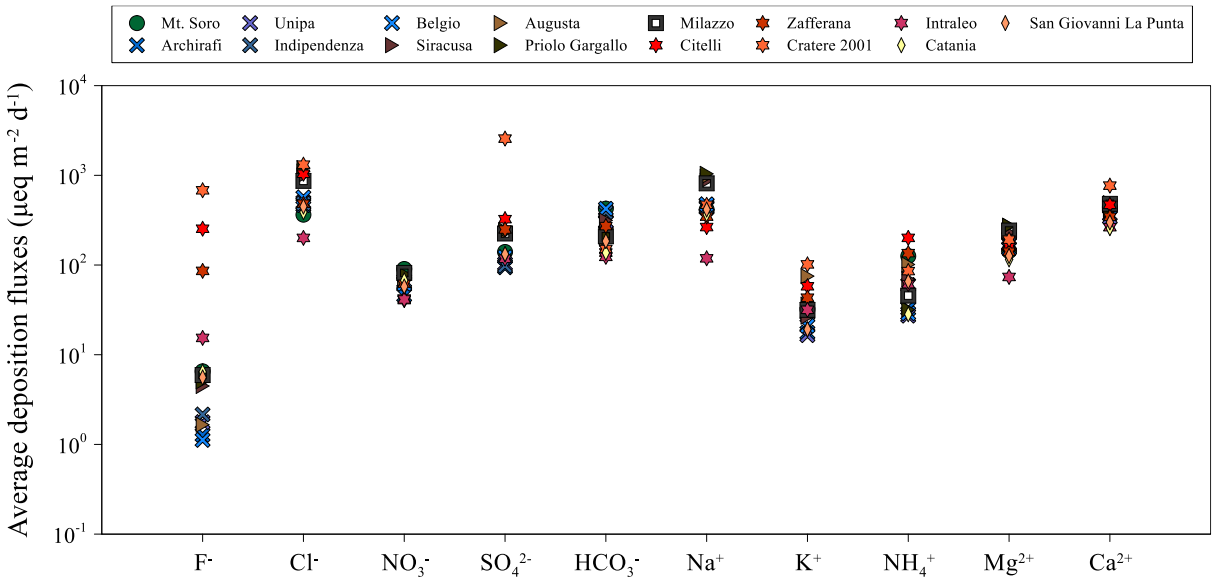

Figure 77 - Average daily deposition rate (µeq m^2 d^{-1}) for each site and each ion.

Fluoride depositions were low in all the sampling sites, with average values between 1.12 µeq m^2 d^{-1} for the site of Belgio, and 6.53 µeq m^2 d^{-1} for the site of Mt. Soro. Exceptions are the sites in the Etna area, for which average values were two orders of magnitude higher than for the other sites. Average values decreased with distance from the active craters, highlighting a prevalent volcanic contribution for this ion to bulk deposition in this area. The deposition rate in the most exposed site (Cratere 2001) was 681 µeq m^2 d^{-1}, one order of magnitude higher than the less exposed site of this area, i.e., Mt. Intraleo, for which an average deposition flux of 15.4 µeq m^2 d^{-1} was calculated. The higher average value calculated for the Mt. Soro site compared to the other sites can be explained by the anomalies in concentrations measured for this ion during the discussed above paroxysmal events of Mt. Etna.

Similar results were observed for chloride. Not considering the Mt. Etna sites, the highest average deposition flux was calculated for the site of Priolo Gargallo (1203 µeq m^2 d^{-1}), one of the most exposed to the contribution of sea-salt aerosols. Deposition fluxes decline moving away from the sea and with increasing altitude, decreasing to an average value of 364 µeq m^2 d^{-1} at the Mt. Soro

sampling site. The sites of San Giovanni La Punta do not follow this rule, indeed, a higher chloride average deposition value (449 μeq m^2 d^{-1}) than at the Catania site (390 μeq m^2 d^{-1}), located at a lower elevation and closer to the coastline, was calculated. As demonstrated above, this site was affected, at least in part, by the influence of Etna's emissions, also for this ion. The average chloride deposition fluxes reached values up to 1315 μeq m^2 d^{-1} at the Cratere 2001 sampling site. A similar value was calculated for the Citelli site (1041 μeq m^2 d^{-1}). The marine influence was treasurable for these sites, therefore the main contribution derived from the dissolution of gaseous volcanic HCl in rainwater. The lowest average value was calculated for the Mt. Intraleo site (201 μeq m^2 d^{-1}), due to the limited exposure to both marine and volcanic sources.

For sodium the main source was the seawater contribution and the average deposition fluxes were between 119 μeq m^2 d^{-1} (Mt. Intraleo) and 1040 μeq m^2 d^{-1} (Priolo Gargallo). For this ion, the volcanic contribution was less significant and, therefore, deposition fluxes comparable to those of other sites less exposed to the marine source have been calculated for the remaining Etna sites.

For sulfate, similar deposition fluxes were calculated for the urban area of Palermo and Catania, between 94.2 and 132 μeq m^2 d^{-1}. A common source, i.e., urban emissions of SOx, was supposed. Higher values were calculated for the two industrial areas, between 225 and 244 μeq m^2 d^{-1}, related to the urban and industrial emissions of SOx. The highest deposition flux was calculated for the Cratere 2001 site, equal to 2567 μeq m^2 d^{-1}, the site most exposed to the volcanic emissions of gaseous SO_2.

Similar deposition fluxes were calculated for nitrate in the two urban areas, with values between 46.1 and 67.4 μeq m^2 d^{-1}. Slightly high values were calculated for the two industrial areas, up to 81.7 μeq m^2 d^{-1} for the site of Milazzo. Nitrogen oxides urban emissions for the Palermo and Catania areas, and urban and industrial emissions for the Priolo Gargallo and Milazzo areas, were the main sources of nitrate in the rainwater. Since volcanic emissions were a negligible source of

nitrogen oxides into the atmosphere, low values were calculated for the Etna sites, with an average of 46.7 μeq m^2 d^{-1}. The highest average value was calculated for the Mt. Soro site, 90.4 μeq m^2 d^{-1}.

The lowest deposition fluxes for K^+ were calculated in the two urban areas, with values from 16.5 μeq m^2 d^{-1} (Unipa) to 29.1 μeq m^2 d^{-1} (Indipendenza). For these areas, the main sources were geogenic and marine. Probably, for the Indipendenza sampling site, an anthropogenic source may be hypothesised, considering the low ss-K^+ fraction (31.9%). A slightly high flux was calculated for the Mt. Soro background area, equal to 31.9 μeq m^2 d^{-1}; dissolution of geogenic material was the main source of K^+ in the area. The highest deposition fluxes for this ion were calculated for the industrial areas (between 26.6 and 75.2 μeq m^2 d^{-1}) and the Mt. Etna area (up to 102 μeq m^2 d^{-1}). Anthropogenic, geogenic, and partially marine sources were involved in the two industrial areas, while a prevalent volcanic origin can be assumed for the Etna area.

Similar results were observed for NH_4^+, for which the lowest deposition fluxes were calculated in the two urban areas, with values from 27.2 μeq m^2 d^{-1} (Unipa) to 65.6 μeq m^2 d^{-1} (San Giovanni La Punta). A higher flux was calculated for the Mt. Soro background area, equal to 126 μeq m^2 d^{-1}, and for the Citelli sampling site (201 μeq m^2 d^{-1}). Anthropogenic sources, i.e., agricultural practices, were the main contributors to ammonium in the two urban areas and the background area.

For Mg^{2+}, the lowest deposition fluxes were calculated for the sites of Mt. Intraleo (73.6 μeq m^2 d^{-1}), Catania (116 μeq m^2 d^{-1}) and San Giovanni La Punta (126 μeq m^2 d^{-1}). Similar values were calculated for the remaining study areas, with average values between 143 μeq m^2 d^{-1} (Mt. Soro) and 274 μeq m^2 d^{-1} (Priolo Gargallo industrial area). Marine and geogenic inputs were involved for this ion.

Similar results were observed for HCO_3^- and Ca^{2+}. The highest deposition fluxes for both ions were calculated for the study areas most affected by the outcrop of rocks and soils with carbonate composition. Average values of 425, 355, 242, 209, 168, and 161 μeq m^2 d^{-1} were calculated for

HCO_3^- for the Mt. Soro, Palermo, Milazzo, Priolo Gargallo, Mt. Etna, and Catania study areas, respectively. For Ca^{2+} average values of 441, 405, 481, 436, 461, and 278 μeq m^2 d^{-1} were calculated for the same areas. The anomalous deposition flux for Ca^{2+} in the Etna area was related to the highest average value (768 μeq m^2 d^{-1}), the maximum calculated in our research, for the Cratere 2001 site. Probably, this flux was linked to the volcanic ash deposition and dissolution in the rainwater.

5.3 Soluble minor and trace elements in rainwater

5.3.1 Concentrations in blank solutions

Three different blank solutions (R I, R II, and R III) were prepared as described in section 3.6 "Quality control assurance". The raw concentrations measured in the various types of blanks, as reported in paragraph 3.6.1, were strongly influenced by the volume of the solution used to prepare them. For this reason, the measured concentrations were normalised to the original solution volume of 0.05 L for R I and 0.30 L for R II and R III. In this way, the weight contribution (μg) of each minor and trace element was calculated for each type of blank solution.

For all the analysed elements, the lowest median contributions were calculated for the R I blank solution, except for Se and Mo (R II for the former and both R II and R III blanks for the latter). The highest median contributions for Li, B, Ti, V, Cr, Mn, Fe, Co, Ni, As, Br, Rb, Sr, Sb, Cs, and Ba were calculated for the blank solution R II, while for the remaining elements for the blank solution R III. Equal median contributions were calculated for Tl in the blank solutions R II and R III.

Comparison of the median amounts of each element present in each of the blanks with the median amounts of the same elements present in the rainwater samples revealed that: (i) the relative contribution of the blank solution R I was less than 1.00% for each element, except for Mo, which was 2.81%; (ii) the relative contribution of the blank solution R II was less than 1.00% for V, As, Se, Sr, Mo, Cd, and Sb, less than 5.00% for Li, B, Mn, Co, Cu, Rb, Ba, and Tl, less than 10.0% for Ni,

Zn, and U, and greater than 10.0%, up to 18.5%, for Al, Ti, Cr, Fe, Br, Cs, and Pb; (iii) the relative contribution of the blank solution R III was less than 1.00% for Li, B, V, Mn, As, Br, Rb, Sr, Mo, and Sb, less than 5.00% for Co, Ni, Se, Cs, Cs, Ba, and Tl, less than 10.0% for Ti, Cr, Fe, Cu, Zn, and U, and greater than 10.0% only for Al (17.3%) and Pb (68.7%). These results are shown graphically in Figure 78.

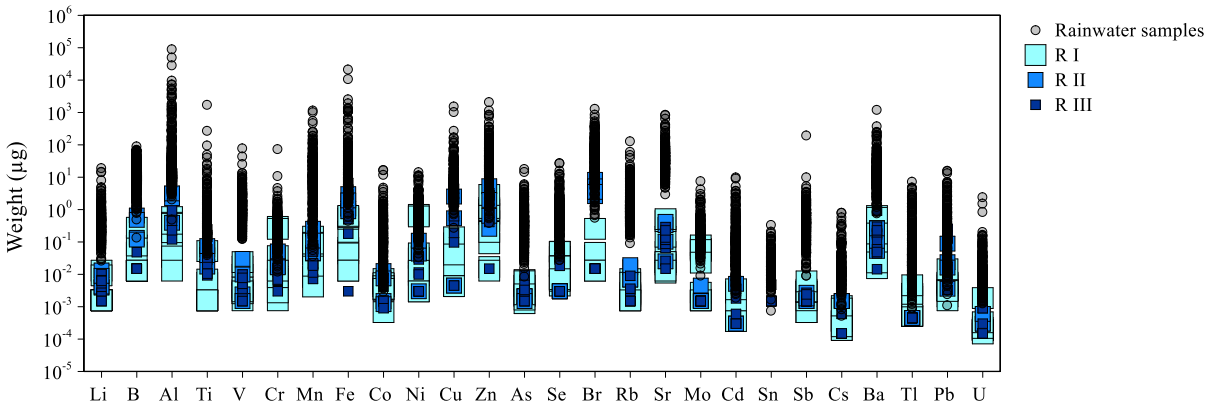

Figure 78 - Quantity, in weight (µg), for each minor and trace element, found in the blank solutions R I, R II, R III, and in the rainwater samples.

Based on the findings, it was decided not to subtract the concentrations of the blank solutions from the concentrations measured in the collected samples. Nevertheless, further investigation will have to be carried out to clarify the sources of contamination of the blank solutions for some problematic elements such as Al and Pb.

5.3.2 Comparison between the study areas

To emphasize the differences among the different sites, minor and trace element volume-weighted mean (VWM) concentrations in the rainwater samples were normalised with respect to their VWM values in the samples from the background site of Mt. Soro. In Figure 79, the dissolved constituents were ordered from the most to the least abundant element in the most enriched study area (Mt. Etna) with respect to the background site.

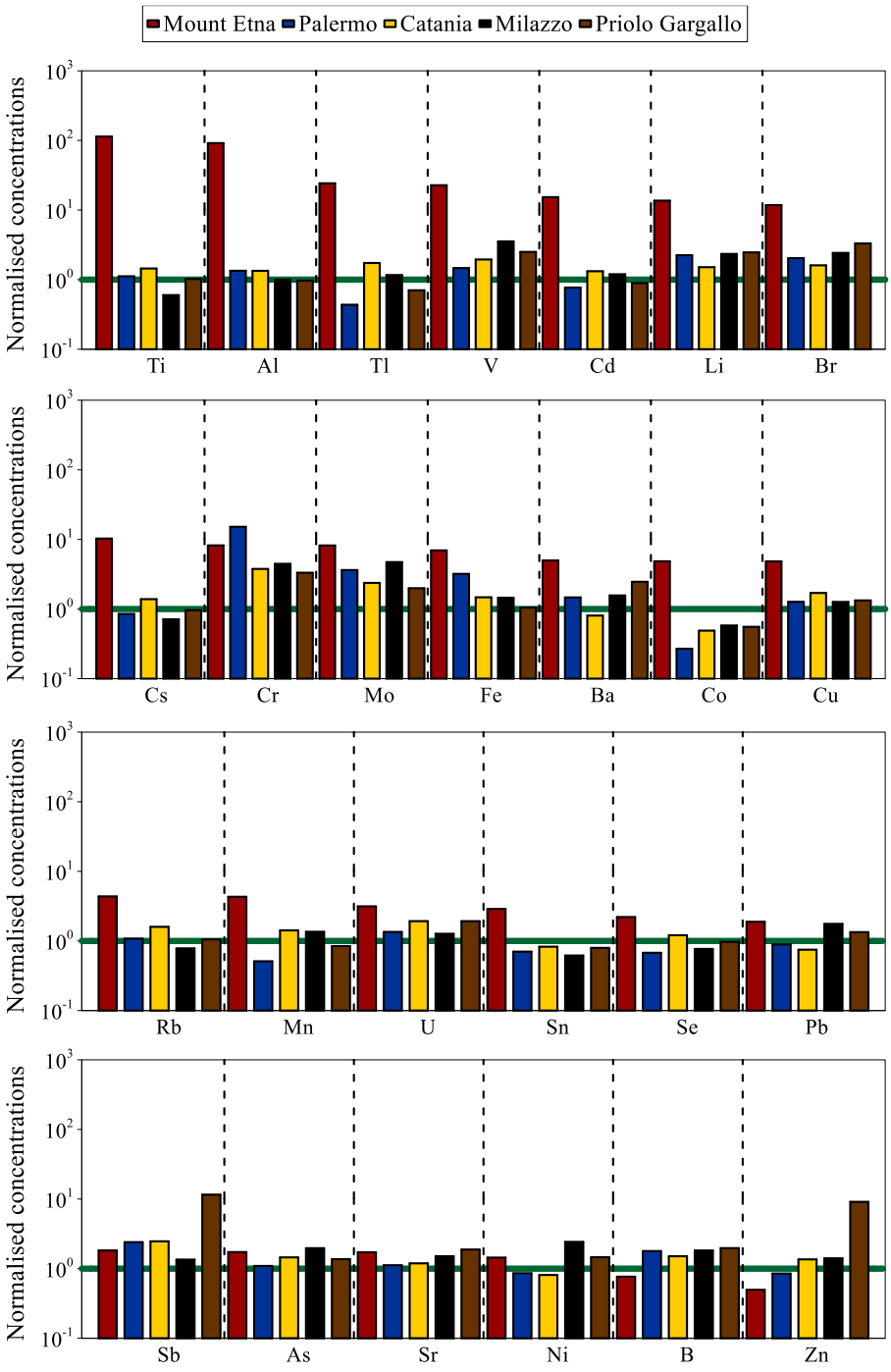

Figure 79 - Normalised minor and trace element concentrations for Mt. Etna, Palermo, Catania, Milazzo, and Priolo Gargallo study areas. The green line is the reference of Mt. Soro.

The greatest enrichments were observed for the Etna study area for most of the elements analysed, i.e., Ti, Al, Tl, V, Cd, Li, Br, Cs, Mo, Fe, Ba, Co, Cu, Rb, Mn, U, Sn, Se and Pb. For Sb, Sr, and Zn, the highest enrichments were calculated for the industrial area of Priolo Gargallo, for Cr

in the urban area of Palermo, and for As in the industrial area of Milazzo. Similar enrichments for the two urban areas (Palermo and Catania) and the two industrial areas (Milazzo and Priolo Gargallo) were calculated for B. Going into the specifics for each study area, it was observed that for all elements, except B and Zn, higher concentrations were measured in rainwater from the Etna area than from the background site (Mt. Soro). For the Palermo area, the highest enrichments were calculated for Cr (15.2), Mo (3.6), Fe (3.2), Sb (2.4), Li (2.3), and Br (2.0). Conversely, lower concentrations were recorded for other elements, specifically Pb, Ni, Cs, Zn, Cd, Sn, Se, Mn, Tl and Co, compared to the background site. Similar evidence emerged for the urban area of Catania, for which the highest enrichments were calculated for Cd (3.8), Sb (2.5), Mo (2.4), and V (2.0). In this case, only for Sn, Ni, Ba, Pb and Co lower concentrations were measured compared to the background site. For the industrial area of Milazzo, the highest enrichments were calculated for Mo (4.7), Cr (4.5), V (3.6), Ni (2.4), Br (2.4), Li (2.3), and As (2.0), while lower concentrations were measured than at the Mt. Soro site for Rb, Se, Cs, Sn, Ti, and Co. Finally, for the industrial area of Priolo Gargallo, the highest enrichments were calculated for Sb (12), Zn (9.1), Cr (3.3), Br (3.3), V (2.5), Li (2.5), Ba (2.5), Mo (2.0), and B (2.0), while lower concentrations were measured than at the Mt. Soro site for Cd, Mn, Sn, Tl, and Co.

From these results, it was possible to draw some preliminary insights into the main sources contributing to the chemistry of rainwater with the emission of certain elements. It was not surprising that refractory elements typical of volcanic emissions, i.e., Ti, Al, Tl, and V were highly enriched in the rainwater of Etna sites. Rainwater samples with low pH values ($3.0 < pH < 4.5$) were frequent in the Mt. Etna area and some metals such as Al and Fe became a significant portion of the total dissolved species, suggesting an efficient dissolution process of the solid phase (volcanic ash and particulate matter) by acid rainwater. The exceptions were the samples from the Mt. Intraleo site, as this is located upwind of the preferred direction of dispersion of gaseous and solid products of volcanic activity. Indeed, these samples had similar concentrations of many minor and trace elements

compared to the background site of Mt. Soro (not shown). Comparable contents of Sr at all study areas point to a prevalent geogenic dust origin of this element, likely in the form of resuspended volcanic ash or soil dust both from local and regional sources. The enrichment observed for Cr, Mo, Fe, and Sb in the urban and industrial areas reflected the contribution of anthropogenic emissions. Especially for Sb and Zn, a very important local source must be identified for the Priolo Gargallo industrial area, considering the concentrations that were even an order of magnitude higher for these two elements than for the other study areas. The enrichments for Br in all the study areas may be attributed to the contribution of sea-salt aerosols and volcanic emissions as regards the Mt. Etna area.

5.3.3 Statistical analysis of soluble minor and trace elements

5.3.3.1 Pearson correlation coefficients

The Pearson's correlation coefficients for each minor and trace element, for each rainwater sample (n = 301), were calculated, and reported in Table 46.

Table 46 - Pearson's correlation coefficients for minor and trace elements in rainwater. Bold values have p-value ≤ 0.0001.

	Li	B	Al	Ti	V	Cr	Mn	Fe	Co	Ni	Cu	Zn	As	Se	Br	Rb	Sr	Mo	Cd	Sn	Sb	Cs	Ba	Tl	Pb	U
Li		**0.556**	**0.760**	0.053	**0.750**	0.005	**0.258**	-0.004	**0.767**	**0.656**	**0.665**	0.004	**0.937**	**0.819**	**0.189**	**0.930**	**0.940**	**0.786**	**0.823**	0.143	0.020	**0.921**	**0.406**	**0.828**	0.124	**0.563**
B	**0.556**		0.421	-0.036	**0.512**	0.092	0.081	0.060	**0.502**	**0.346**	**0.543**	0.077	**0.464**	**0.460**	**0.555**	0.485	**0.650**	**0.542**	**0.444**	**0.313**	**0.224**	**0.500**	**0.326**	**0.432**	0.043	**0.370**
Al	**0.760**	**0.421**		0.074	**0.424**	0.000	**0.402**	-0.002	**0.761**	**0.958**	**0.566**	-0.025	**0.784**	**0.695**	0.106	**0.759**	**0.798**	**0.424**	**0.887**	0.204	-0.016	**0.682**	**0.275**	**0.596**	**0.247**	**0.855**
Ti	0.053	-0.036	0.074		0.090	0.017	**0.574**	0.083	0.152	0.063	0.133	-0.029	0.117	0.124	-0.070	0.051	0.065	0.008	0.083	0.052	0.004	0.127	0.065	0.101	**0.416**	0.125
V	**0.750**	**0.512**	0.424	0.090		0.024	0.065	0.016	**0.644**	**0.185**	**0.675**	-0.009	**0.628**	**0.849**	**0.180**	**0.863**	**0.789**	**0.966**	**0.657**	**0.322**	0.043	**0.803**	**0.343**	**0.879**	0.037	0.130
Cr	0.005	0.092	0.000	0.017	0.024		0.012	**0.897**	0.082	0.004	0.061	-0.011	0.007	0.115	0.013	0.006	0.031	**0.150**	0.003	0.023	0.011	0.061	0.119	0.003	0.080	0.013
Mn	**0.258**	0.081	0.402	**0.574**	0.065	0.012		-0.017	**0.427**	**0.466**	**0.304**	-0.029	0.413	**0.289**	0.008	**0.229**	**0.297**	0.001	**0.437**	0.213	-0.015	**0.351**	**0.216**	**0.307**	**0.624**	**0.689**
Fe	-0.004	0.060	-0.002	0.083	0.016	**0.897**	-0.017		0.017	-0.008	0.012	0.008	-0.020	-0.045	0.005	-0.021	0.029	0.132	-0.017	0.050	0.002	-0.005	0.095	-0.024	0.026	0.010
Co	**0.767**	**0.502**	0.761	0.152	**0.644**	0.082	**0.427**	0.017		0.678	**0.859**	-0.020	**0.828**	**0.888**	0.069	**0.823**	**0.805**	**0.623**	**0.876**	**0.341**	-0.013	**0.835**	**0.344**	**0.822**	**0.324**	**0.607**
Ni	**0.656**	**0.346**	0.958	0.063	**0.185**	0.004	**0.466**	-0.008	**0.678**		**0.460**	-0.026	**0.731**	**0.531**	0.068	**0.597**	**0.667**	**0.206**	**0.787**	0.261	-0.017	**0.560**	**0.230**	**0.429**	**0.299**	**0.918**
Cu	**0.665**	**0.543**	0.566	0.133	**0.675**	0.061	**0.304**	0.012	**0.859**	**0.460**		0.051	**0.679**	**0.854**	0.111	**0.720**	**0.728**	**0.643**	**0.775**	**0.371**	0.072	**0.751**	**0.307**	**0.815**	**0.312**	**0.418**
Zn	0.004	0.077	-0.025	-0.029	-0.009	-0.011	-0.029	0.008	-0.020	-0.026	0.051		-0.036	-0.049	**0.234**	-0.041	-0.002	-0.008	-0.024	-0.022	0.028	-0.042	-0.032	-0.035	0.055	-0.019
As	**0.937**	**0.464**	0.784	0.117	0.628	0.007	**0.413**	-0.020	**0.828**	**0.731**	**0.679**	-0.036		**0.818**	0.094	**0.875**	**0.878**	**0.649**	**0.858**	0.247	-0.002	**0.928**	**0.365**	**0.827**	**0.264**	**0.652**
Se	**0.819**	**0.460**	0.695	0.124	**0.849**	0.115	**0.289**	-0.045	**0.888**	**0.531**	**0.854**	-0.049	**0.818**		0.100	**0.926**	**0.847**	**0.824**	**0.885**	0.238	-0.014	**0.910**	**0.348**	**0.959**	**0.241**	**0.443**
Br	**0.189**	**0.555**	0.106	-0.070	**0.180**	0.013	0.008	0.005	0.069	0.068	0.111	**0.234**	0.094	0.100		0.102	**0.234**	**0.198**	0.116	0.021	**0.162**	0.119	0.082	0.133	-0.061	0.134
Rb	**0.930**	**0.485**	0.759	0.051	**0.863**	0.006	**0.229**	-0.021	**0.823**	**0.597**	**0.720**	-0.041	**0.875**	**0.926**	0.102		**0.925**	**0.863**	**0.877**	0.097	-0.012	**0.923**	**0.372**	**0.911**	0.116	**0.494**
Sr	**0.940**	**0.650**	0.798	0.065	**0.789**	0.031	**0.297**	0.029	**0.805**	**0.667**	**0.728**	-0.002	**0.878**	**0.847**	**0.234**	**0.925**		**0.803**	**0.873**	0.272	0.123	**0.898**	**0.470**	**0.842**	0.146	**0.621**
Mo	**0.786**	**0.542**	0.424	0.008	**0.966**	**0.150**	0.001	0.132	**0.623**	**0.206**	**0.643**	-0.008	**0.649**	**0.824**	**0.198**	**0.863**	**0.803**		**0.634**	0.189	0.041	**0.812**	0.386	**0.851**	-0.013	0.139
Cd	**0.823**	**0.444**	0.887	0.083	**0.657**	0.003	**0.437**	-0.017	**0.876**	**0.787**	**0.775**	-0.024	**0.858**	**0.885**	0.116	**0.877**	**0.873**	**0.634**		**0.284**	-0.017	**0.845**	0.328	**0.857**	**0.305**	**0.711**
Sn	0.143	**0.313**	0.204	0.052	**0.322**	0.023	0.213	0.050	**0.341**	0.261	**0.371**	-0.022	0.247	0.238	0.021	0.097	0.272	0.189	**0.284**		-0.001	0.311	0.119	0.260	**0.297**	**0.341**
Sb	0.020	**0.224**	-0.016	0.004	**0.043**	0.011	-0.015	0.002	-0.013	-0.017	0.072	0.028	-0.002	-0.014	**0.162**	-0.012	0.123	0.041	-0.017	-0.001		-0.017	**0.551**	-0.011	-0.029	0.060
Cs	**0.921**	**0.500**	0.682	0.127	**0.803**	0.061	**0.351**	-0.005	**0.835**	**0.560**	**0.751**	-0.042	**0.928**	**0.910**	0.119	**0.923**	**0.898**	**0.812**	**0.845**	0.311	-0.017		**0.496**	**0.937**	**0.253**	**0.500**
Ba	**0.406**	**0.326**	0.275	0.065	**0.343**	0.119	**0.216**	0.095	**0.344**	**0.230**	**0.307**	-0.032	**0.365**	**0.348**	0.082	**0.372**	**0.470**	**0.386**	**0.328**	0.119	**0.551**	**0.496**		**0.354**	0.118	**0.343**
Tl	**0.828**	**0.432**	0.596	0.101	0.879	0.003	**0.307**	-0.024	**0.822**	**0.429**	**0.815**	-0.035	**0.827**	**0.959**	0.133	**0.911**	**0.842**	**0.851**	**0.857**	0.260	-0.011	**0.937**	**0.354**		**0.242**	**0.378**
Pb	0.124	0.043	0.247	**0.416**	0.037	0.080	**0.624**	0.026	**0.324**	**0.299**	**0.312**	0.055	**0.264**	**0.241**	-0.061	0.116	0.146	-0.013	**0.305**	**0.297**	-0.029	**0.253**	0.118	**0.242**		**0.409**
U	**0.563**	**0.370**	0.855	0.125	0.130	0.013	**0.689**	0.010	**0.607**	**0.918**	**0.418**	-0.019	**0.652**	**0.443**	0.134	**0.494**	**0.621**	0.139	**0.711**	**0.341**	0.060	**0.500**	**0.343**	**0.378**	**0.409**	

For Li, the best correlations were with Sr (0.940), As (0.937), Rb (0.930), and Cs (0.921). Strontium was well correlated with Li and Rb (0.925). Rubidium was correlated, as well as with Li and Sr, also with Se (0.926), Cs (0.923), and Tl (0.911). Arsenic was well correlated with Cs (0.928), and the latter was well correlated with Tl (0.923) and Se (0.910). For Se, the stronger correlations were with Rb, Cs, and Tl (0.959). Boron was well correlated only with Sr (0.650). Aluminium was well correlated with Ni (0.985), Cd (0.887), and U (0.855), and nickel was correlated with U (0.918). Cadmium was well correlated with many trace elements: Al, Se (0.885), Rb (0.877), Co (0.876), Sr (0.873), As (0.858), Tl (0.857), Cs (0.845), and Li (0.823). For Co, the stronger correlations were with Se (0.888), Cd, Cu (0.859), Cs (0.835), As (0.828), Rb (0.823), Tl (0.822), and Sr (0.805). Copper was well correlated with Co, Se (0.854), and Tl (0.815). A good correlation, but not strong, was found between B and Sr (0.650). The stronger correlation for Ti was with Mn (0.574), and the latter was well correlated with U (0.689) and Pb (0.624). For V the best correlations were with Mo

(0.966), Tl (0.879), Rb (0.863), Se (0.849), and Cs (0.803). Strong correlations were found between Mo and V, Rb (0.863), Tl (0.851), Se (0.824), Cs (0.812), and Sr (0.803). Chromium was correlated only with iron (0.897). Bromide was well correlated only with B (0.555), and Sb was correlated with Ba (0.551), but the correlations were not strong. No strong correlations were found between Sn, Zn, and other elements.

5.3.3.2 Principal Component Analysis (PCA)

Relationships between minor and trace elements may be also estimated through the Principal Component Analysis (PCA). For each element, when the concentrations were below the detection limit, values equal to the detection limits (LOD) divided by a factor 2 were considered. It was decided to make the statistical analysis for each study context, separately.

The KMO (Kaiser-Meyer-Olkin) test returned values of 0.830, 0.830, and 0.756 for the volcanic area of Mt. Etna, the two urban areas of Palermo and Catania, and the two industrial areas of Milazzo and Priolo Gargallo. The Bartlett's sphericity test had a significance value of < 0.001, confirming the applicability of PCA, for each of these datasets. The same analysis of the correlation matrix applied to the Mt. Soro background area dataset showed that the matrix cannot be definitively positive and therefore the principal component analysis cannot be applied to this dataset.

The results followed by Varimax rotation to a set of orthogonal axes for a total of 300 rainwater samples are presented in Tables 47a, b, and c. Five principal components were selected for the Mt. Etna area, and the two urban areas, explaining 88.4% and 76.3% of the total variance of the dataset, respectively. Six principal components were found for the urban and industrial areas, explaining 75.2% of the total variance.

Table 47 - The results from Principal Component Analysis (PCA) for Mt. Etna (a), Palermo and Catania (b), and Milazzo and Priolo Gargallo (c) rainwater samples. Factors loadings greater than 0.700 are in bold.

(a) Variable	PC1	PC2	PC3	PC4	PC5
Li	**0.834**	0.444	-0.004	-0.078	0.028
B	**0.749**	0.412	-0.080	0.136	0.405
Al	0.494	**0.830**	0.041	0.010	-0.018
Ti	0.047	-0.108	**0.865**	-0.018	0.087
V	**0.976**	-0.105	0.006	-0.029	0.036
Cr	0.034	0.095	-0.041	0.163	**0.885**
Mn	**0.865**	0.482	0.035	-0.060	0.045
Fe	0.063	0.446	**0.801**	0.139	0.019
Co	0.640	**0.747**	0.132	-0.003	0.014
Ni	**0.714**	0.493	0.071	0.334	0.295
Cu	0.267	**0.941**	0.063	0.050	-0.004
Zn	**0.746**	0.255	0.062	0.316	0.310
As	0.236	0.123	0.192	**0.859**	0.061
Se	**0.741**	0.542	0.090	0.101	0.024
Br	**0.915**	0.254	0.046	0.195	0.110
Rb	**0.847**	0.395	0.125	0.199	0.083
Sr	**0.924**	0.346	-0.037	-0.073	0.054
Mo	**0.975**	-0.068	-0.078	-0.083	0.048
Cd	**0.738**	0.606	0.082	0.119	-0.023
Sn	0.017	-0.061	0.089	**0.857**	0.055
Sb	0.133	-0.137	0.161	-0.055	**0.811**
Cs	**0.893**	0.310	0.125	0.141	0.006
Ba	0.636	0.278	0.198	-0.024	0.099
Tl	**0.948**	0.157	0.093	0.173	-0.012
Pb	0.009	0.254	**0.723**	0.357	0.015
U	0.182	**0.928**	0.274	0.038	-0.011
Variance (%)	58.1	11.4	8.54	5.50	4.82

(b) Variable	PC1	PC2	PC3	PC4	PC5
Li	0.385	0.625	0.182	0.012	0.141
B	0.312	0.652	0.261	0.046	0.489
Al	0.150	0.623	0.150	-0.034	-0.535
Ti	0.398	0.485	0.548	-0.021	-0.352
V	0.352	**0.842**	0.166	0.192	-0.059
Cr	-0.016	-0.031	0.011	**0.987**	-0.004
Mn	0.545	0.392	0.613	0.020	-0.190
Fe	0.019	0.013	0.098	**0.969**	-0.075
Co	0.435	0.371	**0.712**	0.164	-0.162
Ni	0.460	0.206	0.626	0.268	0.180
Cu	0.695	0.522	0.400	0.034	-0.037
Zn	**0.885**	0.063	0.308	0.000	0.134
As	0.602	**0.708**	0.075	0.101	0.082
Se	0.422	0.636	-0.023	0.024	-0.391
Br	0.062	0.090	-0.076	-0.080	**0.723**
Rb	0.542	0.573	0.150	0.026	0.055
Sr	0.186	**0.855**	0.233	0.065	0.095
Mo	0.141	0.510	0.100	**0.775**	-0.073
Cd	**0.847**	0.059	0.258	0.042	-0.015
Sn	0.150	0.224	0.635	0.092	0.086
Sb	0.629	0.381	0.165	0.018	0.260
Cs	**0.770**	0.226	-0.044	-0.024	0.105
Ba	-0.036	0.418	0.090	0.301	0.130
Tl	**0.873**	0.354	0.056	0.051	-0.144
Pb	-0.086	-0.015	**0.789**	-0.030	-0.087
U	0.114	**0.885**	0.150	0.024	-0.060
Variance (%)	45.2	10.4	7.90	6.97	5.76

(c) Variable	PC1	PC2	PC3	PC4	PC5	PC6
Li	**0.935**	0.039	-0.012	0.261	0.025	0.108
B	**0.879**	-0.054	-0.041	-0.019	0.049	0.341
Al	0.334	**0.865**	0.137	-0.055	0.037	0.035
Ti	0.038	**0.956**	0.069	-0.004	-0.033	-0.063
V	**0.815**	0.141	0.004	-0.115	0.079	0.341
Cr	0.395	-0.059	0.402	-0.339	-0.034	0.216
Mn	0.032	0.318	**0.821**	0.138	0.008	-0.090
Fe	0.063	**0.908**	0.249	0.008	-0.067	0.065
Co	0.112	0.144	**0.894**	0.143	-0.059	0.057
Ni	**0.788**	-0.019	0.048	0.093	0.031	0.004
Cu	0.571	0.138	0.409	0.405	0.153	0.308
Zn	0.093	-0.118	0.066	**0.833**	-0.043	-0.020
As	**0.865**	0.051	0.122	0.018	0.103	0.220
Se	**0.849**	0.334	0.188	0.162	0.058	-0.033
Br	0.655	-0.160	-0.311	0.212	-0.100	0.050
Rb	**0.712**	0.127	0.362	0.087	0.077	0.407
Sr	**0.702**	0.087	0.131	-0.105	0.549	0.090
Mo	**0.936**	0.042	0.122	-0.035	0.068	0.067
Cd	0.629	0.054	0.169	0.674	0.018	0.076
Sn	0.350	0.072	0.170	0.071	0.064	**0.783**
Sb	0.155	-0.024	-0.094	0.026	**0.904**	0.162
Cs	0.295	-0.022	-0.146	0.241	0.076	**0.793**
Ba	0.047	-0.011	0.025	-0.068	**0.934**	-0.043
Tl	0.686	0.182	0.323	0.279	0.061	0.110
Pb	0.039	0.036	0.068	0.649	-0.089	0.161
U	**0.877**	0.195	0.012	-0.082	0.100	0.137
Variance (%)	40.4	12.4	8.60	5.42	4.63	3.77

For the Mt. Etna volcanic area, the PC1 accounts for 58.1% of the total variance and has high loadings (> 0.900) for V, Mo, Tl, Sr, Br, Cs, Mn, Rb, and Li. The volcanic source was responsible for the emissions of Tl, and partially Br. Bromide and Cs could arise from the marine source. Vanadium, Sr, Mn, and Li are usually derived from the dissolution of soil and resuspended mineral particles (*Guerzoni et al., 1999*; *Loya-Gonzalez et al., 2020*). Anthropogenic activities, such as agricultural practices, may be responsible for the emissions of Mo and Rb (*Nunziata, 2023*). The PC2 accounts for 11.4% of the total variance and has high loadings for Cu, U, Al, and Co, probably associated with anthropogenic emissions (*Amodio et al., 2014*; *Moreda-Piñeiro et al., 2017*). For Cu,

volcanic emissions might have contributed *(Calabrese et al., 2011*). The PC3 accounts for 8.54% of the total variance and has high loadings for Ti, Fe, and Pb. Volcanic emissions for Ti and Fe (Calabrese et al., 2011), and vehicular emissions for both Fe and Pb (*Amodio et al., 2014*; *Moreda-Piñeiro et al., 2017*; *Loya-Gonzalez et al., 2020*) could be considered. Arsenic and Sn were loaded in PC4, which accounts for 5.50% of the total variance, while Cr and Sb were loaded in PC5 (4.82% of the total variance). These elements were related to the long-range transport of atmospheric particles emitted by anthropogenic sources.

For the two urban areas, the first component (PC1), which is associated with Zn, Cd, Tl, and Cs, explains 45.2% of the total variance. Vehicular emissions were the main source of Zn (tyre wear emissions) and Cd in both the urban areas (*Dongarrà et al., 2007*; *Varrica & Alaimo, 2023*), while Tl and Cs derived from Mt. Etna's volcanic emissions, able to influence the chemical composition of rainwater in the urban area of Catania as well. The second component (PC2) explained 10.4% of the total variance and was associated with crustal elements like Al, V, and Sr. The PC3 accounts for 7.90% of the dataset variance and has high loadings for Pb and Co, both derived from anthropogenic sources, such as vehicular emissions (*Amodio et al., 2014*; *Moreda-Piñeiro et al., 2017*). The PC4 accounts for 6.97% of the total variance and has high loadings for Cr, Fe, and Mo. For the first two elements, a crustal origin could be assumed, although Fe can also derive from brake wear emissions (*Amato et al., 2024*), while Mo could result from vehicular emissions. In the PC5 only Br was loaded with a high loading (0.723) and this component is connected to the marine source.

For the two industrial areas, the first component (PC1), which is associated with Mo, Li, B, U, As, Se, V, Ni, Rb, and Sr, explains 40.4% of the total variance. The PC2 accounts for 12.4% of the dataset variance and has high loadings of crustal elements, i.e., Ti, Fe, and Al. The PC3 accounts for 8.60% of the total variance and has high loadings of Mn and Co, both associated with anthropogenic emissions, such as metallurgical industry emissions (*Amodio et al., 2014*; *Loya-Gonzalez et al., 2020*). Zinc was loaded in PC4, which accounts for 5.42% of the total dataset

variance (tyre wear emissions). The fifth component (PC5), which is associated with Ba and Sb, explains 4.63% of the total variance. These elements were probably derived from urban vehicular emissions, especially form brake wear. Caesium and Sn were loaded in PC6 (3.77% of the total variance).

5.3.4 Atmospheric deposition fluxes for minor and trace elements

Atmospheric deposition fluxes (μg m^{-2} d^{-1}) were calculated by using equation (7). The median values for each minor and trace element and each sampling site are reported in Table 48 and Figure 80. In the latter, the elements are in decreasing order based on the median flux at the Cratere 2001 site.

Table 48 - Median bulk atmospheric deposition fluxes (μg m^{-2} d^{-1}) for minor and trace elements.

	Li	B	Al	Ti	V	Cr	Mn	Fe	Co	Ni	Cu	Zn	As
	μg m^2 d^{-1}	μg m^2 d^{-1}	μg m^2 d^{-1}	μg m^2 d^{-1}	μg m^2 d^{-1}	μg m^2 d^{-1}	μg m^2 d^{-1}	μg m^2 d^{-1}	μg m^2 d^{-1}	μg m^2 d^{-1}	μg m^2 d^{-1}	μg m^2 d^{-1}	μg m^2 d^{-1}
CES	0.270	12.6	17.0	0.490	0.910	0.167	7.79	16.5	0.130	0.544	4.76	12.8	0.204
ARC	0.256	9.30	19.5	0.198	0.588	0.130	0.922	4.71	0.0235	0.216	2.74	8.66	0.163
UNI	0.241	11.4	12.3	0.146	0.637	0.151	1.64	2.85	0.0295	0.238	2.57	8.68	0.173
IND	0.264	12.6	11.2	0.362	0.604	0.164	0.846	6.19	0.0355	0.276	4.24	7.38	0.195
BEL	0.255	14.4	8.42	0.122	0.709	0.235	3.36	3.38	0.0370	0.510	4.12	13.4	0.172
SIR	0.229	10.1	15.9	0.220	1.39	0.204	0.967	4.62	0.0225	0.774	3.76	24.3	0.244
AUG	0.354	13.6	4.79	0.111	0.840	0.0694	5.77	2.96	0.113	0.566	5.54	219	0.165
PRI	0.188	10.5	13.5	0.159	0.976	0.123	0.487	3.82	0.0163	0.436	2.99	9.91	0.157
GAB	0.361	17.9	17.6	0.256	1.97	0.296	10.8	9.15	0.162	1.69	4.87	23.8	0.419
CIT	0.503	5.32	621	2.32	2.24	0.300	37.5	67.5	0.463	0.844	25.9	29.5	0.618
ZAF	0.255	9.06	101	0.966	1.24	0.170	16.6	15.9	0.293	0.480	7.32	20.6	0.380
CRT	0.715	8.24	674	1.08	3.16	0.224	54.6	32.7	0.698	0.817	21.4	32.6	0.732
INT	0.175	5.38	18.4	0.313	0.431	0.115	4.95	9.16	0.0871	0.332	4.74	12.6	0.139
CAT	0.181	8.48	15.7	0.200	0.651	0.107	2.58	6.01	0.0433	0.451	3.25	17.0	0.164
GLP	0.167	6.99	20.3	0.251	1.04	0.146	1.35	6.65	0.0223	0.286	3.47	12.8	0.228

	Se	Br	Rb	Sr	Mo	Cd	Sn	Sb	Cs	Ba	Tl	Pb	U
	μg m^2 d^{-1}	μg m^2 d^{-1}	μg m^2 d^{-1}	μg m^2 d^{-1}	μg m^2 d^{-1}	μg m^2 d^{-1}	μg m^2 d^{-1}	μg m^2 d^{-1}	μg m^2 d^{-1}	μg m^2 d^{-1}	μg m^2 d^{-1}	μg m^2 d^{-1}	μg m^2 d^{-1}
CES	0.462	43.8	0.819	31.7	0.0993	0.0717	0.0924	0.278	0.00908	13.2	0.0201	0.121	0.0118
ARC	0.261	32.0	0.613	24.0	0.108	0.0184	0.0137	0.272	0.00669	10.0	0.0104	0.0487	0.00606
UNI	0.247	47.3	0.519	20.7	0.0892	0.0264	0.00399	0.257	0.00750	9.91	0.0131	0.0428	0.00467
IND	0.236	46.2	0.827	26.2	0.168	0.0253	0.0120	0.339	0.00843	12.7	0.0107	0.0445	0.00559
BEL	0.363	41.6	0.593	26.5	0.167	0.0231	0.00868	0.538	0.00325	12.0	0.00898	0.0310	0.00489
SIR	0.341	27.0	0.649	30.3	0.131	0.0308	0.0195	0.495	0.00763	10.6	0.0189	0.0508	0.00708
AUG	0.295	58.0	0.615	29.7	0.0968	0.0489	0.00395	0.182	0.00695	8.65	0.0209	0.191	0.00435
PRI	0.378	24.4	0.553	33.8	0.119	0.0213	0.0221	0.360	0.00577	9.77	0.0102	0.111	0.00588
GAB	0.605	65.6	0.854	49.8	0.383	0.0806	0.0252	0.346	0.00733	19.0	0.0314	0.224	0.0109
CIT	1.51	48.1	5.81	31.6	0.165	0.554	0.0404	0.269	0.0390	16.9	0.669	0.998	0.0391
ZAF	1.20	32.7	1.60	28.5	0.164	0.162	0.0640	0.301	0.0321	10.2	0.169	0.163	0.00911
CRT	2.83	39.4	6.26	71.9	0.261	0.516	0.0886	0.146	0.0691	21.2	0.679	0.279	0.0315
INT	0.268	13.3	0.487	13.2	0.0515	0.0543	0.0202	0.242	0.00769	6.64	0.0241	0.0970	0.00622
CAT	0.279	22.1	0.923	20.0	0.106	0.0441	0.0118	0.335	0.00627	9.29	0.0238	0.0310	0.00616
GLP	0.408	17.0	0.911	24.1	0.142	0.0325	0.00726	0.382	0.00432	7.94	0.0194	0.0411	0.00732

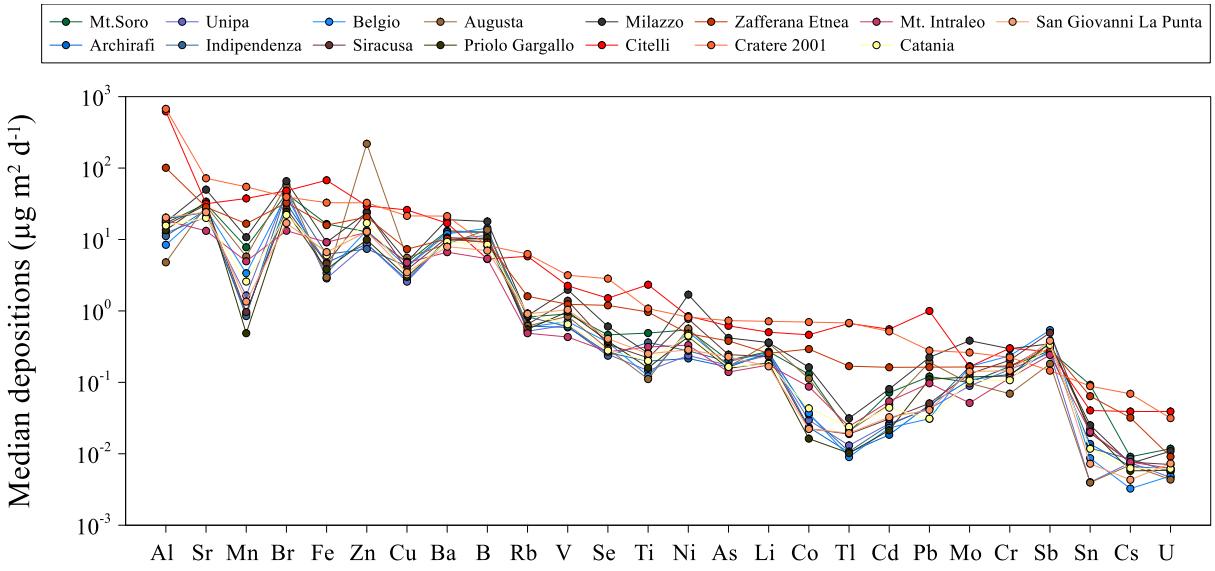

Figure 80 - Median atmospheric deposition fluxes (µg m^{-2} d^{-1}) for each sampling site.

Significantly different levels were found in the atmospheric bulk deposition of the studied territories during the sampling periods. Trace element deposition values varied within one or two orders of magnitudes, especially for Al, Ti, Mn, Fe, Cd, and Pb, in all the sampling sites.

Different values were not only observed between sampling periods but also between monitoring sites. For the background area of Monte Soro, the urban area of Palermo, the industrial area of Milazzo, the Siracusa, the Priolo Gargallo, and the Catania sampling sites, the highest median deposition rates were calculated for Br and Sr. For the former, the marine contribution was prevalent, while for Sr crustal, marine, and volcanic sources could be considered, except for the Palermo urban area and the Milazzo industrial area where the volcanic contributions were not significant. At the Augusta sampling site, the highest median fluxes were calculated for Zn, Br, and Sr. Anthropogenic emissions, such as vehicular transport and metallurgic industry emissions could be responsible for the high Zn fluxes at this site. Very different results were observed for sites in the Etna area. At all sites, the element for which the highest median depositions were calculated was Al. In second place was Br at the Zafferana and Mt. Intraleo sites, Fe at the Citelli site, and Sr at the Cratere 2001 site.

These results can be explained by calling into question the role of the acidity of rainwater in solubilising certain poorly soluble elements such as Al and Fe. The rainwater from these monitoring sites, with the partial exception of the Mt. Intraleo site, had lower average pH values than those from the other study areas. The reason for this is to be found in the interaction of rainwater with acid gases of volcanic origin such as SO_2, HCl, HF, and HBr emitted in large quantities from the summit craters. The volcanic source's contribution to the enrichment of rainwater in many trace elements, such as Al, Fe, Mn, Cu, Ti, Co, Tl, Cd, Sn, Cs, and U, was very impactful but cannot explain alone the observed differences in atmospheric deposition values between monitoring sites. Therefore, it was not surprising that for many of the investigated elements, i.e., Al, Sr, Mn, Zn, Ba, Rb, V, Se, As, Li, Co, Tl, Sn, Cs, U the highest deposition rates were calculated in the Cratere 2001 sampling site, while for Fe, Cu, Ti, Tl, Cd, and Pb, the highest fluxes were obtained for the Citelli rainwater samples.

In the industrial area of Milazzo, the highest deposition fluxes of Br, B, Ni, Mo, and Cr were found. The first two elements were from marine source, while Ni, Mo, and Cr were derived from domestic heating plants, vehicular emissions and, according to Brugnone et al. (2023b), also from the emissions of the industrial hub, especially those related to the activities of the steel plant. For Ni, an important contribution could come from the nearby San Filippo del Mela power plant, located about 4 km east of the monitoring site, which burns fuel oil to produce electricity, a recognised source for this element (*Loya-Gonzalez et al., 2020*). During 2019, from the industrial hub of Milazzo, emission fluxes equal to 586 kg yr^{-1} and 188 kg yr^{-1} were reported by the regional environmental protection agency (Agenzia Regionale per la Protezione dell'Ambiente – ARPA) for Ni and Cr, respectively (*Abita & Basiricò, 2023*). Finally, in the urban area of Palermo, specifically in the Belgio sampling site, the highest flux of Sb was calculated. A widely recognised source for this element in urban areas is the wear of vehicle brakes, and this monitoring site was located near one of the busiest crossroads of the city. The elements for which the lowest median depositions were

calculated were Tl, Sn, Cs, and U, at all monitoring sites. The exceptions were the Etnean sites of Citelli, Zafferana Etnea and Cratere 2001 where, due to the influence of the volcanic source, which was also responsible for the emission of this element, the fluxes were found to be higher.

5.4 Insoluble constituents in bulk atmospheric depositions

The concentration of seventeen minor and trace elements was measured in 300 solutions derived from the microwave-assisted mineralisation of the atmospheric deposition insoluble fraction. Therefore, the chemical composition of insoluble atmospheric particulate matter in rainwater, which also contributes to the total content of the bulk atmospheric deposition, was characterised.

5.4.1 Concentration of minor and trace elements in blank samples

Four different blank solutions (M I, M II, M III, and M IV) were prepared as described in section 3.6. Considering all the samples and the median values of each element analysed, it could be observed that the concentrations in the blank solutions were always much lower than the concentrations in the samples (Fig. 81).

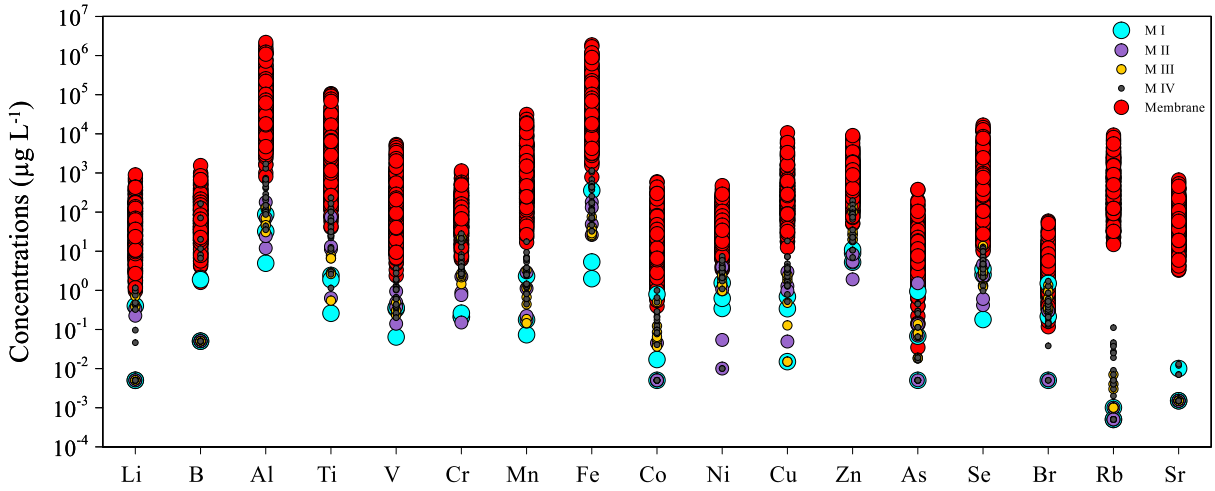

Figure 81 - Raw minor and trace element concentrations (µg L^{-1}) in blank solutions M I, M II, M III, M IV and in the insoluble fraction solutions.

For Li, B, Al, V, Mn, Fe, Co, Ba, and Pb, the concentration measured in the various blanks always corresponded to less than 1% of that measured in the samples. For Ti, Cu, As, and Sr this was always less than 5%, while it was always less than 10% for Cr and Ni. The only elements for which the contamination of the blanks was more significant were Mo and Zn. In the M III blank solution, a median concentration of Mo corresponding to ~ 17% of that measured in the samples under investigation was measured, while in the M IV blank solution, a median concentration of Zn corresponding to ~ 13% of that measured in the samples was measured. Since the contribution of blank solutions was almost always negligible for all the elements analysed, it was decided not to subtract the concentrations of the blanks from those of the samples.

5.4.2 Concentration of minor and trace elements in the insoluble fraction

The measured concentrations were used to calculate the volume-normalised concentrations of minor and trace elements in the insoluble fraction. The normalised concentrations for each element, divided into the four contexts studied (volcanic, urban, industrial, and background) are illustrated in Figure 82.

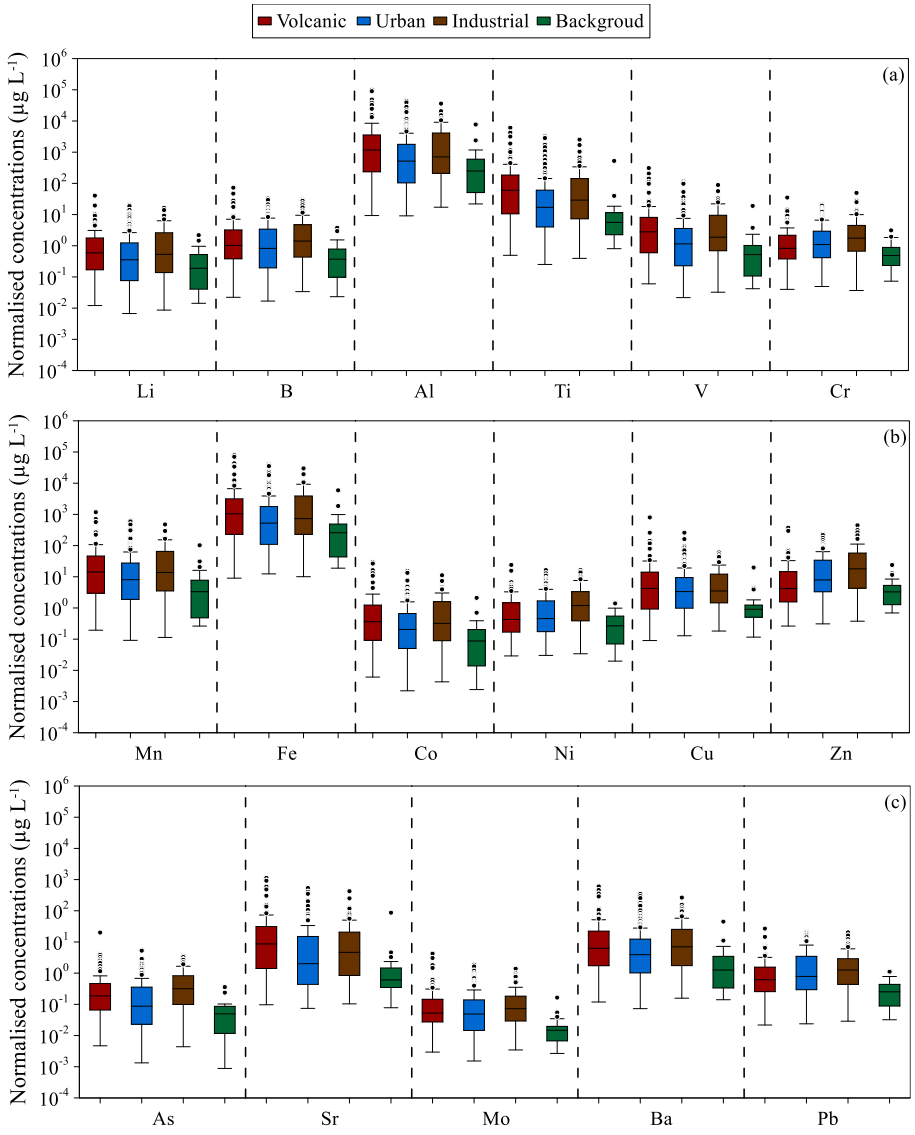

Figure 82 - Volume normalised concentrations (µg L^{-1}) for Li, B, Al, Ti, V, Cr (a), Mn, Fe, Co, Ni, Cu, Zn (b), and As, Sr, Mo, Ba, Pb (c) in the insoluble fraction solutions from the different studied contexts.

The elements for which the highest concentrations were measured were Al and Fe, with values up to 100 mg L^{-1} and 79.4 mg L^{-1}, respectively. In contrast, the least concentrated elements were As and Mo, for which concentrations of up to 20.1 µg L^{-1} and 4.25 µg L^{-1} were measured. For almost all monitoring sites, the order of abundance of the elements analysed was as follows: Al > Fe > Ti > Mn > Sr > Ba > Cu > Zn > V > B > Cr > Li > Pb > Ni > Co > As > Mo.

Considering each sampling site, for all elements analysed, the highest median concentrations were measured at the Cratere 2001 site, and the lowest at the Archirafi sampling site. The exceptions

were Zn and Pb, for which the highest median concentrations of 34.6 µg L^{-1} and 1.87 µg L^{-1} were recorded at the Siracusa site, and Zn, Cu, Ba, and Pb, for which the lowest median concentrations, equal to 2.08 µg L^{-1}, 0.908 µg L^{-1}, 1.26 µg L^{-1}, and 0.252 µg L^{-1}, respectively, were measured in the Zafferana Etnea (for the first two elements) and Mt. Soro sampling sites (for the remaining elements).

Considering the median values for the four contexts studied, it can be observed that the highest concentrations for Li (0.720 µg L^{-1}), Al (1389 µg L^{-1}), Ti (81.1 µg L^{-1}), V (3.18 µg L^{-1}), Mn (16.9 µg L^{-1}), Fe (1138 µg L^{-1}), Co (0.430 µg L^{-1}), Cu (6.37 µg L^{-1}), Sr (11.8 µg L^{-1}), and Ba (7.52 µg L^{-1}), were measured in the volcanic area, while for B (1.26 µg L^{-1}), Cr (1.77 µg L^{-1}), Ni (1.10 µg L^{-1}), Zn (21.1 µg L^{-1}), As (0.265 µg L^{-1}), Mo (0.0740 µg L^{-1}), and Pb (1.19 µg L^{-1}), in the industrial areas. The lowest median concentrations were always measured in the background site of Mt. Soro.

The scientific evidence produced showed that the elements that concentrate in the solid phase during the interaction between atmospheric particulate matter and rainwater were mainly poorly soluble elements such as Fe, Al, Ti, Mn, and Sr. The differences in the concentrations of these elements in the samples collected in different natural and anthropogenic contexts could be attributed to the variety of sources insisting in different areas and, therefore, to the different chemical and/or mineralogical composition of the atmospheric particulate matter emitted. The contributions of the volcanic source and the anthropogenic source, both urban and industrial, were evidenced by the concentrations measured in the samples from the different study areas. In the volcanic area, atmospheric particulate matter consisted mainly of volcanic ash emitted in large quantities, especially during the paroxysmal events that characterised Mt. Etna's activity between 2021 and 2022. This particulate matter was particularly rich in elements such as Al, Fe, and Ti, which were only partially soluble at the pH of rainwater and therefore concentrated in the residual solid material. Industrial activities could be responsible for the emission of atmospheric particulate matter rich in elements, including heavy metals, such as Zn, Cr, Ni, and Pb. At the Mt. Intraleo site, not exposed to

the fallout of volcanic eruption products, and Mt. Soro, an area recognised as a local-scale background, lower concentrations were measured than at the other monitoring sites. Finally, intermediate concentrations were recorded in samples from the urban areas of Palermo and Catania.

5.4.3 Deposition fluxes of minor and trace elements of the insoluble fraction

Atmospheric deposition fluxes (µg m^{-2} d^{-1}) were calculated by using equation (7). The median values for each minor and trace element and each sampling site are reported in Table 49 and Figure 83. In the latter, the elements are ordered from the one with the highest to the lowest median flux at the Cratere 2001 site.

Table 49 - Median bulk atmospheric deposition fluxes (µg m^{-2} d^{-1}) for minor and trace elements in the insoluble fraction solutions.

	Li	B	Al	Ti	V	Cr	Mn	Fe	Co	Ni	Cu	Zn	As	Sr	Mo	Ba	Pb
	µg m^2 d^{-1}	µg m^2 d^{-1}	µg m^2 d^{-1}	µg m^2 d^{-1}	µg m^2 d^{-1}	µg m^2 d^{-1}	µg m^2 d^{-1}	µg m^2 d^{-1}	µg m^2 d^{-1}	µg m^2 d^{-1}	µg m^2 d^{-1}	µg m^2 d^{-1}	µg m^2 d^{-1}	µg m^2 d^{-1}	µg m^2 d^{-1}	µg m^2 d^{-1}	µg m^2 d^{-1}
CES	0.305	0.844	517	14.3	0.830	1.288	7.45	414	0.158	0.500	2.07	6.94	0.126	1.34	0.0362	2.70	0.443
ARC	0.186	0.433	209	6.62	0.485	0.901	4.21	225	0.0951	0.290	1.66	7.02	0.0515	0.789	0.0195	2.06	0.767
UNI	0.424	0.710	511	10.7	0.970	1.06	6.33	471	0.182	0.520	2.53	7.01	0.105	0.895	0.0272	3.38	0.640
IND	0.372	1.22	454	13.2	0.935	2.12	8.28	476	0.252	0.708	5.08	12.0	0.165	1.53	0.0649	4.24	1.29
BEL	0.241	0.595	260	6.28	0.585	1.38	4.20	294	0.111	0.395	3.13	7.16	0.0720	0.731	0.0664	2.25	0.724
SIR	0.676	1.90	1002	40.5	3.07	2.68	15.4	1127	0.500	2.05	4.55	21.7	0.426	4.99	0.0786	7.13	1.65
AUG	0.813	1.91	1206	51.9	3.24	2.37	16.9	1173	0.493	1.38	4.92	33.1	0.350	7.88	0.134	8.92	1.75
PRI	0.690	1.39	931	33.7	2.24	1.61	11.0	949	0.435	1.28	4.37	12.5	0.369	2.88	0.0684	6.70	1.39
GAB	0.442	1.48	498	16.9	1.92	2.66	8.50	597	0.207	1.07	3.13	6.78	0.249	1.76	0.178	4.48	1.30
CIT	0.956	1.87	2217	157	5.34	1.10	24.9	1812	0.741	0.799	6.63	6.66	0.266	17.2	0.108	10.7	0.940
ZAF	0.436	0.714	884	61.2	3.38	0.917	13.8	872	0.348	0.569	3.87	5.13	0.144	5.82	0.0989	6.91	0.664
CRT	2.49	4.74	6203	400	16.4	2.36	73.8	5590	1.80	1.57	22.8	13.7	1.10	56.1	0.180	33.9	2.42
INT	0.450	0.776	571	18.2	1.17	0.846	6.68	526	0.184	0.447	2.85	6.25	0.131	2.25	0.0326	3.03	0.536
CAT	0.629	1.27	962	53.2	2.25	1.30	13.7	907	0.375	0.712	4.89	10.1	0.149	6.29	0.0670	7.32	1.33
GLP	1.53	2.73	2869	157	6.75	2.68	39.6	2860	1.08	1.40	10.1	24.9	0.389	17.1	0.157	18.6	2.25

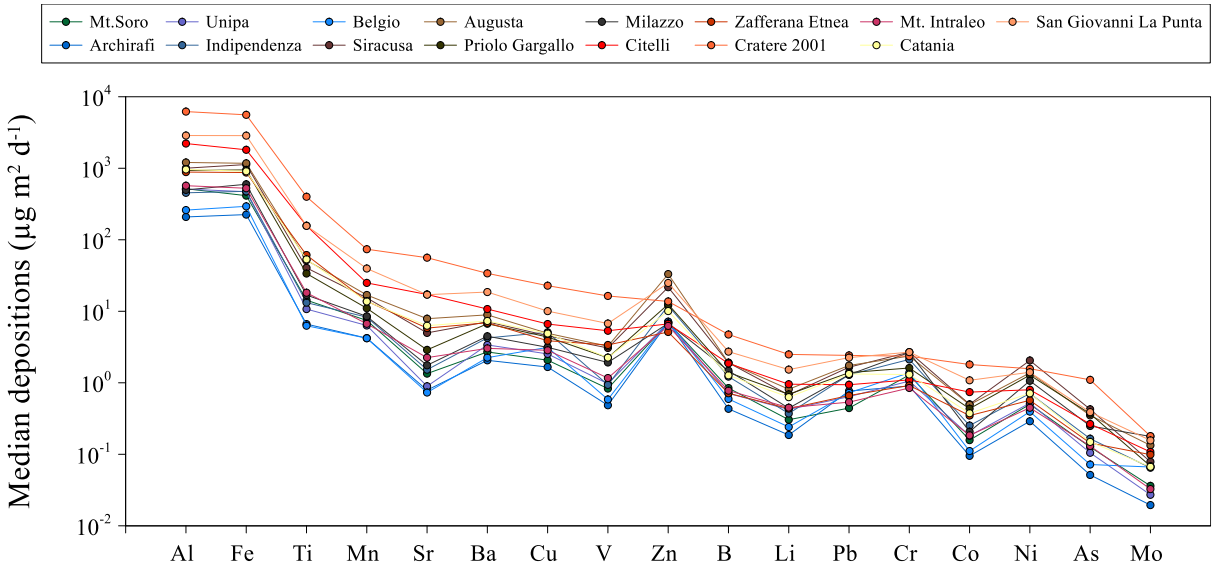

Figure 83 - Median atmospheric deposition fluxes (µg m^{-2} d^{-1}) for minor and trace elements in the insoluble fraction solutions.

Significantly different levels, up to two orders of magnitudes, were found in the atmospheric bulk deposition of the studied territories during the sampling periods. Different values were not only observed between sampling periods but also between monitoring sites. At all monitoring sites, the highest deposition fluxes were calculated for Al and Fe, the most insoluble of the analysed elements. Instead, the lowest fluxes were calculated for the most soluble elements, i.e., As and Mo. For almost all the elements analysed, except Cr, Ni, and Zn, the highest depositions were calculated for the Cratere 2001 site. The other two sites for which the highest deposition values were calculated were Citelli and San Giovanni La Punta. These were the sites most affected by volcanic ash deposition during Etna's 2021-2022 paroxysm sequence. Thus, the products of volcanic activity may constitute a non-negligible fraction of atmospheric deposition, contributing a large suite of minor and trace elements. For some elements, Zn, Ni, and Cr, the contribution of volcanic activity was negligible compared to the contribution of industrial emissions; this explains why the highest fluxes for these elements were calculated in the Priolo Gargallo industrial area.

5.4.4 Comparison between soluble and insoluble fractions

Comparison of the concentrations of minor and trace elements measured in the rainwater and those of the same elements measured in the insoluble solid fraction showed great differences. Based on these, the elements analysed were sorted in order of relative solubility (Fig. 84). The greatest differences were observed for Fe, Ti, Al, and Pb for which 129, 112, ~ 44, and ~ 13 times higher concentrations were measured in the solid insoluble fraction instead of the liquid fraction. Therefore, these elements, during the rainwater-atmospheric particulate interaction process tend to go into solution only partially and concentrate, in contrast, in the solid phase. Other elements, i.e., Ni, Cu, As, and Zn showed similar concentrations between the two different aliquots and, therefore, tend to distribute evenly between the solid and liquid phases. Finally, for Ba, Mo, Sr, and B higher concentrations were measured in the soluble fraction instead of the insoluble one, highlighting the high solubility of these elements, which were concentrated in rainwater and depleted in the residual solid phase.

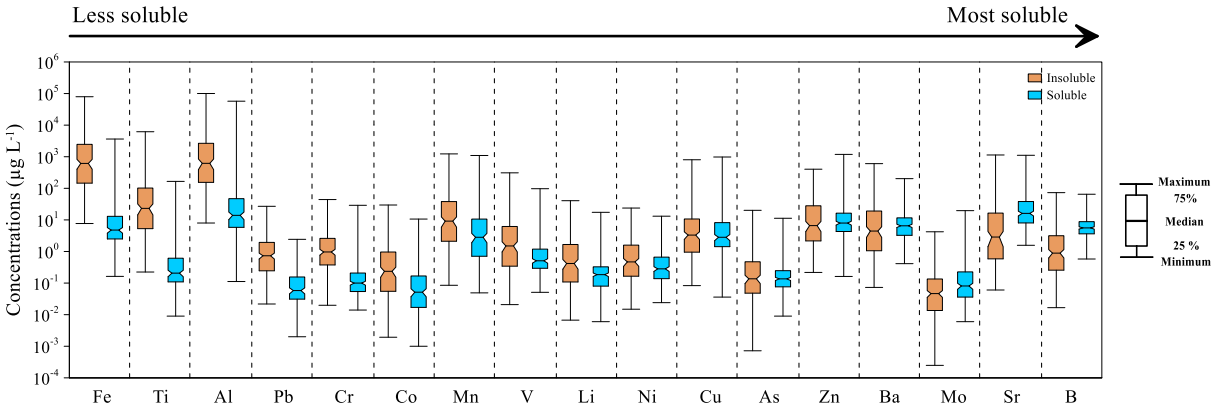

Figure 84 - Concentrations (µg L^{-1}) of minor and trace elements in the insoluble and in the soluble fraction solutions. The elements were sorted according to the difference between the two aliquots analysed.

The relative contribution (%) of each of the two phases to the total concentration of each element is shown in Figure 85. For the less soluble elements, i.e., Fe, Ti, Al, and Pb, the insoluble fraction constituted 99.2%, 99.1%, 97.8%, and 92.7% of the total concentration, respectively. For the

more soluble elements, i.e., Mo, Sr, and B, the contribution of the insoluble fraction was only 36.5%, 15.1%, and 13.7% of the total concentrations. A distribution close to 50-50% between the two fractions was observed for the remaining elements.

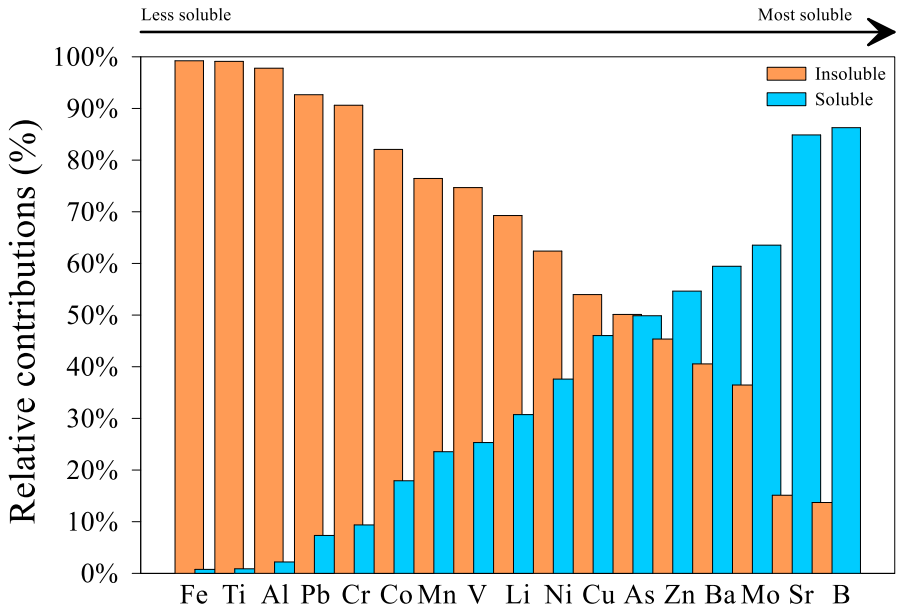

Figure 85 - Relative contributions (%) of minor and trace elements in the insoluble and the soluble fractions.

These ratios were not the same for all monitoring sites. Indeed, it was observed that at Etna sites, such as Cratere 2001 and Citelli, the ratio between the concentration in the soluble fraction and that in the insoluble fraction was higher than at the other monitoring sites. For example, for aluminium, a relative contribution of the soluble fraction of 11.2% and 25.8% was calculated for these two sites, in contrast to the other sites, where an average contribution of 2.37% was calculated. Similar results were observed for Fe, for which a higher relative contribution of the soluble fraction (3.31%) was calculated for the Citelli site than the average of the other monitoring sites (1.01%). The various mineralogical phases in the particulate matter are solubilised in an acid solution, like natural rainwater (pH $\simeq$ 5.6), to varying degrees. It has been shown experimentally (*Wieland & Stumm, 1992*; *Guerzoni et al., 1999*) that the degree of dissolution of both iron and aluminium silicates, such as Kaolinite, is strongly dependent not only on the temperature and acidity conditions of the solution

but also on the abundance of particulate reacting with the solution. Factors controlling Fe and Al solubilities include the differences in the Fe and Al soluble fractions among emission sources (e.g., mineral dust versus anthropogenic aerosol) and atmospheric processes of Fe-Al-bearing particles (*Mahowald et al., 2018*; *Ito et al., 2021*). In addition, numerous studies revealed that the factors have size dependencies because fine aerosol particles yield higher soluble fractions of Fe and Al than coarse aerosol particles (*Baker et al., 2020*; *Kurisu et al., 2021*; *Sakata et al., 2023*). The particle size of Fe-Al-containing particles and the mineralogical phases in which iron and aluminium were found in atmospheric deposition in the study areas will be the subject of future studies. Finally, iron in spherical fly ash particles is almost insoluble in water, even when co-existing with sulfate. Dissolution and oxidation of Fe in spherical fly ash are blocked by the small surface of the sphere and the structure of Fe dispersion in other insoluble aluminosilicates (*Ueda et al., 2023*).

The results showed that the measurement of the concentration of some poorly soluble elements in rainwater can be of fundamental importance in qualitative and quantitative studies of atmospheric deposition. If the contribution of the solid fraction is not considered, significant underestimates in the calculation of total atmospheric deposition of minor and trace elements occur. It is crucial to identify the two contributions of deposition to estimate their absolute amounts and understand the mobility of the elements. The more soluble the species, the easier it is for them to be transferred to the plants and animals in the region. Thus, these analyses play a significant role in modelling the movement of elements in the environment and their potential impact on human health.

5.5 Bulk depositions comparison with previous research

Numerous researchers have been interested in characterising the chemical composition of bulk atmospheric deposition, to assess the state of environmental pollution of the atmosphere in terms of concentration and transport of trace elements, particularly heavy elements. Fernández-Olmo et al., in 2015, carried out a comparison of the composition of bulk atmospheric deposition in Spain

with results reported by various authors for other sites worldwide, dividing them into four different categories according to the environmental characteristics of the sites: urban, industrial, rural, and volcanic. In all these works, the techniques foreseen by the norms UNI EN 14902:2005 and EN 15841:2009 were used regarding the collection of samples to measure the concentration of trace elements in both the soluble (rainwater) and insoluble fractions (mineralisation of the solid material retained by the membrane filter). Therefore, the results reported by all these authors are comparable with those produced during this PhD project, excluding the contribution of the rinse solutions. To the results reported in this work (*Fernández-Olmo et al., 2015*) the following data were added: deposition at a rural site in Cuba (*Morera-Gómez et al., 2019*) and the results of previous research on atmospheric deposition on Mount Etna (*Calabrese et al., 2011*). Overall, the mean daily bulk depositions (μg m^{-2} d^{-1}) of 19 urban, 5 industrial, 12 rural, and 5 volcanic sites were compared with the results of this PhD research (Fig. 86a, b, c, and d). The elements considered were As, Cu, Cr, Ti, Mn, Ni, Pb, V, Mo, and Zn. The number of samples in which depositions were calculated for each context is shown in the same figure.

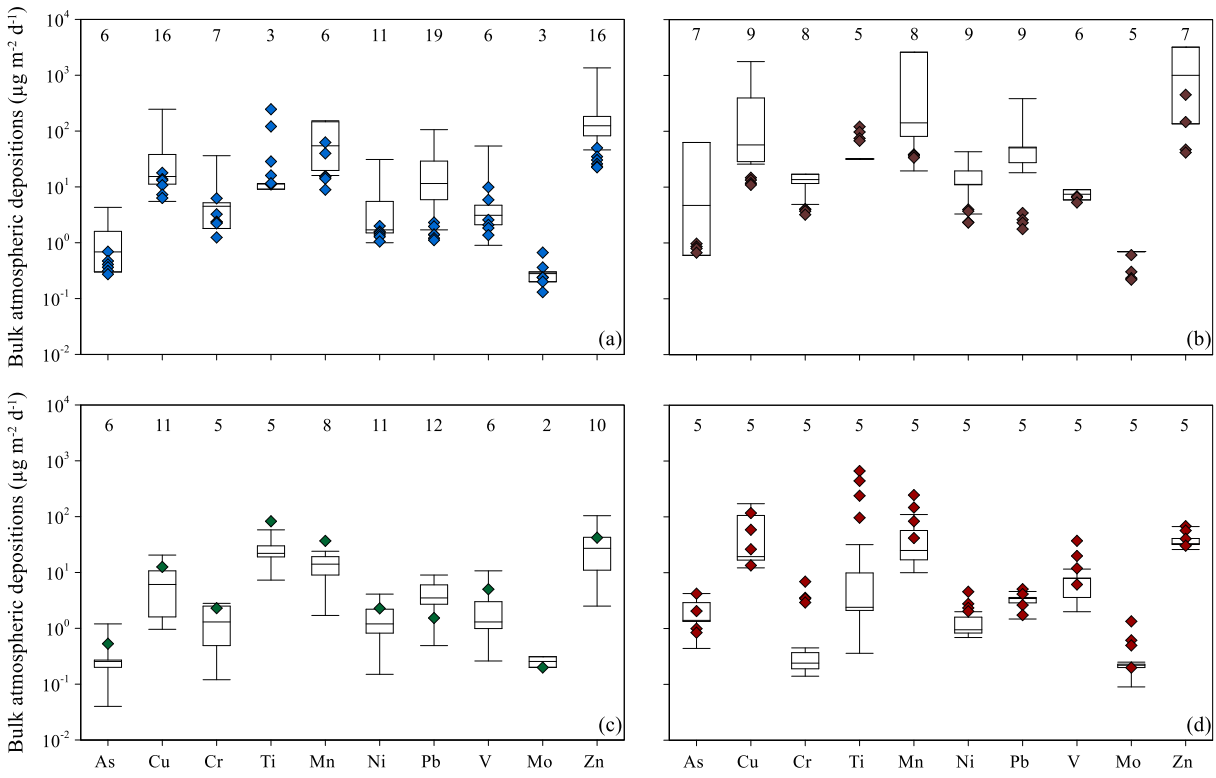

Figure 86 - Comparison of the mean bulk atmospheric depositions (µg m^{-2} d^{-1}) calculated for the samples in this PhD research with values reported by various authors at other urban (a), industrial (b), rural (c), and volcanic (d) sites. The values from previous research are represented by boxes and whiskers. The two whiskers represent the minimum and maximum values, the box encloses the first quartile, the median, and the third quartile. The number of values used for each box is indicated. The values of this research are represented by the rhombuses.

For urban sites, generally lower atmospheric deposition values were calculated in this research than for the other compared sites. For Pb deposition values up to two orders of magnitude lower were calculated for samples from the urban areas of Palermo and Catania. Lower values, -255% on a median basis, were also calculated for Mn. Smaller differences, between -17% (Mo) and -91% (Cr), were observed for the other elements. The only element for which higher atmospheric deposition values were calculated than for the comparison sites was Ti (+49%). Similar results were observed in the industrial context. The only element for which higher deposition fluxes were calculated in the Sicilian samples than those of the other industrial areas considered in the comparison was Ti (+63% on a median basis). A roughly equal median value was calculated for V (-12%). For all other elements, much lower atmospheric deposition values than for the comparison sites were calculated for the Sicilian samples, with differences even of one or two orders of

magnitude, as in the case of Pb (-1947%). For the rural area of Mt. Soro, atmospheric deposition values greater than the median of the rural areas taken as reference were calculated for all elements, with differences ranging from +36% (Zn) to +73% (Ti). Exceptions were only Mo (-28%) and again Pb (-128%). Finally, as regards the Etna sites, median values of atmospheric deposition almost equal to those calculated by Calabrese et al., 2011 were calculated for Pb (-2%) and As (+8%). For all other elements, higher deposition fluxes were calculated than in the previous research, with differences ranging from +32% (Zn) to +99% (Ti).

The previous data used for comparison were from studies conducted between 1999 and 2013, except for values from Morera-Gómez et al. (2019) relating to samples acquired between 2014 and 2016. This comparison has to consider that, in line with the EU's commitments under the Air Convention *(UNECE, Air, 2021*; *UNECE, Protocol on heavy metals, 2021*), specific legislation led to reductions in emissions of heavy metals across Europe from 1990 levels. Between 1990 and 2021, As, Cr, Ni, Pb, and Zn emissions decreased by 90%, 69%, 79%, 95%, and 48%, respectively. The only element for which emissions have remained more or less constant over this period is Cu (+4%). Between 2016 and 2021, emissions have continued to decline, with As, Cu, Cr, Ni, and Pb, emissions decreasing by 18%, 4%, 8%, 14%, and 5% across the EU-27 Member States. In the same period, Zn emissions had increased by 4%. In 2021, Germany, Italy and Poland contributed most to heavy metal emissions in the EU (*EEA-Report-04/2023*).

In summary, in the Sicilian urban and industrial areas, the atmospheric depositions of most of the elements considered were lower than those calculated at other world sites in similar contexts, especially for elements such as Pb, Zn and Mn. The only element enriched in the atmospheric deposition of these areas was Ti. Deposition values from the Mt. Soro background site were higher than those from the rural comparison sites for almost all elements, except for Mo and Pb. Similar results were observed for the Etna area, with equal or greater deposition fluxes calculated for the samples of this research than for those considered for comparison. Contributions from the intense

paroxysmal activity that characterised Etna during the study period could explain the higher fluxes observed for highly volatile elements such as Cr, Ti and V.

5.6 Minor and trace element concentrations in rinse solutions

Rinse solution samples were prepared, as described in paragraph 3.1.3, for the chemical characterisation of materials present on the surface of the bulk collector, which had either not been washed away by the rainwater as it was not soluble or had been deposited after the last rain event before sampling. Twenty-five samples were selected for minor and trace elements determinations, two for each monitoring site, except for the Belgio, Milazzo and Augusta sites for which only one sample was analysed. No samples from the Cratere 2001 site were analysed as part of the PhD research. Fourteen samples were from the period no. 08 (period from 11 October to 03 November 2021), characterised by heavy rainfall in all study areas, with amounts ranging from 107 mm at Palermo to 229 mm for the sites in the industrial area of Priolo Gargallo, in the Etna area and those in the urban area of Catania. Sampling was carried out a few hours (less than 36 hours) after the last rainfall for each monitoring site. The remaining eleven samples were from the period no. 15 (from 26 April to 25 May 2022), characterised by low rainfall, with quantities between 10.8 mm and 67.3 mm at the various monitoring sites, except for Citelli (196 mm) and Zafferana Etnea (145 mm), where rainfall was more abundant. Based on rainfall values measured by automatic weather stations of the "Presidenza della Regione Siciliana Dipartimento della Protezione Civile" (https://www.protezionecivilesicilia.it:8443/aegis/map/map2d), we know that the last rainfall occurred between 09 and 11 May 2022 at all the sampling sites, therefore approximately fifteen days before sampling.

The concentrations of Sn were always below the limit of detection. For all other elements, much higher concentrations were measured in the driest period compared to the wettest one (Fig. 87).

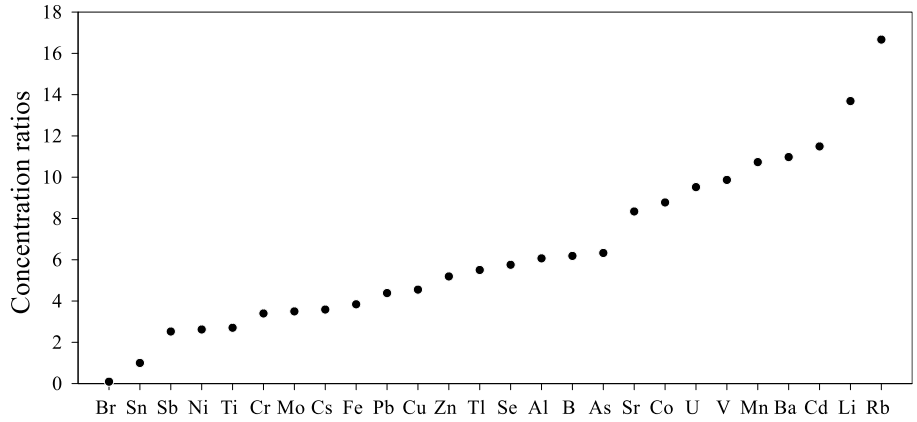

Figure 87 - Minor and trace element concentration ratios between the two sampling periods for which rinse solution samples were analysed.

Concentrations were between 1 and 5 times higher in period no. 15 than in the period no. 08 for Sb, Ni, Ti, Cr, Mo, Cs, Fe, Pb, and Cu. Ratios between 5 and 10 times have been calculated for Zn, Tl, Se, Al, B, As, Sr, Co, U, and V. Finally, ratios of 10.7, 11.0, 11.5, 13.7, and 16.7 were calculated between the concentrations of the two periods for Mn, Ba, Cd, Li, and Rb, respectively. Different results were obtained for Br, often below the detection limit in the samples of period no. 15, while a median concentration of 11.6 μg L^{-1} was calculated for the samples of period no. 08.

The ability of rainwater to leach the solid materials on the surfaces of the bulk collector due to the dry deposition was revealed. These preliminary results show that the concentration of trace elements in this fraction may not be negligible during long periods without precipitation, characterised only by dry deposition. In the absence of rainfall able to dissolve the deposited elements, without recovery of this material, an underestimation of their concentration could also occur in the soluble fraction.

5.7 Relative contributions to Sicilian bulk atmospheric deposition

The atmospheric deposition fluxes were calculated for the soluble fraction, the insoluble fraction, and the rinse solution of the material deposited on the inner sides of the bulk collector. A

comparison of the calculated values for the three fractions can be made to estimate the relative contribution of each in determining the bulk atmospheric deposition. The elements considered were Li, B, Al, Ti, V, Cr, Mn, Fe, Co, Ni, Cu, Zn, As, Sr, Mo, Ba, and Pb, i.e., those analysed in all three different matrices. The comparison was made for the two samples, no.08 and no.15, for which the three different aliquots were analysed.

The results (Fig. 88a) showed that, during the period with a long rain-free phase before sampling, the insoluble fraction constituted most of the atmospheric bulk deposition for all elements considered, except for B, Sr, Mo, and Ba, with relative contributions of up to 98.4% for Ti and Fe. For B the relative contribution from the rinse solution was higher than the other fractions, with a value of 51.9%. Non-negligible contributions were associated with the same fraction for Pb (39.6%), Zn (37.2%), and Cu (30.5%). On the other hand, during the rainy period up to a few hours before sampling, for Ti, Fe, Al, Cr, Li, Pb, Ni, Co, V, and As, the largest contribution to bulk atmospheric deposition came from the insoluble fraction, with relative contributions of up to 98.0% for the first two elements, and for the remaining elements from the soluble fraction. The relative contributions from the recovery fraction were almost negligible, with a maximum value of 9.37% for Pb (Fig. 88b).

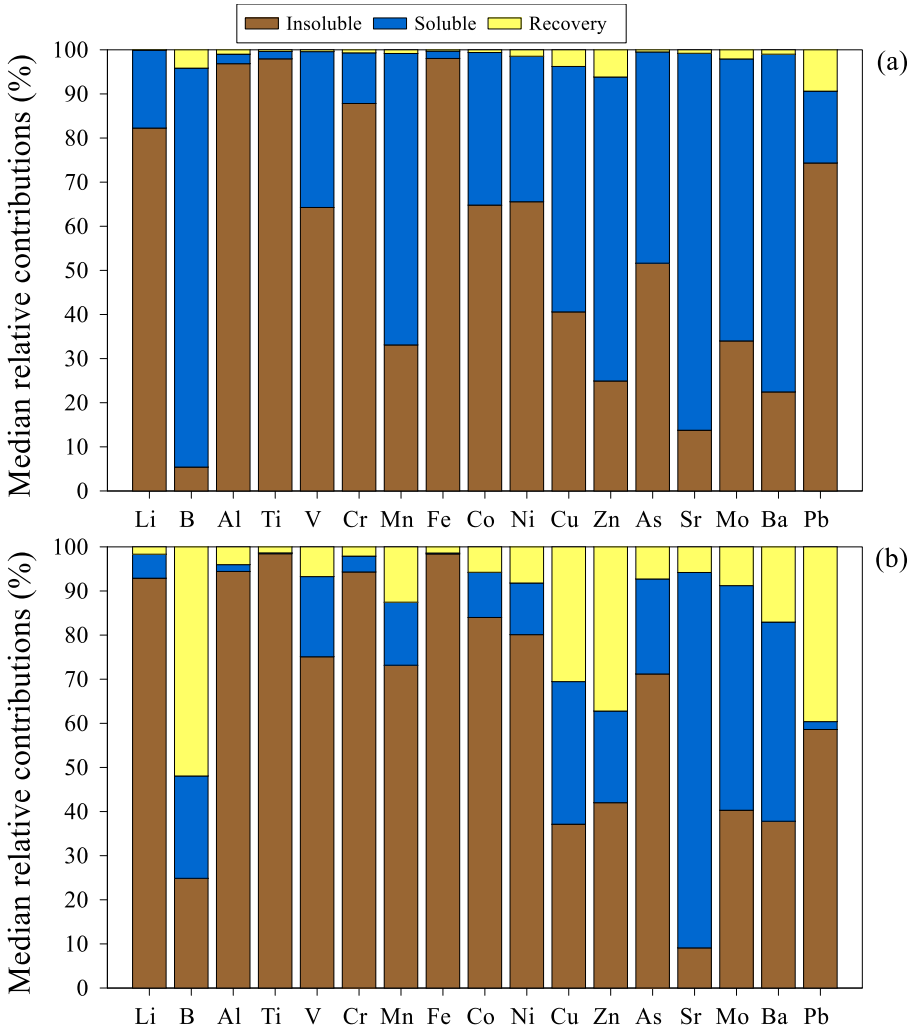

Figure 88 - Trace element median relative contributions (%) to bulk atmospheric depositions from the insoluble, the soluble and the recovery fractions, in two different periods (a = wet; b = dry).

Although it was not possible to analyse all the rinse solutions, the scientific evidence of this PhD highlights the contribution of the dissolution of dry deposition to the chemical composition of the bulk atmospheric deposition. Failure to recover this solid fraction may result in an underestimation of bulk atmospheric deposition fluxes if they are calculated considering only the concentration of the target elements in the soluble and insoluble fractions. This was especially true when sampling was carried out several days after the last rainfall, as the dry deposition that occurred during this time was not dissolved by the rain, remaining confined to the sides of the bulk collector. On the other hand, if the last rain occurred a few days before sampling, only the insoluble fraction of

the dry deposition remained confined on the sides of the bulk collector. This was the reason why the relative contributions to the bulk atmospheric depositions of this fraction were higher in the former case than in the latter.

5.8 Volcanic impact on bulk atmospheric depositions in eastern Sicily

Mt. Etna is known as one of the largest global contributors of magmatic gases such as CO_2, SO_2, and halogens (HF, HCl, HBr) to the atmosphere (*Allard et al., 1991*; *Allard, 1997*; *Bruno et al., 1996*; *Caltabiano et al., 2004*; *Aiuppa et al., 2005*). Detailed research on Mt. Etna demonstrated that volatile heavy metals, such as Bi, Cu, Cd, Sn, Zn, Tl, and Te are also strongly enriched in its gaseous emissions (*Gauthier & Le Cloarec, 1998*). To delineate the influence of Mount Etna on the composition of atmospheric deposition in the eastern sector of Sicily, the median flux values of four key elements, namely fluoride, aluminium, thallium, and tellurium, were evaluated. The considered deposition values are the sum of soluble and insoluble fractions. However, for fluoride, which is highly soluble, the median deposition was only calculated for the soluble fraction. For the considered elements, the highest median deposition values were observed at the Citelli and Cratere 2001 sites (Fig. 89a, b, c, and d). These sites are closest to Etna's summit craters and are more exposed to volcanic plume dispersion and ash fallout and, therefore the most affected by the volcanic source. High levels of deposition of the four elements have also been observed at the Zafferana Etnea site. It is worth noting the high flows of Al calculated for the urban area of Catania and for those of the industrial area of Priolo Gargallo, were comparable to or slightly higher than the value observed at Zafferana Etnea. Especially during the first year of the study, these sites were frequently affected by the fallout of volcanic ash emitted during the long sequence of paroxysms that characterised Etna's activity between December 2020 and February 2022 (Fig. 91). Aluminium is a refractory element that was likely released by the dissolution of volcanic ashes interacting with the rainwater. Furthermore, it is important to consider the contribution of Al from both crustal and anthropogenic

sources. The lowest fluxes were calculated for the Intraleo, Mt. Soro and Milazzo sites. Due to the direction of the prevailing winds (blowing from the western quadrants), these areas were downwind of the volcanic emissions. The median fluoride deposition, slightly higher than the other sites not affected by the volcanic source, observed at the Milazzo site was previously explained by the emissions from ceramic and cement production in this industrial area.

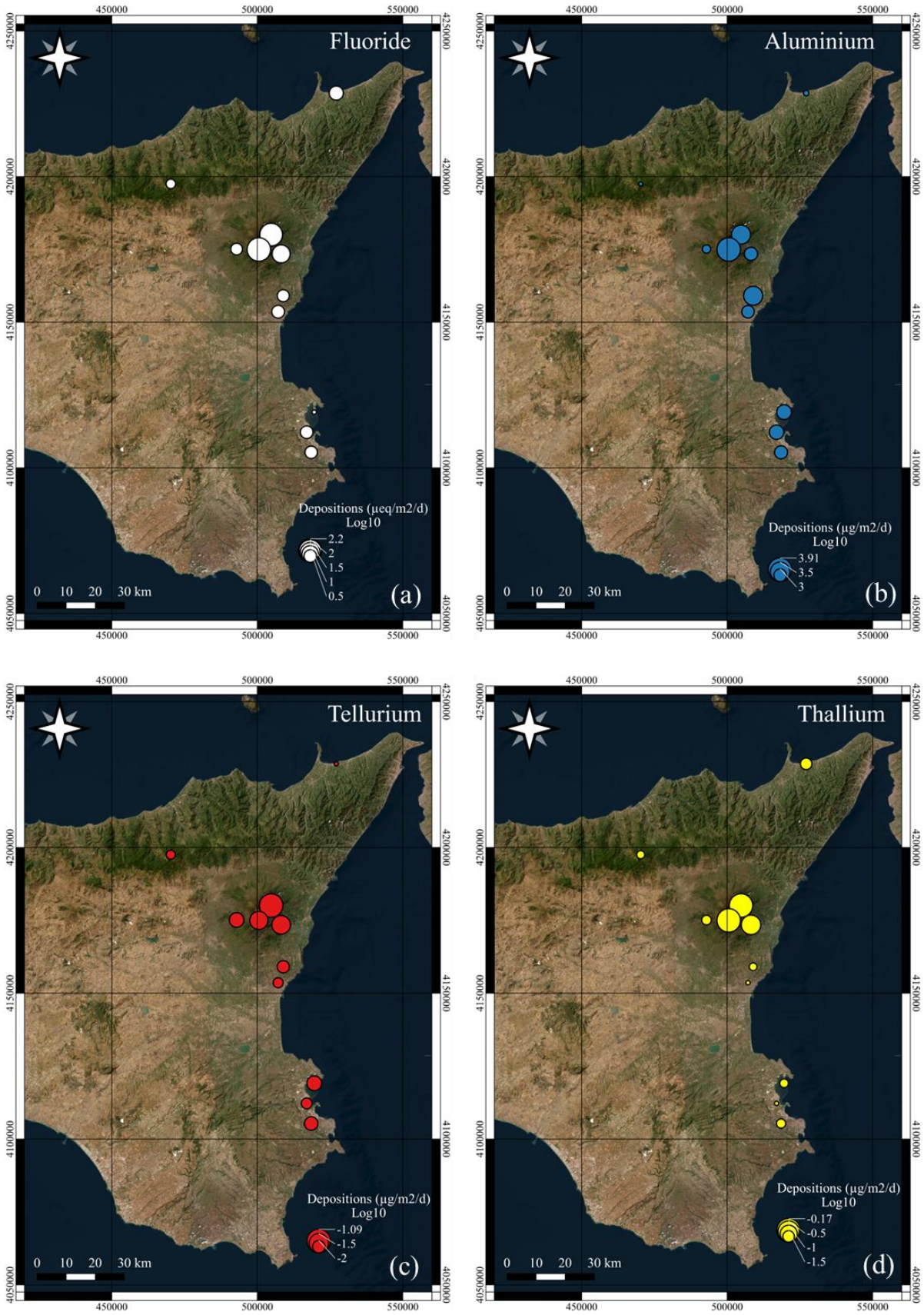

Figure 89 - Median bulk atmospheric depositions of (a) fluoride (µeq m^{-2} d^{-1}),(b) aluminium (µg m^{-2} d^{-1}), (c) tellurium (µg m^{-2} d^{-1}), and (d) thallium (µg m^{-2} d^{-1}) in the monitoring sites of the eastern Sicily. The Log_{10} of the deposition fluxes were used for the graphic representation.

During the volcanic paroxysmal event that occurred between 10 and 11 February 2022, winds blew from the south/south-east. This resulted in ash fallout affecting the north slope of Mt. Etna and the south slope of Mt. Nebrodi. Ash deposits also reached the Mt. Soro site. The median flux values, as shown in Figures 89a, b, c, and d, do not show anomalies associated with this event. This is because median values are not influenced by single extremely anomalous values. To evidence the short-time impact of the volcanic source, the time trends of deposition values calculated at this site for fluoride, aluminium, tellurium, and thallium are shown in Figures 90a, b, c, and d. During the sampling period no. 12, which covers the interval of 18 January - 24 February 2022, a strong anomaly was observed in the atmospheric deposition values of the considered elements, with values more than one order of magnitude greater than the median. Median deposition values of 1.46 μeq m^{-2} d^{-1}, 0.459 mg m^{-2} d^{-1}, 3.32 ng m^{-2} d^{-1}, and 0.0196 μg m^{-2} d^{-1} were calculated for F^-, Al, Te, and Tl, excluding the outlier value of sample no. 12, where deposition values reached 73.0 μeq m^{-2} d^{-1}, 17.6 mg m^{-2} d^{-1}, 15.1 ng m^{-2} d^{-1}, and 0.278 μg m^{-2} d^{-1} were calculated for the same elements. Volcanic emissions may have affected deposition values in other sampling periods, such as periods 7 and 9. In these periods, deposition values higher than the median values were calculated, and in the case of Te, the maximum deposition value for the entire study (30.3 ng m^{-2} d^{-1}) was observed. Etna's activity during these months (September - November 2021) was characterised by frequent paroxysms. An in-depth study of atmospheric circulation at high altitudes during these events could help explain the calculated atmospheric deposition values.

In summary, the chemical composition and the flux values of atmospheric deposition were affected by the volcanic emissions from Etna over a very large area of eastern Sicily. This volcanic impact was observed not only at sites closest to the summit craters but also at sites tens of kilometres away from them, and even at the rural site of Mt. Soro, which is nearly all the time upwind of volcanic emissions.

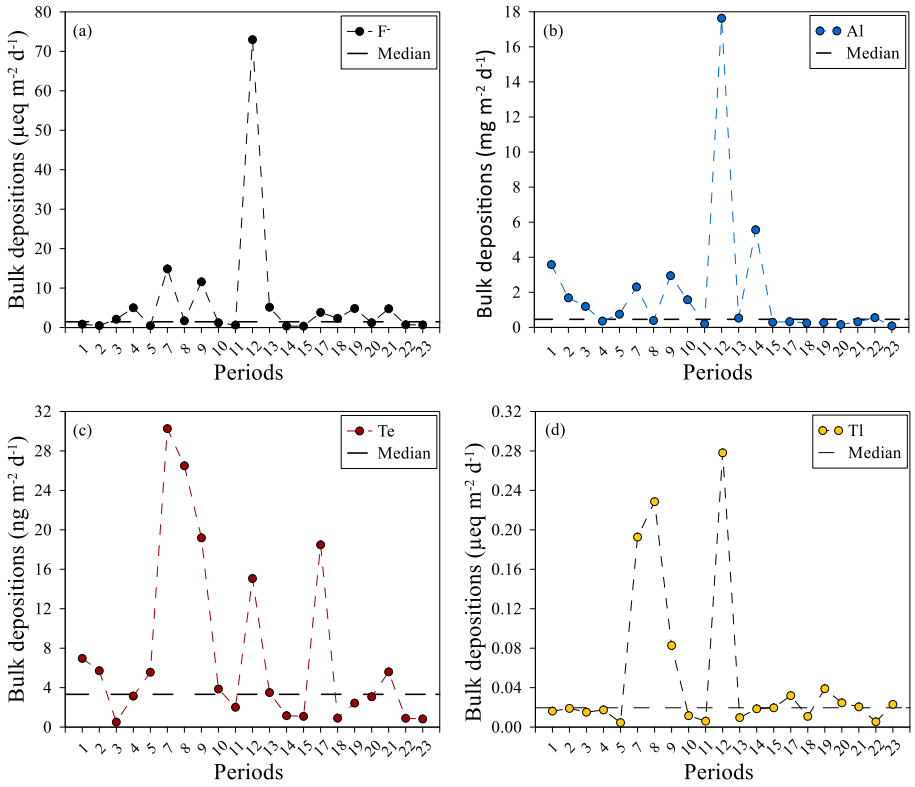

Figure 90 - Bulk atmospheric depositions of (a) fluoride (µeq m^{-2} d^{-1}),(b) aluminium (mg m^{-2} d^{-1}), (c) tellurium (ng m^{-2} d^{-1}), and (c) thallium (µg m^{-2} d^{-1}) in the Mt. Soro monitoring site. The medians were calculated excluding the anomalous value of sample no. 12.

5.8.1 Impact of Etna's paroxysmal sequence of 2021-2022

Mt. Etna's volcanic activity was characterised by a long series of 60 paroxysmal events at the Sud East Crater, from 13 December 2020, up to 21 February 2022. The last two episodes of lesser intensity occurred in May 2022. A graphic representation of the sequence of paroxysms and the atmospheric deposition samples affected by the fallout of volcanic ash is presented in Figure 91.

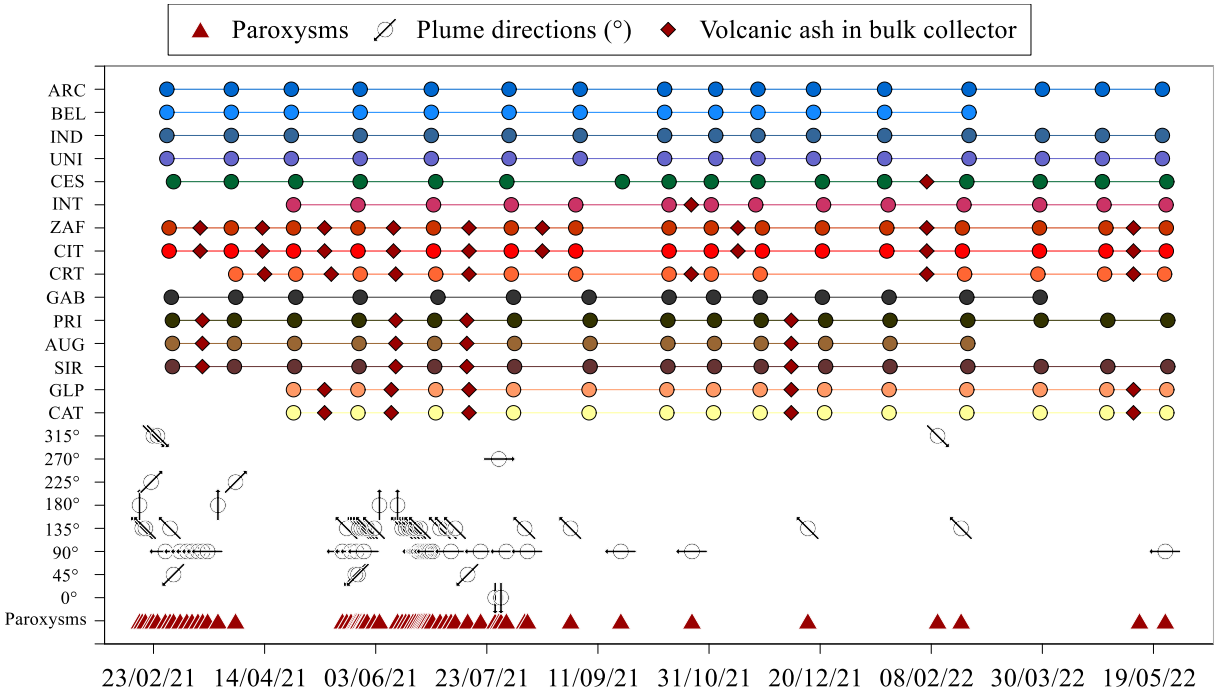

Figure 91 – Etna's paroxysmal sequence. The direction of volcanic plume dispersion and ash fallout is indicated. The red diamonds indicate the samples where ash was found as a constituent of the atmospheric deposition.

During paroxysms, high lava fountains and pyroclastic clouds were produced, resulting in the fallout of volcanic products (ash and lapilli) even at great distances from the point of emission. In several periods, the sampling sites in the Etna area, except for Mt. Intraleo, the sites in the urban area of Catania, and those in the industrial area of Priolo Gargallo, were affected by the fallout of volcanic ash, which thus accounted for a significant fraction of bulk atmospheric deposition during the first year of research. On one occasion, following the paroxysm of 10 February 2022, ash from Etna reached the Mt. Soro background site (sample no. 12).

To characterise, both qualitatively and quantitatively, the contribution of volcanic ash in the chemical composition of atmospheric deposition, a comparison was made between the daily depositions of the previously mentioned monitoring sites (Citelli, Zafferana Etnea, Cratere 2001, Catania, San Giovanni La Punta, Siracusa, and Priolo Gargallo), in the period characterised by abundant ash deposition and the period when it was less abundant or absent. Therefore, the dataset was divided into two periods: the first between 10 March 2021 and 25 February 2022, and the

second between the latter date and the end of the study (20 April 2023). The comparison was made considering the concentration of minor and trace elements in both the soluble and insoluble fractions.

Concerning the soluble fraction, for many elements, there was a reduction in deposition fluxes between the first and second periods (Fig. 92). The largest negative variations, for all the elements, except for Cr, Zn, As, and Br, were observed for the Zafferana Etnea sampling site, up to -65.4% and -68.6% for Mn and Cs, respectively. At the Citelli site, a strong reduction in the deposition flux was observed for Mo (-66.3%), Sn (-46.0%), V (-34.7%), Ba (-33.5%), and U (-33.2%). At Catania and Priolo Gargallo sampling sites, the biggest reductions were observed for Mn, with values of -60.8% and -67.9%, respectively. At San Giovanni La Punta, the largest reduction was observed for Co (-75.6%). No significative variations were observed at the Siracusa sampling site, with values up to -38.3% for Zn. The case of the Cratere 2001 site was peculiar; for all minor and trace elements, except for B (-20.1%) and Sb (-44.7%) there was an increase in flux values between the first and second period, with values up to +3544% and +5532% for Fe and Al, respectively. The cause was traced to the variation in the acidity of rainwater at the same site: from a median pH value of 5.81 to a median value of 4.66 between the first and second study periods. Indeed, it is known from the literature (*Cimino & Toscano, 1998*), that the dissolution of many trace elements from volcanic ash is more intense as the acidity of the interacting rainwater increases. This explained the sharp increase in concentrations and deposition fluxes of normally poorly soluble elements such as Fe and Al. The impact of volcanic ash on the composition of the soluble fraction of atmospheric bulk deposition was very significant at the Mt. Soro background site. For many elements, in sampling no. 12, higher deposition fluxes were calculated than the median of the remaining periods, with enrichments of up to +1591% for Al (276 $\mu g\ m^{-2}\ d^{-1}$ vs 16.3 $\mu g\ m^{-2}\ d^{-1}$).

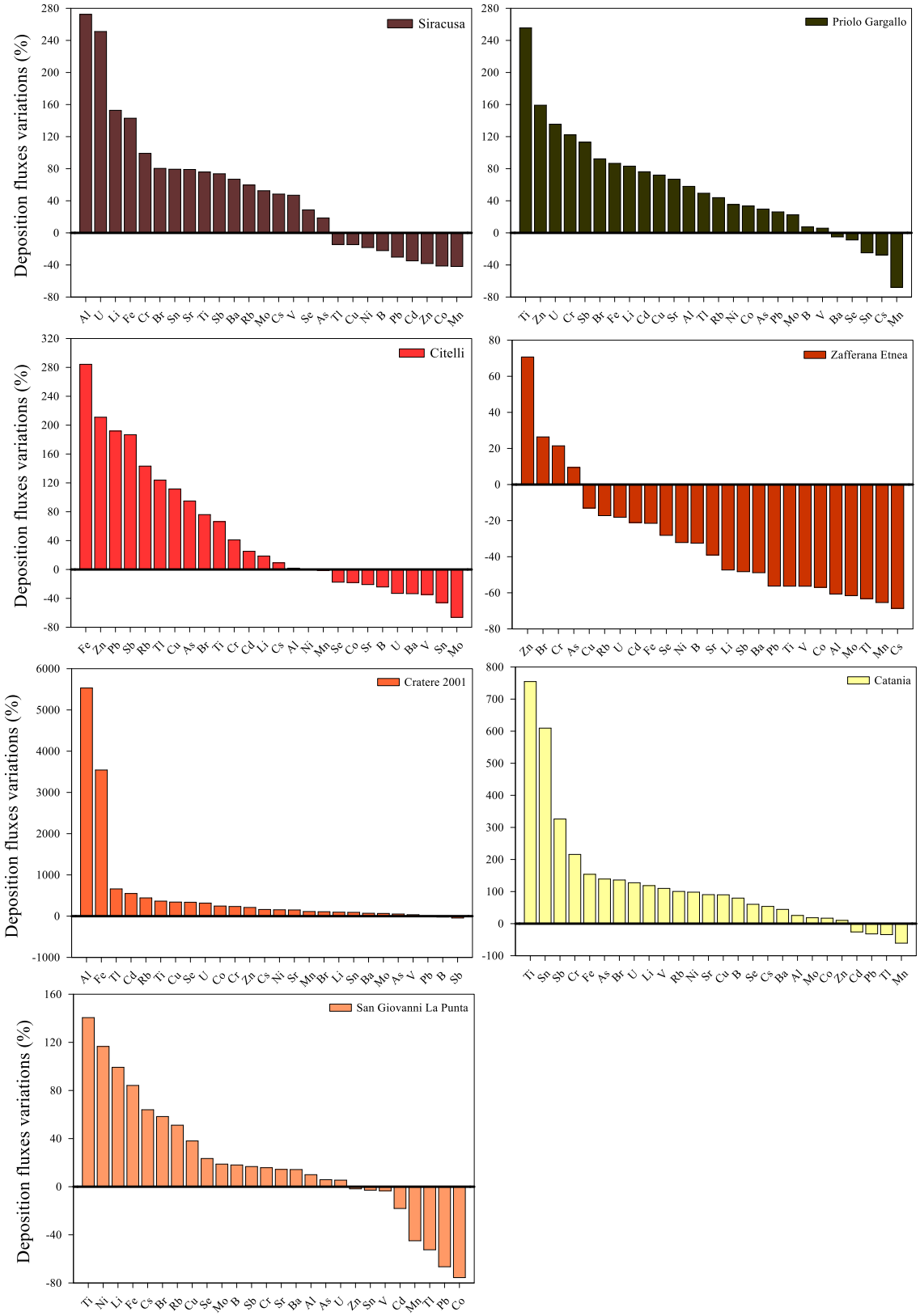

Figure 92 - Variations (%) of minor and trace element daily deposition fluxes, for the soluble fraction, between the period characterised by abundant ash deposition and the period when it was less abundant or absent.

Concerning the insoluble fraction, at the Cratere 2001 site, the only element for which a reduction in the deposition value was observed was Cu (-27.1%). For the other elements, the fluxes between the two periods were comparable or higher in the latter than in the former. Similar results in the Siracusa site, where in the second period only Ti, Co, and Sr deposition fluxes were slightly (up to -18.4%) lower than in the first period. For the other sampling sites, a strong reduction in the insoluble fraction deposition fluxes was observed for almost all the analysed elements, up to -789% for Mn at the Zafferana Etnea sampling site (Fig. 93). This site was the one for which the biggest reductions in trace element deposition fluxes were observed. These changes were caused by a reduction in bulk atmospheric deposition, which in the first period consisted mainly of volcanic ash. The enrichments observed in the soluble fraction of the atmospheric deposition at the Mt. Soro background site due to the Etna paroxysm of 10 February 2022 were also observed in the insoluble fraction, with enrichments of up to +16458% for Sr, by comparing the deposition fluxes calculated for this sample with the median of the other periods (195 μg m^{-2} d^{-1} vs 1.18 μg m^{-2} d^{-1}).

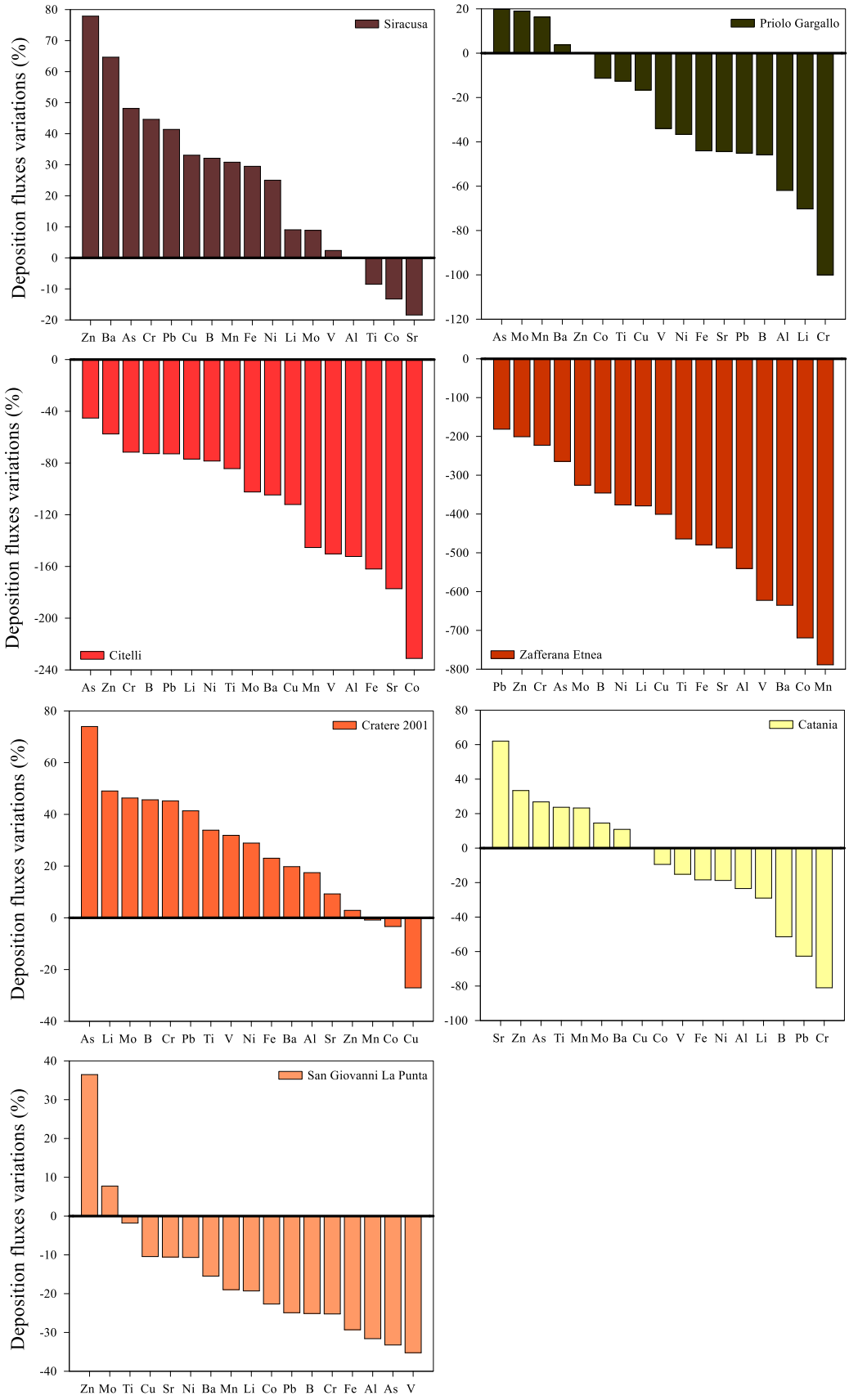

Figure 93 - Variations (%) of minor and trace element daily deposition fluxes, for the insoluble fraction, between the period characterised by abundant ash deposition and the period when it was less abundant or absent.

In conclusion, Etna's paroxysmal activity had a strong influence on the quantity and chemical composition of bulk atmospheric deposition at sites affected by volcanic ash fallout. The greatest differences were observed in the deposition fluxes of trace elements in the insoluble fraction. The site where the greatest differences were observed, both considering the soluble and insoluble fraction was Zafferana Etnea. The concentration and thus the daily atmospheric deposition values of trace elements in the soluble fraction were greatly influenced also by the acidity conditions of the rainwater with which atmospheric particulate, especially volcanic ash, interacted.

5.9 Technology-Critical Elements

The massive requirements of some trace elements led to their extensive extraction from the lithosphere and resulted in their worldwide dispersion and remobilisation within the atmosphere and the biosphere. Indeed, recent studies draw attention to a group of trace elements known as Technology-Critical Elements (TCEs), including tellurium (Te), germanium (Ge), gallium (Ga), indium (In), niobium (Nb), tantalum (Ta), the platinum group elements (PGEs: Pt, Pd, Rh, Os, Ir, Ru), and the rare earth elements (YREEs: La, Ce, Pr, Nd, Sm, Eu, Gd, Tb, Dy, Y, Ho, Er, Tm, Yb, Lu) (*Cobelo-García et al., 2015*).

5.9.1 Concentration of YREEs in blank samples

A blank solution was prepared as described in section 3.6 “Quality control assurance”. Considering all the samples (3) and the median values of each element analysed, it could be observed that the concentrations in the blank solutions were always much lower than the concentrations in the samples (Fig. 94).

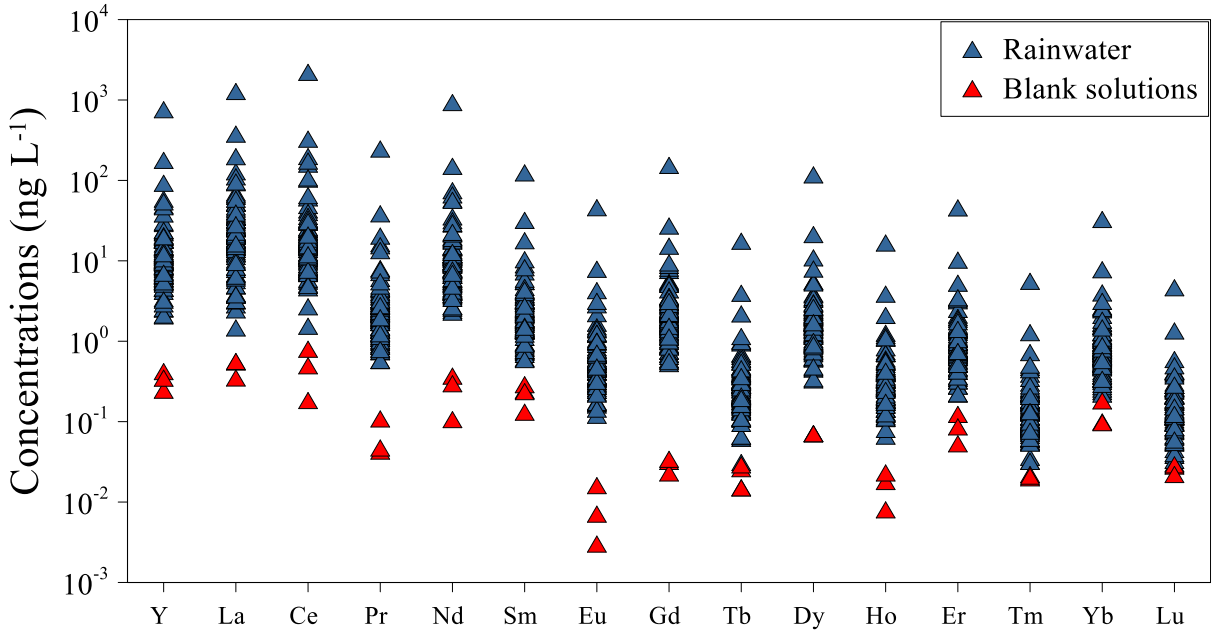

Figure 94 - Raw YREEs concentrations (ng L^{-1}) in blank solution and analysed rainwater samples.

Since the contribution of blank solutions was almost always negligible for all the elements analysed, it was decided not to subtract the concentrations of the blanks from those of the samples.

5.9.2 YREEs

It has recently been recognised that REEs in atmospheric particles and rainwater have a significant impact on the geochemical cycle of REEs in the hydrosphere (*Greaves et al., 1994*; *Yang et al., 2007*; *Klaver et al., 2014*; *Inguaggiato et al., 2015*, *2016*; *Zhu et al., 2016*). The presence of REEs in rainwater is to be found in the multiple interactions between rain droplets and airborne particulates (*Speirs et al., 2023*). Hence, a deep investigation into REE patterns and their distribution could give useful insights into the origin and fate of the particulate matter (PM). REE patterns should be normalized to make them comparable with other case studies. Normalisation to the Post-Archean Australian Shales (PAAS, *McLennan, 1989*) has become one of the most used normalisations to identify element sources, especially when dealing with particles whose composition is potentially similar to the UCC values. REE patterns (Fig. 95) showed a common behaviour with a slight

enrichment in Middle-REE (MREE, from Sm to Dy) with high normalised-concentrations in Eu and Gd. Almost all samples showed also high values in normalised-Y, whereas only in the Palermo urban sites do these values reach the highest peaks. Conversely, samples from the industrial sites showed the highest REE normalised concentrations in La, which in a few observations reached values even larger by a few orders of magnitude. Samples from the Etnean area (excluding the Mt. Intraleo sampling site) showed an almost flat pattern, with the only positive anomalies in Eu and Y.

To investigate the potential interaction of rain droplets with volcanic ash/particulate, the chondrite (*Anders & Grevesse, 1989*) normalised-REE concentrations were compared to the concentrations of Etna's source rocks. These REE concentrations were estimated as average values from alkaline lavas and tephra data reported by Correale et al. (2014) and references therein (Fig. 96). The main trends presented by the Mt. Etna sampling sites seem to follow the main trend of Etna's source rock, with noticeable positive anomalies in Y and a few exceptions of negative anomalies in Ce and Eu in the less concentrated samples. Mt. Intraleo sampling site, already identified as the less affected by volcanic phenomena, showed more consistent patterns in the whole period of sampling instead. However, all their chondrite-normalised patterns presented right-dipping behaviours, indicating a relative enrichment of normalised-LREEs (Light-REEs) concentration over normalised-HREEs (Heavy-REEs), in agreement with the main trend of the area.

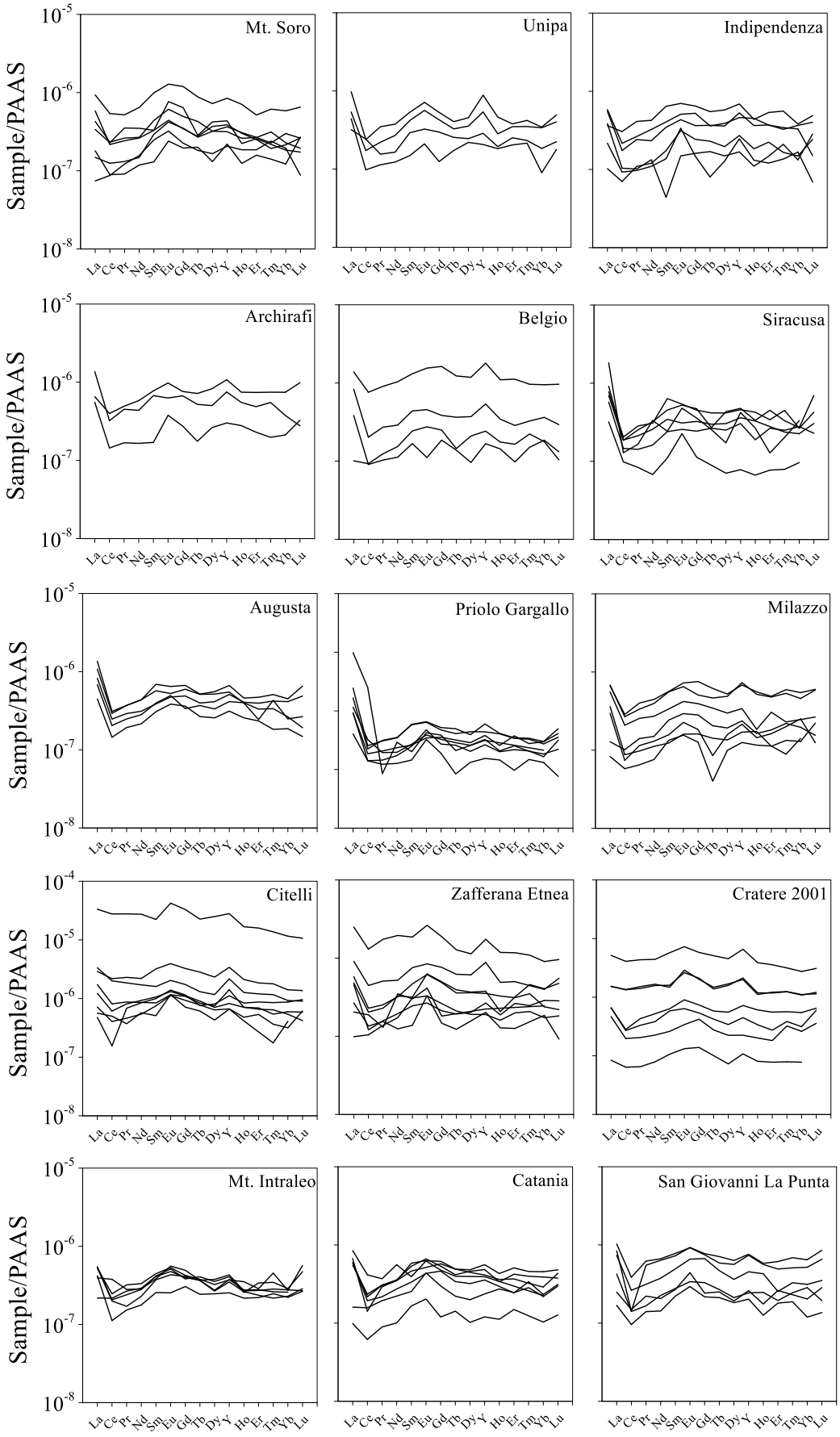

Figure 95 - Shale-normalised pattern of 14 Lanthanoids plus Yttrium.

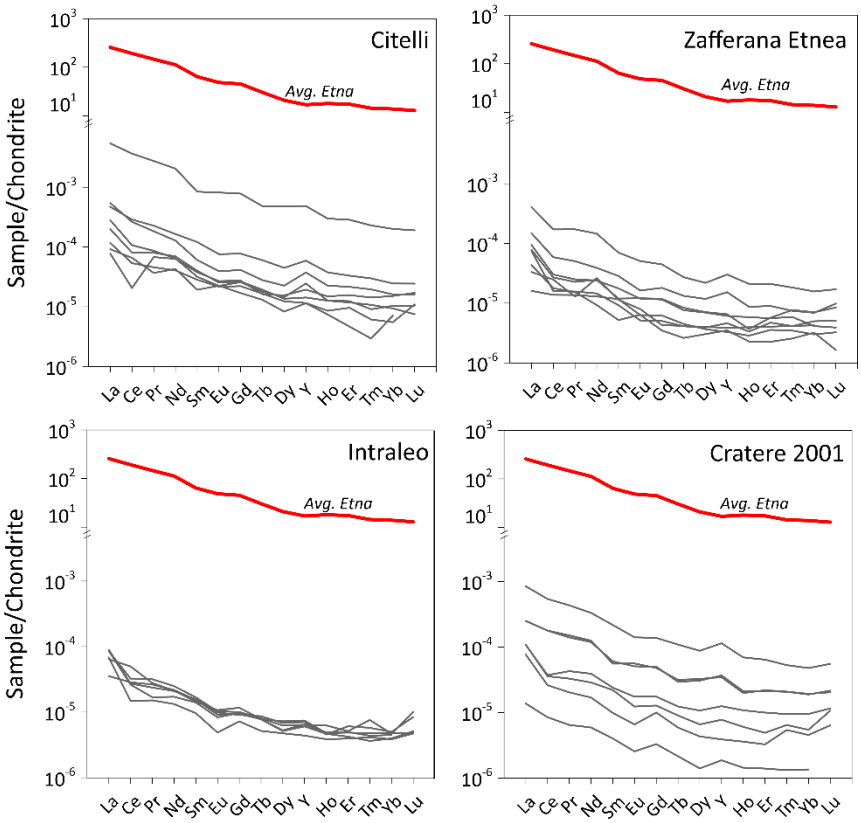

Figure 96 - Chondrite-normalised pattern of 14 Lanthanoids plus Yttrium. Average Etna's data are reported by Correale et al. (2014).

To better understand the relative behaviour of LREEs compared to HREEs, their relationship with other parameters was explored. Since in literature the Middle REEs are arbitrarily split into two groups, it was decided to use the Nd/Yb molar ratio as an indicator of the abundance of light-over-heavy-REEs. As shown in Figure 97a, the Nd/Yb molar ratio showed a slight correlation ($R = 0.60$, p-value < 0.0001) with the total sum of REEs, indicating that the more concentrated samples were also the sample with the higher content in LREEs. This correlation factor rises (from 0.60 to .080) when only the volcanic samples were considered. In Figure 97b the total sum of REEs versus the pH was plotted. It was easy to notice that the more acidic the waters, the more they are enriched in metals. Further, the volcanic rainwater was trendily the most acidic one. A potential cause was given by the higher intensity of leaching of volcanic ashes by the acidic rainwater, which results in rising

REE content. Also, the increase of the Nd/Yb molar ratio was driven directly from the intensity of the weathering, due to the higher relative content of LREEs in Mt. Etna volcanic ash.

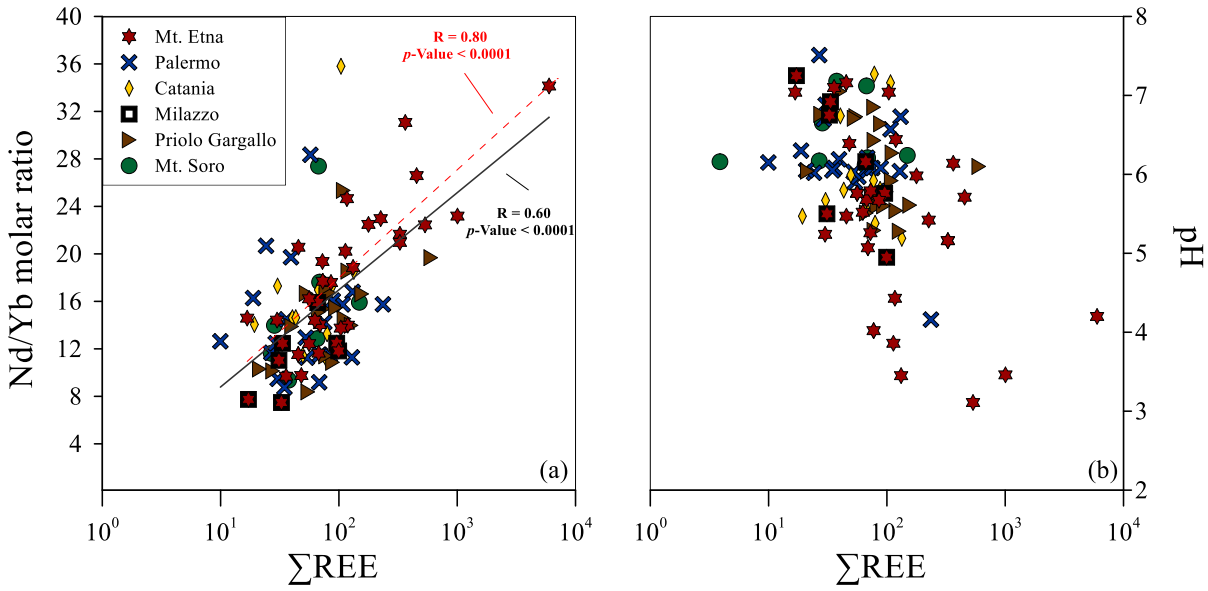

Figure 917 – (a) Nd/Yb molar ratio vs REE total concentration (ng L^{-1}). The black continuous line is the best logarithmic fit for all the samples. The Red dashed line is the best logarithmic fit for volcanic samples only. (b) pH vs REE total concentration (ng L^{-1}).

To recognise the sources of some light REEs, the behaviour of some light REEs was investigated more by assessing the anomaly values. The true Ce anomaly in these samples was discriminated from apparent anomalies, caused by an eventual La enrichment, by comparing (Pr/Pr*)SN and (Ce/Ce*)SN in the binary plot proposed by Bau & Dulski (1996) (Fig. 98). In the graph, the "real" negative Ce anomalies are represented by positive Pr/Pr* and negative Ce/Ce* values (field IIIb). In this study most samples fall in the field of IIa that could be related to a positive La anomaly, able to generate false Ce negative anomalies in normalised patterns. Only a few samples show a positive Ce anomaly, and they were related to urban or volcanic sources. Samples related to the two industrial areas generally fall in the IIa field (positive La, negative Ce) with the lowest values in Ce/Ce*. La anomalies, instead, were estimated according to Lawrence et al. (2006). In Figure 99, La/La*SN is plotted versus the total content of La. Although urban and background

samples do not show any peculiar trend, it was worth noticing the peculiar and different trends of industrial and volcanic samples. Indeed, the latter does not show any relevant increment of La anomalies towards the highest La concentration, indicating an equal enrichment for all LREEs, as can be expected from leaching processes. Conversely, industrial samples displayed a very strong increase in La anomalies, suggesting a non-natural input of this element. A possible candidate for a La source was the cracking catalyst of petrol (*Kulkarni et al., 2007*), but this does not fully explain the anomaly. If the cracking catalyst was the source, a positive Ce anomaly would also be expected, however, there were no Ce anomalies.

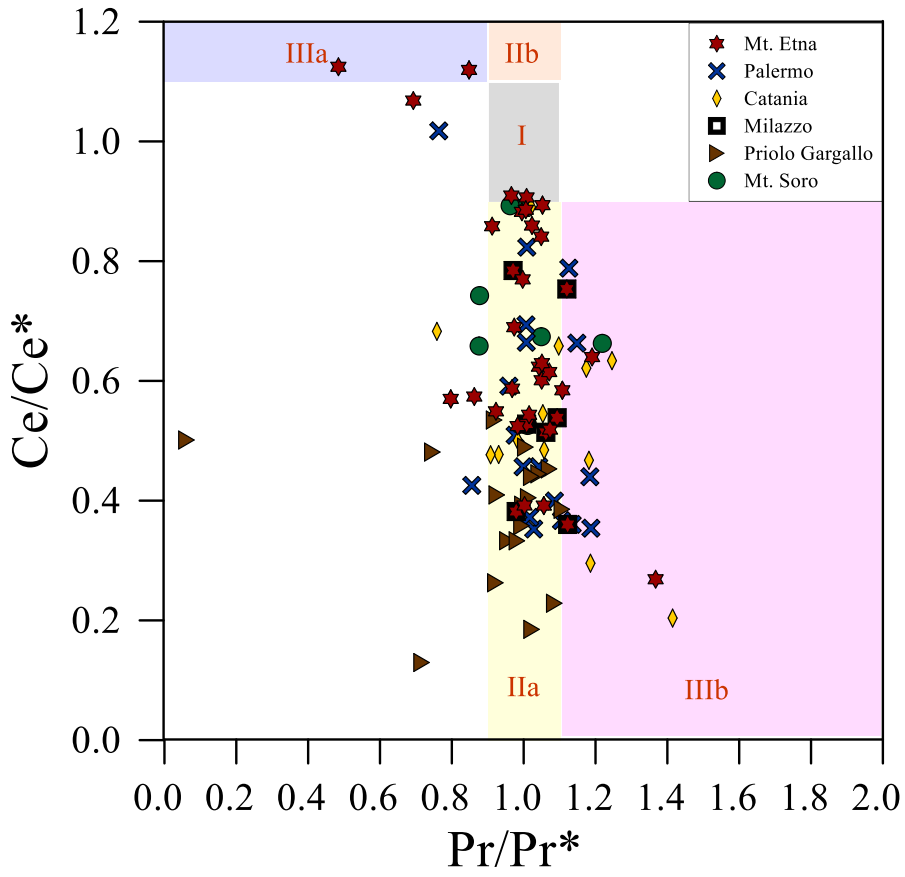

Figure 928 – (Ce/Ce)SN vs (Pr/Pr*)SN graph. Field I: neither CeSN nor LaSN anomaly; field IIa: positive LaSN anomaly, no CeSN anomaly; field IIb: negative LaSN anomaly, no CeSN anomaly; field IIIa: positive CeSN anomaly; field IIIb: negative CeSN anomaly.*

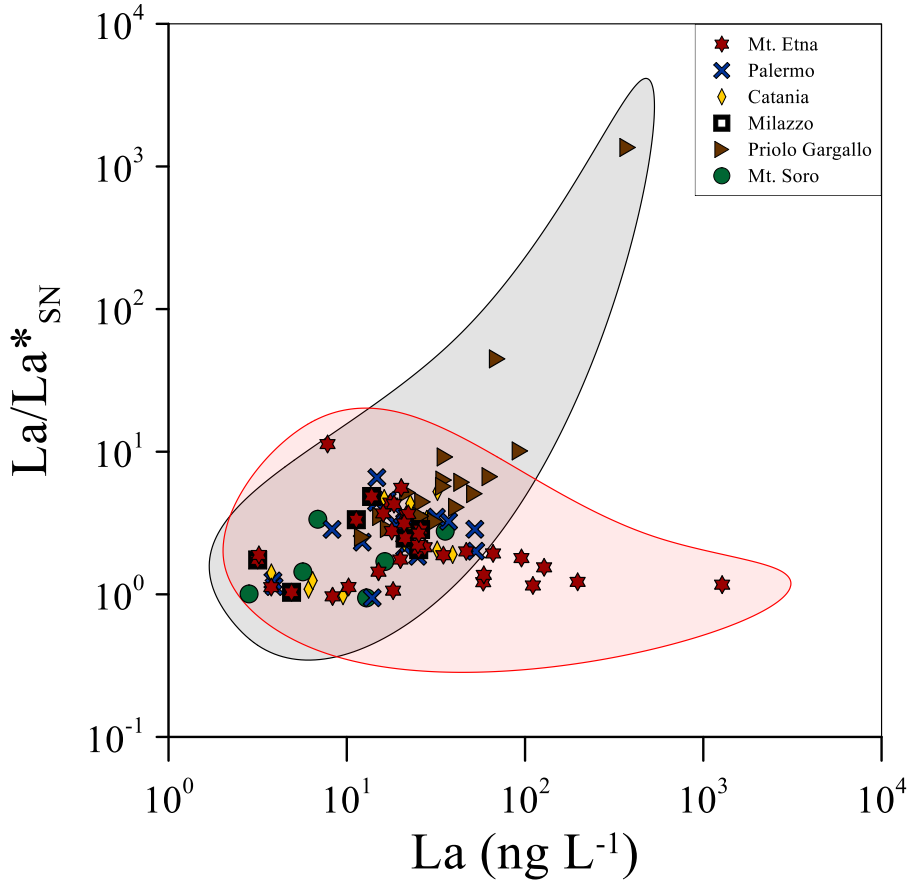

Figure 99 - La anomalies versus La concentrations (ng L^{-1}).

5.9.3 Other TCE concentrations

The concentrations of other TCEs, i.e., Sc, Ge, Zr, Nb, Te, Hf, and Th were measured in the preconcentrated samples. The normalised median concentrations with respect to the median value of the background area of Mt. Soro, are shown in Figure 100.

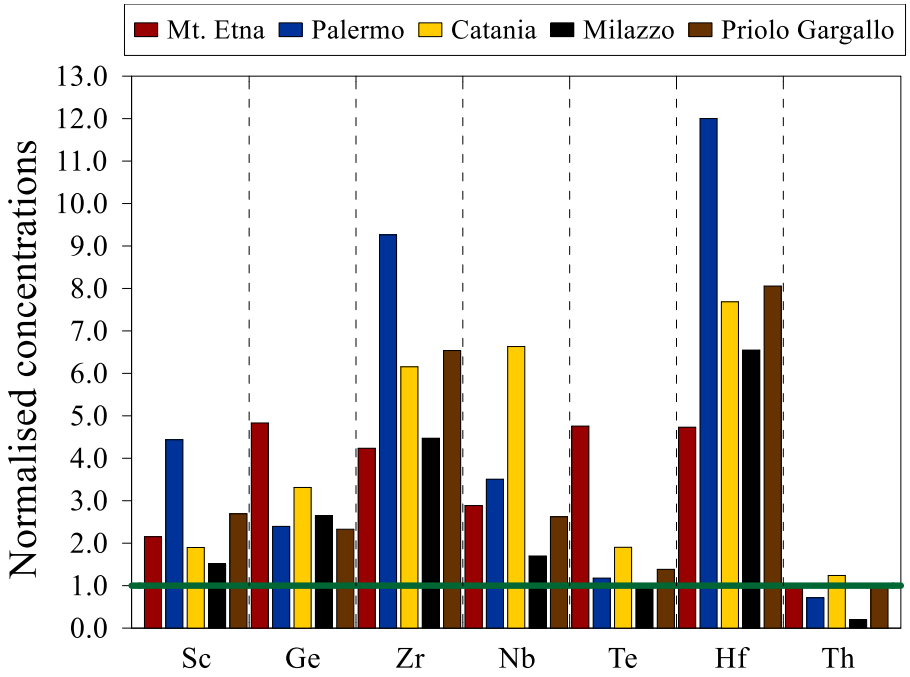

Figure 93 - Normalised concentrations of Sc, Ge, Zr, Nb, Te, Hf, and Th in Mt. Etna, Palermo, Catania, Milazzo, and Priolo Gargallo study areas. The green line is the reference of Mt. Soro.

The volcanic signature was clearly recognisable in the high Te enrichments in the Etna area compared to the background site (ratio of 4.8) and the other study areas. Indeed, Te is a highly volatile element, typically enriched in volcanic emissions. Furthermore, it was not surprising that even in the samples from the Catania area and those from the Priolo Gargallo industrial area, which were influenced by the volcanic source, especially during the paroxysmal events, there was an enrichment of Te, with ratios compared to the background site of 1.9 and 1.4, respectively. Tellurium concentrations were also measured in non-preconcentrated rainwater samples. Considering the samples from Mt. Soro, Palermo, and the industrial area of Milazzo, i.e., the survey sites less or less or not at all influenced by the volcanic source, only in ~ 19% of the cases was the concentration higher than the quantifiable limit (> LOQ). Conversely, considering the rainwater samples most influenced by Etna's volcanic emissions, i.e., three of the four sites in the Etna area (Citelli, Zafferana Etnea, and Cratere 2001), the Mt. Intraleo site, the two sites in the urban area of Catania (Catania and San Giovanni La Punta), and the three sites of the industrial area of Priolo Gargallo

(Siracusa, Augusta, and Priolo Gargallo) it was possible to quantify the concentration of Te in ~ 75%, ~ 52%, ~ 51%, and ~ 30% of the cases, respectively. Another element very enriched in Mt. Etna rainwater samples was Ge (ratio of 4.8). A strong positive correlation was found between Te and Ge ($R = 0.773$, p-value < 0.001), therefore Ge could also be a tracer of the volcanic source.

Very strong enrichments of Hf (ratio of 12) and Zr (ratio of 9.3) were calculated for the urban area of Palermo. Also, in the urban area of Catania and the industrial areas of Priolo Gargallo and Milazzo were observed strong enrichments of these elements with respect to the background site of Mt. Soro. Lower enrichments were calculated for the volcanic area of Mt. Etna. These two elements were strongly correlated with each other, with a Pearson correlation coefficient of 0.983 (significant correlation at the 0.01 level, 2θ). A good Pearson correlation was observed also between Hf and Sc ($R = 0.585$, p-value < 0.001), and between Zr and Sc ($R = 0.615$, p-value < 0.001). This agreed with what was observed in the normalised concentrations; indeed, the highest Sc enrichment was also observed for the urban area of Palermo (median concentration 4.4 higher than the Mt. Soro background site). Therefore, a common source for these three elements may be supposed. No correlations were found between Hf and Zr and other trace elements; instead, high positive correlations were found between Sc and Mn ($R = 0.635$, p-value < 0.001), Cd ($R = 0.622$, p-value <0.001), and Al ($R = 0.599$, p-value < 0.001). An important contribution for Mn and Cd derived from vehicular emissions; Al was a tracer of the crustal source. For Nb the highest normalised median concentrations were calculated in the urban area of Catania (6.6), and the urban area of Palermo (3.5). This element was correlated with Sc ($R = 0.411$, p-value < 0.001), Hf ($R = 0.401$, p-value < 0.001), and Zr ($R = 0.375$, p-value < 0.001). It was well correlated also with Sn ($R = 0.575$, p-value < 0.001). Finally, for Th, higher concentrations were measured in the rainwater samples from the Mt. Soro background area, instead of the other survey areas, except for Catania. This element was well correlated only with Pb ($R = 0.575$, p-value < 0.001).

To summarise, the signature of the volcanic source was recognisable by the high concentrations of Te and Ge in the rainwater, especially in the sites most exposed to the dispersion of volcanic gases and ash. Strong positive correlations were recognised between Hf, Zr, Sc and partly Nb. The highest concentrations of the first two elements were recorded in the two urban and two industrial areas. Anthropogenic sources were the main suspects for the emission of these elements. The highest concentrations of Th were recorded in the urban area of Catania and at the Mt. Soro background site.

5.10 Boron and strontium isotopic composition

At present, the low concentrations of boron in rainwater, usually between 0.2 and 300 µg L^{-1} (*Fogg & Duce, 1985*; *Miyata et al., 2000*), have restricted the use of its isotopes to trace the origin of boron in the atmosphere. Thus, the atmospheric boron cycle is poorly known and complex. The strontium isotope system ($^{87}Sr/^{86}Sr$) was often used to help constrain the different sources of atmospheric Sr (*Pearce et al., 2015*), and has been successfully used as source tracers for sediment provenance, chemical weathering, and long-range transport of aerosols (e.g., *Négrel & Roy, 1998*; *Derry & Chadwick, 2007*; *Négrel et al., 2007*; *Xu et al., 2012*).

In this PhD research, for the first time, boron and strontium isotopic ratios were measured in 29 Sicilian rainwater samples. In the rainwater samples from the urban areas of Palermo and Catania, the B concentrations were between 8.02 and 27.5 µg L^{-1}, with a median concentration of 15.8 µg L^{-1}, while Sr concentrations were between 15.9 and 120 µg L^{-1}, with a median concentration of 68.8 µg L^{-1}. The $\delta^{11}B$ ranged between +22.0‰ and +40.3‰, with a median value of +32.9‰; the $^{87}Sr/^{86}Sr$ ranged between 0.70647 and 0.70992, with a median value of 0.70888. Boron concentrations between 11.8 and 19.5 µg L^{-1} (median of 14.0 µg L^{-1}) and $\delta^{11}B$ from +27.4‰ to +37.8‰ (median of +33.7‰) were measured in the investigated industrial areas. Strontium concentrations between 20.1 and 64.8 µg L^{-1} (median concentration of 34.3 µg L^{-1}), and $^{87}Sr/^{86}Sr$ ratios from 0.70857 to 0.70992

(median of 0.70877) were measured in the same areas. In the rural area of Mt. Soro, the B concentrations were between 4.55 and 30.2 µg L^{-1}, with a median concentration of 9.10 µg L^{-1}; the Sr concentrations were between 9.88 and 94.2 µg L^{-1}, with a median concentration of 30.9 µg L^{-1}. The B and Sr isotopic values were slightly equal in the Mt. Soro rainwater samples, ranging from +38.3 to +40.3‰ for B, and from 0.70885 to 0.70928 for Sr, except for one sample, no. 12, for which a lower $\delta^{11}B$ value of +22.6‰ and an $^{87}Sr/^{86}Sr$ ratio of 0.70719 were measured. Finally, B concentrations between 4.56 and 21.9 µg L^{-1}, with a median value of 8.80 µg L^{-1}, and Sr concentrations between 9.67 and 541 µg L^{-1}, with a median value of 57.8 µg L^{-1}, were measured in the rainwater samples from Mt. Etna. Boron isotopic values from +1.3 and +42.9‰, with a median value of +26.5‰, and $^{87}Sr/^{86}Sr$ ratios from 0.70373 and 0.71036, with a median value of 0.70721, were measured in the same survey sites. The $\delta^{11}B$ values and the $^{87}Sr/^{86}Sr$ ratios for each study context are shown in Figures 101a and b.

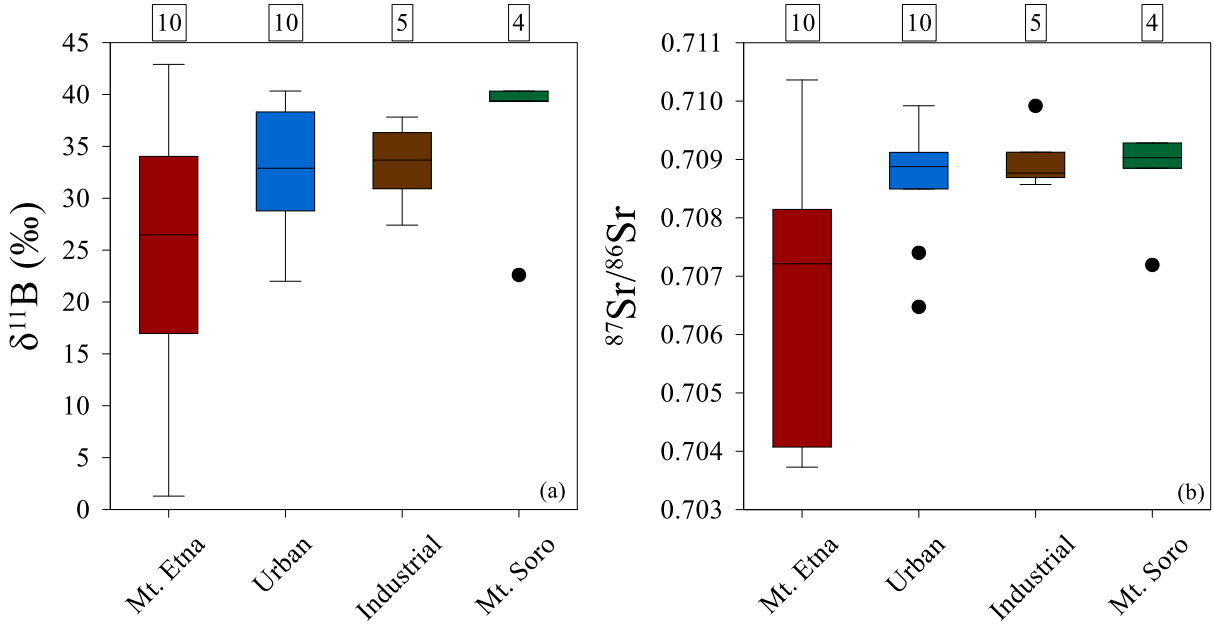

*Figure 94 - (a) Boron ($\delta^{11}B$) and (b) strontium isotopic composition ($^{87}Sr/^{86}Sr$ in Mt. Etna, urban areas, industrial areas, and Mt. Soro rainwater samples. In the box plots, the whiskers coincide with IQR*1.5, the box edges are the first and third quantiles, and the centre lines are the medians. The number of samples used for the construction of the box plots is indicated.*

Previous data on $\delta^{11}B$ in rainwater are sparse but show a wide range of variability. Spivack (1986), measured a $\delta^{11}B$ range from +0.8 to +35‰ over the Pacific Ocean; Xiao et al. (1992), measured a $\delta^{11}B$ of +16.7‰ in Qinghai, China; Eisenhut & Heumann (1997), and Barth (1998) measured a value of +13.1‰ in southeast Germany. In marine rainwater from the North Pacific, Miyata et al. (2000) measured $\delta^{11}B$ from +18.9 to +34.7‰. Higher $\delta^{11}B$ values, between +30.5 and +45‰, were measured by Chetelat et al. (2005) in French Guiana. The boron isotopic composition of instantaneous rain samples from Nepal ranged from -1.5 to +26.0‰, while Californian rainwater had very positive $\delta^{11}B$ of +19.8 and +26.0‰ (*Rose & Koga, 2006*). Zhao & Liu (2010) measured $\delta^{11}B$ in Guiyang City, China, rainwater samples from +2.0 to 30‰. Finally, Millot et al. (2010), in rainwater samples from coastline and inland locations, measured $\delta^{11}B$ between -3.3 and +40.6‰. Previous data on strontium isotopic composition in rainwater samples come from studies carried out in two regions of the planet, France, and China, and show a wide range of variability. Négrel & Roy (1998) and Pearce et al. (2015) measured $^{87}Sr/^{86}Sr$ ratios between 0.70920 and 0.71625 and between 0.70796 and 0.71093 in rainwater samples from the Massif Central and Paris, France. Strontium radiogenic isotopic ratios between 0.70793 and 0.70908, and between 0.70768 and 0.71009 were measured by Han & Liu (2006) and by Han et al. (2012) in Guiyang, China, respectively. In Beijing, China, Xu & Han (2009) and Xu et al. (2012) measured $^{87}Sr/^{86}Sr$ ratios from 0.70912 and 0.71036, and between 0.70920 and 0.71090, respectively. Xu et al. (2009) measured very high $^{87}Sr/^{86}Sr$ ratios, between 0.71025 and 0.71302 in rainwater samples from Lanzhou, Northwest China, Finally, Han et al. (2010), in a karst virgin forest, in the region of Maolan, Southwest China, measured $^{87}Sr/^{86}Sr$ ratios between 0.70746 and 0.71275. Therefore, the $\delta^{11}B$ and the $^{87}Sr/^{86}Sr$ values measured in the rainwater samples analysed in this PhD research fall within the ranges of values previously measured in other areas of the world. Extreme were the Sr isotopic ratios measured in the samples from the Etna area; to the best of my knowledge, never have such low $^{87}Sr/^{86}Sr$ ratios, as low as 0.70373, been measured in rainwater.

The B concentrations (µg L^{-1}) versus $\delta^{11}B$ values (‰), and the Sr concentrations (µg L^{-1}) versus $^{87}Sr/^{86}Sr$ ratios are plotted in Figures 102a and b. There seems to be an inverse relationship between $\delta^{11}B$ and B concentrations and between $^{87}Sr/^{86}Sr$ ratios and Sr concentrations. These results are similar to that described by Millot et al. (2010) for B and by Négrel & Roy (1998) for Sr.

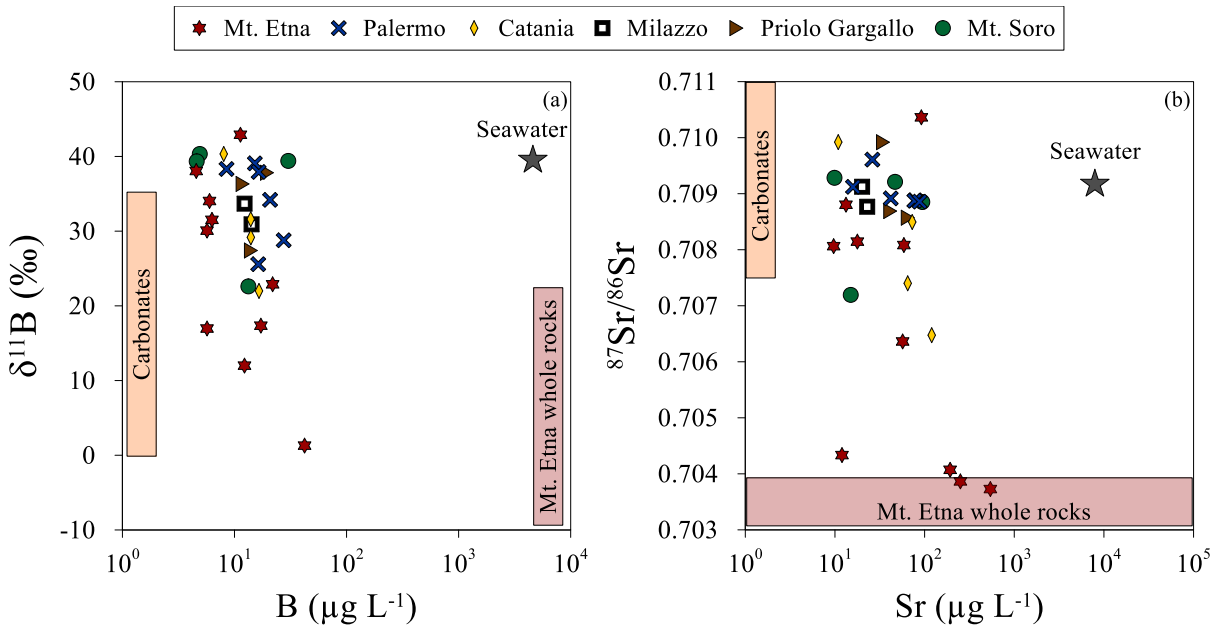

Figure 95 – (a) $\delta^{11}B$ (‰) values and $^{87}Sr/^{86}Sr$ ratios plotted as a function of B and Sr concentrations (µg L^{-1}, log scale), in Sicilian rainwater samples. $\delta^{11}B$ (‰) isotopic composition for carbonates is from Millot et al. (2010), and for Mt. Etna whole rocks is from Pennisi et al. (2000). $^{87}Sr/^{86}Sr$ ratios for carbonates are from Han et al. (2012) and Xu et al. (2012), and for Mt. Etna whole rocks are from Liotta et al. (2017).

Ocean seawater has an $\delta^{11}B$ isotopic composition of +39.5‰ (*Fogg & Duce, 1985*), but through empirical rain-vapour isotopic fractionations, different authors predicted a seawater-derived atmosphere having a $\delta^{11}B$ between +45.0 and +50.0‰ (*Chetelat et al., 2005*; *Zhao & Liu, 2010*). Present-day seawater has an $^{87}Sr/^{86}Sr$ isotope ratio equal to 0.70917 (*Dia et al., 1992*). A non-negligible contribution from the marine source would seem evident, as many rainwater samples, both from rural and urban coastal sites, had a median $\delta^{11}B$ isotopic composition and an $^{87}Sr/^{86}Sr$ isotope ratio very close to that of seawater. Going into more detail, in these areas, the median $\delta^{11}B$ and $^{87}Sr/^{86}Sr$ values closest to the isotopic composition of seawater were calculated at the Mt. Soro

(+39.4‰ and 0.70903), Archirafi (+38.7‰ and 0.70900), Unipa (+37.9‰ and 0.70961), and Catania (+36.0‰ and 0.70921) survey sites. Very high median $\delta^{11}B$ and $^{87}Sr/^{86}Sr$ values were also calculated for the Zafferana Etnea (+38.1‰ and 0.70806) and the Priolo Gargallo (37.8‰ and 0.70992) sampling sites. Although the role of sea-salt degassing as the major source of B in the atmosphere is still debated, several authors have estimated a marine contribution to atmospheric B of between 60% (*Park & Schlesinger, 2002*) and 80% (*Fogg & Duce, 1985*; *Chetelat et al., 2005*). The values of $\delta^{11}B$ measured in the rainwater samples, supported by the results on the chemical composition, suggest that sea-salt degassing could be the prevalent source of B in the atmosphere of the previously mentioned sampling sites. The enrichment of B with respect to the B/Na^+ ratio (by mass) in seawater (Fig. 103a), and the distribution of the samples in the $^{87}Sr/^{86}Sr$ versus Cl^-/Na^+ (mol/mol), highlight that sea-salt aerosol was not the only source of B and Sr in the atmosphere (Fig. 103b).

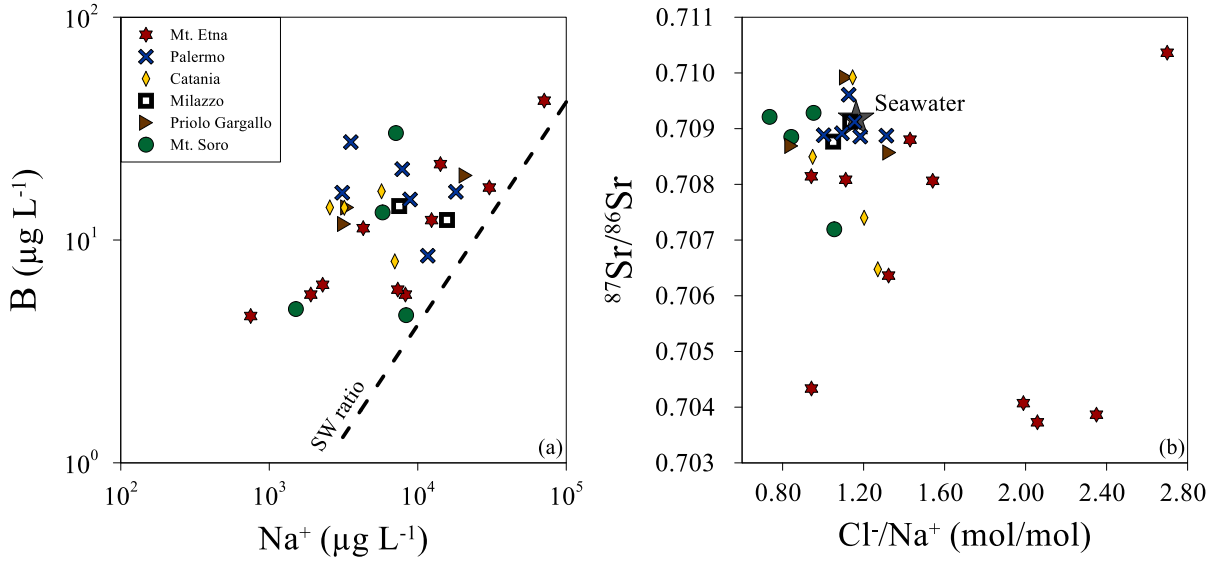

Figure 103 – (a) Boron versus sodium concentrations (µg L^{-1}) and (b) $^{87}Sr/^{86}Sr$ versus Cl^-/Na^+ (mol/mol) in the analysed rainwater samples.

From previous works, Sr isotopes are expected to provide insights into the sources (and their mixtures) of base cations in rainwater, particularly Ca, which is not well-constrained from concentration data alone. Notwithstanding, no strong correlation (R = 0.377; p-value = 0.0837) was

found between Sr and Ca in the analysed rainwater samples (Fig. 104a), and no simple binary mixing correlation was found between $^{87}Sr/^{86}Sr$ ratios and Ca/Sr ratios (Fig. 104b). Accordingly, numerous sources, both local and remote, natural, and anthropogenic inputs, should be responsible for the variation of the Sr isotope and the related element ratios.

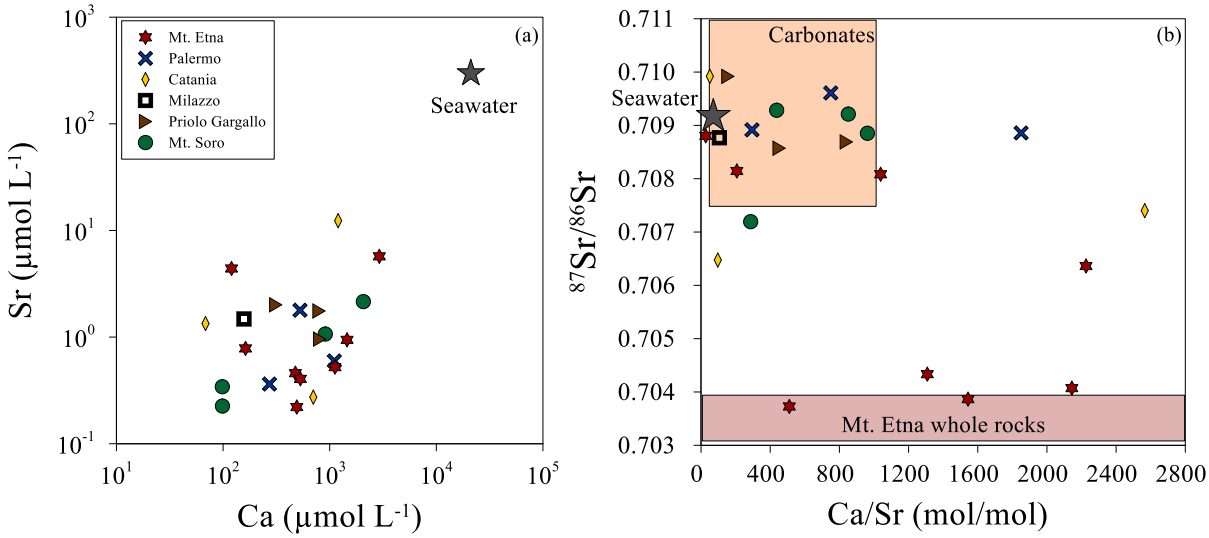

Figure 964 – (a) Strontium versus calcium concentrations (µmol L^{-1}) and (b) $^{87}Sr/^{86}Sr$ versus Ca/Sr (molar ratio) for all the study areas. $^{87}Sr/^{86}Sr$ ratios for carbonates are from Han et al. (2012) and Xu et al. (2012), and for Mt. Etna whole rocks are from Liotta et al. (2017).

Another source for B and Sr, easily distinguishable from the others, was the volcanic one. Very low $\delta^{11}B$ and $^{87}Sr/^{86}Sr$ isotope ratio values were measured in the rainwater samples of Cratere 2001 (from +1.3 to +31.5‰ and from 0.70373 to 0.70808), and of San Giovanni La Punta (from +22.0 to +29.2‰ and from 0.70647 to 0.70740), with median $\delta^{11}B$ values of +17.0 and +25.6‰, and median $^{87}Sr/^{86}Sr$ ratios of 0.70433 and 0.70649, respectively. Although few data on fumarolic condensates of hydrothermal and volcanic systems exist (overall $\delta^{11}B$ ranges from -9.3 to +21.4‰; *Kanzaki et al., 1979*; *Nomura et al., 1982*; *Palmer & Sturchio, 1990*), data on the $^{11}B/^{10}B$ ratio in the volcanic atmosphere (i.e., gas) are extremely scarce. $\delta^{11}B$ values between -5.2 to +25.8‰ were measured by Pennisi et al. (2000) in Mt. Etna groundwaters. Strontium isotope ratios between 0.703226 and 0.703910 were measured in Mt. Etna groundwaters by Pennisi et al. (2000) and Liotta

et al. (2017). The data available in the literature are sufficient to attribute Etna's volcanic source as the major contributor to B and Sr emissions in the atmospheres of these two monitoring sites. Although the rainwater chemistry of the Zafferana Etnea site was partly influenced by the volcanic source, as discussed in the previous chapters, the $\delta^{11}B$ and the $^{87}Sr/^{86}Sr$ values measured at this site showed a strong contribution from the marine source. It is important to highlight the "anomalous" values measured for both boron and strontium isotopes in sample no. 12 at the Mt. Soro background site, equal to +22.6‰ and 0.70719, respectively. Even for this sample, a large part of these two elements was derived from volcanic emissions from Etna; indeed, this sample was collected after the paroxysm of 10 February 2022, whose ash also fell on this area.

The last important natural source for Sr was the geogenic one, especially associated with carbonate dissolution and soil dust, for which $^{87}Sr/^{86}Sr$ ratios between 0.7076 (Han et al., 2012) and 0.7092 (Pearce et al., 2015), and between 0.7111 (Xu & Han, 2009) and 0.7115 (Xu et al., 2012), were measured, respectively.

Low median $\delta^{11}B$ values were measured in Belgio (+28.8‰), Indipendenza (+29.9‰), Siracusa (+31.9‰), and Milazzo (+32.3‰) sampling sites. Several authors (*Fogg & Duce, 1985*; *Park & Schlesinger, 2002*; *Chetelat et al., 2005*; *Millot et al., 2010*; *Zhao & Liu, 2010*) estimated that the contribution of anthropogenic input to the atmospheric boron might be up to 40%. The main anthropogenic inputs for B are biomass and coal burning, use of fertilizers, power plant emissions, and urban aerosols. Boron is widely used as an additive or stuff in many fields including detergent, fertilizer, glass, ceramics, and cosmetics (*Zhou & Liu, 2010*). The same anthropogenic sources may be responsible for the emissions of Sr. For household and automobile exhaust, $^{87}Sr/^{86}Sr$ ratios between 0.7083 and 0.7334 and from 0.7077 to 0.7083 were reported by Négrel et al. (2007). Han et al. (2012) reported an $^{87}Sr/^{86}Sr$ ratio of 0.7076 from fossil fuel combustion. Finally, Négrel & Deschamps (1996) reported $^{87}Sr/^{86}Sr$ ratios between 0.7079 and 0.7087 for fertilisers. Accordingly, gaseous, and particulate anthropogenic contributions may be locally or regionally important. The

chemical composition of the rainwater samples in the above-mentioned sampling sites was influenced by sea-salt aerosols, biomass burning (especially for K^+), urban emissions (vehicular traffic and household), and industrial activities, such as power plant production, refining of fossil fuels, and ceramics production (the latter only for the Milazzo industrial area). Therefore, the $\delta^{11}B$ isotopic composition and the $^{87}Sr/^{86}Sr$ ratios of rainwater samples from the above-mentioned survey sites could be explained by mixing two or more of the above-mentioned sources.

The relationship between the isotopic composition of B and Sr in Sicilian rainwater is shown in Figure 105. Samples conditioned by volcanic emissions are recognisable, characterised by $\delta^{11}B$ below +30‰ and $^{87}Sr/^{86}Sr$ below 0.7075. The "anomalous" sample from the Mt. Soro background site is also evident. The samples influenced by the marine source fall close to its representative point (grey star). The contribution of the anthropogenic sources is masked by the natural contributions.

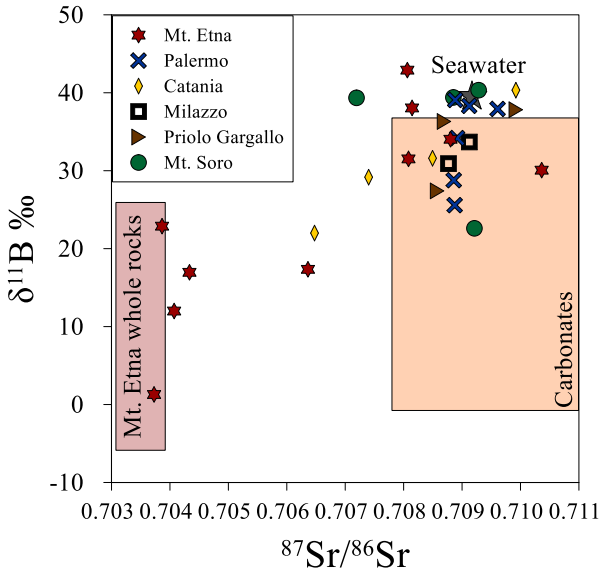

Figure 105 - $\delta^{11}B$(‰) versus $^{87}Sr/^{86}Sr$ isotopic ratios in the analysed rainwater samples. $\delta^{11}B$ (‰) isotopic composition for carbonates is from Millot et al. (2010), and for Mt. Etna whole rocks is from Pennisi et al. (2000). $^{87}Sr/^{86}Sr$ ratios for carbonates are from Han et al. (2012) and Xu et al. (2012), and for Mt. Etna whole rocks are from Liotta et al. (2017).

To summarise, these results provide the first comprehensive study of B and Sr isotopes in Sicilian rainwaters. Sea-salt aerosols, volcanic emissions, and anthropogenic emissions were the

main sources of B and Sr in the study area atmospheres. To the best of my knowledge, these are the first measurements of B and Sr isotopes in rainwater samples affected by the volcanic source. Since the Sr isotope ratios of these possible sources for the rainwaters collected in Sicily have not been characterised, it is difficult to identify the relative contributions for each source for Sr based on its ratio only. The use of other isotope systematic, maybe Pb, could help in discriminating the other sources. This framework could be used in future studies to illustrate how these data for rainwater samples can add to the global understanding of geochemical processes in hydrology. Finally, this work also adds to the potential for the use of B and Sr isotopes as environmental tracers, especially for the volcanic source.

5.11 References

Abita, A. M. & Basiricò, L. (2023). L'inventario delle emissioni in atmosfera della regione siciliana – Sorgenti puntuali. U.O.C. Qualità Dell'aria; ARPA SICILIA: Palermo, Italy, 2023.

Aiuppa, A., Federico, C., Giudice, G., Gurrieri, S., Paonita, A., Valenza, M. (2004). Plume chemistry provides insights into mechanisms of sulfur and halogen degassing in basaltic volcanoes. Earth Planet Sc. Lett., 222(2), pp. 469-483. https://doi.org/10.1016/j.epsl.2004.03.020.

Aiuppa, A., Federico, C., Franco, A., Giudice, G., Guerrieri, S., Inguaggiato, S., Liuzzo, M., McGonigle, A.J.S., Valenza, M. (2005). Emission of bromine and iodine from Mt. Etna volcano. Geochem. Geosyst., 6, Q08008. https://doi.org/10.1029/2005GC000965.

Aiuppa A., Bellomo S., Brusca L., D'Alessandro W. Di Paola R., Longo M. (2006). Major-ion bulk deposition around an active volcano (Mt. Etna, Italy). Bull. Volcanol., 68, pp. 255-265. https://doi.org/10.1007/s00445-005-0005-x.

Alaimo, R. & Ferla, P. (1979) Presenza di palygorskite nella polvere trasportata dallo "scirocco" in Sicilia: Implicazioni geologiche ed ambientali. Ist. Min. Petrol. Geochim., Quaderno n.4.

Allard, P., Carbonelle, J., Dajlevic, D., Le Bronec, J., Morel, P., Robe, M.C., Maurenas, J.M., Faivre-Pierret, R., Martin, R., Sabroux, D., Zettwoog, P. (1991). Eruptive and diffuse emissions of CO_2 from Mt. Etna. Nature, 351, pp. 387-391. https://doi.org/10.1038/351387a0.

Allard, P. (1997). Endogenous magma degassing and storage at Mt. Etna. Geophys. Res. Lett., 24(17), pp. 2219-2222. https://doi.org/10.1029/97GL02101.

Al-Momani, I. F., Ataman, O. Y., Anwari, A. M., Tuncel, S., Köse, C., Tuncel, G. (1995). Chemical composition of precipitation near an industrial area at Izmir, Turkey. Atmos. Environ., 29, pp. 1131–1143. https://doi.org/10.1016/1352-2310(95)00027-V.

Al-Momani, I. F., Momani, K. A., Jaradat, Q. M., Massadeh, A. M., Yousef, Y. A., Alomary, A. A. (2008). Atmospheric deposition of major and trace elements in Amman, Jordan. Environ. Monit. Assess., 136, pp. 209–218. https://doi.org/10.1007/s10661-007-9676-4.

Amato, F., van Drooge, B. L., Jaffrezo, J. L., Favez, O., Colombi, C., Cuccia, E., Reche, C., Ippolito, F., Ridolfo, S., Lara, R., Uzu, G., Ngoc, T. V. D., Dominutti, P., Darfeuil, S., Albinet, A., Srivastava, D., Karanasiou, A., Lanzani, G., Alastuey, A., Querol, X. (2024) Aerosol source apportionment uncertainty linked to the choice of input chemical components. Environ Int., 12, 184, 108441. https://doi: 10.1016/j.envint.2024.108441.

Amodio, M., Catino, S., Dambruoso, P. R., De Gennaro, G., Di Gilio, A., Giungato, P., Laiola, E., Marzocca, A., Mazzone, A., Sardaro, A., Tutino, M. (2014). Atmospheric deposition: Sampling procedures, analytical methods, and main recent findings from the scientific literature. Adv. Meteorol., 2014, 161730. https://doi.org/10.1155/2014/161730.

Anders, E. & Grevesse, N. (1989). Abundances of the elements: Meteoritic and solar. Geochim. Cosmochim. Ac., 53, pp. 197–214. https://doi.org/10.1016/0016-7037(89)90286-X.

Badalamenti, F., Carapezza, M., Dongarrà, G., Macaluso, A., Hauser, S., Parello, F. (1984). Precipitazioni atmosferiche in Sicilia. 1) L'area urbana di Palermo. Rend. Soc. It. Mineral. e Petrol., 39(1), pp. 81-92.

Baker, A. R., Li, M., Chance, R. (2020): Trace metal fractional solubility in size-segregated aerosols from the tropical eastern Atlantic Ocean. Global Biogeochm. Cy., 34, e2019GB006510, https://doi.org/10.1029/2019GB006510.

Barth, S. (1998). $^{11}B/^{10}B$ variations of dissolved boron in a freshwater–seawater mixing plume (Elbe Estuary, North Sea). Mar. Chem., 62, 1-2, pp. 1–14. https://doi.org/10.1016/S0304-4203(98)00023-1.

Bau, M. & Dulski, P. (1996). Distribution of yttrium and rare-earth elements in the Penge and Kuruman iron-formations, Transvaal Supergroup, South Africa. Precambrian Res. 79, pp. 37–55. https://doi.org/10.1016/0301-9268(95)00087-9.

Bellomo, S., D'Alessandro, W., Longo M. (2003). Volcanogenic fluorine in rainwater around active degassing volcanoes: Mt. Etna and Stromboli Island, Italy. Sci. Total Environ., 301, pp. 175–185. https://doi.org/10.1016/S0048-9697(02)00284-X.

Bellomo, S., Aiuppa, A., D'Alessandro, W., Parello, F. (2007). Environmental impact of magmatic fluorine emission in the Mt. Etna area. J. Volcanol. Geoth. Res., 165(1-2), pp. 87-101. https://doi.org/10.1016/j.jvolgeores.2007.04.013.

Berner, E. K. & Berner, R. A. (1987). Global Water Cycle: Chemical Composition and Environment; Prentice-Hall Inc.: Englewood Cliffs, NJ, USA, p. 397. https://scholar.google.com/scholar_lookup?title=Global+Water+Cycle:+Chemical+Composition+and+Environment&author=Berner,+E.K.&author=Berner,+R.A.&publication_year=1987.

Brugnone, F., D'Alessandro, W., Calabrese, S., Li Vigni, L., Bellomo, S., Brusca, L., Prano, V., Saiano, F., Parello, F. (2020). A Christmas gift: Signature of the 24th December 2018 eruption of Mt. Etna on the chemical composition of bulk deposition in eastern Sicily. Italian Journal of Geosciences, 139(3), pp. 1–18. https://doi.org/10.3301/ijg.2020.08.

Brugnone, F., D'Alessandro, W., Parello, F., Liotta, M., Bellomo, S., Prano, V., Li Vigni, L., Sprovieri, M., Calabrese, S. (2023a). Atmospheric Deposition around the Industrial Areas of Milazzo and Priolo Gargallo (Sicily, Italy) - Part A: Major Ions. Int. J. Environ. Res. Public Health, 20, 3898. https://doi.org/10.3390/ijerph20053898.

Brugnone, F., D'Alessandro, W., Parello, F., Brusca, L., Saiano, F., Li Vigni, L., Sprovieri, M., Calabrese, S. (2023b). Atmospheric Deposition around the Industrial Areas of Milazzo and Priolo Gargallo (Sicily–Italy)—Part B: Trace Elements. Atmosphere, 14, 737. https://doi.org/10.3390/atmos14040737.

Bruno, N., Caltabiano, T., Grasso, F., Porto, M., Romano, R. (1996). Degassing of SO_2 and CO_2 at Mt. Etna volcano during the 1991-1993 eruption: correlations and considerations. Acta Vulcanol., 4, pp. 143-147. https://doi.org/10.1016/S0377-0273(01)00201-3.

Calabrese, S., Aiuppa, A., Allard, P., Bagnato, E., Bellomo, S., Brusca, L., Parello, F. (2011). Atmospheric sources and sinks of volcanogenic elements in a basaltic volcano (Etna, Italy). Geochim. Cosmochim. Acta, 75(23), pp. 7401–7425. https://doi.org/10.1016/j.gca.2011.09.040.

Caltabiano, T., Burton, M., Giammanco, S., Allard, P., Bruno, N., Mure, F., Romano, R. (2004). Volcanic gas emissions from the summit craters and flanks of Mt. Etna, 1987–2000. In: Bonaccorso A, Calvari S, Coltelli M, Del Negro C, Falsaperla S (eds). Mt. Etna: Volcano Laboratory. Union Geophys. Monog. Ser., 143. https://doi.org/10.1029/143GM08.

Chesselet, R., Morelli, M., Buat-Menard, P. (1972). Some aspects of the geochemistry of marine aerosols. in D. Dyrssen and D. Jagner, (eds.). The Changing Chemistry of the Oceans, Proceedings of Nobel Symposium 20, Wiley-Interscience, New York, 92pp.

Chetelat, B., Gaillardeta, J., Freydierb, T. R., Négrel, P. (2005). Boron isotopes in precipitation: Experimental constraints and field evidence from French Guiana. Earth Planet Sc. Lett., 235, pp. 16-30. https://doi.org/10.1016/j.epsl.2005.02.014.

Cimino, G., Toscano, G. (1998). Dissolution of trace metals from lava ash: influence on the composition of rainwater in the Mount Etna volcanic area. Environ. Pollut., 99(3), pp. 389-393. https://doi.org/10.1016/S0269-7491(98)00004-9.

Correale, A., Paonita, A., Martelli, M., Rizzo, A., Rotolo, S. G., Corsaro, R. A., Di Renzo, V. (2014). A two-component mantle source feeding Mt. Etna magmatism: Insights from the geochemistry of primitive magmas. Lithos, 184(187), pp. 243–258. https://doi.org/10.1016/J.LITHOS.2013.10.038.

D'Alessandro, W., Katsanou, K., Lambrakis, N., Bellomo, S., Brusca, L., Liotta, M. (2013). Chemical and isotopic characterisation of bulk deposition in the Louros basin (Epirus, Greece). Atmos. Res., 132–133, pp. 399–410. https://doi.org/10.1016/j.atmosres.2013.07.007.

Derry, L. A. & Chadwick, O. A. (2007). Contributions from Earth's atmosphere to soil. Elements, 3(5), pp. 333–338. https://doi.org/10.2113/gselements.3.5.333.

Dia, A., Dupré, B., Allègre, C. J. (1992). Nd isotopes in Indian Ocean sediments used as a tracer of supply to the ocean and circulation paths. Marine Geology, 103(1-3), pp. 349–359. https://doi.org/10.1016/0025-3227(92)90025-D.

Dongarrà, G. & Francofonte, S. (1995). Quality of rainwater: A geochemical process of water-air-rock-life interaction. Geo, 25, pp. 149–155. https://doi.org/10.1007/BF00768544.

Dongarrà, G., Manno, E., Varrica, D., Vultaggio, M. (2007). Mass levels, crustal component and trace elements in PM10 in Palermo, Italy. Atmos. Environ., 41, (36), pp. 7977-7986, https://doi.org/10.1016/j.atmosenv.2007.09.015.

Eisenhut, S. & Heumann, K. G. (1997). Identification of groundwater contaminations by landfills using precise boron isotope ratio measurements with negative thermal ionization mass spectrometry. Freseneius J. Anal. Chem., 359, pp. 375–377. https://doi.org/10.1007/s002160050590.

EN 15841:2009. Ambient air quality - Standard method for determination of arsenic, cadmium, lead and nickel in atmospheric deposition.

Fernández-Olmo, I., Puente, M., Irabien, A. (2015). A comparative study between the fluxes of trace elements in bulk atmospheric deposition at industrial, urban, traffic, and rural sites. Environ. Sci. Pollut. Res., 22, pp. 13427–13441. https://doi.org/10.1007/s11356-015-4562-z.

Fogg, T. R. & Duce, R. A. (1985). Boron in troposphere: distribution and fluxes. J. Geophys. Res. Atmos., 90(D2), pp. 3781-3796. https://doi.org/10.1029/JD090iD02p03781.

Galy-Lacaux, C., Laouali, D., Descroix, L., Gobron, N., Liousse, C. (2009). Long term precipitation chemistry and wet deposition in a remote dry savanna site in Africa (Niger). Atmos. Chem. Phys., 9, pp. 1579–1595. https://doi.org/10.5194/acp-9-1579-2009.

Gauthier, P.-J. & Le Cloarec, M.-F. (1998). Variability of alkali and heavy metal fluxes released by Mt. Etna volcano, Sicily, between 1991 and 1995. J. Volcanol. Geoth. Res., 81, pp. 311–326. https://doi.org/10.1016/S0377-0273(98)00002-X.

Greaves, M. J., Statham, P. J., Elderfield, H. (1994). Rare earth element mobilization from marine atmospheric dust into seawater. Mar. Chem., 46, pp. 255–260. https://doi.org/10.1016/0304-4203(94)90081-7.

Guerzoni, S., Molinaroli, E., Rossini, P., Rampazzo, G., Quarantotto, G., De Falco, G., Cristini, S. (1999). Role of desert aerosol in metal fluxes in the Mediterranean area. Chemosphere, 39, pp. 229–246. https://doi.org/10.1016/S0045-6535(99)00105-8.

Han, G., Liu, C-Q. (2006). Strontium isotope and major ion chemistry of the rainwaters from Guiyang, Guizhou Province, China. Sci. Total. Environ., 364, pp. 165-174. https://doi.org/10.1016/j.scitotenv.2005.06.025.

Han, G., Tang, Y., Wu, Q., Tan, Q. (2010). Chemical and strontium isotope characterization of rainwater in karst virgin forest, Southwest China. Atmos. Environ., 44, pp. 174-181. https://doi.org/10.1016/j.atmosenv.2009.10.019.

Han, G., Wu, Q., Tang, Y. (2012). Acid rain and alkalization in southwestern China: chemical and strontium isotope evidence in rainwater from Guiyang. J. Atmos. Chem., 68, pp. 139-155. https://doi.org/10.1007/s10874-012-9213-x.

Huang, Y. L., Wang, Y. L., Zhang, L. P. (2008). Long-term trend of the chemical composition of wet atmospheric precipitation during 1986-2006 at Shenzhen City, China. Atmos. Environ., 42, 16, pp. 3740-3750. https://doi.org/10.1016/j.atmosenv.2007.12.063.

Inguaggiato, C., Censi, P., Zuddas, P., D'Alessandro, W., Brusca, L., Pecoraino, G., Bellomo, S. (2016). Zirconium–hafnium and rare earth element signatures discriminating the effect of atmospheric fallout from hydrothermal input in volcanic lake water. Chem. Geol., 433, pp. 1–11. https://doi.org/10.1016/j.chemgeo.2016.04.002.

Inguaggiato, C., Censi, P., Zuddas, P., Londoño, J. M., Chacón, Z., Alzate, D., Brusca, L., D'Alessandro, W. (2015). Geochemistry of REE, Zr and Hf in a wide range of pH and water composition: The Nevado del Ruiz volcano-hydrothermal system (Colombia). Chem. Geol., 417, pp. 125–133. https://doi.org/10.1016/j.chemgeo.2015.09.025.

Ito, A., Ye, Y., Baldo, C., Shi, Z. (2021). Ocean fertilization by pyrogenic aerosol iron, npj. Clim. Atmos. Sci., 4(30). https://doi.org/10.1038/s41612-021-00185-8, 2021.

Kanzaki, T., Yoshida, M., Nomura, M., Kakihana, H., Ozawa, T. (1979). Boron isotopic composition of fumarolic condensates and sassolites from Satsuma Iwo-jima, Japan. Geochim. Cosmochim. Ac., 43 (11), pp. 1859–1863. https://doi.org/10.1016/0016-7037(79)90035-8.

Khan, M. F., Latif, M. T., Saw, W. H., Amil, N., Nadzir, M. S. M., Sahani, M., Tahir, N. M., and Chung, J. X. (2016). Fine particulate matter in the tropical environment: monsoonal effects, source apportionment, and health risk assessment, Atmos. Chem. Phys., 16, pp. 597–617. https://doi.org/10.5194/acp-16-597-2016.

Kita, I., Sato, T., Kase, Y., Mitropoulos, P. (2004). Neutral rains at Athens, Greece: A natural safeguard against acidification of rains. Sci. Total Environ., 327, pp. 285–294. https://doi.org/10.1016/j.scitotenv.2004.01.012.

Klaver, G., Verheul, M., Bakker, I., Petelet-Giraud, E., Négrel, P. (2014). Anthropogenic Rare Earth Element in rivers: Gadolinium and lanthanum. Partitioning between the dissolved and particulate phases in the Rhine River and spatial propagation through the Rhine-Meuse Delta

(the Netherlands). Appl. Geochem., 47, pp. 186–197. https://doi.org/10.1016/j.apgeochem.2014.05.020.

Kulkarni, P., Chellam, S., Fraser, M. P. (2007). Tracking petroleum refinery emission events using lanthanum and lanthanides as elemental markers for PM2.5. Environ. Sci. Technol., 41, pp. 6748–6754. https://doi.org/10.1021/es062888i.

Kurisu, M., Sakata, K., Uematsu, M., Ito, A., Takahashi, Y. (2021). Contribution of combustion Fe in marine aerosols over the northwestern Pacific estimated by Fe stable isotope ratios. Atmos. Chem. Phys., 21, pp. 16027–16050. https://doi.org/10.5194/acp-21-16027-2021.

Laouali, D., Galy-Lacaux, C., Diop, B., Delon, C., Orange, D., Lacaux, J. P., Akpo, A., Lavenu, F., Gardrat, E., Castera, P. (2012). Long term monitoring of the chemical composition of precipitation and wet deposition fluxes over three Sahelian savannas. Atmos. Environ., 50, pp. 314–327. https://doi.org/10.1016/j.atmosenv.2011.12.004.

Lawrence, M. G., Greig, A., Collerson, K. D., Kamber, B. S. (2006). Direct quantification of rare earth element concentrations in natural waters by ICP-MS. Appl. Geochem., 21, pp. 839–848. https://doi.org/10.1016/j.apgeochem.2006.02.013.

Liotta, M., D'Alessandro, W., Arienzo, I., Longo, M. (2017). Tracing the circulation of groundwater in volcanic systems using the $^{87}Sr/^{86}Sr$ ratio: Application to Mt. Etna. J. Volcanol. Geoth. Res., 331, pp. 102-107. https://doi.org/10.1016/j.jvolgeores.2017.01.002.

Loya-González, D., López-Serna, D., Alfaro-Barbosa, J. M., López-Reyes, A., González-Rodríguez, H., Cantú-Silva, I. (2020). Chemical Composition of Bulk Precipitation and Its Toxicity Potential Index in the Metropolitan Area of Mt.rrey, Northeastern Mexico. Environments 7, 106. https://doi.org/10.3390/environments7120106.

Mahowald, N. M., Hamilton, D. S., Mackey, K. R. M., Moore, J. K., Baker, A. R., Scanza, R. A. Zhang, Y. (2018). Aerosol trace metal leaching and impacts on marine microorganisms. Nat. Commun., 9, pp. 1–15. https://doi.org/10.1038/s41467-018-04970-7.

McLennan, S. M. (1989). Chapter 7. Rare Earth Elements in Sedimentary Rocks: Influence of Provenance and Sedimentary Processes. Geochemistry and Mineralogy of Rare Earth Elements. De Gruyter, pp. 169–200. https://doi.org/10.1515/9781501509032-010.

Millot, R., Petelet-Giraud, E., Guerrot, C., Négrel, P. (2010). Multi-isotopic composition (^{7}Li– $\delta^{11}B$– δD– $\delta^{18}O$) of rainwaters in France: Origin and spatio-temporal characterization. Appl. Geochem., 25, pp. 1510-1524. https://doi.org/10.1016/j.apgeochem.2010.08.002.

Miyata, Y., Tokieda, T., Amakawa, H., Uematsu, M., Nozaki, Y. (2000). Boron isotope variations in the atmosphere. Tellus, 52B, pp. 1057-1065. https://doi.org/10.3402/tellusb.v52i4.17083.

Morera-Gómez, Y., Santamaría, J. M., Elustondo, D., Lasheras, E., Alonso-Hernández, C. M. (2019). Determination and source apportionment of major and trace elements in atmospheric bulk deposition in a Caribbean rural area, Atmos. Environ., 202, pp. 93-104, https://doi.org/10.1016/j.atmosenv.2019.01.019.

Moreda-Piñeiro, J., Alonso-Rodríguez, E., Turnes-Carou, I., Moscoso-Pérez, C., Blanco-Heras, G., Gómez Tellado, L., López-Mahía, P., Muniategui-Lorenzo, S., Prada-Rodríguez, D. (2017). Inorganic ions and trace metals bulk deposition at an Atlantic Coastal European region. J Atmos. Chem., 74, pp.1–21. https://doi.org/10.1007/s10874-016-9338-4.

Mphepya, J. N., Pienaar, J., Galy-Lacaux, C., Held, G., Turner, C. R., Mphepya, J. N., Pienaar, J. J., Galy-Lacaux, C., Turner, C. R. (2004). Precipitation chemistry in semi-arid areas of Southern Africa: A case study of a rural and an industrial site. J. Atmos. Chem., 47, pp. 1–24. https://doi.org/10.1023/B:JOCH.0000012240.09119.c4.

Négrel, P. & Roy, S. (1998). Chemistry of rainwater in the Massif Central (France): a strontium isotope and major element study. Appl. Geochem., 13(8), pp. 941-952. https://doi.org/10.1016/S0883-2927(98)00029-8.

Négrel, P., Guerrot, C., Millot, R. (2007). Chemical and strontium isotope characterization of rainwater in France: influence of sources and hydrogeochemical implications. Isot. Environ. Health S., 43(3), pp. 179-196. https://doi.org/10.1080/10256010701550773.

Nirel, R. & Dayan, U. (2001). On the Ratio of Sulfur Dioxide to Nitrogen Oxides as an Indicator of Air Pollution Sources. J. Appl. Meteorol. Climatol., 40, pp. 1209–1222. https://doi.org/10.1175/1520-0450(2001)040<1209:OTROSD>2.0.CO;2.

Nomura, M., Kanzaki, T., Ozawa, T., Okamoto, M., Kakihana, H. (1982). Boron isotopic composition of fumarolic condensates from some volcanoes in Japanese island arcs. Geochim. Cosmochim. Ac., 46, 11, pp. 2403–2406. https://doi.org/10.1016/0016-7037(82)90212-5.

Nunziata, G. P. (2023). Trace-elements monitoring of single rainwaters for the environmental risks assessment in the "Land of Fires" located between the provinces of Naples and Caserta. Environ. Earth Sci., 82, 186. https://doi.org/10.1007/s12665-023-10868-5.

Óskarsson, N. (1980). The interaction between volcanic gases and tephra: Fluorine adhering to tephra of the 1970 Hekla eruption. J. Volcanol. Geoth. Res., 8, 2–4, pp. 251-266. https://doi.org/10.1016/0377-0273(80)90107-9.

Palmer, M. R., Sturchio, N. C. (1990). The boron isotope systematics of the Yellowstone National Park (Wyoming) hydrothermal system: A reconnaissance. Geochim. Cosmochim. Ac., 54 (10), pp. 2811–2815. https://doi.org/10.1016/0016-7037(90)90015-D.

Park, H. & Schlesinger, W. H. (2002). Global biogeochemical cycle of boron. Global Biogeochem. Cycles, 16(4), 1072. https://doi.org/10.1029/2001GB001766, 2002.

Pearce, C. R., Parkinson, I. J., Gaillardet, J., Chetelat, B., Burton, K. W. (2015). Characterising the stable ($\delta^{88}/^{86}Sr$) and radiogenic ($^{87}Sr/^{86}Sr$) isotopic composition of strontium in rainwater. Chem. Geol., 409, pp. 54-60. http://dx.doi.org/10.1016/j.chemgeo.2015.05.010.

Pennisi, M. & Le Cloarec, M. F (1998). Variations of Cl, F, and S in Mt. Etna's plume, Italy, between 1992 and 1995. J. Geophys. Res. Solid Earth, 103, pp. 5061–5066. https://doi.org/10.1029/97JB03011.

Pennisi, M., Leeman, W. P., Tonarini S., Pennisi, A., Nabelek, P. (2000). Boron, Sr, O, and H isotope geochemistry of groundwaters from Mt. Etna (Sicily)—hydrologic implications. Geochim. Cosmochim. Ac., 64, 6, pp. 961-974. https://doi.org/10.1016/S0016-7037(99)00382-8.

Rose-Koga, E. F., Sheppard, S. M. F., Chaussidon, M., Carignan, J. (2006). Boron isotopic composition of atmospheric precipitations and liquid–vapour fractionations. Geochim. Cosmochim. Ac., 70, 7, pp. 1603-1615. https://doi.org/10.1016/j.gca.2006.01.003.

Sakata, K., Sakaguchi, A., Yamakawa, Y., Miyamoto, C., Kurisu, M., and Takahashi, Y. (2023). Measurement report: Stoichiometry of dissolved iron and aluminium as an indicator of the factors controlling the fractional solubility of aerosol iron – results of the annual observations of size-fractionated aerosol particles in Japan. Atmos. Chem. Phys., 23, pp. 9815–9836. https://doi.org/10.5194/acp-23-9815-2023.

Schlesinger, W. H., Klein, E. M., Vengosh, A. (2017). Global biogeochemical cycle of vanadium. Proc. Natl. Acad. Sci. USA, 114(52), E11092–E11100. https://doi.org/10.1073/pnas.1715500114.

Seinfeld, J. H., Pandis, S. N. (1998). Atmospheric Chemical Composition and Physics from Air Pollution to Climate Change; John Wiley and Sons, Incorporated: New York, NY, USA. https://scholar.google.com/scholar_lookup?title=Atmospheric+Chemical+Composition+and+Physics+from+Air+Pollution+to+Climate+Change&author=Seinfeld,+J.H.&author=Pandis,+S.N.&publication_year=1998.

Speirs, N. B., Belden, J. L., Hellum, A. M. (2023). The capture of airborne particulates by rain. J. Fluid Mech., 958, A40. https://doi.org/10.1017/jfm.2023.101.

Spivack, A. J. (1986). Boron isotope geochemistry. PhD Thesis. MIT-WHOI Joint Program in Oceanography, Cambridge, Massachusetts, USA. http://hdl.handle.net/1721.1/15187.

Tan, J. H., Duan, J. C., Ma, Y. L., Yang, F. M., Cheng, Y., He, K. B., Yu, Y. C., Wang, J. W. (2014). Source of atmospheric trace elements in winter in Foshan, China. Sci. Total Environ., 493, pp. 262–270. https://doi.org/10.1016/j.scitotenv.2014.05.147.

Thurston, G. D. & Spengler, J. D. (1985). A quantitative assessment of source contributions to inhalable particulate matter pollution in metropolitan Boston. Atmos. Environ., 19(1), pp. 9–25. https://doi.org/10.1016/0004-6981(85)90132-5.

Ueda, S., Iwamoto, Y., Taketani, F., Liu, M., and Matsui, H. (2023). Morphological features and water solubility of iron in aged fine aerosol particles over the Indian Ocean. Atmos. Chem. Phys., 23, pp. 10117–10135. https://doi.org/10.5194/acp-23-10117-2023.

UNECE (2021). Air. United Nations Economic Commission for Europe (https://unece.org/environment-policy/air), accessed on August 3, 2023.

UNECE (2021). Protocol on heavy metals. United Nations Economic Commission for Europe (https://unece-modl.dotsoft.gr/environment-policyair/protocol-heavy-metals), accessed on August 7, 2023.

UNI EN ISO 14902:2005. Ambient air quality - Standard method for the measurement of Pb, Cd, As and Ni in the PM10 fraction of suspended particulate matter.

Varrica, D. & Alaimo, M. G. (2023). Determination of Water-Soluble Trace Elements in the PM10 and PM2.5 of Palermo Town (Italy). Int. J. Environ. Res. Public Health, 20, 724. https://doi.org/10.3390/ijerph20010724.

Wieland, E. & Stumm, W. (1992). Dissolution kinetics of kaolinite in acidic solutions at 25°C. Geochim. Cosmochim. Acta, 56(9), pp. 3339-3355. https://doi.org/10.1016/0016-7037(92)90382-S.

Witham, C. S., Oppenheimer, C., Horwell, C. J. (2005). Volcanic ash-leachates: a review and recommendations for sampling methods. J. Volcanol. Geoth. Res., 141, 3–4, pp. 299-326. https://doi.org/10.1016/j.jvolgeores.2004.11.010.

Xiao, Y., Sun, D., Wang, Y., Qi, H., Jin, L. (1992). Boron isotopic compositions of brine, sediments, and source water in Da Qaidam Lake, Qinghai, China. Geochim. Cosmochim. Ac., 56, 4, pp. 1561-1568. https://doi.org/10.1016/0016-7037(92)90225-8.

Xing, J., Song, J., Yuan, H., Li, X., Li, N., Duan, L., Qu, B., Wang, Q., Kang, X. (2017). Chemical characteristics, deposition fluxes and source apportionment of precipitation components in the Jiaozhou Bay, North China. Atmos. Res., 190, pp. 10–20. https://doi.org/10.1016/j.atmosres.2017.02.001.

Xu, Z. & Han, G. (2009). Chemical and strontium isotope characterization of rainwater in Beijing, China. Atmos. Res., 43, pp. 1954-1961. https://doi.org/10.1016/j.atmosenv.2009.01.010.

Xu, Z., Li, Y., Tang, Y., Han, G. (2009). Chemical and strontium isotope characterization of rainwater at an urban site in Loess Plateau, Northwest China. Atmos. Res., 94, pp. 481-490. https://doi.org/10.1016/j.atmosres.2009.07.005.

Xu, Z., Tang, Y., Ji, J. (2012). Chemical and strontium isotope characterization of rainwater in Beijing during the 2008 Olympic year. Atmos. Res., 107, pp. 115-125. https://doi.org/10.1016/j.atmosres.2012.01.002.

Yang, X., Liu, Y., Li, C., Song, Y., Zhu, H., Jin, X. (2007). Rare earth elements of aeolian deposits in Northern China and their implications for determining the provenance of dust storms in Beijing. Geomorphology, 87, pp. 365–377. https://doi.org/10.1016/j.geomorph.2006.10.004.

Ye, L., Huang, M., Zhong, B., Wang, X., Tu, Q., Sun, H., Wang, C., Wu, L., Chang, M. (2018). Wet and dry deposition fluxes of trace elements in Pearl River Delta Region (China): Characteristics, ecological risk assessment, and source apportionment. J. Environ. Sci., 70, pp. 106–123. https://doi.org/10.1016/j.jes.2017.11.019.

Zhao, Z-Q., Liu, C-Q. (2010). Anthropogenic inputs of boron into urban atmosphere: Evidence from boron isotopes of precipitations in Guiyang City, China. Atmos. Environ., 44, pp. 4165-4171. https://doi.org/10.1016/j.atmosenv.2010.07.035.

Zhu, Z., Liu, C. Q., Wang, Z. L., Liu, X., Li, J. (2016). Rare earth elements concentrations and speciation in rainwater from Guiyang, an acid rain impacted zone of Southwest China. Chem. Geol., 442, pp. 23–34. https://doi.org/10.1016/j.chemgeo.2016.08.038.

6. Conclusions

Atmospheric deposition is a major way in which various chemicals enter terrestrial and aquatic ecosystems. These chemicals include sea spray, geogenic dust, anthropogenic particulate matter, polycyclic aromatic hydrocarbons, and volcanic ash. Recently, research on atmospheric deposition has increased significantly. This is due to its important contribution to explaining pollution phenomena in various environmental compartments. It also allows for evaluating the impacts of pollution sources at both short and long distances, as well as conducting long-term studies to perform health impact assessments on the exposed population.

This PhD study aims to enhance our understanding of the geochemical properties of atmospheric deposition in the Mediterranean basin. The study characterises physical-chemical parameters, major ions, trace and ultra-trace elements, and B and Sr isotopic ratios of bulk atmospheric depositions in four different areas with diverse environmental conditions. These areas include volcanic, urban, industrial, and rural environments, each with varying sources of gaseous species and atmospheric particulate matter. As these areas are located in the middle of the Mediterranean Basin, they are influenced by both local-scale and regional-scale sources such as marine, geogenic (Saharan dust), and anthropogenic sources related to European-scale emissions.

The acidity of rainwater is often neutralised by naturally occurring cations, particularly nss-Ca^{2+} and nss-Mg^{2+}. However, rainwater can be further acidified by nss-SO_4^{2-} and NO_3^-. In the Mt. Etna region, volcanic halogens like HCl, HF, and HBr contribute to rainwater's high acidity levels. This makes it harder to neutralise the acidity of rainwater in this area. The most effective neutralisation of rainwater acidity was observed in Palermo, an urban area where rocks and soils with carbonate composition are prevalent. The results confirm the buffering role of the natural acidity of rainwater by the atmospheric geogenic particulate matter (with a high content of Ca^{2+} and Mg^{2+}), which represents a significant source of CCNs of raindrops.

The study investigated the concentrations and deposition fluxes of major ions in the soluble fraction of bulk atmospheric deposition. The results showed that the Mt. Etna area had significantly higher concentrations and deposition fluxes of most of the investigated ions (F^-, SO_4^{2-}, Cl^-, Mg^{2+}, NH_4^+, and K^+) compared to other study areas. This indicates a large contribution of volcanic activity to rainwater in the Mt. Etna sampling sites, as well as, although to a lesser extent, in the urban area of Catania, the industrial area of Priolo Gargallo, and occasionally in the Mt. Soro rural site. Another significant contributor of ions was the marine source. Statistical techniques such as PCA and PMF were used to identify the contributors of various ions. Sodium and partly Cl^- and Mg^{2+} were found to be derived from the dissolution of sea-salt aerosols, especially in coastal urban and industrial areas. For Ca^{2+}, HCO_3^-, and to some extent Mg^{2+} and K^+, the main contributor was the dissolution of crustal materials, with the highest concentrations and deposition fluxes found in the Palermo study area, which is characterised by carbonate rocks and soils. Anthropogenic sources, such as biomass combustion, agricultural activities, urban emissions, and industrial emissions of NOx and SOx, contributed to the nitrogen species (NH_4^+ and NO_3^-), K^+, and SO_4^{2-} concentrations found in rainwater. The production of ceramics and cement was identified as the primary source of F^- found in rainwater in the Milazzo area.

The study investigated the distribution of trace elements between the soluble and insoluble fractions of atmospheric deposition by determining their concentration and deposition fluxes in both fractions. The study conducted on the soluble fraction of atmospheric deposition at Mt. Etna sites showed that elements commonly found in volcanic emissions such as Ti, Al, Tl, Te, and V were highly enriched. Rainwater samples with low pH values (ranging from 3.0 to 4.5) were frequent in the area, and metals such as Al and Fe contributed significantly to the total dissolved species, indicating that the solid phase (volcanic ash and particulate matter) had efficiently dissolved in acid rainwater. The comparable amounts of Sr found in all study areas suggested that this element originated from geogenic dust, likely in the form of resuspended volcanic ash or soil dust from both

local and regional sources. The urban and industrial areas showed enrichment of Cr, Mo, Fe, and Sb, reflecting the contribution of anthropogenic emissions (brake wear emissions). The Priolo Gargallo industrial area, in particular, was identified as a critical source of Sb and Zn (brake and tyre wear emissions), with deposition fluxes for these two elements even an order of magnitude higher than for the other study areas. Finally, bromide was attributed to a combination of sea-salt aerosols and volcanic emissions. The study found that the abundance order of the analysed elements in the insoluble fraction was as follows: Al > Fe > Ti > Mn > Sr > Ba > Cu > Zn > V > B > Cr > Li > Pb > Ni > Co > As > Mo. This means that elements like Fe, Ti, Al, and Pb that are poorly soluble were concentrated in the solid phase when atmospheric particulate matter interacted with rainwater. On the other hand, highly soluble elements like Mo, Sr, and B were dissolved in rainwater and had lower concentrations in this fraction. Some trace element concentrations were measured in the solutions obtained from the material deposited on the sides of the bulk collector. During the dry period, the concentrations were higher compared to the wettest period, with up to 15 times increase for elements such as Mn, Ba, Cd, Li, and Rb. The more soluble the species, the easier it is for them to be transferred to the plants and animals in the region, with potential impact also on human health.

The trace element concentrations of three solutions were compared to determine the composition of atmospheric bulk deposition. The results showed that during a long rain-free phase before sampling, the majority of atmospheric bulk deposition was made up of the insoluble fraction for all elements except for B, Sr, Mo, and Ba. Titanium and Fe had the highest relative contributions of up to 98.4%. In contrast, during a rainy period up to a few hours before sampling, the largest contribution to bulk atmospheric deposition for Ti, Fe, Al, Cr, Li, Pb, Ni, Co, V, and As came from the insoluble fraction, with relative contributions of up to 98.0% for Ti and Fe, and for the remaining elements from the soluble fraction. The recovery fraction made almost no contribution, with a maximum value of 9.37% for Pb. The results showed that the dissolution of dry deposition contributed to the chemical composition of bulk atmospheric deposition. Failure to recover this solid

fraction can lead to an underestimation of bulk atmospheric deposition fluxes, especially when sampling is carried out several days after the last rainfall. During this time, dry deposition remains confined to the sides of the bulk collector and is not dissolved by the rain.

During the period from 13 December 2020 to 21 February 2022, Mt. Etna experienced a long sequence of paroxysms that led to abundant ash deposition. To understand the impact of this volcanic ash on the chemical composition of atmospheric deposition, a comparison was made between the daily depositions at selected sites during periods of abundant ash deposition and periods when it was less abundant or absent. The selected sites were Citelli, Zafferana Etnea, Cratere 2001, Catania, San Giovanni La Punta, Siracusa, and Priolo Gargallo. The concentration of minor and trace elements in both the soluble and insoluble fractions was considered for the comparison. The results showed that Etna's paroxysmal activity had a significant impact on the chemical composition and quantity of bulk atmospheric deposition at the sites affected by volcanic ash fallout. The differences in deposition fluxes of trace elements in the insoluble fraction were particularly significant. The site where the greatest differences were observed was Zafferana Etnea, both in the soluble and insoluble fractions. The acidity conditions of the rainwater with which atmospheric particulate, especially volcanic ash, interacted, also greatly influenced the concentration and daily atmospheric deposition values of trace elements in the soluble fraction.

The study analysed the concentration of TCEs (Sc, Zr, Nb, Ge, Y, Te, Hf, Th, La, Ce, Pr, Nd, Sm, Eu, Gd, Tb, Dy, Ho, Er, Tm, Yb, and Lu) in rainwater samples that were preconcentrated. The research revealed that the urban areas had the highest concentrations of Sc, Zr, Nb, and Hf, while the rainwater of the Etna area had the highest concentrations of Ge, Y, and Te. The concentration of Th was found to be similar in all the studied environments. The study also highlighted that rainwater from Mt. Etna had the highest concentrations of all lanthanoids. These findings suggest that volcanic sources and the leaching of volcanic ash can enrich rainwater with these elements. This is significant

since these elements are usually present in low concentrations in rainwater and are difficult to quantify.

Finally, B and Sr isotopic ratios were measured in some of the atmospheric deposition samples collected during the research. This provided the first comprehensive study of B and Sr isotopes in Sicilian rainwaters. The study found that sea salt aerosols, anthropogenic emissions, and volcanic emissions were the primary sources of B in the study area atmospheres. On the other hand, geogenic dust was probably the main source of Sr, although the most clearly distinguishable contributions were marine and volcanic. These are the first measurements of B and Sr isotopes in an atmosphere influenced by the volcanic source. This framework could be used in future studies to illustrate how these data for rainwater samples can add to the global understanding of geochemical processes in hydrology. Finally, this work also adds to the potential for the use of B and Sr isotopes as environmental tracers.

The research conducted for this PhD study has provided new insights into the chemical and isotopic compositions of the bulk atmospheric deposition in the Mediterranean Basin. By closely examining the characteristics of different sources present in the study areas and analysing the soluble and insoluble components of atmospheric deposition, as well as the concentrations of TCEs in rainwater and the B and Sr isotopic compositions, this work presents a valuable tool for future investigations into atmospheric deposition in diverse environments and various purposes.

Supplementary materials

Table S. 1 - Number of samples analysed for each aliquot. For each element, the number of samples in which it was measured is indicated. RAIN UN = rain untreated; RAIN F = filtered rainwater; RAIN FA = filtered and acidified rainwater; MEM = mineralised membrane; REC = rinse solutions; PC = preconcentrated samples; RAIN B = rainwater blanks; MEM B = membrane blanks; REC B = recovery blanks; PC B = preconcentrated blanks.

Aliquot	RAIN UN	RAIN F	RAIN FA	MEM	REC	PC	RAIN B	MEM B	REC B	PC B
Total n.	**301**	**301**	**300**	**300**	**25**	**98**	**27**	**38**	**4**	**3**
F^-	/	301	/	/	/	/	/	/	/	/
Cl^-	/	301	/	/	/	/	/	/	/	/
NO_3^-	/	301	/	/	/	/	/	/	/	/
SO_4^{2-}	/	301	/	/	/	/	/	/	/	/
HCO_3^-	297	/	/	/	/	/	/	/	/	/
H^+	301	/	/	/	/	/	/	/	/	/
Na^+	/	301	/	300	/	/	/	/	/	/
K^+	/	/	301	300	/	/	/	/	/	/
NH_4^+	/	/	219	/	/	/	/	/	/	/
Mg^{2+}	/	/	301	300	/	/	/	/	/	/
Ca^{2+}	/	/	301	300	/	/	/	/	/	/
Li	/	/	301	300	25	/	23	38	4	/
B	/	/	301	300	25	/	23	38	4	/
Al	/	/	301	300	25	/	23	38	4	/
Sc	/	/	/	/	/	98	/	/	/	/
Ti	/	/	301	300	25	/	23	38	4	/
V	/	/	301	300	25	/	23	38	4	/
Cr	/	/	301	300	25	/	22	38	4	/
Mn	/	/	301	300	25	/	23	38	4	/
Fe	/	/	301	300	25	/	23	38	4	/
Co	/	/	301	300	25	/	23	38	4	/
Ni	/	/	301	300	25	/	23	38	4	/
Cu	/	/	301	300	25	/	23	38	4	/
Zn	/	/	301	300	25	/	23	38	4	/
Ge	/	/	/	/	/	98	/	/	/	/
As	/	/	301	300	25	/	23	38	4	/
Se	/	/	301	/	25	/	23	38	4	/
Br	/	/	301	/	25	/	19	38	4	/
Rb	/	/	301	/	25	/	23	38	4	/
Sr	/	/	301	300	25	/	23	38	4	/
Y	/	/	/	/	/	98	/	/	/	3
Zr	/	/	/	/	/	98	/	/	/	/
Nb	/	/	/	/	/	98	/	/	/	/
Mo	/	/	301	300	25	/	23	38	4	/
Cd	/	/	301	/	25	/	23	38	4	/
Sn	/	/	301	/	25	/	10	38	/	/
Sb	/	/	301	/	25	/	23	38	4	/
Te	/	/	301	/	/	/	/	/	/	/
Cs	/	/	301	/	25	/	23	38	4	/
Ba	/	/	301	300	25	/	22	38	4	/
La	/	/	/	/	/	98	/	/	/	3
Ce	/	/	/	/	/	98	22	/	/	3
Pr	/	/	/	/	/	98	/	/	/	3
Nd	/	/	/	/	/	98	/	/	/	3
Sm	/	/	/	/	/	98	/	/	/	3
Eu	/	/	/	/	/	98	/	/	/	3
Gd	/	/	/	/	/	98	/	/	/	3
Tb	/	/	/	/	/	98	/	/	/	3
Dy	/	/	/	/	/	98	/	/	/	3
Ho	/	/	/	/	/	98	/	/	/	3
Er	/	/	/	/	/	98	/	/	/	3
Tm	/	/	/	/	/	98	/	/	/	3
Yb	/	/	/	/	/	98	/	/	/	3
Lu	/	/	/	/	/	98	/	/	/	3
Hf	/	/	/	/	/	98	/	/	/	/
Tl	/	/	301	/	25	/	23	38	4	/
Pb	/	/	301	300	25	/	23	38	4	/
Th	/	/	/	/	/	98	/	/	/	/
U	/	/	301	/	25	/	23	38	4	/
$\delta^{11}B$	29	/	/	/	/	/	/	/	/	/
$^{87}Sr/^{86}Sr$	29	/	/	/	/	/	/	/	/	/

Table S. 2 - pH, Electric Conductivity – EC (µS cm^{-1}) and major ions concentrations (µg L^{-1}) in rainwater samples for all the sampling sites.

Sample	pH	EC	F^-	Cl^-	NO_3^-	SO_4^{2-}	Alkalinity as HCO_3^-	Na^+	K^+	NH_4^+	Mg^{2+}	Ca^{2+}
		µS cm^{-1}	µg L^{-1}	µg L^{-1}	µg L^{-1}	µg L^{-1}	µg L^{-1}	µg L^{-1}	µg L^{-1}	µg L^{-1}	µg L^{-1}	µg L^{-1}
CIT 01_Rain	5.71	37.2	1965	6553	<LOQ	6480	3990	1865	979	<LOQ	690	4641
CIT 02_Rain	6.44	63.4	1186	8573	212	8011	2320	1109	825	<LOQ	911	8278
CIT 03_Rain	6.50	68.3	1991	8946	1219	11774	5290	1117	1835	2108	1099	7921
CIT 04_Rain	6.09	29.7	1303	<LOQ	1569	4406	2170	1121	1352	699	632	3853
CIT 05_Rain	7.34	103	2489	5542	1854	24624	<LOQ	3718	6794	3101	1799	13127
CIT 06_Rain	5.98	28.8	1423	3525	1042	15326	<LOQ	2496	1247	2562	800	6036
CIT 07_Rain	3.11	64.0	1001	7295	973	5352	0.00	837	508	534	294	1261
CIT 08_Rain	5.42	33.7	1467	7551	434	4099	4050	2905	606	270	744	3641
CIT 09_Rain	4.43	35.3	200	3997	1029	2285	4150	1778	129	347	295	707
CIT 10_Rain	3.07	386	4598	45958	174	3254	0.00	1622	805	52.7	980	1772
CIT 11_Rain	3.14	140	1490	10757	831	5760	0.00	1277	520	145	401	966
CIT 12_Rain	6.42	23.4	469	4757	1370	3648	<LOQ	2576	411	206	525	2345
CIT 13_Rain	4.14	38.9	14.8	5297	663	3619	4210	1934	473	216	241	649
CIT 14_Rain	6.07	88.5	2550	14626	2561	15336	<LOQ	2693	1103	633	1635	14613
CIT 15_Rain	4.64	23.9	154	2915	812	2371	<LOQ	1090	383	5467	453	1972
CIT 16_Rain	5.73	240	3773	35812	4855	22646	<LOQ	9451	8989	3908	4273	11028
CIT 17_Rain	3.39	148	779	10920	2703	7603	0.00	1017	1570	n.d.	427	2143
CIT 18_Rain	3.09	280	4507	23771	1246	5251	0.00	1348	910	n.d.	660	2218
CIT 19_Rain	3.89	46.8	1062	4991	806	2597	0.00	225	570	n.d.	335	1500
CIT 20_Rain	3.80	109	1425	8218	676	2746	0.00	722	850	n.d.	485	2028
CIT 21_Rain	3.86	42.4	855	6088	446	1454	0.00	847	270	n.d.	191	790
CIT 22_Rain	4.20	136	1991	15737	763	12346	0.00	5015	1620	n.d.	1129	3768
CIT 23_Rain	3.57	84.0	222	6596	632	4243	0.00	1501	340	n.d.	281	1613

Sample	pH	EC	F^-	Cl^-	NO_3^-	SO_4^{2-}	Alkalinity as HCO_3^-	Na^+	K^+	NH_4^+	Mg^{2+}	Ca^{2+}
		$\mu S\ cm^{-1}$	$\mu g\ L^{-1}$	$\mu g\ L^{-1}$	$\mu g\ L^{-1}$	$\mu g\ L^{-1}$	$\mu g\ L^{-1}$	$\mu g\ L^{-1}$	$\mu g\ L^{-1}$	$\mu g\ L^{-1}$	$\mu g\ L^{-1}$	$\mu g\ L^{-1}$
ZAF 01_Rain	6.14	33.8	386	3280	<LOQ	11486	3910	1548	955	<LOQ	675	4576
ZAF 02_Rain	7.10	43.2	49.4	4459	234	3010	2850	2026	695	996	693	3971
ZAF 03_Rain	7.65	75.5	255	4718	3379	12816	<LOQ	2058	5701	4214	1458	9184
ZAF 04_Rain	6.16	146	24130	51550	7800	3862	<LOQ	14213	13327	13406	6854	29160
ZAF 05_Rain	5.91	138	17129	19262	2734	1199	4280	6141	5941	1149	3379	13054
ZAF 06_Rain	6.39	4.50	169	1090	2083	2688	3610	750	1439	389	336	3252
ZAF 07_Rain	3.45	35.2	355	3568	1730	4046	0.00	1240	325	469	271	1128
ZAF 08_Rain	5.68	19.9	58.9	3064	750	1382	2200	1571	207	163	397	1124
ZAF 09_Rain	5.26	24.9	24.7	2510	750	1330	2150	1589	121	272	226	545
ZAF 10_Rain	4.16	18.1	260	2627	<LOQ	1042	0.00	777	54.7	66.3	121	248
ZAF 11_Rain	3.70	52.3	211	5574	2046	3658	0.00	2070	379	763	413	994
ZAF 12_Rain	5.71	55.9	3116	7491	2672	9552	<LOQ	4968	1177	602	999	5030
ZAF 13_Rain	5.30	16.1	7.22	4416	905	2750	2170	2523	137	507	346	521
ZAF 14_Rain	6.91	33.9	133	3862	2703	8851	10090	2233	633	1214	927	9453
ZAF 15_Rain	5.92	27.7	34.2	3117	1445	2054	8890	2206	184	1464	433	2122
ZAF 16_Rain	6.59	53.4	654	1523	2294	8712	5470	1953	2467	1073	793	4048
ZAF 17_Rain	3.42	159	929	8438	1990	5803	0.00	651	530	n.d.	175	838
ZAF 18_Rain	3.76	86.4	492	10210	2883	4459	0.00	4292	400	n.d.	626	1393
ZAF 19_Rain	4.55	49.0	334	6078	2629	3605	<LOQ	1541	440	n.d.	519	2610
ZAF 20_Rain	5.43	30.6	72.2	3014	2065	2333	<LOQ	1081	240	n.d.	338	2670
ZAF 21_Rain	5.24	12.1	60.8	2247	701	1080	<LOQ	1058	80.0	n.d.	171	613
ZAF 22_Rain	5.47	34.4	146	5410	738	1814	<LOQ	2938	130	n.d.	437	1285
ZAF 23_Rain	6.03	24.3	17.1	4367	260	1267	13780	2647	100	n.d.	307	193

Sample	pH	EC	F^-	Cl^-	NO_3^-	SO_4^{2-}	Alkalinity as HCO_3^-	Na^+	K^+	NH_4^+	Mg^{2+}	Ca^{2+}
		$\mu S\ cm^{-1}$	$\mu g\ L^{-1}$	$\mu g\ L^{-1}$	$\mu g\ L^{-1}$	$\mu g\ L^{-1}$	$\mu g\ L^{-1}$	$\mu g\ L^{-1}$	$\mu g\ L^{-1}$	$\mu g\ L^{-1}$	$\mu g\ L^{-1}$	$\mu g\ L^{-1}$
TDF 02_Rain	7.04	43.2	821	2702	292	6086	8820	1222	673	<LOQ	503	5531
TDF 03_Rain	7.24	60.9	401	2442	4526	5818	2220	1308	1360	<LOQ	740	7861
TDF 04_Rain	5.81	16.6	7277	38021	350	61555	9370	12384	11237	10693	4083	22455
TDF 05_Rain	5.82	184	5757	20349	218	38957	7760	10133	9461	5029	2457	13170
TDF 06_Rain	7.04	19.6	591	3926	1581	5626	5520	2289	1001	<LOQ	897	9545
TDF 07_Rain	3.46	77.1	1112	6979	1637	8366	0.00	1274	782	1501	442	2723
TDF 08_Rain	5.76	11.9	60.8	1338	267	912	2130	621	164	51.0	306	1010
TDF 09_Rain	5.67	21.9	22.8	1388	856	1195	2210	922	<LOQ	185	187	1220
TDF 12_Rain	3.92	658	40660	225780	<LOQ	189600	0.00	71070	19538	1307	11402	58517
TDF 13_Rain	4.66	127	7938	12010	1023	52699	4110	8257	4203	622	2520	10637
TDF 14_Rain	6.49	177	3813	13224	2561	34238	6590	4812	2796	380	1926	20898
TDF 15_Rain	5.66	58.5	49541	142689	<LOQ	552341	16720	1387	559	209	502	6707
TDF 16_Rain	5.33	339	<LOQ	<LOQ	<LOQ	<LOQ	5410	89976	30494	13258	18941	147695
TDF 17_Rain	3.36	457	8436.0	61972	3677	34531	0.00	30340	10450	n.d.	2231	9845
TDF 18_Rain	4.45	32.8	703.0	2148	918	4570	<LOQ	641	310	n.d.	247	1140
TDF 19_Rain	4.14	49.8	646.0	1828	1451	7733	0.00	533	220	n.d.	236	1663
TDF 21_Rain	5.16	36.6	870.2	4800	887	3528	<LOQ	1696	390	n.d.	405	2025
TDF 23_Rain	3.12	420	15225	68817	1903	45614	0.00	12261	6080	n.d.	4704	17523

Sample	pH	EC	F^-	Cl^-	NO_3^-	SO_4^{2-}	Alkalinity as HCO_3^-	Na^+	K^+	NH_4^+	Mg^{2+}	Ca^{2+}
		$\mu S\ cm^{-1}$	$\mu g\ L^{-1}$	$\mu g\ L^{-1}$	$\mu g\ L^{-1}$	$\mu g\ L^{-1}$	$\mu g\ L^{-1}$	$\mu g\ L^{-1}$	$\mu g\ L^{-1}$	$\mu g\ L^{-1}$	$\mu g\ L^{-1}$	$\mu g\ L^{-1}$
INT 03_Rain	7.72	48.9	134.9	3007	681	7512	12240	1184	3013	<LOQ	913	8100
INT 04_Rain	7.31	74.1	150.0	4210	3794	11875	<LOQ	1660	13696	10219	2482	6476
INT 05_Rain	7.56	137	2453	5137	4543	10238	<LOQ	2041	14217	3689	2889	11378
INT 06_Rain	7.16	8.20	34.2	543	1724	1310	4240	536	407	683	338	3234
INT 07_Rain	5.07	15.9	<LOQ	1104	1550	2002	<LOQ	771	<LOQ	571	204	1305
INT 08_Rain	5.79	17.2	214.7	2542	<LOQ	1190	<LOQ	706	246	<LOQ	305	1535
INT 09_Rain	5.52	11.4	5.70	824	843	922	2490	552	<LOQ	<LOQ	164	1016
INT 10_Rain	5.11	7.10	17.1	1257	304	576	<LOQ	826	31.3	57.8	116	295
INT 11_Rain	4.59	21.4	36.1	3657	676	1200	<LOQ	2045	184	196	391	938
INT 12_Rain	5.68	37.8	825	16188	2449	7008	4130	7337	606	843	1050	2405
INT 13_Rain	4.14	59.0	251	7934	1860	4133	4120	1904	426	808	370	1495
INT 14_Rain	7.47	68.2	74.1	2052	2691	7690	32510	1599	594	778	868	13108
INT 15_Rain	5.63	58.2	177	9163	1544	7368	5310	812	461	687	657	6429
INT 16_Rain	4.95	187	<LOQ	13472	10441	23477	<LOQ	9117	6815	2963	3833	18717
INT 17_Rain	6.14	27.4	41.8	724	1928	2482	5440	196	210	n.d.	155	980
INT 18_Rain	5.58	17.7	15.2	1523	1271	1378	<LOQ	841	90.0	n.d.	184	1030
INT 19_Rain	5.97	14.7	17.1	639	1358	1099	<LOQ	238	150	n.d.	161	1283
INT 20_Rain	5.64	13.9	15.2	1164	837	1171	<LOQ	636	80	n.d.	210	1095
INT 21_Rain	4.02	44.9	188	6106	601	1330	0.00	1000	280	n.d.	182	860
INT 22_Rain	5.76	60.1	15.2	9830	1011	2088	<LOQ	6189	280	n.d.	778	1450
INT 23_Rain	4.67	17.4	11.4	1402	1135	1382	5530	588	40.0	n.d.	150	430

Sample	pH	EC	F^-	Cl^-	NO_3^-	SO_4^{2-}	Alkalinity as HCO_3^-	Na^+	K^+	NH_4^+	Mg^{2+}	Ca^{2+}
		$\mu S\ cm^{-1}$	$\mu g\ L^{-1}$	$\mu g\ L^{-1}$	$\mu g\ L^{-1}$	$\mu g\ L^{-1}$	$\mu g\ L^{-1}$	$\mu g\ L^{-1}$	$\mu g\ L^{-1}$	$\mu g\ L^{-1}$	$\mu g\ L^{-1}$	$\mu g\ L^{-1}$
ARC 01_Rain	6.96	30.5	<LOQ	5676	157	<LOQ	5000	3229	119	<LOQ	826	3481
ARC 02_Rain	7.15	59.5	<LOQ	4693	447	3278	16730	2532	434	<LOQ	1138	8801
ARC 03_Rain	7.54	117	<LOQ	4704	3840	1834	29650	3098	3634	<LOQ	2721	26338
ARC 04_Rain	7.93	97.3	70	7533	16734	15749	64600	3892	2043	<LOQ	1450	17042
ARC 05_Rain	7.68	89.1	<LOQ	7363	439	4694	52730	4234	1345	<LOQ	1799	24810
ARC 06_Rain	5.61	14.9	114	5772	10224	6307	50460	3485	1060	<LOQ	1135	9772
ARC 07_Rain	6.73	66.3	32	3997	2145	2755	22480	2479	368	<LOQ	812	8413
ARC 08 A_Rain	6.04	11.5	<LOQ	5169	1414	1733	4200	3061	297	340	726	1886
ARC 08 B_Rain	5.90	31.3	68	3479	2071	2736	<LOQ	1815	262	955	633	1976
ARC 09_Rain	5.97	33.9	<LOQ	2240	1693	1718	6240	1417	129	461	391	2491
ARC 10_Rain	5.66	75.8	<LOQ	15989	632	2290	4130	9350	305	153	1223	1032
ARC 11_Rain	6.31	57.6	<LOQ	15301	1606	3221	7000	8993	297	<LOQ	1513	3407
ARC 12_Rain	6.82	118	<LOQ	20839	2840	4147	9270	11684	727	609	1820	4669
ARC 13_Rain	6.48	109	39.9	18740	3801	4930	7630	10909	958	945	1605	4305
ARC 14_Rain	6.78	39.1	<LOQ	3823	1259	1944	7320	2491	192	186	648	2689
ARC 15_Rain	6.10	37.3	<LOQ	476	1370	1747	15340	596	164	50.5	611	4956
ARC 16_Rain	7.40	215	<LOQ	13739	<LOQ	9317	62670	8876	1103	2325	2176	20910
ARC 17_Rain	7.44	62.0	17.1	4913	5679	3106	6240	4990	2165	n.d.	1003	5186
ARC 18_Rain	7.02	62.3	30.4	2769	1228	1733	25900	2003	150	n.d.	634	4673
ARC 19_Rain	6.80	40.4	13.3	2521	1736	1474	9800	1797	90.0	n.d.	541	3028
ARC 20_Rain	5.95	43.1	7.60	6759	1327	1565	7970	4735	285	n.d.	759	2148
ARC 21_Rain	6.30	81.1	20.9	9777	2647	2851	24240	5996	405	n.d.	1146	8173
ARC 22_Rain	6.02	109	7.60	18407	1730	2981	9860	11045	480	n.d.	1521	3815
ARC 23_Rain	5.21	73.9	30.4	13852	763	2486	<LOQ	8540	310	n.d.	1091	1095

Sample	pH	EC	F^-	Cl^-	NO_3^-	SO_4^{2-}	Alkalinity as HCO_3^-	Na^+	K^+	NH_4^+	Mg^{2+}	Ca^{2+}
		$\mu S\ cm^{-1}$	$\mu g\ L^{-1}$	$\mu g\ L^{-1}$	$\mu g\ L^{-1}$	$\mu g\ L^{-1}$	$\mu g\ L^{-1}$	$\mu g\ L^{-1}$	$\mu g\ L^{-1}$	$\mu g\ L^{-1}$	$\mu g\ L^{-1}$	$\mu g\ L^{-1}$
UNI 01_Rain	6.61	23.8	<LOQ	5084	124	<LOQ	3630	2767	100	<LOQ	704	1586
UNI 02_Rain	7.31	53.3	<LOQ	3958	3143	3466	15400	2045	229	411	1008	7576
UNI 03_Rain	7.07	75.5	85.5	7803	11451	8789	38690	4017	2813	1561	1784	11469
UNI 04_Rain	7.34	108	152.0	6017	1854	15926	34770	3344	5861	2798	1970	19017
UNI 05_Rain	7.49	39.4	<LOQ	5850	2530	2635	23940	3190	940	<LOQ	1941	10179
UNI 06_Rain	7.12	16.8	47.5	4193	7769	3682	43010	2749	696	<LOQ	702	6066
UNI 07_Rain	6.57	54.3	60.8	3951	3001	2558	11950	2537	352	<LOQ	968	5557
UNI 08_Rain	6.19	22.2	<LOQ	3806	1128	1637	4860	2330	262	287	582	1531
UNI 09_Rain	6.05	21.4	<LOQ	2166	1891	1819	3310	1364	117	286	390	2455
UNI 10_Rain	6.03	44.1	9.50	14491	626	2035	2170	8597	266	143	1103	790
UNI 11_Rain	6.19	67.4	<LOQ	12496	1370	2501	4180	7360	235	<LOQ	1164	1850
UNI 12_Rain	6.87	113	38.0	17111	2939	3686	8530	10235	637	680	1747	4830
UNI 13_Rain	6.56	183	88.0	31414	6925	8453	3380	18069	1345	1647	2631	5457
UNI 14_Rain	6.81	49.8	28.5	7285	1798	2842	14060	4480	297	222	1247	5613
UNI 15_Rain	6.64	74.0	<LOQ	472	1885	2477	30240	679	192	101	775	9246
UNI 16_Rain	6.97	107	<LOQ	11339	7496	6907	14660	6622	1744	240	1574	9379
UNI 17_Rain	6.99	88.1	24.7	6042	8196	3398	44160	4113	510	n.d.	1368	5860
UNI 18_Rain	6.98	44.1	30.4	2421	3243	2069	14410	1689	140	n.d.	808	3925
UNI 19_Rain	6.54	44.5	9.50	3472	2548	1963	13790	2202	130	n.d.	859	4100
UNI 20_Rain	5.90	55.6	9.50	9837	849	1752	5320	6072	250	n.d.	874	1395
UNI 21_Rain	6.03	82.4	24.7	10749	2982	2870	12930	6513	330	n.d.	1086	4348
UNI 22_Rain	6.05	111	26.6	19188	1742	3384	9350	11574	490	n.d.	1617	2855
UNI 23_Rain	5.08	61.4	17.1	10888	918	2371	<LOQ	6646	190	n.d.	870	823

Sample	pH	EC	F^-	Cl^-	NO_3^-	SO_4^{2-}	Alkalinity as HCO_3^-	Na^+	K^+	NH_4^+	Mg^{2+}	Ca^{2+}
		$\mu S\ cm^{-1}$	$\mu g\ L^{-1}$	$\mu g\ L^{-1}$	$\mu g\ L^{-1}$	$\mu g\ L^{-1}$	$\mu g\ L^{-1}$	$\mu g\ L^{-1}$	$\mu g\ L^{-1}$	$\mu g\ L^{-1}$	$\mu g\ L^{-1}$	$\mu g\ L^{-1}$
IND 01_Rain	6.88	27.6	<LOQ	5123	1277	<LOQ	10850	2734	916	447	836	2701
IND 02_Rain	7.33	70.0	49.4	4158	282	395	7580	2232	1517	3087	1196	9749
IND 03_Rain	7.06	95.1	101	5975	17558	971	47580	3737	9529	<LOQ	2532	16408
IND 04_Rain	7.83	112	135	6284	18141	15379	86090	3101	3832	<LOQ	1906	20034
IND 05_Rain	7.51	27.5	28.5	4743	2530	2726	27270	2449	812	<LOQ	1685	11694
IND 06_Rain	6.59	23.9	95.0	3018	6107	4349	37770	2378	1302	575	1055	6854
IND 07_Rain	6.21	51.4	105	3383	2672	2342	9940	2192	387	318	854	4491
IND 08_Rain	6.08	26.8	<LOQ	3873	1209	1714	3920	2369	305	303	589	1509
IND 09_Rain	6.08	28.1	<LOQ	1999	1674	1694	2520	1279	133	316	418	2132
IND 10_Rain	6.04	33.8	<LOQ	13909	558	1958	4150	8280	266	177	1093	832
IND 11_Rain	6.53	67.3	<LOQ	12212	1352	2674	<LOQ	6900	657	1210	1242	2325
IND 12_Rain	6.81	35.5	20.9	14839	2164	3082	13370	8625	567	451	1771	5491
IND 13_Rain	6.82	125	18.4	24062	4607	6307	10990	13671	1279	1052	2264	6920
IND 14_Rain	6.63	68.4	<LOQ	6837	6758	3096	17720	4285	555	521	1114	10623
IND 15_Rain	6.43	73.3	49.4	472	1159	2165	29440	605	641	96.2	856	9645
IND 16_Rain	7.11	113	95.0	13266	5654	7714	14520	7864	2471	2059	1772	10559
IND 17_Rain	6.94	141	38.0	4079	6008	6677	49250	2848	1060	n.d.	1256	19258
IND 18_Rain	6.84	64.1	38.0	2144	2226	1968	30320	1434	410	n.d.	718	8213
IND 19_Rain	6.73	48.2	13.3	2964	2406	1666	15290	1813	780	n.d.	807	4423
IND 20_Rain	6.73	41.9	13.3	10615	521	1824	5870	6106	240	n.d.	882	2010
IND 21_Rain	6.08	33.9	22.8	10029	1947	2458	15220	5987	430	n.d.	1097	4618
IND 22_Rain	6.15	108	9.50	18002	1897	2923	13340	10478	440	n.d.	1553	3985
IND 23_Rain	5.35	60.9	24.7	10114	899	2208	6530	5950	220	n.d.	949	1878

Sample	pH	EC	F^-	Cl^-	NO_3^-	SO_4^{2-}	Alkalinity as HCO_3^-	Na^+	K^+	NH_4^+	Mg^{2+}	Ca^{2+}
		$\mu S\ cm^{-1}$	$\mu g\ L^{-1}$	$\mu g\ L^{-1}$	$\mu g\ L^{-1}$	$\mu g\ L^{-1}$	$\mu g\ L^{-1}$	$\mu g\ L^{-1}$	$\mu g\ L^{-1}$	$\mu g\ L^{-1}$	$\mu g\ L^{-1}$	$\mu g\ L^{-1}$
BEL 01_Rain	6.70	22.6	<LOQ	4256	173	<LOQ	18270	2291	100	139	823	2455
BEL 02_Rain	7.36	56.1	26.6	3617	2815	2933	19450	1858	368	25.5	1399	9443
BEL 03_Rain	6.59	88.0	43.7	8193	13714	1282	55210	4093	5417	<LOQ	1644	12618
BEL 04_Rain	6.91	92.0	291	6472	14291	17395	85600	3542	325	<LOQ	2179	22156
BEL 05_Rain	7.72	55.6	70.3	10384	5468	7229	65690	6110	310	<LOQ	2423	28615
BEL 06_Rain	6.20	11.3	158	3213	5642	5035	40190	2473	1247	<LOQ	1010	7174
BEL 07_Rain	5.79	28.3	<LOQ	3053	2387	1800	7750	1921	325	<LOQ	635	3094
BEL 08_Rain	6.05	21.7	<LOQ	3419	880	1608	4100	1967	227	281	556	1449
BEL 09_Rain	4.16	79.1	<LOQ	5627	1618	3259	2480	1104	152	617	395	2154
BEL 10_Rain	5.94	26.9	<LOQ	12120	428	1766	4070	7162	297	86.7	969	892
BEL 11_Rain	6.40	59.1	<LOQ	16224	1600	3355	9300	9499	454	<LOQ	1820	4429
BEL 12_Rain	6.82	95.8	24.7	17502	2077	3326	13200	10258	719	326	1894	5291

Sample	pH	EC	F^-	Cl^-	NO_3^-	SO_4^{2-}	Alkalinity as HCO_3^-	Na^+	K^+	NH_4^+	Mg^{2+}	Ca^{2+}
		$\mu S\ cm^{-1}$	$\mu g\ L^{-1}$	$\mu g\ L^{-1}$	$\mu g\ L^{-1}$	$\mu g\ L^{-1}$	$\mu g\ L^{-1}$	$\mu g\ L^{-1}$	$\mu g\ L^{-1}$	$\mu g\ L^{-1}$	$\mu g\ L^{-1}$	$\mu g\ L^{-1}$
CAT 03_Rain	7.14	70.0	<LOQ	10355	7589	9010	37070	2343	3744	1608	1108	10649
CAT 04_Rain	6.74	127	6099	8130	1130	15221	28520	3804	5651	168	2085	18893
CAT 05_Rain	6.16	60.4	3183	2531	5865	8328	14020	2608	2199	<LOQ	1002	9584
CAT 06_Rain	7.27	23.9	219	4686	7440	6898	32000	3202	1009	<LOQ	1150	13802
CAT 07_Rain	5.38	11.2	43.7	2286	1618	2285	<LOQ	1426	<LOQ	<LOQ	303	1331
CAT 08_Rain	5.92	17.5	<LOQ	2897	533	1037	2130	1670	203	189	365	649
CAT 09_Rain	5.56	29.7	<LOQ	2989	930	1325	2150	1950	109	167	304	1136
CAT 10_Rain	5.79	13.8	251	3799	843	2155	<LOQ	2374	199	284	352	1106
CAT 11_Rain	5.59	10.7	66.5	7988	2691	4896	2200	3818	731	420	756	2244
CAT 12_Rain	6.19	105	173	22862	6820	10128	4120	12719	1517	1209	1907	7114
CAT 13_Rain	5.56	73.4	10.3	12386	1717	4277	2120	7004	579	767	849	1371
CAT 14_Rain	7.52	124	<LOQ	3475	6832	8059	33070	1985	493	441	1149	16309
CAT 15_Rain	6.66	160	192	14953	10720	20026	58030	7351	2549	609	2523	29944
CAT 16_Rain	7.81	44.4	<LOQ	387	1259	1651	14450	623	5052	2196	1116	4657
CAT 17_Rain	6.50	305	1372	18268	34255	35165	10720	9996	3430	n.d.	3946	25530
CAT 18_Rain	6.89	65.4	76.0	5815	5258	3984	5610	4096	420	n.d.	855	3963
CAT 19_Rain	7.05	19.6	30.4	1750	2821	1776	5380	1232	170	n.d.	471	2803
CAT 20_Rain	5.98	58.7	135	4363	4365	4315	11540	2479	430	n.d.	725	6288
CAT 21_Rain	5.47	16.5	15.2	2215	670	970	<LOQ	1524	110	n.d.	225	663
CAT 22_Rain	5.78	39.2	36.1	5179	1314	1795	<LOQ	3424	370	n.d.	526	2530
CAT 23_Rain	5.01	72.5	7.60	13749	341	2390	<LOQ	8670	350	n.d.	1023	508

Sample	pH	EC	F^-	Cl^-	NO_3^-	SO_4^{2-}	Alkalinity as HCO_3^-	Na^+	K^+	NH_4^+	Mg^{2+}	Ca^{2+}
		$\mu S\ cm^{-1}$	$\mu g\ L^{-1}$	$\mu g\ L^{-1}$	$\mu g\ L^{-1}$	$\mu g\ L^{-1}$	$\mu g\ L^{-1}$	$\mu g\ L^{-1}$	$\mu g\ L^{-1}$	$\mu g\ L^{-1}$	$\mu g\ L^{-1}$	$\mu g\ L^{-1}$
GLP 03_Rain	7.24	63.1	424	5282	7849	8069	21100	2350	3208	763	1088	8986
GLP 04_Rain	7.53	155	6004	11179	16833	25224	30000	5703	5425	<LOQ	2493	24026
GLP 05_Rain	6.34	46.7	273	2815	4538	7186	21440	2108	1945	<LOQ	921	9276
GLP 06_Rain	7.16	21.7	485	4803	4545	6710	12230	1877	817	699	923	9020
GLP 07_Rain	5.19	23.7	129	2361	1705	3058	<LOQ	1311	<LOQ	381	292	1607
GLP 08_Rain	5.99	20.2	<LOQ	2996	719	1176	2230	1732	211	241	413	1130
GLP 09_Rain	5.81	28.2	<LOQ	2943	1029	1378	2190	1838	109	109	322	1377
GLP 10_Rain	5.72	10.7	112	2432	694	1483	2160	1622	102	214	253	904
GLP 11_Rain	5.59	20.7	34.2	3728	1469	3086	<LOQ	2128	239	252	364	1214
GLP 12_Rain	6.77	146	110	9692	3931	6672	37540	5796	563	<LOQ	1020	17335
GLP 13_Rain	6.14	61.5	7.60	9763	1550	3701	<LOQ	5660	547	930	804	2026
GLP 14_Rain	7.48	71.8	<LOQ	4004	5679	7838	41090	2176	528	42.9	1089	17192
GLP 15_Rain	6.60	30.0	<LOQ	2574	1835	2794	11770	1527	262	3362	562	4753
GLP 17_Rain	7.44	121	466	4746	5524	8986	26860	2557	2050	n.d.	1097	14058
GLP 18_Rain	6.84	79.9	129	6983	6250	4301	11400	4401	540	n.d.	865	5973
GLP 19_Rain	7.20	39.7	39.9	2311	4328	2155	8630	1460	250	n.d.	532	3828
GLP 20_Rain	6.04	50.7	105	3589	3038	3240	9940	1511	410	n.d.	504	4765
GLP 21_Rain	5.67	18.2	22.8	2201	670	1061	<LOQ	1412	130	n.d.	223	965
GLP 22_Rain	5.80	38.8	24.7	4856	1252	1694	5370	3135	130	n.d.	471	1873
GLP 23_Rain	5.33	65.3	13.3	12794	453	2443	<LOQ	7773	380	n.d.	937	675

Sample	pH	EC	F^-	Cl^-	NO_3^-	SO_4^{2-}	Alkalinity as HCO_3^-	Na^+	K^+	NH_4^+	Mg^{2+}	Ca^{2+}
		$\mu S\ cm^{-1}$	$\mu g\ L^{-1}$	$\mu g\ L^{-1}$	$\mu g\ L^{-1}$	$\mu g\ L^{-1}$	$\mu g\ L^{-1}$	$\mu g\ L^{-1}$	$\mu g\ L^{-1}$	$\mu g\ L^{-1}$	$\mu g\ L^{-1}$	$\mu g\ L^{-1}$
GAB 01_Rain	6.75	41.7	70.0	10678	1364	3379	2810	5911	337	427	1237	3354
GAB 02_Rain	7.27	53.3	85.5	8347	3714	6422	20040	4860	942	<LOQ	1572	12763
GAB 03_Rain	7.77	126	245	7444	14198	24384	25600	5543	3029	889	2867	32834
GAB 04_Rain	7.25	19.6	<LOQ	<LOQ	2461	2126	n.d.	2984	547	<LOQ	496	3415
GAB 05_Rain	5.50	7.50	41.8	2968	1395	<LOQ	2170	3487	448	<LOQ	545	2322
GAB 06_Rain	6.92	5.80	<LOQ	2517	1420	1373	3640	1771	<LOQ	<LOQ	342	1962
GAB 07_Rain	5.76	65.2	85.5	12155	2877	6062	<LOQ	7503	<LOQ	490	1118	3146
GAB 08_Rain	6.16	20.6	<LOQ	2858	707	1714	3580	1730	250	248	405	1549
GAB 09_Rain	4.95	24.4	95.0	3827	1445	2477	2150	2206	141	264	378	1335
GAB 10_Rain	5.51	70.4	19.0	20697	527	3739	<LOQ	12213	387	121	1506	968
GAB 11_Rain	5.08	45.7	<LOQ	8201	750	2568	2180	4531	297	309	661	982
GAB 12_Rain	7.55	94.3	26.6	27335	1854	5520	2490	15709	669	466	1993	3327
GAB 13_Rain	5.06	150	23.0	27537	3584	7286	<LOQ	15732	970	1146	1978	2389
GAB 14_Rain	7.33	136	76.0	23568	4073	10526	30500	13637	833	341	2344	13375

Sample	pH	EC	F^-	Cl^-	NO_3^-	SO_4^{2-}	Alkalinity as HCO_3^-	Na^+	K^+	NH_4^+	Mg^{2+}	Ca^{2+}
		$\mu S\ cm^{-1}$	$\mu g\ L^{-1}$	$\mu g\ L^{-1}$	$\mu g\ L^{-1}$	$\mu g\ L^{-1}$	$\mu g\ L^{-1}$	$\mu g\ L^{-1}$	$\mu g\ L^{-1}$	$\mu g\ L^{-1}$	$\mu g\ L^{-1}$	$\mu g\ L^{-1}$
SIR 01_Rain	6.76	66.6	81.7	10284	2164	4910	19120	4281	825	323	1275	8943
SIR 02_Rain	7.40	84.8	64.6	14033	657	7344	20380	5917	1185	359	1653	11805
SIR 03_Rain	7.04	n.d.	41.8	8481	78.4	10421	30940	3332	2680	1244	1208	7927
SIR 04_Rain	7.58	109	673	6841	1727	15384	57260	3342	3357	<LOQ	1635	15891
SIR 05_Rain	7.12	57.4	431	7352	565	10560	81990	3736	3158	6824	1874	14171
SIR 06_Rain	6.73	11.4	93.1	3404	3825	4080	13160	2270	461	<LOQ	581	6938
SIR 07_Rain	5.29	12.7	<LOQ	2251	2083	3202	<LOQ	1543	<LOQ	393	325	2114
SIR 08_Rain	5.60	29.7	<LOQ	5687	527	1925	2270	3204	250	298	601	946
SIR 09_Rain	6.43	26.2	<LOQ	4317	1252	1728	<LOQ	2636	113	289	373	1016
SIR 10_Rain	5.71	17.1	118	4093	477	1594	3610	2553	121	143	355	1585
SIR 11_Rain	5.18	39.3	19.0	5467	1296	3461	2140	3197	285	216	519	2565
SIR 12_Rain	7.19	186	1159	165075	42284	90720	n.d.	49220	3022	<LOQ	6728	30461
SIR 13_Rain	6.37	154	13.1	27097	3732	8510	7460	15566	1177	1142	2000	5445
SIR 14_Rain	7.44	186	114	11907	7979	14357	59270	7089	985	338	1613	27517
SIR 15_Rain	6.38	30.2	28.5	1083	1730	3091	15010	989	211	4004	504	5613
SIR 16_Rain	6.93	50.7	76.0	1629	7074	3926	5500	1185	450	830	815	6443
SIR 17_Rain	6.93	116	91.2	4136	6752	7402	36380	3181	550	n.d.	770	16105
SIR 18_Rain	7.02	107	39.9	11033	3677	5174	26830	6639	470	n.d.	975	9503
SIR 19_Rain	6.95	43.7	26.6	4430	4173	3922	15870	2835	230	n.d.	575	6520
SIR 20_Rain	6.15	98.3	245	6152	6609	9562	13950	4004	430	n.d.	872	9830
SIR 21_Rain	6.04	97.7	13.3	32081	868	5683	7830	18298	750	n.d.	2225	3743
SIR 22_Rain	6.27	123	43.7	8722	3726	6494	29130	5583	380	n.d.	876	10840
SIR 23_Rain	5.30	93.3	11.4	19408	285	3197	<LOQ	11390	340	n.d.	1350	918

Sample	pH	EC	F^-	Cl^-	NO_3^-	SO_4^{2-}	Alkalinity as HCO_3^-	Na^+	K^+	NH_4^+	Mg^{2+}	Ca^{2+}
		$\mu S\ cm^{-1}$	$\mu g\ L^{-1}$	$\mu g\ L^{-1}$	$\mu g\ L^{-1}$	$\mu g\ L^{-1}$	$\mu g\ L^{-1}$	$\mu g\ L^{-1}$	$\mu g\ L^{-1}$	$\mu g\ L^{-1}$	$\mu g\ L^{-1}$	$\mu g\ L^{-1}$
AUG 01_Rain	6.71	55.8	39.9	12805	2294	4910	10890	5237	718	490	1333	4635
AUG 02_Rain	7.19	106	95.0	18936	6219	8822	18960	7599	10774	2421	2029	12156
AUG 03_Rain	6.85	76.6	36.1	14413	838	8722	22650	5926	2943	<LOQ	1601	7307
AUG 04_Rain	7.16	134	128	14225	1133	17918	102080	6508	22681	4964	2130	10810
AUG 05_Rain	6.23	79.2	2622	6060	1228	8952	30530	4043	3960	2103	1434	10510
AUG 06_Rain	6.64	15.9	<LOQ	4129	3317	3509	5640	2668	383	<LOQ	525	3587
AUG 07_Rain	5.28	49.5	<LOQ	8406	2145	4109	<LOQ	5173	<LOQ	452	734	1673
AUG 08_Rain	5.72	48.7	<LOQ	10086	546	2261	2640	5704	332	216	920	1158
AUG 09_Rain	5.92	72.5	<LOQ	8289	936	2222	<LOQ	5023	336	728	715	2663
AUG 10_Rain	5.61	243	<LOQ	59196	1432	9643	<LOQ	34010	1298	320	4122	2190
AUG 11_Rain	6.26	104	<LOQ	26128	2499	7344	13920	15479	1501	1904	2054	3828
AUG 12_Rain	5.53	112	38.0	52185	3819	15408	n.d.	30360	3488	2941	4059	7194

Sample	pH	EC	F^-	Cl^-	NO_3^-	SO_4^{2-}	Alkalinity as HCO_3^-	Na^+	K^+	NH_4^+	Mg^{2+}	Ca^{2+}
		$\mu S\ cm^{-1}$	$\mu g\ L^{-1}$	$\mu g\ L^{-1}$	$\mu g\ L^{-1}$	$\mu g\ L^{-1}$	$\mu g\ L^{-1}$	$\mu g\ L^{-1}$	$\mu g\ L^{-1}$	$\mu g\ L^{-1}$	$\mu g\ L^{-1}$	$\mu g\ L^{-1}$
PRI 01_Rain	7.05	47.8	81.7	8921	1972	3878	11120	3624	446	78.2	1135	5465
PRI 02_Rain	7.27	130	68.4	15208	6863	9144	35900	6341	1184	145	1887	17321
PRI 03_Rain	6.90	61.9	55.1	6639	8773	10858	66310	2774	1764	<LOQ	1113	9566
PRI 04_Rain	7.35	94.0	155	5350	14384	12240	39820	2537	2411	461	1344	15369
PRI 05_Rain	6.82	70.9	15.1	5705	8971	7315	41170	3035	1604	<LOQ	1197	10393
PRI 06_Rain	6.85	9.10	70.3	2801	3367	3240	10390	1999	375	338	507	5423
PRI 07_Rain	5.51	27.2	<LOQ	2446	1978	3456	<LOQ	1617	641	328	383	1643
PRI 08_Rain	5.61	16.3	<LOQ	5034	298	1709	2130	2845	246	214	556	675
PRI 09_Rain	5.54	24.3	39.9	2805	924	1176	<LOQ	1796	109	109	299	533
PRI 10_Rain	5.86	21.5	283	4331	1004	2482	4140	3192	196	360	417	1926
PRI 11_Rain	5.76	43.2	<LOQ	5432	1786	3662	2910	3013	356	396	509	3246
PRI 12_Rain	7.37	1032	701	244595	54002	92160	n.d.	139150	9630	<LOQ	18081	66453
PRI 13_Rain	6.32	199	32.5	35990	5363	11491	2300	20965	1392	1367	2614	6240
PRI 14_Rain	7.45	113	72.2	7863	3515	6845	30280	4940	493	170	1300	14816
PRI 15_Rain	6.50	76.4	41.8	2229	2381	5520	27380	1566	250	268	846	10563
PRI 16_Rain	6.30	38.0	<LOQ	1054	6219	2328	<LOQ	876	274	30.3	530	4277
PRI 17_Rain	6.96	109	143	4651	10521	8736	15510	3413	440	n.d.	907	10910
PRI 18_Rain	7.09	83.6	38.0	11477	3044	4426	9140	7080	310	n.d.	998	4148
PRI 19_Rain	6.62	28.0	24.7	2173	2666	2549	7790	1497	170	n.d.	399	3630
PRI 20_Rain	6.88	165	144	14289	16709	20957	41750	8689	2570	n.d.	2407	21213
PRI 21_Rain	5.60	161	19.0	39490	818	6192	<LOQ	21227	900	n.d.	2563	1763
PRI 22_Rain	6.10	80.2	24.7	8215	1972	3826	14930	4895	560	n.d.	708	5855
PRI 23_Rain	5.53	132	7.60	29927	291	4214	<LOQ	16600	600	n.d.	1988	905

Sample	pH	EC	F^-	Cl^-	NO_3^-	SO_4^{2-}	Alkalinity as HCO_3^-	Na^+	K^+	NH_4^+	Mg^{2+}	Ca^{2+}
		µS cm^{-1}	µg L^{-1}	µg L^{-1}	µg L^{-1}	µg L^{-1}	µg L^{-1}	µg L^{-1}	µg L^{-1}	µg L^{-1}	µg L^{-1}	µg L^{-1}
CES 01_Rain	6.17	15.4	<LOQ	2489	<LOQ	<LOQ	3790	4054	413	<LOQ	462	2953
CES 02_Rain	7.18	33.5	<LOQ	2478	1593	2275	3220	2917	576	1063	714	6287
CES 03_Rain	7.63	87.4	39.9	6578	8798	7574	13810	5794	1531	2533	2717	18229
CES 04_Rain	7.27	121	177	9270	17689	1858	41110	7126	5422	2547	3740	41449
CES 05_Rain	6.65	8.40	<LOQ	<LOQ	1333	<LOQ	2650	1984	385	<LOQ	371	2849
CES 07_Rain	6.21	27.2	39.9	4225	1259	2246	<LOQ	2461	325	306	413	1523
CES 08_Rain	6.12	16.0	<LOQ	1299	657	1531	6730	782	301	978	293	992
CES 09_Rain	6.24	35.1	45.6	2222	2189	2395	<LOQ	1511	246	1090	320	1976
CES 10_Rain	5.93	11.1	<LOQ	4335	651	984	2160	2712	133	109	392	868
CES 11_Rain	5.89	10.1	<LOQ	4615	825	1613	2260	2576	196	462	412	681
CES 12_Rain	6.29	57.9	623	13597	2009	4205	2170	8349	633	529	1081	1970
CES 13_Rain	5.60	28.2	61.4	3713	2288	2587	2190	2100	145	614	376	1790
CES 14_Rain	6.85	71.5	<LOQ	5907	2765	4243	8350	4161	411	438	868	5675
CES 15_Rain	5.69	23.0	<LOQ	1225	1556	2381	9350	2013	270	147	471	3964
CES 17_Rain	5.88	53.5	43.7	3227	2176	2477	71100	2239	170	n.d.	364	1720
CES 18_Rain	6.90	33.7	24.7	2563	2691	1958	35850	1773	180	n.d.	361	2848
CES 19_Rain	6.12	22.8	19.0	2414	1364	1517	<LOQ	1749	150	n.d.	266	940
CES 20_Rain	6.79	9.70	3.80	1732	725	965	6500	1168	190	n.d.	186	743
CES 21_Rain	7.12	14.5	13.3	3184	800	1267	8950	2108	170	n.d.	303	1098
CES 22_Rain	6.16	78.9	7.60	10583	5475	2448	9800	6737	450	n.d.	921	2875
CES 23_Rain	4.46	24.5	7.60	2872	1172	1435	<LOQ	1896	120	n.d.	265	355

Table S. 3 - Minor and trace element concentrations (µg L^{-1}) in rainwater samples for all the sampling sites.

Sample	Li	B	Al	Ti	V	Cr	Mn	Fe	Co	Ni	Cu	Zn	As
	µg L^{-1}	µg L^{-1}	µg L^{-1}	µg L^{-1}	µg L^{-1}	µg L^{-1}	µg L^{-1}	µg L^{-1}	µg L^{-1}	µg L^{-1}	µg L^{-1}	µg L^{-1}	µg L^{-1}
CIT 01_Rain	1.14	1.81	441	0.113	1.36	0.0650	35.7	4.79	0.380	0.168	16.7	5.10	0.0880
CIT 02_Rain	0.163	3.71	56.8	0.118	1.33	0.0630	29.2	2.47	0.0960	0.265	0.307	0.256	0.176
CIT 03_Rain	0.749	4.68	344	10.0	2.03	0.460	51.3	143	0.607	0.666	9.40	13.0	0.461
CIT 04_Rain	0.364	3.28	83.5	0.438	1.24	0.0950	25.9	8.46	0.209	0.682	3.88	17.0	0.317
CIT 05_Rain	1.62	8.37	29.2	0.732	5.57	0.105	0.523	8.64	0.0520	0.161	27.9	2.28	1.17
CIT 06_Rain	0.198	5.28	30.5	0.0810	1.64	0.0420	4.46	3.47	0.0330	0.118	7.90	2.21	0.564
CIT 07_Rain	0.101	3.47	373	2.36	0.823	0.0780	10.6	143	0.195	0.478	17.0	11.7	0.727
CIT 08_Rain	1.16	3.77	393	0.191	3.53	0.0560	37.8	3.77	0.283	0.134	2.13	2.24	0.176
CIT 09_Rain	0.0440	5.68	99.8	0.281	0.448	0.0480	5.84	13.1	0.0930	0.347	1.98	8.91	0.189
CIT 10_Rain	0.381	3.65	2,740	166	7.49	0.0640	52.4	2,040	1.14	0.977	26.1	11.8	1.40
CIT 11_Rain	0.183	0.897	835	42.5	1.95	0.0800	18.0	474	0.432	0.266	16.4	8.52	0.197
CIT 12_Rain	0.145	2.15	122	0.168	0.588	0.0340	11.5	2.92	0.150	0.187	3.22	17.0	0.0720
CIT 13_Rain	0.0870	2.12	86.9	0.336	0.333	0.143	9.61	28.1	0.224	0.146	8.51	2.75	0.438
CIT 14_Rain	0.404	3.01	337	0.118	1.49	0.741	47.8	26.5	0.628	0.938	2.54	6.74	0.422
CIT 15_Rain	<LOQ	<LOQ	85.9	0.0850	0.378	0.0310	5.19	3.07	0.0640	0.214	4.26	7.91	0.151
CIT 16_Rain	2.36	7.67	1,380	1.44	1.53	0.0470	146	43.9	1.69	1.61	47.9	120	1.46
CIT 17_Rain	0.274	4.62	437	1.21	0.672	0.155	19.5	31.7	0.226	0.692	26.8	66.0	1.79
CIT 18_Rain	0.356	4.85	1,420	99.8	4.20	0.258	34.2	937	0.570	0.615	15.5	44.5	0.742
CIT 19_Rain	0.123	1.36	376	2.96	0.496	0.139	12.3	34.3	0.161	0.380	6.68	37.3	0.231
CIT 20_Rain	0.202	3.01	497	10.6	1.13	0.312	17.7	234	0.201	0.453	15.9	34.4	0.501
CIT 21_Rain	0.0500	0.967	127	1.98	0.253	0.0310	5.08	54.5	0.0600	0.153	5.35	12.1	0.277
CIT 22_Rain	0.789	3.48	1,980	2.33	1.96	0.223	47.0	436	0.695	0.527	32.3	44.2	0.134
CIT 23_Rain	0.225	2.18	152	0.743	0.405	0.128	6.53	40.2	0.0980	0.505	9.23	29.3	0.190

Sample	Se	Br	Rb	Sr	Mo	Cd	Sn	Sb	Cs	Ba	Tl	Pb	U
	µg L^{-1}	µg L^{-1}	µg L^{-1}	µg L^{-1}	µg L^{-1}	µg L^{-1}	µg L^{-1}	µg L^{-1}	µg L^{-1}	µg L^{-1}	µg L^{-1}	µg L^{-1}	µg L^{-1}
CIT 01_Rain	0.588	5.89	1.32	38.3	0.243	0.140	<LOQ	0.0360	0.0100	11.4	0.172	<LOQ	0.0140
CIT 02_Rain	0.443	15.2	1.04	36.3	0.0920	0.144	<LOQ	0.350	<LOQ	48.0	0.110	<LOQ	0.0200
CIT 03_Rain	0.656	21.0	2.72	42.0	0.181	0.175	<LOQ	0.104	0.0300	16.3	0.212	0.179	0.0190
CIT 04_Rain	0.886	5.35	1.91	23.8	0.259	0.0800	<LOQ	0.141	0.0240	89.4	0.156	0.0340	0.00300
CIT 05_Rain	1.37	6.98	6.93	70.9	0.778	0.0350	<LOQ	0.394	0.0560	11.2	0.265	<LOQ	0.00900
CIT 06_Rain	1.72	10.8	2.35	51.9	0.442	0.0610	0.0100	0.0880	0.0210	5.89	0.248	0.0440	0.00400
CIT 07_Rain	1.34	23.1	1.90	7.35	0.0800	0.417	0.0270	0.0610	0.0470	4.34	0.591	1.99	0.0150
CIT 08_Rain	0.963	17.7	1.34	34.7	0.339	0.177	<LOQ	0.0740	<LOQ	12.5	0.195	0.0330	0.00400
CIT 09_Rain	0.386	12.8	0.295	4.66	0.0250	0.0500	0.00500	0.0700	0.00400	3.23	0.0210	0.505	0.00700
CIT 10_Rain	1.53	34.9	3.80	32.6	0.166	0.355	<LOQ	0.0150	0.0760	19.6	0.424	1.52	0.0810
CIT 11_Rain	0.831	18.7	2.16	10.6	0.0710	0.447	<LOQ	0.0270	0.0430	7.42	0.555	1.29	0.0350
CIT 12_Rain	0.305	11.3	0.759	9.17	0.0720	0.120	<LOQ	0.0800	0.00500	0.862	0.0420	0.0300	0.00500
CIT 13_Rain	0.475	10.7	1.59	5.37	0.0330	0.430	<LOQ	0.0570	0.0320	3.29	0.403	0.893	0.0140
CIT 14_Rain	0.858	36.8	3.69	75.0	0.185	0.367	<LOQ	0.329	0.00700	21.4	0.393	0.0450	0.0100
CIT 15_Rain	0.236	<LOQ	0.821	8.12	<LOQ	0.136	<LOQ	0.0860	0.00400	3.45	0.169	0.162	0.00400
CIT 16_Rain	4.89	146	32.0	102	0.497	1.85	<LOQ	0.0560	0.148	10.7	2.71	0.205	0.0270
CIT 17_Rain	1.16	41.2	11.3	12.0	0.0810	0.870	<LOQ	0.132	0.127	8.35	0.964	0.863	0.0200
CIT 18_Rain	1.06	58.8	4.44	21.0	0.0870	0.285	0.0210	1.93	0.0370	15.9	0.318	1.36	0.0610
CIT 19_Rain	0.142	14.6	2.20	9.48	0.0170	0.141	<LOQ	0.338	0.00900	6.65	0.115	0.419	0.0160
CIT 20_Rain	0.464	24.2	2.71	12.7	0.0410	0.183	0.00700	1.15	0.00800	7.78	0.138	0.762	0.0210
CIT 21_Rain	0.184	14.5	1.24	5.07	0.0130	0.111	<LOQ	0.0230	0.00800	2.91	0.126	0.338	0.00800
CIT 22_Rain	0.292	40.2	7.16	31.1	0.0290	0.941	<LOQ	0.320	0.0380	14.3	0.633	0.327	0.0510
CIT 23_Rain	0.512	15.7	1.79	9.46	0.0270	0.300	<LOQ	0.0980	0.0120	3.01	0.313	0.791	0.0110

Sample	Li	B	Al	Ti	V	Cr	Mn	Fe	Co	Ni	Cu	Zn	As
	µg L^{-1}	µg L^{-1}	µg L^{-1}	µg L^{-1}	µg L^{-1}	µg L^{-1}	µg L^{-1}	µg L^{-1}	µg L^{-1}	µg L^{-1}	µg L^{-1}	µg L^{-1}	µg L^{-1}
ZAF 01_Rain	0.394	1.91	31.0	<LOQ	2.69	0.0640	26.4	1.88	0.144	0.260	0.558	4.68	0.0550
ZAF 02_Rain	0.149	5.48	2.41	<LOQ	0.508	0.0440	4.33	0.284	0.0250	0.0933	1.72	1.61	0.0990
ZAF 03_Rain	0.230	6.39	29.2	0.632	1.54	0.159	13.0	14.7	0.293	0.642	32.7	7.97	0.311
ZAF 04_Rain	9.49	21.9	816	0.709	11.3	0.146	304	11.4	1.52	1.03	47.4	8.91	0.792
ZAF 05_Rain	4.15	2.54	2,400	47.3	3.85	0.225	182	325	1.77	0.622	41.0	21.5	0.443
ZAF 06_Rain	0.0400	4.56	12.8	0.274	0.659	0.0530	0.414	4.88	0.0210	0.0240	1.45	1.20	0.146
ZAF 07_Rain	0.0440	5.16	124	0.536	0.328	0.0760	6.04	14.5	0.0880	0.210	6.21	11.6	0.280
ZAF 08_Rain	0.0250	3.66	6.07	0.138	0.288	0.0580	4.51	3.63	0.0420	0.167	0.590	1.79	0.115
ZAF 09_Rain	0.00800	4.76	3.62	0.132	0.290	0.0280	2.81	1.82	0.0340	0.128	1.21	6.30	0.0970
ZAF 10_Rain	<LOQ	1.29	113	1.14	0.284	0.0140	2.60	52.3	0.0420	0.240	3.63	2.68	0.107
ZAF 11_Rain	0.330	3.85	176	0.194	0.382	0.143	6.79	68.1	0.160	0.450	9.23	41.0	0.196
ZAF 12_Rain	1.10	4.69	714	1.57	3.55	0.0410	51.6	18.2	0.496	0.322	5.85	9.29	0.212
ZAF 13_Rain	0.0610	3.04	21.6	0.217	0.322	0.0260	5.33	8.74	0.0710	0.0660	0.946	1.77	0.157
ZAF 14_Rain	0.184	2.88	9.20	0.194	0.960	0.147	0.564	5.92	<LOQ	0.435	4.53	3.81	0.279
ZAF 15_Rain	<LOQ	2.23	5.48	<LOQ	0.436	<LOQ	1.99	0.708	<LOQ	0.0940	1.47	1.41	0.0520
ZAF 16_Rain	0.176	1.63	71.1	0.934	2.34	0.302	19.7	13.0	0.120	0.386	23.2	33.5	0.198
ZAF 17_Rain	0.104	3.53	236	4.36	0.503	0.0780	8.32	46.9	0.117	0.167	16.7	18.7	1.11
ZAF 18_Rain	0.191	11.3	218	0.393	0.645	0.208	8.04	70.2	0.130	0.256	9.15	23.5	0.357
ZAF 19_Rain	0.177	3.94	208	0.219	0.377	0.100	11.9	14.3	0.180	0.277	11.4	50.9	0.506
ZAF 20_Rain	0.107	2.00	8.73	0.293	0.428	0.0700	3.53	4.40	0.0150	0.114	1.79	19.5	0.169
ZAF 21_Rain	0.0290	1.37	15.3	0.283	0.142	0.0270	1.96	3.13	0.0230	<LOQ	<LOQ	4.71	0.0600
ZAF 22_Rain	0.119	1.70	37.7	0.129	0.273	0.0500	4.49	5.85	0.0500	0.183	1.26	11.1	0.0300
ZAF 23_Rain	<LOQ	1.09	6.19	0.0870	0.0790	0.0420	0.356	7.21	0.0900	0.0800	2.70	3.92	0.0470

Sample	Se	Br	Rb	Sr	Mo	Cd	Sn	Sb	Cs	Ba	Tl	Pb	U
	µg L^{-1}	µg L^{-1}	µg L^{-1}	µg L^{-1}	µg L^{-1}	µg L^{-1}	µg L^{-1}	µg L^{-1}	µg L^{-1}	µg L^{-1}	µg L^{-1}	µg L^{-1}	µg L^{-1}
ZAF 01_Rain	0.232	4.81	1.15	43.0	0.273	0.0530	<LOQ	0.0490	0.0100	11.6	0.131	<LOQ	0.00700
ZAF 02_Rain	0.411	14.4	0.359	18.3	0.0500	0.0130	<LOQ	0.125	<LOQ	33.9	0.0140	<LOQ	0.00600
ZAF 03_Rain	0.898	21.0	3.49	40.6	2.21	0.0150	<LOQ	0.286	0.0170	4.77	0.0810	0.180	0.0260
ZAF 04_Rain	13.6	40.5	14.6	251	3.36	0.126	<LOQ	0.936	0.309	26.8	1.35	0.0320	0.0110
ZAF 05_Rain	4.72	10.4	8.28	112	1.03	0.399	0.0140	0.169	0.127	27.4	0.887	0.0580	0.0350
ZAF 06_Rain	0.323	14.0	0.524	17.8	0.0810	<LOQ	0.0440	0.160	0.00500	7.06	0.0180	0.0490	0.00200
ZAF 07_Rain	0.647	11.7	0.632	5.58	0.0290	0.145	0.0150	0.269	0.0150	3.19	0.227	1.08	0.00600
ZAF 08_Rain	0.200	10.6	0.263	5.30	0.0190	0.0390	0.00500	0.0790	0.00300	2.46	0.0490	0.0580	0.00200
ZAF 09_Rain	0.101	9.71	0.141	3.59	0.0220	0.0150	<LOQ	0.138	<LOQ	1.65	0.0150	0.0730	0.00100
ZAF 10_Rain	0.165	6.25	0.189	2.63	0.0130	0.0480	<LOQ	0.0170	0.00400	1.24	0.0370	0.200	0.00300
ZAF 11_Rain	0.245	12.6	0.507	5.54	0.0100	0.165	<LOQ	0.363	0.00600	4.93	0.110	0.964	0.00700
ZAF 12_Rain	3.02	14.2	2.75	44.1	0.621	0.201	<LOQ	0.350	0.0460	11.5	0.548	0.0260	0.00700
ZAF 13_Rain	0.173	14.4	0.247	4.15	0.0240	0.0680	<LOQ	0.0940	0.00700	1.71	0.0400	0.163	0.00600
ZAF 14_Rain	0.947	10.4	0.981	50.3	0.0880	0.0710	<LOQ	0.157	<LOQ	12.6	0.0610	0.0320	0.00700
ZAF 15_Rain	0.140	5.59	0.276	9.70	<LOQ	0.0160	<LOQ	0.0700	<LOQ	2.49	0.0180	0.0100	0.00200
ZAF 16_Rain	0.514	<LOQ	4.24	29.4	0.407	0.0790	<LOQ	0.0500	0.00400	2.51	0.118	0.0530	0.0150
ZAF 17_Rain	1.28	26.4	3.73	4.76	0.0960	0.527	<LOQ	0.114	0.0820	4.28	0.783	1.28	0.0160
ZAF 18_Rain	0.773	31.1	1.63	9.67	0.0490	0.181	<LOQ	0.496	0.0240	4.53	0.243	0.400	0.0100
ZAF 19_Rain	0.288	20.4	2.09	12.9	0.0470	0.247	<LOQ	0.111	0.0160	6.28	0.245	0.265	0.00700
ZAF 20_Rain	0.209	8.40	0.703	12.0	0.0540	0.0420	<LOQ	0.110	0.00500	3.40	0.0640	0.00500	0.00400
ZAF 21_Rain	0.155	5.34	0.0420	3.08	0.00600	0.0210	<LOQ	0.0230	0.00100	1.07	0.0140	<LOQ	0.00100
ZAF 22_Rain	0.108	16.5	0.403	8.65	0.0260	0.0260	<LOQ	0.0250	0.00200	2.58	0.0400	0.0360	0.00200
ZAF 23_Rain	0.131	16.8	0.138	2.54	0.0200	0.0240	<LOQ	0.0250	<LOQ	0.412	0.0140	0.123	<LOQ

Sample	Li	B	Al	Ti	V	Cr	Mn	Fe	Co	Ni	Cu	Zn	As
	µg L^{-1}	µg L^{-1}	µg L^{-1}	µg L^{-1}	µg L^{-1}	µg L^{-1}	µg L^{-1}	µg L^{-1}	µg L^{-1}	µg L^{-1}	µg L^{-1}	µg L^{-1}	µg L^{-1}
TDF 02_Rain	0.240	1.35	6.36	<LOQ	1.73	0.267	16.4	5.48	0.284	0.0883	1.18	0.162	0.235
TDF 03_Rain	0.600	3.95	12.7	0.122	2.55	0.0910	1.73	4.39	0.0190	0.348	9.94	2.20	0.608
TDF 04_Rain	5.71	12.3	351	0.230	10.1	0.128	233	8.85	1.65	0.762	39.0	9.87	0.876
TDF 05_Rain	5.20	3.76	594	0.624	3.33	0.0640	140	12.3	1.34	0.443	61.4	13.7	0.341
TDF 06_Rain	0.254	6.30	27.4	0.202	1.08	0.0540	3.37	4.05	0.0610	0.190	4.68	6.35	0.374
TDF 07_Rain	0.257	3.68	626	2.28	1.51	0.0730	19.3	230	0.318	0.312	20.4	13.7	0.915
TDF 08_Rain	0.0640	1.28	11.6	0.206	0.260	0.0530	4.37	3.68	0.0560	0.212	0.518	3.77	0.0730
TDF 09_Rain	0.0490	2.47	5.33	0.271	0.303	0.0440	4.13	2.41	0.0430	0.227	1.30	5.38	0.0840
TDF 12_Rain	12.2	42.2	57,300	0.965	1.18	0.127	733	820	10.6	5.45	980	99.1	2.03
TDF 13_Rain	1.72	5.69	5,640	0.559	3.75	0.129	150	664	2.78	1.68	100	39.6	0.385
TDF 14_Rain	0.527	5.77	94.7	0.206	2.54	0.314	61.0	5.87	0.0400	0.738	2.60	1.16	0.537
TDF 15_Rain	0.143	1.09	19.3	0.229	2.73	0.0220	9.12	4.21	0.0140	0.0840	7.17	4.84	0.535
TDF 16_Rain	17.4	61.0	28,300	2.07	97.2	0.434	1,090	41.6	8.00	6.80	182	227	1.52
TDF 17_Rain	1.64	17.2	4,620	25.6	8.52	1.08	88.9	1,210	1.43	4.52	101	117	11.3
TDF 18_Rain	0.163	2.42	503	0.338	0.874	0.0590	9.66	11.7	0.173	0.117	6.75	7.02	0.556
TDF 19_Rain	0.137	2.11	446	0.604	0.808	0.0830	11.2	122	0.167	0.182	7.22	10.6	1.07
TDF 21_Rain	0.190	1.50	577	0.504	0.722	0.210	15.3	84.9	0.338	0.181	5.20	10.4	0.205
TDF 23_Rain	4.95	14.7	16,900	16.7	1.19	0.735	344	3,630	5.58	2.58	348	55.1	0.840

Sample	Se	Br	Rb	Sr	Mo	Cd	Sn	Sb	Cs	Ba	Tl	Pb	U
	µg L^{-1}	µg L^{-1}	µg L^{-1}	µg L^{-1}	µg L^{-1}	µg L^{-1}	µg L^{-1}	µg L^{-1}	µg L^{-1}	µg L^{-1}	µg L^{-1}	µg L^{-1}	µg L^{-1}
TDF 02_Rain	0.311	8.12	0.782	31.4	0.169	0.0440	<LOQ	0.174	<LOQ	6.32	0.0760	<LOQ	0.00600
TDF 03_Rain	1.33	13.4	1.29	38.1	0.291	0.0190	<LOQ	0.0820	0.0210	63.0	0.117	<LOQ	0.0100
TDF 04_Rain	7.18	73.1	13.7	193	3.76	0.523	<LOQ	0.344	0.356	64.0	1.84	0.0730	0.0190
TDF 05_Rain	3.73	10.0	8.30	108	2.15	0.402	<LOQ	0.0300	0.0700	15.8	0.726	0.0160	0.0190
TDF 06_Rain	0.300	10.5	1.15	58.7	0.112	0.0110	0.00700	0.124	0.00300	9.31	0.0580	0.0310	0.0160
TDF 07_Rain	1.12	16.9	2.61	14.0	0.100	0.677	<LOQ	0.177	0.0550	8.47	0.823	1.24	0.0200
TDF 08_Rain	0.114	3.08	0.239	3.21	0.0210	0.0430	0.00600	0.0250	<LOQ	1.51	0.0430	0.209	0.00200
TDF 09_Rain	0.114	5.45	0.177	4.49	0.0210	<LOQ	0.0120	0.0430	0.00300	2.20	0.0190	0.0550	0.00200
TDF 12_Rain	17.2	217	38.9	541	0.916	6.31	<LOQ	0.0230	0.369	48.4	2.10	0.865	0.979
TDF 13_Rain	4.44	33.4	12.5	91.9	0.429	3.05	<LOQ	0.0470	0.0720	11.9	1.32	0.119	0.0890
TDF 14_Rain	3.47	48.1	12.1	114	0.973	0.775	<LOQ	0.110	0.0430	17.3	1.32	0.0300	0.00800
TDF 15_Rain	0.876	1.52	1.73	41.7	0.252	0.0570	<LOQ	0.0320	0.0210	6.53	0.212	0.0430	0.00900
TDF 16_Rain	17.7	549	84.3	1,110	19.6	6.98	<LOQ	0.565	0.807	110	9.78	0.131	0.141
TDF 17_Rain	7.89	185	30.5	56.9	0.475	1.93	0.0790	0.217	0.282	35.0	3.03	1.66	0.128
TDF 18_Rain	1.17	14.4	1.62	8.47	0.0460	0.134	<LOQ	0.0260	0.0300	5.47	0.184	0.0480	0.0140
TDF 19_Rain	0.386	11.4	1.01	9.59	0.0480	0.0780	<LOQ	0.0440	0.0240	6.35	0.107	0.147	0.0120
TDF 21_Rain	0.437	18.7	1.40	12.4	0.0520	0.109	<LOQ	0.0280	0.0100	6.47	0.128	0.0640	0.0130
TDF 23_Rain	9.16	96.8	43.6	217	0.0340	3.09	<LOQ	0.0190	0.270	82.7	2.46	2.43	0.818

Sample	Li	B	Al	Ti	V	Cr	Mn	Fe	Co	Ni	Cu	Zn	As
	µg L^{-1}	µg L^{-1}	µg L^{-1}	µg L^{-1}	µg L^{-1}	µg L^{-1}	µg L^{-1}	µg L^{-1}	µg L^{-1}	µg L^{-1}	µg L^{-1}	µg L^{-1}	µg L^{-1}
INT 03_Rain	0.146	4.57	18.6	0.824	0.697	0.162	13.7	13.0	0.175	0.597	4.80	5.85	0.151
INT 04_Rain	0.272	12.3	52.9	0.832	0.393	0.229	1.51	22.7	0.129	1.19	17.1	14.9	0.321
INT 05_Rain	0.549	19.1	24.7	0.712	0.626	0.170	1.06	22.2	0.222	0.617	21.3	14.8	0.267
INT 06_Rain	0.0790	3.95	6.08	0.143	0.490	0.0600	1.37	1.58	0.0390	0.102	1.33	1.89	0.0950
INT 07_Rain	0.0460	2.99	3.95	0.0380	0.217	0.0440	2.81	1.81	0.0250	0.139	0.698	3.06	0.0690
INT 08_Rain	0.0620	1.80	53.5	0.137	0.540	0.0240	6.46	2.41	0.0760	0.166	2.01	3.65	0.242
INT 09_Rain	0.0430	1.77	4.25	0.167	0.219	0.0260	3.65	1.39	0.0270	0.108	0.586	2.44	0.0500
INT 10_Rain	0.0240	1.01	1.81	0.0140	0.0510	0.0230	0.697	1.60	0.0110	1.00	0.721	2.68	0.0290
INT 11_Rain	0.272	1.95	12.1	0.0300	0.0740	0.0720	2.97	2.63	0.0940	0.0910	3.86	10.2	0.0200
INT 12_Rain	0.311	5.99	6.88	0.228	0.414	0.0640	3.57	3.16	0.0380	0.121	3.08	8.43	0.0870
INT 13_Rain	0.163	2.14	217	0.243	0.488	0.178	26.5	80.3	0.362	0.346	7.18	11.1	0.469
INT 14_Rain	0.171	2.63	38.2	0.207	0.979	0.238	<LOQ	5.79	<LOQ	0.759	4.14	3.01	0.231
INT 15_Rain	0.0400	0.746	15.4	0.0400	0.649	0.0340	5.25	3.72	<LOQ	0.155	2.97	6.26	0.470
INT 16_Rain	0.562	36.4	99.4	1.08	2.33	5.55	74.1	32.5	0.595	3.43	27.5	102	0.980
INT 17_Rain	0.0430	3.05	9.88	0.170	0.377	0.413	3.54	4.84	0.0180	0.351	2.19	5.38	0.138
INT 18_Rain	0.0350	3.20	3.91	0.0850	0.211	0.0220	2.47	3.46	0.0120	<LOQ	0.935	6.61	0.0490
INT 19_Rain	0.0400	1.80	9.79	0.183	0.205	0.0240	0.737	2.55	<LOQ	0.0270	0.475	7.14	0.0520
INT 20_Rain	0.0620	1.84	7.02	0.163	0.201	0.0810	3.59	4.21	0.0510	0.138	0.976	12.8	0.0250
INT 21_Rain	0.0740	0.612	58.1	0.179	0.141	0.0390	3.68	9.84	0.0570	0.0320	6.85	9.03	0.581
INT 22_Rain	0.246	5.16	15.4	0.301	0.193	0.0830	2.85	7.19	0.0470	0.322	1.59	17.0	0.0920
INT 23_Rain	<LOQ	<LOQ	9.76	0.0690	0.116	0.0680	1.38	15.5	0.0230	0.138	1.94	14.2	0.0640

Sample	Se	Br	Rb	Sr	Mo	Cd	Sn	Sb	Cs	Ba	Tl	Pb	U
	µg L^{-1}	µg L^{-1}	µg L^{-1}	µg L^{-1}	µg L^{-1}	µg L^{-1}	µg L^{-1}	µg L^{-1}	µg L^{-1}	µg L^{-1}	µg L^{-1}	µg L^{-1}	µg L^{-1}
INT 03_Rain	0.210	19.6	1.36	39.0	0.0910	0.0200	<LOQ	0.183	<LOQ	48.6	0.00800	0.0940	0.0240
INT 04_Rain	0.215	12.9	8.77	25.6	0.438	0.0520	0.0500	0.598	0.0420	5.57	0.0680	0.182	0.00500
INT 05_Rain	0.136	15.5	8.11	52.9	0.263	0.0330	0.0450	0.234	0.0320	16.9	0.0360	0.255	0.0370
INT 06_Rain	0.0470	2.83	0.332	13.9	0.0350	<LOQ	<LOQ	0.163	0.00500	7.33	0.00600	0.0260	0.00300
INT 07_Rain	0.227	3.93	0.183	5.60	0.0230	0.0210	0.00900	0.0740	0.00500	2.52	0.0150	0.0500	0.00100
INT 08_Rain	0.216	5.03	0.427	5.53	0.0550	0.0640	<LOQ	0.0220	0.00300	2.58	0.0710	0.0590	0.00300
INT 09_Rain	0.129	3.00	0.102	4.25	0.0110	0.00100	<LOQ	0.0300	<LOQ	2.12	0.00300	0.0240	0.00200
INT 10_Rain	0.0750	3.49	0.0270	1.57	0.00700	0.0590	<LOQ	0.0180	<LOQ	0.477	<LOQ	0.0790	<LOQ
INT 11_Rain	0.129	10.3	0.108	3.03	<LOQ	0.0150	<LOQ	0.198	0.00100	1.62	0.00400	0.0410	0.00200
INT 12_Rain	0.249	30.1	0.352	13.3	0.0590	0.0100	<LOQ	0.151	0.00400	2.21	0.0100	0.0240	0.00400
INT 13_Rain	0.350	11.8	1.23	12.0	0.0160	0.295	<LOQ	0.410	0.0100	8.46	0.200	0.764	0.0250
INT 14_Rain	0.0950	8.85	1.39	67.0	0.0680	0.0470	<LOQ	0.154	<LOQ	13.5	0.0290	0.0480	0.0190
INT 15_Rain	0.919	19.0	2.03	30.5	0.104	0.214	<LOQ	0.193	<LOQ	8.81	0.500	0.0420	0.00400
INT 16_Rain	0.958	71.4	10.7	78.5	0.815	0.234	<LOQ	1.64	0.00800	22.8	0.135	0.195	0.0110
INT 17_Rain	0.102	2.95	0.599	4.44	0.0620	0.0230	<LOQ	0.129	0.0110	2.27	0.0320	0.0150	0.00200
INT 18_Rain	0.323	6.50	0.115	5.58	0.0190	0.00700	<LOQ	0.0370	0.00300	1.61	0.00600	<LOQ	0.00200
INT 19_Rain	<LOQ	3.31	0.0850	6.08	0.0210	0.0280	<LOQ	0.0570	0.00400	2.42	0.0110	0.0510	0.00200
INT 20_Rain	0.102	3.08	0.0430	5.15	0.0200	0.0190	<LOQ	1.40	0.00200	1.89	0.00600	0.0150	0.00500
INT 21_Rain	0.680	18.9	1.88	3.83	0.0270	0.284	<LOQ	0.0240	0.0200	1.97	0.408	0.670	0.00400
INT 22_Rain	0.0280	34.4	0.300	10.6	0.0410	0.0200	<LOQ	0.612	0.00700	2.15	0.00500	0.0780	0.00300
INT 23_Rain	0.302	4.03	0.264	2.67	0.0230	0.0470	<LOQ	0.116	0.00200	1.25	0.0290	0.125	<LOQ

Sample	Li	B	Al	Ti	V	Cr	Mn	Fe	Co	Ni	Cu	Zn	As
	µg L^{-1}	µg L^{-1}	µg L^{-1}	µg L^{-1}	µg L^{-1}	µg L^{-1}	µg L^{-1}	µg L^{-1}	µg L^{-1}	µg L^{-1}	µg L^{-1}	µg L^{-1}	µg L^{-1}
ARC 01_Rain	0.207	6.86	5.64	0.255	0.240	0.0480	1.07	0.853	0.0100	0.169	0.768	3.30	0.0790
ARC 02_Rain	0.231	6.89	8.73	<LOQ	0.622	0.131	0.314	<LOQ	0.0120	0.158	2.15	2.69	0.160
ARC 03_Rain	0.797	23.5	22.1	0.302	1.19	0.295	0.737	4.09	0.0320	0.763	4.31	25.2	0.259
ARC 04_Rain	0.358	7.63	23.3	0.645	1.11	0.283	20.8	18.1	0.172	1.34	7.58	7.39	0.141
ARC 05_Rain	0.259	10.5	91.1	<LOQ	1.03	0.211	0.145	1.31	0.0120	0.0950	1.18	0.380	0.282
ARC 06_Rain	0.366	3.92	47.0	1.62	1.77	0.473	24.6	17.3	0.308	0.857	7.46	33.5	0.151
ARC 07_Rain	0.243	6.61	107	0.371	0.589	0.215	0.628	9.50	0.0110	0.0310	0.890	1.93	0.157
ARC 08 A_Rain	0.101	5.48	8.14	0.126	0.258	0.117	2.83	5.87	0.0410	0.435	2.07	6.47	0.0740
ARC 08 B_Rain	0.0880	7.59	9.52	0.274	0.254	0.145	6.54	7.13	0.0840	0.973	2.87	10.4	0.135
ARC 09_Rain	0.0540	4.66	3.77	0.103	0.378	0.0600	1.58	1.74	0.00500	0.533	1.69	7.17	0.0590
ARC 10_Rain	0.138	6.48	0.680	0.00900	0.0950	0.0180	0.763	0.619	0.00900	0.0590	1.13	6.02	0.0290
ARC 11_Rain	0.178	8.08	3.86	0.0410	0.284	0.0450	0.582	1.24	<LOQ	0.121	1.31	9.77	0.0870
ARC 12_Rain	0.304	8.46	7.04	0.0580	0.357	0.0590	1.21	1.91	0.0180	0.0950	2.43	5.76	0.106
ARC 13_Rain	0.270	9.63	8.93	0.214	0.719	0.147	0.792	4.39	0.0770	0.0980	1.74	2.84	0.145
ARC 14_Rain	<LOQ	3.11	7.34	0.0240	0.325	0.288	0.318	4.02	0.0360	0.797	2.78	14.8	0.106
ARC 15_Rain	<LOQ	3.35	25.8	0.0410	0.405	0.0690	<LOQ	1.86	<LOQ	0.0610	1.51	4.13	0.101
ARC 16_Rain	<LOQ	15.2	135	0.455	2.54	0.469	<LOQ	3.88	<LOQ	0.401	8.71	9.90	0.511
ARC 17_Rain	1.64	6.91	30.4	0.302	0.881	0.157	12.1	10.1	0.114	0.571	12.4	11.8	0.267
ARC 18_Rain	0.111	6.11	56.0	0.156	0.401	0.118	0.196	7.44	0.00500	0.206	2.16	7.52	0.130
ARC 19_Rain	0.0810	4.32	9.18	0.191	0.386	0.0590	0.284	2.37	<LOQ	0.126	1.71	8.59	0.0780
ARC 20_Rain	0.102	4.52	5.20	0.514	0.274	0.0910	0.325	2.55	<LOQ	0.359	2.36	13.4	0.0300
ARC 21_Rain	0.229	5.83	33.5	0.891	0.588	0.0970	0.537	11.1	0.0140	0.165	2.87	5.20	0.137
ARC 22_Rain	0.299	6.18	14.9	0.133	0.220	0.0490	0.593	3.05	0.00600	0.155	2.31	9.38	0.0510
ARC 23_Rain	0.0930	4.74	6.13	0.308	0.0840	0.0780	0.817	4.50	0.0150	0.0600	0.349	4.77	0.0900

Sample	Se	Br	Rb	Sr	Mo	Cd	Sn	Sb	Cs	Ba	Tl	Pb	U
	µg L^{-1}	µg L^{-1}	µg L^{-1}	µg L^{-1}	µg L^{-1}	µg L^{-1}	µg L^{-1}	µg L^{-1}	µg L^{-1}	µg L^{-1}	µg L^{-1}	µg L^{-1}	µg L^{-1}
ARC 01_Rain	<LOQ	17.8	0.241	8.12	0.365	0.0220	<LOQ	0.0750	<LOQ	3.53	0.00900	<LOQ	<LOQ
ARC 02_Rain	0.382	15.5	0.369	23.5	0.153	0.0120	<LOQ	0.175	<LOQ	80.9	0.0140	<LOQ	0.00500
ARC 03_Rain	0.416	23.9	2.03	79.4	0.349	0.0180	<LOQ	0.269	0.0160	24.3	0.0310	<LOQ	0.00700
ARC 04_Rain	<LOQ	20.3	0.766	70.7	0.234	0.0220	<LOQ	0.143	<LOQ	15.7	0.00900	0.0980	0.0150
ARC 05_Rain	<LOQ	19.7	0.949	40.4	0.174	<LOQ	<LOQ	0.149	<LOQ	45.2	0.00600	<LOQ	0.0380
ARC 06_Rain	0.199	3.90	1.71	36.7	0.468	0.0260	0.0440	0.236	0.00800	9.93	0.00500	1.71	0.0120
ARC 07_Rain	0.193	15.2	0.297	18.7	0.431	0.0630	0.00600	0.169	<LOQ	8.47	<LOQ	0.117	0.00800
ARC 08 A_Rain	0.196	16.9	0.288	5.76	0.0440	0.0160	0.0200	0.154	0.00500	2.67	0.0150	0.0780	0.00400
ARC 08 B_Rain	0.215	9.33	0.343	5.91	0.0310	0.0270	0.00600	0.209	0.00800	4.75	0.0270	0.0530	0.00300
ARC 09_Rain	0.0950	10.2	0.210	9.18	0.0360	0.0140	<LOQ	0.391	0.00300	4.43	0.00400	0.0560	0.00200
ARC 10_Rain	0.133	49.2	0.154	9.03	0.0390	0.0130	<LOQ	0.0820	<LOQ	1.52	<LOQ	0.0670	0.00100
ARC 11_Rain	0.190	37.6	0.228	10.4	0.0760	0.0130	<LOQ	0.0990	0.00400	5.66	<LOQ	0.0330	0.00100
ARC 12_Rain	0.209	44.0	0.421	15.9	0.0980	0.0120	<LOQ	0.185	0.00600	4.57	<LOQ	0.0170	0.00300
ARC 13_Rain	0.130	46.8	0.659	19.3	0.211	0.0130	<LOQ	0.370	0.00900	5.63	<LOQ	0.0150	0.00500
ARC 14_Rain	0.239	11.1	0.636	9.15	0.0150	0.0630	<LOQ	0.130	0.00900	4.38	0.00900	0.0560	0.00200
ARC 15_Rain	0.0910	<LOQ	0.375	17.7	0.102	0.0140	<LOQ	0.219	<LOQ	5.15	0.00400	0.0230	0.00200
ARC 16_Rain	0.421	32.2	1.58	78.3	0.407	0.0110	<LOQ	1.28	<LOQ	15.1	0.0100	0.0360	0.0650
ARC 17_Rain	0.223	10.4	10.2	23.5	0.293	0.0220	0.0100	0.150	0.0370	5.22	0.00500	0.109	0.0220
ARC 18_Rain	0.0740	8.61	0.277	12.6	0.0740	0.00900	<LOQ	0.478	0.00200	6.15	0.00800	0.0250	0.00500
ARC 19_Rain	0.0350	11.4	0.291	13.3	0.0470	0.0170	<LOQ	0.208	0.00600	4.66	0.00500	0.0110	0.00100
ARC 20_Rain	0.112	21.8	0.340	8.42	0.0590	0.0130	<LOQ	0.401	0.00300	4.71	0.00400	0.0180	0.00200
ARC 21_Rain	0.259	32.0	0.525	27.4	0.0750	0.0140	<LOQ	0.124	0.00400	8.74	0.00900	0.0380	0.00600
ARC 22_Rain	0.0370	56.2	0.375	16.6	0.0700	0.00700	<LOQ	0.124	0.00300	8.52	0.00600	0.0490	0.00300
ARC 23_Rain	0.131	44.0	0.237	8.62	0.0320	0.00800	<LOQ	0.167	<LOQ	2.08	0.0130	0.0570	<LOQ

Sample	Li	B	Al	Ti	V	Cr	Mn	Fe	Co	Ni	Cu	Zn	As
	µg L^{-1}	µg L^{-1}	µg L^{-1}	µg L^{-1}	µg L^{-1}	µg L^{-1}	µg L^{-1}	µg L^{-1}	µg L^{-1}	µg L^{-1}	µg L^{-1}	µg L^{-1}	µg L^{-1}
UNI 01_Rain	0.101	3.85	1.22	<LOQ	0.191	0.0220	1.26	0.825	0.0110	0.103	0.319	2.50	0.0530
UNI 02_Rain	0.142	6.76	8.14	0.0370	0.700	0.100	0.223	1.17	0.0120	0.251	1.60	5.74	0.164
UNI 03_Rain	0.273	9.19	12.3	0.520	0.839	0.336	24.9	16.0	0.272	0.903	9.58	12.1	0.148
UNI 04_Rain	0.296	13.2	19.4	1.02	1.63	0.394	44.6	19.7	0.510	1.30	23.2	15.5	0.231
UNI 05_Rain	0.194	8.65	16.2	<LOQ	0.316	0.132	0.102	0.373	0.0100	0.0950	2.85	1.89	0.0770
UNI 06_Rain	0.0870	2.58	18.6	0.246	0.578	0.108	13.5	5.51	0.216	0.384	7.83	5.49	0.108
UNI 07_Rain	0.0970	8.33	6.21	0.110	0.390	0.0690	0.205	0.927	0.00600	0.0500	1.39	2.44	0.110
UNI 08_Rain	0.0330	5.32	2.84	0.0950	0.226	0.0640	2.49	1.98	0.0250	0.127	0.637	4.40	0.0600
UNI 09_Rain	0.0480	5.53	2.96	0.136	0.457	0.105	0.646	1.17	<LOQ	0.202	1.18	4.66	0.0760
UNI 10_Rain	0.120	6.65	1.31	0.0360	0.0830	0.0480	0.611	1.21	<LOQ	0.0370	0.877	4.49	0.00900
UNI 11_Rain	0.133	6.57	2.72	0.0190	0.178	0.224	2.43	2.55	0.0140	0.103	1.98	6.73	0.0920
UNI 12_Rain	0.259	9.68	5.43	0.118	0.456	0.0750	0.450	1.63	<LOQ	0.0910	2.85	4.30	0.112
UNI 13_Rain	0.401	16.5	8.73	0.0880	0.554	0.192	2.11	3.19	0.0390	0.269	3.41	11.7	0.222
UNI 14_Rain	<LOQ	3.62	11.7	0.0290	0.345	0.156	<LOQ	2.88	<LOQ	0.449	1.19	2.34	0.0740
UNI 15_Rain	0.0280	2.28	36.3	0.0750	0.423	0.107	<LOQ	1.66	<LOQ	0.133	2.14	3.12	0.0750
UNI 16_Rain	0.0960	16.1	15.2	0.935	0.777	0.273	16.9	14.4	0.159	0.640	19.6	16.8	0.131
UNI 17_Rain	0.226	12.2	16.8	0.157	0.868	0.148	0.328	2.89	0.00600	0.343	12.9	29.2	0.190
UNI 18_Rain	0.152	9.75	11.2	0.195	0.503	0.146	0.760	3.29	0.00300	0.319	4.46	15.3	0.136
UNI 19_Rain	0.122	5.20	8.84	0.0260	0.478	0.0410	0.0870	1.31	<LOQ	<LOQ	0.493	2.10	0.102
UNI 20_Rain	0.121	4.56	2.35	0.230	0.140	2.14	0.978	4.19	0.0390	2.20	0.752	4.59	0.0200
UNI 21_Rain	0.182	7.44	11.3	0.337	0.644	0.0980	0.930	5.21	0.0160	0.0900	1.38	6.57	0.0680
UNI 22_Rain	0.330	7.37	13.5	0.654	0.269	0.0710	0.258	6.43	0.00100	0.172	0.930	6.42	0.0850
UNI 23_Rain	0.0580	3.36	3.75	0.0580	0.0720	0.0630	0.694	3.48	0.0140	0.0810	0.564	6.31	0.109

Sample	Se	Br	Rb	Sr	Mo	Cd	Sn	Sb	Cs	Ba	Tl	Pb	U
	µg L^{-1}	µg L^{-1}	µg L^{-1}	µg L^{-1}	µg L^{-1}	µg L^{-1}	µg L^{-1}	µg L^{-1}	µg L^{-1}	µg L^{-1}	µg L^{-1}	µg L^{-1}	µg L^{-1}
UNI 01_Rain	<LOQ	15.0	0.147	5.99	0.0280	0.0110	<LOQ	0.0640	<LOQ	2.87	0.00300	<LOQ	<LOQ
UNI 02_Rain	0.139	13.3	0.338	22.0	0.0590	0.00900	<LOQ	0.200	<LOQ	114	0.0180	<LOQ	0.00500
UNI 03_Rain	0.374	15.8	1.12	44.3	0.227	0.0280	0.0130	0.461	<LOQ	8.81	0.00700	0.225	0.0170
UNI 04_Rain	0.328	56.3	1.51	68.9	0.269	0.0560	0.0290	0.953	<LOQ	21.4	0.0110	0.292	0.0210
UNI 05_Rain	0.223	14.7	0.332	17.7	0.0890	0.00700	<LOQ	0.130	<LOQ	29.4	0.00500	<LOQ	0.00300
UNI 06_Rain	0.198	3.47	0.539	22.6	0.126	0.0100	0.0110	0.0500	<LOQ	6.54	0.00300	0.153	0.00900
UNI 07_Rain	0.227	14.7	0.263	19.6	0.0610	<LOQ	<LOQ	0.129	0.00300	6.91	0.00500	0.0160	0.00200
UNI 08_Rain	0.162	11.8	0.129	4.63	0.0230	0.0150	<LOQ	0.182	0.00300	4.61	0.00900	0.0580	0.00200
UNI 09_Rain	0.182	10.5	0.203	8.85	0.0320	0.00700	0.00600	0.498	<LOQ	5.04	0.00300	0.0250	0.00300
UNI 10_Rain	0.0370	44.6	0.114	7.67	0.0150	<LOQ	<LOQ	0.333	<LOQ	1.98	<LOQ	0.0770	0.00100
UNI 11_Rain	0.152	31.6	0.174	6.73	0.0240	0.0190	<LOQ	0.223	0.00300	2.91	0.00800	0.0280	0.00200
UNI 12_Rain	0.170	41.4	0.319	15.9	0.0820	0.0120	<LOQ	0.111	0.00200	4.58	<LOQ	0.0390	0.00400
UNI 13_Rain	0.485	82.3	0.667	26.2	0.162	0.0340	0.00700	0.907	0.00900	6.54	0.0140	<LOQ	0.00600
UNI 14_Rain	0.341	24.0	0.280	18.5	0.0110	0.0340	<LOQ	0.0890	<LOQ	6.51	0.00500	0.0250	0.00400
UNI 15_Rain	0.0960	<LOQ	0.420	28.9	0.0240	0.0300	<LOQ	0.417	<LOQ	7.56	0.00400	0.0220	0.00900
UNI 16_Rain	0.337	21.9	1.11	39.1	0.195	0.0300	<LOQ	0.365	<LOQ	7.75	0.00700	0.164	0.0130
UNI 17_Rain	0.323	25.0	0.796	14.6	0.149	0.0330	0.0120	0.251	0.00900	11.4	0.0140	0.00400	0.00500
UNI 18_Rain	0.0350	9.20	0.429	10.9	0.0620	0.0710	<LOQ	1.83	0.00700	6.71	0.0130	0.0500	0.00400
UNI 19_Rain	0.158	13.4	0.265	14.4	0.0470	0.00500	<LOQ	0.103	0.00500	7.09	0.00500	<LOQ	0.00200
UNI 20_Rain	0.0980	29.7	0.0840	6.48	0.0280	0.0140	<LOQ	0.0690	0.00100	2.62	0.00400	<LOQ	0.00100
UNI 21_Rain	0.0960	31.6	0.282	14.8	0.0460	0.0120	<LOQ	0.377	0.00300	4.84	0.00900	0.00600	0.00600
UNI 22_Rain	0.0320	66.0	0.463	14.6	0.0550	0.0110	<LOQ	0.438	0.00400	3.91	0.0120	0.0320	0.00200
UNI 23_Rain	0.118	36.9	0.198	6.26	0.0320	0.0110	<LOQ	0.0570	0.00200	1.88	0.0190	0.0530	<LOQ

Sample	Li	B	Al	Ti	V	Cr	Mn	Fe	Co	Ni	Cu	Zn	As
	µg L^{-1}	µg L^{-1}	µg L^{-1}	µg L^{-1}	µg L^{-1}	µg L^{-1}	µg L^{-1}	µg L^{-1}	µg L^{-1}	µg L^{-1}	µg L^{-1}	µg L^{-1}	µg L^{-1}
IND 01_Rain	0.0910	3.51	2.09	<LOQ	0.228	0.0720	0.912	2.42	0.0100	0.159	1.28	5.26	0.0550
IND 02_Rain	0.230	11.0	4.40	0.140	0.636	0.0990	0.322	0.976	0.0400	0.253	2.56	4.31	0.190
IND 03_Rain	0.661	19.2	28.0	2.19	1.18	0.504	35.5	40.7	0.429	1.46	17.6	18.2	0.220
IND 04_Rain	0.412	16.3	27.4	0.947	1.73	0.599	36.2	20.3	0.396	1.74	18.3	17.8	0.280
IND 05_Rain	0.195	8.74	17.1	<LOQ	0.598	0.162	0.291	1.78	0.0150	0.134	3.53	2.78	0.131
IND 06_Rain	0.193	7.03	25.2	1.18	0.926	0.370	25.3	18.6	0.318	0.881	13.5	18.9	0.0980
IND 07_Rain	0.138	8.80	105	1.67	0.604	0.444	6.98	70.8	0.112	0.303	5.39	9.04	0.103
IND 08_Rain	0.0380	5.55	3.16	0.0710	0.226	0.0650	2.35	2.39	0.0230	0.193	1.17	5.06	0.0750
IND 09_Rain	0.0460	4.85	3.12	0.0730	0.408	0.0390	2.49	1.37	0.0100	0.0930	0.891	3.07	0.0820
IND 10_Rain	0.120	6.46	0.942	0.0830	0.0900	0.0360	0.631	1.06	0.0310	0.0380	0.917	5.80	0.0160
IND 11_Rain	0.330	6.85	3.99	0.109	0.174	0.0340	0.383	2.32	<LOQ	0.0690	1.61	3.34	0.131
IND 12_Rain	0.229	8.45	5.85	0.0360	0.368	0.0610	0.210	1.49	<LOQ	0.0770	2.48	2.89	0.0980
IND 13_Rain	0.323	12.1	13.9	0.132	0.628	0.277	0.986	6.19	0.0770	0.229	6.68	7.52	0.241
IND 14_Rain	<LOQ	4.34	12.2	0.193	0.388	0.235	<LOQ	3.12	0.0130	0.513	3.27	2.46	0.162
IND 15_Rain	0.0190	2.78	21.5	0.0690	0.503	0.109	<LOQ	2.49	<LOQ	0.0950	2.98	3.30	0.0750
IND 16_Rain	0.202	20.8	23.5	0.996	1.03	1.07	6.84	16.9	0.164	1.91	19.1	15.8	0.235
IND 17_Rain	0.350	16.3	58.3	0.425	1.39	0.314	0.247	5.21	0.0150	0.365	12.8	5.77	0.472
IND 18_Rain	0.152	8.19	21.9	0.263	0.280	0.131	0.0820	3.46	0.00300	0.204	3.47	5.30	0.162
IND 19_Rain	0.129	6.07	9.40	0.373	0.388	0.0790	0.438	5.06	<LOQ	0.133	2.77	6.36	0.0790
IND 20_Rain	0.327	5.36	2.48	0.0880	0.161	0.0190	0.442	1.65	<LOQ	0.0570	0.870	4.71	0.0590
IND 21_Rain	0.190	6.79	21.1	0.557	0.493	0.0670	0.187	9.59	<LOQ	0.0420	2.20	5.92	0.107
IND 22_Rain	0.327	9.37	11.8	0.249	0.264	0.0970	0.225	4.54	0.00900	0.191	2.17	10.1	0.0460
IND 23_Rain	0.0700	3.61	3.06	0.169	0.103	0.0570	0.813	2.34	0.0120	0.116	1.10	7.49	0.106

Sample	Se	Br	Rb	Sr	Mo	Cd	Sn	Sb	Cs	Ba	Tl	Pb	U
	µg L^{-1}	µg L^{-1}	µg L^{-1}	µg L^{-1}	µg L^{-1}	µg L^{-1}	µg L^{-1}	µg L^{-1}	µg L^{-1}	µg L^{-1}	µg L^{-1}	µg L^{-1}	µg L^{-1}
IND 01_Rain	<LOQ	15.3	0.332	6.97	0.0580	0.0170	<LOQ	0.141	<LOQ	3.58	<LOQ	<LOQ	<LOQ
IND 02_Rain	0.159	14.0	0.642	23.9	0.122	0.0160	<LOQ	0.143	0.00800	9.39	0.0280	<LOQ	0.00300
IND 03_Rain	0.269	19.3	3.64	54.5	0.679	0.0290	0.0830	0.316	<LOQ	27.3	0.0310	0.746	0.0300
IND 04_Rain	0.121	25.2	1.17	77.0	0.488	0.0320	0.0800	0.364	<LOQ	24.1	0.0110	0.466	0.0240
IND 05_Rain	<LOQ	11.9	0.397	24.0	0.158	<LOQ	<LOQ	0.665	<LOQ	12.9	0.00300	<LOQ	0.00600
IND 06_Rain	0.293	4.35	1.03	25.9	0.277	0.0180	0.0660	0.278	0.00400	8.26	0.00400	0.376	0.0100
IND 07_Rain	0.120	11.2	0.342	13.0	0.0800	0.00900	0.0170	0.173	0.00800	9.89	0.0100	0.800	0.00800
IND 08_Rain	0.174	12.1	0.175	4.90	0.0410	0.0160	0.00700	0.168	0.00300	3.67	0.0100	0.0690	0.00100
IND 09_Rain	0.209	9.53	0.174	8.04	0.0360	0.00700	<LOQ	0.0950	<LOQ	4.44	0.00300	0.0200	0.00200
IND 10_Rain	0.0740	42.9	0.125	7.48	0.0170	0.00700	<LOQ	0.179	<LOQ	1.18	<LOQ	0.0600	0.00100
IND 11_Rain	0.326	32.1	0.350	6.99	0.0490	0.0110	0.00500	0.108	0.00500	3.50	0.00500	0.0200	0.00100
IND 12_Rain	0.249	41.5	0.314	15.2	0.106	0.0110	0.00500	0.249	0.00200	6.71	<LOQ	0.0130	0.00400
IND 13_Rain	0.196	69.6	0.749	21.5	0.226	0.0190	0.0160	0.424	0.0100	7.26	0.0130	0.0270	0.00800
IND 14_Rain	0.170	22.6	0.486	23.4	0.0640	0.0490	<LOQ	0.136	<LOQ	8.44	0.00900	0.0360	0.00300
IND 15_Rain	0.0930	<LOQ	0.870	27.4	0.0800	0.0100	<LOQ	0.188	<LOQ	8.42	0.00400	0.0230	0.00500
IND 16_Rain	0.0910	41.2	1.80	41.9	0.430	0.0140	<LOQ	0.501	<LOQ	8.16	0.00600	0.306	0.0220
IND 17_Rain	0.296	16.2	1.18	34.9	0.375	0.0140	0.0320	0.635	0.00200	18.2	0.0100	0.0450	0.0260
IND 18_Rain	0.0490	7.45	0.561	16.1	0.136	0.0150	<LOQ	0.313	0.00600	8.47	0.0320	0.0310	0.00500
IND 19_Rain	<LOQ	11.7	0.739	13.6	0.0810	0.0180	<LOQ	0.136	0.00200	6.74	0.00800	0.0130	0.00400
IND 20_Rain	<LOQ	34.5	0.169	7.63	0.0380	0.00700	<LOQ	0.0810	0.00100	3.09	0.00200	0.00800	0.00100
IND 21_Rain	0.103	34.4	0.373	14.1	0.0900	0.0160	0.00600	0.118	0.00500	6.95	0.0140	0.00700	0.00300
IND 22_Rain	0.0770	59.1	0.405	16.0	0.0830	0.0170	<LOQ	0.798	0.00400	7.88	0.00300	0.0380	0.00300
IND 23_Rain	0.147	36.8	0.252	7.55	0.0570	0.0210	<LOQ	0.0980	<LOQ	3.27	0.0150	0.0850	<LOQ

Sample	Li	B	Al	Ti	V	Cr	Mn	Fe	Co	Ni	Cu	Zn	As
	µg L^{-1}	µg L^{-1}	µg L^{-1}	µg L^{-1}	µg L^{-1}	µg L^{-1}	µg L^{-1}	µg L^{-1}	µg L^{-1}	µg L^{-1}	µg L^{-1}	µg L^{-1}	µg L^{-1}
BEL 01_Rain	0.101	4.21	1.71	0.0330	0.183	0.0490	1.42	1.03	0.0100	0.162	0.753	4.78	0.0410
BEL 02_Rain	0.169	6.39	8.98	<LOQ	1.63	29.0	2.37	548	0.243	1.32	1.81	1.31	0.166
BEL 03_Rain	0.285	11.8	14.5	0.979	0.782	0.273	13.9	15.3	0.241	0.929	10.9	8.45	0.140
BEL 04_Rain	0.654	27.5	28.9	1.59	1.92	0.571	35.5	22.4	0.328	1.33	17.4	9.68	0.349
BEL 05_Rain	0.564	18.4	39.9	0.118	1.19	0.390	0.366	3.45	0.0380	0.269	8.91	4.06	0.225
BEL 06_Rain	0.209	11.6	23.6	1.16	0.873	0.398	19.3	20.0	0.309	2.24	10.2	22.4	0.110
BEL 07_Rain	0.0570	6.10	4.03	0.0220	0.300	0.150	0.793	5.38	<LOQ	0.104	1.10	4.64	0.0590
BEL 08_Rain	0.0300	5.64	2.92	0.0650	0.168	0.139	2.22	5.29	0.0200	0.173	1.35	7.85	0.0790
BEL 09_Rain	0.0390	4.89	50.4	0.151	0.320	0.0940	9.33	11.6	0.137	0.264	8.24	13.9	0.100
BEL 10_Rain	0.102	5.66	1.21	0.0570	0.0850	0.0330	0.677	1.45	<LOQ	0.346	2.09	6.60	0.0260
BEL 11_Rain	0.296	8.97	3.77	0.0190	0.214	0.0800	0.396	1.76	<LOQ	0.370	4.28	19.8	0.0760
BEL 12_Rain	0.229	9.03	4.39	0.0870	0.305	0.0830	0.310	1.87	0.00300	0.0780	2.39	8.44	0.0770

Sample	Se	Br	Rb	Sr	Mo	Cd	Sn	Sb	Cs	Ba	Tl	Pb	U
	µg L^{-1}	µg L^{-1}	µg L^{-1}	µg L^{-1}	µg L^{-1}	µg L^{-1}	µg L^{-1}	µg L^{-1}	µg L^{-1}	µg L^{-1}	µg L^{-1}	µg L^{-1}	µg L^{-1}
BEL 01_Rain	<LOQ	12.4	0.166	6.00	0.0500	0.0130	<LOQ	0.186	<LOQ	3.24	0.00300	<LOQ	<LOQ
BEL 02_Rain	<LOQ	13.0	0.376	21.0	2.97	0.0130	0.0200	0.178	<LOQ	42.9	0.0120	<LOQ	0.00500
BEL 03_Rain	0.201	22.7	1.67	48.8	0.419	0.0110	0.0370	0.327	<LOQ	30.3	0.00900	0.149	0.0220
BEL 04_Rain	0.612	36.9	1.23	88.0	0.557	0.0330	0.0460	1.58	<LOQ	28.3	0.0190	0.145	0.0330
BEL 05_Rain	0.301	28.3	1.18	63.9	0.481	0.0120	<LOQ	1.32	<LOQ	41.0	0.00800	<LOQ	0.0360
BEL 06_Rain	0.132	5.56	1.06	29.7	0.392	0.263	0.0560	0.579	<LOQ	7.85	0.00300	0.273	0.0130
BEL 07_Rain	0.112	10.7	0.125	9.44	0.0520	<LOQ	<LOQ	0.196	<LOQ	6.56	<LOQ	0.0340	<LOQ
BEL 08_Rain	0.131	11.2	0.134	5.19	0.0350	0.0160	0.00700	0.271	<LOQ	2.57	0.0100	0.0370	0.00100
BEL 09_Rain	0.200	8.13	0.169	8.32	0.0270	0.0250	<LOQ	0.342	0.00300	6.86	0.00400	0.427	0.00600
BEL 10_Rain	0.0640	37.7	0.212	7.09	0.0260	0.0210	<LOQ	0.0660	<LOQ	1.37	<LOQ	0.0690	0.00100
BEL 11_Rain	0.251	46.7	0.267	12.0	0.101	0.0360	0.0100	0.340	0.00200	7.00	<LOQ	0.0210	0.00200
BEL 12_Rain	0.328	46.6	0.338	15.2	0.112	0.0130	0.00800	0.357	0.00300	5.95	<LOQ	0.00900	0.00300

Sample	Li	B	Al	Ti	V	Cr	Mn	Fe	Co	Ni	Cu	Zn	As
	µg L^{-1}	µg L^{-1}	µg L^{-1}	µg L^{-1}	µg L^{-1}	µg L^{-1}	µg L^{-1}	µg L^{-1}	µg L^{-1}	µg L^{-1}	µg L^{-1}	µg L^{-1}	µg L^{-1}
CAT 03_Rain	0.261	18.3	16.4	0.825	0.955	0.360	24.0	22.0	0.413	0.911	11.5	13.0	0.217
CAT 04_Rain	1.10	14.0	179	4.77	2.89	0.370	72.7	32.0	0.585	0.826	40.0	19.2	0.464
CAT 05_Rain	0.655	5.83	183	3.69	2.24	0.332	44.4	46.8	0.429	0.533	25.2	10.4	0.276
CAT 06_Rain	0.244	14.0	42.5	0.136	1.63	0.236	0.806	5.06	0.0630	0.202	4.26	7.88	0.170
CAT 07_Rain	0.0260	3.87	5.82	0.0690	0.223	0.0720	7.04	5.16	0.0790	0.187	1.69	12.6	0.110
CAT 08_Rain	0.0130	3.58	3.41	0.0890	0.177	0.0300	2.73	2.81	0.0380	0.0570	0.187	1.95	0.0630
CAT 09_Rain	0.0280	5.90	3.40	0.120	0.330	0.0380	3.70	1.67	0.0320	0.266	1.40	5.49	0.0760
CAT 10_Rain	0.0850	4.02	74.7	0.101	0.443	0.0340	5.87	6.70	0.0730	0.451	3.35	13.6	0.0730
CAT 11_Rain	0.464	5.59	41.3	0.258	0.363	0.192	8.02	11.1	0.153	0.975	16.6	57.4	0.202
CAT 12_Rain	0.501	15.1	8.76	0.198	1.12	0.139	7.85	5.35	0.0420	0.399	7.51	26.5	0.307
CAT 13_Rain	0.175	8.02	8.25	0.0860	0.461	0.0940	10.7	2.38	0.0740	0.254	1.94	5.32	0.203
CAT 14_Rain	0.214	6.47	31.8	0.176	1.17	3.22	0.0490	78.8	<LOQ	0.547	2.16	0.939	0.271
CAT 15_Rain	0.663	21.2	63.0	0.218	2.55	0.177	0.175	7.40	0.0700	0.618	11.8	6.92	0.363
CAT 16_Rain	<LOQ	9.57	46.4	0.293	0.503	0.0570	5.31	7.32	0.0150	0.112	11.1	7.07	0.0280
CAT 17_Rain	1.11	34.7	68.9	3.56	5.04	1.62	98.3	51.4	0.777	3.26	82.9	140	1.44
CAT 18_Rain	0.204	15.3	7.97	0.627	0.842	0.177	0.324	4.30	0.00400	0.364	5.09	23.4	0.171
CAT 19_Rain	0.105	6.58	4.97	0.243	0.437	0.106	1.21	2.91	0.00600	0.254	3.29	17.9	0.0770
CAT 20_Rain	0.221	8.59	11.9	0.627	0.811	0.221	0.664	6.40	0.0100	0.349	2.52	8.96	0.127
CAT 21_Rain	0.0170	2.22	7.49	0.224	0.116	0.0680	1.43	4.63	0.0380	0.266	0.973	8.66	0.0470
CAT 22_Rain	0.124	4.55	9.46	0.605	0.285	0.0730	1.76	7.46	0.0500	0.222	1.96	13.8	0.0400
CAT 23_Rain	0.0800	4.11	4.32	0.0800	0.0720	0.0450	0.694	3.29	0.0130	0.0620	1.23	5.63	0.0310

Sample	Se	Br	Rb	Sr	Mo	Cd	Sn	Sb	Cs	Ba	Tl	Pb	U
	µg L^{-1}	µg L^{-1}	µg L^{-1}	µg L^{-1}	µg L^{-1}	µg L^{-1}	µg L^{-1}	µg L^{-1}	µg L^{-1}	µg L^{-1}	µg L^{-1}	µg L^{-1}	µg L^{-1}
CAT 03_Rain	0.548	18.2	1.70	49.5	0.335	0.0180	0.0230	0.371	<LOQ	9.23	0.0250	0.214	0.0200
CAT 04_Rain	3.66	6.91	3.59	94.5	0.581	0.0840	0.0310	1.41	0.0110	24.3	0.202	0.0620	0.0450
CAT 05_Rain	3.02	2.20	1.86	53.3	0.592	0.0760	0.0210	0.154	0.0110	8.60	0.127	0.0580	0.0320
CAT 06_Rain	0.442	16.0	0.967	72.7	0.274	<LOQ	0.00900	0.295	<LOQ	21.3	0.0200	0.0530	0.0130
CAT 07_Rain	0.242	8.14	0.265	7.65	0.0400	0.0200	0.00800	0.0890	0.00300	3.83	0.0260	0.0770	0.00200
CAT 08_Rain	0.119	10.00	0.114	3.61	0.00900	0.0100	<LOQ	0.0790	<LOQ	1.59	0.00900	0.0350	0.00100
CAT 09_Rain	0.203	12.9	0.142	5.58	0.0210	0.0110	0.00800	0.0810	<LOQ	2.90	0.00300	0.0750	0.00100
CAT 10_Rain	0.486	11.1	0.522	8.11	0.117	0.0800	0.00500	0.192	0.00700	2.95	0.0620	0.0470	0.00300
CAT 11_Rain	0.352	18.6	0.988	14.2	0.143	0.196	<LOQ	0.194	0.0160	15.0	0.212	0.177	0.00300
CAT 12_Rain	0.441	54.1	1.59	36.3	0.297	0.0480	0.0130	0.377	0.0120	11.0	0.140	0.0390	0.00600
CAT 13_Rain	0.172	34.8	0.417	10.9	0.0530	0.0490	<LOQ	0.148	0.0200	4.00	0.0130	0.0240	0.00700
CAT 14_Rain	0.496	10.6	0.639	79.2	0.116	0.0370	<LOQ	0.229	<LOQ	14.4	0.0110	0.0300	0.0230
CAT 15_Rain	0.475	46.4	3.37	161	0.265	0.0280	<LOQ	0.410	0.00400	24.2	0.0290	0.0670	0.0560
CAT 16_Rain	0.147	<LOQ	4.74	27.4	0.550	0.00800	<LOQ	0.0520	<LOQ	4.63	0.00900	0.0310	0.0110
CAT 17_Rain	3.40	47.2	10.4	131	1.08	0.416	0.0600	4.28	0.0460	29.8	0.525	0.106	0.0540
CAT 18_Rain	0.112	22.5	1.06	22.2	0.110	0.0360	0.00800	0.813	0.00900	8.10	0.0170	0.0160	0.00500
CAT 19_Rain	0.294	7.09	0.430	14.6	0.0560	0.0200	<LOQ	0.603	0.00400	4.32	0.00900	0.0150	0.00200
CAT 20_Rain	0.222	18.1	1.06	31.9	0.0980	0.0170	0.0170	1.50	0.00500	7.54	0.0220	0.0240	0.00500
CAT 21_Rain	0.146	7.55	0.194	3.81	0.0190	0.0140	0.0110	0.147	0.00200	1.90	0.00600	0.0770	0.00200
CAT 22_Rain	0.0330	26.4	0.689	8.48	0.0470	0.0160	<LOQ	0.537	0.00400	4.17	0.00800	0.0380	0.00300
CAT 23_Rain	0.149	51.9	0.230	7.51	0.0200	0.0140	<LOQ	0.0370	<LOQ	1.04	0.00600	0.0850	<LOQ

Sample	Li	B	Al	Ti	V	Cr	Mn	Fe	Co	Ni	Cu	Zn	As
	µg L^{-1}	µg L^{-1}	µg L^{-1}	µg L^{-1}	µg L^{-1}	µg L^{-1}	µg L^{-1}	µg L^{-1}	µg L^{-1}	µg L^{-1}	µg L^{-1}	µg L^{-1}	µg L^{-1}
GLP 03_Rain	0.282	8.63	37.2	2.11	1.06	0.353	31.2	30.0	0.357	0.768	19.2	18.1	0.304
GLP 04_Rain	0.634	16.5	80.9	1.08	4.63	0.174	13.7	10.6	0.168	0.378	21.3	3.93	0.839
GLP 05_Rain	0.498	4.02	99.8	1.89	1.45	0.147	38.2	18.9	0.296	0.262	13.9	6.55	0.154
GLP 06_Rain	0.113	12.0	18.3	0.339	2.08	0.163	0.679	4.79	0.0430	0.189	5.13	8.42	0.478
GLP 07_Rain	0.0460	5.39	61.2	0.356	0.351	0.0920	8.28	9.63	0.114	0.274	2.56	21.2	0.113
GLP 08_Rain	0.0280	3.72	1.61	0.0230	0.214	0.0500	3.25	1.77	0.0210	0.0800	0.277	2.00	0.0490
GLP 09_Rain	0.0240	4.68	3.64	0.116	0.338	0.0400	2.49	3.61	0.0130	0.118	1.11	4.40	0.0830
GLP 10_Rain	0.0380	4.10	14.5	0.121	0.312	0.0410	3.63	2.88	0.0640	0.335	1.66	10.4	0.0590
GLP 11_Rain	0.169	3.60	33.3	0.127	0.338	0.0920	5.84	7.75	0.111	0.273	10.5	29.8	0.140
GLP 12_Rain	0.450	10.5	31.3	0.188	3.28	0.621	0.146	3.56	0.0220	0.131	4.39	1.45	0.336
GLP 13_Rain	0.154	6.51	6.09	0.110	0.525	0.0530	5.08	2.47	0.0230	0.106	0.903	3.11	0.223
GLP 14_Rain	0.186	6.19	47.7	0.218	1.32	0.201	<LOQ	5.66	<LOQ	0.415	3.62	2.60	0.256
GLP 15_Rain	<LOQ	2.00	18.9	<LOQ	0.674	0.0650	<LOQ	1.48	<LOQ	0.117	2.28	4.64	0.0610
GLP 17_Rain	0.233	13.9	46.3	0.981	2.98	0.173	0.215	10.1	0.0440	0.555	19.0	6.46	0.492
GLP 18_Rain	0.252	14.5	14.1	0.231	1.00	0.138	1.06	8.02	0.0100	0.295	4.98	16.5	0.155
GLP 19_Rain	0.166	5.98	7.19	0.200	0.505	0.0840	0.453	2.00	<LOQ	0.0780	3.08	13.5	0.0940
GLP 20_Rain	0.227	6.03	17.0	0.430	0.783	0.248	1.27	7.33	0.0110	0.449	4.97	11.8	0.313
GLP 21_Rain	0.0540	1.84	5.28	0.371	0.186	0.0280	1.73	3.14	0.0150	0.0500	0.180	7.05	0.0610
GLP 22_Rain	0.133	4.29	6.40	0.232	0.261	0.0630	0.763	3.44	0.00600	0.331	1.97	17.0	0.0410
GLP 23_Rain	0.0800	4.24	5.01	0.0870	0.101	0.0630	1.05	4.09	0.0150	0.190	3.20	13.5	0.0560

Sample	Se	Br	Rb	Sr	Mo	Cd	Sn	Sb	Cs	Ba	Tl	Pb	U
	µg L^{-1}	µg L^{-1}	µg L^{-1}	µg L^{-1}	µg L^{-1}	µg L^{-1}	µg L^{-1}	µg L^{-1}	µg L^{-1}	µg L^{-1}	µg L^{-1}	µg L^{-1}	µg L^{-1}
GLP 03_Rain	2.12	11.9	1.94	43.3	0.358	0.0460	0.0140	0.224	<LOQ	14.1	0.0850	0.128	0.0330
GLP 04_Rain	6.84	19.1	4.46	120	1.75	0.0240	0.0160	0.394	0.0120	21.7	0.200	<LOQ	0.0580
GLP 05_Rain	1.50	2.40	1.54	47.5	0.402	0.0450	<LOQ	0.260	<LOQ	8.62	0.0730	<LOQ	0.0300
GLP 06_Rain	0.788	16.2	1.81	49.4	0.262	0.0190	0.159	0.712	0.00600	17.7	0.0970	0.0500	0.0110
GLP 07_Rain	0.234	8.05	0.381	8.01	0.0510	0.0610	0.00500	0.398	0.00700	5.44	0.0690	0.0580	0.00500
GLP 08_Rain	0.167	12.7	0.133	5.09	0.0130	0.0150	<LOQ	0.108	<LOQ	3.85	0.00900	0.0440	0.00100
GLP 09_Rain	0.193	11.4	0.136	6.16	0.0230	0.0100	<LOQ	0.0900	<LOQ	2.94	0.00300	0.0360	0.00200
GLP 10_Rain	0.209	9.03	0.187	5.73	0.0550	0.0440	<LOQ	0.101	<LOQ	1.79	0.0130	0.0290	0.00200
GLP 11_Rain	0.372	10.2	0.558	6.13	0.0610	0.115	<LOQ	0.175	0.0100	10.3	0.129	0.114	0.00200
GLP 12_Rain	0.200	25.9	1.15	40.8	1.28	0.00500	<LOQ	0.573	0.00500	9.02	0.0110	0.0140	0.0790
GLP 13_Rain	0.219	28.4	0.426	9.62	0.0730	0.0280	<LOQ	0.135	0.00600	2.82	0.0110	0.0220	0.00700
GLP 14_Rain	0.417	9.42	0.860	76.9	0.205	0.0410	<LOQ	0.715	<LOQ	12.6	0.0140	0.0320	0.0360
GLP 15_Rain	0.234	2.52	0.481	20.4	0.0310	0.0170	<LOQ	0.0940	<LOQ	5.42	0.000282	0.000529	0.000106
GLP 17_Rain	0.587	8.51	5.72	57.1	0.696	0.0190	0.0120	0.400	0.0150	14.6	0.00103	0.000290	0.000475
GLP 18_Rain	0.106	21.0	1.23	27.3	0.221	0.0190	<LOQ	0.377	0.0110	9.23	0.000260	0.000858	0.000156
GLP 19_Rain	0.358	8.43	0.525	17.0	0.129	0.00800	<LOQ	0.178	0.00400	6.05	0.000192	0.0000873	0.0000349
GLP 20_Rain	<LOQ	14.4	1.19	20.6	0.156	0.0280	0.0100	1.49	0.0130	6.11	0.00220	0.000155	0.000155
GLP 21_Rain	0.102	5.61	0.108	4.01	0.0190	0.0140	<LOQ	0.163	0.00100	1.50	0.000622	0.000415	0.000207
GLP 22_Rain	0.0270	16.4	0.341	9.42	0.0710	0.0160	<LOQ	0.240	0.00200	4.55	0.000160	0.00188	0.0000801
GLP 23_Rain	0.0840	48.5	0.340	7.11	0.0310	0.0200	<LOQ	0.0450	<LOQ	1.50	0.00168	0.0195	0.000840

Sample	Li	B	Al	Ti	V	Cr	Mn	Fe	Co	Ni	Cu	Zn	As
	µg L^{-1}	µg L^{-1}	µg L^{-1}	µg L^{-1}	µg L^{-1}	µg L^{-1}	µg L^{-1}	µg L^{-1}	µg L^{-1}	µg L^{-1}	µg L^{-1}	µg L^{-1}	µg L^{-1}
GAB 01_Rain	0.149	5.38	1.74	<LOQ	0.409	0.197	6.26	1.87	0.0650	0.477	0.491	4.16	0.127
GAB 02_Rain	0.215	7.23	9.35	0.116	0.830	0.102	0.225	1.16	0.00600	0.0850	0.656	1.10	0.172
GAB 03_Rain	0.482	17.8	29.2	<LOQ	2.28	2.54	1.36	11.1	0.0630	2.82	5.24	3.97	0.437
GAB 04_Rain	0.0730	5.11	2.03	<LOQ	2.61	0.158	0.349	0.861	0.0250	0.927	0.779	4.53	0.247
GAB 05_Rain	0.0740	3.83	0.112	<LOQ	0.288	0.0620	3.90	<LOQ	0.0530	0.288	2.04	7.18	0.131
GAB 06_Rain	0.0470	4.50	2.45	0.0440	0.827	0.154	1.50	1.52	0.0100	0.381	1.85	16.4	0.205
GAB 07_Rain	0.239	14.2	6.80	0.214	2.15	0.153	7.33	4.70	0.0620	1.47	6.64	25.2	0.187
GAB 08_Rain	0.0310	2.91	4.80	0.151	0.294	0.140	3.84	6.91	0.0170	0.133	0.510	2.01	0.126
GAB 09_Rain	0.0580	6.73	37.6	0.123	0.364	0.180	6.14	6.06	0.0870	0.496	4.95	21.0	0.256
GAB 10_Rain	0.200	7.58	7.91	0.0230	0.675	0.0490	2.12	7.40	0.0470	1.15	3.04	12.6	0.0580
GAB 11_Rain	0.0870	4.80	13.8	0.0770	0.539	0.0710	1.98	10.8	0.0500	0.756	2.03	6.95	0.125
GAB 12_Rain	0.300	8.89	5.24	0.181	0.450	0.0660	7.67	2.81	0.102	0.922	1.13	14.4	0.129
GAB 13_Rain	0.341	12.3	31.2	0.156	2.02	0.237	5.88	22.3	0.110	1.53	3.46	26.6	0.194
GAB 14_Rain	0.340	6.95	25.8	0.126	1.67	0.230	<LOQ	3.78	<LOQ	0.693	3.94	5.79	0.253

Sample	Se	Br	Rb	Sr	Mo	Cd	Sn	Sb	Cs	Ba	Tl	Pb	U
	µg L^{-1}	µg L^{-1}	µg L^{-1}	µg L^{-1}	µg L^{-1}	µg L^{-1}	µg L^{-1}	µg L^{-1}	µg L^{-1}	µg L^{-1}	µg L^{-1}	µg L^{-1}	µg L^{-1}
GAB 01_Rain	<LOQ	27.8	0.295	15.9	0.100	0.0330	<LOQ	0.0770	<LOQ	5.99	0.0460	<LOQ	0.00400
GAB 02_Rain	0.322	34.9	0.443	48.2	0.130	0.00800	<LOQ	0.428	<LOQ	11.4	0.0170	<LOQ	0.00700
GAB 03_Rain	0.506	30.9	1.52	111	1.24	0.0140	<LOQ	0.347	0.00800	32.4	0.0260	<LOQ	0.0240
GAB 04_Rain	<LOQ	6.81	0.193	9.72	0.264	0.0150	<LOQ	0.136	<LOQ	4.64	0.00600	<LOQ	<LOQ
GAB 05_Rain	<LOQ	6.15	0.109	6.31	0.0540	0.0110	<LOQ	0.100	<LOQ	28.7	0.0100	<LOQ	<LOQ
GAB 06_Rain	0.229	7.79	0.117	11.1	0.116	0.00700	<LOQ	0.211	<LOQ	3.33	0.00500	0.0320	0.00100
GAB 07_Rain	0.125	33.7	0.450	22.9	0.230	0.0430	0.0120	0.156	0.0120	12.6	0.0130	0.0740	0.00600
GAB 08_Rain	0.165	9.60	0.133	6.92	0.0350	0.0150	<LOQ	0.0500	<LOQ	3.77	0.0120	0.0280	0.00100
GAB 09_Rain	0.230	12.2	0.217	8.41	0.0470	0.0500	<LOQ	0.107	<LOQ	10.0	0.0330	0.232	0.00400
GAB 10_Rain	0.143	65.1	0.188	13.8	0.171	0.0270	<LOQ	0.0350	<LOQ	3.13	0.00800	0.156	0.00100
GAB 11_Rain	0.167	20.1	0.0940	5.05	0.0900	0.0260	<LOQ	0.105	0.00200	2.00	0.0170	0.207	0.00100
GAB 12_Rain	0.168	57.9	0.319	20.5	0.124	0.0230	0.00800	0.148	0.00200	4.57	0.0140	0.0630	0.00300
GAB 13_Rain	0.209	67.2	0.399	20.1	0.462	0.0650	<LOQ	0.511	0.00600	3.87	0.0150	1.18	0.00600
GAB 14_Rain	0.142	45.5	0.810	79.5	0.445	0.0470	<LOQ	0.239	<LOQ	19.1	0.00900	0.0370	0.0110

Sample	Li	B	Al	Ti	V	Cr	Mn	Fe	Co	Ni	Cu	Zn	As
	µg L^{-1}	µg L^{-1}	µg L^{-1}	µg L^{-1}	µg L^{-1}	µg L^{-1}	µg L^{-1}	µg L^{-1}	µg L^{-1}	µg L^{-1}	µg L^{-1}	µg L^{-1}	µg L^{-1}
SIR 01_Rain	0.194	7.96	6.07	0.308	0.868	0.166	0.193	1.88	0.00400	0.229	1.60	8.33	0.215
SIR 02_Rain	0.278	13.3	10.7	<LOQ	1.10	0.171	0.0910	2.64	0.0280	0.253	1.93	3.70	0.162
SIR 03_Rain	0.231	6.75	9.97	0.205	0.694	0.188	34.4	12.0	0.265	1.13	6.49	12.0	0.0900
SIR 04_Rain	0.374	14.0	31.6	0.811	3.41	0.436	55.2	18.7	0.583	2.26	9.58	88.3	0.218
SIR 05_Rain	0.264	10.5	48.5	5.23	1.50	0.392	40.6	51.6	0.447	2.07	15.2	11.3	0.181
SIR 06_Rain	0.116	8.93	10.9	0.149	1.05	0.145	0.529	3.01	0.0170	0.672	2.89	83.9	0.228
SIR 07_Rain	0.0400	5.30	2.62	0.0830	0.571	0.134	5.30	2.59	0.0580	0.781	1.74	46.6	0.153
SIR 08_Rain	0.0410	5.04	2.06	0.147	0.216	0.0490	1.73	1.13	0.0280	0.209	1.25	40.8	0.119
SIR 09_Rain	0.0340	6.50	2.94	0.125	0.385	0.0380	2.76	2.20	0.0380	0.186	1.33	23.9	0.0830
SIR 10_Rain	0.0490	3.55	9.02	0.167	0.319	0.0450	2.80	2.19	0.0360	0.597	1.78	12.1	0.0240
SIR 11_Rain	0.149	3.11	2.26	0.0490	0.336	0.0690	3.10	2.17	0.131	9.21	2.73	189	0.103
SIR 12_Rain	2.60	64.9	69.5	0.821	9.36	0.779	1.17	9.45	0.0860	13.1	32.8	145	1.03
SIR 13_Rain	0.340	15.1	11.3	0.176	1.23	2.32	5.43	53.6	0.895	1.33	2.58	59.2	0.393
SIR 14_Rain	0.450	10.7	46.9	0.0570	2.24	0.744	<LOQ	5.87	0.00500	0.981	3.95	4.06	0.399
SIR 15_Rain	<LOQ	1.04	38.8	0.0510	0.733	0.112	0.969	5.43	0.164	0.241	2.56	7.95	0.0730
SIR 16_Rain	<LOQ	6.10	13.8	0.702	0.717	0.198	10.6	9.37	0.0570	0.478	8.20	15.8	0.176
SIR 17_Rain	0.340	11.8	62.3	0.558	4.44	0.500	0.250	3.76	0.0120	0.797	6.42	18.4	0.153
SIR 18_Rain	0.247	15.6	57.1	1.00	2.29	0.183	0.205	6.88	0.00500	0.105	2.48	6.72	0.140
SIR 19_Rain	0.157	6.79	21.4	0.157	1.86	0.0970	0.146	2.34	0.00600	0.261	3.02	9.56	0.117
SIR 20_Rain	0.405	12.0	23.8	0.798	1.91	0.342	1.81	9.84	0.0200	0.704	5.52	28.1	0.218
SIR 21_Rain	0.373	11.0	10.9	0.178	0.219	0.331	1.67	4.62	0.0200	0.440	0.718	78.4	0.314
SIR 22_Rain	0.251	6.57	18.0	0.560	1.23	0.145	0.260	4.33	0.0110	0.878	3.29	27.6	0.0460
SIR 23_Rain	0.141	4.70	1.81	<LOQ	0.159	0.122	0.564	1.42	0.0110	0.210	0.251	28.4	0.134

Sample	Se	Br	Rb	Sr	Mo	Cd	Sn	Sb	Cs	Ba	Tl	Pb	U
	µg L^{-1}	µg L^{-1}	µg L^{-1}	µg L^{-1}	µg L^{-1}	µg L^{-1}	µg L^{-1}	µg L^{-1}	µg L^{-1}	µg L^{-1}	µg L^{-1}	µg L^{-1}	µg L^{-1}
SIR 01_Rain	0.160	28.4	0.484	32.4	0.0940	<LOQ	<LOQ	0.341	<LOQ	10.4	0.0130	<LOQ	0.00500
SIR 02_Rain	<LOQ	28.9	0.501	40.2	0.129	0.0180	<LOQ	0.457	<LOQ	11.0	0.0120	<LOQ	0.00700
SIR 03_Rain	0.219	8.80	0.895	30.8	0.163	0.0170	<LOQ	0.0870	<LOQ	5.30	0.0110	0.272	0.00900
SIR 04_Rain	0.730	9.88	1.13	64.8	0.610	0.0360	0.0210	0.546	<LOQ	22.6	0.0310	0.0980	0.0170
SIR 05_Rain	0.506	7.22	1.27	54.4	0.516	0.0320	0.0180	0.287	<LOQ	7.73	0.0340	0.0460	0.0280
SIR 06_Rain	0.219	11.3	0.415	27.7	0.0970	0.0360	0.0290	0.587	0.00400	16.1	0.0290	0.0610	0.00300
SIR 07_Rain	0.226	7.63	0.184	8.02	0.0380	0.0260	0.0280	0.263	0.00400	6.18	0.0230	0.0870	0.00100
SIR 08_Rain	0.122	17.0	0.0820	4.43	0.0100	0.0100	<LOQ	0.156	<LOQ	3.09	<LOQ	0.0620	<LOQ
SIR 09_Rain	0.100	13.7	0.100	5.18	0.0260	0.0160	<LOQ	0.0800	<LOQ	2.93	0.00300	0.0840	0.00300
SIR 10_Rain	0.167	12.4	0.189	6.39	0.0690	0.0370	0.00800	0.127	0.00300	2.47	0.0180	0.0760	0.00200
SIR 11_Rain	0.151	12.9	0.123	6.80	0.0340	0.0200	<LOQ	0.177	0.00400	5.43	0.0260	0.0330	0.00100
SIR 12_Rain	3.23	233	4.05	181	2.88	0.160	0.0350	9.08	0.0110	43.1	0.154	0.165	0.132
SIR 13_Rain	0.323	77.5	0.680	26.9	0.270	0.0520	0.0200	0.233	0.00700	7.28	0.0260	0.0580	0.0110
SIR 14_Rain	0.240	31.1	0.962	115	0.182	0.0300	<LOQ	0.856	<LOQ	20.2	0.00700	0.0390	0.0640
SIR 15_Rain	0.237	<LOQ	0.316	25.2	<LOQ	0.0180	<LOQ	0.0770	<LOQ	135	0.00400	0.0220	0.00300
SIR 16_Rain	0.230	<LOQ	0.533	23.9	0.104	0.0230	<LOQ	0.165	<LOQ	4.81	0.0320	0.0800	0.00900
SIR 17_Rain	0.454	13.9	1.49	41.3	0.311	0.0250	0.0110	1.44	0.00900	15.4	0.0240	0.0110	0.0380
SIR 18_Rain	0.383	34.3	0.606	28.8	0.161	0.0160	<LOQ	0.637	0.00700	27.3	0.0190	<LOQ	0.0150
SIR 19_Rain	0.104	8.26	0.369	19.3	0.111	0.0180	<LOQ	0.296	0.00500	8.37	0.00700	<LOQ	0.00400
SIR 20_Rain	0.501	64.5	1.04	31.3	0.188	0.0260	0.0100	3.69	0.0180	10.4	0.0690	0.00200	0.0110
SIR 21_Rain	<LOQ	115	0.417	19.5	0.0480	0.00800	0.00600	2.15	0.00200	13.8	0.00500	0.133	0.00400
SIR 22_Rain	0.0550	23.8	0.498	31.3	0.130	0.0170	<LOQ	0.727	0.00400	8.91	0.00700	0.0520	0.0160
SIR 23_Rain	0.108	69.5	0.241	9.67	0.0480	<LOQ	<LOQ	0.212	<LOQ	3.23	<LOQ	0.0730	<LOQ

Sample	Li	B	Al	Ti	V	Cr	Mn	Fe	Co	Ni	Cu	Zn	As
	µg L^{-1}	µg L^{-1}	µg L^{-1}	µg L^{-1}	µg L^{-1}	µg L^{-1}	µg L^{-1}	µg L^{-1}	µg L^{-1}	µg L^{-1}	µg L^{-1}	µg L^{-1}	µg L^{-1}
AUG 01_Rain	0.203	8.37	2.45	0.0750	0.605	0.0410	2.24	1.50	0.0320	0.417	0.555	335	0.103
AUG 02_Rain	0.408	16.8	62.0	1.37	1.54	0.210	12.6	53.3	0.116	0.663	6.89	40.5	0.235
AUG 03_Rain	0.232	6.31	9.53	0.439	0.473	0.199	36.4	13.9	0.263	0.892	8.41	15.1	0.0690
AUG 04_Rain	0.378	18.9	20.9	0.752	1.56	0.170	38.0	23.7	0.749	1.36	23.6	58.9	0.367
AUG 05_Rain	0.530	6.66	96.9	3.02	1.52	0.396	36.8	29.5	0.355	0.928	19.6	7.21	0.260
AUG 06_Rain	0.0680	11.1	5.28	0.218	0.629	0.103	8.83	3.46	0.118	0.899	2.11	312	0.150
AUG 07_Rain	0.0890	7.92	12.4	0.0220	0.373	0.0670	5.04	3.40	0.0770	0.393	2.75	176	0.0660
AUG 08_Rain	0.0790	5.46	0.259	0.0100	0.202	0.0290	1.89	0.163	0.0300	0.0260	0.995	169	0.0360
AUG 09_Rain	0.0680	5.58	3.60	0.106	0.324	0.0250	0.769	1.20	0.00800	0.116	2.32	16.7	0.0760
AUG 10_Rain	0.600	7.57	4.03	0.0650	0.398	0.0400	3.04	1.41	0.103	0.566	2.73	107	0.0700
AUG 11_Rain	0.336	5.37	5.02	0.0900	0.451	0.0420	3.91	3.10	0.0940	0.394	11.9	491	0.144
AUG 12_Rain	0.966	5.76	14.0	0.220	0.633	0.146	14.4	10.2	0.353	1.32	30.0	1,190	0.323

Sample	Se	Br	Rb	Sr	Mo	Cd	Sn	Sb	Cs	Ba	Tl	Pb	U
	µg L^{-1}	µg L^{-1}	µg L^{-1}	µg L^{-1}	µg L^{-1}	µg L^{-1}	µg L^{-1}	µg L^{-1}	µg L^{-1}	µg L^{-1}	µg L^{-1}	µg L^{-1}	µg L^{-1}
AUG 01_Rain	0.152	31.5	0.339	19.9	0.0570	0.0450	<LOQ	0.109	<LOQ	7.73	0.0190	0.00300	0.00400
AUG 02_Rain	0.272	45.5	1.98	52.5	0.147	0.0310	0.0430	0.358	0.0100	13.9	0.0210	0.454	0.0350
AUG 03_Rain	0.148	15.2	0.698	35.5	0.109	0.0270	<LOQ	0.0700	<LOQ	12.0	0.0120	0.168	0.00800
AUG 04_Rain	0.829	21.5	3.99	56.4	0.567	0.0570	0.0240	0.182	<LOQ	15.5	0.0940	0.233	0.00800
AUG 05_Rain	1.43	4.23	1.71	45.4	0.393	0.0670	<LOQ	0.0720	<LOQ	7.08	0.137	<LOQ	0.0240
AUG 06_Rain	0.202	11.5	0.279	14.2	0.0850	0.0350	<LOQ	0.0930	0.00400	6.27	0.0140	0.0410	0.00300
AUG 07_Rain	0.150	27.9	0.181	9.35	0.0490	0.0280	<LOQ	0.319	0.00400	5.62	0.0180	0.397	0.00200
AUG 08_Rain	0.0470	31.4	0.107	7.51	0.0140	0.0170	<LOQ	0.0670	<LOQ	4.02	0.00300	0.0460	<LOQ
AUG 09_Rain	0.232	28.5	0.179	30.8	0.0290	0.0110	<LOQ	0.0890	0.00300	5.20	<LOQ	0.0950	0.00300
AUG 10_Rain	0.161	150	0.504	29.4	0.0560	0.0410	<LOQ	0.200	0.00400	3.74	0.0120	0.129	0.00100
AUG 11_Rain	0.285	59.2	0.508	23.6	0.0830	0.0360	<LOQ	0.165	0.00500	6.87	0.0120	0.176	0.00400
AUG 12_Rain	0.858	63.6	1.39	37.4	0.183	0.164	0.00900	0.157	0.0140	2.97	0.0730	0.692	0.00600

Sample	Li	B	Al	Ti	V	Cr	Mn	Fe	Co	Ni	Cu	Zn	As
	µg L^{-1}	µg L^{-1}	µg L^{-1}	µg L^{-1}	µg L^{-1}	µg L^{-1}	µg L^{-1}	µg L^{-1}	µg L^{-1}	µg L^{-1}	µg L^{-1}	µg L^{-1}	µg L^{-1}
PRI 01_Rain	0.146	6.28	4.59	<LOQ	0.582	0.0520	0.708	1.01	0.00500	0.179	0.467	1.39	0.149
PRI 02_Rain	0.332	15.0	30.6	0.314	1.46	0.139	0.255	4.11	0.0200	0.415	2.52	2.83	0.212
PRI 03_Rain	0.293	5.82	17.1	0.937	1.03	0.654	37.6	17.6	0.351	1.29	17.8	22.1	0.0850
PRI 04_Rain	0.316	7.49	50.6	0.861	1.85	0.370	38.1	13.1	0.333	1.11	10.0	6.51	0.243
PRI 05_Rain	0.321	2.75	200	29.9	1.91	0.236	32.2	205	0.336	1.07	9.48	13.0	0.228
PRI 06_Rain	0.0770	9.19	12.6	0.129	0.839	0.129	0.421	3.04	0.0120	0.138	1.42	3.39	0.128
PRI 07_Rain	0.0330	5.51	3.91	0.0380	0.304	0.0560	4.95	1.62	0.0440	0.300	6.64	3.82	0.154
PRI 08_Rain	0.0380	3.90	5.42	0.0430	0.149	0.0330	2.22	6.01	0.0460	0.161	0.370	3.17	0.0250
PRI 09_Rain	0.0210	3.91	1.50	0.131	0.293	0.0190	3.29	0.982	0.0410	0.203	0.719	3.47	0.0470
PRI 10_Rain	0.0880	3.88	15.9	0.0400	0.462	0.0390	5.01	2.55	0.0660	1.09	3.28	9.40	0.0440
PRI 11_Rain	0.183	3.41	3.99	0.0550	0.502	0.100	3.58	2.20	0.184	0.739	5.48	20.4	0.103
PRI 12_Rain	<LOQ	<LOQ	<LOQ	<LOQ	<LOQ	<LOQ	<LOQ	<LOQ	<LOQ	<LOQ	<LOQ	<LOQ	<LOQ
PRI 13_Rain	0.425	19.5	11.6	0.393	0.868	0.174	4.99	5.60	0.00600	0.509	2.53	7.29	0.352
PRI 14_Rain	0.178	5.04	33.5	0.0850	0.410	0.267	<LOQ	4.31	0.0150	0.458	2.02	1.33	0.169
PRI 15_Rain	0.123	1.44	58.3	<LOQ	0.882	0.190	0.0630	4.45	0.0670	0.0940	4.39	1.78	0.126
PRI 16_Rain	<LOQ	5.40	11.5	0.437	0.406	0.232	11.0	8.27	0.0700	0.479	5.98	19.1	0.0510
PRI 17_Rain	0.279	14.3	24.8	0.613	3.08	0.272	0.169	5.94	0.00800	0.416	12.4	12.9	0.212
PRI 18_Rain	0.192	14.9	8.66	0.266	2.45	0.0830	0.262	2.84	<LOQ	0.464	2.59	12.8	0.0940
PRI 19_Rain	0.101	4.37	8.51	0.113	0.682	0.0500	0.383	2.86	<LOQ	0.130	2.98	14.0	0.0950
PRI 20_Rain	0.664	28.3	39.8	1.88	5.14	0.462	0.828	18.1	0.0500	1.92	32.2	58.4	0.410
PRI 21_Rain	0.405	12.2	6.80	0.491	0.253	0.117	1.81	5.89	0.0620	0.226	0.796	14.6	0.0510
PRI 22_Rain	0.191	6.04	6.92	0.182	0.567	0.0700	0.296	2.78	0.00600	0.484	2.24	11.1	0.0310
PRI 23_Rain	0.254	7.27	1.64	<LOQ	0.0950	0.0370	0.575	1.37	0.00800	0.0310	0.146	3.92	0.0320

Sample	Se	Br	Rb	Sr	Mo	Cd	Sn	Sb	Cs	Ba	Tl	Pb	U
	µg L^{-1}	µg L^{-1}	µg L^{-1}	µg L^{-1}	µg L^{-1}	µg L^{-1}	µg L^{-1}	µg L^{-1}	µg L^{-1}	µg L^{-1}	µg L^{-1}	µg L^{-1}	µg L^{-1}
PRI 01_Rain	0.214	24.9	0.309	22.1	0.0770	0.0140	<LOQ	0.194	<LOQ	6.98	0.0130	<LOQ	0.00400
PRI 02_Rain	0.271	35.0	0.684	66.4	0.160	0.0120	<LOQ	0.677	<LOQ	14.4	0.0110	<LOQ	0.0240
PRI 03_Rain	0.284	5.44	0.763	34.9	0.185	0.0350	<LOQ	0.151	<LOQ	13.1	0.00800	0.202	0.0140
PRI 04_Rain	0.767	7.15	0.959	59.0	0.289	0.0280	<LOQ	0.252	<LOQ	15.0	0.0460	0.0630	0.0210
PRI 05_Rain	1.36	3.20	0.968	40.5	0.303	0.0390	<LOQ	0.0770	<LOQ	8.45	0.0460	0.0920	0.0230
PRI 06_Rain	0.388	11.1	0.289	20.8	0.0840	0.00500	0.0160	0.319	0.00300	9.06	0.0150	0.104	0.00300
PRI 07_Rain	0.137	9.39	0.241	138	0.0520	0.0230	0.00700	32.7	0.00400	202	0.0190	0.0460	<LOQ
PRI 08_Rain	0.140	18.4	0.0670	3.88	0.0140	0.0110	<LOQ	0.0240	<LOQ	1.39	<LOQ	0.0500	0.00200
PRI 09_Rain	0.184	10.9	0.0970	4.51	0.0140	<LOQ	<LOQ	0.0450	<LOQ	2.86	<LOQ	0.0480	0.00100
PRI 10_Rain	0.349	11.0	0.386	8.84	0.146	0.0590	0.0200	0.169	0.00900	3.18	0.0450	0.0800	0.00200
PRI 11_Rain	0.159	11.5	0.173	7.46	0.0640	0.0200	<LOQ	0.142	0.00300	4.10	0.0100	0.0260	0.00200
PRI 12_Rain	<LOQ	<LOQ	<LOQ	<LOQ	<LOQ	<LOQ	<LOQ	<LOQ	<LOQ	<LOQ	<LOQ	<LOQ	<LOQ
PRI 13_Rain	0.440	93.1	0.790	34.3	0.117	0.0410	<LOQ	0.534	0.00700	8.14	0.0450	0.0100	0.00700
PRI 14_Rain	0.0930	22.3	0.542	57.1	0.0910	0.0350	<LOQ	0.472	<LOQ	11.4	0.00400	0.264	0.0200
PRI 15_Rain	0.237	2.04	0.499	48.4	0.0230	0.0140	<LOQ	0.0820	<LOQ	11.1	0.00400	0.128	0.0110
PRI 16_Rain	0.137	<LOQ	0.300	16.1	0.0300	0.0240	<LOQ	0.180	<LOQ	2.76	0.00300	0.0610	0.0100
PRI 17_Rain	0.550	15.5	0.874	35.1	0.225	0.0240	0.0100	0.711	0.00500	10.1	0.0130	<LOQ	0.00900
PRI 18_Rain	0.345	30.8	0.388	16.2	0.150	0.0280	<LOQ	0.882	0.00400	4.39	0.0140	<LOQ	0.00400
PRI 19_Rain	<LOQ	3.71	0.305	11.5	0.0500	0.0160	<LOQ	0.125	0.00400	4.78	0.0150	<LOQ	0.00200
PRI 20_Rain	0.324	52.8	3.05	70.9	0.388	0.0360	0.0430	10.1	0.0270	17.1	0.0440	0.143	0.0320
PRI 21_Rain	<LOQ	128	0.602	20.1	0.0520	0.0290	<LOQ	0.147	0.00300	3.61	0.00700	0.0670	0.00200
PRI 22_Rain	0.0460	23.9	0.496	14.3	0.101	0.0230	<LOQ	0.107	0.00200	5.46	0.00400	0.0280	0.00400
PRI 23_Rain	0.276	105	0.305	14.0	0.0270	0.00900	<LOQ	0.0250	<LOQ	1.12	<LOQ	0.0920	<LOQ

Sample	Li	B	Al	Ti	V	Cr	Mn	Fe	Co	Ni	Cu	Zn	As
	µg L^{-1}	µg L^{-1}	µg L^{-1}	µg L^{-1}	µg L^{-1}	µg L^{-1}	µg L^{-1}	µg L^{-1}	µg L^{-1}	µg L^{-1}	µg L^{-1}	µg L^{-1}	µg L^{-1}
CES 01_Rain	0.0730	1.98	1.43	<LOQ	0.189	0.0310	2.79	0.633	0.0250	0.208	0.0360	1.99	0.0290
CES 02_Rain	0.0890	2.45	3.24	<LOQ	0.288	0.0820	0.233	1.48	0.00600	0.113	0.423	3.61	0.0850
CES 03_Rain	1.11	13.3	15.2	0.260	1.04	0.130	1.03	3.67	0.0320	0.488	4.96	2.08	0.148
CES 04_Rain	0.485	30.2	15.1	<LOQ	2.31	0.316	0.368	3.67	0.0530	1.26	6.68	3.87	0.464
CES 05_Rain	0.0490	4.45	0.556	<LOQ	0.169	0.0300	0.207	<LOQ	0.00700	0.122	0.864	2.42	0.0540
CES 07_Rain	0.0550	3.91	17.7	0.126	0.215	0.124	4.81	12.8	0.0440	0.446	3.96	25.7	0.120
CES 08_Rain	0.00600	1.86	4.46	0.0450	0.122	0.0400	2.99	2.75	0.0250	0.0410	2.88	5.44	0.0770
CES 09_Rain	0.0710	4.89	9.67	0.618	0.503	0.0830	7.51	5.93	0.0530	0.788	2.79	14.9	0.151
CES 10_Rain	0.0350	2.67	5.41	0.394	0.116	0.0380	2.25	3.27	0.0220	0.950	1.03	5.58	0.0230
CES 11_Rain	0.0740	2.64	2.95	0.123	0.122	0.0170	1.81	1.28	0.0230	0.0280	0.853	2.02	0.0460
CES 12_Rain	0.271	4.55	123	0.0470	1.42	0.0310	8.95	2.20	0.0890	0.200	2.37	2.97	0.112
CES 13_Rain	0.0810	2.32	6.74	0.0950	0.335	0.0520	11.4	4.74	0.149	0.700	0.976	2.36	0.127
CES 14_Rain	<LOQ	5.46	12.5	0.230	0.462	0.369	<LOQ	14.1	0.176	0.491	2.29	4.14	0.0960
CES 15_Rain	<LOQ	1.26	7.83	0.0360	0.337	0.0670	0.199	1.62	<LOQ	0.233	2.19	5.13	0.0690
CES 17_Rain	0.0420	5.39	6.53	0.0740	0.303	0.0510	3.67	16.5	<LOQ	0.207	1.41	7.60	0.110
CES 18_Rain	0.0530	6.92	6.50	0.0910	0.433	0.0470	0.706	5.57	<LOQ	0.301	2.77	13.7	0.0740
CES 19_Rain	0.0230	4.65	4.42	0.0990	0.269	0.0540	1.71	2.88	0.0110	0.422	1.62	8.35	0.104
CES 20_Rain	<LOQ	2.47	4.54	0.113	0.108	0.0260	2.91	3.37	0.0280	0.142	1.59	7.60	0.0400
CES 21_Rain	0.0220	1.91	9.49	0.580	0.142	0.0380	1.03	4.81	0.00600	0.113	0.604	7.54	0.0580
CES 22_Rain	0.190	6.36	16.2	0.454	0.265	0.128	0.717	11.5	0.0550	0.232	2.61	7.31	0.0520
CES 23_Rain	<LOQ	0.578	9.52	0.122	0.142	0.0870	6.51	11.5	0.0760	0.141	2.00	11.8	0.0920

Sample	Se	Br	Rb	Sr	Mo	Cd	Sn	Sb	Cs	Ba	Tl	Pb	U
	µg L^{-1}	µg L^{-1}	µg L^{-1}	µg L^{-1}	µg L^{-1}	µg L^{-1}	µg L^{-1}	µg L^{-1}	µg L^{-1}	µg L^{-1}	µg L^{-1}	µg L^{-1}	µg L^{-1}
CES 01_Rain	<LOQ	7.73	0.152	7.14	0.0150	<LOQ	<LOQ	0.132	<LOQ	2.61	0.00300	<LOQ	<LOQ
CES 02_Rain	<LOQ	9.77	0.218	15.5	0.0300	<LOQ	<LOQ	0.0690	<LOQ	4.18	0.00600	<LOQ	0.00500
CES 03_Rain	0.204	21.9	1.07	46.8	0.127	0.0120	<LOQ	0.550	0.00900	13.4	0.0150	<LOQ	0.0100
CES 04_Rain	0.547	37.9	1.69	94.2	0.311	0.0120	0.0140	0.913	0.0130	24.7	0.0320	0.0220	0.0220
CES 05_Rain	<LOQ	5.89	0.0870	4.73	0.0330	<LOQ	<LOQ	0.0500	<LOQ	2.71	<LOQ	<LOQ	<LOQ
CES 07_Rain	0.210	15.7	0.153	20.3	0.0580	0.0330	0.0140	0.0780	0.00400	3.40	0.0270	0.165	0.00200
CES 08_Rain	0.0710	5.10	0.147	2.91	0.0180	0.0200	<LOQ	0.0290	0.00400	2.50	0.0210	0.0480	0.00200
CES 09_Rain	0.333	11.8	0.330	9.88	0.0400	0.0260	0.0600	0.374	0.00600	9.37	0.0170	0.970	0.00600
CES 10_Rain	0.116	13.1	0.0770	3.94	0.0180	0.0330	<LOQ	0.0650	<LOQ	2.47	<LOQ	0.0580	0.00100
CES 11_Rain	0.138	11.5	0.0940	3.07	<LOQ	0.00900	0.00700	0.0380	0.00100	1.02	<LOQ	0.0300	0.00200
CES 12_Rain	0.824	32.0	0.549	15.0	0.132	0.0720	<LOQ	0.124	0.00900	4.49	0.124	0.00900	0.00600
CES 13_Rain	0.165	10.8	0.247	8.34	0.0340	0.0280	<LOQ	0.0970	0.00300	2.72	0.00600	0.0340	0.00800
CES 14_Rain	0.0300	20.7	0.383	29.5	0.0390	0.0430	<LOQ	0.143	<LOQ	7.90	0.00800	0.0250	0.00500
CES 15_Rain	0.235	<LOQ	0.374	16.9	<LOQ	0.0330	<LOQ	0.0670	<LOQ	4.46	0.00900	0.0150	0.00200
CES 17_Rain	0.147	13.0	0.389	7.89	0.0450	0.0260	<LOQ	0.0610	0.00500	2.85	0.0190	0.0140	0.00100
CES 18_Rain	0.229	9.33	0.253	10.7	0.0440	0.0180	<LOQ	0.0630	0.00300	4.19	0.00600	0.0160	0.00200
CES 19_Rain	0.187	10.7	0.201	6.20	0.0380	0.0290	0.0190	0.202	0.00300	3.10	0.00800	0.0620	0.00200
CES 20_Rain	0.0350	6.60	0.153	3.50	0.0190	0.0150	<LOQ	0.0510	0.00200	1.57	0.00400	0.0350	0.00200
CES 21_Rain	0.0360	12.4	0.169	5.96	0.0110	<LOQ	<LOQ	0.0270	0.00200	3.33	0.00300	0.0560	0.00300
CES 22_Rain	0.0470	37.4	0.328	14.2	0.0390	0.00900	<LOQ	0.0730	0.00300	3.25	0.00300	0.0660	0.00500
CES 23_Rain	0.567	7.73	0.180	2.67	0.0260	0.0240	<LOQ	0.136	0.00400	1.35	0.0140	0.189	<LOQ

Table S. 4 - Minor and trace element concentrations (µg L^{-1}) in rinse solutions.

Sample	Li	B	Al	Ti	V	Cr	Mn	Fe	Co	Ni	Cu	Zn	As
	µg L^{-1}	µg L^{-1}	µg L^{-1}	µg L^{-1}	µg L^{-1}	µg L^{-1}	µg L^{-1}	µg L^{-1}	µg L^{-1}	µg L^{-1}	µg L^{-1}	µg L^{-1}	µg L^{-1}
CIT 08	0.180	6.15	507	11.1	1.93	0.0520	10.8	127	0.114	0.0820	28.3	10.1	0.150
CIT 15	0.189	35.8	452	3.88	2.48	0.384	16.1	141	0.116	0.303	23.5	14.1	0.332

Sample	Se	Br	Rb	Sr	Mo	Cd	Sn	Sb	Cs	Ba	Tl	Pb	U
	µg L^{-1}	µg L^{-1}	µg L^{-1}	µg L^{-1}	µg L^{-1}	µg L^{-1}	µg L^{-1}	µg L^{-1}	µg L^{-1}	µg L^{-1}	µg L^{-1}	µg L^{-1}	µg L^{-1}
CIT 08	0.741	32.9	1.20	10.3	0.0850	0.0570	<LOQ	0.0270	0.0280	11.8	0.203	0.717	0.0470
CIT 15	0.878	<LOQ	6.56	12.1	0.110	0.179	<LOQ	0.263	0.0350	9.56	0.263	3.50	0.0590

Sample	Li	B	Al	Ti	V	Cr	Mn	Fe	Co	Ni	Cu	Zn	As
	µg L^{-1}	µg L^{-1}	µg L^{-1}	µg L^{-1}	µg L^{-1}	µg L^{-1}	µg L^{-1}	µg L^{-1}	µg L^{-1}	µg L^{-1}	µg L^{-1}	µg L^{-1}	µg L^{-1}
ZAF 08	<LOQ	6.50	67.0	2.19	0.0620	0.150	1.54	19.4	0.0320	0.228	0.692	12.3	0.0430
ZAF 15	0.174	39.1	691	5.77	2.51	0.274	20.9	133	0.242	0.720	26.5	39.9	0.284

Sample	Se	Br	Rb	Sr	Mo	Cd	Sn	Sb	Cs	Ba	Tl	Pb	U
	µg L^{-1}	µg L^{-1}	µg L^{-1}	µg L^{-1}	µg L^{-1}	µg L^{-1}	µg L^{-1}	µg L^{-1}	µg L^{-1}	µg L^{-1}	µg L^{-1}	µg L^{-1}	µg L^{-1}
ZAF 08	0.133	27.6	0.134	0.499	0.0190	0.0230	<LOQ	0.443	0.00300	0.896	0.0340	0.838	0.00300
ZAF 15	2.10	<LOQ	2.30	18.7	0.0990	0.320	<LOQ	0.208	0.0270	24.5	0.0840	6.49	0.120

Sample	Li	B	Al	Ti	V	Cr	Mn	Fe	Co	Ni	Cu	Zn	As
	µg L^{-1}	µg L^{-1}	µg L^{-1}	µg L^{-1}	µg L^{-1}	µg L^{-1}	µg L^{-1}	µg L^{-1}	µg L^{-1}	µg L^{-1}	µg L^{-1}	µg L^{-1}	µg L^{-1}
INT 08	<LOQ	5.73	28.7	0.737	0.0830	0.0590	0.692	12.9	0.0120	0.193	2.31	1.17	0.0310
INT 15	0.289	41.7	613	5.94	2.77	0.499	17.8	174	0.186	0.446	28.4	23.0	0.559

Sample	Se	Br	Rb	Sr	Mo	Cd	Sn	Sb	Cs	Ba	Tl	Pb	U
	µg L^{-1}	µg L^{-1}	µg L^{-1}	µg L^{-1}	µg L^{-1}	µg L^{-1}	µg L^{-1}	µg L^{-1}	µg L^{-1}	µg L^{-1}	µg L^{-1}	µg L^{-1}	µg L^{-1}
INT 08	0.142	33.2	0.0940	0.292	0.0230	<LOQ	<LOQ	0.0110	0.0170	0.265	0.0240	0.347	0.00300
INT 15	2.10	<LOQ	3.85	17.6	0.143	0.659	<LOQ	0.242	0.0510	14.9	0.768	6.06	0.0900

Sample	Li	B	Al	Ti	V	Cr	Mn	Fe	Co	Ni	Cu	Zn	As
	µg L^{-1}	µg L^{-1}	µg L^{-1}	µg L^{-1}	µg L^{-1}	µg L^{-1}	µg L^{-1}	µg L^{-1}	µg L^{-1}	µg L^{-1}	µg L^{-1}	µg L^{-1}	µg L^{-1}
ARC 08A	<LOQ	7.89	72.4	1.64	0.143	0.110	6.57	21.59	0.0650	0.212	4.38	13.0	0.0280
ARC 15	0.757	36.7	421	4.75	1.14	0.570	30.4	172	0.366	0.959	31.7	86.5	0.238

Sample	Se	Br	Rb	Sr	Mo	Cd	Sn	Sb	Cs	Ba	Tl	Pb	U
	µg L^{-1}	µg L^{-1}	µg L^{-1}	µg L^{-1}	µg L^{-1}	µg L^{-1}	µg L^{-1}	µg L^{-1}	µg L^{-1}	µg L^{-1}	µg L^{-1}	µg L^{-1}	µg L^{-1}
ARC 08A	0.219	<LOQ	0.158	6.07	0.0230	0.0310	<LOQ	0.0820	0.00800	9.63	0.0160	2.38	0.0190
ARC 15	0.657	<LOQ	1.07	17.4	0.0860	0.0970	<LOQ	0.441	0.0210	30.1	0.0230	13.1	0.114

Sample	Li	B	Al	Ti	V	Cr	Mn	Fe	Co	Ni	Cu	Zn	As
	µg L^{-1}	µg L^{-1}	µg L^{-1}	µg L^{-1}	µg L^{-1}	µg L^{-1}	µg L^{-1}	µg L^{-1}	µg L^{-1}	µg L^{-1}	µg L^{-1}	µg L^{-1}	µg L^{-1}
UNI 08	<LOQ	7.76	75.2	0.879	0.130	0.143	4.77	35.2	0.0480	0.159	2.43	8.78	0.0390
UNI 15	0.118	39.4	239	2.57	0.501	0.374	16.1	112	0.175	0.639	11.9	31.5	0.125

Sample	Se	Br	Rb	Sr	Mo	Cd	Sn	Sb	Cs	Ba	Tl	Pb	U
	µg L^{-1}	µg L^{-1}	µg L^{-1}	µg L^{-1}	µg L^{-1}	µg L^{-1}	µg L^{-1}	µg L^{-1}	µg L^{-1}	µg L^{-1}	µg L^{-1}	µg L^{-1}	µg L^{-1}
UNI 08	0.111	1.39	0.0850	3.99	0.0270	0.0190	<LOQ	0.141	0.00500	4.91	<LOQ	2.80	0.0130
UNI 15	0.537	<LOQ	0.654	11.5	0.0560	0.106	<LOQ	0.377	0.0130	17.9	0.0140	5.12	0.0540

Sample	Li	B	Al	Ti	V	Cr	Mn	Fe	Co	Ni	Cu	Zn	As
	µg L^{-1}	µg L^{-1}	µg L^{-1}	µg L^{-1}	µg L^{-1}	µg L^{-1}	µg L^{-1}	µg L^{-1}	µg L^{-1}	µg L^{-1}	µg L^{-1}	µg L^{-1}	µg L^{-1}
IND 08	<LOQ	5.93	84.5	1.58	0.138	0.189	4.61	27.9	0.128	0.178	3.31	48.7	0.0320
IND 15	0.195	42.2	477	3.91	1.24	0.725	52.3	223	0.556	1.28	35.1	91.8	0.260

Sample	Se	Br	Rb	Sr	Mo	Cd	Sn	Sb	Cs	Ba	Tl	Pb	U
	µg L^{-1}	µg L^{-1}	µg L^{-1}	µg L^{-1}	µg L^{-1}	µg L^{-1}	µg L^{-1}	µg L^{-1}	µg L^{-1}	µg L^{-1}	µg L^{-1}	µg L^{-1}	µg L^{-1}
IND 08	0.222	<LOQ	0.124	4.07	0.132	0.0170	<LOQ	0.100	0.00500	5.32	0.00500	2.12	0.0110
IND 15	0.938	1.14	1.45	27.1	0.175	0.211	<LOQ	0.416	0.0140	40.8	0.0150	17.1	0.113

Sample	Li	B	Al	Ti	V	Cr	Mn	Fe	Co	Ni	Cu	Zn	As
	µg L^{-1}	µg L^{-1}	µg L^{-1}	µg L^{-1}	µg L^{-1}	µg L^{-1}	µg L^{-1}	µg L^{-1}	µg L^{-1}	µg L^{-1}	µg L^{-1}	µg L^{-1}	µg L^{-1}
BEL 08	<LOQ	5.81	86.5	0.821	0.131	0.231	5.23	30.7	0.0520	0.276	5.80	16.1	0.0330

Sample	Se	Br	Rb	Sr	Mo	Cd	Sn	Sb	Cs	Ba	Tl	Pb	U
	µg L^{-1}	µg L^{-1}	µg L^{-1}	µg L^{-1}	µg L^{-1}	µg L^{-1}	µg L^{-1}	µg L^{-1}	µg L^{-1}	µg L^{-1}	µg L^{-1}	µg L^{-1}	µg L^{-1}
BEL 08	0.114	<LOQ	0.0790	4.00	0.0400	0.0250	<LOQ	0.157	0.00500	5.06	0.00500	2.33	0.0120

Sample	Li	B	Al	Ti	V	Cr	Mn	Fe	Co	Ni	Cu	Zn	As
	µg L^{-1}	µg L^{-1}	µg L^{-1}	µg L^{-1}	µg L^{-1}	µg L^{-1}	µg L^{-1}	µg L^{-1}	µg L^{-1}	µg L^{-1}	µg L^{-1}	µg L^{-1}	µg L^{-1}
CAT 08	<LOQ	7.42	64.5	0.654	0.0400	0.106	0.864	19.3	0.0120	0.121	1.00	6.20	0.0240
CAT 15	0.342	46.6	940	5.94	4.32	0.590	74.7	247	0.795	1.01	29.8	85.7	0.393

Sample	Se	Br	Rb	Sr	Mo	Cd	Sn	Sb	Cs	Ba	Tl	Pb	U
	µg L^{-1}	µg L^{-1}	µg L^{-1}	µg L^{-1}	µg L^{-1}	µg L^{-1}	µg L^{-1}	µg L^{-1}	µg L^{-1}	µg L^{-1}	µg L^{-1}	µg L^{-1}	µg L^{-1}
CAT 08	0.133	20.5	<LOQ	0.527	0.00900	<LOQ	<LOQ	0.0620	0.00200	1.03	0.00300	1.21	<LOQ
CAT 15	1.42	1.90	3.90	51.6	0.170	0.235	<LOQ	0.326	0.0270	46.3	0.0850	5.51	0.112

Sample	Li	B	Al	Ti	V	Cr	Mn	Fe	Co	Ni	Cu	Zn	As
	µg L^{-1}	µg L^{-1}	µg L^{-1}	µg L^{-1}	µg L^{-1}	µg L^{-1}	µg L^{-1}	µg L^{-1}	µg L^{-1}	µg L^{-1}	µg L^{-1}	µg L^{-1}	µg L^{-1}
GLP 08	<LOQ	6.54	58.2	0.889	0.0330	0.109	1.27	200	0.0210	2.47	19.0	3.05	0.162
GLP 15	0.272	43.6	1037	10.2	4.10	0.435	40.1	227	0.478	0.933	30.6	86.3	0.372

Sample	Se	Br	Rb	Sr	Mo	Cd	Sn	Sb	Cs	Ba	Tl	Pb	U
	µg L^{-1}	µg L^{-1}	µg L^{-1}	µg L^{-1}	µg L^{-1}	µg L^{-1}	µg L^{-1}	µg L^{-1}	µg L^{-1}	µg L^{-1}	µg L^{-1}	µg L^{-1}	µg L^{-1}
GLP 08	0.134	14.3	<LOQ	0.358	0.0150	0.00800	<LOQ	0.119	0.00200	0.762	0.00300	0.772	0.00300
GLP 15	1.39	2.56	2.99	36.1	0.256	0.217	<LOQ	0.219	0.0280	47.5	0.0810	5.11	0.221

Sample	Li	B	Al	Ti	V	Cr	Mn	Fe	Co	Ni	Cu	Zn	As
	µg L^{-1}	µg L^{-1}	µg L^{-1}	µg L^{-1}	µg L^{-1}	µg L^{-1}	µg L^{-1}	µg L^{-1}	µg L^{-1}	µg L^{-1}	µg L^{-1}	µg L^{-1}	µg L^{-1}
GAB 08	0.00500	5.03	17.6	0.381	0.0940	0.0800	0.570	9.78	0.00500	0.0730	0.599	6.17	0.0270

Sample	Se	Br	Rb	Sr	Mo	Cd	Sn	Sb	Cs	Ba	Tl	Pb	U
	µg L^{-1}	µg L^{-1}	µg L^{-1}	µg L^{-1}	µg L^{-1}	µg L^{-1}	µg L^{-1}	µg L^{-1}	µg L^{-1}	µg L^{-1}	µg L^{-1}	µg L^{-1}	µg L^{-1}
GAB 08	0.132	23.3	0.0130	2.43	0.0250	<LOQ	<LOQ	0.0570	0.00200	0.643	<LOQ	0.895	<LOQ

Sample	Li	B	Al	Ti	V	Cr	Mn	Fe	Co	Ni	Cu	Zn	As
	µg L^{-1}	µg L^{-1}	µg L^{-1}	µg L^{-1}	µg L^{-1}	µg L^{-1}	µg L^{-1}	µg L^{-1}	µg L^{-1}	µg L^{-1}	µg L^{-1}	µg L^{-1}	µg L^{-1}
SIR 08	<LOQ	8.13	95.6	1.86	0.112	0.210	1.73	26.3	0.0220	0.188	1.20	12.9	0.0260
SIR 15	0.0900	33.1	360	2.90	2.25	0.376	26.8	97.0	0.274	1.64	11.9	141	0.249

Sample	Se	Br	Rb	Sr	Mo	Cd	Sn	Sb	Cs	Ba	Tl	Pb	U
	µg L^{-1}	µg L^{-1}	µg L^{-1}	µg L^{-1}	µg L^{-1}	µg L^{-1}	µg L^{-1}	µg L^{-1}	µg L^{-1}	µg L^{-1}	µg L^{-1}	µg L^{-1}	µg L^{-1}
SIR 08	0.336	<LOQ	0.0560	1.53	0.0260	0.0290	<LOQ	0.110	0.00500	2.05	0.00500	3.35	0.0130
SIR 15	0.852	1.08	0.936	19.1	0.0870	0.125	<LOQ	0.190	0.0100	114	0.0200	3.84	0.0820

Sample	Li	B	Al	Ti	V	Cr	Mn	Fe	Co	Ni	Cu	Zn	As
	µg L^{-1}	µg L^{-1}	µg L^{-1}	µg L^{-1}	µg L^{-1}	µg L^{-1}	µg L^{-1}	µg L^{-1}	µg L^{-1}	µg L^{-1}	µg L^{-1}	µg L^{-1}	µg L^{-1}
AUG 08	<LOQ	4.32	40.6	0.520	0.0590	0.0690	0.936	10.6	0.0170	0.139	0.935	14.5	0.00600

Sample	Se	Br	Rb	Sr	Mo	Cd	Sn	Sb	Cs	Ba	Tl	Pb	U
	µg L^{-1}	µg L^{-1}	µg L^{-1}	µg L^{-1}	µg L^{-1}	µg L^{-1}	µg L^{-1}	µg L^{-1}	µg L^{-1}	µg L^{-1}	µg L^{-1}	µg L^{-1}	µg L^{-1}
AUG 08	0.130	<LOQ	0.0200	1.80	0.0100	0.0100	<LOQ	0.0660	0.00100	0.880	<LOQ	2.21	0.00400

Sample	Li	B	Al	Ti	V	Cr	Mn	Fe	Co	Ni	Cu	Zn	As
	µg L^{-1}	µg L^{-1}	µg L^{-1}	µg L^{-1}	µg L^{-1}	µg L^{-1}	µg L^{-1}	µg L^{-1}	µg L^{-1}	µg L^{-1}	µg L^{-1}	µg L^{-1}	µg L^{-1}
PRI 08	<LOQ	5.48	24.1	0.341	0.0490	0.136	0.807	13.4	0.00900	0.133	0.887	4.23	0.0180
PRI 15	0.204	43.1	511	3.97	1.79	0.406	33.7	139	0.405	1.07	18.0	68.9	0.236

Sample	Se	Br	Rb	Sr	Mo	Cd	Sn	Sb	Cs	Ba	Tl	Pb	U
	µg L^{-1}	µg L^{-1}	µg L^{-1}	µg L^{-1}	µg L^{-1}	µg L^{-1}	µg L^{-1}	µg L^{-1}	µg L^{-1}	µg L^{-1}	µg L^{-1}	µg L^{-1}	µg L^{-1}
PRI 08	0.141	4.55	<LOQ	0.616	0.0150	0.0110	<LOQ	0.0440	<LOQ	0.615	<LOQ	0.703	<LOQ
PRI 15	1.19	<LOQ	1.41	21.9	0.0970	0.122	<LOQ	0.219	0.0150	28.1	0.0280	3.92	0.100

Sample	Li	B	Al	Ti	V	Cr	Mn	Fe	Co	Ni	Cu	Zn	As
	µg L^{-1}	µg L^{-1}	µg L^{-1}	µg L^{-1}	µg L^{-1}	µg L^{-1}	µg L^{-1}	µg L^{-1}	µg L^{-1}	µg L^{-1}	µg L^{-1}	µg L^{-1}	µg L^{-1}
CES 08	<LOQ	8.31	23.8	0.367	0.0170	0.152	1.10	12.9	0.00500	0.189	1.05	17.6	0.0150
CES 15	<LOQ	41.0	198	1.12	0.290	0.164	21.3	46.5	0.145	0.575	9.79	44.0	0.105

Sample	Se	Br	Rb	Sr	Mo	Cd	Sn	Sb	Cs	Ba	Tl	Pb	U
	µg L^{-1}	µg L^{-1}	µg L^{-1}	µg L^{-1}	µg L^{-1}	µg L^{-1}	µg L^{-1}	µg L^{-1}	µg L^{-1}	µg L^{-1}	µg L^{-1}	µg L^{-1}	µg L^{-1}
CES 08	0.0800	2.76	0.0220	0.903	0.0250	0.0240	<LOQ	0.132	0.00100	1.46	<LOQ	0.362	<LOQ
CES 15	0.469	2.24	1.13	11.7	0.0240	0.158	<LOQ	0.176	0.0100	17.5	0.0160	2.73	0.0420

Table S. 5 - Minor and trace element concentrations (µg L^{-1}) in insoluble fraction solutions. Al, Ti, and Fe concentrations are in mg L^{-1}.

Sample	Li	B	Al	Ti	V	Cr	Mn	Fe	Co	Ni	Cu	Zn	As	Sr	Mo	Ba	Pb	Volume	Material
	µg L^{-1}	µg L^{-1}	mg L^{-1}	mg L^{-1}	µg L^{-1}	µg L^{-1}	µg L^{-1}	mg L^{-1}	µg L^{-1}	µg L^{-1}	µg L^{-1}	µg L^{-1}	µg L^{-1}	µg L^{-1}	µg L^{-1}	µg L^{-1}	µg L^{-1}	L	mg
CIT 01M	165	279	429	24.5	998	137	4.99	338	117	97.9	6.82	804	43.5	3.74	12.1	2.39	117	6.50	128
CIT 02M	620	788	1.20	26.5	1.69	722	9.43	788	278	305	2.82	3.09	114	5.88	8.23	4.46	425	4.00	306
CIT 03M	25.0	41.5	41.8	2.52	108	41.0	523	40.4	15.1	25.3	285	215	4.69	340	2.14	287	27.3	0.300	144
CIT 04M	1.10	<LOQ	0.814	0.0432	24.1	10.9	16.9	0.790	<LOQ	13.7	46.3	52.8	<LOQ	10.1	2.44	16.6	6.56	1.75	93.5
CIT 05M	21.9	39.3	38.6	2.71	105	29.9	643	34.7	16.3	18.3	261	421	5.34	357	1.46	258	15.7	0.200	188
CIT 06M	43.4	93.7	178	10.1	421	30.3	2.28	128	57.9	37.0	494	369	15.8	2.34	6.13	751	37.4	1.50	73.8
CIT 07M	125	203	203	14.6	577	173	2.29	214	68.5	95.8	591	473	32.9	1.48	16.8	691	150	7.14	122
CIT 08M	183	266	399	24.4	1.02	219	4.84	348	126	95.6	5.69	945	43.5	3.16	10.5	2.12	131	5.50	840
CIT 09M	45.9	100	69.3	4.07	185	176	730	66.5	26.7	57.2	166	243	11.8	430	4.51	344	85.7	4.90	68.7
CIT 10M	152	481	1.17	106	2.73	211	15.80	991	283	98.2	1.60	1.13	66.4	11.80	27.1	4.55	100	4.60	631
CIT 11M	16.5	61.4	77.5	9.21	272	40.3	1.15	72.1	30.0	18.0	160	138	9.26	1.20	3.99	581	24.9	1.95	36.1
CIT 12M	75.5	208	348	26.9	953	73.5	4.79	293	116	65.4	864	565	18.4	4.39	11.0	2.57	56.6	1.20	161
CIT 13M	88.6	138	149	8.40	370	140	1.46	126	44.3	82.4	344	366	36.0	842	7.88	700	141	5.80	251
CIT 14M	728	985	1.44	37.9	1.87	993	12.40	986	302	381	2.56	3.57	152	4.19	19.5	5.59	393	2.17	661
CIT 15M	18.3	32.5	20.8	0.619	40.1	32.9	308	17.3	7.05	18.4	103	376	2.57	81.9	1.62	121	13.2	7.60	89.3
CIT 16M	11.8	28.2	26.6	2.18	77.8	14.9	369	25.3	9.92	11.8	273	192	9.25	271	2.47	212	15.5	0.160	13.2
CIT 17M	20.4	35.8	28.6	1.94	79.5	38.6	327	31.4	8.45	22.1	251	205	8.47	159	4.39	135	36.7	0.960	26.1
CIT 18M	50.9	118	114	10.8	337	76.7	1.31	98.8	38.1	41.9	292	367	16.1	1.39	7.31	698	61.0	2.50	97.3
CIT 19M	42.9	85.7	61.3	3.68	156	70.4	622	58.5	17.9	37.5	224	361	11.1	397	4.25	345	50.6	2.40	65.0
CIT 20M	32.9	75.1	62.8	5.60	175	56.0	760	57.3	20.8	32.4	152	333	9.96	581	3.71	415	35.8	2.38	324
CIT 21M	140	237	247	15.0	617	192	2.55	231	71.8	99.1	526	567	40.9	1.94	12.2	1.26	98.1	5.00	115
CIT 22M	84.8	237	361	30.0	966	62.2	4.90	331	106	53.5	842	505	27.6	3.99	14.4	2.35	105	1.47	281
CIT 23M	5.66	9.13	8.05	0.353	19.6	15.8	59.1	8.38	1.77	8.10	26.3	93.5	1.97	24.3	1.28	29.7	7.88	5.00	18.7

Sample	Li	B	Al	Ti	V	Cr	Mn	Fe	Co	Ni	Cu	Zn	As	Sr	Mo	Ba	Pb	Volume	Material
	µg L^{-1}	µg L^{-1}	mg L^{-1}	mg L^{-1}	µg L^{-1}	µg L^{-1}	µg L^{-1}	mg L^{-1}	µg L^{-1}	µg L^{-1}	µg L^{-1}	µg L^{-1}	µg L^{-1}	µg L^{-1}	µg L^{-1}	µg L^{-1}	µg L^{-1}	L	mg
ZAF 01M	299	402	565	30.7	1.36	256	8.88	474	197	132	3.55	1.87	60.9	4.06	37.2	2.37	162	8.83	196
ZAF 02M	24.9	40.8	35.4	1.62	78.0	42.4	519	29.8	13.5	25.2	135	323	5.43	240	1.91	244	23.9	4.90	123
ZAF 03M	117	283	540	37.1	1.24	86.4	7.07	422	159	94.4	1.56	2.25	23.2	6.82	18.4	3.62	87.8	0.120	583
ZAF 04M	2.37	4.36	2.53	0.0842	52.9	29.2	43.0	2.81	0.997	29.7	59.2	104	4.18	14.1	4.14	31.1	12.9	0.200	155
ZAF 05M	80.5	211	366	31.7	1.07	44.9	5.34	326	122	50.3	1.07	546	24.8	4.47	13.6	2.69	58.3	0.150	183
ZAF 06M	92.8	151	135	7.66	350	145	2.30	117	58.4	72.8	531	1.15	21.2	901	5.23	834	80.1	2.20	445
ZAF 07M	15.1	34.3	30.4	2.52	96.2	31.1	396	31.5	11.8	18.0	137	152	6.67	298	3.90	174	34.7	11.6	67.9
ZAF 08M	279	354	379	7.10	576	492	2.67	286	91.5	175	908	1.35	51.0	644	5.99	1.18	232	5.40	653
ZAF 09M	29.4	60.9	39.1	1.48	81.6	132	372	35.1	12.9	42.4	196	330	6.55	144	3.35	180	53.4	4.75	23.5
ZAF 10M	58.7	194	323	27.8	894	104	4.53	287	112	61.4	602	429	15.4	4.06	11.1	1.80	72.6	5.50	471
ZAF 11M	3.46	16.5	14.8	1.58	47.2	28.6	220	13.9	5.59	6.35	55.5	114	1.37	202	0.333	126	12.9	1.35	4.50
ZAF 12M	104	237	338	27.3	1.04	114	4.89	310	120	62.3	1.84	857	34.4	4.00	11.3	2.53	75.9	1.15	407
ZAF 13M	118	184	206	8.35	458	220	2.02	203	58.5	101	484	624	34.1	834	6.90	973	291	6.00	365
ZAF 14M	331	418	407	11.0	702	417	5.73	360	133	242	972	3.12	55.1	1.51	10.6	2.17	181	1.47	209
ZAF 15M	15.8	31.4	20.9	0.923	49.7	46.2	244	18.3	6.66	28.9	118	237	3.27	89.6	0.163	129	16.6	5.00	261
ZAF 16M	4.44	14.3	20.1	1.66	64.8	6.21	287	15.6	7.21	6.60	67.5	110	0.964	287	0.981	143	5.92	0.150	9.20
ZAF 17M	19.6	39.4	30.0	2.77	102	42.3	434	39.5	11.6	24.4	199	234	11.3	220	8.08	160	44.2	3.45	22.3
ZAF 18M	9.74	21.9	20.9	1.81	65.8	19.4	276	20.9	7.51	12.9	106	175	2.54	195	2.73	120	29.0	3.35	21.1
ZAF 19M	15.4	24.7	23.3	1.35	56.3	30.0	228	21.3	6.32	13.7	99.7	111	3.86	119	1.91	117	23.0	0.650	11.9
ZAF 20M	7.03	14.3	15.9	1.17	39.5	13.7	222	14.1	5.62	11.4	65.2	737	4.20	143	0.893	112	13.4	0.700	14.8
ZAF 21M	3.08	5.67	5.90	0.362	15.3	10.2	62.9	6.11	1.55	7.39	23.0	154	1.93	39.8	<LOQ	33.8	5.55	5.10	14.4
ZAF 22M	37.3	87.4	90.5	8.08	290	60.3	1.41	85.1	36.2	31.9	426	372	9.21	1.09	4.14	686	43.6	3.80	436
ZAF 23M	6.26	16.4	20.3	2.10	67.8	14.8	318	20.0	8.01	10.6	90.3	126	2.40	260	1.45	158	15.2	5.50	114

Sample	Li	B	Al	Ti	V	Cr	Mn	Fe	Co	Ni	Cu	Zn	As	Sr	Mo	Ba	Pb	Volume	Material
	µg L^{-1}	µg L^{-1}	mg L^{-1}	mg L^{-1}	µg L^{-1}	µg L^{-1}	µg L^{-1}	mg L^{-1}	µg L^{-1}	µg L^{-1}	µg L^{-1}	µg L^{-1}	µg L^{-1}	µg L^{-1}	µg L^{-1}	µg L^{-1}	µg L^{-1}	L	mg
TDF 02M	185	252	394	19.3	807	166	4.54	304	117	112	1.65	911	32.3	3.42	8.92	2.04	118	2.00	96.5
TDF 03M	76.7	109	93.0	3.89	211	105	1.85	84.5	40.9	72.4	703	499	13.1	569	3.61	655	51.1	0.800	311
TDF 04M	35.6	106	127	12.3	506	33.7	2.14	116	53.4	32.7	1.59	523	26.7	1.67	7.19	1.12	35.0	0.400	565
TDF 05M	91.8	234	385	31.8	1.11	57.2	5.69	354	130	55.6	1.17	576	25.2	4.85	14.7	2.90	64.8	0.200	154
TDF 06M	104	241	361	27.9	1.02	117	5.52	333	128	66.0	1.01	1.09	25.5	3.95	12.4	2.41	85.5	2.70	904
TDF 07M	161	261	301	21.8	762	189	3.41	309	86.9	104	877	528	49.2	2.39	15.7	1.39	252	4.80	168
TDF 08M	469	660	769	23.6	1.33	744	6.29	597	183	254	1.68	1.52	100	2.84	12.0	2.97	336	4.30	1035
TDF 09M	185	311	361	16.8	748	354	3.83	300	102	128	932	1.19	32.3	2.46	8.52	1.94	162	5.40	629
TDF 12M	285	993	1.80	104	5.35	306	31.30	1.88	595	262	4.46	2.39	120	16.70	18.9	6.39	387	1.10	1672
TDF 13M	424	782	1.47	96.2	5.01	206	21.30	1.17	418	167	4.44	1.83	200	14.50	59.0	7.30	399	1.90	988
TDF 14M	897	1.55	2.17	101	4.43	1.13	23.50	1.68	577	476	10.70	5.80	367	12.00	45.4	9.30	662	1.76	973
TDF 15M	109	199	136	6.30	329	158	1.46	108	45.9	72.8	922	669	26.8	720	4.94	708	62.7	3.20	42.4
TDF 16M	304	547	752	45.5	2.32	264	9.22	595	222	180	6.01	2.22	151	6.93	31.9	3.47	202	0.150	260
TDF 17M	193	468	462	33.2	1.29	205	5.60	441	145	128	1.28	885	112	4.57	23.0	2.50	212	1.32	204
TDF 18M	51.4	114	84.6	6.94	269	80.7	1.01	87.9	27.6	41.6	338	278	78.6	641	4.33	478	65.5	6.00	82.7
TDF 19M	191	353	433	27.6	1.05	203	4.93	372	123	118	942	772	79.2	3.74	14.1	2.19	153	3.70	170
TDF 21M	193	383	370	24.1	1.06	267	3.91	373	104	102	1.21	865	184	2.62	11.5	1.98	198	5.70	206
TDF 23M	360	853	1.14	92.8	3.77	277	14.30	1.13	316	198	3.26	1.59	379	12.00	55.5	8.10	531	2.70	395

Sample	Li	B	Al	Ti	V	Cr	Mn	Fe	Co	Ni	Cu	Zn	As	Sr	Mo	Ba	Pb	Volume	Material
	µg L^{-1}	µg L^{-1}	mg L^{-1}	mg L^{-1}	µg L^{-1}	µg L^{-1}	µg L^{-1}	mg L^{-1}	µg L^{-1}	µg L^{-1}	µg L^{-1}	µg L^{-1}	µg L^{-1}	µg L^{-1}	µg L^{-1}	µg L^{-1}	µg L^{-1}	L	mg
INT 03M	17.9	30.6	20.0	0.612	41.5	43.2	281	20.0	7.66	31.5	59.2	154	3.74	123	2.09	158	13.6	0.120	133
INT 04M	10.0	25.0	14.2	0.574	31.8	23.9	307	13.1	5.55	17.6	140	414	3.67	92.9	1.13	112	13.3	0.200	249
INT 05M	4.63	9.47	6.75	0.317	14.7	10.5	126	5.92	2.35	6.01	61.9	236	<LOQ	43.2	0.939	51.7	4.19	0.150	126
INT 06M	102	148	114	2.80	212	181	1.71	96.4	44.7	82.9	286	880	19.2	278	3.76	615	75.4	2.05	532
INT 07M	12.2	25.5	21.4	1.48	59.8	28.5	320	21.8	11.4	18.3	139	249	1.50	186	1.51	127	25.2	6.40	289
INT 08M	376	539	574	25.2	1.22	581	5.68	515	174	237	1.22	1.53	69.9	1.97	9.61	1.66	256	4.80	661
INT 09M	63.2	94.9	74.0	2.06	130	182	609	58.4	21.8	63.8	147	445	10.3	149	1.69	344	60.7	3.90	25.0
INT 10M	15.8	36.4	21.8	0.786	49.6	83.0	194	22.2	6.55	23.4	121	125	4.64	74.4	1.29	85.2	44.7	4.90	50.0
INT 11M	1.28	8.74	3.23	0.306	10.2	37.8	50.0	3.14	0.878	4.10	31.8	86.8	2.65	46.6	0.302	32.2	4.24	2.05	0.600
INT 12M	26.6	71.5	71.8	6.48	217	52.8	1.18	66.8	29.4	29.5	254	401	8.01	864	3.49	601	31.1	0.700	187
INT 13M	5.91	11.0	11.2	0.553	24.3	14.4	94.5	9.75	2.69	7.75	28.8	72.9	1.46	49.1	1.17	48.4	11.6	1.10	149
INT 14M	202	253	198	2.48	325	269	2.96	189	73.2	165	322	960	32.8	429	5.69	1.06	92.1	0.800	103
INT 15M	226	291	254	5.61	428	296	2.81	191	78.3	156	1.11	1.92	44.2	693	4.56	1.09	184	2.25	85.2
INT 16M	7.40	15.9	15.0	0.936	40.0	14.9	201	15.9	5.25	11.0	83.1	262	0.661	130	1.71	90.1	8.42	0.0800	11.2
INT 17M	15.1	27.8	23.8	1.16	51.0	36.2	380	22.4	9.47	24.2	200	515	5.32	124	1.77	143	30.6	3.80	19.8
INT 18M	14.5	36.1	21.5	0.896	43.7	29.3	237	18.7	6.73	18.0	78.1	306	2.65	102	0.964	114	18.1	3.00	7.50
INT 19M	24.6	37.1	29.9	0.824	53.6	44.9	322	24.2	9.21	23.8	82.9	315	5.28	75.4	0.843	156	32.3	1.80	16.1
INT 20M	18.3	34.1	25.9	0.739	48.4	44.9	205	21.0	6.72	21.1	88.3	364	4.04	75.8	0.799	128	29.3	3.10	351
INT 21M	30.4	50.4	35.6	1.01	76.0	64.8	228	34.7	8.55	28.8	152	163	11.1	58.7	4.58	118	38.6	4.75	29.0
INT 22M	18.2	32.4	25.2	1.03	50.7	41.7	219	21.1	6.33	23.2	136	311	9.92	114	1.23	139	27.6	2.15	26.7
INT 23M	1.83	2.17	2.86	0.161	6.82	6.73	25.9	3.44	0.574	3.70	12.6	77.1	<LOQ	16.4	<LOQ	14.9	3.42	0.900	3.60

Sample	Li	B	Al	Ti	V	Cr	Mn	Fe	Co	Ni	Cu	Zn	As	Sr	Mo	Ba	Pb	Volume	Material
	µg L^{-1}	µg L^{-1}	mg L^{-1}	mg L^{-1}	µg L^{-1}	µg L^{-1}	µg L^{-1}	mg L^{-1}	µg L^{-1}	µg L^{-1}	µg L^{-1}	µg L^{-1}	µg L^{-1}	µg L^{-1}	µg L^{-1}	µg L^{-1}	µg L^{-1}	L	mg
ARC 01M	14.9	44.3	17.6	0.705	38.1	42.9	279	16.9	6.45	38.3	96.3	586	5.41	84.2	1.50	320	33.2	4.70	57.4
ARC 02M	55.7	87.9	53.0	1.01	100	101	897	53.7	22.8	64.7	161	920	10.3	116	3.16	391	80.7	1.70	28.4
ARC 03M	1.23	7.68	1.01	0.0410	2.37	6.85	39.2	1.74	0.696	8.87	23.6	639	<LOQ	13.8	0.686	16.1	12.2	0.100	1.10
ARC 04M	56.3	86.5	50.8	0.948	95.7	92.4	642	42.4	17.6	50.4	124	703	11.4	323	2.87	457	69.1	0.130	156
ARC 05M	16.3	48.5	16.2	0.701	41.1	43.1	456	17.5	7.54	21.9	94.0	568	7.32	293	1.82	159	33.4	1.35	43.3
ARC 06M	25.6	47.5	24.8	0.584	48.3	52.2	333	22.7	9.75	27.7	113	660	6.65	202	3.25	271	134	0.150	178
ARC 07M	6.21	15.7	8.30	0.447	22.8	72.4	182	10.9	3.45	16.3	88.1	578	2.65	51.5	1.70	113	53.2	3.50	54.4
ARC 08M	14.7	30.9	23.7	2.25	48.4	64.7	189	19.9	6.92	23.5	148	462	2.74	69.6	2.59	121	36.9	4.25	147
ARC 09M	7.93	18.5	11.1	0.308	24.0	62.6	253	10.9	6.29	18.7	106	251	1.71	36.2	1.31	92.4	34.1	4.00	83.7
ARC 10M	3.11	16.1	4.40	0.148	10.1	102	71.4	5.45	1.75	16.5	83.2	222	<LOQ	37.3	1.45	47.2	29.6	5.87	8.20
ARC 11M	8.25	32.7	11.9	0.482	30.0	99.5	245	16.5	5.91	26.2	238	551	3.87	70.7	3.91	193	89.7	2.35	18.9
ARC 12M	8.66	27.2	13.3	0.458	26.1	78.8	177	13.3	4.37	16.1	106	405	3.01	57.1	1.07	129	123	1.50	55.1
ARC 13M	3.27	7.16	5.06	0.179	9.80	12.1	91.4	4.60	1.40	6.33	30.7	111	<LOQ	19.9	0.510	35.2	11.0	1.15	14.6
ARC 14M	8.94	18.5	10.9	0.355	23.7	27.1	323	11.0	4.63	22.6	126	543	1.73	42.1	1.24	105	46.8	2.60	10.3
ARC 15M	15.1	26.7	15.4	0.422	30.8	34.0	269	14.8	6.05	20.0	90.6	367	3.30	45.9	1.25	113	44.8	1.60	12.5
ARC 16M	9.16	42.8	10.5	0.309	19.8	25.5	184	10.6	3.94	17.5	79.6	380	3.38	51.5	1.01	125	18.2	0.220	11.3
ARC 17M	15.0	26.3	13.7	0.347	28.3	38.8	250	15.6	5.94	24.7	61.4	339	4.23	85.9	1.32	147	34.9	0.150	13.9
ARC 18M	12.7	19.0	13.9	0.445	28.9	25.7	251	13.6	5.17	18.4	110	441	3.18	54.8	1.21	99.3	23.9	1.95	13.8
ARC 19M	5.65	8.64	7.30	0.172	13.6	17.3	83.8	6.11	1.82	9.26	262	243	0.620	18.7	0.512	40.0	11.5	2.20	10.1
ARC 20M	10.5	31.0	14.2	0.413	30.9	59.0	335	16.4	6.51	26.3	260	715	4.85	53.3	2.73	262	62.7	3.00	969
ARC 21M	35.9	58.7	36.7	0.644	66.5	81.6	501	32.9	13.3	37.6	178	509	7.41	75.8	2.70	287	104	0.600	24.1
ARC 22M	26.4	62.1	27.5	0.587	63.4	125	458	33.0	11.9	44.6	505	1.30	11.0	112	7.12	520	132	2.65	40.8
ARC 23M	4.28	6.63	6.08	0.185	10.9	14.4	38.6	5.25	1.09	6.52	26.3	137	0.396	15.4	0.347	33.8	11.9	2.00	8.10

Sample	Li	B	Al	Ti	V	Cr	Mn	Fe	Co	Ni	Cu	Zn	As	Sr	Mo	Ba	Pb	Volume	Material
	µg L^{-1}	µg L^{-1}	mg L^{-1}	mg L^{-1}	µg L^{-1}	µg L^{-1}	µg L^{-1}	mg L^{-1}	µg L^{-1}	µg L^{-1}	µg L^{-1}	µg L^{-1}	µg L^{-1}	µg L^{-1}	µg L^{-1}	µg L^{-1}	µg L^{-1}	L	mg
UNI 01M	51.1	113	58.3	2.72	156	110	894	64.1	25.9	44.0	251	586	11.1	302	3.82	431	83.8	5.20	837
UNI 02M	154	208	131	2.18	244	231	1.98	113	52.3	140	302	1.20	24.4	260	5.60	890	150	1.80	62.5
UNI 03M	19.3	35.7	17.7	0.402	35.8	39.8	220	16.8	5.99	23.7	89.1	268	3.36	117	1.74	167	38.2	0.120	82.7
UNI 04M	121	214	285	19.0	751	139	3.87	264	100	106	1.69	1041	36.3	2.64	10.7	1.66	109	0.130	161
UNI 05M	69.2	124	67.6	1.42	134	138	1.10	61.9	26.6	80.8	317	1.12	16.0	152	4.52	398	110	1.40	353
UNI 06M	19.8	30.3	17.9	0.392	38.9	37.9	269	17.2	7.51	20.5	71.0	339	5.11	149	1.58	220	37.5	0.150	184
UNI 07M	172	255	196	4.50	322	313	2.21	158	56.4	162	549	1.95	37.0	279	7.68	1.01	198	3.60	471
UNI 08M	3.07	6.83	5.77	0.294	13.4	50.0	71.8	5.07	1.72	9.75	43.6	181	<LOQ	33.1	0.478	40.2	10.2	5.60	522
UNI 09M	55.9	84.4	65.0	1.32	113	190	787	54.2	22.6	67.5	224	795	10.9	114	2.95	364	74.7	4.00	57.3
UNI 10M	7.99	24.5	10.4	0.244	21.5	103	107	9.75	2.79	19.5	184	212	3.66	48.0	1.80	84.8	51.5	9.93	81.1
UNI 11M	2.16	9.63	2.90	0.0777	9.48	85.7	96.6	3.20	1.55	10.3	95.2	125	<LOQ	26.3	0.501	59.4	15.8	3.40	10.9
UNI 12M	28.4	247	38.3	1.15	73.5	114	512	36.8	13.7	40.2	169	576	4.44	109	2.03	229	40.3	1.45	19.0
UNI 13M	6.88	12.3	11.2	0.372	19.9	20.8	153	9.46	3.52	11.9	51.7	191	1.45	26.5	0.660	113	14.0	0.520	9.50
UNI 14M	172	248	188	3.00	298	294	2.32	159	55.8	150	460	2.14	32.3	304	6.18	997	213	2.78	71.0
UNI 15M	166	221	147	2.42	248	234	1.93	131	46.4	123	316	1.27	30.8	319	5.78	698	154	1.40	79.9
UNI 16M	6.35	12.8	6.91	0.162	13.7	16.1	97.2	6.48	2.11	9.17	37.3	199	0.145	33.0	0.868	61.9	10.6	0.150	5.20
UNI 17M	1.60	1.61	1.69	0.0579	3.36	7.35	45.9	1.85	<LOQ	7.04	87.7	179	<LOQ	11.4	0.653	22.7	6.99	0.430	1.20
UNI 18M	4.90	8.33	6.49	0.200	12.7	15.7	165	5.66	2.80	10.4	141	331	1.31	23.9	0.900	68.3	18.7	1.75	6.30
UNI 19M	19.6	29.1	22.4	0.402	40.2	40.8	329	19.4	7.90	23.7	69.7	392	4.70	40.7	1.18	138	25.1	1.70	17.3
UNI 20M	7.29	19.3	8.85	0.234	20.0	26.9	158	9.28	3.27	17.6	105	418	3.94	43.3	1.57	104	45.1	5.25	381
UNI 21M	21.2	37.4	23.8	0.493	46.0	49.0	311	21.7	7.89	30.8	89.3	397	6.11	50.5	1.78	156	36.5	1.40	26.0
UNI 22M	4.30	15.4	6.21	0.303	12.6	24.4	59.1	5.60	3.29	11.3	43.0	210	1.25	19.6	<LOQ	34.3	10.4	1.20	503
UNI 23M	3.17	8.03	4.48	0.139	8.55	13.0	35.0	4.29	0.395	6.53	30.0	179	1.20	16.1	1.52	31.3	7.85	2.25	8.80

Sample	Li	B	Al	Ti	V	Cr	Mn	Fe	Co	Ni	Cu	Zn	As	Sr	Mo	Ba	Pb	Volume	Material
	µg L^{-1}	µg L^{-1}	mg L^{-1}	mg L^{-1}	µg L^{-1}	µg L^{-1}	µg L^{-1}	mg L^{-1}	µg L^{-1}	µg L^{-1}	µg L^{-1}	µg L^{-1}	µg L^{-1}	µg L^{-1}	µg L^{-1}	µg L^{-1}	µg L^{-1}	L	mg
IND 01M	94.7	387	99.0	3.42	228	270	1.76	99.0	42.2	73.9	554	1.58	22.2	374	12.4	815	275	5.00	546
IND 02M	56.3	252	51.2	0.984	101	125	1.20	53.7	26.0	66.0	239	1.20	14.2	151	5.05	393	162	1.70	184
IND 03M	32.1	62.2	27.8	0.652	56.0	81.2	374	27.7	9.43	37.6	251	568	9.18	202	4.91	360	125	0.120	215
IND 04M	64.9	90.5	56.3	0.992	105	105	680	49.0	18.8	54.9	144	568	12.9	345	3.67	473	70.1	0.130	159
IND 05M	71.5	121	65.6	1.26	129	207	1.30	73.0	31.9	91.8	528	1.62	19.0	166	10.1	517	242	1.25	181
IND 06M	32.4	57.7	28.0	0.577	56.6	78.3	425	29.2	10.6	34.2	205	693	7.95	208	5.77	348	107	0.150	194
IND 07M	110	184	117	2.34	214	440	1.79	102	47.1	131	942	1.68	23.9	214	12.2	751	226	4.25	655
IND 08M	2.83	7.95	4.81	0.199	9.37	42.2	53.2	4.14	1.01	10.5	67.2	208	<LOQ	18.5	<LOQ	31.1	10.5	4.80	597
IND 09M	24.4	53.1	31.0	0.659	57.1	110	561	28.2	13.6	42.4	189	465	7.00	67.5	2.91	198	53.1	4.00	25.8
IND 10M	3.79	21.1	5.44	0.158	12.6	147	75.5	6.33	1.45	22.3	144	188	<LOQ	32.0	2.54	38.9	30.7	8.60	712
IND 11M	14.3	51.4	18.8	0.569	36.6	181	355	22.7	7.47	37.6	381	543	6.96	74.6	5.34	203	86.8	3.30	98.7
IND 12M	25.4	60.9	33.0	0.958	65.8	134	503	32.2	12.1	40.8	277	654	6.74	111	4.57	265	72.1	1.80	28.0
IND 13M	13.5	33.3	19.7	0.684	44.3	64.5	390	22.4	8.60	35.0	264	590	5.92	75.5	3.66	164	60.6	0.750	23.3
IND 14M	174	257	188	3.36	316	391	2.68	174	58.3	118	1.17	2.65	39.0	429	15.3	1.11	399	3.60	356
IND 15M	86.9	142	72.0	1.33	147	170	1.42	73.0	30.3	83.2	473	1.17	25.9	235	6.39	474	253	1.45	87.1
IND 16M	7.23	21.1	7.80	0.221	16.8	24.8	123	8.11	2.42	12.7	71.3	255	0.621	56.5	2.05	87.2	26.7	0.150	7.10
IND 17M	24.3	51.4	24.2	0.616	53.3	88.0	460	26.6	9.42	37.9	403	1.03	9.44	109	4.17	247	190	0.600	27.0
IND 18M	10.4	23.3	12.6	0.289	33.3	40.4	299	13.9	5.14	21.9	245	603	4.85	56.7	3.12	203	68.9	1.80	15.6
IND 19M	54.7	99.6	70.1	1.10	110	145	884	61.4	21.5	60.5	438	1.13	13.1	122	5.75	358	102	2.20	66.2
IND 20M	16.4	35.4	12.3	0.500	31.6	47.8	228	14.5	33.7	223	336	727	8.05	93.8	3.87	165	89.1	4.30	612
IND 21M	14.0	58.3	17.2	0.381	32.3	46.1	218	15.5	5.42	22.8	108	416	4.42	41.9	2.17	125	29.7	1.40	28.5
IND 22M	5.04	21.0	7.12	0.170	14.3	33.0	96.2	6.48	1.90	14.4	125	379	2.11	30.8	0.426	59.4	22.2	3.60	435
IND 23M	1.76	5.82	2.34	0.0700	4.82	12.1	33.0	2.52	0.730	6.59	53.7	274	0.136	15.7	1.10	25.2	10.9	2.05	15.9

Sample	Li	B	Al	Ti	V	Cr	Mn	Fe	Co	Ni	Cu	Zn	As	Sr	Mo	Ba	Pb	Volume	Material
	µg L^{-1}	µg L^{-1}	mg L^{-1}	mg L^{-1}	µg L^{-1}	µg L^{-1}	µg L^{-1}	mg L^{-1}	µg L^{-1}	µg L^{-1}	µg L^{-1}	µg L^{-1}	µg L^{-1}	µg L^{-1}	µg L^{-1}	µg L^{-1}	µg L^{-1}	L	mg
BEL 01M	101	169	104	3.56	240	289	1.50	109	42.5	95.2	759	1.67	23.4	395	19.8	763	220	5.30	46.6
BEL 02M	94.4	138	82.4	1.59	173	205	1.41	85.7	37.3	107	392	1.27	21.2	195	10.5	606	142	2.10	55.7
BEL 03M	12.2	37.4	11.5	0.299	26.9	39.6	206	13.1	4.73	21.1	119	407	3.44	113	3.82	182	34.6	0.150	138
BEL 04M	77.3	113	64.1	1.11	122	145	849	58.4	22.2	66.9	280	844	15.9	423	6.32	637	148	0.150	177
BEL 05M	11.0	22.0	11.6	0.261	24.4	32.7	229	12.7	5.40	15.7	123	403	1.51	43.2	1.83	103	27.1	0.350	26.9
BEL 06M	27.2	51.2	25.4	0.624	49.8	71.8	311	23.8	8.32	26.5	191	727	8.27	176	6.81	304	49.3	0.150	199
BEL 07M	16.3	44.3	21.2	0.499	46.1	112	404	23.5	9.41	30.2	368	615	3.74	55.2	5.78	211	63.8	7.50	684
BEL 08M	3.11	4.88	4.70	0.113	10.0	55.4	54.7	5.11	1.33	11.7	86.5	181	1.70	42.1	1.33	33.6	13.1	5.80	814
BEL 09M	15.1	28.1	20.0	0.521	42.0	106	160	20.3	5.34	26.1	132	188	3.16	29.5	3.15	82.2	29.0	3.97	11.2
BEL 10M	3.12	22.7	4.23	0.117	10.1	120	57.3	5.75	1.15	21.3	149	144	<LOQ	36.5	2.09	33.9	29.6	9.30	268
BEL 11M	5.85	19.2	7.12	0.203	16.6	81.8	186	10.1	3.04	16.0	1.31	512	1.42	45.8	3.65	131	33.6	2.00	11.8
BEL 12M	8.39	36.8	11.2	0.359	25.5	87.4	229	13.1	5.01	19.9	200	533	<LOQ	60.5	3.28	130	47.2	1.80	61.0

Sample	Li	B	Al	Ti	V	Cr	Mn	Fe	Co	Ni	Cu	Zn	As	Sr	Mo	Ba	Pb	Volume	Material
	µg L^{-1}	µg L^{-1}	mg L^{-1}	mg L^{-1}	µg L^{-1}	µg L^{-1}	µg L^{-1}	mg L^{-1}	µg L^{-1}	µg L^{-1}	µg L^{-1}	µg L^{-1}	µg L^{-1}	µg L^{-1}	µg L^{-1}	µg L^{-1}	µg L^{-1}	L	mg
CAT 03M	26.7	57.9	39.1	2.00	91.2	51.1	589	35.0	14.2	29.8	114	348	6.56	383	3.33	362	39.9	0.130	167
CAT 04M	74.8	138	126	9.36	363	97.2	2.00	118	51.1	54.9	458	711	18.7	1.40	7.81	1.16	75.7	0.130	155
CAT 05M	44.0	87.8	91.2	8.05	274	67.6	1.42	83.9	36.3	38.6	393	438	10.7	1.07	5.44	777	47.9	0.150	51.8
CAT 06M	45.8	80.8	60.9	3.22	140	83.8	1.12	57.7	26.2	52.1	196	683	7.75	397	3.46	477	58.4	0.300	26.8
CAT 07M	59.0	112	82.4	4.95	211	153	1.02	84.2	31.8	53.9	482	647	15.8	497	9.08	597	124	3.77	583
CAT 08M	24.9	44.8	32.5	1.04	65.9	67.9	312	31.2	10.9	36.9	106	288	1.86	2.33	1.83	167	37.5	5.00	169
CAT 09M	33.2	60.8	41.6	1.52	80.4	159	385	34.4	13.8	41.2	189	358	5.97	90.3	2.05	213	50.6	5.20	629
CAT 10M	186	676	1.22	92.1	3.34	322	19.10	1.18	437	259	3.00	2.08	50.0	12.80	12.7	3.46	176	3.15	412
CAT 11M	1.17	11.0	3.34	0.288	9.70	33.2	51.2	3.23	1.04	4.15	78.2	77.0	<LOQ	46.1	0.461	44.9	7.60	0.270	3.30
CAT 12M	15.9	82.4	39.5	3.37	113	55.5	719	39.0	17.1	23.1	197	479	<LOQ	426	2.99	363	39.2	0.150	39.1
CAT 13M	59.9	113	96.8	4.25	229	157	1.54	103	42.4	76.7	338	851	18.4	441	5.62	878	149	3.80	454
CAT 14M	388	502	412	8.44	672	509	5.07	325	123	247	565	1.73	63.7	1.06	9.85	1.87	196	1.20	340
CAT 15M	46.2	82.8	48.4	1.40	114	92.2	436	51.4	14.0	46.3	269	276	9.74	118	3.62	171	46.4	0.150	35.6
CAT 16M	3.37	36.4	5.68	0.399	14.6	7.58	115	5.27	2.09	7.25	38.3	156	0.0349	243	0.930	92.6	4.22	0.150	7.50
CAT 17M	4.71	7.85	8.78	0.563	19.7	13.6	131	8.45	2.85	8.69	105	301	1.37	61.6	0.862	91.8	13.7	0.0700	4.90
CAT 18M	13.8	30.0	23.5	1.38	53.0	36.2	494	22.7	10.3	24.2	194	601	4.36	164	2.09	192	31.1	1.00	14.0
CAT 19M	23.9	42.1	36.6	2.27	86.9	51.9	629	36.0	14.9	32.7	174	714	5.23	261	3.46	277	36.9	0.750	13.5
CAT 20M	20.7	41.8	31.8	1.95	75.3	46.3	528	29.3	12.3	25.8	221	704	6.79	325	2.39	259	43.7	0.850	69.5
CAT 21M	2.70	16.4	4.74	0.268	9.46	12.4	43.9	4.27	0.553	7.53	32.1	245	2.76	27.6	0.382	32.3	5.95	5.00	21.3
CAT 22M	25.8	68.6	51.9	4.19	145	68.0	850	52.2	21.4	38.0	385	769	9.11	547	5.63	586	54.5	2.30	160
CAT 23M	8.72	30.5	24.5	2.48	86.1	36.5	437	28.7	11.0	18.2	153	317	3.20	278	3.47	220	36.4	7.00	427

Sample	Li	B	Al	Ti	V	Cr	Mn	Fe	Co	Ni	Cu	Zn	As	Sr	Mo	Ba	Pb	Volume	Material
	µg L^{-1}	µg L^{-1}	mg L^{-1}	mg L^{-1}	µg L^{-1}	µg L^{-1}	µg L^{-1}	mg L^{-1}	µg L^{-1}	µg L^{-1}	µg L^{-1}	µg L^{-1}	µg L^{-1}	µg L^{-1}	µg L^{-1}	µg L^{-1}	µg L^{-1}	L	mg
GLP 03M	84.4	176	273	19.6	634	76.3	3.80	224	81.0	65.5	572	897	17.4	3.22	11.2	2.08	90.7	0.120	216
GLP 04M	133	216	256	18.4	634	130	4.13	230	87.0	84.0	1.05	1.15	34.3	2.28	12.4	1.91	141	0.130	248
GLP 05M	65.8	128	164	13.0	430	73.0	2.46	156	56.9	49.5	561	678	14.1	1.69	7.51	1.15	59.6	0.150	103
GLP 06M	174	321	342	26.0	844	205	5.86	320	126	127	1.19	1.87	49.8	2.43	14.2	2.50	180	0.700	181
GLP 07M	124	248	286	22.5	820	315	4.14	291	102	114	1.28	1.13	38.4	2.81	17.3	2.15	196	5.15	596
GLP 08M	53.0	87.6	72.7	3.47	170	115	959	70.9	30.1	68.5	182	641	11.6	436	3.10	423	53.5	5.10	290
GLP 09M	155	221	175	6.06	360	353	1.99	140	62.3	115	860	1.45	29.8	627	7.91	989	181	5.10	768
GLP 10M	172	507	833	77.4	2.34	320	12.80	803	296	214	2.28	2.50	45.6	8.55	31.4	3.26	200	6.50	394
GLP 11M	9.82	34.3	31.0	2.85	94.1	60.1	473	31.6	12.0	17.0	264	226	2.31	386	3.76	329	36.6	0.950	10.8
GLP 12M	174	303	404	28.2	971	254	6.11	355	141	163	1.34	2.85	42.1	3.70	24.2	2.47	196	0.700	137
GLP 13M	138	216	256	11.3	518	269	3.19	229	82.1	121	675	1.98	33.9	1.25	8.42	1.59	225	5.70	1006
GLP 14M	437	632	725	32.4	1.40	523	10.70	622	219	224	1.62	3.46	81.3	4.47	28.7	3.88	59.3	1.15	446
GLP 15M	126	180	146	8.55	356	163	2.47	125	59.8	105	430	1.36	22.7	982	7.70	922	84.3	2.55	69.1
GLP 17M	432	680	1.09	68.0	2.04	494	18.20	898	301	288	3.34	9.05	105	7.74	51.4	5.55	458	0.770	370
GLP 18M	69.6	153	221	16.9	559	103	3.39	196	78.3	80.5	678	1.92	18.5	2.46	11.4	1.54	92.3	0.800	71.9
GLP 19M	10.6	19.8	17.0	0.997	38.8	27.9	246	16.6	6.07	15.8	91.4	343	2.87	108	1.60	125	18.8	0.600	19.7
GLP 20M	63.4	126	103	8.22	288	134	2.07	103	48.1	62.5	575	1.85	17.7	820	12.1	845	109	1.15	434
GLP 21M	10.7	22.5	18.1	1.16	40.6	32.5	248	18.2	6.67	18.1	89.9	406	4.92	106	1.16	125	19.0	5.10	32.9
GLP 22M	36.5	84.8	73.1	6.74	229	100	1.50	82.0	36.3	46.5	614	1.21	11.6	890	8.56	915	68.1	2.90	818
GLP 23M	23.7	66.3	62.0	6.42	209	67.6	26.6	69.2	28.0	34.5	286	900	7.64	771	5.69	502	58.5	5.80	566

Sample	Li	B	Al	Ti	V	Cr	Mn	Fe	Co	Ni	Cu	Zn	As	Sr	Mo	Ba	Pb	Volume	Material
	µg L^{-1}	µg L^{-1}	mg L^{-1}	mg L^{-1}	µg L^{-1}	µg L^{-1}	µg L^{-1}	mg L^{-1}	µg L^{-1}	µg L^{-1}	µg L^{-1}	µg L^{-1}	µg L^{-1}	µg L^{-1}	µg L^{-1}	µg L^{-1}	µg L^{-1}	L	mg
GAB 01M	10.3	79.9	12.5	0.652	36.2	58.9	212	14.7	5.61	24.8	70.2	185	4.06	74.3	4.18	111	20.0	3.65	508
GAB 02M	166	210	155	2.97	279	297	2.11	121	53.3	153	281	1.25	25.7	355	8.66	970	134	1.50	58.2
GAB 03M	2.77	6.40	3.29	0.131	8.11	12.5	68.8	3.07	0.946	11.2	21.9	50.2	<LOQ	19.8	0.789	29.5	3.56	0.095	1.40
GAB 04M	118	248	345	25.4	924	139	5.08	308	115	76.7	1.52	1.32	39.9	3.70	14.6	2.66	85.9	1.50	935
GAB 05M	36.1	89.5	43.8	1.72	137	170	599	64.7	17.1	74.3	211	561	14.9	141	12.0	292	70.1	3.85	1630
GAB 06M	38.2	70.0	40.1	1.24	97.1	168	803	49.7	21.1	82.3	374	1.16	21.3	117	6.42	322	91.6	3.40	323
GAB 07M	12.2	35.6	14.9	0.767	116	54.5	268	21.5	7.71	37.9	159	298	7.89	59.1	9.41	211	31.1	2.10	15.1
GAB 08M	109	170	123	2.64	280	347	1.77	134	59.0	100	477	1.47	1.62	2.55	6.30	1.01	177	7.40	1045
GAB 09M	5.02	66.5	6.85	0.340	18.3	101	88.8	8.01	2.69	12.9	64.0	102	17.0	31.4	2.20	104	19.3	2.00	6.80
GAB 10M	2.82	36.8	4.13	0.262	19.7	38.8	78.2	8.57	1.62	16.6	60.9	90.3	<LOQ	29.5	4.71	56.8	34.1	4.80	2.90
GAB 11M	13.1	39.6	16.5	0.569	64.7	156	175	20.2	5.28	46.5	130	167	12.1	42.2	15.0	172	48.6	4.95	8.20
GAB 12M	64.2	298	80.3	2.44	176	303	957	89.7	26.8	135	271	850	15.3	206	13.9	626	129	3.95	69.6
GAB 13M	7.05	42.2	9.78	0.456	75.1	54.8	141	15.8	3.35	34.8	75.6	167	2.84	42.0	11.9	113	82.6	1.30	84.8
GAB 14M	131	192	122	2.76	247	243	1.79	109	43.7	180	304	1.75	23.9	262	9.48	786	116	0.550	63.3

Sample	Li	B	Al	Ti	V	Cr	Mn	Fe	Co	Ni	Cu	Zn	As	Sr	Mo	Ba	Pb	Volume	Material
	µg L^{-1}	µg L^{-1}	mg L^{-1}	mg L^{-1}	µg L^{-1}	µg L^{-1}	µg L^{-1}	mg L^{-1}	µg L^{-1}	µg L^{-1}	µg L^{-1}	µg L^{-1}	µg L^{-1}	µg L^{-1}	µg L^{-1}	µg L^{-1}	µg L^{-1}	L	mg
SIR 01M	239	407	620	29.5	1.35	262	8.55	529	181	179	1.05	4.29	46.3	5.96	15.7	4.30	165	1.83	203
SIR 02M	49.6	84.4	64.3	3.17	159	91.1	1.09	58.9	26.9	62.4	182	890	10.3	459	3.33	483	63.2	0.600	34.4
SIR 03M	35.5	61.6	37.8	1.41	97.9	64.6	539	36.8	15.2	49.4	95.9	385	14.5	364	3.57	458	50.2	0.130	164
SIR 04M	107	148	99.5	1.53	160	182	1.08	74.7	26.9	89.6	340	1.39	21.3	548	9.16	832	132	0.130	148
SIR 05M	52.7	101	78.8	5.06	214	83.4	1.15	69.5	29.6	62.5	178	665	17.1	883	5.77	722	51.9	0.150	121
SIR 06M	80.4	158	100	4.81	255	234	2.12	97.6	50.8	173	381	7.72	34.9	597	8.88	770	238	2.20	443
SIR 07M	2.15	6.77	3.49	0.198	8.32	9.67	40.1	3.11	1.15	7.92	36.4	139	<LOQ	21.6	0.691	31.5	7.55	4.00	98.7
SIR 08M	37.5	61.5	45.5	1.08	106	111	407	47.6	16.2	61.0	104	259	30.5	91.7	2.97	165	66.9	5.75	631
SIR 09M	7.96	18.3	10.8	0.353	25.2	96.0	108	10.4	3.28	22.2	59.8	186	2.92	29.6	1.14	64.6	29.4	5.70	8.70
SIR 10M	88.6	345	494	48.9	1.72	170	7.91	498	219	134	1.45	1.33	22.1	6.14	17.7	1.76	82.6	2.70	188
SIR 11M	7.20	29.6	22.4	1.96	75.0	65.4	335	26.2	9.57	128	186	731	10.4	267	3.21	262	56.9	1.37	8.90
SIR 12M	3.63	51.1	7.21	0.502	31.2	43.6	174	8.10	4.08	28.9	79.1	559	3.39	80.7	1.36	175	28.3	0.0350	6.19
SIR 13M	123	181	169	4.63	328	260	2.69	140	67.2	170	335	3.89	31.9	406	4.54	1.10	174	1.35	254
SIR 14M	265	326	255	4.24	430	357	3.19	214	82.3	208	341	2.70	43.6	580	5.68	1.21	138	0.560	250
SIR 15M	169	231	148	2.91	292	253	2.13	121	57.6	174	388	4.46	31.5	276	4.86	2.86	103	2.57	67.2
SIR 16M	21.3	37.4	25.3	0.701	52.9	42.5	201	22.8	5.66	23.8	124	177	5.13	59.1	1.25	88.3	21.9	0.150	2.50
SIR 17M	34.6	71.4	42.6	1.93	128	95.8	999	46.1	21.6	158	311	3.35	26.8	231	4.29	450	88.4	0.600	29.4
SIR 18M	130	233	163	5.60	415	320	2.84	168	64.3	311	1.01	7.22	53.8	727	11.5	1.93	233	2.90	98.1
SIR 19M	16.8	45.6	19.8	0.633	64.9	44.1	359	22.1	9.35	42.3	227	752	6.37	77.7	1.77	179	34.9	0.550	14.4
SIR 20M	2.64	4.12	4.18	0.146	10.2	8.33	178	3.47	2.96	10.3	45.3	254	3.05	24.5	0.421	33.1	10.1	0.450	15.8
SIR 21M	34.6	144	46.8	1.89	147	413	1.04	74.5	23.4	130	268	4.67	84.1	236	9.24	828	575	4.25	53.7
SIR 22M	15.0	41.5	21.4	0.948	65.7	68.3	426	25.0	10.0	57.8	216	1.56	22.2	209	2.73	364	84.3	0.900	23.0
SIR 23M	4.34	19.4	7.74	0.456	27.2	57.0	97.3	8.88	2.56	21.2	46.0	319	11.6	53.6	1.76	72.2	30.5	5.00	182

Sample	Li	B	Al	Ti	V	Cr	Mn	Fe	Co	Ni	Cu	Zn	As	Sr	Mo	Ba	Pb	Volume	Material
	µg L^{-1}	µg L^{-1}	mg L^{-1}	mg L^{-1}	µg L^{-1}	µg L^{-1}	µg L^{-1}	mg L^{-1}	µg L^{-1}	µg L^{-1}	µg L^{-1}	µg L^{-1}	µg L^{-1}	µg L^{-1}	µg L^{-1}	µg L^{-1}	µg L^{-1}	L	mg
AUG 01M	110	150	119	4.53	268	204	1.56	97.7	43.8	118	208	8.37	19.7	609	9.39	819	176	1.90	52.1
AUG 02M	142	188	139	4.09	289	205	1.73	111	50.2	116	233	3.04	23.4	587	5.07	752	196	0.800	221
AUG 03M	41.4	67.2	47.1	1.71	107	67.6	600	40.9	16.9	45.5	123	328	8.21	376	2.65	371	45.2	0.150	186
AUG 04M	60.3	130	80.6	4.51	220	88.2	1.13	70.7	30.2	61.3	202	2.05	17.8	835	5.54	734	57.6	0.130	198
AUG 05M	47.5	127	155	12.7	422	48.9	2.21	145	55.2	45.0	325	439	12.5	1.88	6.45	1.17	44.7	0.150	163
AUG 06M	56.8	113	76.8	3.87	194	175	1.01	76.5	32.8	82.1	382	3.69	17.0	411	7.38	577	148	2.50	257
AUG 07M	66.2	111	76.6	2.38	171	200	590	68.7	22.1	93.7	450	1.31	19.9	184	11.3	422	279	6.00	325
AUG 08M	103	165	121	2.58	274	345	1.76	135	58.7	97.7	464	1.45	58.8	326	6.26	991	240	5.02	697
AUG 09M	35.1	57.8	42.0	1.20	87.6	132	791	37.0	19.0	61.5	376	1.58	12.0	233	3.19	272	85.5	4.50	291
AUG 10M	1.55	5.52	4.80	0.399	16.0	27.7	64.2	4.36	1.76	9.35	33.7	89.0	3.24	54.9	0.775	39.8	9.12	1.30	2.70
AUG 11M	10.1	52.8	31.3	2.89	104	62.8	489	32.0	13.3	39.3	331	491	11.1	352	3.97	244	37.4	0.500	4.30
AUG 12M	0.966	9.01	1.61	0.138	5.19	24.0	22.8	1.53	0.770	3.42	18.3	224	<LOQ	35.8	0.405	22.8	4.23	0.130	71.1

Sample	Li	B	Al	Ti	V	Cr	Mn	Fe	Co	Ni	Cu	Zn	As	Sr	Mo	Ba	Pb	Volume	Material
	µg L^{-1}	µg L^{-1}	mg L^{-1}	mg L^{-1}	µg L^{-1}	µg L^{-1}	µg L^{-1}	mg L^{-1}	µg L^{-1}	µg L^{-1}	µg L^{-1}	µg L^{-1}	µg L^{-1}	µg L^{-1}	µg L^{-1}	µg L^{-1}	µg L^{-1}	L	mg
PRI 01M	221	366	418	17.8	820	304	5.28	342	113	150	654	1.63	42.8	2.73	10.9	2.37	148	2.35	331
PRI 02M	125	158	129	3.55	256	184	1.68	97.5	43.9	107	235	730	20.7	493	5.24	751	97.9	0.500	51.1
PRI 03M	32.4	57.0	36.5	1.43	93.3	61.8	550	36.3	15.7	50.1	116	516	16.1	350	3.37	347	57.2	0.120	143
PRI 04M	90.8	179	235	16.5	578	90.5	3.10	194	72.8	67.4	418	1.73	22.8	2.76	9.07	1.73	66.4	0.130	241
PRI 05M	37.7	67.8	60.8	4.11	165	68.5	835	52.4	22.7	56.1	158	601	14.5	622	3.81	498	39.5	0.150	57.3
PRI 06M	23.5	44.2	31.3	1.38	74.2	57.3	656	31.9	16.0	51.4	142	562	12.3	140	2.67	217	38.8	1.95	200
PRI 07M	1.73	16.4	5.49	0.0788	6.48	7.34	22.7	2.01	0.857	6.81	333	107	<LOQ	47.2	1.16	87.9	5.76	4.00	229
PRI 08M	24.1	43.5	32.0	1.04	65.4	67.9	312	31.1	10.8	37.2	104	284	4.83	165	1.94	165	45.6	4.50	365
PRI 09M	33.1	52.7	39.5	0.918	76.7	102	298	33.2	12.0	50.8	87.6	285	23.9	75.5	1.84	180	56.3	4.80	16.1
PRI 10M	161	595	1.04	97.5	3.09	227	16.40	993	386	222	2.75	1.96	45.0	11.30	32.0	3.12	130	1.87	352
PRI 11M	6.78	22.0	11.4	0.620	31.2	44.5	156	12.0	4.63	17.9	126	1.55	2.12	72.2	1.67	98.7	38.7	0.750	8.60
PRI 12M	1.85	18.8	3.79	0.283	11.6	29.8	71.4	3.91	1.03	8.58	36.2	268	<LOQ	45.6	0.587	45.1	7.42	0.012	0.900
PRI 13M	30.9	53.7	48.7	1.44	86.6	74.9	829	43.4	18.5	51.6	170	647	8.28	115	2.00	294	42.0	0.900	76.3
PRI 14M	358	811	366	6.36	666	502	5.18	339	127	276	557	2.25	65.9	722	11.9	1.78	186	1.40	302
PRI 15M	176	228	149	2.66	275	239	2.03	115	53.6	143	254	866	32.2	282	4.36	788	77.8	1.20	69.5
PRI 16M	2.86	4.90	3.95	0.200	8.68	7.95	46.3	3.43	0.909	5.92	17.8	101	0.402	28.7	0.118	33.4	3.28	0.150	1.50
PRI 17M	23.1	49.3	33.6	1.28	79.1	63.5	573	28.1	14.1	66.5	279	1.04	22.9	96.2	2.62	212	40.6	0.400	16.4
PRI 18M	6.85	14.2	12.6	0.724	61.0	20.6	219	12.1	5.63	30.6	96.0	381	6.13	70.7	1.75	81.4	14.8	1.20	9.20
PRI 19M	26.3	60.8	35.6	1.62	101	64.8	596	36.3	16.6	63.5	196	1.01	14.1	177	3.67	309	52.9	1.10	25.7
PRI 20M	6.10	11.8	10.0	0.415	22.5	19.1	179	9.32	4.57	25.9	68.2	700	3.68	54.6	1.15	99.0	19.1	0.0850	11.2
PRI 21M	17.2	39.3	25.4	0.825	117	54.8	182	21.2	5.78	35.6	174	510	18.1	134	1.36	290	43.2	5.50	42.4
PRI 22M	11.1	28.1	22.1	0.612	51.5	39.5	282	16.5	6.75	30.3	86.1	478	56.1	73.9	3.08	162	28.6	1.05	13.1
PRI 23M	5.71	14.5	11.1	0.542	39.7	23.2	111	10.7	3.26	22.0	51.5	191	13.8	75.6	1.79	76.3	35.2	5.35	66.0

Sample	Li	B	Al	Ti	V	Cr	Mn	Fe	Co	Ni	Cu	Zn	As	Sr	Mo	Ba	Pb	Volume	Material
	µg L^{-1}	µg L^{-1}	mg L^{-1}	mg L^{-1}	µg L^{-1}	µg L^{-1}	µg L^{-1}	mg L^{-1}	µg L^{-1}	µg L^{-1}	µg L^{-1}	µg L^{-1}	µg L^{-1}	µg L^{-1}	µg L^{-1}	µg L^{-1}	µg L^{-1}	L	mg
CES 01M	173	267	226	5.66	378	266	2.64	210	69.2	113	385	1.11	29.3	801	6.70	1.21	129	6.80	85.8
CES 02M	105	292	101	2.04	194	168	1.75	93.3	45.3	112	121	743	16.4	279	6.58	589	78.9	3.80	53.8
CES 03M	12.5	19.9	15.3	0.517	30.3	25.4	268	12.8	5.06	18.2	55.2	110	3.10	60.9	0.715	93.9	10.1	0.260	46.1
CES 04M	3.64	5.52	4.29	0.120	8.69	12.0	105	4.55	2.16	9.45	29.1	74.9	<LOQ	21.4	<LOQ	36.9	5.08	0.130	1.50
CES 05M	38.0	65.7	44.3	1.80	101	79.3	936	46.0	21.5	57.6	189	544	9.63	184	2.67	274	52.1	3.55	779
CES 07M	70.9	118	77.9	1.94	161	124	966	71.0	24.9	83.4	464	457	13.1	204	4.10	321	112	5.10	439
CES 08M	8.77	19.8	15.2	0.643	30.9	127	139	13.6	6.02	9.49	151	332	<LOQ	44.4	3.34	80.8	19.2	9.60	1633
CES 09M	124	173	142	2.73	239	270	1.45	107	46.8	131	216	1.50	24.4	247	3.94	823	132	4.75	69.5
CES 10M	40.7	86.8	51.8	1.31	99.4	164	423	45.2	14.2	48.9	257	420	7.59	107	2.28	259	60.4	5.20	517
CES 11M	7.95	23.4	14.1	0.653	31.0	154	140	12.5	3.45	20.3	147	214	2.42	101	0.774	96.9	25.5	5.80	526
CES 12M	219	567	1.16	78.9	2.85	163	15.40	889	317	148	2.98	1.96	53.6	13.10	24.8	6.77	168	3.00	285
CES 13M	18.0	30.1	30.7	0.955	49.6	41.7	234	24.6	7.19	24.3	61.2	233	3.51	64.3	0.640	160	26.2	1.90	199
CES 14M	360	486	394	7.00	624	514	5.11	307	117	253	645	3.94	62.2	766	6.59	1.83	188	3.30	184
CES 15M	11.2	24.8	13.6	0.266	26.0	25.0	357	15.1	6.23	19.7	95.1	426	4.06	40.6	0.327	75.8	14.1	2.15	10.6
CES 17M	41.1	70.2	46.5	1.38	99.5	101	1.09	48.4	21.4	65.3	304	928	12.2	149	3.54	240	46.5	4.90	32.5
CES 18M	6.98	41.0	9.04	0.323	18.4	15.6	133	8.79	3.05	17.1	64.0	266	1.04	35.6	1.05	57.4	8.76	1.35	3.70
CES 19M	12.1	29.4	15.2	0.510	27.4	28.9	138	11.7	4.15	18.1	62.4	263	1.48	31.7	1.18	77.7	18.9	6.00	23.5
CES 20M	3.57	7.06	5.48	0.201	10.5	18.6	65.7	4.72	0.605	12.3	73.2	225	0.221	19.5	<LOQ	35.2	10.3	5.00	365
CES 21M	6.64	11.3	9.54	0.258	17.5	18.6	74.3	8.24	2.04	10.5	29.6	200	0.706	23.4	<LOQ	54.4	8.19	5.10	65.3
CES 22M	27.3	52.0	32.6	0.572	61.4	62.9	361	28.9	9.79	33.2	99.7	583	7.82	63.5	0.918	140	27.8	2.20	198
CES 23M	2.55	2.10	3.74	0.165	8.08	10.8	29.8	3.39	0.675	5.92	17.1	115	1.06	13.9	0.409	22.1	7.45	1.80	5.70

Table S. 6 - Technology-Critical Element concentrations (ng L^{-1}), in preconcentrated rainwater samples.

Sample	Sc	Ge	Y	Zr	Nb	Te	La	Ce	Pr	Nd	Sm
	µg L^{-1}	µg L^{-1}	µg L^{-1}	µg L^{-1}	µg L^{-1}	µg L^{-1}	µg L^{-1}	µg L^{-1}	µg L^{-1}	µg L^{-1}	µg L^{-1}
CIT 01_Rain	3.48	8.39	58.5	60.7	0.519	15.3	0.962	0.366	128	159	16.3
CIT 02_Rain	5.33	8.74	30.1	104	0.273	19.6	1.87	0.570	18.2	12.4	6.05
CIT 06_Rain	7.25	3.62	22.3	147	1.97	51.3	3.03	1.83	46.8	48.7	7.14
CIT 07_Rain	23.3	17.6	92.1	293	2.63	75.7	4.95	14.6	111	174	20.3
CIT 08_Rain	5.63	13.8	38.2	52.1	1.90	21.1	0.654	0.394	66.2	64.6	7.70
CIT 09_Rain	<LOQ	9.65	18.0	161	0.546	5.24	2.63	0.962	27.4	32.4	4.08
CIT 21_Rain	5.13	4.30	17.9	57.0	<LOQ	8.78	4.32	12.2	21.6	39.8	3.28
CIT 22_Rain	35.3	50.2	757	162	<LOQ	70.6	2.41	5.41	1276	2208	245

Sample	Eu	Gd	Tb	Dy	Ho	Er	Tm	Yb	Lu	Hf	Th
	µg L^{-1}	µg L^{-1}	µg L^{-1}	µg L^{-1}	µg L^{-1}	µg L^{-1}	µg L^{-1}	µg L^{-1}	µg L^{-1}	µg L^{-1}	µg L^{-1}
CIT 01_Rain	57.9	8.91	2.20	8.10	1.01	5.47	1.26	3.43	0.472	2.61	0.391
CIT 02_Rain	28.7	5.55	1.51	5.37	0.589	3.77	0.829	2.49	0.345	2.46	0.416
CIT 06_Rain	31.5	5.90	1.42	5.20	0.700	3.31	0.702	1.97	0.220	1.68	0.254
CIT 07_Rain	74.5	17.8	4.26	15.2	2.18	10.9	2.09	5.26	0.722	3.98	0.592
CIT 08_Rain	29.2	4.67	1.25	5.08	0.647	3.50	0.702	1.87	0.260	1.52	0.182
CIT 09_Rain	18.4	4.16	1.21	4.35	0.601	2.99	0.476	1.53	0.148	0.895	0.265
CIT 21_Rain	19.4	2.83	1.26	3.33	0.474	2.01	0.412	<LOQ	0.0710	1.15	<LOQ
CIT 22_Rain	929	124	45.7	154	17.5	117	16.6	45.5	5.56	32.7	4.62

Sample	Sc	Ge	Y	Zr	Nb	Te	La	Ce	Pr	Nd	Sm
	µg L^{-1}	µg L^{-1}	µg L^{-1}	µg L^{-1}	µg L^{-1}	µg L^{-1}	µg L^{-1}	µg L^{-1}	µg L^{-1}	µg L^{-1}	µg L^{-1}
ZAF 01_Rain	2.78	5.34	47.0	11.5	<LOQ	6.84	0.266	0.685	95.5	104	15.4
ZAF 02_Rain	2.77	2.33	5.46	5.05	0.0260	2.89	0.0520	1.52	10.2	10.8	1.36
ZAF 06_Rain	4.44	2.99	7.21	153	1.68	5.70	3.31	0.979	17.6	9.65	1.40
ZAF 07_Rain	5.25	7.57	23.8	241	1.14	31.8	3.58	0.959	34.8	35.6	4.49
ZAF 08_Rain	<LOQ	3.15	10.2	80.0	0.378	11.4	0.757	0.497	18.4	16.2	2.03
ZAF 09_Rain	<LOQ	2.80	9.54	117	0.642	3.20	1.59	1.77	22.1	18.2	2.24
ZAF 21_Rain	1.45	1.05	5.13	21.1	<LOQ	3.56	0.164	1.02	3.77	8.31	1.22
ZAF 22_Rain	0.842	<LOQ	6.03	6.53	<LOQ	3.19	<LOQ	2.21	7.80	15.0	1.15

Sample	Eu	Gd	Tb	Dy	Ho	Er	Tm	Yb	Lu	Hf	Th
	µg L^{-1}	µg L^{-1}	µg L^{-1}	µg L^{-1}	µg L^{-1}	µg L^{-1}	µg L^{-1}	µg L^{-1}	µg L^{-1}	µg L^{-1}	µg L^{-1}
ZAF 01_Rain	66.0	10.3	2.84	8.77	0.988	5.31	1.17	3.34	0.442	2.55	0.415
ZAF 02_Rain	4.22	0.767	0.358	0.684	0.0950	0.737	0.127	0.359	0.0620	0.522	0.0400
ZAF 06_Rain	6.59	1.36	0.288	0.988	0.149	0.949	0.186	0.751	0.100	0.811	0.123
ZAF 07_Rain	17.7	4.19	0.912	3.55	0.481	2.86	0.485	1.43	0.180	1.12	0.239
ZAF 08_Rain	11.1	1.76	0.679	2.32	0.304	1.72	0.205	0.909	0.186	1.15	0.206
ZAF 09_Rain	10.8	2.60	0.666	2.27	0.277	1.69	0.324	0.889	0.142	0.672	0.0950
ZAF 21_Rain	5.87	1.72	0.354	1.22	0.163	0.891	0.159	0.568	0.0840	0.488	0.0790
ZAF 22_Rain	11.8	1.68	0.447	0.846	<LOQ	<LOQ	<LOQ	<LOQ	<LOQ	0.691	<LOQ

Sample	Sc	Ge	Y	Zr	Nb	Te	La	Ce	Pr	Nd	Sm
	µg L^{-1}	µg L^{-1}	µg L^{-1}	µg L^{-1}	µg L^{-1}	µg L^{-1}	µg L^{-1}	µg L^{-1}	µg L^{-1}	µg L^{-1}	µg L^{-1}
TDF 02_Rain	1.92	2.75	2.91	10.2	0.160	5.94	0.216	0.224	3.21	5.10	0.576
TDF 06_Rain	6.12	2.81	19.5	140	4.19	3.70	3.09	3.02	25.1	22.5	3.81
TDF 07_Rain	12.7	33.4	178	280	1.67	117	5.29	2.37	197	326	38.4
TDF 08_Rain	4.81	4.68	6.07	100	0.814	6.80	0.863	<LOQ	17.9	15.7	1.81
TDF 09_Rain	3.59	5.44	12.1	173	0.926	1.71	2.43	1.88	25.4	21.5	2.93
TDF 21_Rain	2.59	10.6	54.1	36.1	<LOQ	7.52	0.802	0.435	58.3	107	13.4

Sample	Eu	Gd	Tb	Dy	Ho	Er	Tm	Yb	Lu	Hf	Th
	µg L^{-1}	µg L^{-1}	µg L^{-1}	µg L^{-1}	µg L^{-1}	µg L^{-1}	µg L^{-1}	µg L^{-1}	µg L^{-1}	µg L^{-1}	µg L^{-1}
TDF 02_Rain	2.68	0.591	0.143	0.648	0.0150	0.341	0.0800	0.222	0.0320	0.220	<LOQ
TDF 06_Rain	17.7	3.53	0.974	3.44	0.449	2.60	0.601	1.59	0.229	1.54	0.281
TDF 07_Rain	150	31.8	7.85	27.0	3.95	21.2	3.85	10.2	1.28	7.74	1.34
TDF 08_Rain	7.65	1.45	0.368	1.97	0.214	1.05	0.200	0.519	0.131	0.738	0.155
TDF 09_Rain	13.0	3.24	0.690	2.51	0.327	1.60	0.336	0.780	0.156	0.886	0.259
TDF 21_Rain	56.5	8.20	3.13	9.41	1.14	7.89	1.10	3.47	0.504	3.13	0.495

Sample	Sc	Ge	Y	Zr	Nb	Te	La	Ce	Pr	Nd	Sm
	µg L^{-1}	µg L^{-1}	µg L^{-1}	µg L^{-1}	µg L^{-1}	µg L^{-1}	µg L^{-1}	µg L^{-1}	µg L^{-1}	µg L^{-1}	µg L^{-1}
INT 06_Rain	4.14	1.02	6.86	131	0.766	1.55	2.64	1.56	16.0	8.92	1.35
INT 07_Rain	2.70	3.29	11.0	106	0.921	3.40	1.57	3.85	21.0	16.5	2.12
INT 08_Rain	2.62	3.22	10.0	90.4	0.773	17.0	1.47	<LOQ	20.0	19.6	2.84
INT 09_Rain	1.98	3.92	9.46	181	1.26	2.64	2.48	1.09	20.2	15.9	1.51
INT 21_Rain	1.66	6.18	11.6	25.4	<LOQ	30.6	0.341	2.54	15.1	30.1	2.48
INT 22_Rain	0.987	0.933	10.1	53.6	<LOQ	<LOQ	0.804	1.24	8.32	17.2	2.36

Sample	Eu	Gd	Tb	Dy	Ho	Er	Tm	Yb	Lu	Hf	Th
	µg L^{-1}	µg L^{-1}	µg L^{-1}	µg L^{-1}	µg L^{-1}	µg L^{-1}	µg L^{-1}	µg L^{-1}	µg L^{-1}	µg L^{-1}	µg L^{-1}
INT 06_Rain	6.02	1.42	0.274	1.42	0.188	1.16	0.215	0.629	0.100	0.627	0.115
INT 07_Rain	9.51	2.32	0.554	1.78	0.315	1.66	0.254	0.967	0.140	0.812	0.205
INT 08_Rain	11.3	2.48	0.576	1.98	0.293	1.52	0.349	0.816	0.184	0.766	0.246
INT 09_Rain	7.77	2.07	0.467	1.92	0.283	1.25	0.260	0.674	0.0880	0.647	0.124
INT 21_Rain	9.64	2.13	0.602	2.30	0.285	1.76	0.266	0.776	0.115	<LOQ	0.117
INT 22_Rain	9.86	2.28	0.513	1.86	0.283	1.28	0.274	0.791	0.106	0.729	<LOQ

Sample	Sc	Ge	Y	Zr	Nb	Te	La	Ce	Pr	Nd	Sm
	ng L^{-1}	ng L^{-1}	ng L^{-1}	ng L^{-1}	ng L^{-1}	ng L^{-1}	ng L^{-1}	ng L^{-1}	ng L^{-1}	ng L^{-1}	ng L^{-1}
ARC 07_Rain	17.0	16.2	20.3	350	1.86	1.43	6.08	1.88	52.3	25.6	3.98
ARC 08 A_Rain	24.7	6.36	29.1	1620	3.60	3.40	29.3	5.39	25.0	31.7	4.35
ARC 08 B_Rain	15.9	3.09	8.14	607	1.24	3.96	8.00	0.426	21.2	11.5	1.48
ARC 09_Rain	10.0	4.29	9.72	283	1.35	1.57	4.62	1.02	18.7	12.6	1.79
ARC 21_Rain	<LOQ	0.617	5.32	<LOQ	<LOQ	<LOQ	<LOQ	0.160	3.73	2.68	<LOQ
ARC 22_Rain	0.419	<LOQ	2.51	<LOQ	<LOQ	<LOQ	<LOQ	<LOQ	6.70	10.7	<LOQ

Sample	Eu	Gd	Tb	Dy	Ho	Er	Tm	Yb	Lu	Hf	Th
	ng L^{-1}	ng L^{-1}	ng L^{-1}	ng L^{-1}	ng L^{-1}	ng L^{-1}	ng L^{-1}	ng L^{-1}	ng L^{-1}	ng L^{-1}	ng L^{-1}
ARC 07_Rain	14.8	3.74	0.679	3.12	0.403	2.35	0.546	1.39	0.223	1.06	0.120
ARC 08 A_Rain	19.7	4.30	1.06	3.55	0.556	3.87	0.739	2.11	0.302	2.10	0.427
ARC 08 B_Rain	5.60	0.943	0.408	1.28	0.136	1.23	0.276	0.654	0.0800	0.597	0.141
ARC 09_Rain	7.85	1.79	0.311	1.47	0.180	1.36	0.308	0.761	0.102	0.332	0.125
ARC 21_Rain	6.59	<LOQ	<LOQ	<LOQ	<LOQ	<LOQ	<LOQ	<LOQ	<LOQ	0.486	<LOQ
ARC 22_Rain	4.07	<LOQ	<LOQ	<LOQ	<LOQ	<LOQ	<LOQ	<LOQ	<LOQ	0.236	<LOQ

Sample	Sc	Ge	Y	Zr	Nb	Te	La	Ce	Pr	Nd	Sm
	ng L^{-1}	ng L^{-1}	ng L^{-1}	ng L^{-1}	ng L^{-1}	ng L^{-1}	ng L^{-1}	ng L^{-1}	ng L^{-1}	ng L^{-1}	ng L^{-1}
UNI 07_Rain	13.1	4.84	23.8	285	1.51	6.61	4.91	1.11	37.3	19.0	3.08
UNI 08_Rain	7.73	2.81	5.57	120	0.658	1.58	1.67	0.518	16.9	7.79	1.00
UNI 09_Rain	11.6	1.67	14.6	263	1.43	1.74	4.51	3.55	20.5	13.8	1.95
UNI 21_Rain	2.05	1.86	7.75	28.2	<LOQ	1.10	0.316	1.26	12.2	19.2	1.37
UNI 22_Rain	0.496	<LOQ	2.54	10.7	<LOQ	1.06	<LOQ	1.27	4.87	9.02	<LOQ

Sample	Eu	Gd	Tb	Dy	Ho	Er	Tm	Yb	Lu	Hf	Th
	ng L^{-1}	ng L^{-1}	ng L^{-1}	ng L^{-1}	ng L^{-1}	ng L^{-1}	ng L^{-1}	ng L^{-1}	ng L^{-1}	ng L^{-1}	ng L^{-1}
UNI 07_Rain	12.7	2.96	0.771	2.48	0.313	2.13	0.459	1.08	0.170	0.971	0.213
UNI 08_Rain	4.17	0.826	0.227	0.582	0.134	1.03	0.181	0.581	0.0870	0.254	0.0770
UNI 09_Rain	9.14	2.32	0.609	1.99	0.253	1.66	0.280	0.994	0.142	0.953	0.174
UNI 21_Rain	5.59	1.62	0.351	1.39	0.197	1.15	0.192	0.717	0.0940	0.518	0.0970
UNI 22_Rain	4.17	<LOQ	0.176	<LOQ	<LOQ	<LOQ	<LOQ	<LOQ	<LOQ	<LOQ	<LOQ

Sample	Sc	Ge	Y	Zr	Nb	Te	La	Ce	Pr	Nd	Sm
	ng L^{-1}	ng L^{-1}	ng L^{-1}	ng L^{-1}	ng L^{-1}	ng L^{-1}	ng L^{-1}	ng L^{-1}	ng L^{-1}	ng L^{-1}	ng L^{-1}
IND 01_Rain	2.38	1.80	6.65	42.2	0.146	2.31	0.859	1.79	8.27	7.38	0.857
IND 05_Rain	6.55	1.40	7.34	21.4	0.569	2.96	0.437	0.801	3.91	5.59	0.965
IND 07_Rain	7.81	1.98	14.3	324	1.62	1.60	5.89	1.97	21.1	13.9	2.13
IND 08_Rain	2.11	<LOQ	4.53	147	0.769	2.31	2.20	1.22	14.8	8.26	0.895
IND 09_Rain	7.53	5.76	12.5	252	0.750	2.83	3.76	1.64	22.3	17.2	2.33
IND 21_Rain	2.39	3.74	18.6	25.5	<LOQ	2.91	0.136	0.647	13.9	24.3	3.63
IND 22_Rain	<LOQ	<LOQ	2.06	7.39	<LOQ	<LOQ	<LOQ	0.769	2.45	1.54	<LOQ

Sample	Eu	Gd	Tb	Dy	Ho	Er	Tm	Yb	Lu	Hf	Th
	ng L^{-1}	ng L^{-1}	ng L^{-1}	ng L^{-1}	ng L^{-1}	ng L^{-1}	ng L^{-1}	ng L^{-1}	ng L^{-1}	ng L^{-1}	ng L^{-1}
IND 01_Rain	3.72	0.760	0.364	0.686	0.0620	0.600	0.130	0.344	0.0550	0.471	0.0300
IND 05_Rain	4.07	0.964	0.339	1.13	0.178	0.917	0.182	0.637	0.0670	0.419	0.105
IND 07_Rain	7.90	1.92	0.468	1.70	0.284	1.68	0.361	1.06	0.132	1.03	0.174
IND 08_Rain	4.52	0.244	0.161	0.750	0.131	0.698	0.109	0.421	0.0850	0.374	0.123
IND 09_Rain	11.0	2.25	0.549	2.44	0.279	1.82	0.446	1.05	0.139	0.930	0.0650
IND 21_Rain	14.4	3.57	0.755	3.02	0.425	2.70	0.433	1.53	0.226	1.08	0.211
IND 22_Rain	3.56	<LOQ	<LOQ	<LOQ	<LOQ	<LOQ	<LOQ	<LOQ	<LOQ	0.338	<LOQ

Sample	Sc	Ge	Y	Zr	Nb	Te	La	Ce	Pr	Nd	Sm
	ng L^{-1}	ng L^{-1}	ng L^{-1}	ng L^{-1}	ng L^{-1}	ng L^{-1}	ng L^{-1}	ng L^{-1}	ng L^{-1}	ng L^{-1}	ng L^{-1}
BEL 01_Rain	0.216	1.63	6.53	2.48	<LOQ	1.54	0.0190	0.358	3.86	7.38	1.10
BEL 07_Rain	5.60	1.86	14.5	235	0.959	2.54	3.48	0.466	31.8	16.1	2.40
BEL 08_Rain	2.98	1.04	4.51	118	0.606	2.02	1.90	0.565	14.7	7.22	0.911
BEL 09_Rain	<LOQ	7.69	48.4	264	0.640	2.14	4.20	0.851	52.9	60.6	7.99

Sample	Eu	Gd	Tb	Dy	Ho	Er	Tm	Yb	Lu	Hf	Th
	ng L^{-1}	ng L^{-1}	ng L^{-1}	ng L^{-1}	ng L^{-1}	ng L^{-1}	ng L^{-1}	ng L^{-1}	ng L^{-1}	ng L^{-1}	ng L^{-1}
BEL 01_Rain	5.21	1.35	0.297	1.16	0.112	0.980	0.174	0.469	0.0900	0.501	0.0450
BEL 07_Rain	9.80	2.44	0.492	1.79	0.282	1.74	0.341	0.815	0.132	1.02	0.127
BEL 08_Rain	3.81	0.930	0.120	0.865	0.107	0.450	0.142	0.278	0.0610	0.522	0.0570
BEL 09_Rain	35.1	7.27	1.67	7.58	0.952	5.53	1.089	3.18	0.390	2.68	0.417

Sample	Sc	Ge	Y	Zr	Nb	Te	La	Ce	Pr	Nd	Sm
	ng L^{-1}	ng L^{-1}	ng L^{-1}	ng L^{-1}	ng L^{-1}	ng L^{-1}	ng L^{-1}	ng L^{-1}	ng L^{-1}	ng L^{-1}	ng L^{-1}
CAT 04_Rain	6.97	11.1	6.37	33.2	0.814	13.5	2.02	1.45	6.10	12.5	1.71
CAT 06_Rain	9.58	5.36	15.1	201	3.61	3.95	3.70	3.24	25.5	11.3	2.58
CAT 07_Rain	2.70	3.55	13.1	234	1.08	5.29	4.72	3.98	22.7	17.3	2.68
CAT 08_Rain	5.84	3.34	11.1	133	5.15	3.29	2.11	0.791	21.0	18.6	2.71
CAT 09_Rain	0.379	1.80	9.61	217	0.509	<LOQ	2.38	1.46	22.7	15.4	1.92
CAT 21_Rain	<LOQ	<LOQ	3.24	20.8	<LOQ	<LOQ	0.193	0.357	3.78	4.92	0.787
CAT 22_Rain	0.148	0.525	10.6	14.1	<LOQ	1.06	<LOQ	1.23	32.3	33.0	3.26

Sample	Eu	Gd	Tb	Dy	Ho	Er	Tm	Yb	Lu	Hf	Th
	ng L^{-1}	ng L^{-1}	ng L^{-1}	ng L^{-1}	ng L^{-1}	ng L^{-1}	ng L^{-1}	ng L^{-1}	ng L^{-1}	ng L^{-1}	ng L^{-1}
CAT 04_Rain	7.52	1.41	0.474	1.39	0.171	0.933	0.271	0.700	0.115	0.617	0.129
CAT 06_Rain	11.9	2.57	0.557	2.67	0.379	2.25	0.427	1.45	0.185	1.28	0.208
CAT 07_Rain	12.1	2.96	0.715	2.49	0.322	2.15	0.334	1.20	0.161	1.10	0.163
CAT 08_Rain	11.8	3.24	0.680	2.87	0.381	2.09	0.358	1.05	0.131	0.816	0.188
CAT 09_Rain	9.26	1.86	0.466	2.16	0.263	1.50	0.292	0.695	0.137	0.655	0.135
CAT 21_Rain	3.41	0.919	0.220	0.557	0.110	0.478	0.111	0.425	<LOQ	0.291	0.0550
CAT 22_Rain	19.0	2.18	0.674	2.22	0.308	<LOQ	<LOQ	<LOQ	<LOQ	0.635	<LOQ

Sample	Sc	Ge	Y	Zr	Nb	Te	La	Ce	Pr	Nd	Sm
	ng L^{-1}	ng L^{-1}	ng L^{-1}	ng L^{-1}	ng L^{-1}	ng L^{-1}	ng L^{-1}	ng L^{-1}	ng L^{-1}	ng L^{-1}	ng L^{-1}
GLP 06_Rain	7.98	5.62	20.5	213	5.40	18.8	3.74	2.58	32.2	11.3	4.86
GLP 07_Rain	6.71	3.75	19.9	250	2.53	12.6	4.33	2.16	39.2	30.7	5.48
GLP 08_Rain	2.35	4.00	6.57	111	3.67	3.09	1.96	0.450	16.2	11.2	1.47
GLP 09_Rain	2.39	3.67	12.2	166	0.697	<LOQ	2.74	2.84	28.1	20.9	2.77
GLP 21_Rain	2.21	1.06	5.47	21.8	<LOQ	1.11	0.188	1.91	6.44	7.63	1.24
GLP 22_Rain	1.27	1.36	7.01	54.9	<LOQ	2.43	0.665	1.51	9.53	11.9	1.96

Sample	Eu	Gd	Tb	Dy	Ho	Er	Tm	Yb	Lu	Hf	Th
	ng L^{-1}	ng L^{-1}	ng L^{-1}	ng L^{-1}	ng L^{-1}	ng L^{-1}	ng L^{-1}	ng L^{-1}	ng L^{-1}	ng L^{-1}	ng L^{-1}
GLP 06_Rain	21.6	4.03	1.00	3.61	0.549	2.96	0.576	1.75	0.278	1.82	0.370
GLP 07_Rain	22.6	4.32	0.994	3.49	0.454	2.64	0.558	1.40	0.206	1.46	0.284
GLP 08_Rain	7.66	1.54	0.366	1.53	0.208	0.992	0.245	0.554	0.0990	0.802	0.0840
GLP 09_Rain	12.7	2.74	0.710	3.12	0.363	1.70	0.424	0.724	0.133	0.882	0.152
GLP 21_Rain	4.84	1.23	0.317	1.01	0.164	0.854	0.125	0.514	0.0760	0.336	0.0590
GLP 22_Rain	7.00	1.49	0.477	1.13	0.194	0.898	0.174	0.745	<LOQ	0.574	0.123

Sample	Sc	Ge	Y	Zr	Nb	Te	La	Ce	Pr	Nd	Sm
	ng L^{-1}	ng L^{-1}	ng L^{-1}	ng L^{-1}	ng L^{-1}	ng L^{-1}	ng L^{-1}	ng L^{-1}	ng L^{-1}	ng L^{-1}	ng L^{-1}
GAB 01_Rain	2.65	2.52	5.81	88.8	0.111	4.60	1.62	0.124	11.3	5.89	1.01
GAB 04_Rain	1.11	1.43	3.38	12.7	0.0430	1.91	0.124	0.0930	3.16	4.62	0.574
GAB 05_Rain	1.66	1.24	6.40	11.8	0.296	1.64	0.280	0.126	4.90	8.07	1.24
GAB 06_Rain	2.66	2.86	4.59	98.7	0.535	1.72	1.96	0.425	13.8	6.97	0.86
GAB 07_Rain	5.36	5.52	19.7	392	2.16	2.84	6.43	2.79	25.9	21.3	2.96
GAB 08_Rain	6.40	5.50	9.19	159	1.95	1.56	2.13	1.54	21.3	16.6	2.25
GAB 09_Rain	2.50	7.24	18.4	263	0.670	6.91	4.26	<LOQ	25.3	22.8	3.54

Sample	Eu	Gd	Tb	Dy	Ho	Er	Tm	Yb	Lu	Hf	Th
	ng L^{-1}	ng L^{-1}	ng L^{-1}	ng L^{-1}	ng L^{-1}	ng L^{-1}	ng L^{-1}	ng L^{-1}	ng L^{-1}	ng L^{-1}	ng L^{-1}
GAB 01_Rain	4.42	0.873	0.245	0.857	0.0660	0.739	0.143	0.463	0.0810	0.709	0.0540
GAB 04_Rain	2.58	0.743	0.168	0.590	0.0310	0.465	0.115	0.322	0.0360	0.399	0.00500
GAB 05_Rain	5.09	1.35	0.317	1.32	0.159	0.900	0.162	0.518	0.0890	0.553	0.0670
GAB 06_Rain	3.79	0.685	0.173	0.752	0.110	0.632	0.172	0.320	0.0540	0.365	0.0960
GAB 07_Rain	13.4	3.09	0.702	2.37	0.360	2.29	0.514	1.36	0.216	1.29	0.255
GAB 08_Rain	9.21	1.87	0.453	1.83	0.267	1.40	0.183	0.873	0.0930	0.695	0.115
GAB 09_Rain	15.1	3.13	0.781	3.52	0.477	2.45	0.552	1.39	0.241	1.54	0.260

Sample	Sc	Ge	Y	Zr	Nb	Te	La	Ce	Pr	Nd	Sm
	ng L^{-1}	ng L^{-1}	ng L^{-1}	ng L^{-1}	ng L^{-1}	ng L^{-1}	ng L^{-1}	ng L^{-1}	ng L^{-1}	ng L^{-1}	ng L^{-1}
SIR 01_Rain	2.27	2.49	2.11	70.7	0.511	1.88	1.38	1.06	12.2	7.85	0.738
SIR 06_Rain	4.24	2.94	8.22	155	1.10	7.67	2.86	1.30	21.9	11.7	1.26
SIR 07_Rain	5.95	2.72	9.76	172	0.897	3.26	2.76	1.47	34.9	14.9	1.88
SIR 08_Rain	10.0	2.95	12.4	164	0.681	1.58	2.23	0.301	29.6	16.3	2.50
SIR 09_Rain	12.8	5.47	12.8	290	0.895	3.91	4.37	0.0500	26.6	14.8	2.23
SIR 21_Rain	<LOQ	<LOQ	<LOQ	<LOQ	<LOQ	<LOQ	<LOQ	<LOQ	9.68	8.53	<LOQ
SIR 22_Rain	1.62	1.42	11.4	51.3	<LOQ	<LOQ	1.26	2.36	69.7	10.3	1.46

Sample	Eu	Gd	Tb	Dy	Ho	Er	Tm	Yb	Lu	Hf	Th
	ng L^{-1}	ng L^{-1}	ng L^{-1}	ng L^{-1}	ng L^{-1}	ng L^{-1}	ng L^{-1}	ng L^{-1}	ng L^{-1}	ng L^{-1}	ng L^{-1}
SIR 01_Rain	2.30	0.611	0.244	0.527	0.00200	0.330	0.0660	0.220	0.0320	0.272	<LOQ
SIR 06_Rain	5.47	1.33	0.277	1.13	0.205	1.18	0.187	0.755	0.101	0.784	0.0990
SIR 07_Rain	8.72	1.92	0.334	1.51	0.231	1.42	0.325	0.794	0.0960	0.636	0.132
SIR 08_Rain	10.4	3.52	0.583	2.10	0.322	1.95	0.421	0.970	0.182	0.748	0.184
SIR 09_Rain	10.9	2.52	0.566	2.20	0.209	2.02	0.331	1.28	0.134	0.761	0.302
SIR 21_Rain	2.71	<LOQ	<LOQ	<LOQ	<LOQ	<LOQ	<LOQ	<LOQ	<LOQ	0.315	<LOQ
SIR 22_Rain	11.3	1.34	0.517	1.67	0.198	0.806	0.264	0.365	0.0820	0.933	<LOQ

Sample	Sc	Ge	Y	Zr	Nb	Te	La	Ce	Pr	Nd	Sm
	ng L^{-1}	ng L^{-1}	ng L^{-1}	ng L^{-1}	ng L^{-1}	ng L^{-1}	ng L^{-1}	ng L^{-1}	ng L^{-1}	ng L^{-1}	ng L^{-1}
AUG 01_Rain	3.20	2.67	8.44	14.4	0.0820	2.50	0.157	0.616	17.0	11.5	1.70
AUG 06_Rain	5.66	1.66	13.8	217	1.79	4.28	4.48	3.79	31.3	19.7	2.57
AUG 07_Rain	5.98	2.84	17.9	155	0.820	3.36	2.67	2.92	51.9	24.7	3.27
AUG 08_Rain	3.97	2.97	11.2	92.7	1.64	1.61	1.28	1.01	26.0	16.3	2.19
AUG 09_Rain	2.34	4.16	14.8	161	0.715	1.52	2.62	2.26	41.1	23.3	3.26

Sample	Eu	Gd	Tb	Dy	Ho	Er	Tm	Yb	Lu	Hf	Th
	ng L^{-1}	ng L^{-1}	ng L^{-1}	ng L^{-1}	ng L^{-1}	ng L^{-1}	ng L^{-1}	ng L^{-1}	ng L^{-1}	ng L^{-1}	ng L^{-1}
AUG 01_Rain	7.30	1.71	0.415	1.69	0.206	1.20	0.254	0.666	0.0740	0.525	0.0640
AUG 06_Rain	10.6	2.14	0.511	2.28	0.307	1.93	0.402	1.12	0.170	1.17	0.211
AUG 07_Rain	14.8	3.82	0.697	3.11	0.400	2.59	0.455	1.34	0.206	1.27	0.282
AUG 08_Rain	9.53	2.20	0.533	1.57	0.285	1.56	0.396	0.945	0.136	0.744	0.0830
AUG 09_Rain	14.8	3.16	0.566	2.77	0.396	2.42	0.393	0.694	0.174	0.701	0.115

Sample	Sc	Ge	Y	Zr	Nb	Te	La	Ce	Pr	Nd	Sm
	ng L^{-1}	ng L^{-1}	ng L^{-1}	ng L^{-1}	ng L^{-1}	ng L^{-1}	ng L^{-1}	ng L^{-1}	ng L^{-1}	ng L^{-1}	ng L^{-1}
PRI 01_Rain	2.00	1.88	4.17	61.5	0.396	2.32	1.20	0.364	15.4	11.2	1.09
PRI 06_Rain	5.06	2.70	10.3	118	1.30	5.17	2.25	1.84	34.7	14.8	1.82
PRI 07_Rain	6.43	1.69	7.13	240	0.790	3.37	4.08	0.0740	35.5	11.2	1.28
PRI 08_Rain	9.22	2.70	16.1	247	0.762	1.50	3.73	0.287	93.6	20.3	2.71
PRI 09_Rain	9.88	3.09	11.9	170	0.763	1.52	1.98	0.727	63.4	18.0	2.77
PRI 21_Rain	1.32	1.52	8.78	28.5	<LOQ	1.08	0.239	0.827	44.0	25.8	1.71
PRI 22_Rain	1.68	0.862	8.50	25.9	<LOQ	<LOQ	<LOQ	5.17	376	198	0.750

Sample	Eu	Gd	Tb	Dy	Ho	Er	Tm	Yb	Lu	Hf	Th
	ng L^{-1}	ng L^{-1}	ng L^{-1}	ng L^{-1}	ng L^{-1}	ng L^{-1}	ng L^{-1}	ng L^{-1}	ng L^{-1}	ng L^{-1}	ng L^{-1}
PRI 01_Rain	4.31	0.806	0.351	0.880	0.0650	0.619	0.144	0.276	0.0600	0.372	0.0330
PRI 06_Rain	7.98	1.45	0.373	1.65	0.247	1.34	0.255	1.07	0.112	0.839	0.178
PRI 07_Rain	5.86	1.39	0.513	1.26	0.201	0.955	0.199	0.621	0.0840	0.466	0.137
PRI 08_Rain	11.7	3.27	0.705	2.42	0.384	1.84	0.409	0.990	0.138	0.847	0.215
PRI 09_Rain	11.9	3.22	0.690	2.20	0.317	2.07	0.402	0.968	0.133	0.771	0.154
PRI 21_Rain	6.67	1.50	0.420	1.52	0.222	1.21	0.206	0.721	0.0830	0.518	0.0960
PRI 22_Rain	9.86	1.12	0.457	1.80	0.163	<LOQ	<LOQ	<LOQ	<LOQ	0.601	<LOQ

Sample	Sc	Ge	Y	Zr	Nb	Te	La	Ce	Pr	Nd	Sm
	ng L^{-1}	ng L^{-1}	ng L^{-1}	ng L^{-1}	ng L^{-1}	ng L^{-1}	ng L^{-1}	ng L^{-1}	ng L^{-1}	ng L^{-1}	ng L^{-1}
CES 01_Rain	0.482	1.04	5.58	2.02	<LOQ	1.29	<LOQ	0.153	2.83	6.93	1.07
CES 02_Rain	1.28	0.922	8.54	7.46	0.315	1.81	0.109	1.96	5.67	9.93	1.16
CES 05_Rain	2.11	0.834	5.94	9.75	0.250	1.85	0.299	1.02	6.88	7.10	0.802
CES 07_Rain	4.99	4.44	10.4	107	0.987	4.24	1.10	1.79	22.3	17.3	2.14
CES 08_Rain	1.94	<LOQ	9.85	74.0	0.296	2.43	1.06	2.64	16.3	18.5	2.31
CES 09_Rain	4.61	5.18	22.9	202	2.18	3.94	3.73	7.89	35.7	42.9	4.59
CES 21_Rain	1.56	1.12	11.7	15.5	<LOQ	0.815	0.171	0.491	12.9	18.2	3.11
CES 22_Rain	0.967	<LOQ	<LOQ	28.6	<LOQ	<LOQ	0.243	0.917	1.46	<LOQ	<LOQ

Sample	Eu	Gd	Tb	Dy	Ho	Er	Tm	Yb	Lu	Hf	Th
	ng L-1	ng L-1	ng L-1	ng L-1	ng L-1	ng L-1	ng L-1	ng L-1	ng L-1	ng L-1	ng L-1
CES 01_Rain	5.30	1.37	0.348	1.05	0.141	0.774	0.184	0.529	0.0970	0.547	0.0380
CES 02_Rain	5.02	1.63	0.454	1.63	0.208	1.50	0.258	0.760	0.127	0.643	0.0840
CES 05_Rain	4.01	0.722	0.259	0.911	0.155	0.613	0.123	0.451	0.0570	0.344	0.117
CES 07_Rain	8.90	1.83	0.478	1.61	0.213	1.73	0.299	0.714	0.0780	0.606	0.114
CES 08_Rain	9.06	2.44	0.661	2.31	0.331	1.50	0.305	0.762	0.0920	0.845	0.113
CES 09_Rain	21.9	5.50	1.39	5.57	0.681	3.39	0.701	1.47	0.249	1.65	0.282
CES 21_Rain	11.9	1.83	0.828	2.99	0.220	1.98	0.221	0.732	<LOQ	0.519	0.0750
CES 22_Rain	2.40	<LOQ	<LOQ	<LOQ	<LOQ	<LOQ	<LOQ	<LOQ	<LOQ	<LOQ	<LOQ

Table S. 7 - Boron and strontium isotopic composition in rainwater samples. S.D. = Standard Deviation.

Sample	$^{87}Sr/^{86}Sr$	Std. Err.	$\delta^{11}B$ (‰)	S.D.
ZAF 04	0.7038650	0.000005	22.88	0.323
ZAF 06	0.7081444	0.000012	38.05	0.103
ZAF 18	0.7080635	0.000005	42.90	0.202
TDF 04	0.7040719	0.000007	12.00	0.175
TDF 04 REP 1	n.d.	n.d.	10.64	0.423
TDF 04 REP 2	n.d.	n.d.	11.45	0.070
TDF 06	0.7080832	0.000007	31.51	0.182
TDF 12	0.7037281	0.000008	1.289	0.302
TDF 13	0.7043343	0.000009	16.96	0.111
TDF 13 CHEM2	0.7043430	0.000007	16.86	0.154
TDF 17	0.7063621	0.000004	17.34	0.245
INT 12	0.7088030	0.000007	34.04	0.118
INT 13	0.7103627	0.000006	30.07	0.065

Sample	$^{87}Sr/^{86}Sr$	Std. Err.	$\delta^{11}B$ (‰)	S.D.
ARC 12	0.7091222	0.000009	38.32	0.264
ARC 12 REP	n.d.	n.d.	38.15	0.127
ARC 16	0.7088823	0.000009	39.07	0.240
UNI 13	0.7096083	0.000008	37.93	0.091
IND 04	0.7088737	0.000011	25.58	0.279
IND 16	0.7089158	0.000006	34.19	0.141
BEL 04	0.7088578	0.000008	28.78	0.052
CAT 06	0.7084946	0.000007	31.60	0.172
CAT 13	0.7099210	0.000007	40.33	0.165
GLP 04	0.7064746	0.000008	22.00	0.345
GLP 17	0.7074008	0.000012	29.17	0.193

Sample	$^{87}Sr/^{86}Sr$	Std. Err.	$\delta^{11}B$ (‰)	S.D.
GAB 07	0.7087676	0.000009	30.91	0.000
GAB 13	0.7091249	0.000010	33.68	0.157
SIR 04	0.7085717	0.000011	27.41	0.121
SIR 04 REP	0.7085570	0.000015	n.d.	n.d.
SIR 17	0.7086902	0.000006	36.32	0.262
PRI 13	0.7099191	0.000005	37.82	0.228
PRI 13 CHEM2	0.7099265	0.000008	n.d.	n.d.

Sample	$^{87}Sr/^{86}Sr$	Std. Err.	$\delta^{11}B$ (‰)	S.D.
CES 03	0.7092115	0.000010	22.61	0.195
CES 04	0.7088513	0.000015	39.40	0.223
CES 09	0.7092833	0.000006	40.33	0.056
CES 12	0.7071935	0.000009	39.35	0.141
CES 12 REP 1	n.d.	n.d.	38.30	0.139
CES 12 REP 2	n.d.	n.d.	38.85	0.229

Table S. 8 - Minor, trace, and Technology-Critical Element concentrations in blank solutions.

Sample	Li	B	Al	Ti	V	Cr	Mn	Fe	Co	Ni	Cu	Zn	As	Se	Br	Rb	Sr	Mo	Cd	Sn	Sb	Cs	Ba	Tl	Pb	U
	µg L^{-1}	µg L^{-1}	µg L^{-1}	µg L^{-1}	µg L^{-1}	µg L^{-1}	µg L^{-1}	µg L^{-1}	µg L^{-1}	µg L^{-1}	µg L^{-1}	µg L^{-1}	µg L^{-1}	µg L^{-1}	µg L^{-1}	µg L^{-1}	µg L^{-1}	µg L^{-1}	µg L^{-1}	µg L^{-1}	µg L^{-1}	µg L^{-1}	µg L^{-1}	µg L^{-1}	µg L^{-1}	µg L^{-1}
R I_01	<LOQ	<LOQ	0.146	<LOQ	0.0360	0.154	0.222	0.293	0.0150	0.0460	0.281	2.36	0.0150	0.217	0.160	0.00900	0.211	<LOQ	<LOQ	<LOQ	0.00200	0.00100	0.257	<LOQ	0.0110	<LOQ
R I_02	<LOQ	<LOQ	0.348	<LOQ	<LOQ	0.0260	0.177	0.235	0.0180	0.0350	0.168	4.13	0.00700	0.146	0.199	0.00700	0.0950	<LOQ	<LOQ	<LOQ	0.00200	0.00100	0.579	<LOQ	0.0160	<LOQ
R I_03	<LOQ	<LOQ	0.150	<LOQ	0.0110	<LOQ	0.268	0.190	0.0260	0.132	0.205	5.56	0.00400	0.213	1.28	0.00800	0.693	0.00900	<LOQ	<LOQ	0.00200	0.00100	0.325	<LOQ	0.0110	<LOQ
R I_04	<LOQ	<LOQ	1.25	0.0193	0.0137	0.00925	0.0308	1.01	0.00200	<LOQ	0.415	6.44	0.00737	0.0157	<LOQ	<LOQ	2.33	0.270	<LOQ	<LOQ	<LOQ	<LOQ	3.47	<LOQ	0.00675	<LOQ
R I_05	<LOQ	0.205	3.19	0.228	0.0684	0.0300	0.698	2.79	0.0107	0.190	0.663	17.8	0.0157	0.0246	<LOQ	0.0259	2.71	0.230	<LOQ	<LOQ	0.0100	<LOQ	3.01	<LOQ	0.0198	<LOQ
R I_06	<LOQ	<LOQ	0.986	<LOQ	0.00876	1.49	0.435	3.21	0.0190	3.79	0.0448	0.417	0.0241	0.0711	<LOQ	<LOQ	0.0802	0.353	0.00926	<LOQ	0.00964	0.00319	0.0605	0.00836	0.0186	0.000382
R I_07	<LOQ	<LOQ	2.06	<LOQ	0.00861	1.28	0.408	3.50	0.0118	3.36	0.175	1.01	0.0220	0.0694	<LOQ	<LOQ	0.0973	0.248	0.00916	<LOQ	0.0115	0.00264	0.0948	0.00675	0.0554	0.000585
R I_08	0.0500	0.351	1.90	0.0250	0.0100	0.0500	0.0685	0.0500	0.0150	0.0495	<LOQ	0.0661	0.00529	<LOQ	<LOQ	0.0197	0.0428	0.0931	0.00500	<LOQ	0.0100	<LOQ	0.891	0.00825	0.00500	0.000910
R I_09	0.0346	1.40	<LOQ	<LOQ	0.0970	<LOQ	0.0146	0.0500	0.0122	<LOQ	<LOQ	<LOQ	0.00796	<LOQ	<LOQ	<LOQ	<LOQ	<LOQ	0.0118	<LOQ	0.0217	<LOQ	<LOQ	0.0160	0.0103	0.00596

Sample	Li	B	Al	Ti	V	Cr	Mn	Fe	Co	Ni	Cu	Zn	As	Se	Br	Rb	Sr	Mo	Cd	Sn	Sb	Cs	Ba	Tl	Pb	U
	µg L^{-1}	µg L^{-1}	µg L^{-1}	µg L^{-1}	µg L^{-1}	µg L^{-1}	µg L^{-1}	µg L^{-1}	µg L^{-1}	µg L^{-1}	µg L^{-1}	µg L^{-1}	µg L^{-1}	µg L^{-1}	µg L^{-1}	µg L^{-1}	µg L^{-1}	µg L^{-1}	µg L^{-1}	µg L^{-1}	µg L^{-1}	µg L^{-1}	µg L^{-1}	µg L^{-1}	µg L^{-1}	µg L^{-1}
R II_01	0.0130	2.19	1.31	0.0580	0.00800	0.0590	0.148	3.59	<LOQ	<LOQ	<LOQ	0.849	0.00700	<LOQ	27.7	0.0230	0.0840	<LOQ	<LOQ	<LOQ	<LOQ	<LOQ	0.177	<LOQ	0.0120	0.00100
R II_02	0.0440	1.61	10.3	0.194	0.100	0.139	0.855	10.0	0.0420	0.163	8.44	17.6	0.00700	<LOQ	17.4	0.0550	1.11	0.0150	<LOQ	<LOQ	0.00900	<LOQ	0.900	<LOQ	0.0790	0.00200
R II_03	0.0140	0.448	7.51	0.131	<LOQ	0.0550	0.150	2.96	0.00400	0.146	<LOQ	2.15	0.00700	<LOQ	8.68	0.0230	0.340	<LOQ	<LOQ	<LOQ	<LOQ	<LOQ	0.362	<LOQ	0.0540	0.00100
R II_04	0.0300	0.396	10.5	0.249	0.0330	0.170	0.368	6.42	0.0250	0.365	1.80	6.64	0.00500	<LOQ	11.8	0.0640	1.40	<LOQ	0.0170	<LOQ	0.00600	<LOQ	0.877	<LOQ	0.296	0.00200

Sample	Li	B	Al	Ti	V	Cr	Mn	Fe	Co	Ni	Cu	Zn	As	Se	Br	Rb	Sr	Mo	Cd	Sn	Sb	Cs	Ba	Tl	Pb	U
	µg L^{-1}	µg L^{-1}	µg L^{-1}	µg L^{-1}	µg L^{-1}	µg L^{-1}	µg L^{-1}	µg L^{-1}	µg L^{-1}	µg L^{-1}	µg L^{-1}	µg L^{-1}	µg L^{-1}	µg L^{-1}	µg L^{-1}	µg L^{-1}	µg L^{-1}	µg L^{-1}	µg L^{-1}	µg L^{-1}	µg L^{-1}	µg L^{-1}	µg L^{-1}	µg L^{-1}	µg L^{-1}	µg L^{-1}
R III_01	0.0120	<LOQ	1.91	0.0360	<LOQ	0.252	0.0660	0.0100	<LOQ	<LOQ	1.51	3.56	<LOQ	<LOQ	<LOQ	<LOQ	0.0870	<LOQ	0.0120	<LOQ	<LOQ	<LOQ	0.147	<LOQ	0.0110	<LOQ
R III_02	0.0340	0.161	1.48	0.0960	<LOQ	0.0310	0.267	1.72	0.0140	0.0380	0.636	2.72	<LOQ	<LOQ	<LOQ	<LOQ	0.217	<LOQ	<LOQ	0.0160	<LOQ	<LOQ	0.627	<LOQ	0.0510	0.00100
R III_03	<LOQ	<LOQ	23.0	0.0690	<LOQ	0.0840	0.0690	3.21	<LOQ	0.108	2.09	6.19	<LOQ	<LOQ	<LOQ	<LOQ	0.292	<LOQ	<LOQ	<LOQ	<LOQ	<LOQ	3.09	<LOQ	0.436	0.00300
R III_04	0.00900	4.19	34.9	0.480	0.0150	0.289	0.208	13.8	0.00500	0.0960	14.7	9.13	0.00800	0.112	<LOQ	0.0110	0.522	<LOQ	<LOQ	<LOQ	<LOQ	<LOQ	0.570	<LOQ	0.854	0.00600
R III_05	0.00700	4.72	43.9	0.810	0.0120	0.0530	0.0730	22.0	<LOQ	0.119	10.0	6.82	0.0170	0.0950	<LOQ	0.00900	0.475	<LOQ	<LOQ	<LOQ	<LOQ	<LOQ	0.337	<LOQ	0.510	0.00300
R III_06	<LOQ	<LOQ	0.401	0.0310	0.0170	0.0210	0.0240	0.604	0.0260	<LOQ	0.323	<LOQ	0.00900	0.201	<LOQ	<LOQ	0.389	<LOQ	0.00200	<LOQ	<LOQ	<LOQ	0.198	<LOQ	0.0260	<LOQ
R III_07	0.0220	27.6	43.0	0.196	0.0330	0.0400	0.196	7.41	<LOQ	0.0330	7.83	9.28	0.0310	0.102	<LOQ	0.0120	0.962	<LOQ	0.0100	<LOQ	0.00900	0.00200	0.988	<LOQ	0.436	0.00800
R III_08	<LOQ	<LOQ	0.767	0.0350	0.00600	0.0100	0.0380	1.68	<LOQ	<LOQ	<LOQ	1.65	<LOQ	<LOQ	<LOQ	<LOQ	0.458	<LOQ	0.0120	<LOQ	<LOQ	<LOQ	0.0480	<LOQ	0.0570	<LOQ
R III_09	<LOQ	<LOQ	3.14	0.110	<LOQ	0.0230	0.0620	2.05	<LOQ	<LOQ	<LOQ	1.38	<LOQ	0.145	<LOQ	<LOQ	<LOQ	<LOQ	0.00600	<LOQ	<LOQ	<LOQ	0.163	<LOQ	0.0250	<LOQ
R III_10	0.0210	35.0	27.7	0.545	0.0260	0.0510	0.169	9.74	0.00300	0.495	5.76	10.7	0.0110	0.0610	<LOQ	0.0300	0.760	0.00500	0.0210	<LOQ	0.00800	0.00200	0.761	<LOQ	0.507	0.00500

Sample	Li	B	Al	Ti	V	Cr	Mn	Fe	Co	Ni	Cu	Zn	As	Se	Br	Rb	Sr	Mo	Cd	Sn	Sb	Cs	Ba	Tl	Pb	U
	µg L^{-1}	µg L^{-1}	µg L^{-1}	µg L^{-1}	µg L^{-1}	µg L^{-1}	µg L^{-1}	µg L^{-1}	µg L^{-1}	µg L^{-1}	µg L^{-1}	µg L^{-1}	µg L^{-1}	µg L^{-1}	µg L^{-1}	µg L^{-1}	µg L^{-1}	µg L^{-1}	µg L^{-1}	µg L^{-1}	µg L^{-1}	µg L^{-1}	µg L^{-1}	µg L^{-1}	µg L^{-1}	µg L^{-1}
M I_01	<LOQ	1.87	4.91	0.258	0.0640	0.213	0.0730	1.98	0.0170	0.343	<LOQ	8.92	0.0670	<LOQ	<LOQ	0.0180	0.179	1.50	0.0250	0.127	0.0310	0.00100	0.101	0.0100	0.0410	0.0330
M I_02	0.398	<LOQ	32.0	2.40	0.335	0.206	0.176	5.30	<LOQ	0.622	0.338	5.20	<LOQ	<LOQ	<LOQ	<LOQ	2.53	<LOQ	<LOQ	<LOQ	<LOQ	<LOQ	0.342	<LOQ	0.882	<LOQ
M I_03	<LOQ	<LOQ	87.0	1.87	0.361	0.260	2.30	355	0.791	1.54	0.686	10.9	0.941	<LOQ	<LOQ	<LOQ	3.50	0.213	<LOQ	<LOQ	<LOQ	<LOQ	0.886	<LOQ	1.06	<LOQ

Sample	Li	B	Al	Ti	V	Cr	Mn	Fe	Co	Ni	Cu	Zn	As	Se	Br	Rb	Sr	Mo	Cd	Sn	Sb	Cs	Ba	Tl	Pb	U
	µg L^{-1}	µg L^{-1}	µg L^{-1}	µg L^{-1}	µg L^{-1}	µg L^{-1}	µg L^{-1}	µg L^{-1}	µg L^{-1}	µg L^{-1}	µg L^{-1}	µg L^{-1}	µg L^{-1}	µg L^{-1}	µg L^{-1}	µg L^{-1}	µg L^{-1}	µg L^{-1}	µg L^{-1}	µg L^{-1}	µg L^{-1}	µg L^{-1}	µg L^{-1}	µg L^{-1}	µg L^{-1}	µg L^{-1}
M II_01	<LOQ	<LOQ	11.9	0.631	0.140	0.883	0.173	48.8	0.0448	3.92	2.98	5.14	0.0693	<LOQ	<LOQ	0.0100	0.416	0.291	0.0235	0.0200	0.272	0.00100	2.48	<LOQ	0.134	0.00100
M II_02	0.340	<LOQ	178	74.7	0.936	0.754	2.87	179	<LOQ	1.06	1.28	5.40	0.00500	<LOQ	<LOQ	<LOQ	4.55	0.295	<LOQ	<LOQ	<LOQ	<LOQ	1.70	<LOQ	0.634	<LOQ
M II_03	0.223	<LOQ	24.3	11.3	0.488	0.150	0.221	25.9	<LOQ	0.0538	0.0490	1.90	0.135	<LOQ	<LOQ	<LOQ	2.30	<LOQ	<LOQ	<LOQ	<LOQ	<LOQ	0.224	<LOQ	0.542	<LOQ
M II_04	<LOQ	<LOQ	69.6	13.1	0.372	2.23	1.12	132	<LOQ	<LOQ	0.975	8.30	1.51	<LOQ	<LOQ	<LOQ	0.600	<LOQ	<LOQ	<LOQ	<LOQ	<LOQ	0.881	<LOQ	0.988	<LOQ

Sample	Li	B	Al	Ti	V	Cr	Mn	Fe	Co	Ni	Cu	Zn	As	Se	Br	Rb	Sr	Mo	Cd	Sn	Sb	Cs	Ba	Tl	Pb	U
	μg L^{-1}	μg L^{-1}	μg L^{-1}	μg L^{-1}	μg L^{-1}	μg L^{-1}	μg L^{-1}	μg L^{-1}	μg L^{-1}	μg L^{-1}	μg L^{-1}	μg L^{-1}	μg L^{-1}	μg L^{-1}	μg L^{-1}	μg L^{-1}	μg L^{-1}	μg L^{-1}	μg L^{-1}	μg L^{-1}	μg L^{-1}	μg L^{-1}	μg L^{-1}	μg L^{-1}	μg L^{-1}	μg L^{-1}
M III_01	<LOQ	<LOQ	30.6	0.544	0.262	1.44	0.184	24.2	0.0534	1.42	<LOQ	20.1	0.0190	<LOQ	<LOQ	0.0430	1.33	1.35	0.0824	0.0380	0.114	0.00100	3.17	<LOQ	0.168	0.00500
M III_02	<LOQ	<LOQ	62.8	2.75	0.247	2.15	0.438	41.6	0.123	2.01	0.478	98.9	0.0677	<LOQ	<LOQ	0.0980	2.44	0.634	0.0849	0.119	0.426	0.00400	3.19	<LOQ	0.374	0.00800
M III_03	<LOQ	<LOQ	118	7.72	0.491	2.76	1.26	75.2	0.0850	2.63	1.81	138	0.136	<LOQ	<LOQ	0.236	3.40	1.04	0.0748	0.231	0.184	0.00700	3.42	<LOQ	0.623	0.0140
M III_04	<LOQ	<LOQ	131	2.82	0.247	19.3	0.144	25.9	0.0406	1.58	0.127	26.9	0.0182	<LOQ	<LOQ	0.0240	1.31	0.397	0.0437	0.0510	0.217	0.00100	2.41	<LOQ	0.0900	0.00100
M III_05	0.427	<LOQ	47.6	6.56	0.246	20.8	0.669	33.8	0.0645	2.39	<LOQ	19.5	0.0182	<LOQ	<LOQ	0.0500	1.23	0.301	0.0588	0.0440	0.151	0.00300	2.52	<LOQ	0.163	0.00500
M III_06	0.374	<LOQ	69.3	2.60	0.232	2.35	3.25	35.1	0.503	0.956	2.16	25.8	0.0833	<LOQ	<LOQ	0.0500	2.93	0.345	0.0756	0.227	0.144	0.00100	3.15	<LOQ	0.190	0.0740
M III_07	0.701	<LOQ	46.2	6.52	0.306	22.3	1.12	28.7	0.0363	1.33	2.48	31.3	0.0800	<LOQ	<LOQ	0.0660	13.6	0.931	0.0908	0.0700	0.164	0.00100	6.86	<LOQ	1.45	0.0170

Sample	Li	B	Al	Ti	V	Cr	Mn	Fe	Co	Ni	Cu	Zn	As	Se	Br	Rb	Sr	Mo	Cd	Sn	Sb	Cs	Ba	Tl	Pb	U
	μg L^{-1}	μg L^{-1}	μg L^{-1}	μg L^{-1}	μg L^{-1}	μg L^{-1}	μg L^{-1}	μg L^{-1}	μg L^{-1}	μg L^{-1}	μg L^{-1}	μg L^{-1}	μg L^{-1}	μg L^{-1}	μg L^{-1}	μg L^{-1}	μg L^{-1}	μg L^{-1}	μg L^{-1}	μg L^{-1}	μg L^{-1}	μg L^{-1}	μg L^{-1}	μg L^{-1}	μg L^{-1}	μg L^{-1}
M IV_01	0.746	11.6	115	31.8	0.409	5.94	2.36	121	0.117	3.76	0.511	22.5	0.270	<LOQ	15.4	0.322	4.10	0.859	0.130	0.350	0.178	0.0270	7.02	<LOQ	0.579	0.0220
M IV_02	0.968	8.02	1.3	231	3.60	6.09	17.5	1.05	0.497	3.16	2.97	18.4	0.465	<LOQ	71.7	1.16	12.7	0.562	0.0580	0.471	0.232	0.0410	13.0	0.0120	0.837	0.0450
M IV_03	0.420	<LOQ	406	29.7	1.21	4.43	7.04	371	0.272	2.97	1.36	10.8	0.447	<LOQ	8.97	0.547	6.03	0.300	0.0420	0.322	0.192	0.0190	9.60	<LOQ	0.375	0.0180
M IV_04	0.437	<LOQ	436	49.7	1.32	3.41	6.73	435	0.217	2.05	1.35	6.90	0.296	<LOQ	<LOQ	0.559	4.64	0.123	0.0471	0.323	0.197	0.0250	7.85	0.00700	0.519	0.0170
M IV_05	1.15	<LOQ	1.7	62.1	2.74	8.15	9.32	1.14	0.988	3.81	7.25	28.3	0.292	<LOQ	<LOQ	2.05	4.11	0.450	0.0227	0.492	0.148	0.111	8.09	0.0130	0.815	0.252
M IV_06	0.481	<LOQ	732	40.8	1.20	7.10	3.46	504	0.287	6.43	18.2	17.1	0.256	<LOQ	15.8	0.845	3.93	0.270	0.0328	0.523	0.758	0.0460	10.2	0.00700	4.84	0.0340
M IV_07	0.0957	6.59	121	21.9	0.420	3.03	3.42	158	0.651	1.72	4.76	18.6	0.113	<LOQ	10.9	0.133	4.52	0.223	0.0168	0.169	0.126	0.00500	7.31	<LOQ	0.529	0.232
M IV_08	<LOQ	<LOQ	111	2.97	0.241	21.3	0.443	46.6	0.0798	2.30	1.79	196	0.0627	<LOQ	<LOQ	0.0670	1.31	0.324	0.0118	0.101	1.88	0.00300	2.69	<LOQ	0.598	0.00800
M IV_09	<LOQ	<LOQ	98.2	12.6	0.331	12.7	0.606	72.6	0.0764	3.05	0.783	18.0	0.0182	<LOQ	18.1	0.106	2.30	0.0380	0.0202	0.0940	0.148	0.00500	3.47	<LOQ	0.277	0.00800
M IV_10	0.322	<LOQ	587	25.2	1.08	22.7	2.81	434	0.144	4.24	7.23	34.9	0.113	<LOQ	<LOQ	0.723	2.18	0.142	0.0202	0.256	0.142	0.0370	4.47	<LOQ	0.580	0.0150
M IV_11	<LOQ	<LOQ	44.1	2.57	0.259	27.9	0.855	92.9	0.123	4.27	1.26	10.6	0.0182	<LOQ	<LOQ	0.0770	0.964	0.135	0.0328	0.0590	0.120	0.00400	2.69	<LOQ	0.239	0.00300
M IV_12	<LOQ	<LOQ	35.3	1.14	0.199	17.2	0.808	32.3	0.0406	3.22	2.65	22.6	0.0190	<LOQ	<LOQ	0.0570	7.27	0.156	0.0202	0.0610	0.130	0.00200	5.87	<LOQ	1.06	0.0140
M IV_13	0.0459	20.1	623	10.5	0.657	21.2	6.45	676	0.173	2.87	3.75	87.8	0.0652	<LOQ	<LOQ	0.215	7.24	1.28	0.0546	0.451	0.139	0.00400	8.51	<LOQ	1.15	0.0130
M IV_14	<LOQ	<LOQ	214	23.9	0.611	3.81	3.14	528	0.203	6.21	3.32	106	0.0173	<LOQ	25.1	0.296	4.16	0.372	0.0689	0.325	0.161	0.00900	4.35	<LOQ	0.933	0.0140
M IV_15	<LOQ	163	114	10.4	0.365	2.84	1.15	67.3	0.0969	2.89	1.63	80.1	0.0165	<LOQ	<LOQ	0.196	2.85	0.479	0.143	0.170	0.142	0.00700	3.35	<LOQ	0.580	0.00800
M IV_16	<LOQ	<LOQ	99.7	11.7	0.389	2.28	1.25	71.4	0.0824	2.20	1.39	65.1	0.0190	<LOQ	<LOQ	0.155	3.49	1.71	0.0933	0.133	0.171	0.00500	3.52	<LOQ	0.523	0.00900
M IV_17	<LOQ	<LOQ	287	125	1.01	3.39	3.77	252	<LOQ	7.33	3.66	152	<LOQ	<LOQ	<LOQ	<LOQ	5.73	0.194	<LOQ	<LOQ	<LOQ	<LOQ	2.55	<LOQ	1.42	<LOQ
M IV_18	<LOQ	<LOQ	200	121	1.04	2.75	2.64	183	<LOQ	3.73	2.95	113	<LOQ	<LOQ	<LOQ	<LOQ	5.07	0.433	<LOQ	<LOQ	<LOQ	<LOQ	2.28	<LOQ	1.95	<LOQ
M IV_19	<LOQ	<LOQ	617	71.4	1.82	3.36	5.30	441	<LOQ	5.14	3.96	94.5	<LOQ	<LOQ	<LOQ	<LOQ	11.6	0.142	<LOQ	<LOQ	<LOQ	<LOQ	5.31	<LOQ	1.22	<LOQ
M IV_20	<LOQ	<LOQ	235	25.0	0.660	3.03	2.49	173	<LOQ	2.09	2.28	121	<LOQ	<LOQ	<LOQ	<LOQ	5.80	0.00500	<LOQ	<LOQ	<LOQ	<LOQ	2.72	<LOQ	0.828	<LOQ
M IV_21	<LOQ	<LOQ	87.0	31.3	0.599	2.40	1.38	115	<LOQ	<LOQ	1.31	84.8	<LOQ	<LOQ	<LOQ	<LOQ	4.70	0.595	<LOQ	<LOQ	<LOQ	<LOQ	1.20	<LOQ	0.367	<LOQ
M IV_22	<LOQ	<LOQ	148	59.2	0.433	2.65	1.46	109	<LOQ	<LOQ	2.85	95.4	<LOQ	<LOQ	<LOQ	<LOQ	4.70	0.00500	<LOQ	<LOQ	<LOQ	<LOQ	1.83	<LOQ	1.26	<LOQ
M IV_23	<LOQ	<LOQ	530	100	1.82	4.93	6.10	450	<LOQ	1.09	3.36	87.7	<LOQ	<LOQ	<LOQ	<LOQ	9.83	0.519	<LOQ	<LOQ	<LOQ	<LOQ	4.93	<LOQ	1.06	<LOQ
M IV_24	<LOQ	70.8	687	165	1.91	4.01	6.54	433	<LOQ	5.81	3.62	73.5	<LOQ	<LOQ	<LOQ	<LOQ	9.73	0.207	<LOQ	<LOQ	<LOQ	<LOQ	6.52	<LOQ	1.02	<LOQ

Sample	La	Ce	Pr	Nd	Sm	Eu	Gd	Tb	Dy	Y	Ho	Er	Tm	Yb	Lu
	ng L^{-1}	ng L^{-1}	ng L^{-1}	ng L^{-1}	ng L^{-1}	ng L^{-1}	ng L^{-1}	ng L^{-1}	ng L^{-1}	ng L^{-1}	ng L^{-1}	ng L^{-1}	ng L^{-1}	ng L^{-1}	ng L^{-1}
BLK1	0.551	0.495	0.0430	0.368	0.288	0.00300	0.0320	0.0260	0.0707	0.419	0.0180	0.123	0.0220	0.0990	0.0280
BLK2	0.349	0.183	0.0470	0.106	0.131	0.00707	0.0230	0.0290	0.0707	0.246	0.0230	0.0860	0.0200	0.0970	0.0290
BLK3	0.561	0.795	0.108	0.296	0.236	0.016	0.0340	0.0150	0.0707	0.347	0.00800	0.0530	0.0210	0.181	0.0220